UBIQUITIN AND UBIQUITIN-LIKE MODIFICATIONS IN VIRAL INFECTION AND INNATE IMMUNITY

EDITED BY: Soham Gupta, Konstantin Sparrer and Éric Bergeron
PUBLISHED IN: Frontiers in Immunology

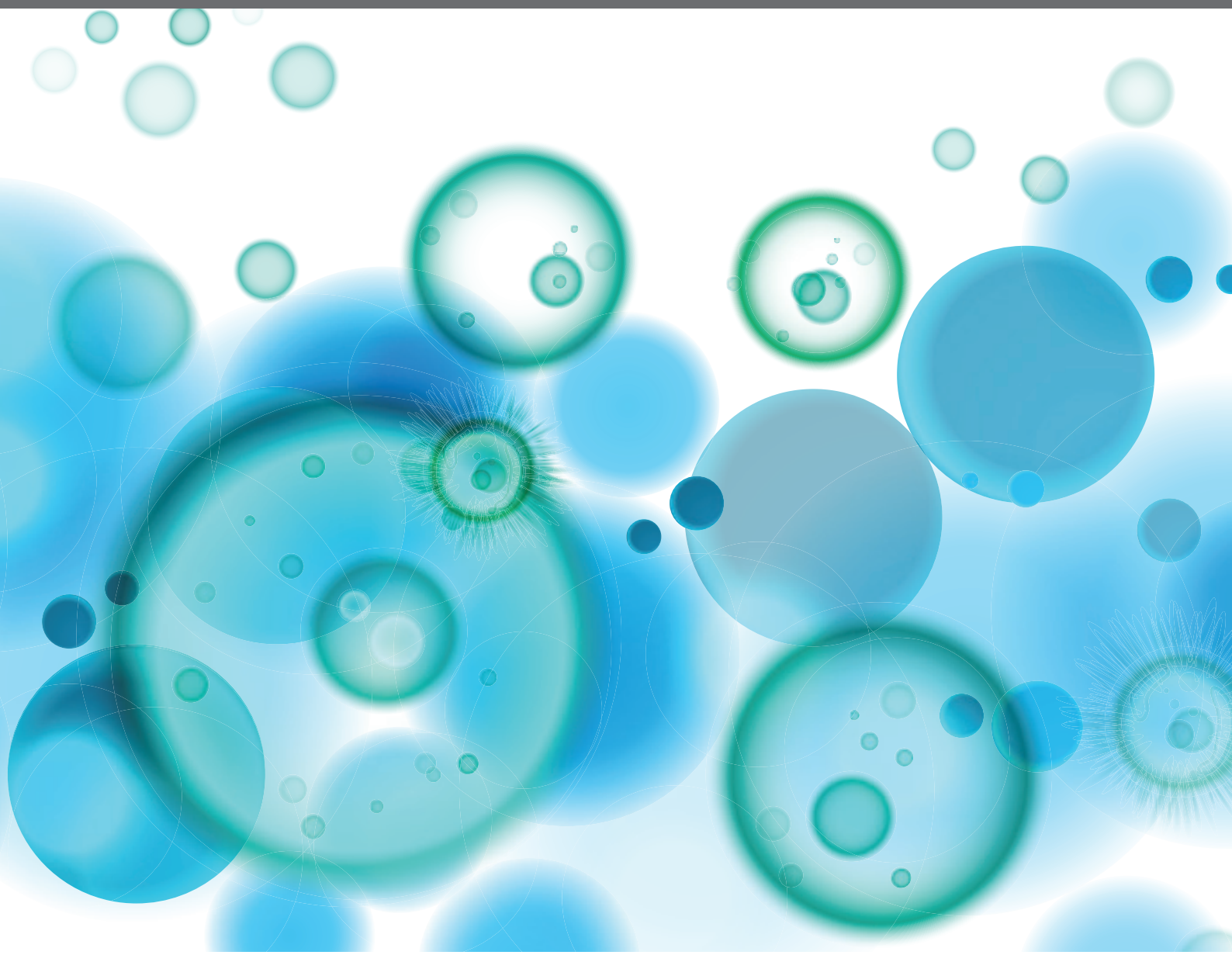

frontiers Research Topics

ISSN 1664-8714
ISBN 978-2-88976-056-5
DOI 10.3389/978-2-88976-056-5

About Frontiers

Frontiers is more than just an open-access publisher of scholarly articles: it is a pioneering approach to the world of academia, radically improving the way scholarly research is managed. The grand vision of Frontiers is a world where all people have an equal opportunity to seek, share and generate knowledge. Frontiers provides immediate and permanent online open access to all its publications, but this alone is not enough to realize our grand goals.

Frontiers Journal Series

The Frontiers Journal Series is a multi-tier and interdisciplinary set of open-access, online journals, promising a paradigm shift from the current review, selection and dissemination processes in academic publishing. All Frontiers journals are driven by researchers for researchers; therefore, they constitute a service to the scholarly community. At the same time, the Frontiers Journal Series operates on a revolutionary invention, the tiered publishing system, initially addressing specific communities of scholars, and gradually climbing up to broader public understanding, thus serving the interests of the lay society, too.

Dedication to Quality

Each Frontiers article is a landmark of the highest quality, thanks to genuinely collaborative interactions between authors and review editors, who include some of the world's best academicians. Research must be certified by peers before entering a stream of knowledge that may eventually reach the public - and shape society; therefore, Frontiers only applies the most rigorous and unbiased reviews.
Frontiers revolutionizes research publishing by freely delivering the most outstanding research, evaluated with no bias from both the academic and social point of view. By applying the most advanced information technologies, Frontiers is catapulting scholarly publishing into a new generation.

What are Frontiers Research Topics?

Frontiers Research Topics are very popular trademarks of the Frontiers Journals Series: they are collections of at least ten articles, all centered on a particular subject. With their unique mix of varied contributions from Original Research to Review Articles, Frontiers Research Topics unify the most influential researchers, the latest key findings and historical advances in a hot research area! Find out more on how to host your own Frontiers Research Topic or contribute to one as an author by contacting the Frontiers Editorial Office: frontiersin.org/about/contact

UBIQUITIN AND UBIQUITIN-LIKE MODIFICATIONS IN VIRAL INFECTION AND INNATE IMMUNITY

Topic Editors:
Soham Gupta, Karolinska Institutet (KI), Sweden
Konstantin Sparrer, Ulm University Medical Center, Germany
Éric Bergeron, Centers for Disease Control and Prevention (CDC), United States

Citation: Gupta, S., Sparrer, K., Bergeron, É., eds. (2023). Ubiquitin and Ubiquitin-like Modifications in Viral Infection and Innate Immunity. Lausanne: Frontiers Media SA. doi: 10.3389/978-2-88976-056-5

Table of Contents

frontiers | Frontiers in Immunology

TYPE Editorial
PUBLISHED 02 February 2023
DOI 10.3389/fimmu.2023.1148296

OPEN ACCESS

EDITED AND REVIEWED BY
Pei-Hui Wang,
Shandong University, China

*CORRESPONDENCE
Konstantin M.J. Sparrer
konstantin.sparrer@uni-ulm.de
Éric Bergeron
exj8@cdc.gov
Soham Gupta
soham.gupta@ki.se

†These authors have contributed equally to this work

SPECIALTY SECTION
This article was submitted to Viral Immunology, a section of the journal Frontiers in Immunology

RECEIVED 19 January 2023
ACCEPTED 23 January 2023
PUBLISHED 02 February 2023

CITATION
Sparrer KMJ, Bergeron É and Gupta S (2023) Editorial: Ubiquitin and ubiquitin-like modifications in viral infection and innate immunity.
Front. Immunol. 14:1148296.
doi: 10.3389/fimmu.2023.1148296

Editorial: Ubiquitin and ubiquitin-like modifications in viral infection and innate immunity

Konstantin M. J. Sparrer[1*†], Éric Bergeron[2,3*†] and Soham Gupta[4*†]

[1]Institute of Molecular Virology, Ulm University Medical Center, Ulm, Germany, [2]Viral Special Pathogens Branch, Division of High-Consequence Pathogens and Pathology, Centers for Disease Control and Prevention, Atlanta, GA, United States, [3]Department of Pharmaceutical and Biomedical Sciences, College of Pharmacy, University of Georgia, Athens, GA, United States, [4]Division of Clinical Microbiology, Department of Laboratory Medicine, Karolinska Institutet, Stockholm, Sweden

KEYWORDS

ubiquitin, ISG15, Nedd8, ubiquitin-like modifications, E3-ubiquitin ligase, deubiquitinases, innate immunity, viral mimicry

Editorial on the Research Topic
Ubiquitin and ubiquitin-like modifications in viral infection and innate immunity

The Research Topic '*ubiquitin and ubiquitin-like modifications in viral infection and innate immunity*' aimed to advance our knowledge and understanding of the regulation of innate immune signaling by ubiquitin and ubiquitin-like modifiers during infection, its interplay with viral proteins and the application of modern techniques to decode these interactions. Six original research papers, three mini-reviews, one review article, and one perspective article that covered various aspects of the Research Topic were eventually part of the collection.

Innate immune responses are our first line of defense against invading pathogens. Multiple signaling pathways work in concert to eliminate the invading pathogen (1). However, to mediate a rapid but balanced defensive response, the innate immune system itself has to be intricately regulated. The fate and function of the individual key signalling factors is often regulated by post-translational modifications (PTMs) (2). Most prominently among them are ubiquitin (Ub) and ubiquitin-like (UbLs) modifications such as ISGylation, Neddylation, UFMylation, SUMOylation (3, 4). These modifications virtually control all aspects of innate immune signaling (5, 6). A concerted series of enzymatic processes leads to the covalent attachment of Ub/UbLs to mainly lysine residue of substrate proteins. It involves an activation enzyme (E1), a conjugation enzyme (E2), and ligating enzyme (E3). E3-Ub ligases recognize the substrate simultaneously interacts with the Ub-conjugated E2 and the substrate protein and mediates the isopeptide bond formation between the Ub and a lysine residue of the substrate protein (7). Modification of a signaling protein by Ub or UbLs eventually impacts its functional activity and/or stability.

More than 600 human E3-ligases have been identified so far, among them are members of the tripartite motif (TRIM) family that are encoded within the MHC-I locus of the human DNA (8). The review by Jia et al. highlights the role of TRIMs in regulating innate immunity that impacts infections or auto-inflammatory conditions. Beyond classical ubiquitination, TRIM proteins like TRIM38 mediate SUMOylation in RNA-sensing (RIG-I/MDA5) and DNA-sensing (cGAS/STING) pathways. A role of TRIM7 in the negative regulation of innate

immune response upon RNA-virus infection was revealed by the study of Yang et al. TRIM7, also known as E3 ubiquitin-protein ligases RING-finger protein 90 (RNF90) promotes K48-linked ubiquitination of the important RNA-sensing signaling adaptor MAVS. This eventually leads to the proteasomal degradation of MAVS and consequently decreased innate immune signaling in response to RNA viruses. Of note, the negative regulation of MAVS by TRIM7 may protect against aberrant spontaneous activation of immune responses under physiological conditions.

Ubiquitin has seven lysine residues (Lys6, Lys11, Lys27, Lys29, Lys33, Lys48, and Lys63). The mode of Ub lysine-lysine interconnection determines the fate of the substrate protein (9). In addition to lysine-linked chains, linear chains can be formed that are linked *via* the N-terminal first methionine. This is mediated by the specialized E3-ligase complex Linear ubiquitin chain assembly complex (LUBAC) (10, 11). The study by Miyashita et al. shows that the autophagy cargo, Nuclear dot protein 52 kDa (NDP52, also known as calcium binding and coiled-coil domain 2, CALCOCO2) interacts with the LUBAC complex *via* the HOIP subunit. Although this interaction did not affect the E3-ligase activity of the LUBAC, NDP52 negatively regulates TNF-α secretion, antiviral signaling, and apoptosis, as well as xenophagosome formation.

Despite forming a covalent bond between the substrate and ubiquitin chain, modifications by ubiquitination are reversible. Homeostasis is maintained by a balance between PTM formation by E3-ligases and the removal of ubiquitin chains by deubiquitinases (DUBs) (12). Currently, more than 100 human DUBs have been identified, and the role of major DUBs in type-I IFN signaling during viral infection was comprehensively reviewed by Qian et al. In addition, it was highlighted that the DUBs are not always required to be catalytically active to regulate signal transduction. DUBs can also have specific antiviral activity, as shown by Gao et al. Specifically, the DUB ubiquitin-specific protease 8 (USP8) may suppress HIV-1 infectivity by counteracting Vif-induced APOBEC3G degradation. Their work also revealed other DUBs like USP7, USP33, and USP37 that play a role as host-encoded restriction factors to prevent degradation facilitated by HIV-1 accessory proteins Vpr, Vpu, and Vpx.

However, viruses have evolved strategies to interfere with the ubiquitin system to counteract the host defenses and promote their replication. To this end, viruses encode proteins that mimic key components of Ub and UbL ligases or deubiquitinates (13, 14). For example, poxviruses encode E3-ubiquitin ligase and adaptor proteins belonging to PRANC, ANK/BC, BBK, P28/RING, and MARCH proteins. Cui et al. reviewed the role of these five categories of proteins in host immune evasion. Accessory proteins of HIV, such as Nef exploit ubiquitin regulatory factors to dampen innate signaling. Castro-Gonzalez et al. provide a perspective on Nef's impact on autophagy and apoptotic pathways triggered by Nef-promoted mono-ubiquitination of BCL-2 by PRKN. Mono-ubiquitination enhances the interaction of BCL-2 with BECN1, thereby diminishing autophagy initiation (15).

While ubiquitination is undoubtedly among the most studied PTMs, UbL modifications like ISGylation, SUMOylation, and Neddylation etc. have recently gained increased attention. In principle, similar cascades as classical ubiquitination are required to mediate conjugation to substrates. In their review, Thery et al. discussed different mass-spectrometry-based approaches to identify the substrates of Interferon-stimulated gene 15 (ISG15) and ISGylation sites. Mohanty et al. studied interaction dynamics between NEDD8 and E3-ligase Culling-RING ligases (CRLs). All-atom MD simulations combined with NMR spectroscopy revealed the interactions that stabilize the open and closed conformation of NEDDylated-Cul5^{CTD}. In addition, they define the role of NEDD8 in the catalytic confirmation of Cullin-Rbx1 and the effect of NEDD8 deamidation on CRL activity.

Although a significant focus of the Research Topic is Ub and UbL proteins in the human system, we did not restrict ourselves to one species only. In shrimps, Wang et al. identify a viral serine/threonine protein kinase WSV083 that phosphorylates the nuclear transcription factor Tcf, triggering its ubiquitination and proteasome mediated degradation. Thus, the antiviral function of Tcf is reduced. Shephard et al. studied the structure of chicken 2'-5' oligoadenylate synthetase-like proteins (OASL), a key enzyme in innate immunity, whose UbL tandem domain shares similarity to human ISG15 and, unlike mammalian OASL, it can be conjugated to proteins. This led them to speculate that OASL may have a similar function as ISG15 in the absence of the latter.

In this collection we have assembled novel research and overview articles covering different stages of the ubiquitination and deubiquitination cascades, non-ubiquitin modifiers, and extending our understanding of the role of Ub and UbLs in innate immune regulation of non-human species. State-of-the-art proteomics-based and NMR spectroscopy-based technologies that could be applied to study interactions and structural conformations were presented. Although our collection has certainly expanded our knowledge about the role of Ub and UbL modifications in antiviral innate immune responses, there are still a lot of open questions. Are specific ubiquitin chains more prevalent for one or another innate immune pathway? Are the known conjugated proteins the only UbL proteins? How important are the mixed linkage-type chains in innate immunity? Can the proteolysis-targeting chimera (PROTAC) technology be used in the therapeutic regulation of innate immune response? Thus, we are also looking forward to exciting future work on Ub and UbL modifiers as the major regulatory PTMs in innate immunity.

Author contributions

All the authors equally contributed in drafting, reviewing, and editing the manuscript critically for intellectual components and approved it for final submission. Original draft by SG.

Funding

KS was supported by the German Research Foundation (DFG grants SPP1923, SP 1600/5-1 and CRC1279, INST 40/623-1) as well as the German Ministry for Education and Research (BMBF grant IMMUNOMOD, 01KI2014). EB was funded through NIAID (R01AI151006) and DTRA (HDTRA12210007). SG received support from the Swedish Research Council grant (2021-03035), Karolinska Institutet Stiftelser och Fonder grant (2020-02153), The Center for Medical Innovation grant (CIMED-FoUI-093304), and Åke Wiberg Stiftelse grant (M20-0220).

Acknowledgments

We acknowledge the support of the contributors, and time and effort of the reviewers for critically reviewing and providing valuable comments and suggestions to improve the submitted manuscripts in this topic.

Conflict of interest

The authors declare that the research was conducted in the absence of any commercial or financial relationships that could be construed as a potential conflict of interest.

Publisher's note

Disclaimer

Opinions, interpretations, conclusions, and recommendations are those of the author and not necessarily endorsed by the Centers for Disease Control and Prevention.

References

1. Kanneganti TD, Lamkanfi M, Amer AO. Innate immune pathways in host defense. *Mediators Inflammation* (2012) 2012:708972. doi: 10.1155/2012/708972

2. Karve TM, Cheema AK. Small changes huge impact: The role of protein posttranslational modifications in cellular homeostasis and disease. *J Amino Acids* (2011) 2011:207691. doi: 10.4061/2011/207691

3. Cappadocia L, Lima CD. Ubiquitin-like protein conjugation: Structures, chemistry, and mechanism. *Chem Rev* (2018) 118(3):889–918. doi: 10.1021/acs.chemrev.6b00737

4. Davis ME, Gack MU. Ubiquitination in the antiviral immune response. *Virology* (2015) 479-480:52–65. doi: 10.1016/j.virol.2015.02.033

5. Liu X, Wang Q, Chen W, Wang C. Dynamic regulation of innate immunity by ubiquitin and ubiquitin-like proteins. *Cytokine Growth Factor Rev* (2013) 24(6):559–70. doi: 10.1016/j.cytogfr.2013.07.002

6. Zinngrebe J, Montinaro A, Peltzer N, Walczak H. Ubiquitin in the immune system. *EMBO Rep* (2014) 15(1):28–45. doi: 10.1002/embr.201338025

7. Glickman MH, Ciechanover A. The ubiquitin-proteasome proteolytic pathway: Destruction for the sake of construction. *Physiol Rev* (2002) 82(2):373–428. doi: 10.1152/physrev.00027.2001

8. Koepke L, Gack MU, Sparrer KM. The antiviral activities of TRIM proteins. *Curr Opin Microbiol* (2021) 59:50–7. doi: 10.1016/j.mib.2020.07.005

9. Swatek KN, Komander D. Ubiquitin modifications. *Cell Res* (2016) 26(4):399–422. doi: 10.1038/cr.2016.39

10. Kirisako T, Kamei K, Murata S, Kato M, Fukumoto H, Kanie M, et al. A ubiquitin ligase complex assembles linear polyubiquitin chains. *EMBO J* (2006) 25(20):4877–87. doi: 10.1038/sj.emboj.7601360

11. Fiil BK, Gyrd-Hansen M. The Met1-linked ubiquitin machinery in inflammation and infection. *Cell Death Differ* (2021) 28(2):557–69. doi: 10.1038/s41418-020-00702-x

12. Snyder NA, Silva GM. Deubiquitinating enzymes (DUBs): Regulation, homeostasis, and oxidative stress response. *J Biol Chem* (2021) 297(3):101077. doi: 10.1016/j.jbc.2021.101077

13. Masucci MG. Viral ubiquitin and ubiquitin-like deconjugases-Swiss army knives for infection. *Biomolecules* (2020) 10(8):1137. doi: 10.3390/biom10081137

14. Wimmer P, Schreiner S. Viral mimicry to usurp ubiquitin and SUMO host pathways. *Viruses* (2015) 7(9):4854–72. doi: 10.3390/v7092849

15. Castro-Gonzalez S, Shi Y, Colomer-Lluch M, Song Y, Mowery K, Almodovar S, et al. HIV-1 nef counteracts autophagy restriction by enhancing the association between BECN1 and its inhibitor BCL2 in a PRKN-dependent manner. *Autophagy* (2021) 17(2):553–77. doi: 10.1080/15548627.2020.1725401

frontiers in Immunology

ORIGINAL RESEARCH
published: 19 March 2021
doi: 10.3389/fimmu.2021.635475

Crosstalk Between NDP52 and LUBAC in Innate Immune Responses, Cell Death, and Xenophagy

Hirohisa Miyashita[1†], *Daisuke Oikawa*[1†], *Seigo Terawaki*[1], *Daijiro Kabata*[2], *Ayumi Shintani*[2] *and Fuminori Tokunaga*[1*]

[1] Department of Pathobiochemistry, Graduate School of Medicine, Osaka City University, Osaka, Japan, [2] Department of Medical Statistics, Graduate School of Medicine, Osaka City University, Osaka, Japan

Nuclear dot protein 52 kDa (NDP52, also known as CALCOCO2) functions as a selective autophagy receptor. The linear ubiquitin chain assembly complex (LUBAC) specifically generates the N-terminal Met1-linked linear ubiquitin chain, and regulates innate immune responses, such as nuclear factor-κB (NF-κB), interferon (IFN) antiviral, and apoptotic pathways. Although NDP52 and LUBAC cooperatively regulate bacterial invasion-induced xenophagy, their functional crosstalk remains enigmatic. Here we show that NDP52 suppresses canonical NF-κB signaling through the broad specificity of ubiquitin-binding at the C-terminal UBZ domain. Upon TNF-α-stimulation, NDP52 associates with LUBAC through the HOIP subunit, but does not disturb its ubiquitin ligase activity, and has a modest suppressive effect on NF-κB activation by functioning as a component of TNF-α receptor signaling complex I. NDP52 also regulates the TNF-α-induced apoptotic pathway, but not doxorubicin-induced intrinsic apoptosis. A chemical inhibitor of LUBAC (HOIPIN-8) cancelled the increased activation of the NF-κB and IFN antiviral pathways, and enhanced apoptosis in *NDP52*-knockout and -knockdown HeLa cells. Upon *Salmonella*-infection, colocalization of *Salmonella*, LC3, and linear ubiquitin was detected in parental HeLa cells to induce xenophagy. Treatment with HOIPIN-8 disturbed the colocalization and facilitated *Salmonella* expansion. In contrast, HOIPIN-8 showed little effect on the colocalization of LC3 and *Salmonella* in *NDP52*-knockout cells, suggesting that NDP52 is a weak regulator in LUBAC-mediated xenophagy. These results indicate that the crosstalk between NDP52 and LUBAC regulates innate immune responses, apoptosis, and xenophagy.

Keywords: NDP52, ubiquitin, LUBAC, NF-κB, apoptosis, xenophagy

OPEN ACCESS

Edited by:
Soham Gupta,
Karolinska Institutet (KI), Sweden

Reviewed by:
Henning Walczak,
Imperial College London, United Kingdom
Domagoj Vucic,
Genentech, Inc., United States
Rudi Beyaert,
Ghent University, Belgium
Konstanze F. Winklhofer,
Ruhr University Bochum, Germany

***Correspondence:**
Fuminori Tokunaga
ftokunaga@med.osaka-cu.ac.jp

[†]*These authors have contributed equally to this work*

Specialty section:
This article was submitted to Molecular Innate Immunity, a section of the journal Frontiers in Immunology

Received: *30 November 2020*
Accepted: *03 March 2021*
Published: *19 March 2021*

Citation:
Miyashita H, Oikawa D, Terawaki S, Kabata D, Shintani A and Tokunaga F (2021) Crosstalk Between NDP52 and LUBAC in Innate Immune Responses, Cell Death, and Xenophagy. Front. Immunol. 12:635475. doi: 10.3389/fimmu.2021.635475

INTRODUCTION

Protein ubiquitination, a crucial post-translational modification, is catalyzed by ubiquitin-activating enzyme (E1), ubiquitin-conjugating enzyme (E2), and ubiquitin ligase (E3), and regulates numerous cellular functions, including proteasomal degradation, membrane trafficking, DNA repair, and signal transduction, by generating various types of ubiquitin linkages in the "ubiquitin code" (1, 2). Linear ubiquitin chain assembly complex (LUBAC) is composed of the HOIL-1L (also known as

RBCK1), HOIP (RNF31), and SHARPIN subunits, and generates the N-terminal Met1-linked linear polyubiquitin chain (3–5). LUBAC is required for the regulation of the canonical nuclear factor-κB (NF-κB) activation pathway, interferon (IFN) regulatory factor 3 (IRF3)-mediated antiviral response, and cell death (5). Moreover, dysfunctions in LUBAC and linear ubiquitin-binding proteins, such as NF-κB-essential modulator (NEMO), optineurin (OPTN), and A20, are associated with various disorders (6–10). Indeed, we previously reported that OPTN selectively binds to linear ubiquitin through the UBAN domain, and plays a crucial role in the suppression of NF-κB activity (8). Furthermore, the amyotrophic lateral sclerosis-associated *OPTN* mutations, such as E478G and Q398X, abrogated the inhibitory effects on LUBAC-mediated NF-κB activation, and increased caspase activation (7, 8). These results suggested that LUBAC affects the physiological functions of OPTN.

To modulate the LUBAC activity, we developed α,β-unsaturated carbonyl-containing compounds, HOIPIN-1 (from HOIP-inhibitor-1) and its potent derivative HOIPIN-8 (11–13). HOIPINs are powerful and specific LUBAC inhibitors that suppress the LUBAC-mediated proinflammatory cytokine-induced NF-κB activation and pathogen-associated molecular patterns-induced IFN antiviral pathways, by modifying the active site Cys885 and thus specifically inhibiting the RING-HECT-hybrid reaction in HOIP (13). Indeed, we showed that HOIPINs suppressed the enhanced NF-κB activation in *OPTN*-deficient cells.

Nuclear dot protein 52 kDa (NDP52, also known as calcium binding and coiled-coil domain 2, CALCOCO2) was originally identified as an antigen protein localized in nuclear domain 10 (14, 15). NDP52, as well as OPTN, p62/SQSTM1, NBR1, and Tax1-binding protein 1 (TAX1BP1), functions as an autophagy cargo receptor that recognizes substrates for selective autophagy, including proteins, organelles, and pathogens, in a ubiquitin-dependent or independent manner, and links to ATG8/LC3 *via* LC3-interacting regions (LIRs) (16). In particular, NDP52 and OPTN are critical for the selective autophagy of damaged mitochondria (mitophagy) and invading microorganisms (xenophagy) (16–18). Bacteria that have invaded mammalian cells are initially restricted in vacuoles or phagosomes; however, some escape to the cytoplasm by disruption of the phagosomal or vacuolar membrane (19). NDP52 binds to galectin 8 (Gal8) (20), which recognizes bacterial carbohydrates in the cytoplasm and bridges to LC3 in autophagosomes. Moreover, ubiquitinated and ruptured phagosomal and bacterial membranes are recognized by NDP52 for autophagic degradation (21–23). Importantly, Noad and co-workers reported that LUBAC is recruited to the bacterial surface *via* HOIP, and linear ubiquitin is part of the ubiquitin coat of invading *Salmonella* (24). Subsequently, the recruited NEMO and OPTN, linear ubiquitin-binding UBAN domain-containing proteins, function in NF-κB and xenophagy, respectively. Furthermore, van Wijk et al. reported that OTULIN, a linear ubiquitin chain-specific deubiquitinase, plays a major role in the regulation of linear ubiquitin in the bacterial coat, which affects the recruitment of NEMO and the activation of canonical IKK (25). A more recent report showed that the linear ubiquitination of ATG13 by LUBAC and the deubiquitination by OTULIN are associated with autophagy initiation (26). Thus, NDP52 and linear ubiquitination are closely correlated in xenophagy; however, the detailed physiological crosstalk between NDP52 and LUBAC has remained elusive. In this study, we investigated the physiological roles of the crosstalk between NDP52 and LUBAC in innate immune responses, cell death, and xenophagy, using the LUBAC inhibitors, HOIPINs.

MATERIALS AND METHODS

Reagents

The following reagents were obtained as indicated: zVAD-FMK (ZVAD) (ENZO Life Sciences), recombinant human TNF-α and IL-1β (BioLegend), poly(I:C) (HMW) (Invivogen), doxorubicin (Calbiochem), DAPI (Dojindo), blasticidin (Wako), pepstatin A, chloroquine, and cycloheximide (Sigma), E64d (Tokyo Chemical Industry), monoubiquitin, eight kinds of diubiquitins, linear (M1)-, K11-, K48-, and K63-tetraubiquitins (Boston Biochem), control siRNA (sc-37007) and *NDP52*-siRNA (sc-93738) (Santa Cruz Biotechnology), and BV6 (Genentech). HOIPIN-1 (2-[(1*E*)-3-(2-methoxyphenyl)-3-oxoprop-1-en-1-yl] benzoic acid sodium salt) and HOIPIN-8 (2-{(E)-3-[2,6-difluoro-4-(1H-pyrazol-4-yl)-phenyl]-3-oxo-propenyl}-4-(1-methyl-1H-pyraol-4-yl)-benzoic acid sodium salt) were prepared as described (11, 12).

Plasmids

The open reading frames of cDNAs were amplified by reverse-transcription PCR. Mutants of these cDNAs were prepared by the QuikChange method, and the nucleotide sequences were verified. The cDNAs were ligated to the appropriate epitope sequences and cloned into the pcDNA3.1 (Invitrogen), pMAL-c2x (New England Biolabs), and pGEX6p-1 (Addgene) vectors. For lentiviral transduction, pCSII-CMV-RfA-IRES-Blast (RIKEN BioResource Research Center) was used.

Cell Culture and Transfection

HeLa cells (ATCC), HEK293T cells (ATCC), A549 cells (ATCC), and *ATG7*$^{-/-}$ HeLa cells (27) (a generous gift from Prof. Yoshimori) were cultured in DMEM containing 10% fetal bovine serum (FBS) and antibiotics. Transfection experiments were performed using PEI (polyethylenimine) or lipofectamine RNAiMAX (Thermo Fisher). For the stable expression of the FLAG-His_6-tagged NDP52-wild type (WT) or -D439R mutant in *NDP52*$^{-/-}$ HeLa cells, lentiviral infection followed by selection with 5 μg/ml blasticidin was performed.

Luciferase Assay

HEK293T and A549 cells were cultured in 24-well plates, and co-transfected with the pGL4.32 [*luc2P*/NF-κB-RE/Hygro] vector (Promega) and the pRL-TK *Renilla* Luciferase control reporter vector (Promega). At 24 h after transfection by PEI, the cells were lysed and the luciferase activity was measured with a GloMax 20/

20 luminometer (Promega), using the Dual-Luciferase Reporter Assay System (Promega). At 18 h after transfection, TNF-α (10 ng/ml) or IL-1β (1 ng/ml) was added to the medium. The cultures were incubated further for 6 h and then the cells were analyzed.

Immunoprecipitation, SDS-PAGE, and Immunoblotting

Cells were lysed with 50 mM Tris-HCl, pH 7.5, 150 mM NaCl, 1% Triton X-100, 2 mM PMSF, and complete protease inhibitor cocktail (Sigma). Immunoprecipitation was performed using appropriate antibodies followed by Protein G agarose beads (GE Healthcare) at 4°C with gentle rotation. Immunoprecipitates were washed five times with the lysis solution. The samples were then separated by SDS-PAGE and transferred to PVDF membranes. After blocking in Tris-buffered saline containing 0.1% Tween-20 (TBS-T) with 5% skim-milk or bovine serum albumin (BSA), the membrane was incubated with the appropriate primary antibodies, diluted in TBS-T containing 5% w/v BSA, and then with horseradish peroxidase-conjugated secondary antibodies (GE Healthcare). The chemiluminescent images were obtained with an LAS4000 imaging analyzer (GE Healthcare) or a Fusion Solo S imaging system (Vilber).

Antibodies

The following antibodies were used for immunoblot analyses: NDP52 (#9036; 1:1,000), P-IκBα (#9246; 1:1,000), IκBα (#4812; 1:1,000), P-p105 (#4806; 1:1,000), p105 (#3035; 1:1,000), P-p65 (#3033; 1:1,000), p65 (#8242; 1:1,000), P-IKKα/β (#2697; 1:1,000), P-IRF3 (#4947; 1:2,000), IRF3 (#4302; 1:1,000), P-TBK1 (#5483; 1:1000), TBK1 (#3504; 1:1000), caspase 8 (#4790; 1:1,000), cleaved caspase 8 (#9496; 1:1,000), caspase 3 (#9662; 1:1,000), cleaved caspase 3 (#9661; 1:1,000), caspase 9 (#9502; 1:1,000), Bid (#8762; 1:1,000), PARP (#9542; 1:1,000), and Atg7 (#8558; 1:1000) were obtained from Cell Signaling. HOIL-1L (sc-393754; 1:250), ubiquitin (P4D1) (sc-8017; 1:1,000), TNFR1 (sc-8436; 1:1,000), β-actin (sc-47778; 1:1,000), MAVS (sc-166583; 1:1,000), and IKKα/β (sc-7607; 1:1,000) were purchased from Santa Cruz Biotechnology. HOIP (ab125189; 1:1,000) and NEMO (ab178872; 1:3,000) were purchased from Abcam. RIP1 (BD Biosciences, 610458; 1:1,000), tubulin (Cedarlane, CLT9002; 1:3,000), SHARPIN (Proteintech, 14626-1-AP; 1:3,000), linear ubiquitin (Millipore, clone LUB9, MABS451; 1:1,000), HA (Roche, 11867423001; 1:1,000), Myc (MBL, HRP-Conjugate, M192-7; 1:20,000), and DYKDDDDK (Wako, 1E6, 015-22391; HRP-Conjugate; 1:20,000) were also used. For immunoprecipitation, c-Myc (Santa Cruz Biotechnology, sc-40; 1μg), FLAG (Sigma-Aldrich, clone M2, F1840; 1μg), FADD (Proteintech, 14906-1-AP; 2μg), NDP52 (Abcam, ab68588; 2 μg), and normal rabbit IgG (MBL, PM035; 2 μg) were used. For immunofluorescence analyses, LC3 (MBL, clone 4E12; 1:100), linear ubiquitin (Genentech, 1F11/3F5/Y102L; 5 μg/ml), and NDP52 (abcam, ab68588; 1:200) were used as primary antibodies, and then anti-mouse IgG Alexa Fluor 488, anti-human IgG Alexa Fluor 647, and anti-rabbit Alexa Fluor 647 (Thermo Fisher, goat polyclonal; 1:1000) were used as secondary antibodies, respectively.

Recombinant Proteins

Expression vectors of maltose-binding protein (MBP)-fused wild type (WT)-NDP52 and the NDP52-D439R mutant, and MBP-LacZ were expressed in *Escherichia coli* Rosetta 2 (DE3) (Novagen) and purified using amylose resin (New England Biolabs). The glutathione *S*-transferase (GST)-fused NDP52-UBZ domain was expressed in *E. coli* BL21 (DE3)pLysS (Promega) and purified with a GSTrap column (GE Healthcare).

Pulldown Assay

Linear polyubiquitin was prepared as described previously (28). Briefly, reaction mixture, containing 40 mM Tris-HCl, pH 7.5, 10 mM $MgCl_2$, 0.6 mM dithiothreitol, 10 mM ATP, 1.4 mM ubiquitin (Boston Biochem), 1 μM baculovirus-expressed His-E1, 8 μM *E. coli*-expressed His-UbcH5c, and baculovirus-expressed His-HOIP/Myc-SHARPIN complex was incubated at 37°C for 3 h, and then heated at 60°C for 15 min. After centrifugation at 14,000 rpm for 30 min, the supernatant containing linear polyubiquitin was used. MBP-fusion proteins (0.8 μM) and tetraubiquitin (2 μM), diubiquitin (1 μM), monoubiquitin (1 μM), and linear polyubiquitin (1 μg) were incubated in reaction buffer (50 mM Tris-HCl, pH 7.5, 150 mM NaCl, 1 mM dithiothreitol, 0.1% NP-40 and 0.25 mg/ml BSA) at 37°C for 1 h, followed by the addition of amylose resin. Similarly, GST-fusion proteins were incubated with tetraubiquitin (3.4 μg), followed by glutathione Sepharose (GE Healthcare). The samples were further incubated at 4°C for 1 h with gentle rotation, and then the beads were washed three times with the reaction buffer without BSA, and analyzed by SDS–PAGE. The bound ubiquitin was detected by immunoblotting using an anti-ubiquitin antibody, and MBP- and GST-fusion proteins were stained with Coomassie Brilliant Blue (CBB).

For the pulldown assay with cell lysates, HEK293T cells were transiently transfected with plasmids encoding HA-tagged ubiquitin or its single-Lys mutants (K6, K11, K27, K29, K33, K48, and K63), and lysed with buffer containing 50 mM Tris-HCl, pH 7.5, 150 mM NaCl, 1 mM dithiothreitol, 0.1% NP-40, 2 mM PMSF, and protease inhibitor cocktails (Sigma). The lysates were incubated with MBP-fusion proteins in the reaction buffer for 1 h at 37°C, followed by the addition of amylose resin. The samples were further incubated at 4°C for 1 h with gentle rotation, and then the beads were washed three times with the reaction buffer without BSA.

For the pulldown assay with M1-TUBE (Tandem Ubiquitin Binding Entity), parental and *NDP52*$^{-/-}$-HeLa cells (1×10^7 cells) were stimulated with 1 μg/ml FLAG-tagged TNF-α, and lysed in 1 ml RIPA buffer, containing 50 mM Tris-HCl, pH 7.5, 150 mM NaCl, 1% NP-40, 0.5% sodium deoxycholate, 0.1% SDS, 2 mM EDTA, 2 mM PMSF, and protease inhibitor cocktails (Sigma), for 15 min on ice. The cell lysates were subjected to the pulldown with M1-TUBE Biotin (LifeSensors, UM306), and Dynabeads M-280 Streptavidin (Invitrogen) overnight at 4°C, and washed five times.

Construction of Knockout HeLa Cells

The gRNA cloning vector and the pCAG-hCas9 vector were obtained from Addgene. The nucleotide sequence 5'-GAAGTTCTACATCCCTGGAGG-3' in exon 2 of the human *NDP52* gene was selected as the target. These plasmids and a puromycin-resistant vector (pXS-Puro) were co-transfected into HeLa cells, and puromycin-resistant cell clones were selected by limiting dilution. Genome editing of the *NDP52* gene was screened by a BstNI digestion assay, and the mutations were confirmed by sequencing. The deficiency of the NDP52 protein was confirmed by immunoblotting.

For the knockout of the *RNF31* gene, which encodes HOIP, the nucleotide sequence 5'-TCAACCCTCAGGAAGCTCAGC-3' in exon 2 of the human *RNF31* gene was selected as the target. Genome editing of the *RNF31* gene was screened by a BtsCI digestion assay, and the mutations were confirmed by sequencing. The deficiency of the HOIP protein was confirmed by immunoblotting.

Quantitative PCR (qPCR)

Cell lysis, reverse-transcription, and qPCR were performed with a SuperPrep Cell Lysis RT Kit for qPCR (TOYOBO) and Power SYBR Green PCR Master Mix (Life Technologies), according to the manufacturers' instructions. Quantitative real-time PCR was performed with a Step-One-Plus PCR system (Applied Biosystems) by the ΔΔCT method, using the following oligonucleotides: human *IL-6* sense, 5'-AGCCACTCA CCTCTTC-3', and human *IL-6* anti-sense, 5'-GCCTCTTTGC TGCTTT-3'; human *ICAM1* sense, 5'-GTGGTAGCAGC CGCAGT-3', and human *ICAM1* anti-sense, 5'-TTCGGTT TCATGGGGGT-3'; human *TNF-α* sense, 5'-GCCGCATCGC CGTCTC-3', and human *TNF-α* anti-sense, 5'-CCTCAGC CCCCTCTGG-3'; human *BIRC3* sense, 5'-AGATG AAAATGCAGAGTCATCAAT-3', and human *BIRC3* anti-sense, 5'-CATGATTGCATCTTCTGAATGG-3'; human *IFIT2* sense, 5'-TGGTGGCAGAAGAGGAAGAT-3', and human *IFIT2* anti-sense, 5'-GTAGGCTGCTCTCCAAGGAA-3'; human *ISG15* sense, 5'-GCGAACTCATCTTTGCCAGTA-3', and human *ISG15* anti-sense, 5'-CCAGCATCTTCA CCGTCAG-3'; and human *GAPDH* sense, 5'-AGCAACAGGG TGGTGGAC-3', and human *GAPDH* anti-sense, 5'-GTGTG GTGGGGGACTGAG-3'.

TNF Receptor Complex I and Complex II Analyses

The TNFR complex I analysis was performed as described previously (10). Briefly, parental, *NDP52*$^{-/-}$-HeLa cells, and *HOIP*$^{-/-}$-HeLa cells (2×10^7 cells) were stimulated with 1 μg/ml FLAG-tagged TNF-α, and lysed in 1 ml lysis buffer, containing 50 mM Tris-HCl, pH 7.5, 150 mM NaCl, 1% Triton X-100, 2 mM PMSF, and protease inhibitor cocktails (Sigma), for 15 min on ice. The cell lysates were then immunoprecipitated with anti-FLAG M2 magnetic beads (Sigma) overnight at 4°C, and immunoprecipitates were washed five times with the lysis solution.

For the complex II analysis, parental and *NDP52*$^{-/-}$–HeLa cells (2×10^7 cells) were stimulated with 20 μg/ml CHX, 20 ng/ml TNF-α, with or without 30 μM HOIPIN-8, and lysed in 1 ml lysis buffer, containing 50 mM Tris-HCl, pH 7.5, 150 mM NaCl, 1% Triton X-100, 2 mM PMSF, and protease inhibitor cocktails (Sigma), for 15 min on ice. The cell lysates were then immunoprecipitated using an anti-FADD antibody, followed by Protein G agarose beads (GE Healthcare) at 4°C for 2 h with gentle rotation. Subsequently, the samples were washed five times.

Cell Survival Assay

The number of viable cells was measured with a Cell Counting Kit-F (DOJINDO), based on the degradation of Calcein-AM, and an ATP-based CellTiter-Glo Luminescent Cell Viability Assay (Promega). For quantifying cellular cytotoxicity, a trypan blue exclusion assay and a Cytotoxicity LDH Assay Kit-WST (DOJINDO), which is based on lactate dehydrogenase (LDH) release from damaged cells to the media, were used. Cell proliferation was measured with an xCELLigence RTCA S16 instrument (ACEA Biosciences, Inc.). For the experiments, the parental and *NDP52*$^{-/-}$-HeLa cells were seeded in E-Plate VIEW 16 plates (ACEA Biosciences) at 20,000 cells/well, and monitored every 15 min for 24 h. The cells were then stimulated with TNF-α and CHX, and monitored every 15 min for 24 h. The data were analyzed with real-time cell analysis (RTCA) software and exported for statistical analysis.

Xenophagy Assay

The xenophagy assay was basically performed as described (29) with minor modifications. Briefly, 1×10^5 HeLa cells were seeded in 24-well plates, one day before infection. The cells were infected with *Salmonella enterica* serovar Typhimurium SR-11 χ3181 in penicillin/streptomycin-free cell culture medium, at a multiplicity of infection (MOI) of 100, for 15 min. The extracellular *Salmonella* cells were washed away with PBS, and then the residual bacteria were killed by culturing the cells in medium containing 50 μg/ml gentamicin for 40 min. The *Salmonella*-infected cells were cultured in medium with 10 μg/ml gentamicin, and lysed with extraction buffer (1% Triton X-100, 0.1% SDS in PBS) at the indicated times. The cell lysates were serially diluted with PBS, and small aliquots were spotted onto LB agar plates in quadruplicate. After 12 h incubation at 37°C, *Salmonella* colonies were counted manually to calculate the total number of bacteria in each well.

Immunofluorescence Analysis

HeLa cells (5×10^4) were seeded on collagen I-coated coverslips in 24-well plates, one day before infection. The cells were infected with mCherry-labeled *Salmonella* at a MOI of 300, and treated with gentamicin as described in the xenophagy assay protocol. The cells were fixed with phosphate buffered 4% paraformaldehyde at room temperature for 15 min, and then permeabilized/blocked in staining buffer (0.05% saponin, 10% FBS, 10 mM glycine in PBS) for 30 min. The cells were sequentially incubated with primary and secondary antibodies, diluted with the staining buffer, in a humidity box for 1 h. The stained cells were counterstained with DAPI and mounted onto glass slides with FluorSave (Millipore). The confocal fluorescence images of the prepared slides were captured with an

LSM800 system (Carl Zeiss) using the following excitation laser, detection range and pinhole settings: DAPI (Laser: 405 nm, Detection range: 400-600 nm, Pinhole = 49 μm), Alexa488 (Laser: 488 nm, Detection range: 450-580 nm, Pinhole = 52 μm), mCherry (Laser: 561 nm, Detection range: 570-650 nm, Pinhole = 60 μm), and Alexa647 (Laser: 640 nm, Detection range: 645-700 nm, Pinhole = 66 μm). All images were acquired as 16-bit depth images with a 63X water-immersion objective lens by scanning each channel four separate times, at a speed of 3.18 μsec/pixel, for averaging. These images were analyzed with the accompanying ZEN software to depict the intensity profile plots and to calculate the mean fluorescence intensity of interest. *Pearson's* and *Manders'* correlation coefficient between two independent channels were also determined using the ZEN software by thresholding with the signals obtained from negative control sample (non-infected cells stained with the secondary antibodies and DAPI only) as backgrounds. The captured images were processed with Fiji (ImageJ).

Statistical Analysis

To examine the differences in the outcomes between the mutant groups, linear regression analyses were performed for each outcome variable separately. All pairwise comparisons were derived from the linear regression analyses. Furthermore, in order to compare the change of the normalized cell index over time among mutant groups, we conducted a multivariable non-linear regression analysis including a two-way interaction term between the indicator variable for the mutant groups and the time variable in addition to their main effect terms as explanatory variables. Moreover, the non-linear effect of the time variable on the outcome was considered using a restricted-cubic-spline with knot 5. In all regression models, we estimated the heteroskedasticity corrected standard errors and 95% confidence intervals using the Huber-White sandwich estimators for a robust variance-covariance matrix (30). Normality of the residuals of all regression models was assessed graphically. All residual plots appeared to show a good degree of normally or no meaningful skewness was detected. All p-values were adjusted for multiplicity using the Bonferroni method. All hypothesis tests were performed with a two-sided 5% significance level using R software (https://cran.r-project.org/).

RESULTS

Ubiquitin-Binding Domain of NDP52 Is Crucial to Suppress Canonical NF-κB Signaling

Human NDP52 consists of the SKIP carboxyl homology (SKICH), LC3-interacting region (LIR), coiled-coil, galectin-8 binding (GALBI), and C-terminal ubiquitin-binding zinc finger (UBZ) domains (17, 19) (**Figure 1A**). The substitution of Asp439 by Arg (D439R) in the UBZ domain reportedly abolishes the ubiquitin-binding (31). Moreover, the genetic variant of Val248 to Ala (V248A) is associated with Crohn's disease, a chronic inflammatory bowel disease (32). To confirm the ubiquitin-selectivity of NDP52, we initially performed pulldown experiments. Although MBP-fused NDP52-WT failed to pulldown either mono- or eight different kinds of diubiquitins (**Supplementary Figure 1A**), MBP-fused NDP52-WT, but not the D439R mutant, coprecipitated with linear (M1)-, K48-, or K63-tetraubiquitins with an affinity order of K63>M1>K48 (**Figure 1B**). The GST-fused UBZ domain (a.a. 394-446) of NDP52 also precipitated tetraubiquitins with a similar affinity order of K63>M1>K48>K11-tetraubiquitin (**Supplementary Figure 1B**). When we expressed the N-terminally HA-tagged single Lys mutants of ubiquitin in HEK293T cells, MBP-NDP52-WT, but not MBP-NDP52-D439R, bound all of the Lys-linked polyubiquitin chains, and seemed to have higher affinity toward K27- and K29-polyubiquitin chains, followed by K63-chain (**Figure 1C**). Since linear ubiquitination cannot be evaluated with an N-terminally tagged ubiquitin (3), we performed an *in vitro* MBP pulldown experiment using LUBAC-generated linear polyubiquitin (**Figure 1D**). The results revealed that MBP-NDP52-WT, but not the D439R mutant, coprecipitated long (>130 kDa) linear polyubiquitin chains. These results suggested that the UBZ domain of NDP-52 shows broad specificity to ubiquitin-linkages, including linear chains, although it may have higher affinity toward some atypical ubiquitin chains. Moreover, the mutation of Asp439 to Arg drastically abolishes the ubiquitin-binding of NDP52, including the M1-chain.

Next, to investigate the physiological functions of NDP52, we examined the effect of NDP52 overexpression on TNF-α- and LUBAC-mediated NF-κB activation, by a luciferase assay (**Figure 1E**). The increasing expression of NDP52-WT dose-dependently suppressed the NF-κB activation, whereas the overexpression of the D439R mutant failed to suppress, and rather increased, the NF-κB activity in HEK293T cells. Since the increasing expression of the WT-, or D439R- and ΔUBZ-mutants of NDP52 with LUBAC subunits showed no effect on the LUBAC-mediated linear ubiquitination (**Figure 1F**), NDP52 does not seem to directly inhibit the E3 activity of LUBAC. We previously showed that the C-terminally tetraubiquitin-fused NEMO (NEMO-Ub4), a mimic of linear ubiquitinated NEMO, fully activates the canonical NF-κB pathway (33). The NEMO-Ub4-induced NF-κB activation was suppressed by the WT and V248A variant of NDP52, but not by the ΔUBZ mutant (**Figure 1G**). In contrast, the noncanonical NF-κB activation pathway by NF-κB-inducing kinase (NIK) was not suppressed by the WT and mutants of NDP52. We further examined the effects of the overexpression of NDP52-WT, and V248A, D439R, and ΔUBZ mutants on the basal NF-κB activity. The increased expression of NDP52-WT and V248A had no effect on the basal NF-κB activity in HEK293T cells, whereas the overexpression of the D439R and ΔUBZ mutants dose-dependently enhanced the basal NF-κB activity (**Supplementary Figure 2A**). Similar effects of the NDP52-WT and D439R mutant were detected by a luciferase assay in A549 cells (**Supplementary Figure 2B**). These results suggested that the overexpression of ubiquitin-binding-defective mutants of NDP52 may affect the basal NF-κB activity. The V248A variant in *NDP52* is associated with Crohn's disease, and thus the increased pathogen-induced NF-κB activation may contribute to the pathogenesis (31, 34). However, there were no differences in the canonical and noncanonical NF-κB

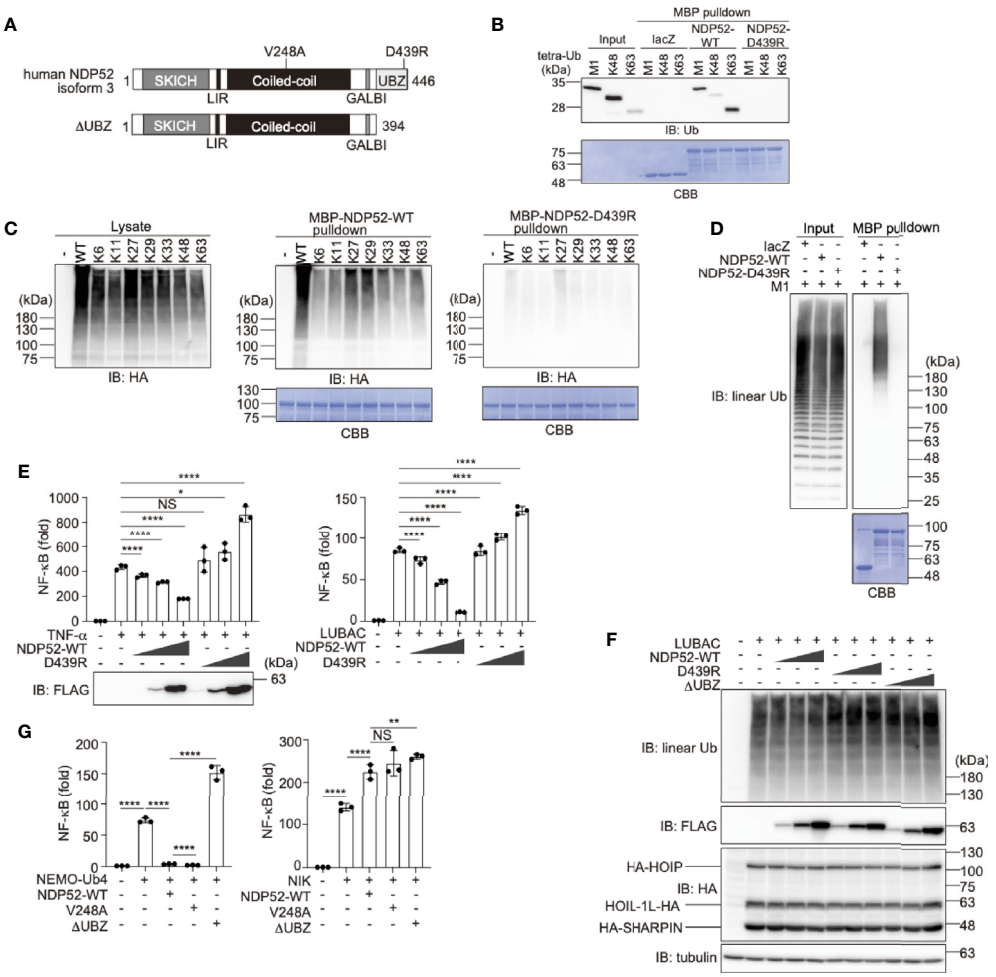

FIGURE 1 | The ubiquitin-binding activity of NDP52 is indispensable for NF-κB suppression. **(A)** Domain structure of Wild-type (WT) human NDP52 isoform 3 and its ΔUBZ mutant. V248A is associated with Crohn's disease (31), and the D439R substitution causes the defect in ubiquitin-binding (32). SKICH, SKIP carboxyl homology; LIR, LC3-interacting region; GALBI, galectin-8 binding; and UBZ, ubiquitin-binding zinc finger. **(B)** The UBZ domain of NDP52 functions as the ubiquitin-binding site. *In vitro* MBP pulldown experiments using linear (M1)-, K48-, or K63-linked tetraubiquitins and MBP-fused lacZ, NDP52-WT, and D439R mutant were performed, and the bound ubiquitin chain was detected by immunoblotting. The precipitated MBP-fusion proteins were visualized by Coomassie Brilliant Blue (CBB) staining. **(C)** Low ubiquitin selectivity of NDP52. HA-tagged single Lys mutants of ubiquitin were expressed in HEK293T cells, and the lysates were pulled down by MBP-NDP52-WT or -D439R mutant. The precipitated ubiquitin was detected by an anti-HA antibody, and the precipitated MBP-fusion proteins were detected by CBB staining. **(D)** Linear polyubiquitin-binding of NDP52. LUBAC-generated linear polyubiquitin was pulled down by the MBP-NDP52-WT or -D439R mutant *in vitro*. The precipitated ubiquitin was detected by an anti-linear ubiquitin antibody, and the precipitated MBP-fused proteins were detected by CBB staining. **(E)** NDP52-WT, but not the D439R mutant, suppresses NF-κB activity. Effects of increasing amounts (0.025 μg, 0.075 μg, and 0.25 μg/well) of WT and D439R mutant of FLAG-NDP52 were examined, in the presence of either 10 ng/ml TNF-α or the co-expression of LUBAC subunits in HEK293T cells, by the NF-κB luciferase assay. **(F)** NDP52 does not inhibit the linear ubiquitination activity of LUBAC. HA-tagged LUBAC subunits (1.0 μg HA-HOIP, 0.2 μg HOIL-1L-HA, and 0.2 μg HA-SHARPIN/well) and increasing amounts (0.1 μg, 0.3 μg, and 1.0 μg/well) of FLAG-NDP52-WT, -D439R, and -ΔUBZ were co-expressed in HEK293T cells, and cell lysates were immunoblotted with the indicated antibodies. **(G)** NDP52 suppresses the canonical NF-κB pathway. The C-terminally tetraubiquitin-fused NEMO (NEMO-Ub4), WT and mutants of NDP52, and/or NIK were co-transfected with the NF-κB luciferase reporter, as indicated, and luciferase activity was measured at 24 h-post transfection. **(E, G)** Data are shown as Means ± SD (n = 3) by Huber-White Sandwich estimators for variance-covariance structures corrected with Bonferroni method. $^{*}P < 0.05$, $^{**}P < 0.01$, $^{****}P < 0.0001$, NS, not significant.

activations with the V248A variant and NDP52-WT, suggesting that a different cellular phenomenon underlies this disease.

NDP52 Binds NF-κB Signaling Factors, Including LUBAC

At present, 269 unique interactors and 409 raw interactions of NDP52 (CALCOCO2) are listed on the BioGRID site (https://thebiogrid.org/115535/summary/homo-sapiens/calcoco2.html). Intriguingly, the interaction of HOIL-1L (RBCK1) with NDP52 can be characterized by affinity capture mass spectrometry (35). Moreover, NF-κB signaling factors, such as TANK-binding kinase 1 (TBK1) (36), TBK1-binding protein 1 (TBKBP1) (36), MAVS (37), c-IAP2 (BIRC3) (38), IκB kinase (IKK)β (IKBKB) (39), IKKϵ (IKBKE) (21), NEMO (IKBKG) (40), TAB3 (21), A20

(TNFAIP3) (41), TRAF2 (42), TRAF3 (35), TRAF4 (43), and TRAF6 (40) are included as physiological interactors of NDP52. At present, NDP52 is reportedly involved in the TNF-α-induced NF-κB signal transduction pathway through binding with a ubiquitin editing complex, such as A20 (21), but it may play a more important role in the regulation of the NF-κB signaling pathway through binding with multiple factors, including LUBAC.

To examine the binding of NDP52 with LUBAC, we performed a co-immunoprecipitation followed by an immunoblotting analysis in HEK293T cells (**Figure 2A**). To avoid the linear ubiquitin-mediated interaction, we used the active site mutant (C885A) of HOIP with HOIL-1L and SHARPIN. As a result, NDP52, as well as NEMO, a known substrate of LUBAC (44), efficiently coprecipitated with three components of the LUBAC complex. Among the LUBAC subunits, NDP52 bound HOIP alone, but not HOIL-1L or SHARPIN. The endogenous association of NDP52 and HOIP was also detected in HeLa cells (**Figure 2B**). The deletions of the zinc finger domains (a.a. 300-438) and UBA-flanking region (a.a. 575-698) of HOIP reduced NDP52-binding (**Figures 2C, D**). Furthermore, the deletion of either SKICH (a.a. 1-127) or the UBZ domain (a.a. 395-446) of NDP52 disturbed the HOIP-binding, whereas the coiled-coil region alone (a.a. 128-350) showed no affinity for HOIP (**Figures 2E, F**). These results indicated that NDP52 principally associates with LUBAC through HOIP, by biphasic interactions through the SKICH and UBZ domains.

To further confirm the binding of NDP52 with NF-κB signaling factors, we performed a co-immunoprecipitation assay using the WT and ΔUBZ mutant of NDP52 in HEK293T cells (**Supplementary Figure 3**). NDP52-WT efficiently associated with the reported NF-κB signaling factors, such as IKKβ, NEMO, IKKα, TRAF6, and A20. The deletion of the UBZ domain drastically reduced the association with NEMO, TRAF6, and A20. In contrast, IKKβ and IKKα substantially bound the

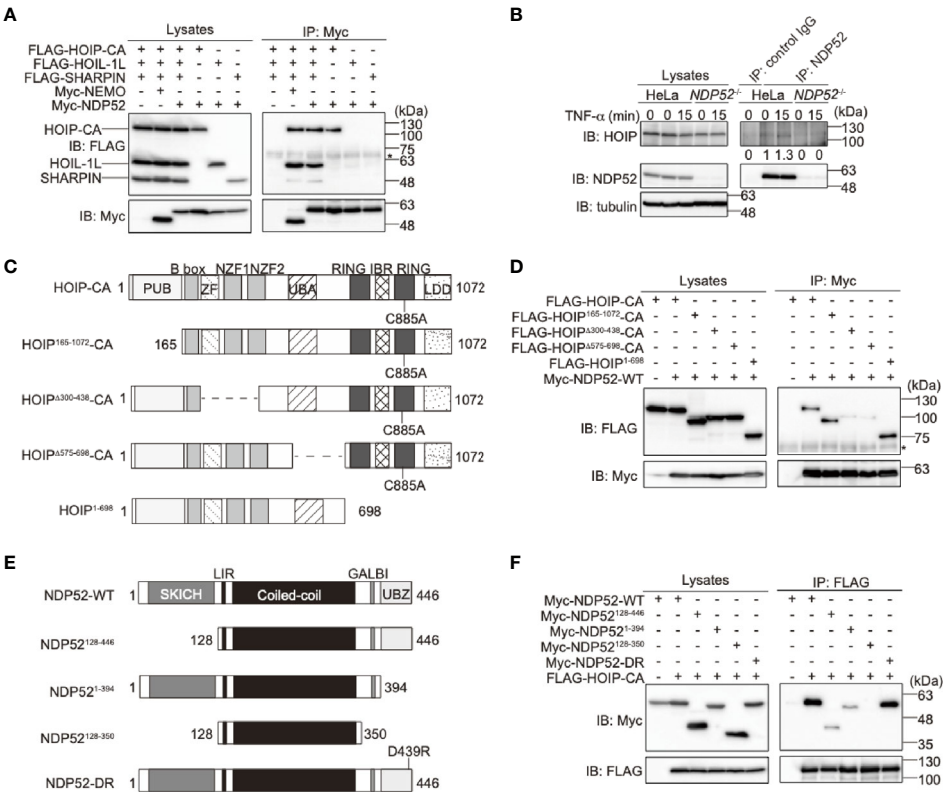

FIGURE 2 | NDP52 binds LUBAC through HOIP. **(A)** HOIP binds NDP52. The FLAG-tagged HOIP C885A mutant (HOIP-CA), HOIL-1L, SHARPIN, and Myc-tagged NEMO or NDP52 were co-expressed in HEK293T cells, as indicated. The cell lysates and anti-Myc immunoprecipitates were immunoblotted with the indicated antibodies. *: nonspecific signal. **(B)** NDP52 physiologically interacts with LUBAC. Parental and *NDP52*$^{-/-}$-HeLa cells were stimulated with 1 μg/ml FLAG-TNF-α, and cell lysates and anti-NDP52 immunoprecipitates were subjected to immunoblotting with the indicated antibodies. Taking the intensity in control IgG immunoprecipitates as the background and the anti-NDP52 immunoprecipitates of HeLa without TNF-α stimulation as 1.0, the relative intensities of HOIP are shown. **(C)** Domain structure and mutants of HOIP. PUB: peptide:N-glycanase/UBA or UBX-containing proteins; ZF: zinc finger; NZF: Npl4-type zinc finger; UBA: ubiquitin-associated; RING: really interesting new gene; IBR: in-between RING; and LDD: linear ubiquitin determining. **(D)** The zinc fingers and UBA-flanking regions of HOIP are crucial for NDP52-binding. The full length and various mutants of FLAG-tagged HOIP were co-expressed with Myc-NDP52-WT in HEK293T cells, and immunoprecipitations followed by immunoblotting analyses were performed as indicated. *: nonspecific signal. **(E)** Domain structure and mutants of NDP52. **(F)** The SKICH and UBZ domains of NDP52 bind HOIP. A similar analysis to that in **(D)** was performed, using the WT and various mutants of Myc-NDP52 and FLAG-HOIP-CA.

ΔUBZ mutant of NDP52. Therefore, these different binding profiles of the WT- and ΔUBZ mutant of NDP52 with NF-κB signaling factors may correlate with the enhanced NF-κB activity by the overexpression of ubiquitin-binding defective mutants of NDP52.

NDP52 Is a Negative Regulator of TNF-α and Antiviral Signaling pathways

To further clarify the physiological functions of NDP52, we constructed *NDP52*-knockout (*NDP52*$^{-/-}$) HeLa cells by the CRIPSR/Cas9 method (**Supplementary Figure 4A**). The siRNA-mediated knockdown of *NDP52* had no effect on the background immunoreactive bands in the parental and *NDP52*$^{-/-}$-HeLa cells, suggesting the specific ablation of *NDP52* (**Supplementary Figure 4B**), Upon stimulation with TNF-α or IL-1β, the NF-κB luciferase activity was significantly up-regulated in *NDP52*$^{-/-}$-HeLa cells as compared to the parental cells (**Figure 3A**). Moreover, the expression of NF-κB target genes, such as *IL-6* and *BIRC3* (c-IAP2), was enhanced in TNF-α- and IL-1β-treated *NDP52*$^{-/-}$-HeLa cells (**Figure 3B**, **Supplementary Figure 4C**). We restored the NDP52-WT and D439R mutant into *NDP52*$^{-/-}$-HeLa cells, with comparable expression to that of the parental cells (**Supplementary Figure 4D**). Although the enhanced *IL-6* expression in *NDP52*$^{-/-}$ cells was significantly suppressed in NDP52-WT-restored cells, the restoration of the D439R mutant had minimal suppressive effects after TNF-α- and IL-1β-

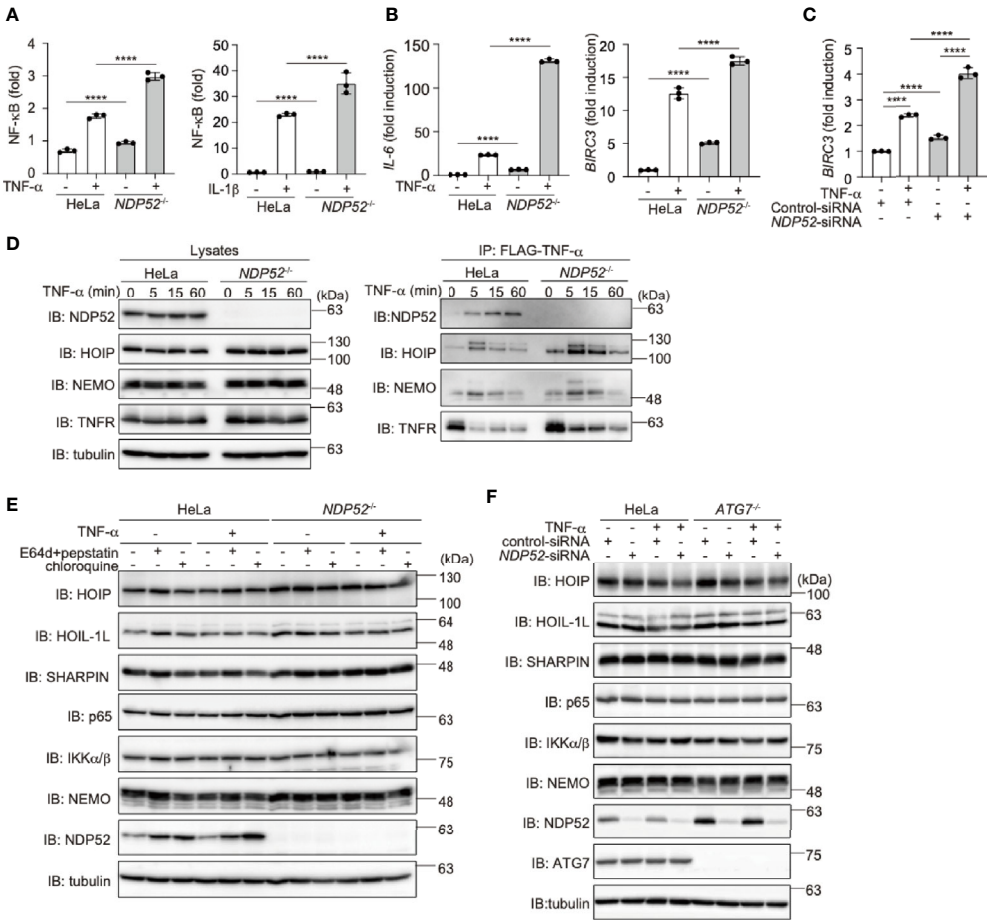

FIGURE 3 | Genetic ablation of *NDP52* enhances canonical NF-κB activation. **(A)** Enhanced NF-κB activation in *NDP52*$^{-/-}$-HeLa cells. The NF-κB luciferase reporter was transfected into parental and *NDP52*$^{-/-}$-HeLa cells. The cells were then treated with or without 10 ng/ml TNF-α and 1 ng/ml IL-1β for 6 h, and the luciferase activity was measured. **(B)** Enhanced expression of NF-κB target genes in TNF-α-treated *NDP52*$^{-/-}$-HeLa cells. Parental- and *NDP52*$^{-/-}$-HeLa cells were stimulated with 10 ng/ml TNF-α for 1 h, and qPCR analyses of *IL-6* and *BIRC3* were performed. **(C)** Enhanced expression of *BIRC3* in *NDP52*-silenced HeLa cells. HeLa cells were transfected with control- or *NDP52*-siRNA and stimulated with 10 ng/ml TNF-α for 1 h, and then qPCR analysis was performed. **(A–C)** Data are shown as Means ± SD (n = 3) by Huber-White Sandwich estimators for variance-covariance structures corrected with Bonferroni method. ****P < 0.0001. **(D)** NDP52 is a component of TNFR complex I. Parental and *NDP52*$^{-/-}$-HeLa cells were stimulated with 1 μg/ml FLAG-TNF-α for the indicated periods, and cell lysates and anti-FLAG immunoprecipitates were subjected to immunoblotting with the indicated antibodies. **(E)** Lysosomal inhibitors do not affect the protein levels of LUBAC subunits or NF-κB signaling factors. Parental and *NDP52*$^{-/-}$-HeLa cells were treated with E64d (10 μg/ml) and pepstatin A (10 μg/ml), or chloroquine (50 μM) for 8 h. Cell lysates were immunoblotted with the indicated antibodies. **(F)** *ATG7*-deficiency showed no effect on the turnover of NF-κB signaling factors. Parental and *ATG7*$^{-/-}$-HeLa cells were transfected with control- or *NDP52*-siRNA and stimulated with 20 ng/ml TNF-α for 8 h. Cell lysates were immunoblotted by the indicated antibodies.

stimulation (**Supplementary Figures 4E, F**). In addition to *NDP52*$^{-/-}$-HeLa cells, the TNF-α-induced expression of *BIRC3* was upregulated in *NDP52*-siRNA-transfected HeLa cells, as compared to the control-siRNA-transfected cells (**Figure 3C**). These results suggested the inhibitory effect of NDP52 on the canonical NF-κB activation pathway.

Upon TNF-α stimulation, multiple proteins, such as receptor-interacting serine/threonine-protein kinase 1 (RIP1), IKK complex, and LUBAC, are recruited to the TNF receptor (TNFR) to form signaling complex I, which is crucial for TNF-α-mediated canonical NF-κB activation (45, 46). Importantly, we identified that NDP52 was recruited upon the FLAG-TNF-α treatment of the parental HeLa cells, but not *NDP52*$^{-/-}$cells, clearly indicating that NDP52 is a component of TNFR signaling complex I (**Figure 3D**). Furthermore, the recruitment of NDP52 to TNFR complex I was partially suppressed in *HOIP*$^{-/-}$ cells (**Supplementary Figure 4G**), suggesting that the linear ubiquitination by LUBAC affects the association of NDP52 with TNFR upon TNF-α stimulation. Since the M1-TUBE pulldowns of linear ubiquitin from TNF-α-stimulated parental and *NDP52*$^{-/-}$-HeLa cells showed similar levels of intracellular linear ubiquitin, NDP52 does not seem to inhibit the E3 activity of LUBAC (**Supplementary Figure 4H**).

To further examine whether NDP52 mediates the autophagic degradation of LUBAC and NF-κB signaling factors, we treated parental and *NDP52*$^{-/-}$-HeLa cells with lysosomal inhibitors, such as E64d+pepstatin or chloroquine (**Figure 3E**). However, these inhibitors had no effect on the protein levels of LUBAC subunits and NF-κB signaling factors in either the presence or absence of TNF-α stimulation. Moreover, the *NDP52* knockdown in *ATG7*$^{-/-}$-HeLa cells had minimal effects on the intracellular amounts of LUBAC subunits and NF-κB signaling factors, in either the presence or absence of TNF-α stimulation (**Figure 3F**). Collectively, these results indicated that autophagy-induced lysosomal degradation is not involved in NDP52-mediated NF-κB regulation.

To investigate the crosstalk between NDP52 and LUBAC, we treated parental and *NDP52*$^{-/-}$-HeLa cells with LUBAC inhibitors, HOIPINs. The phosphorylation of p105, p65, and IKK, hallmarks of NF-κB activation, was upregulated in *NDP52*$^{-/-}$-HeLa cell lysates as compared to the parental cells. However, the enhanced phosphorylation of NF-κB factors was dose-dependently cancelled in the presence of HOIPIN-8 or HOIPIN-1 (**Figure 4A**, **Supplementary Figure 5**). Moreover, the enhanced expression of NF-κB targets, such as *ICAM1* and *TNF*-α, in *NDP52*$^{-/-}$-HeLa cells was suppressed in the presence of HOIPIN-8 (**Figure 4B**), suggesting that LUBAC inhibitors negated the increased NF-κB activation in *NDP52*$^{-/-}$-HeLa cells.

When we transfected poly(I:C), a mimic of viral dsRNA, to activate the RIG-I-like receptors-mediated antiviral response, the phosphorylation of TBK1 and IRF3 was enhanced in *NDP52*$^{-/-}$-cells, as compared to that in parental cells (**Figure 4C**), indicating the augmented activation of the IFN antiviral pathway by the genetic ablation of *NDP52*. However, we could not detect the degradation of TBK1, MAVS, and IRF3 after a 4 h-treatment with poly(I:C). In the presence of HOIPIN-8, the phosphorylation of TBK1 and IRF3 in parental and *NDP52*$^{-/-}$-HeLa cells was partially suppressed. Furthermore, the expression of IRF3-target genes, such as *IFIT2* and *ISG15*, was upregulated in *NDP52*$^{-/-}$-HeLa cells and suppressed by HOIPIN-8 (**Figure 4D**). These results indicated that NDP52 has a physiologically inhibitory effect on innate immune responses, such as the canonical NF-κB and type I IFN antiviral pathways.

NDP52 Regulates TNF-α-Induced Apoptosis

TNF-α stimulation induced not only NF-κB activation but also cell death, when the expression of NF-κB targets was prohibited in the presence of cycloheximide (CHX), a protein synthesis inhibitor (47, 48). To investigate the role of NDP52 in the regulation of cell death, we treated parental and *NDP52*$^{-/-}$-HeLa cells with TNF-α+CHX, and found that the number of trypan blue-positive dead cells was increased among *NDP52*$^{-/-}$ cells, as compared to the parental HeLa cells (**Figure 5A**). Since the pan-caspase inhibitor ZVAD suppressed the enhanced cell death, it seemed to be mediated by the apoptosis pathway. The increased TNF-α+CHX-induced cell death was detected in *NDP52*-silenced HeLa cells, as compared to the control siRNA-transfected cells (**Figure 5B**). The ATP-based cell viability assay also indicated the enhanced cell death in *NDP52*$^{-/-}$ cells after TNF-α+CHX or TNF-α+Smac mimetic BV6 treatment (**Figure 5C**). Furthermore, a real time cell analysis revealed that *NDP52*$^{-/-}$-HeLa cells died more rapidly than the parental cells after TNF-α+CHX-treatment, and cell death was accelerated in the presence of HOIPIN-8 (**Figure 5D**). Indeed, the cleavages of PARP, caspase 8, and caspase 3, which are hallmarks of apoptosis, were increased in *NDP52*$^{-/-}$-HeLa cells and dose-dependently enhanced by HOIPIN-8 or HOIPIN-1 (**Figure 5E**, **Supplementary Figure 6A, B**). During the course of TNF-α-induced cell death, TNFR complex II, composed of RIP1, caspase 8, and Fas-associated death domain protein (FADD), plays a crucial role to activate the apoptosis pathway (49). The anti-FADD immunoprecipitation indicated that TNF-α+CHX-induced TNFR complex II formation was upregulated in *NDP52*$^{-/-}$ cells as compared to the parental cells, and was further increased in the presence of HOIPIN-8 (**Figure 5F**). These data indicated that NDP52 physiologically functions as an anti-apoptotic factor in the TNF-α-induced apoptotic pathway.

Doxorubicin, a genotoxic agent, activates the Bcl-2/Bax-mediated intrinsic apoptosis pathway (50). In contrast to the TNF-α+CHX treatment, the cleavages of PARP, Bid, and caspases 9, 8, and 3 were similar between the doxorubicin-treated parental and *NDP52*$^{-/-}$-HeLa cells (**Figure 5G**). In the presence of HOIPIN-8, the doxorubicin-induced cleavages of Bid, and caspases 8 and 3, but not PARP and caspase 9, were suppressed in parental and *NDP52*$^{-/-}$-HeLa cells. However, cell viability and toxicity assessments by CellTiter-Glo, Calcein-AM, and lactate dehydrogenase analyses did not reveal a significant anti-apoptotic effect of HOIPIN-8 in doxorubicin-treated cells (**Figures 5C, H**, **Supplementary Figure 6C**). These results suggested that, in contrast to the TNF-α-induced apoptotic pathway, the intrinsic apoptotic pathway is not affected by the

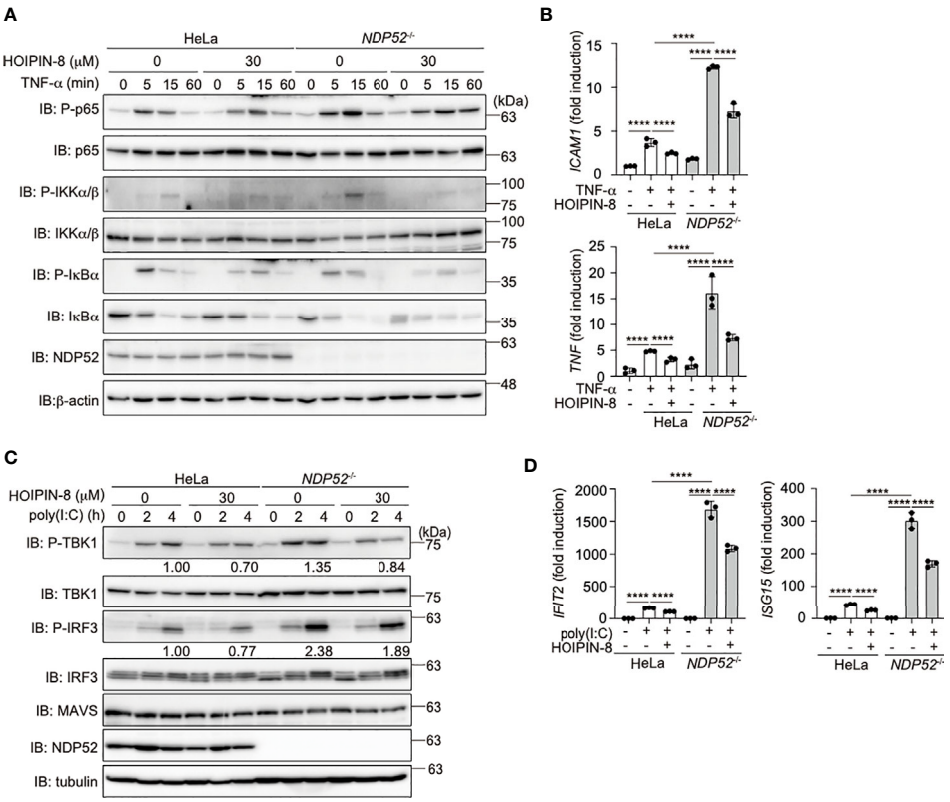

FIGURE 4 | HOIPIN-8 suppresses the enhanced NF-κB and IFN antiviral signaling pathways in *NDP52*$^{-/-}$ cells. **(A)** HOIPIN-8 cancels the enhanced TNF-α signaling in *NDP52*$^{-/-}$-HeLa cells. Parental and *NDP52*$^{-/-}$-HeLa cells were stimulated with 10 ng/ml TNF-α for the indicated periods, in the absence or presence of 30 μM HOIPIN-8. Cell lysates were immunoblotted with the indicated antibodies. **(B)** The enhanced expression of NF-κB target genes in TNF-α-treated *NDP52*$^{-/-}$-HeLa cells is suppressed by HOIPIN-8. Parental and *NDP52*$^{-/-}$-HeLa cells were stimulated with TNF-α as in **(A)** for 1 h, and qPCR analyses of *ICAM1* and *TNF* were performed. **(C)** Poly (I:C)-mediated type I IFN signaling is enhanced in *NDP52*$^{-/-}$-HeLa cells. Parental and *NDP52*$^{-/-}$-HeLa cells were stimulated with 10 μg/ml poly(I:C) in either the presence or absence of 30 μM HOIPIN-8 for the indicated periods, and cell lysates were subjected to immunoblotting with the indicated antibodies. Taking the intensities of P-TBK1 and P-IRF3 in 4 h poly (I:C)-treated HeLa cells without HOIPIN-8 as 1.0, the relative intensities are shown. **(D)** Enhanced expression of IRF3 targets in *NDP52*$^{-/-}$-HeLa cells. The mRNA levels of *IFIT2* and *ISG15* in parental and *NDP52*$^{-/-}$-HeLa cells, treated as indicated for 4 h, were examined by qPCR. **(B, D)** Data are shown as Means ± SD (n = 3) by Huber-White Sandwich estimators for variance-covariance structures corrected with Bonferroni method. ****$P < 0.0001$.

genetic ablation of *NDP52* and/or the inhibition of LUBAC activity.

Effect of HOIPINs on NDP52-Mediated Xenophagy

To evaluate the importance of the crosstalk between NDP52 and LUBAC, we next investigated the effects of HOIPIN-8 on the xenophagy triggered by *Salmonella typhimurium* infection in HeLa cells. At 1 h after infection, LC3-positive membranes were recruited to *Salmonella* foci, and most of them were also positive for linear ubiquitin (**Supplementary Figures 7A, 8**) in accordance with previous reports (24, 25). In contrast, the majority of the invaded *Salmonella* cells were devoid of LC3, and the colocalization between LC3 and linear ubiquitin, which were shown by *Pearson's* and *Manders'* correlation coefficients and mean fluorescence intensities, was significantly diminished in HOIPIN-8-treated cells (**Supplementary Figures 7B, C, 8**). At 8 h after infection, *Salmonella* escaped from the clearance system of the host cells and started to explosively proliferate in the cytoplasm, even in the non-treated cells. At this time point, the bacterial cells were covered with a trace amount of linear ubiquitin, but the LC3 positive membranes were not well recruited to the expanding bacterial foci, in both the non-treated and HOIPIN-8-treated cells (**Supplementary Figures 7D, E, 8**). The colony forming assay indicated that the entry into HeLa cells was not affected by HOIPIN-8, whereas the *Salmonella* expansion was facilitated by the suppression of LUBAC (**Supplementary Figure 7F**). Thus, the compromised elimination of bacteria in HOIPIN-8-treated cells can be attributed to the defects in the initial responses against *Salmonella*, including the linear ubiquitination and LC3 recruitment.

We next examined whether NDP52 affects the linear ubiquitination of the invaded *Salmonella*. *NDP52*$^{-/-}$-HeLa cells were infected with *Salmonella* as described previously (29), and the colocalization of linear ubiquitin and *Salmonella* foci in

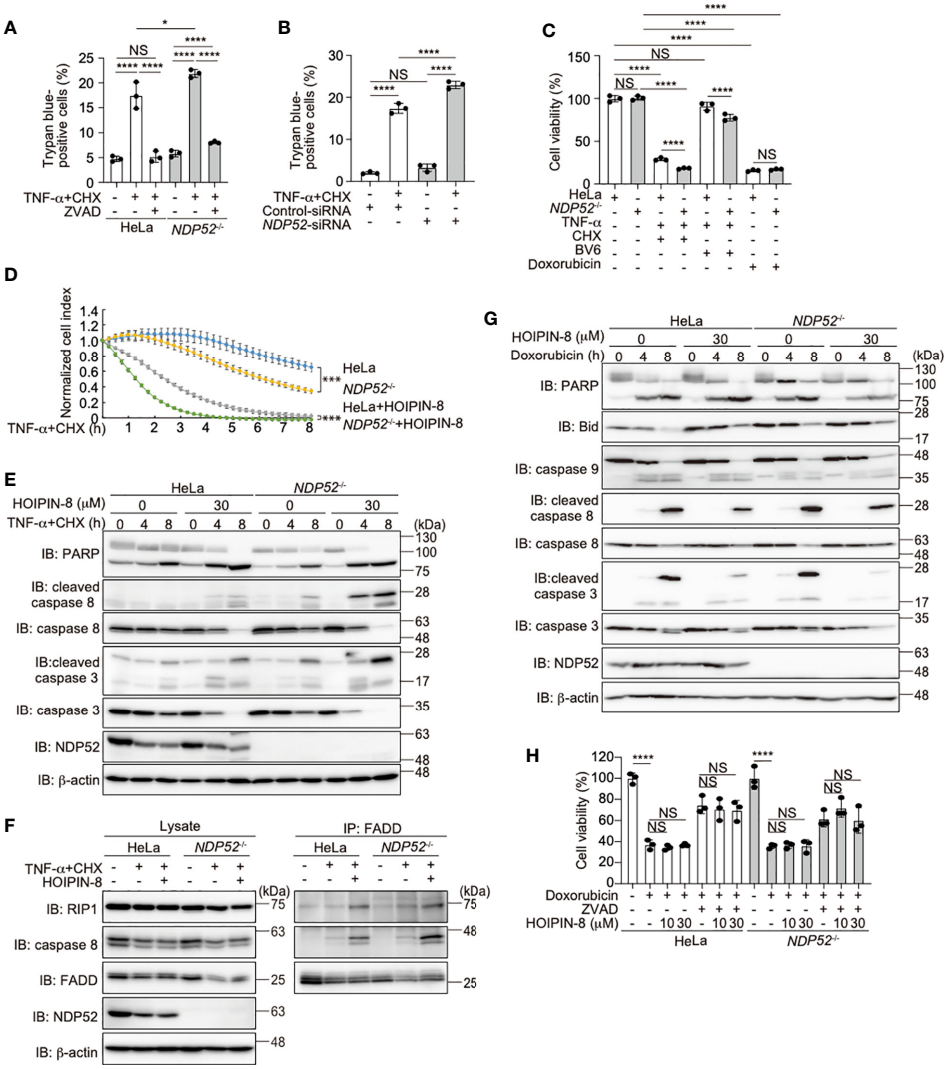

FIGURE 5 | NDP52 suppresses the TNF-α-induced apoptosis. **(A)** TNF-α+CHX-induced cell death is enhanced in *NDP52*$^{-/-}$-HeLa cells. Parental and *NDP52*$^{-/-}$-HeLa cells were treated with 10 ng/ml TNF-α, 10 μg/ml CHX, and/or 20 μM ZVAD for 12 h, as indicated, and trypan-blue positive cells were counted. **(B)** Increased TNF-α-induced cell death in *NDP52*-silenced cells. Control- or *NDP52*-siRNA was transfected into HeLa cells, which were then treated with 10 ng/ml TNF-α+10 μg/ml CHX as indicated. Trypan-blue positive cells were counted as in **(A)**. **(C)** Reduced viability of *NDP52*$^{-/-}$ cells. Parental and *NDP52*$^{-/-}$-HeLa cells were treated with 10 ng/ml TNF-α, 10 μg/ml CHX, 4 μM BV6, and/or 25 μM doxorubicin as indicated for 24 h. The cell viability was then analyzed by an ATP-based assay. **(D)** HOIPIN-8 accelerated cell death. Parental and *NDP52*$^{-/-}$-HeLa cells were treated with 10 ng/ml TNF-α, 10 μg/ml CHX, and/or 30 μM HOIPIN-8, and analyzed by an xCELLigence real-time cell analyzer. Data are shown as mean ± s.e.m. (n = 4), and P-values for the comparison of the change of the normalized cell index over time between parental and *NDP52*$^{-/-}$-HeLa cells in the absence and presence of HOIPIN-8, respectively. ***$P < 0.001$. **(E)** Enhanced cleavages of caspases and PARP in TNF-α+CHX- and HOIPIN-8-treated *NDP52*$^{-/-}$-HeLa cells. Parental and *NDP52*$^{-/-}$-HeLa cells were treated with 10 ng/ml TNF-α, 10 μg/ml CHX, and/or 30 μM HOIPIN-8 as indicated, and cell lysates were analyzed by immunoblotting with the indicated antibodies. **(F)** Increased TNFR complex II formation in *NDP52*$^{-/-}$ cells. Parental and *NDP52*$^{-/-}$-HeLa cells were treated with 20 ng/ml TNF-α, 20 μg/ml CHX, and/or 30 μM HOIPIN-8 as indicated for 2.5 h, and cell lysates and anti-FADD immunoprecipitates were immunoblotted with the indicated antibodies. **(G)** NDP52 and HOIPIN-8 exert minimal effects on the doxorubicin-induced intrinsic apoptotic pathway. Cells were treated with 25 μM doxorubicin and analyzed as in **(E)**. **(H)** HeLa cells were treated with 25 μM doxorubicin, 20 μM ZVAD, and/or HOIPIN-8 as indicated, and cell viability was analyzed by a Calcein-AM assay. **(A–C, H)** Data are shown as Means ± SD (n = 3) by Huber-White Sandwich estimators for variance-covariance structures corrected with Bonferroni method. *$P < 0.05$, ****$P < 0.0001$, NS, not significant.

either the absence or presence of HOIPIN-8 was evaluated and compared with that in parental HeLa cells. Interestingly, the linear ubiquitination of *Salmonella*, which was observed in parental HeLa cells, was profoundly suppressed in *NDP52*$^{-/-}$ cells (**Figure 6A**, **Supplementary Figure 9**). Quantitative imaging analyses of *Salmonella* and linear ubiquitin colocalization revealed that NDP52 plays an important role in the linear ubiquitination of invaded *Salmonella* (**Figure 6B**). We also tested the effects of HOIPIN-8 on *Salmonella* elimination in *NDP52*$^{-/-}$-HeLa cells. In the *NDP52*-deficient background, no

additional effects of LUBAC inhibition on the reduction of colocalization or linear ubiquitination were found (**Figure 6B**), but the HOIPIN-8 treatment strikingly exacerbated *Salmonella* elimination in *NDP52*$^{-/-}$-HeLa cells, while the NDP52 defect showed minimal adverse effects in non-treated cells (**Figure 6C**). These results suggested that NDP52 substantially contributes to the elimination of invading bacteria in collaboration with LUBAC.

We finally investigated the effect of a LUBAC inhibitor on the NDP52 localization in *Salmonella*-infected cells. At 1 h after infection, NDP52 was selectively accumulated in *Salmonella*-encapsulating xenophagosomes (**Supplementary Figures 10A, 11**). As expected, either the inhibition of LUBAC or the genetic loss of *NDP52*, or both caused poor xenophagosome formation (**Supplementary Figures 10B-D, 11**), while their effects on the colocalization correlation between *Salmonella* and LC3 were limited (**Supplementary Figure 10E**). In contrast to the reduction in LC3-positive xenophagosome formation, the NDP52 recruitment to *Salmonella* was not affected by the HOIPIN-8 treatment (**Supplementary Figure 10F**).

These xenophagy analyses indicated that LUBAC plays an important role in xenophagosome formation, and thus the suppression of LUBAC attenuates the clearance of invaded bacteria. In addition, the genetic deletion of *NDP52* also

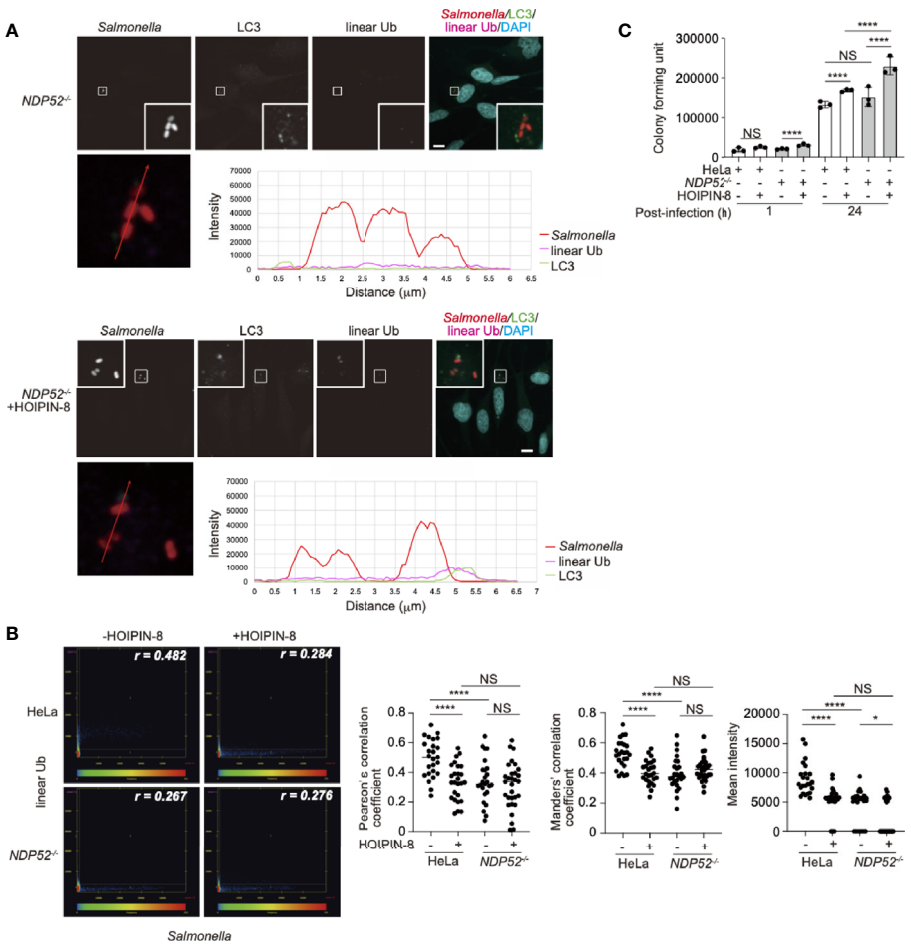

FIGURE 6 | Effect of LUBAC inhibitor on xenophagosome formation in *NDP52*$^{-/-}$-HeLa cells. **(A)** Colocalization of linear ubiquitin with *Salmonella* xenophagosomes. *NDP52*$^{-/-}$-HeLa cells were infected with mCherry-labeled *Salmonella*. The recruitments of endogenous LC3 and linear ubiquitin chains were visualized by immunofluorescence analyses. Representative confocal images of each condition are shown. *Insets*: Enlarged images of boxed regions with *Salmonella* foci. Lower panels: Intensity profile plot of *Salmonella*, linear ubiquitin, and LC3 signals on the line across *Salmonella* foci shown in the left panel. *Bars*: 10 μm. **(B)** Colocalization analysis of *Salmonella* foci and linear ubiquitin. Representative dot plots from *Salmonella*-infected wild type and *NDP52*$^{-/-}$-HeLa cells with or without HOIPIN-8 treatment are shown. *Pearson's* correlation coefficient (*r*) is indicated in the upper right corner of each panel. Scatter plots of *Pearson's* and *Manders'* correlation coefficients, and mean intensities calculated from multiple images of *Salmonella* foci of each group are shown on the right side. Data are shown by scatter plots using HeLa without HOIPIN-8, (n = 25); HeLa with HOIPIN-8, (n = 28); *NDP52*$^{-/-}$ without HOIPIN-8, (n = 25); and *NDP52*$^{-/-}$ with HOIPIN-8, (n = 30). **(C)** Colony formation assay of cells infected with *Salmonella*. Parental and *NDP52*$^{-/-}$-HeLa cells were infected with *Salmonella* at a MOI of 100 in triplicate, and cultured in the absence or presence of 30 μM HOIPIN-8. The invaded intracellular bacteria were grown on LB agar plates in quadruplicate and their colonies were counted at the indicated timepoints. Data are shown as Means ± SD (n = 3). **(B, C)** Data was analyzed by Huber-White Sandwich estimators for variance-covariance structures corrected with Bonferroni method. *P < 0.05, ****P < 0.0001, NS, not significant.

curtailed both the linear ubiquitination of *Salmonella* and LC3 recruitment, indicating that the collaboration between LUBAC and NDP52 takes a part in xenophagy. In summary, the crosstalk between NDP52 and LUBAC contributes to several cellular responses, including NF-κB-mediated inflammation, apoptosis, and xenophagy regulation.

DISCUSSION

NDP52 is a multifunctional regulatory protein that predominantly works in selective autophagy (17, 18). Although linear (de) ubiquitination is involved in the NDP52-mediated xenophagy of invading *Salmonella* (24, 25), little is known about the crosstalk between NDP52 and LUBAC in innate immune responses. In terms of the regulation of the NF-κB signaling pathway, NDP52 is reportedly involved in the TNF-α-induced NF-κB signal transduction network (41), and only slightly inhibited the TRAF6-mediated NF-κB activation (51). Furthermore, NDP52 suppressed the lipopolysaccharide-induced NF-κB and IRF3 activation pathways by mediating the autophagic degradations of Toll/interleukin-1 receptor homology domain-containing adaptor inducing interferon (TRIF) and TRAF6 (52). In this study, we showed that NDP52 down-regulates the canonical NF-κB pathway through ubiquitin-binding *via* the C-terminal UBZ domain, which is centered on a crucial Asp439 residue (**Figure 1**). The V248A variant of NDP52 is reportedly associated with Crohn's disease, and the variant affects Toll-like receptor-mediated NF-κB signaling through the ubiquitin-binding at this region. However, V248A of NDP52 showed no effect on NF-κB activation, suggesting that it may affect other cellular functions, including selective autophagy. NDP52 reportedly associates with NF-κB signaling factors, such as the IKK complex (39, 40), TRAFs (35, 40, 42, 43), A20 (41), c-IAP2 (38), and HOIL-1L (35), and we identified HOIP as the primary NDP52-binding subunit in LUBAC (**Figure 2**). The ubiquitin-binding defective mutants of NDP52 may have a positive effect on the NF-κB activity through their different binding affinities for NF-κB signaling factors, such as by the substantial binding with IKKα/β. Importantly, NDP52 is a component of TNFR signaling complex I (**Figure 3**). At present, K11-, K63-, and M1-ubiquitin chains, which are produced by the E3s of c-IAP-1/2, TRAF2/5, and LUBAC, are known to be involved in TNFR signaling complex I (45, 53, 54). Moreover, the linear ubiquitination of NEMO functions as a scaffold to recruit multiple IKK molecules through the UBAN domain of NEMO, and induces the *trans*-activation of canonical IKK (44, 55). The ubiquitin-binding of NDP52 through the UBZ domain showed its broad specificity in ubiquitin-linkages (32), although it also appeared to have affinities toward atypical linkages, such as K27-, K29-, K63-, and M1-chains (**Figure 1**). Therefore, NDP52 seems to be recruited to TNFR by binding with a wide variety of ubiquitin chains, including the M1 chain, and thus regulates the canonical NF-κB activation pathway (**Figure 7**). Indeed, the recruitment of NDP52 to TNFR complex I was suppressed in *HOIP*-deficient cells (**Supplementary Figure 4**).

In addition to its role in NF-κB signaling, NDP52 partly regulates the type I IFN production pathway, and a LUBAC inhibitor cancelled the enhanced antiviral signaling in *NDP52*-deficient cells (**Figure 4**). Since NDP52 reportedly associates with several antiviral signaling factors, such as TBK1 (36), TBKBP1 (36), MAVS (37), and IKKε (21), it seems to function as a crucial regulator in innate immune responses.

Furthermore, we showed that the TNF-α-induced apoptotic pathway, but not doxorubicin-mediated intrinsic apoptosis, was enhanced in *NDP52*$^{-/-}$-HeLa cells as compared to parental HeLa cells (**Figure 5**). When TNFR signaling complex I fails to activate NF-κB, cells activate the apoptotic pathway with the formation of a second complex, complex II, composed of RIP1, FADD, and caspase 8 (49). Indeed, we identified the facilitated complex II formation in *NDP52*-deficient cells upon TNF-α+CHX treatment (**Figure 5**). In the course of complex II formation, RIP1 deubiquitination by CYLD, a deubiquitinase that cleaves linear- and K63-ubiquitin chains, plays a crucial role (56, 57). Therefore, NDP52 may prevent the CYLD-mediated deubiquitination of RIP1, resulting in the suppression of the TNF-α-induced apoptotic pathway (**Figure 7**). Since HOIPIN-8 inhibits the LUBAC-mediated linear ubiquitination of RIP1 upon TNF-α stimulation, it also seems to facilitate the complex II formation.

In addition to NDP52, other multiple autophagy receptors, including OPTN, p62 and TAX1BP1, are also involved in xenophagy, although NDP52 seems to play a major role in *Salmonella* elimination (21–23, 58). Moreover, LUBAC and OTULIN are crucial regulators of xenophagy (24, 25), and LUBAC linearly ubiquitinates proteins in the inner membrane of invading *Salmonella*, and preferentially recruits linear ubiquitin-specific UBAN domain-containing OPTN and NEMO, which facilitate xenophagy and NF-κB activation, respectively (24). LUBAC and OTULIN are reportedly regulates the initiation of autophagy by the linear (de)ubiquitination of ATG13 (26), suggesting the crosstalk between linear ubiquitination and selective autophagy. In this study, we showed that *Salmonella*, LC3, and linear ubiquitin are colocalized 1 h after infection, and HOIPIN-8 treatment suppressed the recruitment of linear ubiquitin and LC3 to the bacteria, thereby allowing increased colony formation (**Supplementary Figure 7**). On the other hand, NDP52 recruitment was scarcely disturbed by HOIPIN-8 treatment (**Supplementary Figure 10**), consistent with previous findings that OPTN recruitment to *Salmonella* was abrogated in *HOIP*-deficient cells, in contrast to NDP52 (24). Intriguingly, the ablation of *NDP52* significantly reduced the linear ubiquitination of *Salmonella* (**Figure 6**), suggesting that NDP52 is not an inhibitor of LUBAC in xenophagy progression, but is required for the effective linear ubiquitination of invading bacteria and xenophagosome formation. Thus, apart from its adaptor function, the NDP52 recruited to bacterial foci might work cooperatively with LUBAC in forming xenophagosomes and killing bacteria (**Figure 7**). Since the *NDP52*-deficiency alone seemed to have a minor effect, OPTN may play a dominant role in xenophagy, as reported previously (24). Further analyses of xenophagy receptors, such as the effects of the combined deletion of *NDP52* and *OPTN*, will be necessary.

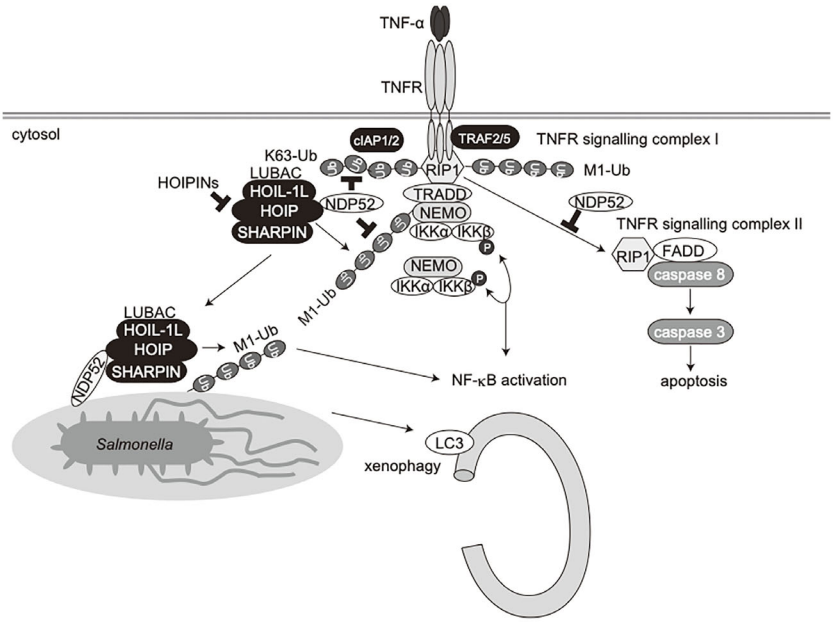

FIGURE 7 | Schematic model of innate immune responses, apoptosis, and xenophagy by crosstalk between NDP52 and LUBAC.

Collectively, we have shown that NDP52 functions in innate immune responses, such as the NF-κB and type I IFN antiviral signaling pathways, apoptosis, and selective autophagy such as xenophagy (**Figure 7**). Therefore, the crosstalk between NDP52 and LUBAC may represent an attractive therapeutic target to develop anti-inflammatory agents.

DATA AVAILABILITY STATEMENT

The original contributions presented in the study are included in the article/**Supplementary Material**. Further inquiries can be directed to the corresponding author.

ETHICS STATEMENT

The protocols were approved by the Safety Committee for Recombinant DNA Experiments and the Safety Committee for Bio-Safety Level 2 (BSL-2) Experiments of Osaka City University.

AUTHOR CONTRIBUTIONS

HM, DO, and ST performed cell biological experiments, DK and AS performed statistical analyses, and FT coordinated the study. All authors wrote and commented on the manuscript, and discussed the results. All authors contributed to the article and approved the submitted version.

FUNDING

This work was partly supported by MEXT/JSPS KAKENHI grants (Nos. JP16H06276 (AdAMS), JP16H06575, JP18H02619, and JP19K22541 to FT, JP18K06967, JP19H05296, and JP20H05337 to DO, and JP18K06937 to ST), a grant from the Takeda Science Foundation (to FT and ST), and a Grant for Research Program on Hepatitis from the Japan Agency for Medical Research and Development (AMED – 19fk0210050h0001 to FT).

ACKNOWLEDGMENTS

Salmonella enterica serovar Typhimurium SR-11 χ3181 was originally obtained from Dr. Hidenori Matsui of Kitasato University. The same strain of mCherry-labeled *Salmonella* and ATG7$^{-/-}$ HeLa cells were kindly provided from Prof. Tamotsu Yoshimori of Osaka University. We thank Drs. Kiyosei Iio and Shingo Obika of JT, Inc. for HOIPINs, Ms. Wakana Koeda, Ms. Shiori Motoyama, and Ms. Ayana Sugihara for technical assistance, and the Research Support Platform of Osaka City University Graduate School of Medicine for technical support. We also thank Genentech, Inc. for the anti-linear ubiquitin antibody and BV6, and Dr. Kazuki Kato of The University of Tokyo for helpful discussion.

SUPPLEMENTARY MATERIAL

The Supplementary Material for this article can be found online at: https://www.frontiersin.org/articles/10.3389/fimmu.2021.635475/full#supplementary-material

REFERENCES

1. Hershko A, Ciechanover A. The ubiquitin system for protein degradation. *Annu Rev Biochem* (1992) 61:761–807. doi: 10.1146/annurev.bi.61.070192.003553
2. Komander D, Rape M. The ubiquitin code. *Annu Rev Biochem* (2012) 81:203–29. doi: 10.1146/annurev-biochem-060310-170328
3. Kirisako T, Kamei K, Murata S, Kato M, Fukumoto H, Kanie M, et al. A ubiquitin ligase complex assembles linear polyubiquitin chains. *EMBO J* (2006) 25(20):4877–87. doi: 10.1038/sj.emboj.7601360
4. Iwai K, Fujita H, Sasaki Y. Linear ubiquitin chains: NF-κB signalling, cell death and beyond. *Nat Rev Mol Cell Biol* (2014) 15(8):503–8. doi: 10.1038/nrm3836
5. Oikawa D, Sato Y, Ito H, Tokunaga F. Linear Ubiquitin Code: Its Writer, Erasers, Decoders, Inhibitors, and Implications in Disorders. *Int J Mol Sci* (2020) 21(9):3381. doi: 10.3390/ijms21093381
6. Doffinger R, Smahi A, Bessia C, Geissmann F, Feinberg J, Durandy A, et al. X-linked anhidrotic ectodermal dysplasia with immunodeficiency is caused by impaired NF-κB signaling. *Nat Genet* (2001) 27(3):277–85. doi: 10.1038/85837
7. Maruyama H, Morino H, Ito H, Izumi Y, Kato H, Watanabe Y, et al. Mutations of optineurin in amyotrophic lateral sclerosis. *Nature* (2010) 465 (7295):223–6. doi: 10.1038/nature08971
8. Nakazawa S, Oikawa D, Ishii R, Ayaki T, Takahashi H, Takeda H, et al. Linear ubiquitination is involved in the pathogenesis of optineurin-associated amyotrophic lateral sclerosis. *Nat Commun* (2016) 7:12547. doi: 10.1038/ncomms12547
9. Kato M, Sanada M, Kato I, Sato Y, Takita J, Takeuchi K, et al. Frequent inactivation of A20 in B-cell lymphomas. *Nature* (2009) 459(7247):712–6. doi: 10.1038/nature07969
10. Tokunaga F, Nishimasu H, Ishitani R, Goto E, Noguchi T, Mio K, et al. Specific recognition of linear polyubiquitin by A20 zinc finger 7 is involved in NF-κB regulation. *EMBO J* (2012) 31(19):3856–70. doi: 10.1038/emboj.2012.241
11. Katsuya K, Hori Y, Oikawa D, Yamamoto T, Umetani K, Urashima T, et al. High-Throughput Screening for Linear Ubiquitin Chain Assembly Complex (LUBAC) Selective Inhibitors Using Homogenous Time-Resolved Fluorescence (HTRF)-Based Assay System. *SLAS Discovery* (2018) 23 (10):1018–29. doi: 10.1177/2472555218793066
12. Katsuya K, Oikawa D, Iio K, Obika S, Hori Y, Urashima T, et al. Small-molecule inhibitors of linear ubiquitin chain assembly complex (LUBAC), HOIPINs, suppress NF-κB signaling. *Biochem Biophys Res Commun* (2019) 509(3):700–6. doi: 10.1016/j.bbrc.2018.12.164
13. Oikawa D, Sato Y, Ohtake F, Komakura K, Hanada K, Sugawara K, et al. Molecular bases for HOIPINs-mediated inhibition of LUBAC and innate immune responses. *Commun Biol* (2020) 3(1):163. doi: 10.1038/s42003-020-0882-8
14. Korioth F, Gieffers C, Maul GG, Frey J. Molecular characterization of NDP52, a novel protein of the nuclear domain 10, which is redistributed upon virus infection and interferon treatment. *J Cell Biol* (1995) 130(1):1–13. doi: 10.1083/jcb.130.1.1
15. Sternsdorf T, Jensen K, Zuchner D, Will H. Cellular localization, expression, and structure of the nuclear dot protein 52. *J Cell Biol* (1997) 138(2):435–48. doi: 10.1083/jcb.138.2.435
16. Morishita H, Mizushima N. Diverse Cellular Roles of Autophagy. *Annu Rev Cell Dev Biol* (2019) 35:453–75. doi: 10.1146/annurev-cellbio-100818-125300
17. Fan S, Wu K, Zhao M, Zhu E, Ma S, Chen Y, et al. The Role of Autophagy and Autophagy Receptor NDP52 in Microbial Infections. *Int J Mol Sci* (2020) 21 (6):2008. doi: 10.3390/ijms21062008
18. Viret C, Rozieres A, Faure M. Novel Insights into NDP52 Autophagy Receptor Functioning. *Trends Cell Biol* (2018) 28(4):255–7. doi: 10.1016/j.tcb.2018.01.003
19. Kwon DH. Song HK. A Structural View of Xenophagy, a Battle between Host and Microbes. *Mol Cells* (2018) 41(1):27–34. doi: 10.14348/molcells.2018.2274
20. Falcon B, Noad J, McMahon H, Randow F, Goedert M. Galectin-8-mediated selective autophagy protects against seeded tau aggregation. *J Biol Chem* (2018) 293(7):2438–51. doi: 10.1074/jbc.M117.809293
21. Thurston TL, Ryzhakov G, Bloor S, von Muhlinen N, Randow F. The TBK1 adaptor and autophagy receptor NDP52 restricts the proliferation of ubiquitin-coated bacteria. *Nat Immunol* (2009) 10(11):1215–21. doi: 10.1038/ni.1800
22. Cemma M, Kim PK, Brumell JH. The ubiquitin-binding adaptor proteins p62/SQSTM1 and NDP52 are recruited independently to bacteria-associated microdomains to target Salmonella to the autophagy pathway. *Autophagy* (2011) 7(3):341–5. doi: 10.4161/auto.7.3.14046
23. Tumbarello DA, Manna PT, Allen M, Bycroft M, Arden SD, Kendrick-Jones J, et al. The Autophagy Receptor TAX1BP1 and the Molecular Motor Myosin VI Are Required for Clearance of Salmonella Typhimurium by Autophagy. *PloS Pathog* (2015) 11(10):e1005174. doi: 10.1371/journal.ppat.1005174
24. Noad J, von der Malsburg A, Pathe C, Michel MA, Komander D, Randow F. LUBAC-synthesized linear ubiquitin chains restrict cytosol-invading bacteria by activating autophagy and NF-κB. *Nat Microbiol* (2017) 2:17063. doi: 10.1038/nmicrobiol.2017.63
25. van Wijk SJL, Fricke F, Herhaus L, Gupta J, Hotte K, Pampaloni F, et al. Linear ubiquitination of cytosolic Salmonella Typhimurium activates NF-κB and restricts bacterial proliferation. *Nat Microbiol* (2017) 2:17066. doi: 10.1038/nmicrobiol.2017.66
26. Chu Y, Kang Y, Yan C, Yang C, Zhang T, Huo H, et al. LUBAC and OTULIN regulate autophagy initiation and maturation by mediating the linear ubiquitination and the stabilization of ATG13. *Autophagy* (2020) 1–16. doi: 10.1080/15548627.2020.1781393
27. Nakamura S, Shigeyama S, Minami S, Shima T, Akayama S, Matsuda T, et al. LC3 lipidation is essential for TFEB activation during the lysosomal damage response to kidney injury. *Nat Cell Biol* (2020) 22(10):1252–63. doi: 10.1038/s41556-020-00583-9
28. Tokunaga F, Nakagawa T, Nakahara M, Saeki Y, Taniguchi M, Sakata S, et al. SHARPIN is a component of the NF-κB-activating linear ubiquitin chain assembly complex. *Nature* (2011) 471(7340):633–6. doi: 10.1038/nature09815
29. Kageyama S, Omori H, Saitoh T, Sone T, Guan JL, Akira S, et al. The LC3 recruitment mechanism is separate from Atg9L1-dependent membrane formation in the autophagic response against Salmonella. *Mol Biol Cell* (2011) 22(13):2290–300. doi: 10.1091/mbc.E10-11-0893
30. Long JS, Ervin LH. Using heteroscedasticity consistent standard errors in the linear regression model. *Am Statistician* (2000) 54(3):217–24. doi: 10.2307/2685594
31. Ellinghaus D, Zhang H, Zeissig S, Lipinski S, Till A, Jiang T, et al. Association between variants of PRDM1 and NDP52 and Crohn's disease, based on exome sequencing and functional studies. *Gastroenterology* (2013) 145(2):339–47. doi: 10.1053/j.gastro.2013.04.040
32. Xie X, Li F, Wang Y, Wang Y, Lin Z, Cheng X, et al. Molecular basis of ubiquitin recognition by the autophagy receptor CALCOCO2. *Autophagy* (2015) 11(10):1775–89. doi: 10.1080/15548627.2015.1082025
33. Kensche T, Tokunaga F, Ikeda F, Goto E, Iwai K, Dikic I. Analysis of nuclear factor-kappaB (NF-κB) essential modulator (NEMO) binding to linear and lysine-linked ubiquitin chains and its role in the activation of NF-κB. *J Biol Chem* (2012) 287(28):23626–34. doi: 10.1074/jbc.M112.347195
34. Till A, Lipinski S, Ellinghaus D, Mayr G, Subramani S, Rosenstiel P, et al. Autophagy receptor CALCOCO2/NDP52 takes center stage in Crohn disease. *Autophagy* (2013) 9(8):1256–7. doi: 10.4161/auto.25483
35. Newman AC, Kemp AJ, Drabsch Y, Behrends C, Wilkinson S. Autophagy acts through TRAF3 and RELB to regulate gene expression via antagonism of SMAD proteins. *Nat Commun* (2017) 8(1):1537. doi: 10.1038/s41467-017-00859-z
36. Huttlin EL, Bruckner RJ, Paulo JA, Cannon JR, Ting L, Baltier K, et al. Architecture of the human interactome defines protein communities and disease networks. *Nature* (2017) 545(7655):505–9. doi: 10.1038/nature22366
37. Li S, Wang L, Berman M, Kong YY, Dorf ME. Mapping a dynamic innate immunity protein interaction network regulating type I interferon production. *Immunity* (2011) 35(3):426–40. doi: 10.1016/j.immuni.2011.06.014
38. Lee SH, Mayr C. Gain of Additional BIRC3 Protein Functions through 3'-UTR-Mediated Protein Complex Formation. *Mol Cell* (2019) 74(4):701–712 e709. doi: 10.1016/j.molcel.2019.03.006
39. Liu K, Zhang L, Zhao Q, Zhao Z, Zhi F, Qin Y, et al. SKP2 attenuates NF-κB signaling by mediating IKKbeta degradation through autophagy. *J Mol Cell Biol* (2018) 10(3):205–15. doi: 10.1093/jmcb/mjy012
40. Wang J, Huo K, Ma L, Tang L, Li D, Huang X, et al. Toward an understanding of the protein interaction network of the human liver. *Mol Syst Biol* (2011) 7:536. doi: 10.1038/msb.2011.67
41. Van Quickelberghe E, De Sutter D, van Loo G, Eyckerman S, Gevaert K. A protein-protein interaction map of the TNF-induced NF-κB signal transduction pathway. *Sci Data* (2018) 5:180289. doi: 10.1038/sdata.2018.289

42. Rual JF, Venkatesan K, Hao T, Hirozane-Kishikawa T, Dricot A, Li N, et al. Towards a proteome-scale map of the human protein-protein interaction network. *Nature* (2005) 437(7062):1173–8. doi: 10.1038/nature04209
43. Rozan LM, El-Deiry WS. Identification and characterization of proteins interacting with Traf4, an enigmatic p53 target. *Cancer Biol Ther* (2006) 5 (9):1228–35. doi: 10.4161/cbt.5.9.3295
44. Tokunaga F, Sakata S, Saeki Y, Satomi Y, Kirisako T, Kamei K, et al. Involvement of linear polyubiquitylation of NEMO in NF-κB activation. *Nat Cell Biol* (2009) 11(2):123–32. doi: 10.1038/ncb1821
45. Haas TL, Emmerich CH, Gerlach B, Schmukle AC, Cordier SM, Rieser E, et al. Recruitment of the linear ubiquitin chain assembly complex stabilizes the TNF-R1 signaling complex and is required for TNF-mediated gene induction. *Mol Cell* (2009) 36(5):831–44. doi: 10.1016/j.molcel.2009.10.013
46. Dondelinger Y, Darding M, Bertrand MJ, Walczak H. Poly-ubiquitination in TNFR1-mediated necroptosis. *Cell Mol Life Sci* (2016) 73(11-12):2165–76. doi: 10.1007/s00018-016-2191-4
47. Cabal-Hierro L, Lazo PS. Signal transduction by tumor necrosis factor receptors. *Cell Signal* (2012) 24(6):1297–305. doi: 10.1016/j.cellsig.2012.02.006
48. Zamaraev AV, Kopeina GS, Zhivotovsky B, Lavrik IN. Cell death controlling complexes and their potential therapeutic role. *Cell Mol Life Sci* (2015) 72 (3):505–17. doi: 10.1007/s00018-014-1757-2
49. Micheau O, Tschopp J. Induction of TNF receptor I-mediated apoptosis via two sequential signaling complexes. *Cell* (2003) 114(2):181–90. doi: 10.1016/s0092-8674(03)00521-x
50. Tacar O, Sriamornsak P, Dass CR. Doxorubicin: an update on anticancer molecular action, toxicity and novel drug delivery systems. *J Pharm Pharmacol* (2013) 65(2):157–70. doi: 10.1111/j.2042-7158.2012.01567.x
51. Morriswood B, Ryzhakov G, Puri C, Arden SD, Roberts R, Dendrou C, et al. T6BP and NDP52 are myosin VI binding partners with potential roles in cytokine signalling and cell adhesion. *J Cell Sci* (2007) 120(Pt 15):2574–85. doi: 10.1242/jcs.007005
52. Inomata M, Niida S, Shibata K, Into T. Regulation of Toll-like receptor signaling by NDP52-mediated selective autophagy is normally inactivated by A20. *Cell Mol Life Sci* (2012) 69(6):963–79. doi: 10.1007/s00018-011-0819-y
53. Dynek JN, Goncharov T, Dueber EC, Fedorova AV, Izrael-Tomasevic A, Phu L, et al. c-IAP1 and UbcH5 promote K11-linked polyubiquitination of RIP1 in TNF signalling. *EMBO J* (2010) 29(24):4198–209. doi: 10.1038/emboj.2010.300
54. Emmerich CH, Schmukle AC, Haas TL, Gerlach B, Cordier SM, Rieser E, et al. The linear ubiquitin chain assembly complex forms part of the TNF-R1 signalling complex and is required for effective TNF-induced gene induction and prevents TNF-induced apoptosis. *Adv Exp Med Biol* (2011) 691:115–26. doi: 10.1007/978-1-4419-6612-4_12
55. Fujita H, Rahighi S, Akita M, Kato R, Sasaki Y, Wakatsuki S, et al. Mechanism underlying IκB kinase activation mediated by the linear ubiquitin chain assembly complex. *Mol Cell Biol* (2014) 34(7):1322–35. doi: 10.1128/MCB.01538-13
56. Vucic D, Dixit VM, Wertz IE. Ubiquitylation in apoptosis: a post-translational modification at the edge of life and death. *Nat Rev Mol Cell Biol* (2011) 12 (7):439–52. doi: 10.1038/nrm3143
57. Wright A, Reiley WW, Chang M, Jin W, Lee AJ, Zhang M, et al. Regulation of early wave of germ cell apoptosis and spermatogenesis by deubiquitinating enzyme CYLD. *Dev Cell* (2007) 13(5):705–16. doi: 10.1016/j.devcel.2007.09.007
58. von Muhlinen N, Thurston T, Ryzhakov G, Bloor S, Randow F. NDP52, a novel autophagy receptor for ubiquitin-decorated cytosolic bacteria. *Autophagy* (2010) 6(2):288–9. doi: 10.4161/auto.6.2.11118

Conflict of Interest: The authors declare that the research was conducted in the absence of any commercial or financial relationships that could be construed as a potential conflict of interest.

frontiers in Immunology

PERSPECTIVE
published: 06 May 2021
doi: 10.3389/fimmu.2021.682624

HIV Nef-mediated Ubiquitination of BCL2: Implications in Autophagy and Apoptosis

Sergio Castro-Gonzalez[*†], *Sydney Simpson*[†], *Yuhang Shi*, *Yuexuan Chen*, *Jared Benjamin* and *Ruth Serra-Moreno*[*]

Microbiology and Immunology, University of Rochester Medical Center, Rochester, NY, United States

Ubiquitination is a process that acts upon every step of the HIV replication cycle. The activity, subcellular localization, and stability of HIV dependency factors as well as negative modulators can be affected by ubiquitination. These modifications consequently have an impact on the progression and outcome of infection. Additionally, recent findings suggest new roles for ubiquitination in the interplay between HIV and the cellular environment, specifically in the interactions between HIV, autophagy and apoptosis. On one hand, autophagy is a defense mechanism against HIV that promotes the degradation of the viral protein Gag, likely through ubiquitination. Gag is an essential structural protein that drives virion assembly and release. Interestingly, the ubiquitination of Gag is vital for HIV replication. Hence, this post-translational modification in Gag represents a double-edged sword: necessary for virion biogenesis, but potentially detrimental under conditions of autophagy activation. On the other hand, HIV uses Nef to circumvent autophagy-mediated restriction by promoting the ubiquitination of the autophagy inhibitor BCL2 through Parkin/PRKN. Although the Nef-promoted ubiquitination of BCL2 occurs in both the endoplasmic reticulum (ER) and mitochondria, only ER-associated ubiquitinated BCL2 arrests the progression of autophagy. Importantly, both mitochondrial BCL2 and PRKN are tightly connected to mitochondrial function and apoptosis. Hence, by enhancing the PRKN-mediated ubiquitination of BCL2 at the mitochondria, HIV might promote apoptosis. Moreover, this effect of Nef might account for HIV-associated disorders. In this article, we outline our current knowledge and provide perspectives of how ubiquitination impacts the molecular interactions between HIV, autophagy and apoptosis.

Keywords: autophagy, apoptosis, HIV, Nef, BCL2, BECN1, PRKN

OPEN ACCESS

Edited by:
Konstantin Sparrer, Ulm University Medical Center, Germany

Reviewed by:
Daniel Sauter, University Hospital Tübingen, Germany
Michael A. Mandell, University of New Mexico, United States

***Correspondence:**
Ruth Serra-Moreno
ruth_serra-moreno@urmc.rochester.edu
Sergio Castro-Gonzalez
sergio_gonzalez@urmc.rochester.edu

[†]*These authors have contributed equally to this work*

Specialty section:
This article was submitted to Viral Immunology, a section of the journal Frontiers in Immunology

Received: *18 March 2021*
Accepted: *21 April 2021*
Published: *06 May 2021*

Citation:
Castro-Gonzalez S, Simpson S, Shi Y, Chen Y, Benjamin J and Serra-Moreno R (2021) HIV Nef-mediated Ubiquitination of BCL2: Implications in Autophagy and Apoptosis. Front. Immunol. 12:682624. doi: 10.3389/fimmu.2021.682624

UBIQUITINATION IN THE MUTUAL ANTAGONISM BETWEEN HIV AND AUTOPHAGY

Ubiquitination post-translational modifications are used for multiple purposes including signaling transduction, enhancing protein function, driving protein subcellular localization and targeting proteins for degradation (1–3). One of these degradation pathways is autophagy, which targets components in the cytosol, including subcellular organelles and microbial pathogens, for lysosomal degradation. Whereas Lys-48 polyubiquitination commonly directs substrates to the proteasome (4–7), autophagy cargos are usually tagged with Lys-63 ubiquitin chains (4, 7, 8). Specifically, Lys-63 polyubiquitinated molecules are recognized by the ubiquitin binding domain (UBD) of different specialized autophagic receptors, including SQSTM1/p62. These receptors can simultaneously bind to ubiquitinated cargo and autophagosomal markers (i.e., LC3), allowing for the encapsulation of substrates into elongating autophagosomes (9–11).

Autophagy itself is highly regulated, in part through ubiquitination, as well as other post-translational modifications (1). For instance, ULK1, a serine/threonine kinase responsible for inducing autophagy under conditions of amino acid withdrawal, is ubiquitinated by the E3 ubiquitin ligase TRAF6, which enhances ULK1's function and stability (12). Moreover, TRAF6 ubiquitinates Beclin1/BECN1, which promotes autophagy induced by Toll-like receptor 4 signaling (13). p62 activity can similarly be regulated through E2-supported ubiquitination by UB2D2/UB2D3, which allows for this receptor to recognize cargo (14) (**Figure 1**). In addition to triggering autophagy, ubiquitination can also down-regulate this pathway by targeting components of this cascade for degradation (15). Particularly, the ubiquitination of (i) ULK1 and VPS34 by the E3 ligase Cul3-KLHL20, (ii) BECN1 by RNF216, and (iii) AMBRA1 by Cullin-4, promotes the proteasomal degradation of these autophagy regulators and, thus, reduces autophagy flux (16–19) (**Figure 1**). Additionally, many members of the tripartite motif (TRIM) family of E3 ligases regulate autophagy, although their mode of action does not always involve ubiquitination. Among the TRIM proteins that positively modulate autophagy we find TRIM5α, TRIM6, TRIM16, TRIM17, TRIM20, TRIM21, TRIM22, TRIM23, TRIM49 and TRIM50. These molecules trigger autophagy in response to stimuli such as viral infections, cell damage, IFNγ stimulation and pattern recognition receptor (PRR) engagement (20–28). Examples of TRIM members that down-regulate autophagy are TRIM17, TRIM28, TRIM37 and TRIM59. Despite its ability to promote autophagy of midbodies, TRIM17 can also hinder autophagy by stabilizing the autophagy inhibitor MCL1. In an analogous manner, TRIM37 increases the stability of mTOR, which naturally keeps autophagy off (29–31). By contrast, rather than enhancing the activity of autophagy inhibitors, TRIM28 and TRIM59 prevent autophagy through the ubiquitination and subsequent degradation of the positive regulators AMPK1α and TRAF6, respectively (32, 33) (**Figure 1**). Although not through ubiquitination, LC3 – a key player in autophagy initiation, progression and execution – is regulated through a ubiquitin-

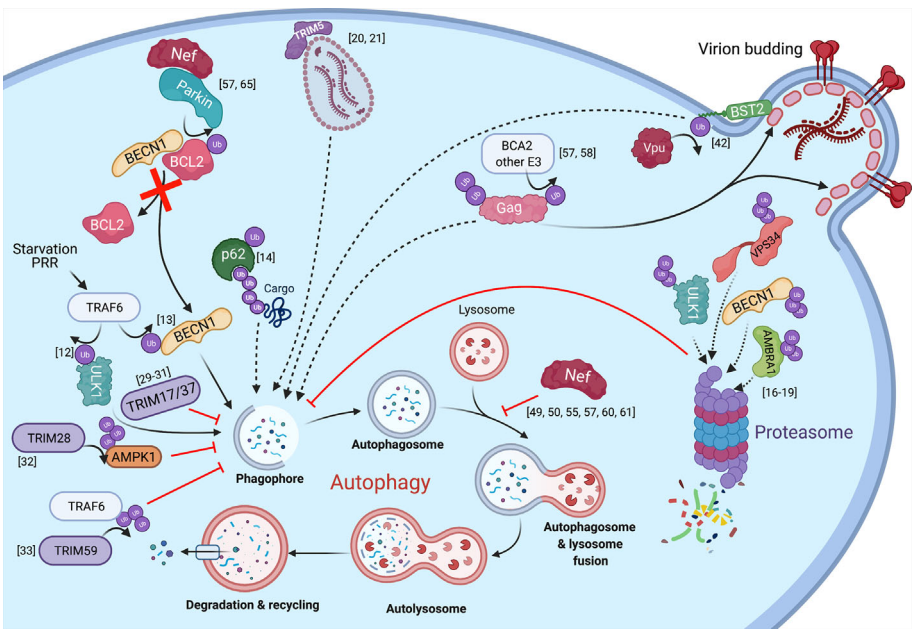

FIGURE 1 | The intersections between HIV infection and autophagy mediated by ubiquitination. The autophagy pathway and known interactions with HIV proteins are shown with regards to ubiquitination. Solid arrows represent the transfer of a ubiquitin group, direct contribution to the autophagy pathway, or show the steps of the autophagy cycle. Dotted lines represent substrates targeted for elimination. Red lines or arrows represent autophagy inhibition at corresponding steps in the pathway.

like process. Particularly, LC3 becomes lipidated and this post-translational modification requires the concerted action of enzymes that mimic the function of the E1, E2 and E3 enzymes involved in ubiquitination, and they are often referred to as E3-like ligases (34–36).

Ubiquitination also plays a role in viral infections, including HIV. On one hand, the HIV accessory proteins Vif, Vpr, Vpx and Vpu usurp ubiquitination signaling to target host factors – which would otherwise limit virion production – for proteasomal or lysosomal degradation (37–41), and also for autophagy-mediated clearance (42). For instance, Vpu has been reported to re-route the restriction factor Tetherin/BST2 to autophagosomes in a non-canonical manner (**Figure 1**). On the other hand, ubiquitination can cause the degradation of HIV proteins through the proteasomal, lysosomal and/or autophagy pathways. For example, the ubiquitination of the HIV core by TRIM5α promotes the proteasomal degradation of the capsid and premature termination of reverse transcription. In addition to this well-known activity, TRIM5α also triggers autophagy in response to HIV infection and leads to the autophagic degradation of the HIV core (20, 21) (**Figure 1**). Another example of ubiquitin-dependent degradation is that of the HIV protein Tat, which is responsible for switching from a state of viral latency to one of productive replication. Tat is ubiquitinated by the E3 ligase CHIP, which consequently causes its proteasomal degradation, and thus, negatively impacts viral transcription (43). However, Tat is also susceptible to ubiquitination in a non-degradative manner by the E3 ligase PJA2. Specifically, PJA2 adds atypical ubiquitin chains to Tat that increase its transactivating potential (44). Besides being degraded at the proteasome, Tat has also been found as an autophagy target in $CD4^+$ T cells, although its ubiquitination is not required to route it to autophagosomes (45). Conversely, Tat has been reported to down-regulate autophagy in neurons (46). Similar to Tat, Vif is also directed for autophagy-mediated clearance in a ubiquitin-independent manner through an association with the HDAC6 deacetylase (47). Paradoxically, Vif has been reported to inhibit canonical autophagy by associating with LC3 and preventing its incorporation into autophagosomal structures. Although the underlying mechanism by which Vif achieves this is not well understood, it does not seem to rely on LC3 ubiquitination or degradation (48).

The dichotomy of Tat and Vif in their relationship with the autophagy machinery underscores that the autophagy-HIV interactions are complex. Actually, conflicting reports exist regarding this interplay, with studies supporting that autophagy enhances or inhibits the progression of infection, depending on cell type (20, 45, 49–56). However, our group recently found that the HIV Gag polyprotein, the immature precursor of several structural proteins required for virion maturation, is degraded through autophagy regardless of cell type (57). Since Gag is susceptible to ubiquitination, which is part of its role in facilitating virion budding, it is likely that the targeting of Gag to autophagosomal membranes requires ubiquitination as well. In fact, our previous work on breast cancer-associated gene 2 (BCA2), a RING finger E3 ubiquitin ligase, showed that this protein promotes the ubiquitination and subsequent lysosomal degradation of HIV Gag (58). Hence, Gag ubiquitination could similarly tag this protein for autophagy-mediated clearance (**Figure 1**). Despite the antiviral potential of autophagy against HIV, our work also revealed that the virus has evolved mechanisms to counteract the autophagy-mediated destruction of viral elements needed for replication, including Gag. In particular, the HIV protein Nef counteracts the antiviral effects of autophagy. Importantly, while Nef is not required for replication *in vitro*, it enhances infection and contributes to pathogenesis *in vivo* by affording immune evasion through multiple mechanisms, including MHC-I down-regulation and counteraction of the restriction factors SERINC3 and SERINC5 [reviewed in (59)]. Besides these roles, Nef was also known to prevent viral degradation caused by autophagy through (i) a physical association with BECN1, inhibiting in turn autophagolysosomal biogenesis, and (ii) by promoting the cytosolic sequestration of the transcription factor TFEB, a master regulator of autophagy genes (49, 50, 55, 60, 61). In both models, the ultimate outcome is a defect in the fusion between autophagosomes and lysosomes. In support of these findings, we also found that Nef blocks autophagy maturation. However, we uncovered an additional mechanism by which Nef blocks autophagy at early stages of the cascade, and that requires a physical association between Nef and the E3 ubiquitin ligase Parkin/PRKN. Specifically, Nef recruits PRKN to promote the mono-ubiquitination of BCL2, an autophagy inhibitor (**Figure 1**) (57). Under normal conditions, BCL2 interacts with the autophagy initiator BECN1 to prevent autophagosome formation. However, under conditions of stress, BECN1 dissociates from BCL2 to initiate autophagosome biogenesis (62–64). Remarkably, the sequestration of BECN1 by BCL2 is enhanced if BCL2 is mono-ubiquitinated (65). In fact, we found that the Nef-mediated recruitment of PRKN not only increases BCL2 ubiquitination but also BECN1-BCL2 association. As a consequence of this, autophagosome formation is severely inhibited, while Gag levels and virion production are restored (**Figure 1**) (57). Based on these observations, we conclude that, besides its already described roles in autophagy maturation, Nef circumvents the autophagy block by intersecting with an early event in the autophagy cascade.

EFFECTS OF THE NEF-PROMOTED UBIQUITINATION OF BCL2 ON AUTOPHAGY AND APOPTOSIS

The increased levels of ubiquitinated BCL2 promoted by Nef may have further implications for infected cells. BCL2 is found in multiple subcellular compartments, including the endoplasmic reticulum (ER) and the mitochondria (66–68). ER-associated BCL2 is mainly involved in the regulation of autophagy through its interaction with BECN1, as stated above. Specifically, BCL2 binds to the BCL2 homology domain 3 (BH-3 domain) of BECN1 and sequesters this molecule, which in turn impairs

autophagy at both initiation and maturation stages. Autophagy initiation and maturation are dependent on the respective formation of the protein complexes PI3K-C1 and PI3K-C2 (class III PI 3-kinase complex 1 and complex 2). The core structure of PI3K-C1 consists of VPS34, BECN1, VPS15, and ATG14. PI3K-C2 core structure differs from C1 by the absence of ATG14 and the addition of UVRAG. The presence of ATG14 or UVRAG targets each complex towards phagophore membranes or autophagosomal membranes, which helps modulate autophagy initiation and maturation, respectively (69–71). Besides its role in sequestering BECN1, BCL2 may additionally intersect with C1/C2 and inhibit VPS34 kinase activity by blocking BECN1 interactions with ATG14 and UVRAG in their respective complexes (57, 69, 72, 73). The resulting effect of BCL2 binding to BECN1 is an overall antagonization of autophagy. Although this phenomenon has been described in more detail for C1 formation, the sequestration of free BECN1 might also impact the biogenesis of C2 and, thus, autophagy maturation (**Figure 2A**). Therefore, a major point of regulation in autophagy is the promotion and reduction of BECN1-BCL2 complexes.

Besides its ability to associate with the ER, BCL2 and other members of the BCL2 family can also be found at the mitochondria, where they regulate apoptosis by controlling the permeabilization of the outer mitochondrial membrane. Apoptosis is an essential process that removes damaged or infected cells in an orderly fashion. Under conditions of extreme stress or damage, pro-apoptotic effector proteins, such as BCL2-associated X protein (BAX) or BCL2 antagonist/killer-1 (BAK), homo-oligomerize to form pores on the outer mitochondrial membrane (74–77). The formation of these pores allows for cytochrome C to escape from the mitochondrial lumen. The release of cytochrome C to the cytosol enables its binding to the apoptotic protease activating factor (Apaf-1) and consequently triggers multiple caspase cascades that lead to this controlled death fate (77–79). Conversely, under healthy conditions, BCL2 pro-survival proteins directly bind to the BH3 domain in BAX to prevent pore formation on the outer mitochondrial membrane, which in turn prevents apoptosis (80, 81). Due to the importance of maintaining a healthy cell survival/cell death equilibrium, there are other relevant cellular factors involved in this apoptotic regulation. In particular, the BH3 domain of BCL2-associated agonist of cell death (BAD) is able to directly bind to mitochondria-associated BCL2 to hamper its anti-apoptotic function (82–84) (**Figure 2B**). Therefore, the BCL2-mediated inactivation of BAX, as well as its own regulation *via* BAD interaction, are crucial to control mitochondrial membrane integrity and consequently cell survival.

Whereas its subcellular localization dictates which cellular pathway will be susceptible for BCL2-mediated inhibition (autophagy *vs.* apoptosis), post-translational modifications of BCL2 will regulate the degree of restriction exerted over these two pathways. From this perspective, BCL2 is susceptible to become phosphorylated at Ser70 by the JNK1 kinase (85–87). When this phosphorylation occurs at the ER, it causes a reduction in the association between BCL2 and BECN1 and thus, it facilitates autophagy activation and progression by increasing the availability of BECN1 (62, 64, 85) (**Figure 2A**; top). Alternatively, JNK1 as well as other kinases have been

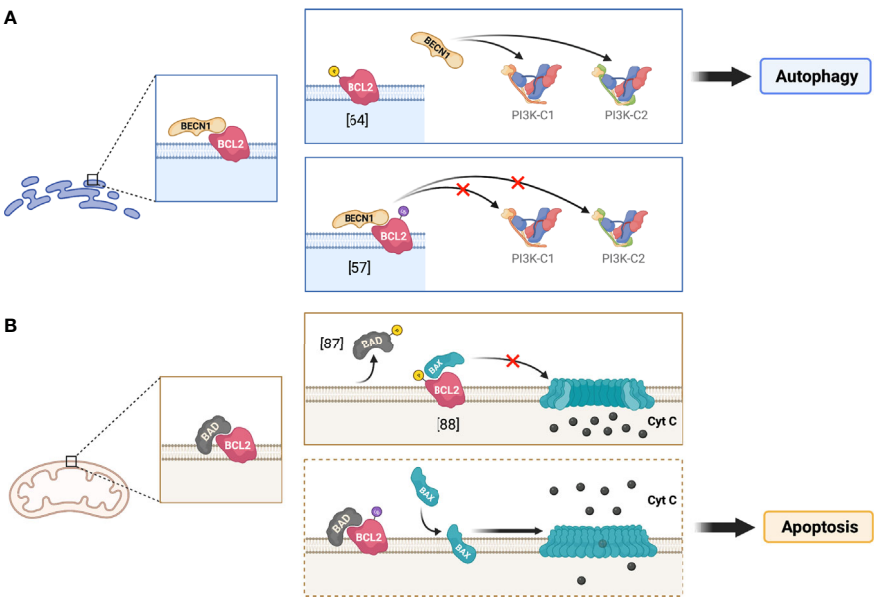

FIGURE 2 | Implications of the phosphorylation and ubiquitination of BCL2 at the ER and mitochondria. The figure illustrates the regulation of BCL2 functions through its post-translational modifications at different subcellular localizations, depicting the potential effect of BCL2 ubiquitination on autophagy and apoptosis. **(A)** presents the roles of BCL2 in the endoplasmic reticulum (ER), whereas **(B)** depicts the roles of BCL2 at the mitochondria. The dotted frame in **(B)** represents putative roles.

reported to mediate the phosphorylation of both BCL2 and its inhibitor BAD at the outer mitochondrial membrane (86, 88). This phosphorylation can promote the dissociation of BCL2 from BAD, which enables BCL2 anti-apoptotic function by increasing the ratio BCL2 to BAX (86, 88) (**Figure 2B**; top).

As noted above, in addition to phosphorylation, BCL2 is mono-ubiquitinated by PRKN. Of note, PRKN primarily localizes at the mitochondria where it helps regulate mitochondrial quality control, namely through mitophagy – the autophagy of mitochondria – when these organelles are impaired (89–91). The Nef-promoted mono-ubiquitination of BCL2 at the ER increases its stability and enhances its association with BECN1 to further restrict the early stages and progression of the autophagy pathway (57, 65) (**Figure 2A**; bottom). Besides facilitating BCL2 mono-ubiquitination at the ER, HIV Nef also increases mono-ubiquitination and stability of the BCL2 isoform in the mitochondria, although it does not cause an enhancement in its association with BECN1 (57). However, the potential impacts of mitochondrial BCL2 mono-ubiquitination on mitophagy and apoptosis are yet to be determined. One could speculate in this matter that, analogously to what applies for the ER in terms of BCL2-BECN1 interactions, the mono-ubiquitination of BCL2 at the mitochondria might promote BCL2-BAD association and consequently, facilitate cell death through apoptosis (**Figure 2B**; bottom).

DISCUSSION AND CONCLUDING REMARKS

The effects of the Nef-dependent mono-ubiquitination of BCL2 could have strong implications in our understanding of the role of Nef in the development of pathologies associated with HIV^+ individuals. First of all, the fact that not only Nef impacts autophagy restriction but also might facilitate apoptotic events through the PRKN-dependent mono-ubiquitination of BCL2 could provide mechanistic support to previous studies that connect Nef expression and apoptosis in different cell types, such as cardiomyocytes, brain endothelial cells or $CD4^+$ T cells (92–94). Importantly, this Nef-mediated apoptosis may be responsible, at least in part, for the depletion of infected as well as bystander $CD4^+$ T cells, which is the main cause of the immunodeficiency observed in infected individuals. Additionally, the effect of the Nef-enhanced ubiquitination of BCL2 on autophagy could also account for the development of other HIV-associated pathologies, including HIV-associated neurological disorders (HAND) or HIV-associated pulmonary hypertension (HIV-PH) (95–97). These conditions are not only relevant because of their undesired symptomatology and prognosis, but also because they are usually associated with persons living with HIV, even those controlling the infection due to their adherence to the antiretroviral regimens. Whereas Nef expression has been linked to the development of these pathologies, the underlying mechanisms still remain unknown. Remarkably, several studies have demonstrated that autophagic dysfunction is directly associated with pulmonary hypertension as well as numerous neurological and cognitive conditions, including HAND (96, 98, 99). In fact, autophagy dysregulation by HIV Tat has been linked with neuronal degeneration (46), so the effect of Nef on BCL2 ubiquitination and its role in autophagy might exacerbate neuronal damage. In addition, malfunction of the ubiquitin ligase PRKN seems to be associated with neurological disorders (100, 101). Therefore, Nef's capacity to intersect with autophagy through the recruitment of PRKN to drive the mono-ubiquitination of BCL2 might be a key driver in the development of these HIV-associated conditions.

Ubiquitin has a relevant position in the arms-race between HIV and the host cell environment. Despite being required for viral particle assembly, the ubiquitination of HIV Gag might be tagging this protein for the so-called 'kiss of death' fate. Conversely, HIV has evolved a strategy to hijack the cellular ubiquitin machinery in order to overcome this hurdle. This mechanism involves the mono-ubiquitination of BCL2 that, in addition to preventing the degradation of Gag, might also be lifting the endogenous control over apoptosis. This in turn could have a wide range of implications for the pathogenesis and prognosis of HIV^+ individuals. Therefore, further elucidation of the role of ubiquitin within the interplay between HIV and the host could be promising for the identification of new therapeutic targets against this virus.

AUTHOR CONTRIBUTIONS

SC-G, SS, and RS-M outlined the perspectives paper. SC-G, SS, YS, YC, JB, and RS-M researched specific sections of the perspectives article and provided the literature referenced here. SC-G wrote the abstract. SC-G and SS designed the figures. SC-G, SS and RS-M wrote the manuscript. All authors contributed to the article and approved the submitted version.

FUNDING

We thank the University of Rochester Medical Center (URMC) for supporting our work. SC-G is supported by a NIH HARC collaboration grant (P50AI150476; subcontract award 12310sc; Serra-Moreno PI), YS is supported by NIH R21AI138589 (Serra-Moreno, PI), YC is supported by NSF RAPID MCB-2032518 (Serra-Moreno, PI). JB and SS are supported by RS-M startup funds. RS-M is supported by URMC, P50AI150476, R21AI138589, and MCB-2032518.

ACKNOWLEDGMENTS

The figures presented in this manuscript were created with BioRender.com

REFERENCES

1. Chen RH, Chen YH, Huang TY. Ubiquitin-Mediated Regulation of Autophagy. *J BioMed Sci* (2019) 26:80. doi: 10.1186/s12929-019-0569-y
2. Kulathu Y, Komander D. Atypical Ubiquitylation - the Unexplored World of Polyubiquitin Beyond Lys48 and Lys63 Linkages. *Nat Rev Mol Cell Biol* (2012) 13:508–23. doi: 10.1038/nrm3394
3. Yau R, Rape M. The Increasing Complexity of the Ubiquitin Code. *Nat Cell Biol* (2016) 18:579–86. doi: 10.1038/ncb3358
4. Kwon YT, Ciechanover A. The Ubiquitin Code in the Ubiquitin-Proteasome System and Autophagy. *Trends Biochem Sci* (2017) 42:873–86. doi: 10.1016/j.tibs.2017.09.002
5. Tai HC, Schuman EM. Ubiquitin, the Proteasome and Protein Degradation in Neuronal Function and Dysfunction. *Nat Rev Neurosci* (2008) 9:826–38. doi: 10.1038/nrn2499
6. Grice GL, Nathan JA. The Recognition of Ubiquitinated Proteins by the Proteasome. *Cell Mol Life Sci* (2016) 73:3497–506. doi: 10.1007/s00018-016-2255-5
7. Nathan JA, Kim HT, Ting L, Gygi SP, Goldberg AL. Why do Cellular Proteins Linked to K63-polyubiquitin Chains Not Associate With Proteasomes? *EMBO J* (2013) 32:552–65. doi: 10.1038/emboj.2012.354
8. Tan JM, Wong ES, Kirkpatrick DS, Pletnikova O, Ko HS, Tay SP, et al. Lysine 63-Linked Ubiquitination Promotes the Formation and Autophagic Clearance of Protein Inclusions Associated With Neurodegenerative Diseases. *Hum Mol Genet* (2008) 17:431–9. doi: 10.1093/hmg/ddm320
9. Wooten MW, Geetha T, Babu JR, Seibenhener ML, Peng J, Cox N, et al. Essential Role of Sequestosome 1/p62 in Regulating Accumulation of Lys63-ubiquitinated Proteins. *J Biol Chem* (2008) 283:6783–9. doi: 10.1074/jbc.M709496200
10. Wurzer B, Zaffagnini G, Fracchiolla D, Turco E, Abert C, Romanov J, et al. Oligomerization of p62 Allows for Selection of Ubiquitinated Cargo and Isolation Membrane During Selective Autophagy. *Elife* (2015) 4:e08941. doi: 10.7554/eLife.08941
11. Pankiv S, Clausen TH, Lamark T, Brech A, Bruun JA, Outzen H, et al. p62/SQSTM1 Binds Directly to Atg8/LC3 to Facilitate Degradation of Ubiquitinated Protein Aggregates by Autophagy. *J Biol Chem* (2007) 282:24131–45. doi: 10.1074/jbc.M702824200
12. Nazio F, Strappazzon F, Antonioli M, Bielli P, Cianfanelli V, Bordi M, et al. mTOR Inhibits Autophagy by Controlling ULK1 Ubiquitylation, Self-Association and Function Through AMBRA1 and TRAF6. *Nat Cell Biol* (2013) 15:406–16. doi: 10.1038/ncb2708
13. Shi CS, Kehrl JH. TRAF6 and A20 Regulate Lysine 63-Linked Ubiquitination of Beclin-1 to Control TLR4-induced Autophagy. *Sci Signal* (2010) 3:ra42. doi: 10.1126/scisignal.2000751
14. Peng H, Yang J, Li G, You Q, Han W, Li T, et al. Ubiquitylation of p62/sequestosome1 Activates its Autophagy Receptor Function and Controls Selective Autophagy Upon Ubiquitin Stress. *Cell Res* (2017) 27:657–74. doi: 10.1038/cr.2017.40
15. Kocaturk NM, Gozuacik D. Crosstalk Between Mammalian Autophagy and the Ubiquitin-Proteasome System. *Front Cell Dev Biol* (2018) 6:128. doi: 10.3389/fcell.2018.00128
16. Liu CC, Lin YC, Chen YH, Chen CM, Pang LY, Chen HA, et al. Cul3-KLHL20 Ubiquitin Ligase Governs the Turnover of ULK1 and VPS34 Complexes to Control Autophagy Termination. *Mol Cell* (2016) 61:84–97. doi: 10.1016/j.molcel.2015.11.001
17. Gomez-Diaz C, Ikeda F. Roles of Ubiquitin in Autophagy and Cell Death. *Semin Cell Dev Biol* (2019) 93:125–35. doi: 10.1016/j.semcdb.2018.09.004
18. Xu C, Feng K, Zhao X, Huang S, Cheng Y, Qian L, et al. Regulation of Autophagy by E3 Ubiquitin Ligase RNF216 Through BECN1 Ubiquitination. *Autophagy* (2014) 10:2239–50. doi: 10.4161/15548627.2014.981792
19. Antonioli M, Albiero F, Nazio F, Vescovo T, Perdomo AB, Corazzari M, et al. AMBRA1 Interplay With Cullin E3 Ubiquitin Ligases Regulates Autophagy Dynamics. *Dev Cell* (2014) 31:734–46. doi: 10.1016/j.devcel.2014.11.013
20. Mandell MA, Kimura T, Jain A, Johansen T, Deretic V. TRIM Proteins Regulate Autophagy: TRIM5 is a Selective Autophagy Receptor Mediating HIV-1 Restriction. *Autophagy* (2014) 10:2387–8. doi: 10.4161/15548627.2014.984278
21. Ribeiro CM, Sarrami-Forooshani R, Setiawan LC, Zijlstra-Willems EM, van Hamme JL, Tigchelaar W, et al. Receptor Usage Dictates HIV-1 Restriction by Human TRIM5alpha in Dendritic Cell Subsets. *Nature* (2016) 540:448–52. doi: 10.1038/nature20567
22. Chauhan S, Kumar S, Jain A, Ponpuak M, Mudd MH, Kimura T, et al. Trims and Galectins Globally Cooperate and TRIM16 and Galectin-3 Co-Direct Autophagy in Endomembrane Damage Homeostasis. *Dev Cell* (2016) 39:13–27. doi: 10.1016/j.devcel.2016.08.003
23. Fusco C, Mandriani B, Di Rienzo M, Micale L, Malerba N, Cocciadiferro D, et al. TRIM50 Regulates Beclin 1 Proautophagic Activity. *Biochim Biophys Acta Mol Cell Res* (2018) 1865:908–19. doi: 10.1016/j.bbamcr.2018.03.011
24. Kimura T, Jain A, Choi SW, Mandell MA, Schroder K, Johansen T, et al. TRIM-Mediated Precision Autophagy Targets Cytoplasmic Regulators of Innate Immunity. *J Cell Biol* (2015) 210:973–89. doi: 10.1083/jcb.201503023
25. Mandell MA, Jain A, Arko-Mensah J, Chauhan S, Kimura T, Dinkins C, et al. TRIM Proteins Regulate Autophagy and can Target Autophagic Substrates by Direct Recognition. *Dev Cell* (2014) 30:394–409. doi: 10.1016/j.devcel.2014.06.013
26. Di Rienzo M, Romagnoli A, Antonioli M, Piacentini M, Fimia GM. TRIM Proteins in Autophagy: Selective Sensors in Cell Damage and Innate Immune Responses. *Cell Death Differ* (2020) 27:887–902. doi: 10.1038/s41418-020-0495-2
27. Sparrer KMJ, Gableske S, Zurenski MA, Parker ZM, Full F, Baumgart GJ, et al. TRIM23 Mediates Virus-Induced Autophagy Via Activation of TBK1. *Nat Microbiol* (2017) 2:1543–57. doi: 10.1038/s41564-017-0017-2
28. Lou J, Wang Y, Zheng X, Qiu W. TRIM22 Regulates Macrophage Autophagy and Enhances Mycobacterium Tuberculosis Clearance by Targeting the Nuclear Factor-Multiplicity kappaB/beclin 1 Pathway. *J Cell Biochem* (2018) 119:8971–80. doi: 10.1002/jcb.27153
29. Brigant B, Metzinger-Le Meuth V, Rochette J, Metzinger L. Trimming Down to TRIM37: Relevance to Inflammation, Cardiovascular Disorders, and Cancer in MULIBREY Nanism. *Int J Mol Sci* (2018) 20:1–14. doi: 10.3390/ijms20010067
30. Wang W, Xia Z, Farre JC, Subramani S. TRIM37 Deficiency Induces Autophagy Through Deregulating the MTORC1-TFEB Axis. *Autophagy* (2018) 14:1574–85. doi: 10.1080/15548627.2018.1463120
31. Mandell MA, Jain A, Kumar S, Castleman MJ, Anwar T, Eskelinen EL, et al. TRIM17 Contributes to Autophagy of Midbodies While Actively Sparing Other Targets From Degradation. *J Cell Sci* (2016) 129:3562–73. doi: 10.1242/jcs.190017
32. Pineda CT, Ramanathan S, Fon Tacer K, Weon JL, Potts MB, Ou YH, et al. Degradation of AMPK by a Cancer-Specific Ubiquitin Ligase. *Cell* (2015) 160:715–28. doi: 10.1016/j.cell.2015.01.034
33. Han T, Guo M, Gan M, Yu B, Tian X, Wang JB. TRIM59 Regulates Autophagy Through Modulating Both the Transcription and the Ubiquitination of BECN1. *Autophagy* (2018) 14:2035–48. doi: 10.1080/15548627.2018.1491493
34. Fujita N, Itoh T, Omori H, Fukuda M, Noda T, Yoshimori T. The Atg16L Complex Specifies the Site of LC3 Lipidation for Membrane Biogenesis in Autophagy. *Mol Biol Cell* (2008) 19:2092–100. doi: 10.1091/mbc.e07-12-1257
35. Lescouzeres L, Bomont P. E3 Ubiquitin Ligases in Neurological Diseases: Focus on Gigaxonin and Autophagy. *Front Physiol* (2020) 11:1022. doi: 10.3389/fphys.2020.01022
36. Scrivo A, Codogno P, Bomont P. Gigaxonin E3 Ligase Governs ATG16L1 Turnover to Control Autophagosome Production. *Nat Commun* (2019) 10:780. doi: 10.1038/s41467-019-08331-w
37. Iwabu Y, Fujita H, Kinomoto M, Kaneko K, Ishizaka Y, Tanaka Y, et al. HIV-1 Accessory Protein Vpu Internalizes Cell-Surface BST-2/Tetherin Through Transmembrane Interactions Leading to Lysosomes. *J Biol Chem* (2009) 284:35060–72. doi: 10.1074/jbc.M109.058305
38. Mehle A, Strack B, Ancuta P, Zhang C, McPike M, Gabuzda D. Vif Overcomes the Innate Antiviral Activity of APOBEC3G by Promoting its Degradation in the Ubiquitin-Proteasome Pathway. *J Biol Chem* (2004) 279:7792–8. doi: 10.1074/jbc.M313093200
39. Mitchell RS, Katsura C, Skasko MA, Fitzpatrick K, Lau D, Ruiz A, et al. Vpu Antagonizes BST-2-mediated Restriction of HIV-1 Release Via beta-TrCP and Endo-Lysosomal Trafficking. *PloS Pathog* (2009) 5:e1000450. doi: 10.1371/journal.ppat.1000450

40. Seissler T, Marquet R, Paillart JC. Hijacking of the Ubiquitin/Proteasome Pathway by the HIV Auxiliary Proteins. *Viruses* (2017) 9:1–21. doi: 10.3390/v9110322
41. Yu X, Yu Y, Liu B, Luo K, Kong W, Mao P, et al. Induction of APOBEC3G Ubiquitination and Degradation by an HIV-1 Vif-Cul5-SCF Complex. *Science* (2003) 302:1056–60. doi: 10.1126/science.1089591
42. Madjo U, Leymarie O, Fremont S, Kuster A, Nehlich M, Gallois-Montbrun S, et al. LC3C Contributes to Vpu-Mediated Antagonism of BST2/Tetherin Restriction on HIV-1 Release Through a Non-canonical Autophagy Pathway. *Cell Rep* (2016) 17:2221–33. doi: 10.1016/j.celrep.2016.10.045
43. Ali A, Farooqui SR, Banerjea AC. The Host Cell Ubiquitin Ligase Protein CHIP is a Potent Suppressor of HIV-1 Replication. *J Biol Chem* (2019) 294:7283–95. doi: 10.1074/jbc.RA118.007257
44. Faust TB, Li Y, Jang GM, Johnson JR, Yang S, Weiss A, et al. PJA2 Ubiquitinates the HIV-1 Tat Protein With Atypical Chain Linkages to Activate Viral Transcription. *Sci Rep* (2017) 7:45394. doi: 10.1038/srep45394
45. Sagnier S, Daussy CF, Borel S, Robert-Hebmann V, Faure M, Blanchet FP, et al. Autophagy Restricts HIV-1 Infection by Selectively Degrading Tat in CD4+ T Lymphocytes. *J Virol* (2015) 89:615–25. doi: 10.1128/JVI.02174-14
46. Fields J, Dumaop W, Eleuteri S, Campos S, Serger E, Trejo M, et al. Hiv-1 Tat Alters Neuronal Autophagy by Modulating Autophagosome Fusion to the Lysosome: Implications for HIV-associated Neurocognitive Disorders. *J Neurosci* (2015) 35:1921–38. doi: 10.1523/JNEUROSCI.3207-14.2015
47. Valera MS, de Armas-Rillo L, Barroso-Gonzalez J, Ziglio S, Batisse J, Dubois N, et al. The HDAC6/APOBEC3G Complex Regulates HIV-1 Infectiveness by Inducing Vif Autophagic Degradation. *Retrovirology* (2015) 12:53. doi: 10.1186/s12977-015-0181-5
48. Borel S, Robert-Hebmann V, Alfaisal J, Jain A, Faure M, Espert L, et al. HIV-1 Viral Infectivity Factor Interacts With Microtubule-Associated Protein Light Chain 3 and Inhibits Autophagy. *AIDS* (2015) 29:275–86. doi: 10.1097/QAD.0000000000000554
49. Campbell GR, Rawat P, Bruckman RS, Spector SA. Human Immunodeficiency Virus Type 1 Nef Inhibits Autophagy Through Transcription Factor EB Sequestration. *PloS Pathog* (2015) 11:e1005018. doi: 10.1371/journal.ppat.1005018
50. Campbell GR, Spector SA. Inhibition of Human Immunodeficiency Virus Type-1 Through Autophagy. *Curr Opin Microbiol* (2013) 16:349–54. doi: 10.1016/j.mib.2013.05.006
51. Daussy CF, Beaumelle B, Espert L. Autophagy Restricts HIV-1 Infection. *Oncotarget* (2015) 6:20752–3. doi: 10.18632/oncotarget.5123
52. Denizot M, Varbanov M, Espert L, Robert-Hebmann V, Sagnier S, Garcia E, et al. Hiv-1 gp41 Fusogenic Function Triggers Autophagy in Uninfected Cells. *Autophagy* (2008) 4:998–1008. doi: 10.4161/auto.6880
53. Dinkins C, Pilli M, Kehrl JH. Roles of Autophagy in HIV Infection. *Immunol Cell Biol* (2015) 93:11–7. doi: 10.1038/icb.2014.88
54. Espert L, Beaumelle B, Vergne I. Autophagy in Mycobacterium Tuberculosis and HIV Infections. *Front Cell Infect Microbiol* (2015) 5:49. doi: 10.3389/fcimb.2015.00049
55. Kyei GB, Dinkins C, Davis AS, Roberts E, Singh SB, Dong C, et al. Autophagy Pathway Intersects With HIV-1 Biosynthesis and Regulates Viral Yields in Macrophages. *J Cell Biol* (2009) 186:255–68. doi: 10.1083/jcb.200903070
56. Nardacci R, Ciccosanti F, Marsella C, Ippolito G, Piacentini M, Fimia GM. Role of Autophagy in HIV Infection and Pathogenesis. *J Intern Med* (2017) 281:422–32. doi: 10.1111/joim.12596
57. Castro-Gonzalez S, Shi Y, Colomer-Lluch M, Song Y, Mowery K, Almodovar S, et al. HIV-1 Nef Counteracts Autophagy Restriction by Enhancing the Association Between BECN1 and its Inhibitor BCL2 in a PRKN-dependent Manner. *Autophagy* (2020) 17(2):1–25. doi: 10.1080/15548627.2020.1725401
58. Nityanandam R, Serra-Moreno R. BCA2/Rabring7 Targets HIV-1 Gag for Lysosomal Degradation in a Tetherin-Independent Manner. *PloS Pathog* (2014) 10:e1004151. doi: 10.1371/journal.ppat.1004151
59. Buffalo CZ, Iwamoto Y, Hurley JH, Ren X. How HIV Nef Proteins Hijack Membrane Traffic To Promote Infection. *J Virol* (2019) 93:1–18. doi: 10.1128/JVI.01322-19
60. Chang C, Young LN, Morris KL, von Bulow S, Schoneberg J, Yamamoto-Imoto H, et al. Bidirectional Control of Autophagy by BECN1 Bara Domain Dynamics. *Mol Cell* (2019) 73:339–353 e6. doi: 10.1016/j.molcel.2018.10.035
61. Shoji-Kawata S, Sumpter R, Leveno M, Campbell GR, Zou Z, Kinch L, et al. Identification of a Candidate Therapeutic Autophagy-Inducing Peptide. *Nature* (2013) 494:201–6. doi: 10.1038/nature11866
62. Decuypere JP, Parys JB, Bultynck G. Regulation of the Autophagic bcl-2/beclin 1 Interaction. *Cells* (2012) 1:284–312. doi: 10.3390/cells1030284
63. Pattingre S, Tassa A, Qu X, Garuti R, Liang XH, Mizushima N, et al. Bcl-2 Antiapoptotic Proteins Inhibit Beclin 1-Dependent Autophagy. *Cell* (2005) 122:927–39. doi: 10.1016/j.cell.2005.07.002
64. Wei Y, Pattingre S, Sinha S, Bassik M, Levine B. JNK1-Mediated Phosphorylation of Bcl-2 Regulates Starvation-Induced Autophagy. *Mol Cell* (2008) 30:678–88. doi: 10.1016/j.molcel.2008.06.001
65. Chen D, Gao F, Li B, Wang H, Xu Y, Zhu C, et al. Parkin Mono-Ubiquitinates Bcl-2 and Regulates Autophagy. *J Biol Chem* (2010) 285:38214–23. doi: 10.1074/jbc.M110.101469
66. Akao Y, Otsuki Y, Kataoka S, Ito Y, Tsujimoto Y. Multiple Subcellular Localization of bcl-2: Detection in Nuclear Outer Membrane, Endoplasmic Reticulum Membrane, and Mitochondrial Membranes. *Cancer Res* (1994) 54:2468–71.
67. Janiak F, Leber B, Andrews DW. Assembly of Bcl-2 Into Microsomal and Outer Mitochondrial Membranes. *J Biol Chem* (1994) 269:9842–9. doi: 10.1016/S0021-9258(17)36960-0
68. Krajewski S, Tanaka S, Takayama S, Schibler MJ, Fenton W, Reed JC. Investigation of the Subcellular Distribution of the Bcl-2 Oncoprotein: Residence in the Nuclear Envelope, Endoplasmic Reticulum, and Outer Mitochondrial Membranes. *Cancer Res* (1993) 53:4701–14.
69. Hurley JH, Young LN. Mechanisms of Autophagy Initiation. *Annu Rev Biochem* (2017) 86:225–44. doi: 10.1146/annurev-biochem-061516-044820
70. McKnight NC, Zhenyu Y. Beclin 1, an Essential Component and Master Regulator of PI3K-III in Health and Disease. *Curr Pathobiol Rep* (2013) 1:231–8. doi: 10.1007/s40139-013-0028-5
71. Brier LW, Ge L, Stjepanovic G, Thelen AM, Hurley JH, Schekman R. Regulation of LC3 Lipidation by the Autophagy-Specific Class III Phosphatidylinositol-3 Kinase Complex. *Mol Biol Cell* (2019) 30:1098–107. doi: 10.1091/mbc.E18-11-0743
72. Kang R, Zeh HJ, Lotze MT, Tang D. The Beclin 1 Network Regulates Autophagy and Apoptosis. *Cell Death Different* (2011) 18:571–80. doi: 10.1038/cdd.2010.191
73. Chang NC, Nguyen M, Germain M, Shore GC. Antagonism of Beclin 1-Dependent Autophagy by BCL-2 At the Endoplasmic Reticulum Requires NAF-1. *EMBO J* (2010) 29:606–18. doi: 10.1038/emboj.2009.369
74. Westphal D, Dewson G, Czabotar PE, Kluck RM. Molecular Biology of Bax and Bak Activation and Action. *Biochim Biophys Acta* (2011) 1813:521–31. doi: 10.1016/j.bbamcr.2010.12.019
75. Westphal D, Kluck RM, Dewson G. Building Blocks of the Apoptotic Pore: How Bax and Bak are Activated and Oligomerize During Apoptosis. *Cell Death Differ* (2014) 21:196–205. doi: 10.1038/cdd.2013.139
76. Wei MC, Zong WX, Cheng EH, Lindsten T, Panoutsakopoulou V, Ross AJ, et al. And BAK: A Requisite Gateway to Mitochondrial Dysfunction and Death. *Science* (2001) 292:727–30. doi: 10.1126/science.1059108
77. Eskes R, Desagher S, Antonsson B, Martinou JC. Bid Induces the Oligomerization and Insertion of Bax Into the Outer Mitochondrial Membrane. *Mol Cell Biol* (2000) 20:929–35. doi: 10.1128/MCB.20.3.929-935.2000
78. Cai J, Yang J, Jones DP. Mitochondrial Control of Apoptosis: The Role of Cytochrome C. *Biochim Biophys Acta* (1998) 1366:139–49. doi: 10.1016/S0005-2728(98)00109-1
79. Li P, Nijhawan D, Budihardjo I, Srinivasula SM, Ahmad M, Alnemri ES, et al. Cytochrome C and dATP-dependent Formation of Apaf-1/caspase-9 Complex Initiates an Apoptotic Protease Cascade. *Cell* (1997) 91:479–89. doi: 10.1016/S0092-8674(00)80434-1
80. Czabotar PE, Lessene G, Strasser A, Adams JM. Control of Apoptosis by the BCL-2 Protein Family: Implications for Physiology and Therapy. *Nat Rev Mol Cell Biol* (2014) 15:49–63. doi: 10.1038/nrm3722
81. Skommer J, Brittain T, Raychaudhuri S. Bcl-2 Inhibits Apoptosis by Increasing the Time-to-Death and Intrinsic Cell-to-Cell Variations in the Mitochondrial Pathway of Cell Death. *Apoptosis* (2010) 15:1223–33. doi: 10.1007/s10495-010-0515-7
82. Howells CC, Baumann WT, Samuels DC, Finkielstein CV. The Bcl-2-associated Death Promoter (BAD) Lowers the Threshold At Which the

Bcl-2-interacting Domain Death Agonist (BID) Triggers Mitochondria Disintegration. *J Theor Biol* (2011) 271:114–23. doi: 10.1016/j.jtbi.2010.11.040
83. Yu Y, Zhong Z, Guan Y. The Downregulation of Bcl-xL/Bcl-2-associated Death Promoter Indicates Worse Outcomes in Patients With Small Cell Lung Carcinoma. *Int J Clin Exp Pathol* (2015) 8:13075–82.
84. Hsu SY, Kaipia A, Zhu L, Hsueh AJ. Interference of BAD (Bcl-xL/Bcl-2-associated Death Promoter)-Induced Apoptosis in Mammalian Cells by 14-3-3 Isoforms and P11. *Mol Endocrinol* (1997) 11:1858–67. doi: 10.1210/me.11.12.1858
85. Wei Y, Sinha S, Levine B. Dual Role of JNK1-mediated Phosphorylation of Bcl-2 in Autophagy and Apoptosis Regulation. *Autophagy* (2008) 4:949–51. doi: 10.4161/auto.6788
86. Ruvolo PP, Deng X, May WS. Phosphorylation of Bcl2 and Regulation of Apoptosis. *Leukemia* (2001) 15:515–22. doi: 10.1038/sj.leu.2402090
87. Zha J, Harada H, Yang E, Jockel J, Korsmeyer SJ. Serine Phosphorylation of Death Agonist BAD in Response to Survival Factor Results in Binding to 14-3-3 Not BCL-X(L). *Cell* (1996) 87:619–28. doi: 10.1016/S0092-8674(00)81382-3
88. Ito T, Deng X, Carr B, May WS. Bcl-2 Phosphorylation Required for Anti-Apoptosis Function. *J Biol Chem* (1997) 272:11671–3. doi: 10.1074/jbc.272.18.11671
89. Narendra D, Tanaka A, Suen DF, Youle RJ. Parkin is Recruited Selectively to Impaired Mitochondria and Promotes Their Autophagy. *J Cell Biol* (2008) 183:795–803. doi: 10.1083/jcb.200809125
90. Yang Y, Gehrke S, Imai Y, Huang Z, Ouyang Y, Wang JW, et al. Mitochondrial Pathology and Muscle and Dopaminergic Neuron Degeneration Caused by Inactivation of Drosophila Pink1 is Rescued by Parkin. *Proc Natl Acad Sci USA* (2006) 103:10793–8. doi: 10.1073/pnas.0602493103
91. Araya J, Tsubouchi K, Sato N, Ito S, Minagawa S, Hara H, et al. PRKN-Regulated Mitophagy and Cellular Senescence During COPD Pathogenesis. *Autophagy* (2019) 15:510–26. doi: 10.1080/15548627.2018.1532259
92. Rasola A, Gramaglia D, Boccaccio C, Comoglio PM. Apoptosis Enhancement by the HIV-1 Nef Protein. *J Immunol* (2001) 166:81–8. doi: 10.4049/jimmunol.166.1.81
93. Acheampong EA, Parveen Z, Muthoga LW, Kalayeh M, Mukhtar M, Pomerantz RJ. Human Immunodeficiency Virus Type 1 Nef Potently Induces Apoptosis in Primary Human Brain Microvascular Endothelial Cells Via the Activation of Caspases. *J Virol* (2005) 79:4257–69. doi: 10.1128/JVI.79.7.4257-4269.2005
94. Lenassi M, Cagney G, Liao M, Vaupotic T, Bartholomeeusen K, Cheng Y, et al. Hiv Nef is Secreted in Exosomes and Triggers Apoptosis in Bystander CD4+ T Cells. *Traffic* (2010) 11:110–22. doi: 10.1111/j.1600-0854.2009.01006.x
95. Lamers SL, Fogel GB, Liu ES, Barbier AE, Rodriguez CW, Singer EJ, et al. Brain-Specific HIV Nef Identified in Multiple Patients With Neurological Disease. *J Neurovirol* (2018) 24:1–15. doi: 10.1007/s13365-017-0586-0
96. Cheney L, Guzik H, Macaluso FP, Macian F, Cuervo AM, Berman JW. Hiv Nef and Antiretroviral Therapy Have an Inhibitory Effect on Autophagy in Human Astrocytes That May Contribute to HIV-Associated Neurocognitive Disorders. *Cells* (2020) 9:1–25. doi: 10.3390/cells9061426
97. Almodovar S, Hsue PY, Morelli J, Huang L, Flores SC, Lung HIVS. Pathogenesis of HIV-associated Pulmonary Hypertension: Potential Role of HIV-1 Nef. *Proc Am Thorac Soc* (2011) 8:308–12. doi: 10.1513/pats.201006-046WR
98. Zhang CF, Zhao FY, Xu SL, Liu J, Xing XQ, Yang J. Autophagy in Pulmonary Hypertension: Emerging Roles and Therapeutic Implications. *J Cell Physiol* (2019) 234:16755–67. doi: 10.1002/jcp.28531
99. Dever SM, Rodriguez M, Lapierre J, Costin BN, El-Hage N. Differing Roles of Autophagy in HIV-associated Neurocognitive Impairment and Encephalitis With Implications for Morphine Co-Exposure. *Front Microbiol* (2015) 6:653. doi: 10.3389/fmicb.2015.00653
100. Ge P, Dawson VL, Dawson TM. PINK1 and Parkin Mitochondrial Quality Control: A Source of Regional Vulnerability in Parkinson's Disease. *Mol Neurodegener* (2020) 15:20. doi: 10.1186/s13024-020-00367-7
101. Wasner K, Grunewald A, Klein C. Parkin-Linked Parkinson's Disease: From Clinical Insights to Pathogenic Mechanisms and Novel Therapeutic Approaches. *Neurosci Res* (2020) 159:34–9. doi: 10.1016/j.neures.2020.09.001

Conflict of Interest: The authors declare that the research was conducted in the absence of any commercial or financial relationships that could be construed as a potential conflict of interest.

The handling editor has declared a past collaboration with one of the authors [RS-M].

frontiers in Immunology

MINI REVIEW
published: 10 June 2021
doi: 10.3389/fimmu.2021.687102

Emerging Roles of MHC Class I Region-Encoded E3 Ubiquitin Ligases in Innate Immunity

Xiuzhi Jia, Chunyuan Zhao and Wei Zhao *

Department of Pathogenic Biology, School of Basic Medical Science, Cheeloo College of Medicine, Shandong University, Jinan, China

The major histocompatibility complex (MHC) class I (MHC-I) region contains a multitude of genes relevant to immune response. Multiple E3 ubiquitin ligase genes, including tripartite motif 10 (*TRIM10*), *TRIM15*, *TRIM26*, *TRIM27*, *TRIM31*, *TRIM38*, *TRIM39*, *TRIM40*, and RING finger protein 39 (*RNF39*), are organized in a tight cluster, and an additional two TRIM genes (namely *TRIM38* and *TRIM27*) telomeric of the cluster within the MHC-I region. The E3 ubiquitin ligases encoded by these genes possess important roles in controlling the intensity of innate immune responses. In this review, we discuss the E3 ubiquitin ligases encoded within the MHC-I region, highlight their regulatory roles in innate immunity, and outline their potential functions in infection, inflammatory and autoimmune diseases.

Keywords: MHC class I region, E3 ubiquitin ligases, innate immunity, post-translational modifications, autoimmune diseases

OPEN ACCESS

Edited by:
Konstantin Sparrer, Ulm University Medical Center, Germany

Reviewed by:
Katrin Rittinger, Francis Crick Institute, United Kingdom
Sébastien Nisole, UMR9004 Institut de Recherche en Infectiologie de Montpellier (IRIM), France

***Correspondence:**
Wei Zhao
wzhao@sdu.edu.cn

Specialty section:
This article was submitted to Molecular Innate Immunity, a section of the journal Frontiers in Immunology

Received: *29 March 2021*
Accepted: *27 May 2021*
Published: *10 June 2021*

Citation:
Jia X, Zhao C and Zhao W (2021) Emerging Roles of MHC Class I Region-Encoded E3 Ubiquitin Ligases in Innate Immunity. Front. Immunol. 12:687102. doi: 10.3389/fimmu.2021.687102

INTRODUCTION

Innate immunity is the first line of defense against invading pathogens and cancers. A variety of germline-encoded pattern recognition receptors (PRRs) recognize conserved structures present in pathogenic microorganisms (termed as pathogen-associated molecular patterns) and danger signals (termed as damage-associated molecular patterns), in turn initiating innate immune responses. The different types of PRRs include Toll-like receptors (TLRs), retinoic acid-inducible gene-I (RIG-I)-like receptors (RLRs), and cytosolic DNA sensors [e.g., cyclic GMP-AMP synthase (cGAS)]. These PRRs transduce activation signals by recruiting cellular adaptors including myeloid differentiation factor 88, Toll/IL-1 receptor (TIR) domain-containing adapter inducing interferon (IFN)-β (TRIF), mitochondrial antiviral signaling protein (MAVS), and stimulator of interferon genes (STING). These activation signals then activate the transcription factors nuclear factor kappa-B (NF-κB) and interferon regulatory factor 3 (IRF3), leading to the expression of proinflammatory cytokines and type I IFNs (1–3).

Optimal activation of innate immunity is crucial for the elimination of invading pathogens and mutant cells, as well as for the maintenance of immune homeostasis. A magnitude of sophisticated strategies have been developed by our body to manipulate the intensity of innate immune response, including epigenetic regulation and post-translational modifications (PTMs) of key immune signaling adaptors (4). Ubiquitination is an important PTM that is dynamically controlled by multiple E3 ubiquitin ligases and deubiquitinases, and it has been implicated in innate immune

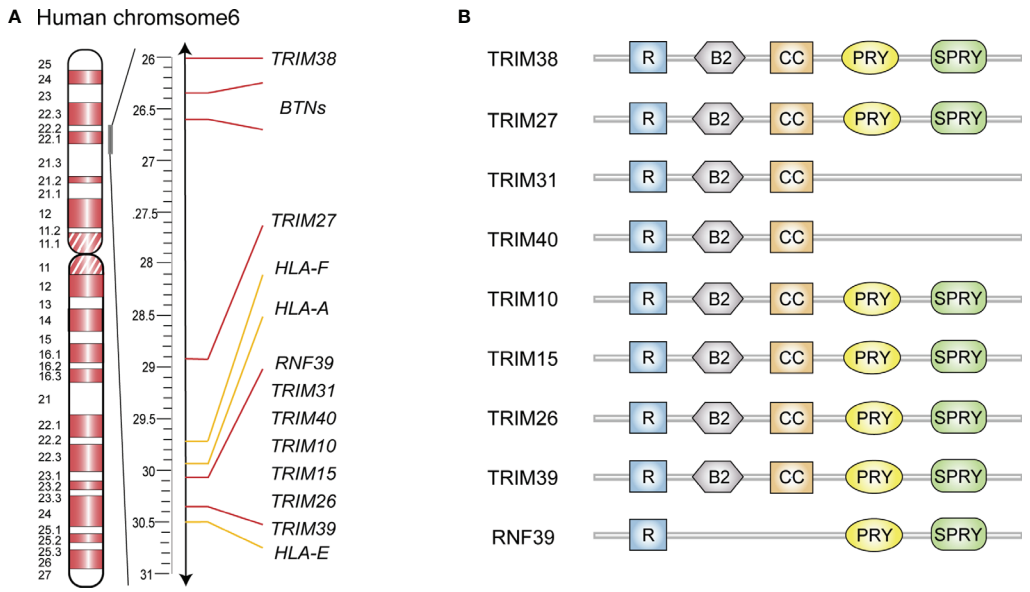

FIGURE 1 | Schematic representation of gene clusters and structure domain of MHC-I region encoded E3 ubiquitin ligases. **(A)** Gene cluster of human MHC-I region. **(B)** Schematic diagram of structure domain of MHC-I region encoded E3 ubiquitin ligases. R, RING finger; B, B-box; CC, coiled-coil.

response (5). Recently, a series of E3 ubiquitin ligases encoded within the MHC-I region (**Figure 1**) have been reported as important regulators of innate immunity. In this review, we will introduce the MHC-I region genes encoded E3 ubiquitin ligases, highlight their regulatory roles in innate immunity and potential functions in infection, inflammatory and autoimmune diseases.

CLUSTER OF E3 UBIQUITIN LIGASES GENES IN THE MHC-I REGION

MHC-I region contains a large number of immune-related genes, which are often polymorphic and closely linked as a result of their genomic proximity (6). In addition, many of these genes are associated with infections and autoimmune diseases, such as rheumatoid arthritis (RA) and systemic lupus erythematosus (SLE) (6). The human MHC-I genomic region locates on chromosome 6p21.33-6p22.2, known as human leukocyte antigen (HLA) class I region which contains HLA gene loci and several non-HLA gene clusters (7). Several E3 ubiquitin ligase genes in this region are organized in a tight cluster from HLA-E to HLA-A (**Figure 1A**), and they comprise six TRIM family members (including *TRIM10, TRIM15, TRIM26, TRIM31, TRIM39* and *TRIM40*) as well as *RNF39* (8). Two additional TRIM genes (namely *TRIM27* and *TRIM38*) are found telomeric from this cluster and near to the butyrophilin genes (8). In the mouse genome, *Trim10, Trim15, Trim26, Trim31, Trim39, Trim40* and *Rnf39* are located on chromosome 17 in the B1 region within the histocompatibility(H)2-I genetic group, while *Trim27* and *Trim38*, are located on chromosome 13 in the A3.1 region.

STRUCTURE OF MHC-I REGION-ENCODED E3 UBIQUITIN LIGASES

Most MHC-I region encoded E3 ubiquitin ligases are members of the TRIM protein family and possess RING finger, B-box 2, and coiled-coil (CC) domain (**Figure 1B**) (9, 10). The N-terminal RING finger domain confers the E3 ubiquitin ligase activity, which is essential for TRIMs to exert their antiviral effects and regulate innate immune signaling pathways (11). Specifically, the RING domain functions by recognizing E2 ubiquitin-conjugating enzymes *via* zinc finger motifs, subsequently transferring the ubiquitins or ubiquitin-like proteins to their substrates (11). The second signature sequence of MHC-I region encoded TRIM proteins is the B-box 2 domain, which also exhibits zinc-finger motifs similar to RING domain. Currently, the unified function of B-box 2 remains unclear, but there is evidence that it can potentiate the ability of TRIM5α to mediate human immunodeficiency virus 1 (HIV-1) restriction; lead to higher-order self-assembly of TRIM5α; and offer an E2 binding site resembling RING, which endows E3 ligase activity in some TRIMs lacking a RING domain (12–14). Following the B-box 2 domain is the CC domain, a typical hyper-secondary structure that can assemble with other CC structures to mediate homo- or hetero- oligomeric interactions among TRIM proteins (15). This oligomerization promotes the generation of high-molecular-mass complexes that are compartmentalized either in distinct cellular compartments such as nuclear bodies (PML/TRIM19) or microtubules (MID1/TRIM18) (16). In addition, structural analyses of several TRIM CC dimers have indicated that they are formed by antiparallel dimeric architecture, which places the RING and B-box domains on opposite sides of the CC domain.

This architecture permits the dimerization of RING domains in some cases, endowing E3 ligase activity to some TRIM proteins (15). Furthermore, TRIM10, TRIM15, TRIM26, TRIM27, TRIM38, TRIM39 and RNF39 share a C-terminal PRY-SPRY domain (**Figure 1B**) that binds with high specificity to a diverse set of substrates, including peptides and proteins, and even RNA molecules (17, 18).

EMERGING ROLES OF MHC-I REGION ENCODED E3 UBIQUITIN LIGASES IN INNATE IMMUNITY

Increasing evidences indicate that the MHC-I region encoded E3 ubiquitin ligase genes possess moderate levels of polymorphism, play regulatory roles in innate immune responses (**Figure 2**), and their expressions are associated with a variety of autoimmune diseases (8).

TRIM38

TRIM38 may be involved in the development of various autoimmune diseases and generally in the innate immune response. In one study, the presence of autoantibodies to TRIM38 significantly correlated with disease severity in patients with primary Sjögren's syndrome (SS, a disease in which circulating autoantibodies react with multiple cellular proteins to cause glandular dysfunction) (19). Similarly, in patients with dermatomyositis (DM, an autoimmune connective tissue disease characterized by erythema in the eyes and hands, and weakness in the proximal muscles), skin and muscle biopsy analyses showed that *TRIM38* gene expression was upregulated (20). In fact, TRIM38 is an intriguing regulator of innate immunity (21). As a negative regulator, TRIM38 mediates lysine 48 (K48)-linked polyubiquitination of TNF receptor associated factor 6, TRIF and NF-κB-activating kinase-associated protein 1 to promote their proteasomal degradation, resulting in the inhibition of TLR and RLR pathways (22–24). In addition, TRIM38 facilitates the

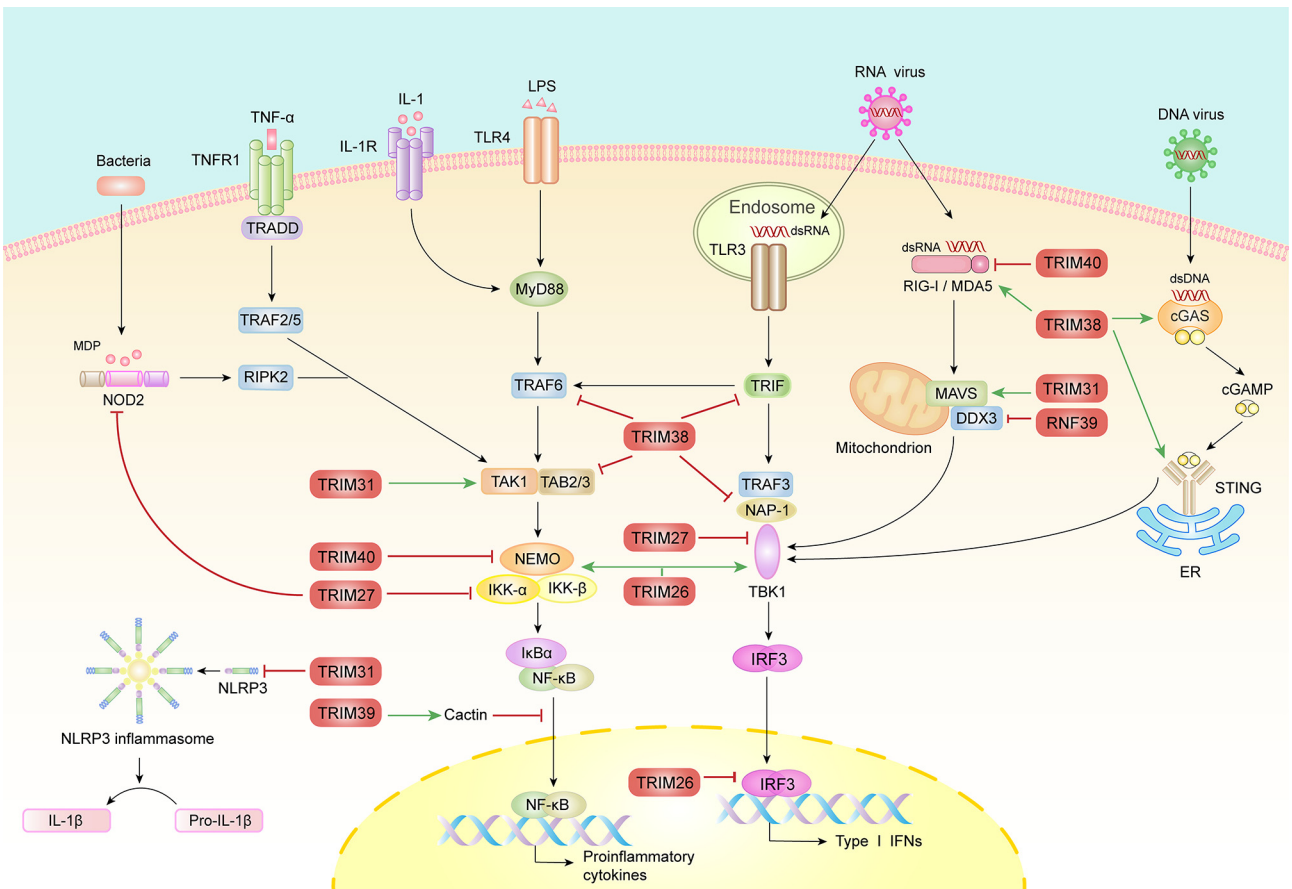

FIGURE 2 | The roles of MHC-I region encoded E3 ubiquitin ligases in innate immunity. Multiple PRRs including TLRs, RLRs, NLRs and DNA sensors detect the invasion of pathogen and trigger downstream complex signaling pathways that culminate in the activation of transcription factor, IRF3 and NF-κB, resulting in the induction of type I IFNs and proinflammatory factors. Conversely, inflammatory cytokines, such as TNFα and IL-1β further active NF-κB signaling pathway. During these processes, E3 ubiquitin ligases catalyze diverse molecules including polyubiquitin, SUMO and Nedd8 to adaptors to ensure optimal activation or timely turned-off of signals. This figure has displayed the positive (green arrows) and negative (red lines) function of the MHC-I region encoded E3 ubiquitin ligases in PRR-mediated innate immune signaling pathways.

lysosome-dependent degradation of TAK1-binding protein 2 (TAB2) in TNF- and IL-1β-triggered signaling, independent of its E3 ubiquitin ligase activity; however, the specific mechanism remains to be explored (25). Notably, the interaction between TRIM38 and TAB2/3 is weakened in RA, resulting in an excess expression of TAB2/3 and proinflammatory cytokines, indicating the essential roles of TRIM38 in modulating autoimmune disease severity (26).

Besides its E3 ubiquitin ligase activity, TRIM38 has also been identified as an E3 small ubiquitin-like modifier (SUMO) ligase and mediates the SUMOylation of RIG-I and MDA5 (27). First, TRIM38 catalyzes the SUMOylation of RIG-I and MDA5, subsequently inhibiting K48-linked ubiquitination and degradation through steric hindrance both in rest and infection states (27). Second, this SUMOylation of RIG-I and MDA5 at K96/K889 and K43/K865 mediated by TRIM38 facilitates PP1-mediated dephosphorylation and K63-linked polyubiquitination of RIG-I/MDA5, leading to RLRs activation (27). Third, the SUMOylation of RIG-I/MDA5 impaired and the K48-linked ubiquitination increased in the late phase of viral infection, restricting both the intensity and duration of RLRs activation (27). This may also explain why in a different study, Enterovirus 71, another RNA virus, escaped immune surveillance through promoting degradation of TRIM38 (28). In DNA-sensing signaling pathways, TRIM38 also regulates the activation and expression of both cGAS and STING by mediating their SUMOylation by different mechanisms (29). Thus, TRIM38 may be the key in establishing an efficient antiviral state in the early phase of viral infection, while also terminating the activation of RLRs and cGAS/STING in the late phase. These results indicate that TRIM38 is a multifunctional molecule in innate immunity, and even affects the same pathway through different mechanisms (such as RLRs).

TRIM27

TRIM27, also known as RET finger protein, plays important regulatory roles in innate immune responses; its dysregulation may cause several inflammatory diseases. TRIM27 binds to NOD2 *via* its PRY-SPRY domain, subsequently promoting K48-linked polyubiquitination and degradation of NOD2 and leading to the inhibition of NF-κB signal (30). An immunohistological inspection indicated that when compared to healthy tissue, *TRIM27* expression appeared higher in tissue derived from patients with Crohn disease (CD), implying that *TRIM27* has a role in CD, which is a known NOD2-related inflammatory disease (30). Additionally, in a model of hepatic ischemia-reperfusion injury (IRI, which initiates from oxidative stress and inflammation caused by insufficient blood supply and subsequent reperfusion owing to trauma, resection or transplantation of the liver), TRIM27 alleviated liver damage and inflammation by suppressing the recruitment of TAK1 *via* TAB2/3 degradation (31). Moreover, TRIM27 interacts with multiple IKKs, including IKKα, IKKβ, IKKε and TBK1, to attenuate both NF-κB and IRF triggered IFN-β expression (32). Furthermore, TRIM27 promotes IL-6-induced STAT3 activation by mediating ubiquitination of protein inhibitor of activated STAT3, thereby aggravating psoriasis (a chronic inflammatory disease that predominantly affects the skin and joints), colitis, and colitis-associated cancer (33, 34). In addition, it has been reported that TRIM27 is a host restriction factor that suppresses the survival of *Mycobacterium tuberculosis* in macrophages by upregulating the NF-κB and JNK/p38 pathways (35). Another study showed that TRIM27 could serve as a potential biomarker for discriminating active tuberculosis from latent tuberculosis infection and healthy people (36).

Recently, TRIM27 was reported to promote K48-linked ubiquitination at Lys251/372 and protein degradation of TBK1 during Vesicular stomatitis virus (VSV) infection (37). Furthermore, TRIM27 facilitates hepatitis C virus (HCV) replication through inhibiting IRF3 and NF-κB pathway (38). However, TRIM27 possesses contrary roles in Herpes simplex virus type 1 (HSV-1), HIV-1 and N-tropic murine leukemia virus (N-MLV)-infected cells; the contrary effects of TRIM27 may be related to varying effects of TRIM27 upon the lifecycles of different viruses (39, 40). While TRIM27 may regulate different innate immune pathways to control a type I IFN response during RNA virus and DNA virus infection, its effect during retrovirus infection may depend on direct interaction with viral components. Moreover, considering its vital role in regulating host antiviral immune responses, TRIM27 turn out to be the evasion target of HSV-1. The ICP0 protein of HSV-1, which has its own RING domain and E3 ubiquitin ligase activity, has been shown to interact with TRIM27 to promote its polyubiquitination and degradation (41). These contradictory results suggest complex roles of TRIM27 in innate immunity.

TRIM31

Single nucleotide polymorphisms (SNPs) of *TRIM31*, also called hemochromatosis candidate gene I, are associated with a variety of inflammatory diseases including inflammatory bowel disease (IBD, a chronic nonspecific inflammatory disease characterized by recurrent inflammation of the intestinal mucosa, comprising two main distinctive entities, ulcerative colitis and CD) and irritant contact dermatitis (ICD, a kind of skin inflammatory reaction after contact with exogenous irritants) (42, 43). Additionally, TRIM31 expression correlates with reduced risk of nasopharyngeal carcinoma associated with Epstein–Barr virus infection (44). These evidences suggest the potential roles of TRIM31 in antiviral immune responses and autoimmune disorders. A confirmatory study identified that TRIM31 suppressed NLR family pyrin domain containing 3 (NLRP3) inflammasome activation by promoting K48-linked ubiquitination and proteasomal degradation of NLRP3 (45). The study also showed that *Trim31* deficiency aggravates alum-induced peritonitis and attenuates the severity of DSS-induced colitis (45). Furthermore, TRIM31 reduces the risk of other NLRP3 inflammasome-associated diseases such as apical periodontitis (AP, an acute suppurative inflammation caused by endodontic microbial infections) and age-related macular degeneration (AMD, a major cause of blindness in the elderly in developed countries, induced by dysfunction of retinal pigment epithelial cells, which constitute the immune defense barrier of the macula) (46, 47). In addition, TRIM31 is involved

in the development of sepsis and colorectal cancer through regulating the NF-κB signaling pathway (48, 49).

In addition to its role in inflammation, TRIM31 has been shown to modify multiple MAVS sites with K63-linked polyubiquitin, leading to its aggregation and thus the enhancement of IFN-I expression upon RNA virus infection (50). The PB1-F2 protein of avian influenza A (H7N9) virus, scaffold protein FAF1 and Rho family small guanosine triphosphatase Rac1 limit the interaction between MAVS and TRIM31, resulting in the inhibition of MAVS ubiquitination, aggregation, and activation (51–53). TRIM31 also triggers ubiquitination and degradation of the hepatitis B virus (HBV) component HBx and therefore plays a potential role in IFN-resistant HBV infection (54). Furthermore, while TRIM31 can inhibit HIV-1 entry, downregulation of endogenously expressed *TRIM 31* inhibits both HIV-1 and MLV release, suggesting that TRIM31 plays different roles at early and late stages of the retroviral lifecycle (40). Overall, these findings provide the possibility of TRIM31 as a potential antiviral drug target.

TRIM40

Genome-wide association studies show strong association between genetic variants of *TRIM40* and common diseases. For example, one of *TRIM40* SNPs, *rs757262*, can balance the risk of developing different autoimmune diseases (55). Accordingly, several functional studies indicate that TRIM40 is a regulator of innate immunity. TRIM40 physically combines with Nedd8 to promote the neddylation of IKKγ, thereby preventing gastrointestinal neoplasia caused by chronic inflammation; reduces inflammation and liver injury in septic mice *via* attenuating the activation of TLR4 pathway; and suppresses RLRs pathway by promoting both K27- and K48-linked polyubiquitination of RIG-I and MDA5, thus enhancing their proteasomal degradation (56–58). As RIG-I and MDA5 are associated with autoimmune diseases including Aicardi-Goutières syndrome (AGS, a severe autoimmune encephalopathy caused by aberrant activation of the IFN-I axis), Singleton–Merten syndrome(SMS, a type I interferonopathy characterized by aortic calcifications, psoriasis, glaucoma and skeletal abnormalities) and type 1 diabetes (T1D), TRIM40 may attenuate the pathogenesis of autoimmune diseases by regulating the activation of RIG-I and MDA5 (59–61).

TRIM26

TRIM26, also called RNF95 or ZNF173, exhibits polymorphisms associated with several autoimmune disorders including T1D and multiple sclerosis (MS, an autoimmune disease characterized by inflammatory demyelination of the central nervous system) and with nasopharyngeal carcinoma caused by viral disease (62–64). In antiviral immunity, TRIM26 mediates the K48-linked polyubiquitination and protein degradation of nuclear IRF3, attenuating the antiviral response (65). However, another study reported that TRIM26 actually enhanced innate immunity against RNA viruses, by recruiting NEMO to facilitate the interaction between TBK1 and MAVS (66). Furthermore, a genome-wide CRISPR-Cas9 screening identified TRIM26 as a critical HCV host factor, where it mediates K27-linked ubiquitination of HCV-encoded NS5B protein, enhances the interaction between NS5B-NS5A, and ultimately promotes HCV genome replication (67). Thus, as a key E3 ubiquitin ligase, TRIM26 plays multiple roles through catalyzing the conjugation of multiple ubiquitin chains to variety of substrates.

RNF39

Emerging evidences indicate that RNF39 is a potential immune regulator. Genetic variants of *RNF39* are associated with a variety of viral diseases and autoimmune diseases, such as the progression of HIV-1 and Behcet's disease (BD, a chronic systemic vasculitis resulting in ulcerative in the oral cavity and on the genitals, as well as inflammatory damage of the eyes) (68). The DNA methylation state of *RNF39* impacts autoimmune disorders, including MS, SLE and allergic rhinitis (AR, a delayed hypersensitivity nasal mucosa reaction to environmental allergens, caused by IgE mediated release of autacoids) and confers poor responsiveness to HBV vaccination (69–72). Furthermore, *RNF39* genetic variants are related to HIV-1 plasma viral loads, $CD4^+$ T cell count, and the clinical course of HIV-1 infection (73–75). Besides its role in DNA viruses and retrovirus infection, RNF39 has also been identified as a feedback suppressor of RNA virus-induced signaling and antiviral immunity. RNF39 mediates K48-linked polyubiquitination and proteasomal degradation of DDX3X, a scaffold vital for the formation of the MAVS-TRAF3 complex, to subsequently inhibit the RLR pathway (76). *Rnf39* deficiency enhances RLR activation and inhibits RNA viral replication (76). Further studies will identify more immune targets of RNF39, which will help to explain the regulatory roles of RNF39 in antiviral and autoimmune responses.

Other MHC-I Region Encoded E3 Ubiquitin Ligases

Several other MHC-I region-encoded E3 ubiquitin ligases have also been reported to regulate viral infection and innate immunity. SNPs in *TRIM15* show a correlation with lupus nephritis (LN, an autoimmune disease characterized by the hypersecretion of autoantibodies and deposition of immune complexes in the kidneys); this correlation varies significantly according to ethnicity (77). Furthermore, human TRIM15 interferes with the release of HIV-1 and MLV from cells (40). TRIM15 targets adaptors upstream of MAVS to potentiate RIG-I-mediated IFN-β production and suppress viral infection (78). TRIM39 stabilizes Cactin to attenuate TLR- and TNF-α-mediated RelA/p65 translocation, inhibiting the expression of IL-6 and IL-8 (79). SNP analyses indicate that the genetic variants of *TRIM39* are also associated with inflammatory diseases including psoriasis, and autoimmune diseases including BD and cutaneous lupus erythematosus (CLE, an autoimmune connective tissue disease with cutaneous lesion) (68, 80, 81). Another study found a differentially methylated site in the promoter region of TRIM39-RPP2 that was associated with IBD patients (82). Lastly, TRIM39 also regulates the type I IFN response to exert its antiviral functions (83). TRIM10 contributes to the restriction of HIV-1 entry and shows high correlation with the risk of developing MS, RA, LN, ankylosing

spondylitis (AS, a chronic autoimmune-mediated arthritis that predominantly affects the axial skeleton and peripheral joints), autoimmune thyroid disease (AITD, various conditions caused by autoantibodies attacking the thyroid, including Hashimoto's thyroiditis and Graves' disease) and T1D, although its exact functions in these conditions remain unknown (40, 77, 84). In summary, the detailed mechanisms of action of these lesser-studied MHC-I region-encoded E3 ubiquitin ligases (including TRIM10, TRIM15 and TRIM39) need to be further investigated.

CONCLUSION AND PERSPECTIVE

Many MHC-I region-encoded E3 ubiquitin ligases are highly polymorphic, participate in the regulation of inflammation and antiviral innate immunity, and play a key role in the interaction between virus and host. At present, the known mechanisms of action include ubiquitination and SUMOylation; however, more mechanisms will be elucidated with further study. Concordantly, these MHC-I region genes are related to a variety of inflammatory, viral and autoimmune diseases. Nonetheless, their exact roles in the development of these diseases remain largely unclarified. In addition, same E3 ubiquitin ligases may play contrary roles in different inflammatory diseases. So, how does the organism regulate the action of the same MHC-I region-encoded E3 ubiquitin ligase (such as TRIM26 and TRIM38) to exert multiple or even opposing activities in different pathways? Further studies with varied cell types and disease models using gene-deficient mice are required to answer these questions. Given the important role of MHC-I region-encoded E3 ubiquitin ligases in antiviral innate immunity, it is tempting to speculate that viruses have evolved immune escape mechanisms by manipulating TRIM proteins. In addition, as some viruses are known to participate in oncogenesis or cancer progression, whether these E3 ubiquitin ligases could regulate the development of virus-related cancer deserves further investigation.

In this review, we have focused on the roles of MHC-I region-encoded E3 ubiquitin ligases in controlling the intensity of innate immune responses; however, whether these MHC-I region-encoded E3 ubiquitin ligases could modulate adaptive immunity requires further investigation. Elucidating their specific functions and molecular details in immune regulation will help us to further understand the vital roles of MHC-I region genes in immunity and provide promising diagnostic and therapeutic targets for diseases characterized by aberrant activation of innate immunity.

AUTHOR CONTRIBUTIONS

XJ drafted the manuscript and figures, CZ and WZ edited the manuscript, WZ supervised and edited the figures. All authors contributed to the article and approved the submitted version.

FUNDING

This work was supported by grants from the National Natural Science Foundation of China (81622030, 31870866 and 81901609). WZ is a Newton Advanced Fellow awarded by the Academy of Medical Sciences.

REFERENCES

1. Fitzgerald KA, Kagan JC. Toll-Like Receptors and the Control of Immunity. *Cell* (2020) 180:1044–66. doi: 10.1016/j.cell.2020.02.041
2. Rehwinkel J, Gack MU. Rig-I-like Receptors: Their Regulation and Roles in RNA Sensing. *Nat Rev Immunol* (2020) 20:537–51. doi: 10.1038/s41577-020-0288-3
3. Zhang X, Bai XC, Chen ZJ. Structures and Mechanisms in the Cgas-STING Innate Immunity Pathway. *Immunity* (2020) 53:43–53. doi: 10.1016/j.immuni.2020.05.013
4. Zhang Q, Cao X. Epigenetic Remodeling in Innate Immunity and Inflammation. *Annu Rev Immunol* (2021) 39:279–311. doi: 10.1146/annurev-immunol-093019-123619
5. Liu J, Qian C, Cao X. Post-Translational Modification Control of Innate Immunity. *Immunity* (2016) 45:15–30. doi: 10.1016/j.immuni.2016.06.020
6. Al Naqbi H, Mawart A, Alshamsi J, Al Safar H, Tay GK. Major Histocompatibility Complex (MHC) Associations With Diseases in Ethnic Groups of the Arabian Peninsula. *Immunogenetics* (2021) 73:131–52. doi: 10.1007/s00251-021-01204-x
7. Ruddy DA, Kronmal GS, Lee VK, Mintier GA, Quintana L, Domingo RJr, et al. A 1.1-Mb Transcript Map of the Hereditary Hemochromatosis Locus. *Genome Res* (1997) 7:441–56. doi: 10.1101/gr.7.5.441
8. Meyer M, Gaudieri S, Rhodes DA, Trowsdale J. Cluster of TRIM Genes in the Human MHC Class I Region Sharing the B30.2 Domain. *Tissue Antigens* (2003) 61:63–71. doi: 10.1034/j.1399-0039.2003.610105.x
9. Nisole S, Stoye JP, Saïb A. TRIM Family Proteins: Retroviral Restriction and Antiviral Defence. *Nat Rev Microbiol* (2005) 3:799–808. doi: 10.1038/nrmicro1248
10. van Gent M, Sparrer K, Gack MU. Trim Proteins and Their Roles in Antiviral Host Defenses. *Annu Rev Virol* (2018) 5:385–405. doi: 10.1146/annurev-virology-092917-043323
11. Joazeiro CA, Weissman AM. RING Finger Proteins: Mediators of Ubiquitin Ligase Activity. *Cell* (2000) 102:549–52. doi: 10.1016/s0092-8674(00)00077-5
12. Diaz-Griffero F, Qin XR, Hayashi F, Kigawa T, Finzi A, Sarnak Z, et al. A B-box 2 Surface Patch Important for TRIM5alpha Self-Association, Capsid Binding Avidity, and Retrovirus Restriction. *J Virol* (2009) 83:10737–51. doi: 10.1128/JVI.01307-09
13. Wagner JM, Roganowicz MD, Skorupka K, Alam SL, Christensen D, Doss G, et al. Mechanism of B-box 2 Domain-Mediated Higher-Order Assembly of the Retroviral Restriction Factor TRIM5α. *Elife* (2016) 5:e16309. doi: 10.7554/eLife.16309
14. Bell JL, Malyukova A, Holien JK, Koach J, Parker MW, Kavallaris M, et al. TRIM16 Acts as an E3 Ubiquitin Ligase and can Heterodimerize With Other TRIM Family Members. *PloS One* (2012) 7:e37470. doi: 10.1371/journal.pone.0037470
15. Esposito D, Koliopoulos MG, Rittinger K. Structural Determinants of TRIM Protein Function. *Biochem Soc Trans* (2017) 45:183–91. doi: 10.1042/BST20160325
16. Reymond A, Meroni G, Fantozzi A, Merla G, Cairo S, Luzi L, et al. The Tripartite Motif Family Identifies Cell Compartments. *EMBO J* (2001) 20:2140–51. doi: 10.1093/emboj/20.9.2140
17. James LC, Keeble AH, Khan Z, Rhodes DA, Trowsdale J. Structural Basis for PRYSPRY-mediated Tripartite Motif (TRIM) Protein Function. *Proc Natl Acad Sci USA* (2007) 104:6200–5. doi: 10.1073/pnas.0609174104
18. Choudhury NR, Heikel G, Trubitsyna M, Kubik P, Nowak JS, Webb S, et al. RNA-Binding Activity of TRIM25 is Mediated by its PRY/SPRY Domain and

is Required for Ubiquitination. *BMC Biol* (2017) 15:105. doi: 10.1186/s12915-017-0444-9
19. Wolska N, Rybakowska P, Rasmussen A, Brown M, Montgomery C, Klopocki A, et al. Brief Report: Patients With Primary Sjögren's Syndrome Who Are Positive for Autoantibodies to Tripartite Motif-Containing Protein 38 Show Greater Disease Severity. *Arthritis Rheumatol* (2016) 68:724–9. doi: 10.1002/art.39497
20. Aljabban J, Syed S, Syed S, Rohr M, Weisleder N, McElhanon KE, et al. Investigating Genetic Drivers of Dermatomyositis Pathogenesis Using Meta-Analysis. *Heliyon* (2020) 6:e04866. doi: 10.1016/j.heliyon.2020.e04866
21. Hu MM, Shu HB. Multifaceted Roles of TRIM38 in Innate Immune and Inflammatory Responses. *Cell Mol Immunol* (2017) 14:331–8. doi: 10.1038/cmi.2016.66
22. Xue Q, Zhou Z, Lei X, Liu X, He B, Wang J, et al. TRIM38 Negatively Regulates TLR3-mediated Ifn-β Signaling by Targeting TRIF for Degradation. *PloS One* (2012) 7:e46825. doi: 10.1371/journal.pone.0046825
23. Zhao W, Wang L, Zhang M, Wang P, Yuan C, Qi J, et al. Tripartite Motif-Containing Protein 38 Negatively Regulates TLR3/4- and RIG-I-mediated Ifn-β Production and Antiviral Response by Targeting NAP1. *J Immunol* (2012) 188:5311–8. doi: 10.4049/jimmunol.1103506
24. Zhao W, Wang L, Zhang M, Yuan C, Gao C. E3 Ubiquitin Ligase Tripartite Motif 38 Negatively Regulates TLR-mediated Immune Responses by Proteasomal Degradation of TNF Receptor-Associated Factor 6 in Macrophages. *J Immunol* (2012) 188:2567–74. doi: 10.4049/jimmunol.1103255
25. Hu MM, Yang Q, Zhang J, Liu SM, Zhang Y, Lin H, et al. TRIM38 Inhibits Tnfα- and IL-1β-Triggered NF-κb Activation by Mediating Lysosome-Dependent Degradation of TAB2/3. *Proc Natl Acad Sci USA* (2014) 111:1509–14. doi: 10.1073/pnas.1318227111
26. Lin Y, Luo Z. NLRP6 Facilitates the Interaction Between TAB2/3 and TRIM38 in Rheumatoid Arthritis Fibroblast-Like Synoviocytes. *FEBS Lett* (2017) 591:1141–9. doi: 10.1002/1873-3468.12622
27. Hu MM, Liao CY, Yang Q, Xie XQ, Shu HB. Innate Immunity to RNA Virus is Regulated by Temporal and Reversible SUMOylation of RIG-I and MDA5. *J Exp Med* (2017) 214:973–89. doi: 10.1084/jem.20161015
28. Liu X, Lei X, Zhou Z, Sun Z, Xue Q, Wang J, et al. Enterovirus 71 Induces Degradation of TRIM38, a Potential E3 Ubiquitin Ligase. *Virol J* (2011) 8:61. doi: 10.1186/1743-422X-8-61
29. Hu MM, Yang Q, Xie XQ, Liao CY, Lin H, Liu TT, et al. Sumoylation Promotes the Stability of the DNA Sensor cGAS and the Adaptor STING to Regulate the Kinetics of Response to DNA Virus. *Immunity* (2016) 45:555–69. doi: 10.1016/j.immuni.2016.08.014
30. Zurek B, Schoultz I, Neerincx A, Napolitano LM, Birkner K, Bennek E, et al. TRIM27 Negatively Regulates NOD2 by Ubiquitination and Proteasomal Degradation. *PloS One* (2012) 7:e41255. doi: 10.1371/journal.pone.0041255
31. Chen SY, Zhang HP, Li J, Shi JH, Tang HW, Zhang Y, et al. Tripartite Motif-Containing 27 Attenuates Liver Ischemia/Reperfusion Injury by Supressing Transforming Growth Factor β-Activated Kinase 1 (TAK1) by TAK1 Binding Protein 2/3 Degradation. *Hepatology* (2020) 73:738–58. doi: 10.1002/hep.31295
32. Zha J, Han KJ, Xu LG, He W, Zhou Q, Chen D, et al. The Ret Finger Protein Inhibits Signaling Mediated by the Noncanonical and Canonical IkappaB Kinase Family Members. *J Immunol* (2006) 176:1072–80. doi: 10.4049/jimmunol.176.2.1072
33. Zhang HX, Xu ZS, Lin H, Li M, Xia T, Cui K, et al. TRIM27 Mediates STAT3 Activation At Retromer-Positive Structures to Promote Colitis and Colitis-Associated Carcinogenesis. *Nat Commun* (2018) 9:3441. doi: 10.1038/s41467-018-05796-z
34. Miao X, Xiang Y, Mao W, Chen Y, Li Q, Fan B. TRIM27 Promotes IL-6-induced Proliferation and Inflammation Factor Production by Activating STAT3 Signaling in HaCaT Cells. *Am J Physiol Cell Physiol* (2020) 318:C272–81. doi: 10.1152/ajpcell.00314.2019
35. Wang J, Teng JL, Zhao D, Ge P, Li B, Woo PC, et al. The Ubiquitin Ligase TRIM27 Functions as a Host Restriction Factor Antagonized by Mycobacterium Tuberculosis PtpA During Mycobacterial Infection. *Sci Rep* (2016) 6:34827. doi: 10.1038/srep34827
36. Chen Y, Cao S, Sun Y, Li C. Gene Expression Profiling of the TRIM Protein Family Reveals Potential Biomarkers for Indicating Tuberculosis Status. *Microb Pathog* (2018) 114:385–92. doi: 10.1016/j.micpath.2017.12.008
37. Zheng Q, Hou J, Zhou Y, Yang Y, Xie B, Cao X. Siglec1 Suppresses Antiviral Innate Immune Response by Inducing TBK1 Degradation Via the Ubiquitin Ligase TRIM27. *Cell Res* (2015) 25:1121–36. doi: 10.1038/cr.2015.108
38. Zheng F, Xu N, Zhang Y. Trim27 Promotes Hepatitis C Virus Replication by Suppressing Type I Interferon Response. *Inflammation* (2019) 42:1317–25. doi: 10.1007/s10753-019-00992-5
39. Wan W, Wang L, Chen X, Zhu S, Shang W, Xiao G, et al. A Subcellular Quantitative Proteomic Analysis of Herpes Simplex Virus Type 1-Infected HEK 293t Cells. *Molecules* (2019) 24:4215. doi: 10.3390/molecules24234215
40. Uchil PD, Quinlan BD, Chan WT, Luna JM, Mothes W. Trim E3 Ligases Interfere With Early and Late Stages of the Retroviral Life Cycle. *PloS Pathog* (2008) 4:e16. doi: 10.1371/journal.ppat.0040016
41. Conwell SE, White AE, Harper JW, Knipe DM. Identification of TRIM27 as a Novel Degradation Target of Herpes Simplex Virus 1 ICP0. *J Virol* (2015) 89:220–9. doi: 10.1128/JVI.02635-14
42. Onoufriadis A, Stone K, Katsiamides A, Amar A, Omar Y, de Lange KM, et al. Exome Sequencing and Genotyping Identify a Rare Variant in NLRP7 Gene Associated With Ulcerative Colitis. *J Crohns Colitis* (2018) 12:321–6. doi: 10.1093/ecco-jcc/jjx157
43. Yucesoy B, Talzhanov Y, Michael Barmada M, Johnson VJ, Kashon ML, Baron E, et al. Association of MHC Region SNPs With Irritant Susceptibility in Healthcare Workers. *J Immunotoxicol* (2016) 13:738–44. doi: 10.3109/1547691X.2016.1173135
44. Ning L, Ko JM, Yu VZ, Ng HY, Chan CK, Tao L, et al. Nasopharyngeal Carcinoma MHC Region Deep Sequencing Identifies HLA and Novel non-HLA TRIM31 and TRIM39 Loci. *Commun Biol* (2020) 3:759. doi: 10.1038/s42003-020-01487-y
45. Song H, Liu B, Huai W, Yu Z, Wang W, Zhao J, et al. The E3 Ubiquitin Ligase TRIM31 Attenuates NLRP3 Inflammasome Activation by Promoting Proteasomal Degradation of NLRP3. *Nat Commun* (2016) 7:13727. doi: 10.1038/ncomms13727
46. Huang P, Liu W, Chen J, Hu Y, Wang Y, Sun J, et al. TRIM31 Inhibits NLRP3 Inflammasome and Pyroptosis of Retinal Pigment Epithelial Cells Through Ubiquitination of NLRP3. *Cell Biol Int* (2020) 44:2213–19. doi: 10.1002/cbin.11429
47. Wu X, Lu M, Ding S, Zhong Q. Tripartite Motif 31 Alleviates IL-1ß Secretion Via Promoting the Ubiquitination of Pyrin Domain Domains-Containing Protein 3 in Human Periodontal Ligament Fibroblasts. *Odontology* (2020) 108:424–32. doi: 10.1007/s10266-020-00519-7
48. Yang X, Sun J, Sun F, Yao Y, Tian T, Zhou J, et al. TRIM31 Promotes Apoptosis Via TAK1-mediated Activation of NF-κb Signaling in Sepsis-Induced Myocardial Dysfunction. *Cell Cycle* (2020) 19:2685–700. doi: 10.1080/15384101.2020.1826235
49. Wang H, Yao L, Gong Y, Zhang B. TRIM31 Regulates Chronic Inflammation Via NF-κb Signal Pathway to Promote Invasion and Metastasis in Colorectal Cancer. *Am J Transl Res* (2018) 10:1247–59. doi: 10.1080/15384101.2020.1826235
50. Liu B, Zhang M, Chu H, Zhang H, Wu H, Song G, et al. The Ubiquitin E3 Ligase TRIM31 Promotes Aggregation and Activation of the Signaling Adaptor MAVS Through Lys63-linked Polyubiquitination. *Nat Immunol* (2017) 18:214–24. doi: 10.1038/ni.3641
51. Cheung PH, Lee TT, Kew C, Chen H, Yuen KY, Chan CP, et al. Virus Subtype-Specific Suppression of MAVS Aggregation and Activation by PB1-F2 Protein of Influenza A (H7N9) Virus. *PloS Pathog* (2020) 16:e1008611. doi: 10.1371/journal.ppat.1008611
52. Dai T, Wu L, Wang S, Wang J, Xie F, Zhang Z, et al. Faf1 Regulates Antiviral Immunity by Inhibiting MAVS But Is Antagonized by Phosphorylation Upon Viral Infection. *Cell Host Microbe* (2018) 24:776–90. doi: 10.1016/j.chom.2018.10.006
53. Yang S, Harding AT, Sweeney C, Miao D, Swan G, Zhou C, et al. Control of Antiviral Innate Immune Response by Protein Geranylgeranylation. *Sci Adv* (2019) 5:eaav7999. doi: 10.1126/sciadv.aav7999
54. Tan G, Yi Z, Song H, Xu F, Li F, Aliyari R, et al. Type-I-Ifn-Stimulated Gene Trim5γ Inhibits Hbv Replication by Promoting Hbx Degradation. *Cell Rep* (2019) 29:3551–63.e3. doi: 10.1016/j.celrep.2019.11.041
55. Cagliani R, Riva S, Pozzoli U, Fumagalli M, Comi GP, Bresolin N, et al. Balancing Selection is Common in the Extended MHC Region But Most Alleles With Opposite Risk Profile for Autoimmune Diseases are Neutrally Evolving. *BMC Evol Biol* (2011) 11:171. doi: 10.1186/1471-2148-11-171

56. Noguchi K, Okumura F, Takahashi N, Kataoka A, Kamiyama T, Todo S, et al. TRIM40 Promotes Neddylation of Ikkγ and is Downregulated in Gastrointestinal Cancers. *Carcinogenesis* (2011) 32:995–1004. doi: 10.1093/carcin/bgr068
57. Yang H, Meng L, Ai D, Hou N, Li H, Shuai X, et al. Acetic Acid Alleviates the Inflammatory Response and Liver Injury in Septic Mice by Increasing the Expression of TRIM40. *Exp Ther Med* (2019) 17:2789–98. doi: 10.3892/etm.2019.7274
58. Zhao C, Jia M, Song H, Yu Z, Wang W, Li Q, et al. The E3 Ubiquitin Ligase TRIM40 Attenuates Antiviral Immune Responses by Targeting MDA5 and RIG-I. *Cell Rep* (2017) 21:1613–23. doi: 10.1016/j.celrep.2017.10.020
59. Nejentsev S, Walker N, Riches D, Egholm M, Todd JA. Rare Variants of IFIH1, a Gene Implicated in Antiviral Responses, Protect Against Type 1 Diabetes. *Science* (2009) 324:387–9. doi: 10.1126/science.1167728
60. Oda H, Nakagawa K, Abe J, Awaya T, Funabiki M, Hijikata A, et al. Aicardi-Goutières Syndrome is Caused by IFIH1 Mutations. *Am J Hum Genet* (2014) 95:121–5. doi: 10.1016/j.ajhg.2014.06.007
61. Jang MA, Kim EK, Now H, Nguyen NT, Kim WJ, Yoo JY, et al. Mutations in DDX58, Which Encodes RIG-I, Cause Atypical Singleton-Merten Syndrome. *Am J Hum Genet* (2015) 96:266–74. doi: 10.1016/j.ajhg.2014.11.019
62. Nyaga DM, Vickers MH, Jefferies C, Perry JK, O'Sullivan JM. Type 1 Diabetes Mellitus-Associated Genetic Variants Contribute to Overlapping Immune Regulatory Networks. *Front Genet* (2018) 9:535. doi: 10.3389/fgene.2018.00535
63. Lyu XM, Zhu XW, Zhao M, Zuo XB, Huang ZX, Liu X, et al. A Regulatory Mutant on TRIM26 Conferring the Risk of Nasopharyngeal Carcinoma by Inducing Low Immune Response. *Cancer Med* (2018) 7:3848–61. doi: 10.1002/cam4.1537
64. Cree BA, Rioux JD, McCauley JL, Gourraud PA, Goyette P, McElroy J, et al. A Major Histocompatibility Class I Locus Contributes to Multiple Sclerosis Susceptibility Independently From HLA-DRB1*15:01. *PloS One* (2010) 5:e11296. doi: 10.1371/journal.pone.0011296
65. Wang P, Zhao W, Zhao K, Zhang L, Gao C. TRIM26 Negatively Regulates Interferon-β Production and Antiviral Response Through Polyubiquitination and Degradation of Nuclear IRF3. *PloS Pathog* (2015) 11:e1004726. doi: 10.1371/journal.ppat.1004726
66. Ran Y, Zhang J, Liu LL, Pan ZY, Nie Y, Zhang HY, et al. Autoubiquitination of TRIM26 Links TBK1 to NEMO in RLR-mediated Innate Antiviral Immune Response. *J Mol Cell Biol* (2016) 8:31–43. doi: 10.1093/jmcb/mjv068
67. Liang Y, Zhang G, Li Q, Han L, Hu X, Guo Y, et al. TRIM26 is a Critical Host Factor for HCV Replication and Contributes to Host Tropism. *Sci Adv* (2021) 7:eabd9732. doi: 10.1126/sciadv.abd9732
68. Kurata R, Nakaoka H, Tajima A, Hosomichi K, Shiina T, Meguro A, et al. TRIM39 and RNF39 are Associated With Behçet's Disease Independently of HLA-B*51 and -a*26. *Biochem Biophys Res Commun* (2010) 401:533–7. doi: 10.1016/j.bbrc.2010.09.088
69. Lu Y, Cheng Y, Yan W, Nardini C. Exploring the Molecular Causes of Hepatitis B Virus Vaccination Response: An Approach With Epigenomic and Transcriptomic Data. *BMC Med Genomics* (2014) 7:12. doi: 10.1186/1755-8794-7-12
70. Renauer P, Coit P, Jeffries MA, Merrill JT, McCune WJ, Maksimowicz-McKinnon K, et al. DNA Methylation Patterns in Naïve CD4+ T Cells Identify Epigenetic Susceptibility Loci for Malar Rash and Discoid Rash in Systemic Lupus Erythematosus. *Lupus Sci Med* (2015) 2:e000101. doi: 10.1136/lupus-2015-000101
71. Maltby VE, Lea RA, Sanders KA, White N, Benton MC, Scott RJ, et al. Differential Methylation At MHC in CD4+ T Cells is Associated With Multiple Sclerosis Independently of HLA-DRB1. *Clin Epigenet* (2017) 9:71. doi: 10.1186/s13148-017-0371-1
72. Morin A, Laviolette M, Pastinen T, Boulet LP, Laprise C. Combining Omics Data to Identify Genes Associated With Allergic Rhinitis. *Clin Epigenet* (2017) 9:3. doi: 10.1186/s13148-017-0310-1
73. Fellay J, Shianna KV, Ge D, Colombo S, Ledergerber B, Weale M, et al. A Whole-Genome Association Study of Major Determinants for Host Control of HIV-1. *Science* (2007) 317:944–7. doi: 10.1126/science.1143767
74. Fellay J, Ge D, Shianna KV, Colombo S, Ledergerber B, Cirulli ET, et al. Common Genetic Variation and the Control of HIV-1 in Humans. *PloS Genet* (2009) 5:e1000791. doi: 10.1371/journal.pgen.1000791
75. Lin YJ, Chen CY, Jeang KT, Liu X, Wang JH, Hung CH, et al. Ring Finger Protein 39 Genetic Variants Associate With HIV-1 Plasma Viral Loads and its Replication in Cell Culture. *Cell Biosci* (2014) 4:40. doi: 10.1186/2045-3701-4-40
76. Wang W, Jia M, Zhao C, Yu Z, Song H, Qin Y, et al. RNF39 Mediates K48-linked Ubiquitination of DDX3X and Inhibits RLR-dependent Antiviral Immunity. *Sci Adv* (2021) 77:eabe5877. doi: 10.1126/sciadv.abe5877
77. Lanata CM, Nititham J, Taylor KE, Chung SA, Torgerson DG, Seldin MF, et al. Genetic Contributions to Lupus Nephritis in a Multi-Ethnic Cohort of Systemic Lupus Erythematous Patients. *PloS One* (2018) 13:e0199003. doi: 10.1371/journal.pone.0199003
78. Uchil PD, Hinz A, Siegel S, Coenen-Stass A, Pertel T, Luban J, et al. TRIM Protein-Mediated Regulation of Inflammatory and Innate Immune Signaling and its Association With Antiretroviral Activity. *J Virol* (2013) 87:257–72. doi: 10.1128/JVI.01804-12
79. Suzuki M, Watanabe M, Nakamaru Y, Takagi D, Takahashi H, Fukuda S, et al. TRIM39 Negatively Regulates the Nfκb-Mediated Signaling Pathway Through Stabilization of Cactin. *Cell Mol Life Sci* (2016) 73:1085–101. doi: 10.1007/s00018-015-2040-x
80. Kisiel B, Kisiel K, Szymański K, Mackiewicz W, Biało-Wójcicka E, Uczniak S, et al. The Association Between 38 Previously Reported Polymorphisms and Psoriasis in a Polish Population: High Predicative Accuracy of a Genetic Risk Score Combining 16 Loci. *PloS One* (2017) 12:e0179348. doi: 10.1371/journal.pone.0179348
81. Kunz M, König IR, Schillert A, Kruppa J, Ziegler A, Grallert H, et al. Genome-Wide Association Study Identifies New Susceptibility Loci for Cutaneous Lupus Erythematosus. *Exp Dermatol* (2015) 24:510–5. doi: 10.1111/exd.12708
82. McDermott E, Ryan EJ, Tosetto M, Gibson D, Burrage J, Keegan D, et al. Dna Methylation Profiling in Inflammatory Bowel Disease Provides New Insights Into Disease Pathogenesis. *J Crohns Colitis* (2016) 10:77–86. doi: 10.1093/ecco-jcc/jjv176
83. Kurata R, Tajima A, Yonezawa T, Inoko H. TRIM39R, But Not TRIM39B, Regulates Type I Interferon Response. *Biochem Biophys Res Commun* (2013) 436:90–5. doi: 10.1016/j.bbrc.2013.05.064
84. Sirota M, Schaub MA, Batzoglou S, Robinson WH, Butte AJ. Autoimmune Disease Classification by Inverse Association With SNP Alleles. *PloS Genet* (2009) 5:e1000792. doi: 10.1371/journal.pgen.1000792

Conflict of Interest: The authors declare that the research was conducted in the absence of any commercial or financial relationships that could be construed as a potential conflict of interest.

frontiers in Immunology

ORIGINAL RESEARCH
published: 02 August 2021
doi: 10.3389/fimmu.2021.698697

Phosphorylation of Shrimp Tcf by a Viral Protein Kinase WSV083 Suppresses Its Antiviral Effect

Chuanqi Wang[1,2], *Lingwei Ruan*[1]*, *Hong Shi*[1], *Wenyang Lin*[1,2], *Linmin Liu*[1] *and Sujie Li*[1]

[1] State Key Laboratory Breeding Base of Marine Genetic Resources, Key Laboratory of Marine Genetic Resources of Ministry of Natural Resources, Third Institute of Oceanography, Ministry of Natural Resources, Fujian Key Laboratory of Marine Genetic Resources, Xiamen, China, [2] School of Life Science, Xiamen University, Xiamen, China

Nuclear DNA-binding TCF proteins, which act as the main downstream effectors of Wnt signaling, are essential for the regulation of cell fate and innate immunity. However, their role during viral infection in shrimp remains unknown. Herein, we demonstrated that *Litopenaeus vannamei* TCF (LvTcf) acts independently of Lvβ-catenin to promote interferon-like protein LvVago1 production, thus mounting the response to WSSV infection. Further, we observed that WSV083, a WSSV serine/threonine protein kinase, bound to LvTcf and phosphorylated it. Phosphorylated LvTcf was then recognized and degraded *via* the ubiquitin-proteasome pathway. Moreover, mass spectrometry analyses indicated that the T39 and T104 residues of LvTcf were target sites phosphorylated by WSV083. Point mutation analyses suggested that additional sites of LvTcf may undergo phosphorylation *via* WSV083. Taken together, the current work provides valuable insights into host immunity and viral pathogenesis. LvTcf is not only a modulator of shrimp innate immunity but is also an important target for WSSV immune evasion. Thus, the current findings will help improve disease control in shrimps.

Keywords: Wnt signaling pathway, LvTcf, LvVago1, WSV083, phosphorylation, ubiquitin-proteasome pathway

OPEN ACCESS

Edited by:
Soham Gupta,
Karolinska Institutet (KI), Sweden

Reviewed by:
Shihao Li,
Institute of Oceanology (CAS), China
Kenneth Michael Cadigan,
University of Michigan, United States

***Correspondence:**
Lingwei Ruan
ruanlingwei@tio.org.cn

Specialty section:
This article was submitted to Viral Immunology, a section of the journal Frontiers in Immunology

Received: *22 April 2021*
Accepted: *21 July 2021*
Published: *02 August 2021*

Citation:
Wang C, Ruan L, Shi H, Lin W, Liu L and Li S (2021) Phosphorylation of Shrimp Tcf by a Viral Protein Kinase WSV083 Suppresses Its Antiviral Effect. Front. Immunol. 12:698697. doi: 10.3389/fimmu.2021.698697

INTRODUCTION

White spot syndrome virus (WSSV) is the only species within the Whispovirus genus of the *Nimaviridae* family (1–3). It is a large double-stranded circular DNA virus with a genome of approximately 300 kb containing 181 open reading frames (ORFs). This virus is a major crustacean pathogen, causing a cumulative mortality of up to 100% in cultured shrimp (4, 5). Due to the current lack of effective treatment, understanding the mechanisms of host immunity and host-virus interactions is of great importance for improving WSSV control.

WSSV triggers pattern recognition upon cell entry as the initial step of the innate immune response (6). Shrimp mount humoral and cellular immune responses (7) to defend against viral infection. These rely on several key cell signaling cascades, including the Toll/IMD-NF-κB and JAK/STAT pathways, among others, which transduce extracellular signals into cells and promote the expression of antimicrobial peptides or other immune effector molecules to combat WSSV infection (8–10). In its shrimp host, WSSV employs a number of mechanisms to ensure propagation. To this end, the virus hijacks host proteins to facilitate gene transcription. Shrimp NF-κB and STAT were

reported to bind the promoter of the WSSV immediate early gene *ie1*, promoting its expression (11–13). Viral transcription factor IE1 then drives host JNK autophosphorylation to activate c-Jun and stimulate *ie1*, *wsv056*, *wsv249*, as well as *wsv403* expression (14). Through the cell cycle, IE1 and WSV056 competitively interact with Rb to promote the transition from G0/G1 to S phase, providing a favorable environment for viral replication (15). In addition, WSSV employs several strategies to evade host immunity. For example, viral microRNA WSSV-miR-22 restricts host STAT expression by targeting its 3′UTR, which allows for subverting the JAK/STAT-driven antiviral response (16). WSSV can also manipulate metabolic programming to induce the Warburg effect, counteracting reactive oxygen species (17–19). Moreover, WSSV regulates the degradation of host proteins *via* ubiquitination-related enzymes encoded by *wsv222*, *wsv249*, and *wsv403*, facilitating viral replication and proliferation (20–24).

Within research on the relationship between host signaling and viral infection, the Wnt pathway has attracted increasing attention. It is evolutionarily conserved in metazoan animals, regulating cell fate during embryonic development as well as in adult tissues (25–27). In addition, Wnt/β-catenin/TCF signaling participates in immune regulation. In particular, TCF-1 initiates TFH differentiation, thus promoting the B cell-mediated response to acute viral infections (28). With regard to innate immunity, β-catenin/TCF promotes the expression of type I IFN and interferon-stimulated genes to suppress viral infection (29–32). In Drosophila, the Dally-mediated Wnt signaling pathway is involved in S2 phagocytosis of WSSV (33). Our previous work showed that the expression of LvWnt5b was initially suppressed in shrimp as a proapoptotic response against WSSV infection. Moreover, Lvβ-catenin tends to translocate to the nucleus following WSSV infection where it activates the expression of several antimicrobial peptides (34, 35). However, how WSSV regulates the Wnt signaling pathway in shrimp remains unclear. Therefore, further research is necessary in order to determine the relationship between shrimp Wnt signaling and WSSV infection.

Nuclear DNA-binding TCF/LEF proteins from the high-mobility group (HMG) box family are the main downstream effectors of the Wnt pathway. In humans, the TCF/LEF family consists of four members designated TCF7, LEF1, TCF7L1, and TCF7L2 (also known as TCF1, LEF1, TCF3, and TCF4, respectively) (36). The majority of TCF isoforms possess a conserved β-catenin-binding domain at the N-terminus and a monomeric HMG domain that recognizes the Wnt response element (5'-ACATCAAAG-3') to mediate DNA binding (37–39). Importantly, isoforms exhibit different functional properties. In this study, we found that shrimp TCF, referred to as LvTcf, plays a protective role against WSSV infection by promoting the production of shrimp interferon-like protein LvVago1 in an Lvβ-catenin-independent manner. Furthermore, we uncovered a new mechanism through which WSSV regulates the Wnt signaling pathway. WSV083, a serine/threonine protein kinase encoded by WSSV (40), was found to bind and phosphorylate LvTcf. Phosphorylated LvTcf was then degraded *via* the ubiquitin-proteasome pathway. Thus, WSV083 suppressed the antiviral effect mediated by LvTcf. The current findings highlight novel therapeutic targets for WSSV control.

MATERIALS AND METHODS

Shrimp and Virus

L.vannamei, about 15-20 g, were purchased from a market in Xiamen, China, and kept in air-pumped circulating seawater for 3 days before experiments. WSSV particles (a Chinese isolated) were extracted from hemocytes of infected crayfish *Procambarus clarkii* and quantified according to Yang's description (41, 42).

Cell Lines, Reagents and Antibodies

High Five cells were cultured in Express Five SFM (Gibco, USA; Cat. No. 10486025) with 10% L-Glutamine (Gibco, USA; Cat. No. 25030081). S2 cells were maintained in complete Schneider's Drosophila Medium. Complete Schneider's Drosophila Medium was prepared as follows: Schneider's Drosophila Medium (Gibco, USA; Cat. No. R69007) was supplemented with 10% fetal bovine serum (Gibco, USA; Cat. No. 16140071) and 1% Penicillin-Streptomycin (Gibco, USA; Cat. No. 15070063). Sf9 cells were cultured in Sf-900 III SFM (Gibco, USA; Cat. No. 10902104) with 10% fetal bovine serum and 1% Penicillin-Streptomycin. MG132 (Merck, USA; Cat. No. 474790) were used for treating cells. Calf intestinal alkaline phosphatase (CIAP, Thermo Fisher Scientific, USA; Cat. No. 18009-019) were used for dephosphorylation assay *in vitro*. Protein A-coupled Sepharose (GE Healthcare, USA; Cat. No. 17-5280-04) was used for antibody purification and immunoprecipitation. Primary Antibodies used in this study were anti-flag (Sigma, USA; Cat. No. F3165; Abcam, USA; Cat. No. ab205606), anti-V5 (Thermo Fisher Scientific, USA; Cat. No. R961-25), anti-myc (Cell Signaling Technology, USA; Cat. No. 2276S), anti-α-tubulin (Sigma, USA; Cat. No. T5168). Anti-c-myc Agarose Affinity Gel (Sigma, USA; Cat. No. A7470) and Anti-FLAG M2 Affinity Gel (Sigma, USA; Cat. No. A2220) were used for immunoprecipitation or protein purification. Secondary antibodies used in this work including Goat anti-Mouse IgG antibody (Thermo Fisher Scientific, USA; Cat. No. 31430), Goat anti-Rabbit IgG antibody (Life technologies, USA, Cat. No. A16110), FITC goat anti-mouse antibody (Life technologies, USA, Cat. No. A11029) and Rhodamine Red^{TM}-X goat anti-rabbit antibody (Life technologies, USA, Cat. No. R6394).

RNA Extraction, cDNA Synthesis and Genomic DNA Extraction

Total RNA was extracted with TRIzol reagent (Molecular Research Center, Inc, USA; Cat. No. TR118) according to the manufacturer's instruction. Total RNA was treated with DNaseI(Takara, Japan; Cat. No. 2270A) at 37°C for 0.5 h to remove residual genomic DNA. The first-strand cDNA was synthesized by reverse transcriptase M-MLV (Takara, Japan; Cat. No. 2641A) with Oligo(dT)$_{18}$ primer (Thermo Fisher Scientific, USA; Cat. No. SO131). TIANGEN Marine Animal DNA Kit (TIANGEN, Beijing, China; Cat. No. GD3311-02) was used to extract the shrimp genomic DNA according to the manufacturer's instructions.

WSSV Challenge

Each batch of 40 healthy shrimps was injected with 1×10^5 WSSV virions diluted in 100 μl PBS (140 mM NaCl, 3 mM KCl, 8 mM Na_2HPO_4, 1.5 mM KH_2PO_4, pH 7.4). Shrimps injected with 100 μl PBS were set as negative control. Samples of four individuals collected at different time points post injection (0, 6, 12, 24, 48 h) were used for analysis by qRT-PCR.

RNAi Assay

We used RNAi to knock down the expression of LvTcf in order to explore its role in shrimp innate immunity. DsLvTcf and dsEGFP (control) were synthesized using the T7 RiboMAX Express RNAi System (Promega, USA; Cat. No. P1700), according to the manufacturer's instructions. dsRNA was diluted in PBS, and 100 μL of PBS containing 20 μg dsRNA was injected into shrimps twice after 24 h. Another 12 h later, shrimp of the two groups were injected with 1×10^5 WSSV virions. Shrimp hemocytes (n = 8) were collected at 48 h post-infection (hpi). The transcriptional levels of *LvTcf* and the number of WSSV copies were then analyzed. siRNA was used to reduce the expression of endogenous β-catenin in S2 cells. SiDmβ-catenin was synthesized by GenePharma based on the following sequences: (5′-3′) GCUUGCAAAUUCUGGCCUAT and UAGGCCAGAAUUUGCAAGCTT.

qRT-PCR

qRT-PCR was performed using TB Green Premix Ex Taq (Cat. No. RR820) in a Rotor-Gene™ 6000 (Corbett Life Science) with the following program: 1 cycle of pre-denaturation for 1 min at 95°C, followed by 40 cycles of 95°C for 10 s, 56°C for 15 s, and 72°C for 15 s. Primers are listed in **Table S1**. We used *LvEF-1α* (GenBank accession No. GU136229) as an internal control, and each sample was analyzed in triplicate. Relative expression was determined *via* the $2^{-\Delta\Delta Ct}$ method. Statistical significance was set at $p<0.05$.

Absolute q-PCR

We performed absolute q-PCR to monitor viral loads in shrimp. Briefly, we collected gills from shrimp at 48 hpi (n = 8 in the *LvTcf* knockdown experiment). Gill genomic DNA was extracted as described above. Primers for WSSV genomic DNA-F and WSSV genomic DNA-R (**Table S1**) were used to measure WSSV genomic copies *via* absolute q-PCR according to a previously described method (43). The WSSV copy number in 1 μg of shrimp genomic DNA was then calculated.

Plasmid Construction

GST protein was expressed *via* the pGEX-4T-2 vector (stored in our laboratory). The ORF of WSV083 was cloned into pGEX-4T-2 to express the WSV083-GST fusion protein. The ORFs of LvTcf and Lvβ-catenin were cloned into the pIEx-4 vector (Novagen), with a c-Myc tag or FLAG tag fused to the N-terminus. The LvTcf catenin-binding domain deletion mutant (LvTcf57-556) was inserted into pIEx-4 with a c-Myc tag fused to the N-terminus. EGFP with a c-Myc, V5, or FLAG tag fused to the N-terminus was cloned into pIEx-4 vector at the same time. The ORFs of WSV056, WSV069 (IE1), WSV079, WSV100, WSV249, WSV403, wild-type (WT) WSV083, kinase domain deletion mutant WSV083DM, and kinase domain point mutant D459A WSV083PM were introduced into a pIEx-4 vector with a V5 tag fused to the N-terminus. FLAG-tagged ubiquitin was cloned into the pIEx-4 vector. The point mutations of LvTcf, including LvTcf2MuA (T39AT104A), LvTcf4MuA (T39AT10 4AT311AS315A), and LvTcf5MuA (T39AT104AT311AS315AS 356A) were introduced into the wild-type LvTcf expression plasmid using the Mut Express® II Fast Mutagenesis Kit V2 (Vazyme, Nanjing, China; Cat. No. C214). The promoters of LvVago1-5 were cloned into the pGL3-Basic vector (stored in our laboratory).

Co-Immunoprecipitation (Co-IP) and Western Blotting Analyses

High Five cells were maintained in Express Five SFM medium with 10% L-glutamine. CellfectinTM II reagent (Thermo Fisher Scientific, USA; Cat. No. 10362100) was used for cell transfection according to the manufacturer's instructions. High Five cells (cultured in a six-well plate) were harvested at 48 h post-transfection and lysed in Western and IP cell lysis buffer (Beyotime, Shanghai, China; Cat. No. P0013) with the addition of 1 mM phenylmethylsulfonylfluoride (PMSF; BBI Life Sciences, China, Cat. No. A610425) and a protease inhibitor cocktail (Calbiochem, USA; Cat. No. 539134) or a phosphatase inhibitor cocktail (Roche, USA; Cat. No. 04906837001) for 30 min on ice. Ten percent of the cell lysates were used for input analysis, and the rest were immunoprecipitated with an antibody affinity gel for 4 h at 4°C. Alternatively, lysates were preincubated with protein A-coupled Sepharose (GE Healthcare, USA; Cat. No. 17-5280-04) to remove nonspecific protein binding for 1 h at 4°C. Lysates were then immunoprecipitated with Sepharose and the indicated antibodies for at least 4 h. The gel or beads were washed sequentially with lysis buffer five times and boiled in 5×SDS loading buffer (Solarbio, Beijing, China; Cat. No. P1040) for western blot analysis. The protein samples were separated on SDS-PAGE gel and transferred to a nitrocellulose blotting membrane (Millipore, USA; Cat. No. IPVH00010). The membrane was blocked in 5% (w/v) skim milk in TBST (20 mM Tris-HCl, 150 mM NaCl, 0.1% Tween 20, pH 7.6) at room temperature for 1 h. The membrane was then incubated with a primary antibody for 1 h at room temperature. A horseradish peroxidase (HRP)-conjugated secondary antibody was then incubated with the membrane for 1 h at room temperature. SuperSignalTM West Pico PLUS Chemiluminescent Substrate (Thermo Fisher Scientific, USA; Cat. No. 34578) was used for signal detection.

GST Pull-Down

A GST or GST-WSV083 expression plasmid was transformed into *Escherichia coli* BL21, and single colonies were selected on plates supplemented with ampicillin (100 μg/mL). *E. coli* were then cultured and induced with 1 mM isopropyl-B-D-thiogalactopyranoside (Thermo Fisher Scientific, USA; Cat. No. R0392) for 16 h at 16°C in LB medium during the mid-

exponential growth phase. Cells were harvested, sonicated, and protein was solubilized in PBS. Solubilized proteins were incubated with GST-Sepharose beads (GE Healthcare, USA; Cat. No. 17-5132-01) with rotation for 1 h at 4°C, collected by centrifugation, and washed five times with PBS. To determine whether the GST-WSV083 fusion protein binds to LvTcf, a pIEx-4-LvTcf-myc plasmid was transfected into High Five cells and harvested after 48 h, as mentioned above. The cell lysate was incubated with GST or GST-WSV083 fusion protein-bound beads with rotation at 4°C for 9 h, followed by five washes with PBS. Bound proteins were eluted in SDS loading buffer for Coomassie blue staining or western blotting.

Dual-Luciferase Reporter Assay

Dual-luciferase reporter assays were performed in *Drosophila* S2 cells. Briefly, S2 cells were seeded into 48-well plates and cultured at 27°C in *Schneider's Drosophila* Medium (Gibco, USA; Cat. No. R69007) supplemented with 10% fetal bovine serum (Gibco, USA; Cat. No. 16140071) and 1% Penicillin-Streptomycin (Gibco, USA; Cat. No. 15070063). Once cells grew to 60-80% confluence, transient transfection was performed. Using the FuGENE HD Transfection Reagent (Promega, USA; Cat. No. E2311), each well was transfected with 500 ng Firefly luciferase reporter plasmid (pGL3-Basic, pGL3-LvVago1-5, respectively), 500 ng of target protein expression plasmid (pIEx-LvTcf-Myc, pIEx-Lvβ-catenin-FLAG), and 5 ng pRL-OpIE2 Renilla luciferase plasmid (internal control). The transfection ratio of the three plasmids was 100:100:1. The cells were lysed 48 h after transfection, and luciferase activity was detected using the Dual-Luciferase® Reporter Assay System (Promega, USA; Cat. No. E1910) on a GloMaxTM20/20 Luminometer (Promega, USA). Relative luciferase activity was calculated by normalizing Firefly luciferase activity to Renilla luciferase activity. Western blotting was performed to confirm protein expression. All experiments were repeated at least three times.

Immunofluorescence Assay

Sf9 cells were transfected with the target plasmids and cultured for 24 h at 27°C in 35-mm dishes (Cellvis, USA; Cat. No. D35-20-1-N). The cells were washed twice with PBS, fixed with 4% paraformaldehyde at room temperature for 20 min, and were then permeabilized with 0.5% TritonX-100 (diluted in PBS) for 1 min. After washing three times, cells were blocked with 5% bovine serum albumin (diluted in TBST) for 1 h, followed by incubation for 1.5 h at room temperature or overnight (about 10 h) at 4°C with a mouse anti-myc antibody (Cell Signaling Technology, USA; Cat. No. 2276S; 1:250) and a rabbit anti-FLAG antibody (Abcam, USA; Cat. No. ab205606; 1:200) or a rabbit anti-V5 antibody (Thermo Fisher Scientific, USA; Cat. No. R961-25; 1:200). After washing with PBS four times, the cells were subsequently incubated with mixed FITC goat anti-mouse (Life technologies, USA, Cat. No. A11029; 1:500) and rhodamine goat anti-rabbit secondary antibodies (Life technologies, USA, Cat. No. R6394, 1:500) for 1 h at room temperature. The cells were washed with PBS five times before nuclei were stained with 0.5 μg/mL Hoechst (Beyotime, Nanjing, China; Cat. No. C1028) for 1 min. Finally, the cells were observed under a confocal laser-scanning microscope (Leica SP2).

Calf Intestinal Alkaline Phosphatase (CIAP) Assay

LvTcf was co-expressed with EGFP, WSV083, or its mutants in High Five cells for 48 h. A spot of the cell lysate was used as input. The remaining proteins were immunoprecipitated with an anti-myc antibody and washed with lysis buffer three times as well as with phosphatase buffer (50 mM Tris-HCl, 0.1 mM EDTA, pH 8.5) three times. The bound beads in 30 μl phosphatase buffer were treated with CIAP (Thermo Fisher Scientific, USA; Cat. No. 18009-019) at 37°C for 1 h. The reaction was stopped with SDS loading buffer, and the beads were boiled for 5 min for western blotting.

Ubiquitination Assay

Ubiquitination assays were performed in High Five cells. Expression plasmids, including ubiquitin, were co-transfected into cells. After 12 h, the cells were treated with 10 μM protease inhibitor MG132 (Merck, USA; Cat. No. 474790) for 24 h and harvested with Western and IP cell lysis buffer [20 mM Tris (pH7.5), 150 mM NaCl, 1% Triton X-100] (Beyotime, Nanjing, China; Cat. No. P0013). The supernatants were immunoprecipitated as described above. The input and immunoprecipitates were subjected to western blot analysis.

Mass Spectrum Analysis

FLAG-LvTcf samples were collected from High Five cells co-expressing WSV083WT or WSV083DM. After SDS-PAGE analysis, FLAG-LvTcf bands were recovered for mass spectrometry analysis by Novogene (Beijing, China).

RESULTS

Effects of LvTcf on WSSV Infection

We obtained full-length *LvTcf* from the *Litopenaeus vannamei* transcriptome analyzed in our laboratory (unpublished). The *LvTcf* gene was 2220 bp in length (GenBank accession No. MT241372), which included a 1671 bp ORF encoding 556-amino acid protein with a predicted molecular mass of 60.214 kDa. A catenin-binding domain, a conserved High Mobility group (HMG) domain, and a C-clamp domain were found at positions 1-56 aa, 288-358 aa, and 381-411 aa respectively (**Figures S1A, B**). Multiple sequence alignment suggested that the LvTcf HMG domain had several highly-conserved Ser/Thr/Lys phosphorylation sites (**Figure S1C**). Phylogenetic analysis revealed that LvTcf was evolutionarily associated with arthropods, including crustaceans and insects (**Figure S1D**).

To investigate the relationship between LvTcf and WSSV infection, we performed time-course analysis of LvTcf expression in hemocytes. The expression of viral gene *ie1* was used as an index of WSSV infection level, increasing gradually, which suggested successful infection (**Figure 1A**). *LvTcf* expression was significantly upregulated approximately 6-fold at 24 hpi

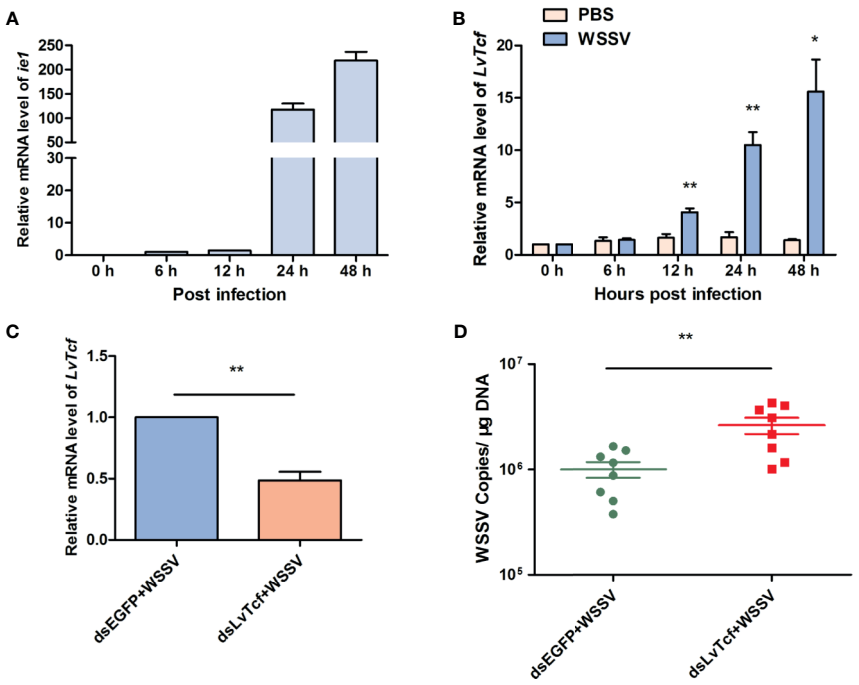

FIGURE 1 | LvTcf played a protective role against WSSV infection. **(A, B)** LvTcf expression following WSSV infection. Expression of WSSV immediately early gene *ie1* **(A)** and *LvTcf* **(B)** after WSSV challenge, as determined using qRT-PCR. Hemocytes were collected at 0, 6, 12, 24, 48 h post-WSSV injection. *LvEF-1α* was used as internal control. **(C, D)** Effects of LvTcf on WSSV infection. **(C)** The expression level of *LvTcf* after RNAi. **(D)** Silencing of *LvTcf* facilitated WSSV proliferation. DsRNA-LvTcf and dsRNA-eGFP (control group) were injected into shrimp. After 24 h, the two groups were infected with 1×10^5 WSSV virions. The number of WSSV copies in gills (n = 8) were assessed at 48 h post-infection by absolute q-PCR. *LvEF-1α* was used as internal control. All the experiments were performed in triplicate. The data were statistically analyzed *via* the student's *t*-test (*p < 0.05, ** p < 0.01).

and 11-fold at 48 hpi (**Figure 1B**). These results indicated that WSSV infection positively regulated *LvTcf* expression. Further, we employed RNAi to knock down the expression of LvTcf in order to investigate its role during WSSV infection. Healthy shrimps were injected with dsLvTcf or dsEGFP (as control). Both groups were subsequently challenged with WSSV. 48 h after the injection of shrimp with WSSV, gill *LvTcf* was suppressed at the mRNA level compared to the control group (**Figure 1C**). The number WSSV copies in gills increased after LvTcf silencing (**Figure 1D**). Taken together, these results suggested that LvTcf plays a protective role against WSSV infection.

LvTcf Promotes the Production of LvVago1 Independently of Lvβ-Catenin

β-catenin and TCF usually form a complex in order to activate gene expression (37, 44, 45). As we predicted that the β-catenin-binding domain is located in the N-terminus of LvTcf, we sought to determine whether Lvβ-catenin could bind to LvTcf. Co-IP experiments indicated that Lvβ-catenin interacted with LvTcf in High Five cells (**Figures 2A, B**). Moreover, immunofluorescence analysis further revealed a strong colocalization of Lvβ-catenin with wild-type LvTcf, but not with its catenin-binding domain deletion mutation (LvTcf57-556) (**Figure 2C**). Lvβ-catenin expressed alone was mainly localized in the cytoplasm, while LvTcf, a nuclear protein, was present in the nucleus. When Lvβ-catenin and LvTcf were co-expressed in cells, Lvβ-catenin translocated into the nucleus and colocalized with LvTcf (**Figure 2C**).

According to previous reports, the β-catenin/TCF pathway facilitates interferon production following viral infection (30–32). Thus, we hypothesized that the Lvβ-catenin/LvTcf pathway could promote the expression of shrimp interferon-like protein Vago during WSSV infection. As five isoforms of Vago have been identified in shrimp to date (46, 47), we performed dual luciferase reporter gene assays in Drosophila S2 cells to confirm the Lvβ-catenin/LvTcf-mediated transcriptional regulation at Vago promoters. To our surprise, the results indicated that LvTcf, but not Lvβ-catenin, could significantly promote *LvVago1* promoter activity, and Lvβ-catenin/LvTcf together had a less effect (**Figures 2D**). Further, knockdown of LvTcf led to decreased *LvVago1* expression after WSSV infection (**Figures 2E, F**). We found that LvTcf57-556, a catenin-binding domain deletion mutant, could still activate the LvVago1 promoter (**Figure 2G**). This activation was not reduced under Lvβ-catenin co-expression (**Figure 2H**). To determine the influence of endogenous β-catenin in S2 cells, we silenced the expression of β-catenin *via* siRNA and detected the effect of LvTcf on the *LvVago1* promoter. The knockdown of endogenous Dmβ-catenin did not affect *LvVago1* promoter activity, which was regulated by LvTcf (**Figure 2I**).

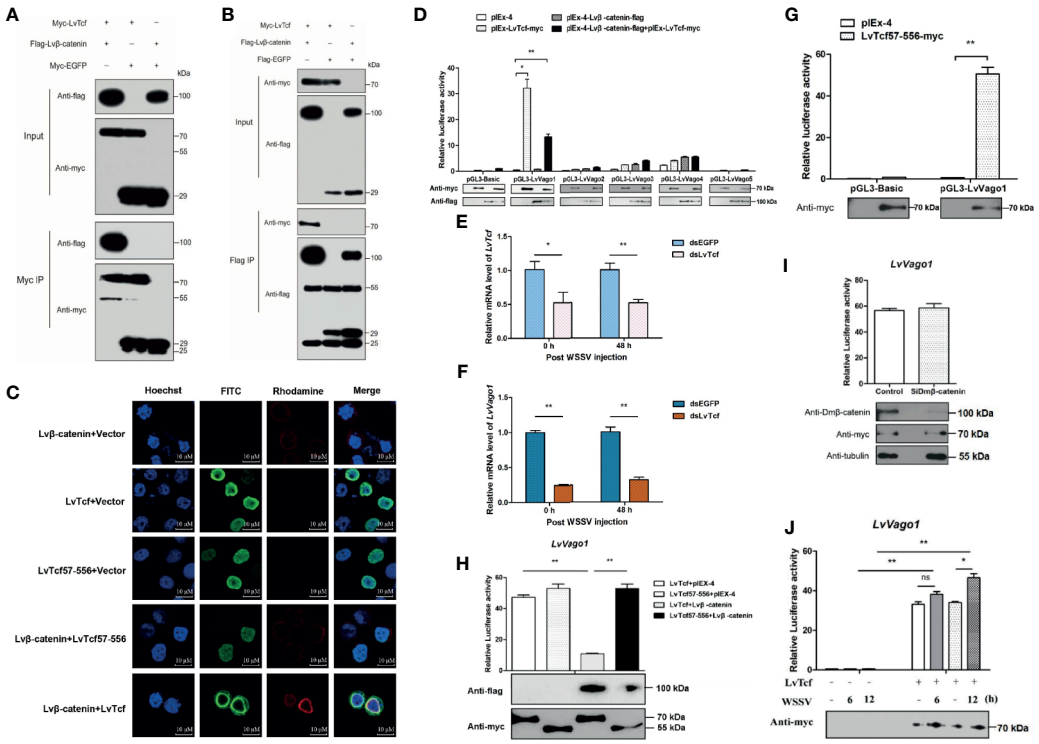

FIGURE 2 | LvTcf was involved in regulating LvVago1 expression independently of Lvβ-catenin. **(A, B)** Co-IP analysis in High Five cells indicated that LvTcf interacted with Lvβ-catenin. Cell lysates were immunoprecipitated using rabbit anti-c-Myc agarose affinity Gel **(A)** or mouse anti-FLAG M2 affinity gel **(B)**. **(C)** Immunofluorescence analysis revealed that LvTcf colocalized with Lvβ-catenin. Cells were transfected with Myc-LvTcf, FLAG-Lvβ-catenin, or both. After 36 h, immunofluorescence analysis was performed with primary mouse anti-Myc, rabbit anti-FLAG, as well as secondary FITC anti-mouse and rhodamine anti-rabbit antibodies. Finally, the cells were observed under a confocal laser-scanning microscope. The scale bar = 10 μm. **(D–I)** LvTcf activated the *LvVago1* promoter independently of Lvβ-catenin. **(D)** The effects of Lvβ-catenin/LvTcf expression on the promoter activity of *LvVago1-5* were analyzed *via* a dual-luciferase reporter assay. **(E, F)** Silencing of *LvTcf* led to a decrease in *LvVago1* expression after WSSV infection. **(G, H)** The effect of LvTcf57-556/Lvβ-catenin on the promoter activity of *LvVago1* was analyzed *via* a dual-luciferase reporter assay. **(I)** Knockdown of Dmβ-catenin did not affect the LvTcf-induced activation of *LvVago1* promoter activity. **(J)** The effect of LvTcf on *LvVago1* upon WSSV stimulation. Data were analyzed *via* the student's *t*-test (ns, No Significant, *p < 0.05, ** p < 0.01).

Based on the above-described results, we suggest that LvTcf activates the expression of *LvVago1* independently of Lvβ-catenin. We further detected the regulatory activity of LvTcf on the *LvVago1* promoter upon WSSV stimulation. pGL3-LvVago1 was co-transfected with an empty vector or LvTcf expression plasmids in *Drosophila* S2 cells. WSSV was added at 36 and 42 h after transfection. After culturing for 48 h, the cells were lysed, and fluorescence activity was detected. WSSV stimulation increased *LvVago1* promoter activity, which was regulated by LvTcf (**Figure 2J**). Taken together, these results revealed that LvTcf could promote the expression of interferon-like protein LvVago1 independently of Lvβ-catenin, thus having a protective role against WSSV infection.

LvTcf Interacts With WSV083

TCF is the main downstream nuclear transcription factor of the Wnt pathway and is involved in immune regulation. It is usually a target of diverse viruses (48). To reveal the regulatory effect of WSSV on host LvTcf, we sought to identify LvTcf-associated viral proteins. As key viral regulatory factors, WSSV immediate-early proteins play important roles in successful infection and replication. In addition, these proteins mainly localize to the host cell nucleus. Therefore, we selected WSSV immediate-early proteins with known functions to study their relationship with LvTcf. In High Five cells, viral immediate-early protein expression plasmids of WSV403, WSV249, WSV079, WSV083, WSV069, WSV100, and WSV056 were co-transfected with the LvTcf-myc expression plasmid. The results indicated that LvTcf may interact with WSV083 and WSV069 (**Figure S2**). Transient transfection and Co-IP further indicated that WSV083 interacted with LvTcf (**Figure 3A**). Moreover, WSV083-GST was expressed in *E. coli* BL21, while LvTcf-myc was expressed in High Hive cells due to its difficult expression in prokaryotic cells. A GST-pull-down was then performed, indicating that WSV083-GST, but not GST alone, could bind to LvTcf *in vitro* (**Figures 3B, C**). These results revealed that WSV083 interacted with LvTcf directly.

WSV083 Phosphorylates LvTcf

While exploring the interaction between LvTcf and WSV083, we found that LvTcf displayed an upshift in mobility on the SDS-

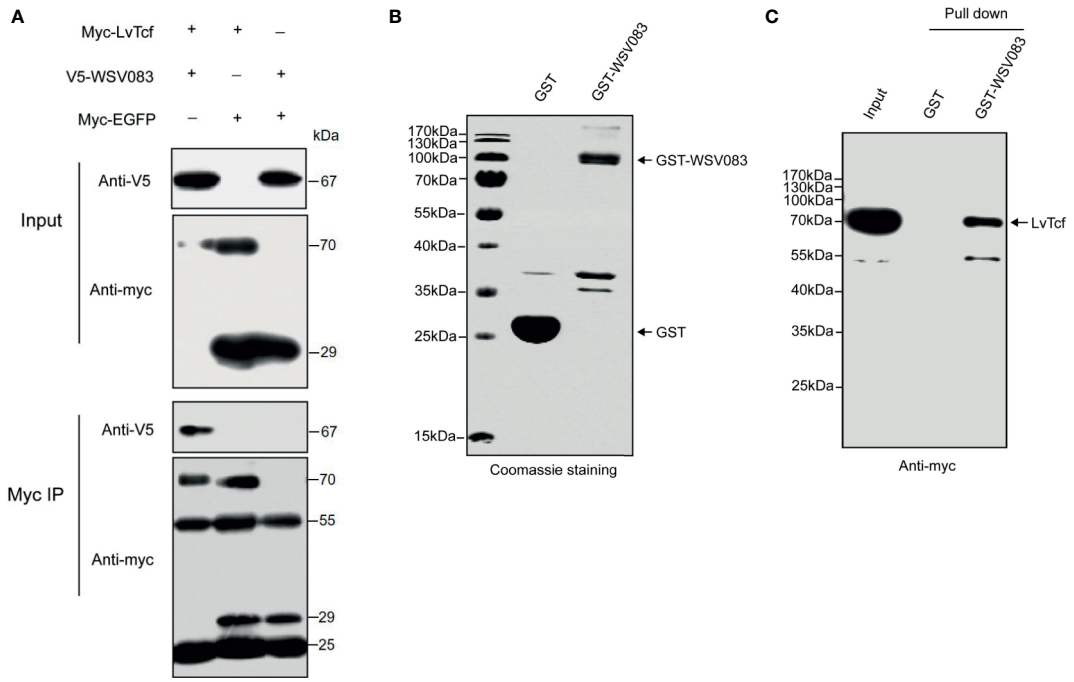

FIGURE 3 | Interaction between LvTcf and WSV083. **(A)** Co-IP experiments indicated that LvTcf interacted with WSV083 in High Five cells. Myc co-IP was performed using a mouse anti-Myc antibody. Western blotting was performed using a mouse anti-Myc or anti-V5-HRP antibody. **(B, C)** GST pull-down analysis of the interaction between LvTcf and WSV083. **(B)** GST and GST-WSV083 were expressed in E. coli BL21 cells and purified using GST-Sepharose beads. Identical proteins were assessed by SDS-PAGE with Coomassie staining. **(C)** High Five cells transfected with Myc-LvTcf expression plasmids were lysed and incubated with GST Sepharose beads coupled with GST or GST-WSV083, respectively. The immunoprecipitates were analyzed via western blot using an anti-Myc antibody.

PAGE gel when co-expressed with WSV083 (**Figure 3A**). As WSV083 is essentially a serine/threonine protein kinase, we hypothesized that this phenomenon was caused by the WSV083-mediated phosphorylation of LvTcf. At the same time, WSV083 kinase domain deletion mutant WSV083DM and kinase domain ATP-binding point mutant D459A WSV083PM expression plasmids were constructed (**Figure 4A**). We then co-expressed both LvTcf and WSV083 or its mutants in High Five cells. The LvTcf immunoprecipitated *via* anti-myc agarose was subjected to treatment with or without CIAP. The results revealed that LvTcf co-expressed with WSV083WT exhibited slower mobility through the gel compared to LvTcf co-expressed with the control vector. WSV083DM nor WSV083PM affected the mobility of LvTcf (**Figure 4B**). After CIAP treatment, the mobility difference of LvTcf disappeared (**Figure 4B**), indicating that WSV083 phosphorylated LvTcf.

WSV083 Increases the Degradation of LvTcf Through the Ubiquitin-Proteasome Pathway

In addition, we found that LvTcf protein levels were reduced in the presence of WSV083WT (**Figures 3A**, **4B**). To validate this observation, we transfected High Five cells with equal amounts of LvTcf plasmid and increasing amounts of WSV083WT plasmid, while decreasing amounts of EGFP plasmid were added to maintain the same amount of transfection. Western blotting results indicated that WSV083 decreased the level of LvTcf in a dose-dependent manner (**Figure 5A**). To further confirm whether WSV083 promoted the degradation of LvTcf through the proteasome pathway after its phosphorylation, we co-transfected LvTcf with pIEx-4, WSV083WT, WSV083DM, and WSV083PM expression plasmids into High Five cells. The proteasome inhibitor MG132 was used to block protein degradation. MG132 completely inhibited LvTcf degradation by WSV083WT, while the empty vector, WSV083DM, or WSV083PM, had no effect on LvTcf (**Figure 5B**). This suggests that phosphorylation of LvTcf by functional WSV083 is necessary for its proteasome-mediated degradation.

Since protein degradation is usually related to ubiquitination, we further determined whether LvTcf underwent ubiquitylation as a result of WSV083-mediated phosphorylation. LvTcf was co-transfected with EGFP, WSV083, and ubiquitin into High Five cells for intracellular ubiquitination assays. In the presence of WSV083WT, which possesses kinase activity, a polyUb-LvTcf smear of greater molecular mass was observed compared to the control group (**Figure 5C**), indicating that WSV083 promoted the ubiquitylation of LvTcf. Moreover, immunofluorescence analysis indicated that LvTcf colocalized with WSV083, and the latter could change the subcellular localization of LvTcf upon addition of MG132 (**Figure 5D**). We believe that WSV083-phosphorylated LvTcf was transferred to the

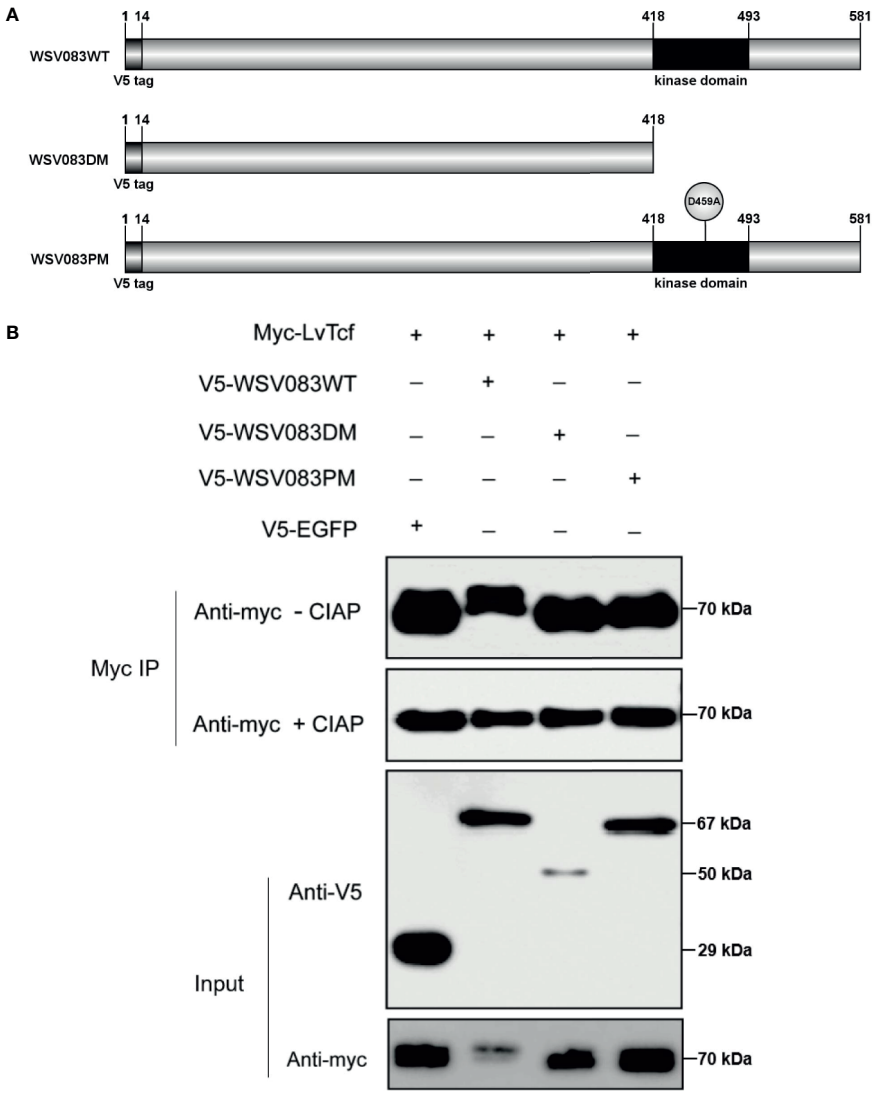

FIGURE 4 | LvTcf phosphorylation by WSV083. **(A)** Schematic diagram of WSV083 and its kinase activity deficiency mutant expression vectors. **(B)** High Five cells were co-transfected with Myc-LvTcf and V5-EGFP, V5-WSV083WT, V5-WSV083DM, V5-WSV083PM, respectively. After 48 h, whole-cell extracts were immunoprecipitated with anti-Myc and protein A beads. Immunoprecipitates were then subjected to CIAP treatment and immunoblotting as indicated.

cytoplasm for degradation. The current results suggested that WSV083 increased the degradation of LvTcf *via* the ubiquitin-proteasome pathway. In addition, WSV083 inhibited the LvTcf-mediated activity of the *LvVago1* promoter (**Figure 5E**). While our data cannot rule out an indirect mechanism where WSV083 regulates a kinase that in turn directly phosphorylates LvTCF, we favor a model where WSV083 phosphorylates LvTCF directly, on multiple residues that remain to be identified, leading to its degradation by the ubiquitin-proteasome pathway.

Identification of WSV083-Targeted LvTcf Phosphorylation Sites

Based on the results described above, we speculated that an E3 ligase might recognize the specific LvTcf residues that were phosphorylated by WSV083. To locate these, we employed mass spectrometry in LvTcf samples gathered from High Five cells co-expressing LvTcf with WSV083WT or WSV083DM (**Figure S3**). The Thr39 and Thr104 LvTcf residues were found to be phosphorylated in cells co-transfected with WSV083WT, but not WSV083DM (**Figures 6A, B**). We therefore suggest that WSV083 phosphorylates LvTcf at Thr39 and Thr104. However, the LvTcfT39AT104A mutant (LvTcf2MuA) retained a mobility shift in SDS-PAGE gel when co-expressed with WSV083WT (**Figure 6C**). LvTcf might therefore contain other residues that are phosphorylated by WSV083, in addition to Thr39 and Thr104. Thus, we continued to substitute some potentially conserved phosphorylated serine or threonine residues (Thr311, Ser315, and Ser356) with alanine. When T39, T104,

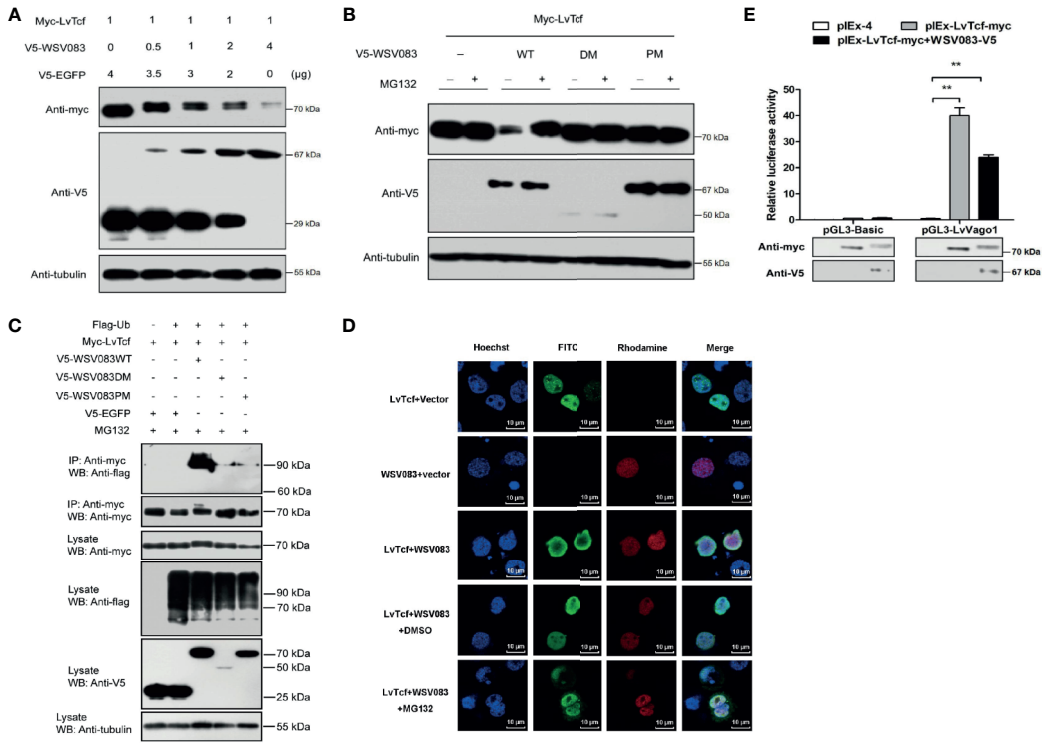

FIGURE 5 | WSV083 promotes the degradation of LvTcf *via* the ubiquitin-proteasome pathway. **(A)** High Five cells were transfected with Myc-LvTcf and increasing doses of V5-WSV083 expression plasmid (0, 0.5, 1, 2, and 4 μg), as indicated. After 48 h, the cells were lysed and analyzed by western blotting. **(B)** High Five cells were co-transfected with Myc-LvTcf, pIEx-4, V5-WSV083WT, or its mutants. After 24 h, the cells were treated with or without 10 μM MG132 as indicated. Anti-Myc, anti-V5, and anti-tubulin antibodies were used for western blotting. **(C)** WSV083 promoted the polyubiquitination of LvTcf. High Five cells were co-transfected with Myc-LvTcf, FLAG-Ub, and V5-WSV083, as indicated. After 24 h, the cells were treated with 10 μM MG132 for 12 h. Whole-cell extracts were immunoprecipitated with anti-Myc and protein A beads followed by western blotting with anti-FLAG. **(D)** WSV083-phosphorylated LvTcf was transferred into the cytoplasm for degradation. Cells were transfected with Myc-LvTcf, V5-WSV083, or both. After 24 h, cells co-transfected with Myc-LvTcf and V5-WSV083 were treated with MG132 or DMSO for 18 h. Immunofluorescence experiments were performed with a primary mouse anti-Myc, rabbit anti-V5 as well as secondary FITC anti-mouse and rhodamine anti-rabbit antibodies. Finally, the cells were observed under a confocal laser-scanning microscope. Scale bar = 10 μm. **(E)** Dual-luciferase reporter assays indicated that WSV083 inhibited the effect of LvTcf on the *LvVago1* promoter. Data were analyzed *via* the student's *t*-test (**$p < 0.01$).

Thr311, Ser315 and Ser356 (LvTcf5MuA) were simultaneously mutated, a mobility shift still occurred (**Figure 6D**). CIAP treatment abolished the mobility difference of LvTcf mutants (**Figure 6E**). These results indicated that a series of serine or threonine sites of LvTcf, including T39 and T104, could be phosphorylated by WSV083.

DISCUSSION

TCF, the key transcription factor of the Wnt signaling pathway, drives the development of lymphocytes (T cells, B cells), NK cells, and innate lymphoid cells (49, 50). Further, TCF-1 is essential for both the initiation of TFH differentiation and the effector function of differentiated TFH during acute viral infection by promoting the expression of Bcl-6 (28). In addition, the β-catenin/TCF signaling pathway functions in innate defense mechanisms to defend against diverse pathogens *via* phagocytosis, autophagy, reactive oxygen species production, and antimicrobial peptide production (31). Thus, TCF plays a critical role in innate and adaptive immune responses. Various studies have confirmed the involvement of Wnt signaling in WSSV infection (33–35, 51–54). However, little is known regarding the relationship between shrimp Tcf and WSSV. In the current study, we demonstrated for the first time that LvTcf exerts antiviral effects by promoting the production of interferon-like protein LvVago1 independently of Lvβ-catenin. Further, this antiviral effect was suppressed by WSSV protein kinase WSV083.

WSSV triggered expression changes in diverse host molecules, including LvTcf. As shown in **Figure 1**, LvTcf mRNA was significantly increased following WSSV infection (**Figures 1A, B**), indicative of a close relationship between LvTcf and WSSV infection. RNAi experiments revealed that LvTcf knockdown resulted in greater WSSV proliferation (**Figures 1C, D**), suggesting that the former plays a protective role against WSSV infection. A recent research found that two isoforms of LvPangolin, LvPangolin1 (LvTcf in this work) and LvPangolin2, had antiviral properties against WSSV, which is compatible with our findings (55).

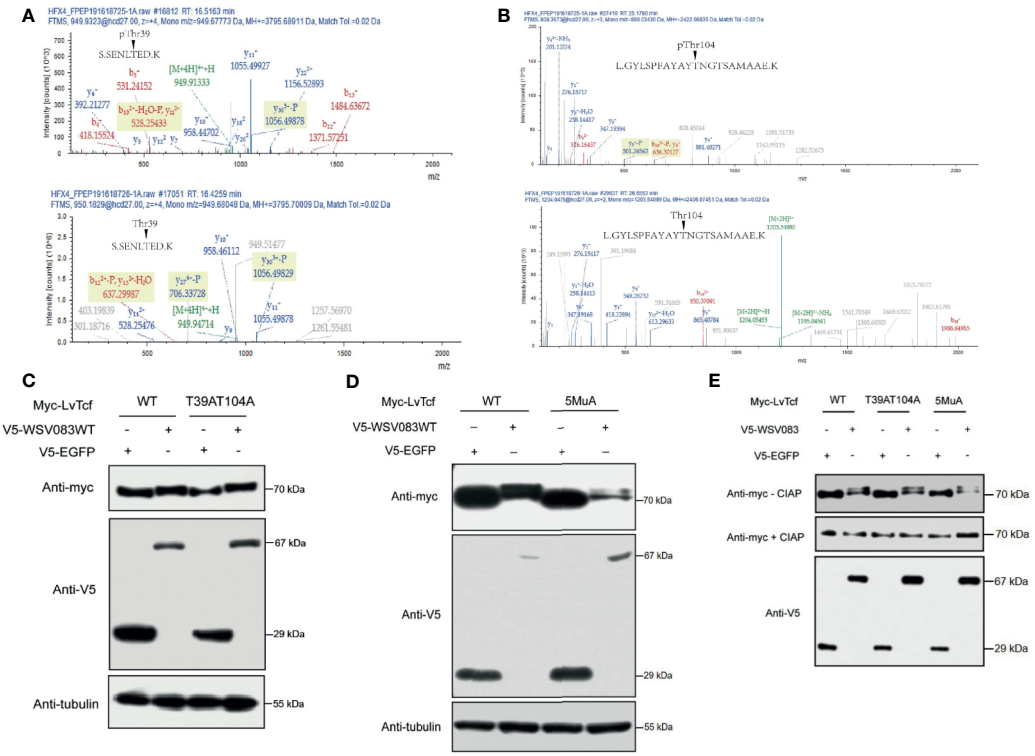

FIGURE 6 | Identification of WSV083 phosphorylation sites on LvTcf. **(A, B)** Mass spectrometry analysis of LvTcf immunoprecipitates revealed that Thr39 and Thr104 in LvTcf were phosphorylation sites targeted by WSV083. **(A)** or **(B)** upper panel: Spectrum analysis of LvTcf immunoprecipitated from cells co-expressing WSV083WT; lower panel: from cells co-expressing WSV083DM. **(C, D)** Myc-LvTcfT-39AT104A or Myc-LvTcf5MuA (T39A/T104A/T311A/S315A/S356A) still displayed their mobility shift when co-expressed with WSV083WT. Myc-LvTcfWT, Myc-LvTcfT39AT104A **(C)**, Myc-LvTcf5MuA **(D)** were co-expressed with V5-EGFP or V5-WSV083WT in High Five cells. After 36 h, cell lysates were subjected to western blotting, as indicated. **(E)** CIAP abolished the mobility shift of LvTcf mutants when co-expressed with WSV083WT. Myc-LvTcfWT, Myc-LvTcfT39AT104A, or Myc-LvTcf5MuA were co-expressed with V5-EGFP or V5-WSV083WT, respectively. At 36 h post-transfection, cell lysates were subjected to immunoprecipitation, CIAP treatment, and immunoblotting, as indicated.

Wnt/β-catenin/TCF signaling pathway-mediated responses to bacterial and viral infections have been the subject of extensive study, highlighting the cascade's roles in orchestrating phagocytosis, antimicrobial or interferon defense, as well as inflammatory cytokine production (56–58). In the current study, we sought to explore the LvTcf-mediated regulation of downstream immune-related genes in shrimp. Interferons, a family of immune proteins which spearhead antiviral defense, are regulated by β-catenin/TCF in an interferon regulatory factor-independent manner (59). There are five interferon-like proteins in shrimp. Among them, the interferon regulatory factor-mediated antiviral effects of LvVago1, LvVago4, and LvVago5, have been previously characterized (47, 60). Sequence analysis revealed that LvTcf harbors several possible binding sites in the promoters of LvVago-encoding genes. LvTcf promoted the activity of the *LvVago1* promoter during WSSV infection (**Figures 2D–F, H, J**). In a recent study, β-catenin was shown to activate gene expression by binding to other transcription factors such as FOXO4 without TCF (61). We found that LvTcf initiated the production of LvVago1 independently Lvβ-catenin even though they could interact with each other. Moreover, cooperation with Lvβ-catenin reduced the effect of LvTcf on *LvVago1* promoter activity. It is suggested that LvTcf acts by itself or cooperates with other transcription factors to activate LvVago1 expression, whereas the Lvβ-catenin/LvTcf complex might upregulate the transcription of other shrimp target genes. Taken together, our study clarified one of the mechanisms through which LvTcf defends against WSSV infection.

Host immune molecules are often targeted by viruses. The regulation of post-translational modifications, especially the ubiquitination of host immune molecules, is an effective means of immune evasion (20, 62). For instance, IpaH9.8, an E3 ubiquitin ligase of Shigella flexneri, could target human GBP-1 to induce its ubiquitination and degradation, thus suppressing host defense (63). Kaposi's sarcoma-associated herpesvirus encodes an E3 ligase RTA that suppresses innate immunity *via* the ubiquitin-mediated degradation of MyD88 (64). As pivotal nuclear co-activators of the Wnt signaling pathway, TCFs are regulated by various factors. LEF1, TCF7L1, and TCF7L2 are phosphorylated by HIPK2 at their HMG box domain (65). These are also phosphorylated by NLK, as the first step for ubiquitylation by NARF, and are subsequently degraded *via* the proteasome (66). Various reports have indicated that SUMOylation and acetylation of TCFs regulate their

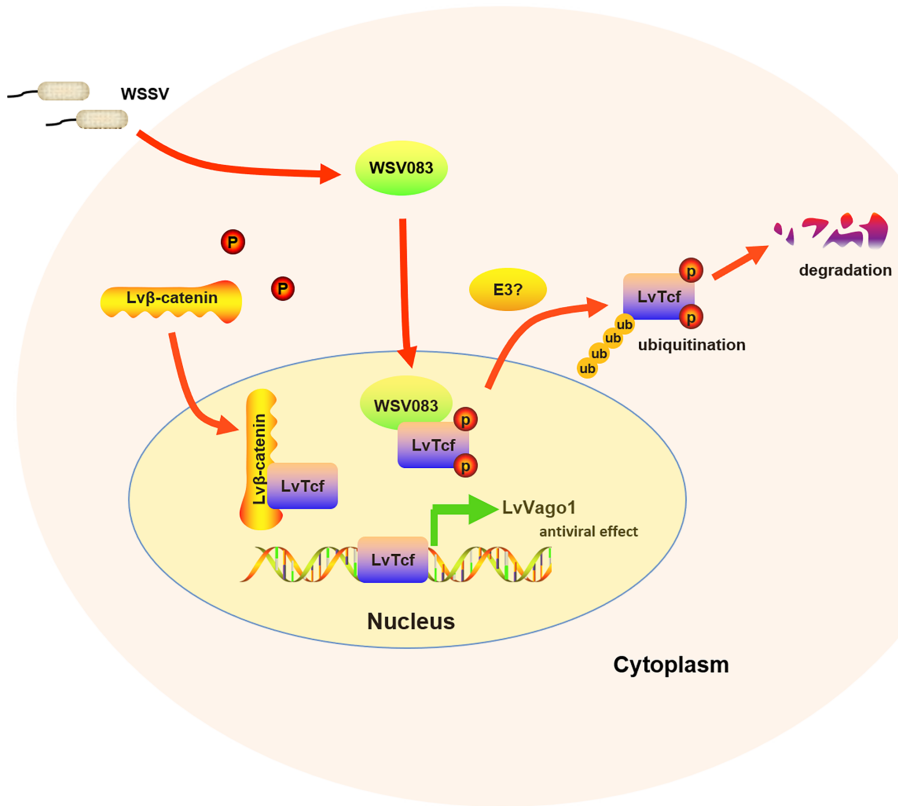

FIGURE 7 | Model of the relationship between LvTcf and WSSV infection. WSSV infection (pathogenic stress) induced the LvTcf-driven production of interferon-like protein LvVago1 independently of Lvβ-catenin, as an antiviral defense mechanism. However, WSSV encodes a serine/threonine protein kinase, WSV083, which phosphorylates LvTcf. Phosphorylated LvTcf is translocated to the cytoplasm, recognized by an E3 ligase, and degraded *via* the ubiquitin-proteasome pathway.

subcellular localization and transcriptional activity (67, 68). In the present study, we discovered that LvTcf was modulated by the viral Ser/Thr protein kinase WSV083. WSV083 caused the phosphorylation of LvTcf and delayed its mobility in SDS-PAGE due to changes in molecular weight and isoelectric point (**Figure 4B**). WSV083-mediated LvTcf phosphorylation could impact the latter's protein stability (**Figures 5A–C**). Phosphorylated LvTcf was transferred into the cytoplasm for degradation *via* the ubiquitin-proteasome pathway (**Figure 5D**). Some E3 ligases mediate the degradation of target proteins necessary for the recognition of specific phosphorylated amino acid residues (69–71). We speculated that an E3 ligase might recognize the LvTcf residues phosphorylated by WSV083 prior to its ubiquitination. However, mass spectrometry analysis did not identify all LvTcf residues targeted by WSV083 (**Figure 6**). In addition, although over-expression of WSV083 downregulated LvTcf protein and inhibited its ability to activate *Lv*Vago1 promoter (**Figure 5E**), this did not contradict the findings in **Figure 2J** that WSSV infection induced LvTcf activation of the *Lv*Vago1. In contrast to WSV083 overexpression, the amount of WSV083 in S2 cells was insufficient to cause LvTcf breakdown in a WSSV-stimulated manner. S2 cells, on the other hand, were capable of receiving and responding to WSSV infection. In response to WSSV stimulation, LvTcf in S2 cells was likely to upregulate the activity of the *Lv*Vago1 promoter.

In summary, our work showed that LvTcf promoted the expression of shrimp interferon-like protein Vago1 following WSSV infection, whereas WSSV protein kinase WSV083 could directly bind to and phosphorylate LvTcf, promoting its degradation *via* the ubiquitin-proteasome pathway (**Figure 7**). The current findings provide new insight into the response against WSSV, thus having implications for disease control.

DATA AVAILABILITY STATEMENT

The datasets presented in this study can be found in online repositories. The names of the repository/repositories and accession number(s) can be found in the article/**Supplementary Material**.

AUTHOR CONTRIBUTIONS

CW, LR, and HS designed the experiments. CW, WL, LL, and SL performed the experiments and data analysis. CW and LR were

responsible for writing, finalizing, and submitting the manuscript. All the authors discussed the results. All authors contributed to the article and approved the submitted version.

FUNDING

This work was funded by Natural Science Foundation of Fujian Province of China (2020J06031), National Natural Science Foundation of China (No. 31972816) and China Agriculture Research System of MOF and MARA (CARS-48).

ACKNOWLEDGMENTS

The authors would like to thank Feng Yang, Fang Li, Yueling Zhang, and Defu Yao for their help in providing experimental supplies.

SUPPLEMENTARY MATERIAL

The Supplementary Material for this article can be found online at: https://www.frontiersin.org/articles/10.3389/fimmu.2021.698697/full#supplementary-material

REFERENCES

1. Yang F, He J, Lin X, Li Q, Pan D, Zhang X, et al. Complete Genome Sequence of the Shrimp White Spot Bacilliform Virus. *J Virol* (2001) 75:1902(23). doi: 10.3389/fimmu.2017.01902
2. Sanchez-Paz A. White Spot Syndrome Virus: An Overview on an Emergent Concern. *Vet Res* (2010) 41(6):43. doi: 10.1051/vetres/2010015
3. Huang PH, Huang TY, Cai PS, Chang LK. Role of *Litopenaeus Vannamei* Yin Yang 1 in the Regulation of the White Spot Syndrome Virus Immediate Early Gene Ie1. *J Virol* (2017) 91(6):e02314–16. doi: 10.1128/JVI.02314-16
4. Escobedo-Bonilla CM, Alday-Sanz V, Wille M, Sorgeloos P, Nauwynck HJ. A Review on the Morphology, Molecular Characterization, Morphogenesis and Pathogenesis of White Spot Syndrome Virus. *J Fish Dis* (2008) 31(1):1–18. doi: 10.1111/j.1365-2761.2007.00877.x
5. Sedeh FM, Afsharnasab M, Heidarieh M, Shafaee SK, Razavi MH. Titration of the Iranian White Spot Virus Isolate, on Crayfish Astacus Leptodactylus and Penaeus Semisulcatus. *Iran J Fish Sci* (2012) 11(1):145–55. doi: 10.1007/s00267-003-2709-z
6. Akira S, Uematsu S, Takeuchi O. Pathogen Recognition and Innate Immunity. *Cell* (2006) 124(4):783–801. doi: 10.1016/j.cell.2006.02.015
7. Tassanakajon A, Somboonwiwat K, Supungul P, Tang S. Discovery of Immune Molecules and Their Crucial Functions in Shrimp Immunity. *Fish Shellfish Immunol* (2013) 34(4):954–67. doi: 10.1016/j.fsi.2012.09.021
8. Li F, Xiang J. Signaling Pathways Regulating Innate Immune Responses in Shrimp. *Fish Shellfish Immunol* (2013) 34(4):973–80. doi: 10.1016/j.fsi.2012.08.023
9. Deepika A, Sreedharan K, Paria A, Makesh M, Rajendran KV. Toll-Pathway in Tiger Shrimp (*Penaeus Monodon*) Responds to White Spot Syndrome Virus Infection: Evidence Through Molecular Characterisation and Expression Profiles of MyD88, TRAF6 and TLR Genes. *Fish Shellfish Immunol* (2014) 41(2):441–54. doi: 10.1016/j.fsi.2014.09.026
10. Wen R, Li F, Li S, Xiang J. Function of Shrimp STAT During WSSV Infection. *Fish Shellfish Immunol* (2014) 38(2):354–60. doi: 10.1016/j.fsi.2014.04.002
11. Huang XD, Zhao L, Zhang HQ, Xu XP, Jia XT, Chen YH, et al. Shrimp NF-κb Binds to the Immediate-Early Gene Ie1 Promoter of White Spot Syndrome Virus and Upregulates its Activity. *Virology* (2010) 406(2):176–80. doi: 10.1016/j.virol.2010.06.046
12. Liu WJ, Chang YS, Wang AH, Kou GH, Lo CF. White Spot Syndrome Virus Annexes a Shrimp STAT to Enhance Expression of the Immediate-Early Gene Ie1. *J Virol* (2007) 81(3):1461–71. doi: 10.1128/JVI.01880-06
13. Yao D, Ruan L, Lu H, Shi H. Shrimp STAT Was Hijacked by White Spot Syndrome Virusimmediate-Early Protein IE1 Involved in Modulation of Viral Genes. *Fish Shellfish Immunol* (2016) 59:268–75. doi: 10.1016/j.fsi.2016.10.051
14. Wang S, Li H, Weng S, Li C, He J. White Spot Syndrome Virus Establishes a Novel IE1/JNK/c-Jun Positive Feedback Loop to Drive Replication. *iScience* (2020) 23(1):100752. doi: 10.1016/j.isci.2019.100752
15. Ran X, Bian X, Ji Y, Yan X, Yang F, Li F. White Spot Syndrome Virus IE1 and WSV056 Modulate the G1/S Transition by Binding to the Host Retinoblastoma Protein. *J Virol* (2013) 87(23):12576–82. doi: 10.1128/JVI.01551-13
16. Ren Q, Huang Y, He Y, Wang W. A White Spot Syndrome Virus microRNA Promotes Thevirus Infection by Targeting the Host STAT. *Sci Rep* (2015) 5:18384. doi: 10.1038/srep18384
17. Chen IT, Aoki T, Huang YT, Hirono I, Chen TC, Huang JY, et al. White Spot Syndrome Virus Induces Metabolic Changes Resembling the Warburg Effect in Shrimp Hemocytes in the Early Stage of Infection. *J Virol* (2011) 85 (24):12919–28. doi: 10.1128/JVI.05385-11
18. Su MA, Huang YT, Chen IT, Lee DY, Hsieh YC, Li CY, et al. An Invertebrate Warburg Effect: A Shrimp Virus Achieves Successful Replication by Altering the Host Metabolome *via* the PI3K-Akt-mTOR Pathway. *PloS Pathog* (2014) 10(6):e1004196. doi: 10.1371/journal.ppat.1004196
19. Chen IT, Lee DY, Huang YT, Kou GH, Wang HC, Chang GD, et al. Six Hours After Infection, the Metabolic Changes Induced by WSSV Neutralize the Host's Oxidative Stress Defenses. *Sci Rep* (2016) 6:27732. doi: 10.1038/srep27732
20. Isaacson MK, Ploegh HL. Ubiquitination, Ubiquitin-Like Modifiers, and Deubiquitination in Viral Infection. *Cell Host Microbe* (2009) 5(6):559–70. doi: 10.1016/j.chom.2009.05.012
21. Wang Z, Chua HK, Gusti AA, He F, Fenner B, Manopo I, et al. RING-H2 Protein WSSV249 From White Spot Syndrome Virus Sequesters a Shrimp Ubiquitin-Conjugating Enzyme, PvUbc, for Viral Pathogenesis. *J Virol* (2005) 79(14):8764–72. doi: 10.1128/JVI.79.14.8764-8772.2005
22. He F, Kwang J. Identification and Characterization of a New E3 Ubiquitin Ligase in White Spot Syndrome Virus Involved in Virus Latency. *Virol J* (2008) 5:151. doi: 10.1186/1743-422X-5-151
23. He F, Fenner BJ, Godwin AK, Kwang J. White Spot Syndrome Virus Open Reading Frame 222 Encodes a Viral E3 Ligase and Mediates Degradation of a Host Tumor Suppressor *via* Ubiquitination. *J Virol* (2006) 80(8):3884–92. doi: 10.1128/JVI.80.8.3884-3892.2006
24. He F, Syed SM, Hameed ASS, Kwang J. Viral Ubiquitin Ligase WSSV222 Is Required for Efficient White Spot Syndrome Virus Replication in Shrimp. *J Gen Virol* (2009) 90(Pt 6):1483–90. doi: 10.1099/vir.0.008912-0
25. Reya T, Clevers H. Wnt Signalling in Stem Cells and Cancer. *Nature* (2005) 434(7035):843–50. doi: 10.1038/nature03319
26. Freese JL, Pino D, Pleasure SJ. Wnt Signaling in Development and Disease. *Neurobiol Dis* (2010) 38(2):148–53. doi: 10.1016/j.nbd.2009.09.003
27. Komiya Y, Habas R. Wnt Signal Transduction Pathways. *Organogenesis* (2008) 4(2):68–75. doi: 10.4161/org.4.2.5851
28. Xu L, Cao Y, Xie Z, Huang Q, Bai Q, Yang X, et al. The Transcription Factor TCF-1 Initiates the Differentiation of T(FH) Cells During Acute Viral Infection. *Nat Immunol* (2015) 16(9):991–9. doi: 10.1038/ni.3229
29. Harmon B, Bird SW, Schudel R, Hatch AV, Rasley A. Negrete OA. A Genome-Wide RNA Interference Screen Identifies a Role for Wnt/β-Catenin Signaling During Rift Valley Fever Virus Infection. *J Virol* (2016) 90(16):7084–97. doi: 10.1128/JVI.00543-16
30. Gantner BN, Jin H, Qian F, Hay N, He B, Ye RD. The Akt1 Isoform is Required for Optimal IFN-β Transcription Through Direct Phosphorylation of β-Catenin. *J Immunol* (2012) 189(6):3104–11. doi: 10.4049/jimmunol.1201669
31. Ljungberg JK, Kling JC, Tran TT, Blumenthal A. Functions of the WNT Signaling Network in Shaping Host Responses to Infection. *Front Immunol* (2019) 10:2521. doi: 10.3389/fimmu.2019.02521
32. Zwezdaryk KJ, Combs JA, Morris CA, Sullivan DE. Regulation of Wnt/β-Catenin Signaling by Herpesviruses. *World J Virol* (2016) 5(4):144–54. doi: 10.5501/wjv.v5.i4.144
33. Zhu F, Zhang X. The Wnt Signaling Pathway is Involved in the Regulation of Phagocytosis of Virus in Drosophila. *Sci Rep* (2013) 3:2069. doi: 10.1038/srep02069
34. Zhang S, Shi L, Li H, Wang S, He J, Li C. Cloning, Identification and Functional Analysis of a β-Catenin Homologue From Pacific White Shrimp, *Litopenaeus Vannamei*. *Fish Shellfish Immunol* (2016) 54:411–8. doi: 10.1016/j.fsi.2016.03.162

35. Sun J, Ruan L, Zhou C, Shi H, Xu X. Characterization and Function of a β-Catenin Homolog From *Litopenaeus Vannamei* in WSSV Infection. *Dev Comp Immunol* (2017) 76:412–9. doi: 10.1016/j.dci.2017.07.003
36. Hrckulak D, Kolar M, Strnad H, Korinek V. TCF/LEF Transcription Factors: An Update From the Internet Resources. *Cancers (Basel)* (2016) 8(7):70. doi: 10.3390/cancers8070070
37. van de Wetering M, Cavallo R, Dooijes D, van Beest M, van Es J, Loureiro J, et al. Armadillo Coactivates Transcription Driven by the Product of the Drosophila Segment Polarity Gene dTCF. *Cell* (1997) 88(6):789–99. doi: 10.1016/s0092-8674(00)81925-x
38. van Beest M, Dooijes D, van De Wetering M, Kjaerulff S, Bonvin A, Nielsen O, et al. Sequence-Specific High Mobility Group Box Factors Recognize 10-12-Base Pair Minor Groove Motifs. *J Biol Chem* (2000) 275(35):27266–73. doi: 10.1074/jbc.M004102200
39. Atcha FA, Syed A, Wu B, Hoverter NP, Yokoyama NN, Ting JH, et al. A Unique DNA Binding Domain Converts T-Cell Factors Into Strong Wnt Effectors. *Mol Cell Biol* (2007) 27(23):8352–63. doi: 10.1128/MCB.02132-06
40. Lu H, Ruan L, Xu X. An Immediate-Early Protein of White Spot Syndrome Virus Modulates the Phosphorylation of Focal Adhesion Kinase of Shrimp. *Virology* (2011) 419(2):84–9. doi: 10.1016/j.virol.2011.07.021
41. Xie X, Li H, Xu L, Yang F. A Simple and Efficient Method for Purification of Intact White Spot Syndrome Virus (WSSV) Viral Particles. *Virus Res* (2005) 108(1-2):63–7. doi: 10.1016/j.virusres.2004.08.002
42. Zhou Q, Qi YP, Yang F. Application of Spectrophotometry to Evaluate the Concentration of Purified White Spot Syndrome Virus. *J Virol Methods* (2007) 146(1-2):288–92. doi: 10.1016/j.jviromet.2007.07.007
43. Shi H, Yan X, Ruan L, Xu X. A Novel JNK From Litopenaeus Vannamei Involved in White Spot Syndrome Virus Infection. *Dev Comp Immunol* (2012) 37(3-4):421–8. doi: 10.1016/j.dci.2012.03.002
44. Cadigan KM, Waterman ML. TCF/LEFs and Wnt Signaling in the Nucleus. *Cold Spring Harb Perspect Biol* (2012) 4(11):a007906. doi: 10.1101/cshperspect.a007906
45. Behrens J, von Kries JP, Kühl M, Bruhn L, Wedlich D, Grosschedl R, et al. Functional Interaction of Beta-Catenin With the Transcription Factor LEF-1. *Nature* (1996) 382(6592):638–42. doi: 10.1038/382638a0
46. Yang L, Luo M, He J, Zuo H, Weng S, He J, et al. A JAK-STAT Pathway Target Gene Encoding a Single WAP Domain (SWD)-Containing Protein From *Litopenaeus Vannamei*. *Fish Shellfish Immunol* (2019) 89:555–63. doi: 10.1016/j.fsi.2019.04.046
47. Li C, Li H, Chen Y, Chen Y, Wang S, Weng SP, et al. Activation of Vago by Interferon Regulatory Factor (IRF) Suggests an Interferon System-Like Antiviral Mechanism in Shrimp. *Sci Rep* (2015) 5:15078. doi: 10.1038/srep15078
48. van Zuylen WJ, Rawlinson WD, Ford CE. The Wnt Pathway: A Key Network in Cell Signalling Dysregulated by Viruses. *Rev Med Virol* (2016) 26(5):340–55. doi: 10.1002/rmv.1892
49. De Obaldia ME, Bhandoola A. Transcriptional Regulation of Innate and Adaptive Lymphocyte Lineages. *Annu Rev Immunol* (2015) 33:607–42. doi: 10.1146/annurev-immunol-032414-112032
50. Raghu D, Xue HH, Mielke LA. Control of Lymphocyte Fate, Infection, and Tumor Immunity by TCF-1. *Trends Immunol* (2019) 40(12):1149–62. doi: 10.1016/j.it.2019.10.006
51. Chen X, Zeng D, Chen X, Xie D, Zhao Y, Yang C, et al. Transcriptome Analysis of *Litopenaeus Vannamei* in Response to White Spot Syndrome Virus Infection. *PloS One* (2013) 8(8):e73218. doi: 10.1371/journal.pone.0073218
52. Zhang S, Li CZ, Yang QH, Dong XH, Chi SY, Liu HY, et al. Molecular Cloning, Characterization and Expression Analysis of Wnt4, Wnt5, Wnt6, Wnt7, Wnt10 and Wnt16 From *Litopenaeus Vannamei*. *Fish Shellfish Immunol* (2016) 54:445–55. doi: 10.1016/j.fsi.2016.04.028
53. Ruan L, Sun J, Zhou C, Shi H. Cloning, Identification and Function Analysis of a Chibby Homolog From *Litopenaeus Vannamei*. *Fish Shellfish Immunol* (2018) 78:114–20. doi: 10.1016/j.fsi.2018.04.039
54. Du J, Zhang X, Yuan J, Zhang X, Li F, Xiang J. Wnt Gene Family Members and Their Expression Profiling in *Litopenaeus Vannamei*. *Fish Shellfish Immunol* (2018) 77:233–43. doi: 10.1016/j.fsi.2018.03.034
55. Zhu L, Zhang S, Hou C, Liang X, Saif Dehwah MA, Tan B, et al. The T Cell Factor, Pangolin, From *Litopenaeus Vannamei* Play a Positive Role in the Immune Responses Against White Spot Syndrome Virus Infection. *Dev Comp Immunol* (2021) 119:104041. doi: 10.1016/j.dci.2021.104041
56. Maiti G, Naskar D, Sen M. The Wingless Homolog Wnt5 Stimulates Phagocytosis But Not Bacterial Killing. *Proc Natl Acad Sci U.S.A.* (2012) 109(41):16600–5. doi: 10.1073/pnas.1207789109
57. Zhao W, Sun Z, Wang S, Li Z, Zheng L. Wnt1 Participates in Inflammation Induced by Lipopoly-Saccharide Through Upregulating Scavenger Receptor A and NF-kB. *Inflammation* (2015) 38(4):1700–6. doi: 10.1007/s10753-015-0147-8
58. Chen K, Fu Q, Li D, Wu Y, Sun S, Zhang X. Wnt3a Suppresses Pseudomonas Aeruginosa-Induced Inflammation and Promotes Bacterial Killing in Macrophages. *Mol Med Rep* (2016) 13(3):2439–46. doi: 10.3892/mmr.2016.4869
59. Marcato V, Luron L, Laqueuvre LM, Simon D, Mansuroglu Z, Flamand M, et al. β-Catenin Upregulates the Constitutive and Virus-Induced Transcriptional Capacity of the Interferon Beta Promoter Through T-Cell Factor Binding Sites. *Mol Cell Biol* (2015) 36(1):13–29. doi: 10.1128/MCB.00641-15
60. Chen YH, Jia XT, Zhao L, Li CZ, Zhang S, Chen YG, et al. Identification and Functional Characterization of Dicer2 and Five Single VWC Domain Proteins of *Litopenaeus Vannamei*. *Dev Comp Immunol* (2011) 35(6):661–71. doi: 10.1016/j.dci.2011.01.010
61. Doumpas N, Lampart F, Robinson MD, Lentini A, Nestor CE, Cantù C, et al. TCF/LEF Dependent and Independent Transcriptional Regulation of Wnt/β-Catenin Target Genes. *EMBO J* (2019) 38(2):e98873. doi: 10.15252/embj.201798873
62. Li C, Weng S, He J. WSSV-Host Interaction: Host Response and Immune Evasion. *Fish Shellfish Immunol* (2019) 84:558–71. doi: 10.1016/j.fsi.2018.10.043
63. Li P, Jiang W, Yu Q, Liu W, Zhou P, Li J, et al. Ubiquitination and Degradation of GBPs by a Shigella Effector to Suppress Host Defence. *Nature* (2017) 551(7680):378–83. doi: 10.1038/nature24467
64. Zhao Q, Liang D, Sun R, Jia B, Xia T, Xiao H, et al. Kaposi's Sarcoma-Associated Herpesvirus-Encoded Replication and Transcription Activator Impairs Innate Immunity *via* Ubiquitin-Mediated Degradation of Myeloid Differentiation Factor 88. *J Virol* (2015) 89(1):415–27. doi: 10.1128/JVI.02591-14
65. Hikasa H, Sokol SY. Phosphorylation of TCF Proteins by Homeodomain-Interacting Protein Kinase 2. *J Biol Chem* (2011) 286(14):12093–100. doi: 10.1074/jbc.M110.185280
66. Yamada M, Ohnishi J, Ohkawara B, Iemura S, Satoh K, Hyodo-Miura J, et al. NARF, an Nemo-Like Kinase (NLK)-Associated Ring Finger Protein Regulates the Ubiquitylation and Degradation of T Cell Factor/Lymphoid Enhancer Factor (TCF/LEF). *J Biol Chem* (2006) 281(30):20749–60. doi: 10.1074/jbc.M602089200
67. Sachdev S, Bruhn L, Sieber H, Pichler A, Melchior F, Grosschedl R. PIASy, a Nuclear Matrix-Associated SUMO E3 Ligase, Represses LEF1 Activity by Sequestration Into Nuclear Bodies. *Genes Dev* (2001) 15(23):3088–103. doi: 10.1101/gad.944801
68. Yamamoto H, Ihara M, Matsuura Y, Kikuchi A. Sumoylation is Involved in Beta-Catenin-Dependent Activation of Tcf-4. *EMBO J* (2003) 22(9):2047–59. doi: 10.1093/emboj/cdg204
69. Willems AR, Goh T, Taylor L, Chernushevich I, Shevchenko A, Tyers M. SCF Ubiquitin Protein Ligases and Phosphorylation-Dependent Proteolysis. *Philos Trans R Soc Lond B Biol Sci* (1999) 354(1389):1533–50. doi: 10.1098/rstb.1999.0497
70. Won KA, Reed SI. Activation of Cyclin E/CDK2 is Coupled to Site-Specific Autophosphorylation and Ubiquitin-Dependent Degradation of Cyclin E. *EMBO J* (1996) 15(16):4182–93. doi: 10.1002/j.1460-2075.1996.tb00793.x
71. Yost C, Torres M, Miller JR, Huang E, Kimelman D, Moon RT. The Axis-Inducing Activity, Stability, and Subcellular Distribution of Beta-Catenin is Regulated in Xenopus Embryos by Glycogen Synthase Kinase 3. *Genes Dev* (1996) 10(12):1443–54. doi: 10.1101/gad.10.12.1443

Conflict of Interest: The authors declare that the research was conducted in the absence of any commercial or financial relationships that could be construed as a potential conflict of interest.

this article, or claim that may be made by its manufacturer, is not guaranteed or endorsed by the publisher.

frontiers in Immunology

MINI REVIEW
published: 10 August 2021
doi: 10.3389/fimmu.2021.720765

Proteomics Mapping of the ISGylation Landscape in Innate Immunity

Fabien Thery[1,2†], *Denzel Eggermont*[1,2†] *and Francis Impens*[1,2,3*]

[1] VIB-UGent Center for Medical Biotechnology, VIB, Ghent, Belgium, [2] Department of Biomolecular Medicine, Ghent University, Ghent, Belgium, [3] VIB Proteomics Core, VIB, Ghent, Belgium

During infection, pathogen sensing and cytokine signaling by the host induce expression of antimicrobial proteins and specialized post-translational modifications. One such protein is ISG15, a ubiquitin-like protein (UBL) conserved among vertebrates. Similar to ubiquitin, ISG15 covalently conjugates to lysine residues in substrate proteins in a process called ISGylation. Mice deficient for ISGylation or lacking ISG15 are strongly susceptible to many viral pathogens and several intracellular bacterial pathogens. Although ISG15 was the first UBL discovered after ubiquitin, the mechanisms behind its protective activity are poorly understood. Largely, this stems from a lack of knowledge on the ISG15 substrate repertoire. To unravel the antiviral activity of ISG15, early studies used mass spectrometry-based proteomics in combination with ISG15 pulldown. Despite reporting hundreds of ISG15 substrates, these studies were unable to identify the exact sites of modification, impeding a clear understanding of the molecular consequences of protein ISGylation. More recently, a peptide-based enrichment approach revolutionized the study of ubiquitin allowing untargeted discovery of ubiquitin substrates, including knowledge of their exact modification sites. Shared molecular determinants between ISG15 and ubiquitin allowed to take advantage of this technology for proteome-wide mapping of ISG15 substrates and modification sites. In this review, we provide a comprehensive overview of mass spectrometry-based proteomics studies on protein ISGylation. We critically discuss the relevant literature, compare reported substrates and sites and make suggestions for future research.

Keywords: ISG15, mass spectrometry, infection, interferon, ubiquitin-like modification

OPEN ACCESS

Edited by:
Soham Gupta,
Karolinska Institutet (KI), Sweden

Reviewed by:
Akos Vegvari,
Karolinska Institutet (KI), Sweden
Yuchen Nan,
Northwest A and F University, China

***Correspondence:**
Francis Impens
francis.impens@vib-ugent.be

†These authors have contributed equally to this work

Specialty section:
This article was submitted to Molecular Innate Immunity, a section of the journal Frontiers in Immunology

Received: *04 June 2021*
Accepted: *16 July 2021*
Published: *10 August 2021*

Citation:
Thery F, Eggermont D and Impens F (2021) Proteomics Mapping of the ISGylation Landscape in Innate Immunity. Front. Immunol. 12:720765. doi: 10.3389/fimmu.2021.720765

INTRODUCTION

ISG15, a Ubiquitin-Like Protein of the Immune System

Host cellular immunity arises from the intricate network of cell types and signaling molecules which confer resistance to pathogenic infections. As part of both the innate and adaptive immune system, interferons (IFNs) are a family of proteins released by host cells upon encounter of foreign invaders. Acting as a cytokine, IFNs signal to other cells to induce the expression of interferon-stimulated genes (ISGs) whose products control pathogenic infections. The evolutionary conserved ubiquitin-like protein (UBL) ISG15 is one of the genes most strongly induced by IFNs and has a profound role

in the antimicrobial response. For instance, ISG15 is known to counteract both viral, bacterial and fungal infections (1). To exert this function, ISG15 depends on three molecular activities which include i) negative control of interferon-α/-β signaling as a free intracellular molecule (2, 3), ii) induction of IFN-γ secretion as an extracellular cytokine and iii) ubiquitin-like protein conjugation in a process called ISGylation (4, 5) (**Figure 1**). Similar to ubiquitylation, ISGylation is mediated by the consecutive action of an E1-activating enzyme (UBA7), an E2-conjugating enzyme (UBE2L6) and E3 ligases (ARIH1, TRIM25 or hHERC5/mHERC6) that covalently link ISG15 to lysine residues of target proteins (14–18). In addition, ISGylation can be reversed through the action of a deconjugating protease, the ubiquitin-like carboxy-terminal hydrolase USP18 (6, 19).

Although its discovery dates back to the 1980s, ISG15 only recently regained attention as an UBL involved in a plethora of biological pathways. Aside from the immune system, ISG15 also plays a role in the progression of cancers, exosome secretion, the DNA damage response, telomere shortening, autophagy, hypoxia and ischemia (20–28). However, its main and most studied function lies within the host response against viral infection [recently reviewed in (1)]. ISG15 acts antiviral by covalently modifying host and viral proteins which interferes with viral assembly or function (29). Accordingly, mice lacking ISG15 are unable to control various pathogens including clinically relevant etiologic agents such as influenza, herpes-, noro- and coxsackievirus (30–32). This crucial antiviral function of ISG15 is further supported by effective immune evasion strategies of specific pathogens which express ISG15 proteases (e.g. SARS/MERS virus) or interfere with ISG15 conjugation (e.g. influenza virus) (33–35). Notably, also the coronavirus pandemic led to renewed interest in ISG15 since the papain-like protease (PLpro) from SARS-CoV-2 actively targets and deconjugates ISGylated proteins to dismantle the host immune response (36, 37). In line with this, molecular inhibition of PLpro restores ISGylation levels in infected cells concomitant with reduced viral replication and virus-induced cytopathogenic effects (10).

Although ISG15 and ISGylation have been primarily characterized in the context of viral infection, it was recently shown that ISG15 also protects against infections by intracellular bacteria such as *Listeria monocytogenes* (*L. monocytogenes*) and *Mycobacterium tuberculosis* (*M. tuberculosis*) or predominantly extracellular bacteria like *Pseudomonas aeruginosa* (38–40). Concordantly, individuals with an inherited ISG15 deficiency show an increased susceptibility to weakly virulent *M. tuberculosis*, a condition known as Mendelian susceptibility to mycobacterial disease (MSMD) (4). Although this phenotype was first ascribed to the extracellular function of ISG15, it was later shown that ISG15 conjugation is also upregulated during *M. tuberculosis* infection *in vivo* (39). Likewise, our laboratory and others have shown that increased levels of ISGylation protect against *L. monocytogenes in vitro* and *in vivo* (38). Meanwhile beyond bacteria, ISGylation was also found to be critical to control *Toxoplasma gondii* (*T. gondii*) infection in human cells (41).

Clearly, ISG15 and ISGylation harbor a broad antimicrobial effect against several major classes of pathogens. Evidently, this raises the question how one single protein modification can target such a diverse set of disease agents. One model suggests that cotranslational modification of newly translated proteins is the basis of ISG15's far-reaching antimicrobial function. Indeed, the dominant ISG15 E3 ligase HERC5 associates with polyribosomes and preferentially modifies proteins that are being synthesized during the active stages of the conjugation machinery (29). Considering that during viral infection mainly viral proteins are translated, ISGylation will preferentially target viral proteins thus disturbing their folding and activity. As such mechanism does not require affinity for specific viral components, ISG15 cotranslational tagging likely contributes to the ability of ISG15 to counteract a broad range of viruses. While this model contributes to our understanding of the antiviral activity of ISG15, it does not explain how ISGylation counteracts bacterial infections. In addition, viral infection or type I interferons (IFN-I) signaling also leads to strong ISGylation of host proteins for which the functional role is still unknown. To gain insights into the biological implications of ISGylation, research has focused on identifying the targets and sites of ISGylation induced upon infection.

Like many other protein post-translational modifications (PTMs), research on UBLs has benefited greatly from recent advances in mass spectrometry (MS)-based proteomics. Aside from shotgun proteomics experiments to profile protein changes upon ISG15 modulation (42–44), several MS screens were performed in the past two decades to identify targets and sites of ISG15 with increasing levels of ingenuity, but also with their own set of shortcomings. In this review, we provide a comprehensive overview of MS-based studies on protein ISGylation. We critically discuss the relevant literature and make suggestions for future developments and research.

MS-Based Approaches to Identify ISG15 Substrates

Despite its early classification as an UBL, it was not until 2002 when the first substrates of ISG15-conjugation were discovered. Following immune challenge of murine macrophages with bacterial DNA, Hamerman and colleagues identified Serpin2a as a bacteria-induced host protein with unexpected higher molecular mass forms on western blot (45). The authors expressed a tagged version of Serpin2a in macrophages followed by immunoprecipitation (IP) and separation on SDS-PAGE to isolate these modified forms of Serpin2a. Subsequent MS analysis then revealed mouse ISG15 as the PTM that conjugates to Serpin2a during macrophage activation. One year later, four additional ISG15-substrates were reported using a high-throughput western blot screen on human thymus samples (46).

In the years that followed, different research groups continued using untargeted MS-based approaches to identify targets of ISGylation. In 2005, a research team led by Robert M Krug was the first to report a comprehensive catalog of 156 human ISGylated proteins (47). The authors overexpressed doubly tagged His-FLAG-ISG15 along with E1/E2 enzymes in HeLa cells treated with IFN-I. ISGylated proteins were isolated from cellular lysates by affinity pulldown and separated by SDS-PAGE prior to their MS identification from specific gel bands. *Bona fide* ISGylated

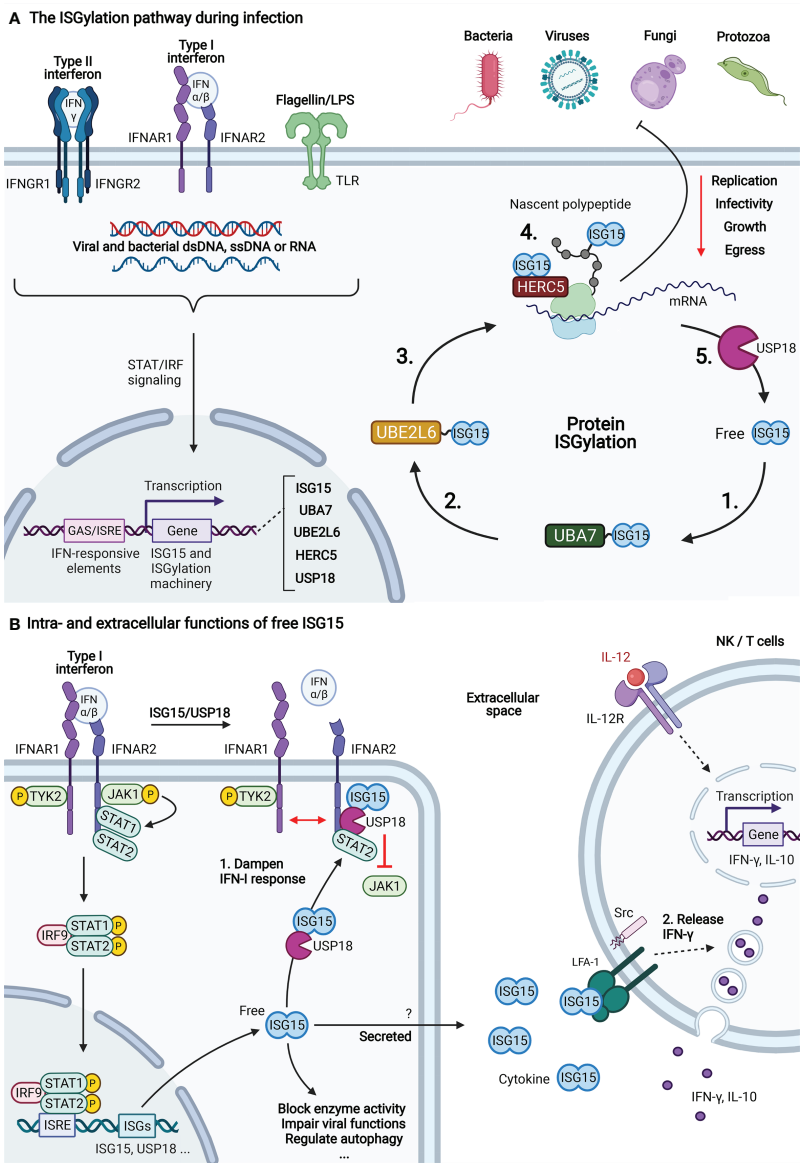

FIGURE 1 | The three functions of ISG15. **(A)** The ISGylation pathway during infection. After detecting the presence of an intra- or extracellular pathogen, several antimicrobial signaling pathways lead to the expression of ISGs, including ISG15 and its conjugation machinery. The covalent attachment of ISG15 to substrate proteins, also called ISGylation, relies on the activities of an E1 (UBA7) (1), E2 (UBE2L6) (2) and E3 (hHERC5/mHERC6) (3) enzyme. The product of the ISG15-conjugation pathway is an ISGylated host or viral protein (4). Target modification by ISG15 has a widespread negative effect on the replication, growth, egress and infectivity of four major classes of pathogens, including viruses, bacteria, fungi and protozoa (1). Deconjugation is catalyzed by USP18 which releases ISG15 from its substrate (5) (6). **(B)** Intra- and extracellular functions of free ISG15. Apart from its activity as a ubiquitin-like conjugate, ISG15 also exists in a free form with functions both inside and outside the cell. (1) Type I interferon (IFN-I) signaling is the main pathway for induction of ISG15 and the ISGylation machinery, including the deISGylase USP18. Binding of IFN-I to the dimeric IFN-I receptor (IFNAR1/2) results in recruitment and activation of Janus activated kinases (JAKs) and tyrosine kinase 2 (TYK2). Consequently, the JAKs phosphorylate STAT1 and STAT2 which dimerize and form a three-protein complex with IRF9. This complex translocates to the nucleus where it binds to IFN-responsive regulatory elements (ISRE) to initiate transcription of IFN-stimulated genes (ISGs). Among these genes is *Usp18*, which, in addition to its enzymatic activity, also functions as a negative regulator of IFN-I signaling by binding to IFNAR2 (7). There, it prevents dimerization of the receptor and blocks recruitment of JAKs which puts a brake on IFN-I-signaling (8). There, it prevents dimerization of the receptor and blocks recruitment of JAKs which puts a brake on IFN-I-signaling (8). In humans, this function depends on direct interaction with ISG15 which protects USP18 from proteasomal degradation (3). Apart from its role in IFN-I signaling, free ISG15 also blocks the activity of certain enzymes, impairs viral functions by sequestering viral proteins, regulates autophagy (9). (2) When ISG15 is not conjugated to other proteins, it also becomes secreted through an unknown non-canonical secretion pathway (10, 11). In the extracellular space, it acts as a cytokine for NK and T cells where it binds to LFA-1 and induces the secretion of IFN-γ and IL-10 from secretory granules (5). The mechanism relies on a synergy between IL-12 and ISG15 where IL-12 triggers the expression of IFN-γ and ISG15 promotes the secretion of IFN-γ through downstream activation of SRC kinases. In addition, ISG15 was shown to enhance secretion of other pro-inflammatory cytokines such as CXCL1, CXCL5, IL-1 and IL-6 (12, 13). Figure created with BioRender.com.

proteins were distinguished from potential contaminants by applying the same procedure on untransfected control cells. Similarly, Takeuchi and colleagues relied on overexpression of FLAG-ISG15 and the ISGylation machinery (E1/E2 enzymes) in HeLa cells to identify six additional substrates of ISG15 (48).

Although new insights were gained into the functions of ISG15, both studies suffered from the use of transient transfection to overexpress the ISGylation machinery. This was known to introduce artefacts through modification of collateral proteins that are not endogenous ISG15-conjugates (29). To overcome these limitations, alternative strategies were devised based on antibodies recognizing endogenous ISG15 or on cell lines stably expressing tagged ISG15. Wong et al. engineered A549 cells to express FLAG-ISG15 which was leveraged to isolate ISGylated proteins from IFN-I-treated cells (49). They identified 168 ISGylation targets of which 24 were biochemically validated. Moreover, the use of A549 instead of HeLa cells elegantly expanded the repertoire of ISG15 targets in epithelial cells. Also during that time, the first ISG15 substrates derived from professional immune cells were uncovered thanks to the lab of Dong-Er Zhang. Here, the authors relied on antibodies raised against human and mouse ISG15 to isolate and map ISG15 substrates in human U937 monocytes and *Usp18*$^{-/-}$ mouse embryonic fibroblast (MEF) cells treated with IFN-I (50). In total, 76 ISGylation targets were discovered of which 21 were found in both human and mouse cells, suggesting a core set of ISGylated proteins shared across different species and cell types. More recently, Care et al. applied the same antibody-based strategy to draft the first catalog of ISG15 substrates in primary human cells (51). The authors investigated how ISG15-conjugation is involved in the maturation of plasmablasts into immunoglobulin-secreting plasma cells. To this end, primary B cells were isolated from human donors, treated with IFN-I and immunoprecipitated with anti-ISG15 antibodies. MS analysis and comparison with control-IP samples revealed 52 ISGylated substrates, several of which are known regulators of B cell maturation.

Nonetheless, the identification of endogenous ISG15 substrates through IP remains suboptimal due to the inefficiency of ISG15 antibodies to enrich for ISGylated proteins (47, 52). As a result, Yan et al. recently developed a novel approach to map ISG15 targets based on adenoviral delivery and stable overexpression of FLAG-ISG15 into primary *Isg15*$^{-/-}$ adipocytes treated with LPS (52). In this way, potent anti-FLAG antibodies could be used to fish for ISGylated proteins, similar to the early screens of Takeuchi and Wong. Following standard IP and MS analysis, the authors eventually identified 527 murine ISG15 substrates, hitherto the highest number of ISGylated proteins reported in a single experiment. One of the reasons for their high coverage is the incorporation of state-of-the-art proteomics tools, including peptide isotopic labeling by Tandem Mass Tags (TMT) and high-resolution orbitrap MS analysis.

Together, these studies made important contributions to the field by expanding the landscape of potential ISGylation functions beyond the scope of microbial infections. Nevertheless, ISG15's antimicrobial activity is still considered as its foremost function which prompted additional proteomics studies in the context of infection. In 2015, Radoshevich et al. demonstrated that ISG15 counteracts infection with the intracellular bacterial pathogen *L. monocytogenes in vitro* and *in vivo* (38). To work out the molecular determinants underlying the antilisterial activity, the authors developed a quantitative proteomics approach to identify ISG15 substrates. Using HeLa cells stably expressing FLAG-His-ISG15, they isolated ISGylated proteins by His pulldown and quantitatively measured the levels of ISG15-conjugates with Stable Isotope Labeling by Amino acids in Cell culture (SILAC). Unlike previous screens where in-gel digestion was used without any isotopic labeling approach, this report was the first to combine contemporary in-solution sample preparation with SILAC-based quantification. With their approach, the authors identified 42 new ISG15 substrates of which two were validated at the endogenous level during *L. monocytogenes* infection. Similarly, Bhushan and colleagues investigated the role of ISGylation signaling during autophagy-mediated growth restriction of intracellular *T. gondii* (41). The authors found that ISG15 is part of the proxisome of the Autophagy Gene 5 (ATG5) where it mediates recruitment of autophagy adaptors to the pathogen-containing vacuole (PV). Accordingly, deletion of ISG15 blocked PV-recruitment which impaired IFN-γ-dependent control of *T. gondii*. To discern the function of ISG15-conjugation during this process, the authors mapped ISG15 substrates in A549 cells upon IFN-γ treatment. Their protocol used A549 cells stably expressing wild-type or non-conjugatable ISG15 (control) that were subjected to ISG15 IP and on-bead trypsin digestion followed by MS analysis. 239 ISGylated proteins were identified, making up the first list of ISGylated proteins induced upon IFN-γ treatment in an epithelial cell line. Finally, one study identified ISG15 substrates during influenza A viral infection (53). Here, A549 cells were cultured in presence or absence (control) of the virus to induce a physiological ISGylation response. After 24h, cells were lysed and ISGylated proteins were pulled down prior to on-bead trypsin digestion and LC-MS/MS analysis. Among 22 ISGylated proteins, the authors picked up the influenza A non-structural protein 1 as a known viral target of ISGylation (54, 55).

Together, just 20 years after the initial discovery of the first ISG15 substrate, MS-based methods led to the successful identification of hundreds of ISGylation substrates in various cell types upon different stimuli. However, many of these studies relied on artificial systems that used ectopic overexpression of ISG15 in cultured cells, leading to overexpression artefacts, and on treatment with IFNs which could induce a stronger ISGylation response than what is physiologically induced during infection. In addition, none of the above screens was able to pinpoint the exact modification site on substrate proteins, making it difficult to investigate how ISG15-conjugation affects the function of the identified substrates.

Proteome-Wide Mapping of ISG15 Modification Sites

To overcome the inability to map ISG15 modification sites and inspired by recent developments in the ubiquitin field, we recently devised a novel approach to study protein ISGylation (56). When trypsin cleaves proteins into peptides, also conjugated ISG15 becomes proteolyzed which leaves a diglycine tag (GG) attached

to the original modified lysine residue. As a result, peptides that were modified by ISG15 can be isolated from the bulk of unmodified peptides using anti-K-ε-GG antibodies. Hence, the modified peptides including the exact site of modification can be identified by LC-MS/MS. Without any further comparison, however, GG peptide pulldown is unable to distinguish ISG15 sites from ubiquitin and NEDD8 sites since trypsin digestion leaves the same diglycine adduct for all three PTMs. One evident solution is to include an *Isg15*$^{-/-}$ control condition where all enriched sites either correspond to NEDD8 or ubiquitin sites. In this way, sites that are uniquely identified in the wild-type correspond to *bona fide* ISG15 sites. Using this comparative approach, we were able to map 930 ISG15 sites on 434 proteins in the liver of mice infected with *L. monocytogenes*, the first study reporting on the proteome-wide identification of ISG15 modification sites, directly in an *in vivo* model of bacterial infection.

Last year, the group of Benedikt Kessler published a similar strategy to map ISG15 modification sites in the chronic myeloid leukemia (CML)-derived cell line HAP1 (57). Here, the authors used *Usp18*$^{-/-}$ cells instead of *Isg15*$^{-/-}$ cells to control for the ubiquitin/NEDD8 signal spillover. Knockout of USP18 as the major deISGylation enzyme leads to massive accumulation of ISGylated proteins after IFN-I treatment. Hence, sites differentially regulated between *Usp18*$^{-/-}$ and wild-type cells correspond to actual ISG15 sites, assuming that ubiquitylation and NEDDylation are not affected in *Usp18*$^{-/-}$ cells. Their approach eventually uncovered 796 ISG15 modification sites on 476 substrate proteins. In addition, the authors validated 110 of the identified targets in the same cellular system by ISG15 IP followed by LC-MS/MS. Together, both approaches led to the joint discovery of 679 USP18-dependent substrates of ISG15.

Finally, a recent proteomics study on ISGylation generated the first list of porcine ISG15 substrates in a porcine alveolar macrophage cell line treated with IFN-I (58). Similar to previous studies, the authors relied on an antibody against porcine ISG15 to isolate ISGylated proteins prior to in-solution digestion and MS analysis. Even without specific enrichment, MS analysis allowed to identify GG-modified peptides and map 190 ISGylation sites on 97 substrate proteins. Evidently, this study demonstrates the capacity of contemporary MS-based proteomics to map ISG15 modification sites directly after ISG15 pulldown, albeit with a lower efficiency compared to standard GG-peptidomics.

COMMON SUBSTRATES AND FUTURE PERSPECTIVES

In the above studies two strategies were used to map ISG15 substrates: i) enrichment of ISGylated proteins on the protein level and ii) pulldown of GG-modified peptides to identify the protein along with the modification site(s) (**Figure 2A**). Together, both strategies led to the discovery of 1,563 ISG15 substrates of which 64 were validated by orthogonal approaches (**Supplementary Table S1**), with a coverage increasing over time thanks to more performant MS technologies and improved methods to study ISG15 (**Figures 2B, C**). For example, GG-peptidomics alone resulted in more identified ISGylation substrates than all previous approaches combined. By looking at the overlap across all screens, 29 ISG15 substrates were identified in half of the studies, suggesting that despite the different species, cell types and strategies employed, there is a degree of selectivity for certain ISG15 substrates (**Figure 2D**). Among these 29 proteins are many metabolic proteins, especially glycolytic enzymes, and ISGs such as STAT1 and IFIT1, in line with previous reports (44, 52, 56, 59).

Aside from protein substrates, three studies additionally uncovered 1,916 ISG15 modification sites (**Supplementary Table S2**). However, unlike SUMOylation (60), these studies did not report any sequence motif that would drive the specificity for ISG15 conjugation (56, 57). We ranked ISG15 substrates based on their number of identified GG sites, which allowed us to highlight the top most modified ISG15 substrates in each study (**Figures 2E–H**). By looking at the overlap, the molecular chaperone HSPA8 and the glycolytic enzyme GAPDH were found as most modified ISG15 substrates. GAPDH was found in six out of fourteen screens, while HSPA8 was found in eleven screens, so far without any further characterization. Likely, ISGylation of these key proteins regulates their activity or interaction state, influencing the cellular processes in which they are involved.

Despite the gain of knowledge through ISG15 site-seeing, studies by Zhang and Pinto-Fernandez relied on genetic approaches with *Isg15*$^{-/-}$ animals or *Usp18*$^{-/-}$ cells to discern *bona fide* ISG15 sites. Since both proteins are regulators of IFN-I signaling, but also other processes (3, 61) (**Figure 1**), their absence could potentially introduce artefacts which might also affect the identification of ISG15 sites. Future studies will need to address this caveat by developing novel genetic approaches that preserve both IFN-I signaling and endogenous ISG15 conjugation. In analogy to strategies employed for the identification of SUMO sites (62, 63), one could envision to mutate ISG15's C-terminal sequence to LRL**K**GG, which after endopeptidase Lys-C digestion will generate ISG15-derived GG-modified peptides that can be specifically enriched and identified by MS. However, such genetic approaches cannot easily be used in a clinical setting.

To overcome the need for genetic approaches and expand the repertoire of applicable samples, alternative approaches could be based on novel antibodies or technologies that combine enzymatic and chemical methods. Unlike trypsin digestion which generates the same GG-modified peptides for ubiquitin, NEDD8 and ISG15, digestion with endopeptidase Lys-C leads to remnants that are specific for each UBL. Hence, antibodies developed against this fragment could be used to fish for ISG15-modified peptides. In the case of ubiquitin, this strategy led to the proteome-wide identification of 63,000 unique modification sites (64). Another elegant strategy would be to include a treatment with USP2 (a ubiquitin-specific protease) ahead of trypsin digestion and GG-peptide enrichment to deplete the sample from ubiquitin-modification sites. Similarly, the specificity of proteases such as USP18 could be leveraged to reveal free lysine residues at ISG15 modification sites available for chemical labeling and enrichment by affinity precipitation

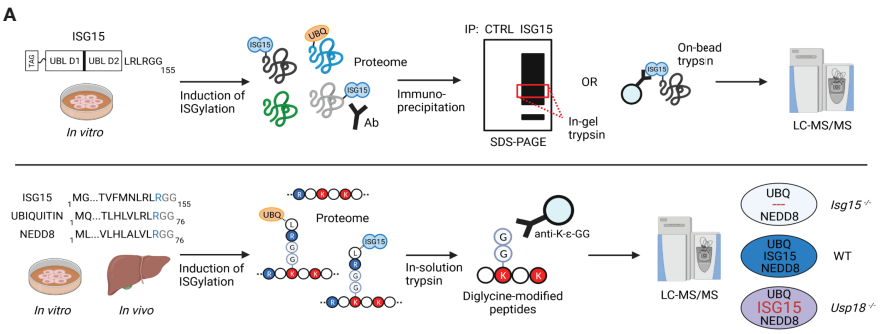

B

Reference	# Substrates	# Sites	Treatment/infection	Organism	Sample type	ISG15 expression	Purification method
Zhao 2005	156	none	IFN-β	human	HeLa cell	His-FLAG-ISG15 overexpression	His PD + FLAG IP
Giannakopoulos 2005[a]	43	none	IFN-α	human	U937 cell	endogenous ISG15	ISG15 IP
Giannakopoulos 2005[b]	52	none	IFN-β	murine	MEF USP18-/- cell	endogenous ISG15	ISG15 IP
Wong 2006	168	none	IFN-β	human	A549 cell	FLAG-ISG15 transduction	FLAG IP
Takeuchi 2006	10	none	untreated	human	HeLa cell	FLAG-ISG15 overexpression	FLAG IP
Radoshevich 2015	42	none	IFN-α; untreated	human	HeLa cell	FLAG-His-ISG15 transduction	His PD
Peng 2016	22	none	Influenza A (H3N2); untreated	human	A549 cell	endogenous ISG15	ISG15 IP
Care 2016	52	none	IFN-α	human	Plasmablast	endogenous ISG15	ISG15 IP
Zhang 2019	434	930	*Listeria monocytogenes*	murine	liver	endogenous ISG15	GG-peptide IP
Bhushan 2020	239	none	IFN-γ	human	A549 cell	HA-ISG15GG/AA transduction	ISG15 IP
Pinto-Fernandez 2020[a]	476	796	IFN-α	human	HAP1 cell	endogenous ISG15	GG-peptide IP
Pinto-Fernandez 2020[b]	313	none	IFN-α	human	HAP1 cell	endogenous ISG15	ISG15 IP
Zhu 2021	97	190	IFN-α	porcine	CRL-2843	endogenous ISG15	ISG15 IP
Yan 2021	527	none	LPS	murine	Beige adipocyte	FLAG-ISG15 transduction	FLAG IP

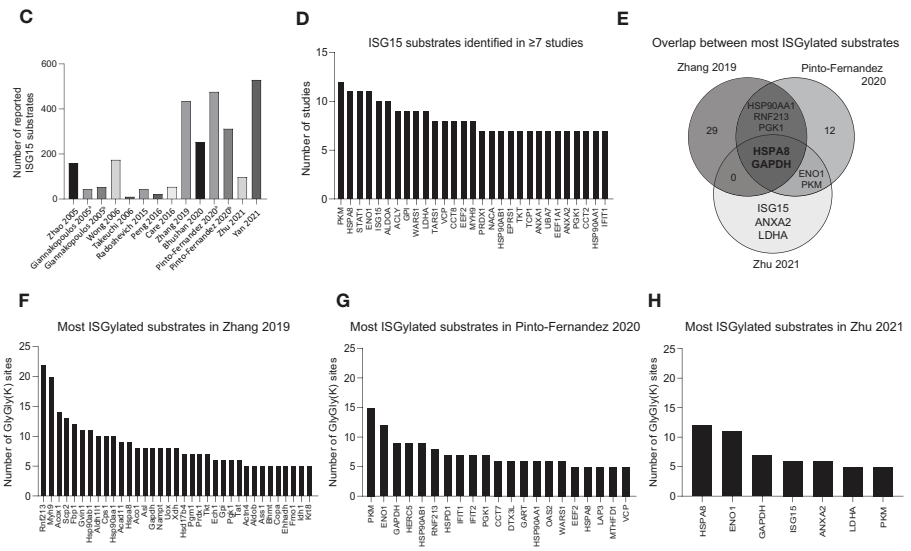

FIGURE 2 | MS-based discovery of ISG15 substrates. **(A)** Commonly used workflows to identify ISG15 substrates by mass spectrometry. Upper panel: many studies rely on pulldown of ISGylated proteins from induced cells using antibodies or resins against endogenous or overexpressed (tagged) ISG15. Pulled down proteins are separated by SDS-PAGE to trypsinize specific gel bands. Alternatively, proteins are digested directly on-bead. In both cases, the released peptides are analyzed by liquid chromatography-tandem mass spectrometry (LC-MS/MS). Non-specific binders can be controlled by parallel analysis of cells expressing no ISG15 or non-conjugatable ISG15 (e.g. ISG15AA) or by using an antibody isotype control. Lower panel: to identify exact sites of ISG15 modification, recent studies applied diglycine (GG) peptide enrichment from induced cells or tissues. Here, trypsin digestion of extracted proteins generates GG-modified peptides derived from conjugated ISG15, ubiquitin or NEDD8. These GG-modified peptides can be captured with specific anti-K-ε-GG antibodies prior to their identification by LC-MS/MS. To distinguish ISG15 modification sites from ubiquitin and NEDD8 sites, genetic controls are included such as *Isg15*$^{-/-}$ mice or *Usp18*$^{-/-}$ cells. Consequently, comparison with a wild-type condition allows to pinpoint *bona fide* ISG15 sites based on their absence in *Isg15*$^{-/-}$ or increased abundance in *Usp18*$^{-/-}$ conditions. Figure created with BioRender.com. **(B)** Overview of MS-based proteomics studies reporting ISG15 substrates, listing relevant information on the number of identified substrates and the experimental design. **(C)** Bar chart showing the increase of identified ISG15 substrates in the different studies over time. **(D)** Bar chart showing 29 ISG15 substrates that were reported in ≥7 studies. **(E)** Venn diagram showing the overlap between the most modified ISG15 substrates listed in panel **(F–H)**. **(F–H)** Bar charts showing the most modified ISG15 substrates (substrates with ≥5 sites) in the three GG-peptidomics screens.

(65) or diagonal chromatography (66). Beyond label-free quantification, improvements in quantification methods also have the potential to increase site identification by GG-peptidomics, as demonstrated by the incorporation of SILAC and TMT-labeling in several ubiquitin studies (67, 68).

AUTHOR CONTRIBUTIONS

FT and DE wrote the manuscript. DE conceived **Figure 1**. FT conceived **Figure 2** and the supplementary tables. FI supervised FT and DE and edited the manuscript. All authors contributed to the article and approved the submitted version.

FUNDING

FI acknowledges funding from Odysseus grant G0F8616N from the Research Foundation Flanders (FWO) and ERANET Infect-ERA BacVIRISG15. DE is supported by the FWO PhD fellowship 1167221N for fundamental research.

SUPPLEMENTARY MATERIAL

The Supplementary Material for this article can be found online at: https://www.frontiersin.org/articles/10.3389/fimmu.2021.720765/full#supplementary-material

REFERENCES

1. Perng YC, Lenschow DJ. ISG15 in Antiviral Immunity and Beyond. *Nat Rev Microbiol* (2018) 16(7):423–39. doi: 10.1038/s41579-018-0020-5
2. Speer SD, Li Z, Buta S, Payelle-Brogard B, Qian L, Vigant F, et al. ISG15 Deficiency and Increased Viral Resistance in Humans But Not Mice. *Nat Commun* (2016) 7:11496. doi: 10.1038/ncomms11496
3. Zhang X, Bogunovic D, Payelle-Brogard B, Francois-Newton V, Speer SD, Yuan C, et al. Human Intracellular ISG15 Prevents Interferon-Alpha/Beta Over-Amplification and Auto-Inflammation. *Nature* (2015) 517(7532):89–93. doi: 10.1038/nature13801
4. Bogunovic D, Byun M, Durfee LA, Abhyankar A, Sanal O, Mansouri D, et al. Mycobacterial Disease and Impaired IFN-Gamma Immunity in Humans With Inherited ISG15 Deficiency. *Sci (New York N.Y.)* (2012) 337 (6102):1684–8. doi: 10.1126/science.1224026
5. Swaim CD, Scott AF, Canadeo LA, Huibregtse JM. Extracellular ISG15 Signals Cytokine Secretion Through the LFA-1 Integrin Receptor. *Mol Cell* (2017) 68(3):581–90.e5. doi: 10.1016/j.molcel.2017.10.003
6. Malakhov MP, Malakhova OA, Kim KI, Ritchie KJ, Zhang DE. UBP43 (USP18) Specifically Removes ISG15 From Conjugated Proteins. *J Biol Chem* (2002) 277(12):9976–81. doi: 10.1074/jbc.M109078200
7. Malakhova OA, Kim KI, Luo JK, Zou W, Kumar KG, Fuchs SY, et al. UBP43 is a Novel Regulator of Interferon Signaling Independent of Its ISG15 Isopeptidase Activity. *EMBO J* (2006) 25(11):2358–67. doi: 10.1038/sj.emboj.7601149
8. Arimoto KI, Lochte S, Stoner SA, Burkart C, Zhang Y, Miyauchi S, et al. STAT2 is an Essential Adaptor in USP18-Mediated Suppression of Type I Interferon Signaling. *Nat Struct Mol Biol* (2017) 24(3):279–89. doi: 10.1038/nsmb.3378
9. Freitas BT, Scholte FEM, Bergeron E, Pegan SD. How ISG15 Combats Viral Infection. *Virus Res* (2020) 286:198036. doi: 10.1016/j.virusres.2020.198036
10. Swaim CD, Canadeo LA, Monte KJ, Khanna S, Lenschow DJ, Huibregtse JM. Modulation of Extracellular ISG15 Signaling by Pathogens and Viral Effector Proteins. *Cell Rep* (2020) 31(11):107772. doi: 10.1016/j.celrep.2020.107772
11. Knight E Jr, Cordova B. IFN-Induced 15-kDa Protein is Released From Human Lymphocytes and Monocytes. *J Immunol (Baltimore Md.: 1950)* (1991) 146(7):2280–4.
12. Ostvik AE, Svendsen TD, Granlund AVB, Doseth B, Skovdahl HK, Bakke I, et al. Intestinal Epithelial Cells Express Immunomodulatory ISG15 During Active Ulcerative Colitis and Crohn's Disease. *J Crohns Colitis* (2020) 14 (7):920–34. doi: 10.1093/ecco-jcc/jjaa022
13. Dos Santos PF, Mansur DS. Beyond ISGlylation: Functions of Free Intracellular and Extracellular Isg15. *J Interferon Cytokine Res* (2017) 37 (6):246–53. doi: 10.1089/jir.2016.0103
14. Yuan W, Krug RM. Influenza B Virus NS1 Protein Inhibits Conjugation of the Interferon (IFN)-Induced Ubiquitin-Like ISG15 Protein. *EMBO J* (2001) 20 (3):362–71. doi: 10.1093/emboj/20.3.362
15. Kim KI, Giannakopoulos NV, Virgin HW, Zhang DE. Interferon-Inducible Ubiquitin E2, Ubc8, is a Conjugating Enzyme for Protein ISGylation. *Mol Cell Biol* (2004) 24(21):9592–600. doi: 10.1128/MCB.24.21.9592-9600.2004
16. Dastur A, Beaudenon S, Kelley M, Krug RM, Huibregtse JM. Herc5, an Interferon-Induced HECT E3 Enzyme, is Required for Conjugation of ISG15 in Human Cells. *J Biol Chem* (2006) 281(7):4334–8. doi: 10.1074/jbc.M512830200
17. Zou W, Zhang DE. The Interferon-Inducible Ubiquitin-Protein Isopeptide Ligase (E3) EFP Also Functions as an ISG15 E3 Ligase. *J Biol Chem* (2006) 281 (7):3989–94. doi: 10.1074/jbc.M510787200
18. Okumura F, Zou W, Zhang DE. ISG15 Modification of the Eif4e Cognate 4EHP Enhances Cap Structure-Binding Activity of 4EHP. *Genes Dev* (2007) 21(3):255–60. doi: 10.1101/gad.1521607
19. Basters A, Geurink PP, El Oualid F, Ketscher L, Casutt MS, Krause E, et al. Molecular Characterization of Ubiquitin-Specific Protease 18 Reveals Substrate Specificity for Interferon-Stimulated Gene 15. *FEBS J* (2014) 281 (7):1918–28. doi: 10.1111/febs.12754
20. Villarroya-Beltri C, Guerra S, Sanchez-Madrid F. ISGylation - a Key to Lock the Cell Gates for Preventing the Spread of Threats. *J Cell Sci* (2017) 130 (18):2961–9. doi: 10.1242/jcs.205468
21. Villarroya-Beltri C, Baixauli F, Mittelbrunn M, Fernandez-Delgado I, Torralba D, Moreno-Gonzalo O, et al. ISGylation Controls Exosome Secretion by Promoting Lysosomal Degradation of MVB Proteins. *Nat Commun* (2016) 7:13588. doi: 10.1038/ncomms13588
22. Park JH, Yang SW, Park JM, Ka SH, Kim JH, Kong YY, et al. Positive Feedback Regulation of P53 Transactivity by DNA Damage-Induced ISG15 Modification. *Nat Commun* (2016) 7:12513. doi: 10.1038/ncomms12513
23. Raso MC, Djoric N, Walser F, Hess S, Schmid FM, Burger S, et al. Interferon-Stimulated Gene 15 Accelerates Replication Fork Progression Inducing Chromosomal Breakage. *J Cell Biol* (2020) 219(8):e202002175. doi: 10.1083/jcb.202002175
24. Lou Z, Wei J, Riethman H, Baur JA, Voglauer R, Shay JW, et al. Telomere Length Regulates ISG15 Expression in Human Cells. *Aging (Albany NY)* (2009) 1(7):608–21. doi: 10.18632/aging.100066
25. Xu D, Zhang T, Xiao J, Zhu K, Wei R, Wu Z, et al. Modification of BECN1 by ISG15 Plays a Crucial Role in Autophagy Regulation by Type I IFN/Interferon. *Autophagy* (2015) 11(4):617–28. doi: 10.1080/15548627.2015.1023982
26. Nakashima H, Nguyen T, Goins WF, Chiocca EA. Interferon-Stimulated Gene 15 (ISG15) and ISG15-Linked Proteins can Associate With Members of the Selective Autophagic Process, Histone Deacetylase 6 (HDAC6) and SQSTM1/P62. *J Biol Chem* (2015) 290(3):1485–95. doi: 10.1074/jbc.M114.593871
27. Nakka VP, Lang BT, Lenschow DJ, Zhang DE, Dempsey RJ, Vemuganti R. Increased Cerebral Protein ISGylation After Focal Ischemia Is Neuroprotective. *J Cereb Blood Flow Metab* (2011) 31(12):2375–84. doi: 10.1038/jcbfm.2011.103
28. Yeh YH, Yang YC, Hsieh MY, Yeh YC, Li TK. A Negative Feedback of the HIF-1alpha Pathway *via* Interferon-Stimulated Gene 15 and ISGylation. *Clin Cancer Res* (2013) 19(21):5927–39. doi: 10.1158/1078-0432.CCR-13-0018
29. Durfee LA, Lyon N, Seo K, Huibregtse JM. The ISG15 Conjugation System Broadly Targets Newly Synthesized Proteins: Implications for the Antiviral

Function of ISG15. *Mol Cell* (2010) 38(5):722–32. doi: 10.1016/j.molcel.2010.05.002
30. Lenschow DJ, Lai C, Frias-Staheli N, Giannakopoulos NV, Lutz A, Wolff T, et al. IFN-Stimulated Gene 15 Functions as a Critical Antiviral Molecule Against Influenza, Herpes, and Sindbis Viruses. *Proc Natl Acad Sci USA* (2007) 104(4):1371–6. doi: 10.1073/pnas.0607038104
31. Rodriguez MR, Monte K, Thackray LB, Lenschow DJ. ISG15 Functions as an Interferon-Mediated Antiviral Effector Early in the Murine Norovirus Life Cycle. *J Virol* (2014) 88(16):9277–86. doi: 10.1128/JVI.01422-14
32. Rahnefeld A, Klingel K, Schuermann A, Diny NL, Althof N, Lindner A, et al. Ubiquitin-Like Protein ISG15 (Interferon-Stimulated Gene of 15 kDa) in Host Defense Against Heart Failure in a Mouse Model of Virus-Induced Cardiomyopathy. *Circulation* (2014) 130(18):1589–600. doi: 10.1161/CIRCULATIONAHA.114.009847
33. Yang X, Chen X, Bian G, Tu J, Xing Y, Wang Y, et al. Proteolytic Processing, Deubiquitinase and Interferon Antagonist Activities of Middle East Respiratory Syndrome Coronavirus Papain-Like Protease. *J Gen Virol* (2014) 95(Pt 3):614–26. doi: 10.1099/vir.0.059014-0
34. Lindner HA, Lytvyn V, Qi H, Lachance P, Ziomek E, Menard R. Selectivity in ISG15 and Ubiquitin Recognition by the SARS Coronavirus Papain-Like Protease. *Arch Biochem Biophys* (2007) 466(1):8–14. doi: 10.1016/j.abb.2007.07.006
35. Chang YG, Yan XZ, Xie YY, Gao XC, Song AX, Zhang DE, et al. Different Roles for Two Ubiquitin-Like Domains of ISG15 in Protein Modification. *J Biol Chem* (2008) 283(19):13370–7. doi: 10.1074/jbc.M800162200
36. Shin D, Mukherjee R, Grewe D, Bojkova D, Baek K, Bhattacharya A, et al. Papain-Like Protease Regulates SARS-CoV-2 Viral Spread and Innate Immunity. *Nature* (2020) 587(7835):657–62. doi: 10.1038/s41586-020-2601-5
37. Liu G, Lee JH, Parker ZM, Acharya D, Chiang JJ, van Gent M, et al. ISG15-Dependent Activation of the Sensor MDA5 Is Antagonized by the SARS-CoV-2 Papain-Like Protease to Evade Host Innate Immunity. *Nat Microbiol* (2021) 6(4):467–78. doi: 10.1038/s41564-021-00884-1
38. Radoshevich L, Impens F, Ribet D, Quereda JJ, Nam Tham T, Nahori MA, et al. ISG15 Counteracts Listeria Monocytogenes Infection. *Elife* (2015) 4:e06848. doi: 10.7554/eLife.06848
39. Kimmey JM, Campbell JA, Weiss LA, Monte KJ, Lenschow DJ, Stallings CL. The Impact of ISGylation During Mycobacterium Tuberculosis Infection in Mice. *Microb Infect* (2017) 19(4-5):249–58. doi: 10.1016/j.micinf.2016.12.006
40. Gao N, Me R, Dai C, Yu FX. ISG15 Acts as a Mediator of Innate Immune Response to Pseudomonas Aeruginosa Infection in C57BL/6J Mouse Corneas. *Invest Ophthalmol Vis Sci* (2020) 61(5):26. doi: 10.1167/iovs.61.5.26
41. Bhushan J, Radke JB, Perng YC, McAllaster M, Lenschow DJ, Virgin HW, et al. ISG15 Connects Autophagy and IFN-Gamma-Dependent Control of Toxoplasma Gondii Infection in Human Cells. *mBio* (2020) 11(5):e00852–20. doi: 10.1128/mBio.00852-20
42. Real CI, Megger DA, Sitek B, Jahn-Hofmann K, Ickenstein LM, John MJ, et al. Identification of Proteins That Mediate the Pro-Viral Functions of the Interferon Stimulated Gene 15 in Hepatitis C Virus Replication. *Antiviral Res* (2013) 100(3):654–61. doi: 10.1016/j.antiviral.2013.10.009
43. Baldanta S, Fernandez-Escobar M, Acin-Perez R, Albert M, Camafeita E, Jorge I, et al. ISG15 Governs Mitochondrial Function in Macrophages Following Vaccinia Virus Infection. *PloS Pathog* (2017) 13(10):e1006651. doi: 10.1371/journal.ppat.1006651
44. Kespohl M, Bredow C, Klingel K, Voss M, Paeschke A, Zickler M, et al. Protein Modification With ISG15 Blocks Coxsackievirus Pathology by Antiviral and Metabolic Reprogramming. *Sci Adv* (2020) 6(11):eaay1109. doi: 10.1126/sciadv.aay1109
45. Hamerman JA, Hayashi F, Schroeder LA, Gygi SP, Haas AL, Hampson L, et al. Serpin 2a is Induced in Activated Macrophages and Conjugates to a Ubiquitin Homolog. *J Immunol* (2002) 168(5):2415–23. doi: 10.4049/jimmunol.168.5.2415
46. Malakhov MP, Kim KI, Malakhova OA, Jacobs BS, Borden EC, Zhang DE. High-Throughput Immunoblotting. Ubiquitiin-Like Protein ISG15 Modifies Key Regulators of Signal Transduction. *J Biol Chem* (2003) 278(19):16608–13. doi: 10.1074/jbc.M208435200
47. Zhao C, Denison C, Huibregtse JM, Gygi S, Krug RM. Human ISG15 Conjugation Targets Both IFN-Induced and Constitutively Expressed Proteins Functioning in Diverse Cellular Pathways. *Proc Natl Acad Sci USA* (2005) 102(29):10200–5. doi: 10.1073/pnas.0504754102
48. Takeuchi T, Inoue S, Yokosawa H. Identification and Herc5-Mediated ISGylation of Novel Target Proteins. *Biochem Biophys Res Commun* (2006) 348(2):473–7. doi: 10.1016/j.bbrc.2006.07.076
49. Wong JJ, Pung YF, Sze NS, Chin KC. HERC5 Is an IFN-Induced HECT-Type E3 Protein Ligase That Mediates Type I IFN-Induced ISGylation of Protein Targets. *Proc Natl Acad Sci USA* (2006) 103(28):10735–40. doi: 10.1073/pnas.0600397103
50. Giannakopoulos NV, Luo JK, Papov V, Zou W, Lenschow DJ, Jacobs BS, et al. Proteomic Identification of Proteins Conjugated to ISG15 in Mouse and Human Cells. *Biochem Biophys Res Commun* (2005) 336(2):496–506. doi: 10.1016/j.bbrc.2005.08.132
51. Care MA, Stephenson SJ, Barnes NA, Fan I, Zougman A, El-Sherbiny YM, et al. Network Analysis Identifies Proinflammatory Plasma Cell Polarization for Secretion of ISG15 in Human Autoimmunity. *J Immunol* (2016) 197(4):1447–59. doi: 10.4049/jimmunol.1600624
52. Yan S, Kumari M, Xiao H, Jacobs C, Kochumon S, Jedrychowski M, et al. IRF3 Reduces Adipose Thermogenesis *via* ISG15-Mediated Reprogramming of Glycolysis. *J Clin Invest* (2021) 131(7):e144888. doi: 10.1172/JCI144888
53. Peng Q, Wang Z, Wu D, Li X, Liu X, Sun W, et al. Analysis of ISG15-Modified Proteins From A549 Cells in Response to Influenza Virus Infection by Liquid Chromatography-Tandem Mass Spectrometry. *Chin J Analytical Chem* (2016) 44(6):850–6. doi: 10.1016/S1872-2040(16)60936-2
54. Tang Y, Zhong G, Zhu L, Liu X, Shan Y, Feng H, et al. Herc5 Attenuates Influenza A Virus by Catalyzing ISGylation of Viral NS1 Protein. *J Immunol* (2010) 184(10):5777–90. doi: 10.4049/jimmunol.0903588
55. Zhao C, Hsiang TY, Kuo RL, Krug RM. ISG15 Conjugation System Targets the Viral NS1 Protein in Influenza A Virus-Infected Cells. *Proc Natl Acad Sci USA* (2010) 107(5):2253–8. doi: 10.1073/pnas.0909144107
56. Zhang Y, Thery F, Wu NC, Luhmann EK, Dussurget O, Foecke M, et al. The *In Vivo* ISGylome Links ISG15 to Metabolic Pathways and Autophagy Upon Listeria Monocytogenes Infection. *Nat Commun* (2019) 10(1):5383. doi: 10.1038/s41467-019-13393-x
57. Pinto-Fernandez A, Salio M, Partridge T, Chen J, Vere G, Greenwood H, et al. Deletion of the Deisgylating Enzyme USP18 Enhances Tumour Cell Antigenicity and Radiosensitivity. *Br J Cancer* (2021) 124(4):817–30. doi: 10.1038/s41416-020-01167-y
58. Zhu C, Li J, Tian C, Qin M, Wang Z, Shi B, et al. Proteomic Analysis of ISGylation in Immortalized Porcine Alveolar Macrophage Cell Lines Induced by Type I Interferon. *Vaccines (Basel)* (2021) 9(2):164. doi: 10.3390/vaccines9020164
59. Ganesan M, Poluektova LY, Tuma DJ, Kharbanda KK, Osna NA. Acetaldehyde Disrupts Interferon Alpha Signaling in Hepatitis C Virus-Infected Liver Cells by Up-Regulating Usp18. *Alcohol Clin Exp Res* (2016) 40(11):2329–38. doi: 10.1111/acer.13226
60. Hendriks IA, Vertegaal AC. A Comprehensive Compilation of SUMO Proteomics. *Nat Rev Mol Cell Biol* (2016) 17(9):581–95. doi: 10.1038/nrm.2016.81
61. Goldmann T, Zeller N, Raasch J, Kierdorf K, Frenzel K, Ketscher L, et al. USP18 Lack in Microglia Causes Destructive Interferonopathy of the Mouse Brain. *EMBO J* (2015) 34(12):1612–29. doi: 10.15252/embj.201490791
62. Impens F, Radoshevich L, Cossart P, Ribet D. Mapping of SUMO Sites and Analysis of SUMOylation Changes Induced by External Stimuli. *Proc Natl Acad Sci USA* (2014) 111(34):12432–7. doi: 10.1073/pnas.1413825111
63. Tammsalu T, Matic I, Jaffray EG, Ibrahim AF, Tatham MH, Hay RT. Proteome-Wide Identification of SUMO Modification Sites by Mass Spectrometry. *Nat Protoc* (2015) 10(9):1374–88. doi: 10.1038/nprot.2015.095
64. Akimov V, Barrio-Hernandez I, Hansen SVF, Hallenborg P, Pedersen AK, Bekker-Jensen DB, et al. UbiSite Approach for Comprehensive Mapping of Lysine and N-Terminal Ubiquitination Sites. *Nat Struct Mol Biol* (2018) 25(7):631–40. doi: 10.1038/s41594-018-0084-y
65. Hendriks IA, D'Souza RC, Chang JG, Mann M, Vertegaal AC. System-Wide Identification of Wild-Type SUMO-2 Conjugation Sites. *Nat Commun* (2015) 6:7289. doi: 10.1038/ncomms8289

66. Stes E, Laga M, Walton A, Samyn N, Timmerman E, De Smet I, et al. A COFRADIC Protocol to Study Protein Ubiquitination. *Proteome Res* (2014) 13(6):3107–13. doi: 10.1021/pr4012443
67. Udeshi ND, Mani DR, Eisenhaure T, Mertins P, Jaffe JD, Clauser KR, et al. Methods for Quantification of *In Vivo* Changes in Protein Ubiquitination Following Proteasome and Deubiquitinase Inhibition. *Mol Cell Proteomics* (2012) 11(5):148–59. doi: 10.1074/mcp.M111.016857
68. Udeshi ND, Mani DC, Satpathy S, Fereshetian S, Gasser JA, Svinkina T, et al. Rapid and Deep-Scale Ubiquitylation Profiling for Biology and Translational Research. *Nat Commun* (2020) 11(1):359. doi: 10.1038/s41467-019-14175-1

Conflict of Interest: The authors declare that the research was conducted in the absence of any commercial or financial relationships that could be construed as a potential conflict of interest.

Publisher's Note: All claims expressed in this article are solely those of the authors and do not necessarily represent those of their affiliated organizations, or those of the publisher, the editors and the reviewers. Any product that may be evaluated in this article, or claim that may be made by its manufacturer, is not guaranteed or endorsed by the publisher.

frontiers in Immunology

ORIGINAL RESEARCH
published: 17 August 2021
doi: 10.3389/fimmu.2021.695331

NEDD8 Deamidation Inhibits Cullin RING Ligase Dynamics

*Priyesh Mohanty, Kiran Sankar Chatterjee and Ranabir Das**

National Center for Biological Sciences, Tata Institute of Fundamental Research (TIFR), Bangalore, India

Cullin-RING ligases (CRLs) are a significant subset of Ubiquitin E3 ligases that regulate multiple cellular substrates involved in innate immunity, cytoskeleton modeling, and cell cycle. The glutamine deamidase Cycle inhibitory factor (Cif) from enteric bacteria inactivates CRLs to modulate these processes in the host cell. The covalent attachment of a Ubiquitin-like protein NEDD8 catalytically activates CRLs by driving conformational changes in the Cullin C-terminal domain (CTD). NEDDylation results in a shift from a compact to an open CTD conformation through non-covalent interactions between NEDD8 and the WHB subdomain of CTD, eliminating the latter's inhibitory interactions with the RING E3 ligase-Rbx1/2. It is unknown whether the non-covalent interactions are sufficient to stabilize Cullin CTD's catalytic conformation. We studied the dynamics of Cullin-CTD in the presence and absence of NEDD8 using atomistic molecular dynamics (MD) simulations. We uncovered that NEDD8 engages in non-covalent interactions with 4HB/αβ subdomains in Cullin-CTD to promote open conformations. Cif deamidates glutamine 40 in NEDD8 to inhibit the conformational change in CRLs by an unknown mechanism. We investigated the effect of glutamine deamidation on NEDD8 and its interaction with the WHB subdomain post-NEDDylation using MD simulations and NMR spectroscopy. Our results suggest that deamidation creates a new intramolecular salt bridge in NEDD8 to destabilize the NEDD8/WHB complex and reduce CRL activity.

Keywords: bacterial effector, deamidation, protein dynamics (molecular dynamics), NMR spectroscopy, Cullin RING E3 ligases, enteropathogenic *E. coli*, cycle inhibitory factor

OPEN ACCESS

Edited by:
Éric Bergeron, Centers for Disease Control and Prevention (CDC), United States

Reviewed by:
Kevin Haubrich, University of Dundee, United Kingdom
Chen Wang, China Pharmaceutical University, China

****Correspondence:***
Ranabir Das
rana@ncbs.res.in

Specialty section:
This article was submitted to Molecular Innate Immunity, a section of the journal Frontiers in Immunology

Received: *14 April 2021*
Accepted: *29 July 2021*
Published: *17 August 2021*

Citation:
Mohanty P, Chatterjee KS and Das R (2021) NEDD8 Deamidation Inhibits Cullin RING Ligase Dynamics. Front. Immunol. 12:695331. doi: 10.3389/fimmu.2021.695331

INTRODUCTION

Ubiquitination is a post-translational modification that involves the sequential transfer of Ubiquitin (Ub) by E1, E2, and E3 enzymes onto the lysine residue of a substrate protein or another Ub molecule. E3 ligases catalyze the transfer of Ub from the E2~Ub thioester conjugate to the substrate. E3 may belong to RING or HECT classes. RING-E3s (~600) use a RING domain to catalyze the Ub transfer from the E2~Ub thioester onto the substrate lysine (1). A significant subset of RING E3 ligases (25-30%), known as Cullin-RING ligases (CRLs), tightly regulates the levels of various cellular substrates (2). CRLs are large, multi-modular machines comprising of an N-terminal domain ($Cullin^{NTD}$) for substrate recognition and a C-terminal domain ($Cullin^{CTD}$) to associate with the RING ligase Rbx1/2 (3). CRLs require the covalent attachment of a Ub-like protein - NEDD8, for catalytic activation (4, 5). The NEDDylation effect can be reversed by the COP9 signalosome, which cleaves NEDD8 to regulate CRL activity (6).

Crystal structures suggest that NEDDylation promotes the Cullin^{CTD} transition from a closed, inactive state to an open, active state (7). Rbx1/2 interacts with the Winged-helix B subdomain (WHB^{SD}) of Cullin^{CTD} in the closed, inactive form. Post-NEDDylation, NEDD8 engages in non-covalent interactions with the WHB^{SD} and masks its interaction with Rbx1/2. Moreover, it also triggers a domain rotation WHB^{SD} to promote interactions between WHB^{SD} and the four-helix bundle subdomain (4HB^{SD}). Consequently, the Rbx RING domain (Rbx^{RING}) transitions from a compact to an extended catalytic conformation (**Figure 1**). In silico models have proposed that in the full-length NEDDylated-Cullin, NEDD8 and Cullin^{NTD} may also interact (7). A recent structure of full-length, NEDDylated-CRL bound to E2~Ub conjugate reveals that NEDD8 interacts with Cullin^{NTD}, Cullin^{CTD}, and the E2~Ub to nucleate an active CRL/E2~Ub complex (8). However, the interaction dynamics between NEDD8 and Cullin in the absence of E2~Ub are unknown. These interactions are fundamental to the NEDD8-induced conformational change in CRL, which is the precursor to E2~Ub binding and activity.

Secreted bacterial effectors optimize the host cellular environment for replication. Glutamine deamidases convert glutamine to glutamate in their substrate proteins (9). The deamidase Cycle Inhibiting Factor (Cif) secreted by enteropathogenic *E. Coli* specifically deamidates the glutamine at position 40 (Q40) in NEDD8 to convert it to glutamate (10, 11). CRL facilitate the proteasomal degradation of CDK inhibitors p21/27, promoting timely progression through the G1/S and G2/M transition points of the eukaryotic cell cycle (2). Deamidated-NEDD8 (dNEDD8) drastically lowers the

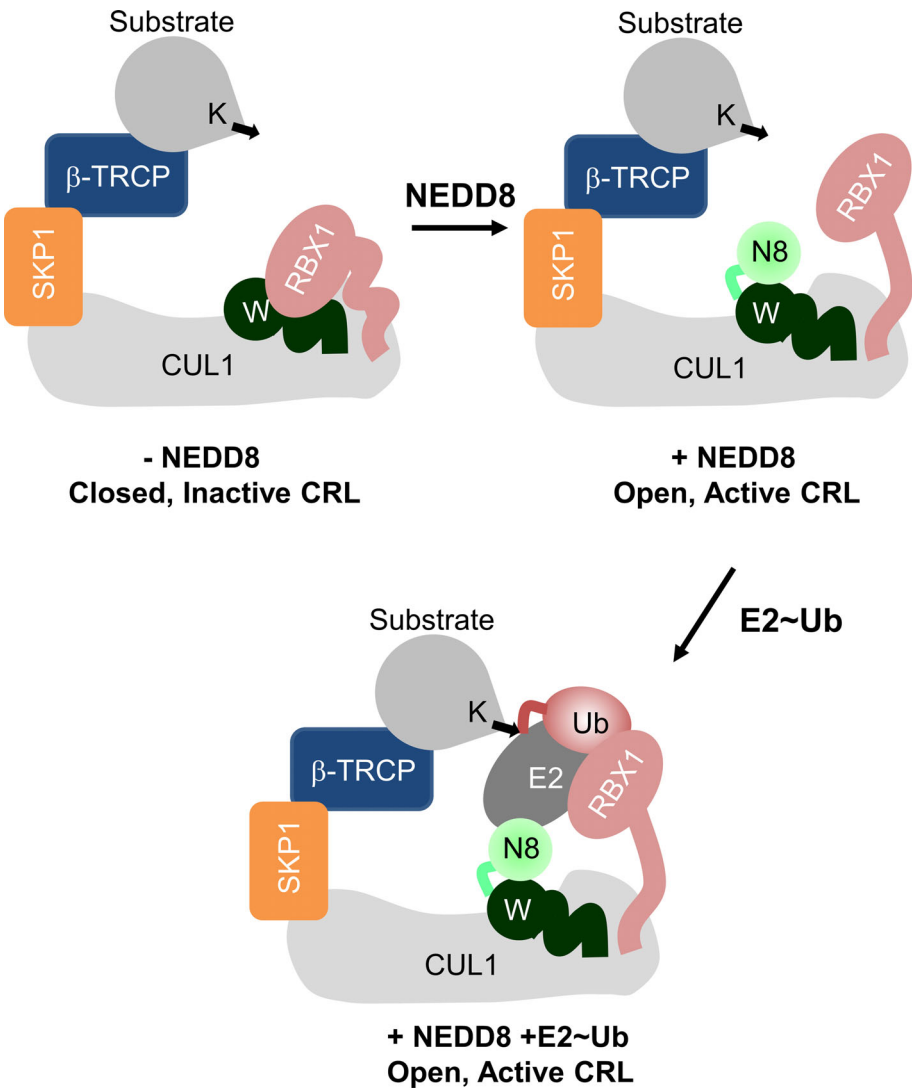

FIGURE 1 | Role of NEDD8 in the activation of Cullin RING ligases. Schematic illustration showing the mechanism of Cullin RING ligase activation by NEDDylation. Conjugation of NEDD8 (N8) to the WHB^{SD} (W) triggers a change in its orientation which frees the Rbx^{RING} domain from inhibitory interactions.

polyubiquitination activity of CRLs and blocks p21/p27 degradation, leading to cell cycle arrest (10). The Cullin family of E3 ligases also regulates the IκBα ubiquitination and degradation, activating the NFκB inflammatory responses (12). Cullin inhibition by NEDD8 deamidation could be instrumental in depleting the host inflammatory response. Cross-linking and Mass spectrometry experiments indicate that dNEDD8 prevents structural reconfiguration of Cullin^{CTD} necessary for CRL activation (13). A recent NEDD8~CUL1/Substrate/E2~Ub structure postulated that deamidation destabilizes the NEDD8/WHB^{SD} interface (8). A thorough understanding of how dNEDD8 prevents the structural reconfiguration in Cullin^{CTD} is currently lacking.

We report (i) NEDD8's role in promoting Cullin-Rbx1 open/catalytic conformations and (ii) the mechanistic basis behind CRL inactivation by dNEDD8, using all-atom MD simulations and NMR spectroscopy. The NEDDylated-Cul5^{CTD} open conformation is stabilized by transient interactions between NEDD8 and 4HB/αβ-subdomains of Cullin^{CTD}. NEDD8/Cullin^{CTD} interactions inhibit WHB^{SD}'s tendency to associate with the Rbx1^{RING} domain and stabilize the closed conformation. NEDD8 deamidation results in an intramolecular salt-bridge formation, which competes with intermolecular interactions formed during NEDD8/WHB^{SD} association. Consequently, the dNEDD8/WHB^{SD} complex is unstable, and dNEDD8 cannot induce the CRL open/active conformation. Overall, this study provides valuable atomistic insights into NEDD8's role in maintaining CRLs in an active conformation and the mechanism underlying its inhibition by bacterial deamidation.

METHODS

Starting Structures and Molecular Modeling

Starting structures for MD simulations were obtained from the Protein Data Bank (PDB). Structures for closed and open conformations of Cul5^{CTD}-Rbx1 were PDB id: 3DPL (chain: C/R) and PDB id: 3DQV (chain: A/B/C), respectively. The structure for dNEDD8 was taken from PDB id: 1NDD. Complexes of NEDD8~Cul1/5-WHB^{SD} were obtained from PDB id: 6TTU (Chain: C/N) and PDB id: 3DQV (Chain: A/C), respectively. NEDD8~Cul1-WHB^{SD} extended conformation was modeled from PDB id: 4P50 (chain A/K). Glutamine to glutamate substitutions in NEDD8 was introduced by replacing existing sidechains with best aligning rotamers from the Dunbrack rotamer library (14) in UCSF Chimera (15).

MD Simulation Protocol

All systems except the extended conformation of NEDD8~Cul1-WHB^{SD} were parameterized using the AMBER99SB*-ILDN force field (16–18) with CUFIX (19–22) corrections. For extended NEDD8~Cul1-WHB^{SD}, the AMBER99SBws (23) were used to prevent overestimation of protein-protein interactions and improve conformational sampling. All simulations were performed using the Gromacs 5.1.2 package (24, 25). Zinc coordination sites in the Rbx1^{RING} domain were modeled based on the Zinc AMBER force field (26) (ZAFF). The isopeptide bond between NEDD8-G76 and Cul1^{CTD}-K721/Cul5^{CTD}-K724 was modeled based on peptide bond parameters inAMBER99.

The starting structures were solvated in suitable cubic boxes by adding TIP3P/TIP4P2005 water molecules and 0.1 M NaCl. Cul5CTD-Rbx1 structures (closed/open) were simulated in a rhombic dodecahedral box with an edge length of 14.2 nm. dNEDD8 was simulated in a cubic box with an edge length of 6.5 nm. NEDD8/Cul1-WHB^{SD} association simulations were performed in a cubic box with an edge length of 12.0 nm. NEDD8~Cul1-WHB^{SD} complex variants were simulated in rectangular boxes with dimensions (nm): 9 x 8 x 8. Counter ions were added to neutralize the residual charge of the system. The electrically neutral system was then subjected to energy minimization using the steepest descent method for a maximum of 5000 steps until the maximum force on any atom was <1000 kJ mol^{-1}nm^{-1}.

Temperature and pressure equilibration was performed with harmonic positional restraints on all heavy protein atoms (k=1000 kJ mol^{-1}nm^{-1}) using periodic boundary conditions. Production MD simulations were carried out at 300 K and 1 bar pressure (NPT ensemble). Temperature control was achieved using the Berendsen thermostat (27) with a coupling constant (τt) of 2.0 ps. The Parrinello-Rahman barostat (28) was employed for pressure control using a coupling constant (τp) of 5 ps. All bond lengths were constrained using the LINCS (Hess, 2008) algorithm. Virtual interaction sites (29) were employed for hydrogen atoms, which permitted a 4 fs time step. The mass of water oxygen was reduced from 16 to 2 amu to improve sampling efficiency. Short-range electrostatics and van der Waals interactions were calculated using a 1.2 nm cutoff. Long-range electrostatics were calculated using Particle Mesh Ewald (30, 31) summation. SMD simulations of NEDD8~Cul5-WHB^{SD}~NEDD8 complexes were carried out in a rectangular box of dimensions (nm): 12 x 9 x 9. Dissociation of the complexes was performed for 16 ns at a pull rate of 0.25 nm ns^{-1} using a moving harmonic potential (force constant = 1500 kJ mol^{-1} nm^{-2}) applied to the NEDD8 (aa:1-70) COM. The COM motion of WHB^{SD} was removed every 100 fs to promote the build-up of the unbinding force.

Structure and MD Trajectory Analysis

Nonbonded interactions in crystal structures were identified using the contact analysis tool in UCSF chimera. MD trajectories were analyzed using analysis tools available within the Gromacs package. Conventional MD trajectories were analyzed for snapshots saved at 200/240 ps intervals. 'gmx gyrate' was used to calculate the radius of gyration for various Cullin^{CTD}-Rbx1 complexes. Inter-atomic distances and the number of contacts were analyzed using the 'gmx mindist.' 'gmx hbond' script was used to analyze hydrogen bonds. For SMD trajectories, force and COM separation values were recorded every 4 ps. Mean Force-time and work-time profiles

were calculated over twelve independent trajectories to obtain mean F_{max} and W for enforced dissociation. Two-dimensional free energy landscapes for $Cul5^{CTD}$-Rbx1 with and without NEDD8 were computed using a bin width of 0.03 nm, and the normalized free energy (ΔG) for each bin was determined using the relation:

$$\Delta G(R1, R2) = -k_B T [ln\ P_i - ln\ P_{max}],$$

where R1/R2 are reaction coordinates, k_B is the Boltzmann constant, T is the temperature, P_i is the joint probability of R1/R2 for a given bin, and P_{max} is the maximum probability. The lowest free energy state corresponds to ΔG = 0.

Protein Expression and Purification

Plasmid for NEDD8 for bacterial expression was procured from Addgene. For N-terminal His-tag addition, the plasmid DNA was subcloned in Kanamycin resistance pet28b vector. Substitutions were done using Site-directed mutagenesis, and the corresponding clone was verified by sequencing. For overexpression and purification, clones were transformed in BL21 (DE3) bacterial cells and grown in an M9 medium containing $^{15}NH_4Cl$ and ^{13}C-glucose. Cells were grown at 37°C, and protein expression was induced at OD_{600} of 0.8 by adding IPTG (isopropyl this-β-d-thiogalactoside) final concentration of 0.25mM. After five hours of further growth, the cells were harvested by centrifugation. NEDD8 and Q40E NEDD8 were purified from inclusion bodies by unfolding and refolding, according to the previously reported method (32). The cells were re-suspended in the lysis buffer [50 mM Tris, (pH 8.0), 300 mM NaCl], lysed by sonication. The lysate was centrifuged at 15000 rpm at 4°C, and the supernatant was discarded. The remaining inclusion bodies were washed and dissolved in denaturant buffer (8M Urea, 25 mM Tris, 150 mM NaCl) and sonicated further until the solution became clear. The solution was mixed with pre-equilibrated Ni^{2+} NTA-agarose beads (Protino) for 30 minutes. The slurry mixture (lysate with beads) was loaded to an open column, washed extensively with high salt lysis buffer for removing DNA impurities, and eluted with different imidazole concentrations present in denaturant buffer (pH 8.0). The eluted fraction was dialyzed overnight at 4°C in 0 M Urea buffer (25 mM Tris, pH 7.6, 150 mM NaCl) for refolding. Further purification was done by gel filtration (Superdex 75 16/600) column. The final protein was obtained in PBS containing 1 mM DTT at pH 7.4.

NMR Spectroscopy

The NMR experiments were recorded at 298K on an 800 MHz Bruker Avance III HD spectrometer with a cryoprobe head. The samples were prepared in PBS with 1 mM DTT, pH 7.4. The protein sample was supplemented by 10% D2O. The standard triple resonance experiments HNCA and HN(CO)CA were used for assigning the chemicals shifts of ^{13}C, ^{15}N, and ^{1}H backbone atoms. 95% (69 out of 73) of the non-proline backbone amide resonances were assigned in the protein. The assignment is deposited in BMRB with id 50948. Backbone assignment for wt NEDD8 was already available from BMRB (Entry 10062) (33).

RESULTS

Both the apo-$Cullin^{CTD}$ and NEDDylated-$Cullin^{CTD}$ Are Dynamic

Cullin C-terminal domain comprises of four-helix bundle (4HB), α/β, and winged-helix B (WHB) subdomains (**Figure 2A**). The open and closed $Cul5^{CTD}$-Rbx1 structures suggest that NEDDylation drives a reorientation of the WHB^{SD} (**Figure 2A**). NEDD8 masks the $Rbx1^{RING}$ interaction surface on WHB^{SD} (helix-29/ECTD) to promote the WHB^{SD} reorientation. Consequently, the WHB^{SD}-$Rbx1^{RING}$ interaction is disrupted, and Rbx1 adopts open and flexible/dynamic conformations, essential for the CRL activity (7). In the open conformation, helix-29 of WHB^{SD} interacts with $4HB/\alpha\beta^{SD}$. However, there are no short-range interactions between NEDD8 and $4HB/\alpha\beta^{SD}$ subdomains (**Figure 2B**). Moreover, unlike the closed conformation, there are no interactions between ECTD and $4HB^{SD}$ in the open conformation (**Figure 2B**). In the NEDD8~$Cul5^{CTD}$ crystal structure, the open conformation appears to be stabilized through mutual interactions between two NEDD8~$Cul5^{CTD}$-Rbx1 conformers in the asymmetric unit (**Figure S1**). Altogether, whether the NEDD8~$Cul5^{CTD}$-Rbx1 open conformation observed in crystal structures represents a stable structure in solution is unclear.

The stability of $Cul5^{CTD}$-Rbx1 open/closed conformations was studied using atomistic MD simulations with explicit solvent (Materials and Methods). The simulations were carried out both in the presence and absence of NEDD8. Overall dimensions of complexes were analyzed by their average radius of gyration (<Rg>), and their probability distributions were compared (**Figure 3**). <Rg> values calculated for the closed and open ensembles remain close to their crystal structures (**Figure 3A**). Simulations initiated from the closed conformation exhibited a narrow distribution of Rg about ~2.65 nm (**Figure 3B**). Simulations of the open conformation in the presence of NEDD8 showed a bimodal Rg distribution ranging from 2.7 to 3.1 nm. In the absence of NEDD8, the Rg distribution of the open conformation exhibited a shift towards closed-like conformations (**Figure 3B**).

The conformation of $Cul5^{CTD}$ was analyzed by measuring the distance between Cα-atoms of two residues chosen for convenience, S567 and R714, which reduces from 5.3 nm to 3.6 nm as $Cul5^{CTD}$-Rbx1 transitions from the open to closed conformation (**Figure 2A**). Simulations of the closed conformation generated a restricted $Cul5^{CTD}$ ensemble, which was predominantly populated at an S567-R714 distance of ~3.6 nm (**Figure 3C**). In contrast, NEDD8~$Cul5^{CTD}$-Rbx1 has an ensemble of $Cul5^{CTD}$ conformations where the S567-R714 distance has an extended range of 4.0-6.0 nm (**Figure 3C**), which correlates well with its broad Rg distribution. NEDD8 removal causes a shift towards more compact $Cul5^{CTD}$ conformations. The conformational heterogeneity observed in NEDD8~$Cul5^{CTD}$ indicates that WHB^{SD} may adopt a range of orientations instead of a single orientation observed in the crystal structure. The multiple WHB^{SD} orientations result from frequent rupture of the short-range interactions that stabilize the orientation of WHB^{SD} against $4HB^{SD}$. The mean WHB^{SD}/$4HB^{SD}$ contact occupancies were merely 50%-75% during the

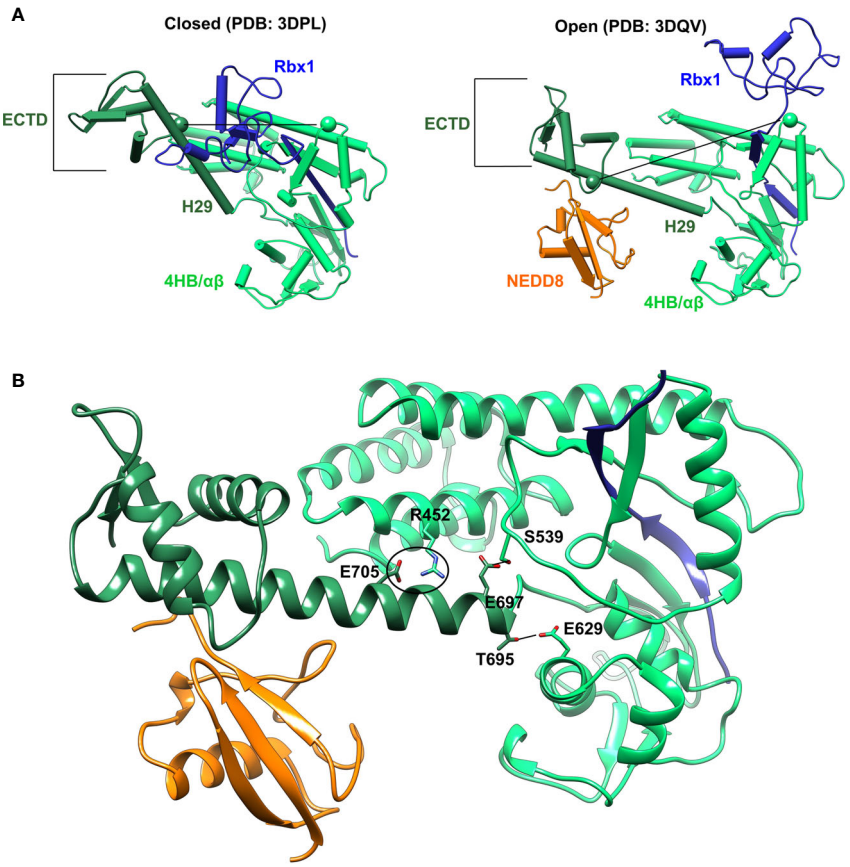

FIGURE 2 | Crystal conformations of Cul5^{CTD} closed and open states. **(A)** Crystal structures of Cul5^{CTD}-Rbx1 in the closed/open state were used to initiate independent MD simulations. Dotted black lines connect the Cα atoms (spheres) of S567 and R714 in Cul5^{CTD}. ECTD in both complexes refers to the extreme C-terminal domain, which comprises aa:726-780. **(B)** Non-covalent interactions between WHB^{SD} and 4HB/αβ^{SD} in the open conformation of NEDD8~Cul5^{CTD}-Rbx1 are shown in **(A)**. The black circle represents the R452/E705 salt bridge, while black lines correspond to S539/E697 and E629/T695 hydrogen bonds. The RING domain of Rbx1 (blue) is omitted for the sake of clarity.

simulation (**Figure S2**). Overall, the simulations underline the dynamic nature of the Cullin^{CTD} ensemble before and after NEDDylation. The dynamic Cullin^{CTD} ensembles may play a significant role in CRL activity by modulating its interaction with regulatory co-factors (34, 35).

Transient Interactions Between NEDD8 and 4HB/αβ Subdomain Promotes the Extended Conformations of NEDD8~Cullin^{CTD}

Although interactions between ECTD and Rbx1^{RING} are absent in the crystallographic open conformation, MD simulations indicate a tendency for such interactions to occur both in the presence and absence of NEDD8 (**Figures S3, S4**). Such interactions arise due to the dynamics of WHB^{SD} in the open conformation. NEDD8~Cul5^{CTD} was mostly open across all eight trajectories, and ECTD/RING interactions could be observed in only two trajectories (**Figure S3**). DeNEDDylation leads to compact Cul5^{CTD} for more extended periods, which increases the frequency of ECTD/RING interaction, as observed in four of the eight trajectories (**Figure S4**). The compact Cul5^{CTD} conformations stabilized by ECTD/RING interactions were observed in two of these trajectories (**Figure S5**). From the 2-D plots and the trajectories, it is clear that NEDD8 promotes extended conformations of Cul5^{CTD} to minimize ECTD/RING interaction (**Figure 4A** and **Movies S1, S2**). NEDD8~Cul5^{CTD}-Rbx1 contact analysis indicates that NEDD8 had frequent contacts with 4HB/αβ^{SD} of Cul5^{CTD}, including hydrogen bonds (**Figure S6**). The mean number of ECTD/RING contacts increased by more than two-fold upon removing NEDD8, indicating that NEDD8 inhibits the ECTD/RING interactions (**Figure 4B**). A representative NEDD8~Cul5^{CTD}-Rbx1 conformation, wherein NEDD8 interacts with 4HB/αβ^{SD} is shown in **Figure 4C**. The occurrence of ECTD/RING interactions in NEDD8~Cul5^{CTD}-Rbx1 simulations strongly suggests that partial masking of WHB^{SD} by NEDD8 is insufficient to maintain the open conformation. In summary, NEDDylated-Cullin^{CTD} exists as an ensemble of open conformations *via* transient interactions between NEDD8 and 4HB/αβ^{SD}.

A

	Rg (nm)		S567-R714 distance (nm)	
Complex	Crystal	MD	Crystal	MD
Cul5^{CTD}-Rbx1 (closed)	2.62	2.65 (±0.03)	3.61	3.63 (±0.18)
NEDD8~Cul5^{CTD}-Rbx1 (open)	2.97	2.88 (±0.08)	5.27	5.07 (±0.44)
Cul5^{CTD}-Rbx1 (open)	2.85	2.78 (±0.06)	5.27	4.65 (±0.42)

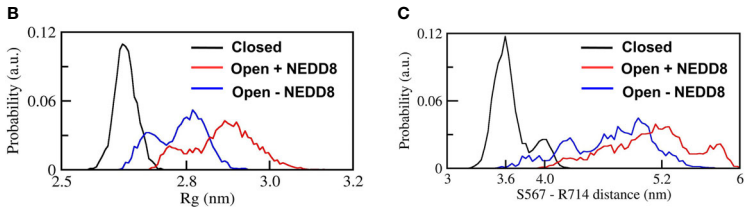

FIGURE 3 | Dynamic ensembles of Cul5^{CTD} closed, and open states were observed from simulations. **(A)** Radius of gyration for Cul5^{CTD}-Rbx1 variants and S567-R714 separation in Cul5^{CTD} calculated from MD simulations. Mean ± std deviation for each variant is calculated over eight independent MD trajectories performed for 200 ns. **(B)** Probability distributions for the radius of gyration (Rg) of closed/open states of Cul5^{CTD}-Rbx1 calculated from the 1.6 μs macro trajectory for each state. The macro trajectory was obtained by combining eight independent 200 ns runs. **(C)** Probability distribution of S567-R714 distance in Cul5^{CTD} calculated from the 1.6 μs macro trajectory for each state.

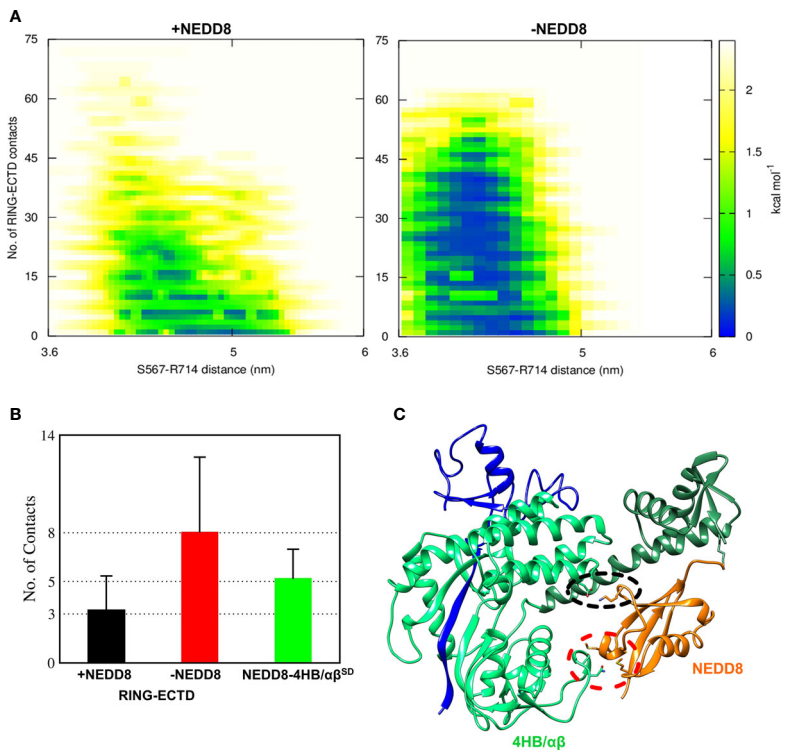

FIGURE 4 | NEDDylation biases the conformational landscape of Cullin^{CTD}-Rbx1 towards an ensemble of open conformations which minimize RING/ECTD interaction. **(A)** 2D-free energy landscapes calculated for the open state of Cul5^{CTD}-Rbx1 with and without NEDD8 from 1.6 μs macro trajectories obtained by combining eight independent 200 ns trajectories for each state. Upon removal of NEDD8, ECTD/RING interaction is more favorable. **(B)** Mean + SEM for several ECTD/Rbx1^{RING} and 4HB/αβ^{SD}-NEDD8 contacts across all Cul5^{CTD}-Rbx1 trajectories initiated from the open state with and without NEDD8. Contact cutoff was chosen to be 0.4 nm. **(C)** A representative conformation of NEDD8~Cul5^{CTD}-Rbx1 showing NEDD8 interacting with 4HB/αβ^{SD}. Interacting atoms are shown as sticks. A black dotted circle indicates a salt bridge between NEDD8 (K48) and 4HB^{SD} (E407). The red dotted circle indicates van der Waals interactions between NEDD8 (M1/M62) and αβ^{SD} (N655/S656).

NEDD8 Deamidation Creates a New Intramolecular Salt-Bridge

NEDD8 deamidation disfavours open CRL conformations and reduces CRL activity. As a first step towards understanding how NEDD8 deamidation affects CRL activation, dNEDD8 (Q40E) was simulated for 500 ns. Intriguingly, an intramolecular salt bridge formed frequently between E40 and R74, located in the flexible C-terminal tail (**Figures 5A, B**). Solution NMR spectroscopy was used to probe the deamidation effect on NEDD8. Uniformly ^{13}C, ^{15}N labeled NEDD8, and dNEDD8 were grown and purified from E. coli. The dNEDD8 backbone amide resonances in the ^{1}H-^{15}N Heteronuclear Single Quantum Coherence (HSQC) NMR spectra were well separated, indicating that the molecule is folded (**Figure S7**). The chemical shifts of backbone amide resonances in NEDD8 were retrieved from previous data stored in the Biological Magnetic Resonance Bank (BMRB entry 10062) (33). The standard triple resonance experiments were used to assign the backbone amide chemical shifts in dNEDD8. An overlay of NEDD8 and dNEDD8 ^{1}H -^{15}N HSQC spectra shows minor changes in chemical shifts for a few backbone resonances (**Figure S7**). A chemical shift perturbation (CSP) plot revealed changes in two distinct regions in dNEDD8 (**Figure 5C**). The residues between 39 and 45 have significant CSP, with the highest CSP at E40 (**Figure 5C**), which is expected to be the deamidation site. Interestingly, the second set of residues affected by deamidation spans the C terminal tail in NEDD8. Residues 68 to 74 exhibit significant perturbation in their chemical shifts, with the highest CSP at 74 (**Figure 5C**). The high CSPs at these regions support the implication from MD studies that a new salt bridge is formed between E40-R74 dNEDD8 (**Figure 5D**).

NEDD8 Deamidation Enhances Its Dissociation From WHB^{SD}

In the NEDDylated Cul5^{CTD}-Rbx1 complex, R74 in NEDD8 interacts with K764/Y765, located in ECTD of WHB^{SD} (**Figure 6A**). The E40/R74 interaction in dNEDD8 could disrupt the intermolecular contacts of R74 and thereby destabilize the non-covalent complex. Steered MD simulations (12 independent runs) were performed to dissociate NEDD8 variants from WHB^{SD}. The rupture force (F_{max}) and cumulative work (W_{unbind}) required for each variant's dissociation were determined from these runs. As shown in **Figure 6B**, F_{max} and W_{unbind} were highest for the NEDD8 complex. Compared to

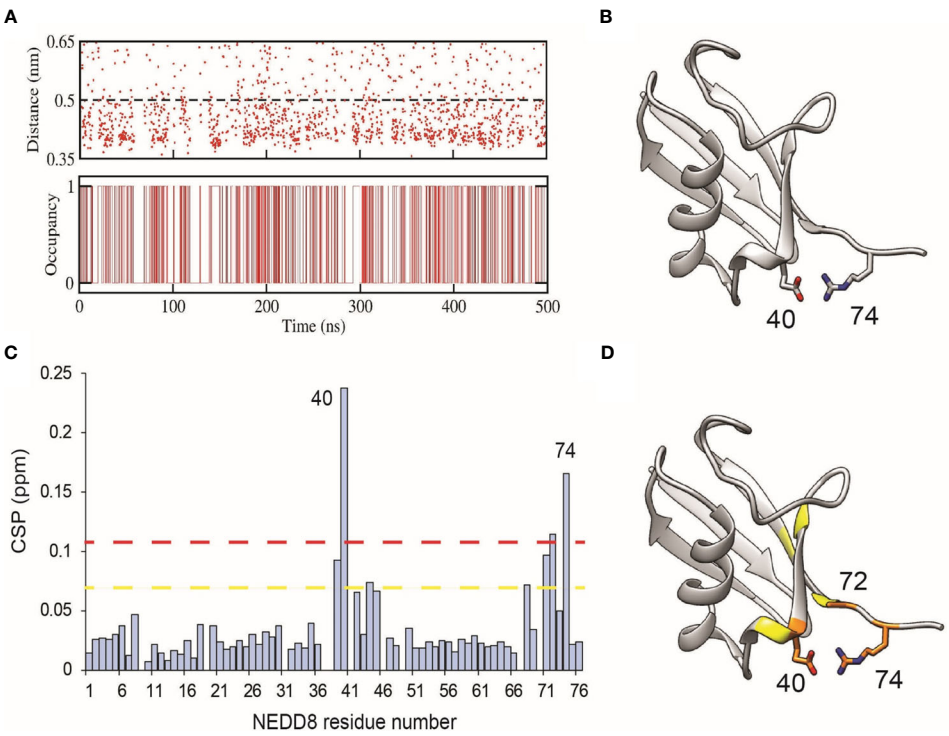

FIGURE 5 | Formation of an intramolecular salt-bridge in dNEDD8. **(A)** Salt-bridge stability as a function of time in a 500 ns MD simulation of dNEDD8. In the bottom plot, salt-bridge occupancy is shown as either 1 or 0 to indicate the presence or absence of a salt-bridge, respectively. Salt-bridge occupancy was calculated using a 0.5 nm cutoff. The occupancy of the salt-bridge was calculated to be 44.2%. **(B)** MD snapshot showing the formation of R74-E40 salt-bridge in dNEDD8. **(C)** The NMR CSP plot showing the effect of Q40E substitution in NEDD8. The CSP = $[(\delta H_{NEDD8} - \delta H_{dNEDD8})2 + (\delta N_{NEDD8} - \delta N_{dNEDD8})2/25]1/2$, where δH_{NEDD8} and δH_{dNEDD8} are amide proton chemical shifts of residue in wt-NEDD8 and dNEDD8, respectively. The dashed yellow line and red line denote Mean+SD and Mean+2*SD, respectively. **(D)** The residues with high CSPs are mapped onto the NEDD8 structure. The residues with CSP above Mean+SD are colored yellow, and the residues with CSP above Mean+2*SD are colored orange.

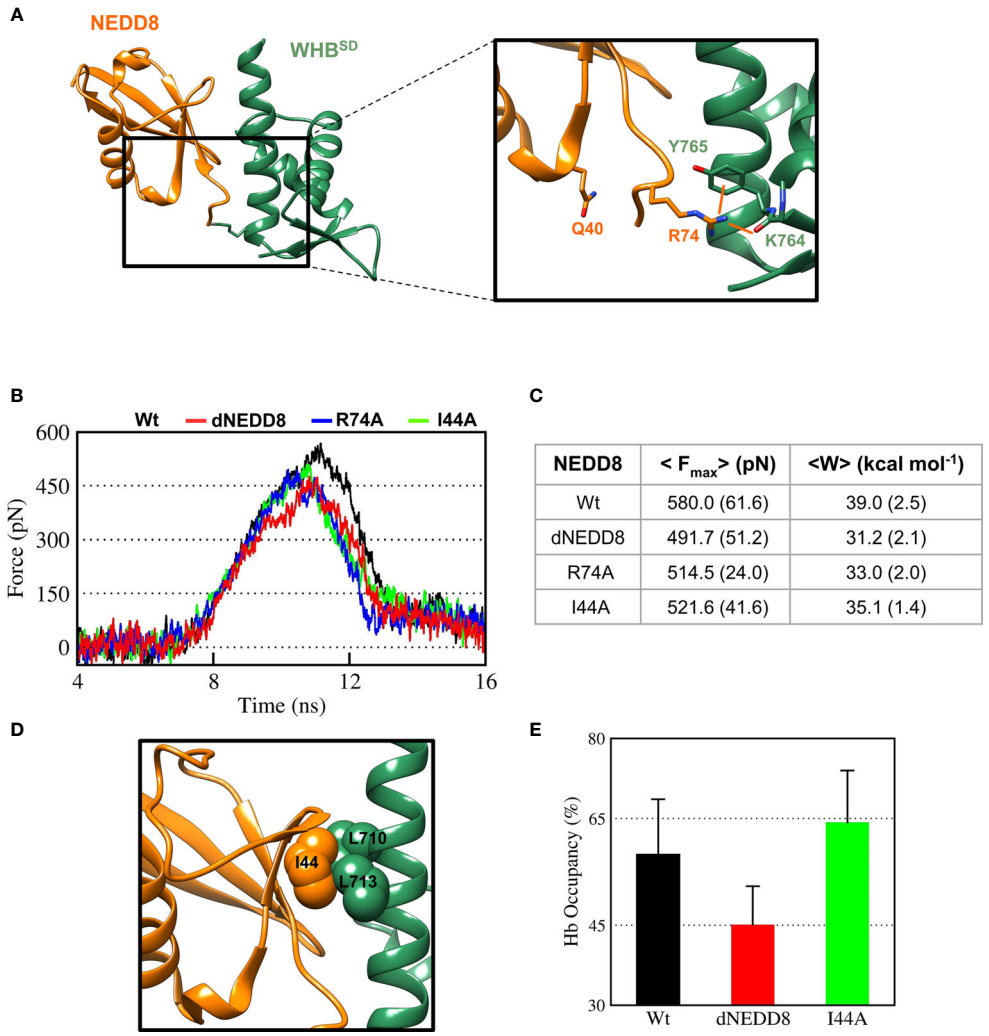

NEDD8	< F_{max}> (pN)	<W> (kcal mol^{-1})
Wt	580.0 (61.6)	39.0 (2.5)
dNEDD8	491.7 (51.2)	31.2 (2.1)
R74A	514.5 (24.0)	33.0 (2.0)
I44A	521.6 (41.6)	35.1 (1.4)

FIGURE 6 | Deamidation of NEDD8 enhances its dissociation from WHB^{SD}. **(A)** R74-mediated interactions in the Cul5-WHB^{SD}~NEDD8 complex (PDB: 3DQV). Orange lines indicate interactions of R74 with and K764 (backbone) and Y765 (sidechain). **(B)** Mean force-time profile for the dissociation of NEDD8-wt and its mutants from WHB^{SD} obtained from steered MD (SMD) simulations. Twelve independent SMD runs were performed for 20 ns in the case of each complex. **(C)** F_{max} and unbinding work (W) determined from average profiles obtained by steered MD. One standard error of mean is indicated in ( ). **(D)** I44-mediated hydrophobic interactions in the Cul5-WHB^{SD}~NEDD8 complex. **(E)** Mean occupancy of the R74-K764 hydrogen bond from NEDD8-wt, dNEDD8, and NEDD8-I44A SMD runs.

NEDD8, F_{max} and W_{unbind} for dNEDD8 were reduced by ~90 pN and 8 kcal/mol, respectively, indicating a destabilized dNEDD8-WHB^{SD} complex (**Figure 6C**). I44 in NEDD8 engages in hydrophobic interactions with WHB^{SD} in the NEDD8-WHB^{SD} complex (**Figure 6D**). The F_{max} and W_{unbind} reduced when the I44 mediated contacts were disrupted (I44A substitution) (**Figure 6C**). However, dNEDD8 was more unstable compared to the I44A complex (**Figures 6B, C**). Moreover, destabilization of the dNEDD8 complex was comparable to the NEDD8-R74A complex, which suggested that E40 disrupted R74-mediated interactions during dNEDD8 dissociation.

Concomitantly, the R74/K764 hydrogen bond's mean stability was reduced by 13-15% for dNEDD8 compared to NEDD8 or I44A-NEDD8 complex (**Figure 6E**). The R74/K764 hydrogen bond dynamics during the SMD in NEDD8 and dNEDD8 complexes are shown in **Figures S8, S9**. In a few dNEDD8 trajectories, transient salt-bridges (<0.5 nm) were observed between E40 and R74 from 8-16 ns (**Figure S9**), which appeared to compete with and destabilize the R74-K764 hydrogen bond. In conclusion, SMD simulations suggest that the intramolecular interaction between E40 and R74 in dNEDD8 may destabilize the NEDD8-WHB^{SD} complex.

Intramolecular E40-R74 Interaction Interferes With the NEDD8/Cullin-WHB^{SD} Association

The E40-R74 interaction may also inhibit the association between dNEDD8 and WHB^{SD}. An extended open conformation structure of NEDD8~Cullin-WHB^{SD} with no contacts between NEDD8 and WHB^{SD} is required as the

starting structure to study the association, which is currently unavailable for Cul5 but available for Cul1. Hence, the NEDD8~Cul1-WHB^{SD} structure (PDB id: 4P5O) was chosen for this purpose (**Figure S10A**). Unbiased MD simulations were initiated from an extended NEDD8~Cul1-WHB^{SD} conformation to determine if E40 in dNEDD8 could compete for R74 during association with WHB^{SD}. Five independent runs were performed (300 ns) for NEDD8 and dNEDD8-conjugated Cul1-WHB^{SD}. For all NEDD8~WHB^{SD} variants, a range of extended conformations was observed across all trajectories with minimal interaction between NEDD8 (aa: 1-70) and WHB^{SD} (**Figure S10B**). In the NEDD8/dNEDD8 trajectories, R74 formed a hydrogen bond with E760, which corresponds to the same position as K764 in Cul5-WHB^{SD} (**Figure S11**). The mean occupancy of R74/E760 hydrogen bond calculated over NEDD8/dNEDD8 trajectories indicates a slight destabilization (>15%) for dNEDD8~WHB^{SD} due to competition with R74/E40 salt-bridge (**Figure 7A**). In dNEDD8 trajectories, E40 was found to compete for R74 in four of the five trajectories (**Figure S11C**). A representative WHB^{SD}~dNEDD8 conformation with an E40/R74 salt-bridge is shown in **Figure 7B**. In the NEDD8~Cul1-WHB^{SD} and NEDD8~Cul5-WHB^{SD} complex structures, R74-mediated interactions stabilize the compact conformation of the C-terminal tail (**Figures 7A** and **S11A**), which likely reduces the range of motion for NEDD8 around WHB^{SD} and enhances non-covalent binding between NEDD8 and WHB^{SD}. The conformation adopted by the C-terminal tail was determined by measuring the Cα distance between A72 and G76, which is 0.75 nm in the NEDD8~Cul5-WHB^{SD} crystal structure. The combined probability distributions of the C-terminal conformations from all wt-NEDD8, dNEDD8, and NEDD8-R74A trajectories are shown in **Figure 7C**. The probability distributions indicate that the C-terminal tail populates both compact and extended conformations to a similar extent in wt-NEDD8. In contrast, the dNEDD8 C-terminal tail has a strong bias towards extended conformations (**Figures 7C, D**). Similar to dNEDD8, NEDD8-R74A conjugate populates extended conformations of the C-terminal tail, confirming that R74-mediated hydrogen bonding is required for compact conformations. To summarize, R74-mediated hydrogen bonds with E760 of WHB^{SD} played a crucial role in NEDD8/WHB^{SD} non-covalent interaction. MD simulations suggest that intramolecular attraction between E40 and R74 in the dNEDD8~WHB^{SD} complex may disrupt R74 contacts with WHB^{SD} and destabilize dNEDD8~WHB^{SD} association.

Deamidation Also Destabilizes the NEDD8~WHB^{SD}/E2~Ub Complex

When E2~Ub binds to NEDD8~Cul1-Rbx1, NEDD8 is no longer associated with WHB^{SD} through its I44 patch (as in **Figure S11A**) (8). Instead, the I44 patch interacts with the 'backside' of E2. In this complex, NEDD8 Q40 is close to R717, located on helix-29 of WHB^{SD} (**Figure 8A**). The effect of deamidation was also investigated in the NEDD8~WHB^{SD}

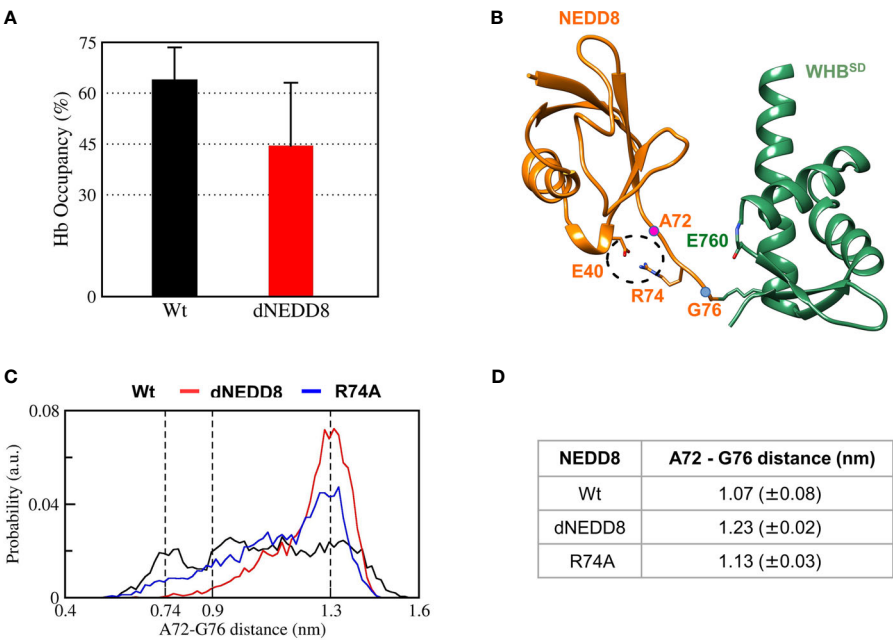

NEDD8	A72 - G76 distance (nm)
Wt	1.07 (±0.08)
dNEDD8	1.23 (±0.02)
R74A	1.13 (±0.03)

FIGURE 7 | R74-E40 salt-bridge may hinder NEDD8/WHB^{SD} association by disallowing compact conformations of the NEDD8 C-terminal tail. **(A)** Mean± one standard error of R74/E760 hydrogen bond occupancy for NEDD8-wt and dNEDD8 conjugates. **(B)** Snapshot from trajectory 1 of Cul1-WHB^{SD}~NEDD8 showing an intramolecular salt-bridge involving R74/E40. The Cα atom positions of A72/G76 are shown as pink spheres. **(C)** Combined probability distribution of the C-terminal tail conformation obtained from five 300 ns trajectories for each conjugate. The A72-G76 distance varies from 0.74 to 0.9 nm in crystal complexes of Cul1/5-WHB^{SD}~NEDD8. **(D)** Mean ± one standard error of the C-terminal tail conformation across all five trajectories for each conjugate.

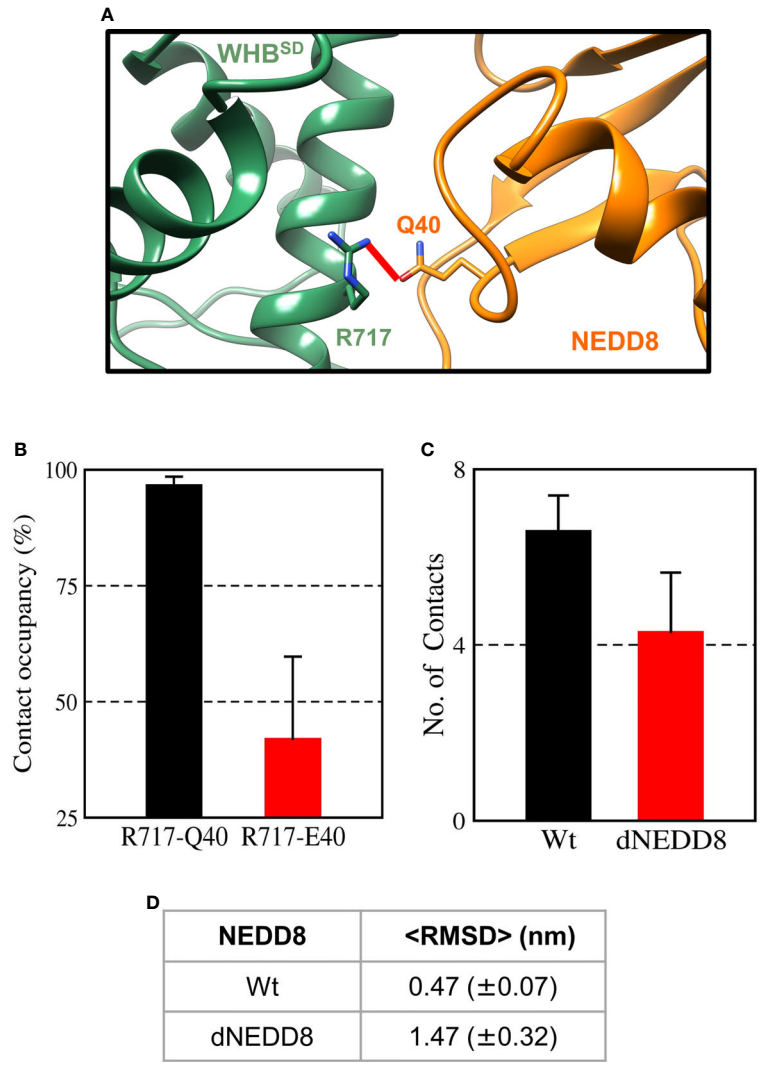

D

NEDD8	<RMSD> (nm)
Wt	0.47 (±0.07)
dNEDD8	1.47 (±0.32)

FIGURE 8 | An intermolecular salt-bridge involving E40 destabilizes the Cul1-WHB^{SD}~NEDD8 complex. **(A)** Relative positions of R717 and Q40 in the Cul1-WHB^{SD}~NEDD8. The red line connects the Nη1 atom of R717 to the Oϵ atom of Q40 and has a length of 0.41 nm. The distance between the atoms drops below 0.32 nm in NEDD8-wt simulations, indicating a hydrogen bond formation. **(B)** Contact occupancies of R717-Q40 hydrogen bond, and R717-E40 salt-bridge were calculated using cutoffs of 0.32 and 0.5 nm, respectively. Mean ± std. Error is calculated for over three independent 200 ns trajectories. **(C)** Mean ± std error of the number of contacts formed between NEDD8 (I36/L71) and Cul1-WHB^{SD} (helix-29) sidechains using a cutoff of 0.45 nm. **(D)** Average RMSDs of Cul1-WHB^{SD}~NEDD8 complexes over three independent 200 ns trajectories. ± One std. Error is indicated in ( ).

portion of this complex by simulations. The E2~Ub, Rbx1 & Cullin 4HB, α/β subdomains were removed before simulations to reduce the size of the system. In triplicate simulations, a stable hydrogen bond forms between Q40 and R717 across all trajectories (**Figures 8B** and **S12A**). Overall, the wt-complex maintained native hydrophobic interactions (**Figures 8C** and **S12C**) and had a mean RMSD below 0.5 nm (**Figures 8D** and **S12D**), indicating a stable complex. In contrast, the dNEDD8 complex was unstable, resulting in increased RMSD beyond 1 nm across all replicates (**Figure S12D**). Destabilization of dNEDD8 complex correlated with the lower contact occupancy of the R717-E40 contact (**Figures 8D** and **S12D**) and hydrophobic interactions (**Figure 8C**), which disrupted the orientation between NEDD8 and WHB^{SD}, leading to an inactive Cul1-Rbx complex.

DISCUSSION

Our study provides atomistic insights into the role of NEDD8 in stabilizing the open, catalytically-active Cullin^{CTD} conformation and how its function is impaired by deamidation. Unlike a single conformation observed in crystal structures, NEDD8~Cul5^{CTD}-Rbx1 exists as an ensemble of interconverting closed and open conformations. The orientation between WHB^{SD} and 4HB^{SD} observed in the crystal structure was unstable and adopted

multiple orientations across independent simulations. The MD simulations suggest that NEDD8 activates Cullin^{CTD}-Rbx1 through a combination of two mechanisms, (i) steric hindrance of interactions between Rbx1 and WHB/4HB^{SD}, and (ii) transient interactions between NEDD8 and Cullin 4HB/$\alpha\beta^{SD}$. The steric hindrance induces the open conformation. The transient interactions minimize ECTD/RING interaction, which also promotes the open/active conformation. These observations are supported by *in vitro* activity assays, which showed that in the absence of NEDD8, the ECTD deletion is sufficient to convert CRLs from an inactive to a constitutively active state (36).

Our results also uncover the underlying mechanism by which bacterial deamidation of NEDD8 inactivates CRLs. We have previously shown that the deamidation of the E2 enzyme-UBC13 by the *Shigella flexneri* deamidase – OspI triggers an intramolecular salt-bridge formation, inhibiting its association with the cognate RING E3 ligase - TRAF6 (37). We show here by MD simulations that deamidation at Q40 triggers the formation of an intramolecular salt bridge between E40 and R74. The NMR CSPs supported the observation. However, due to the low solubility of NEDD8 in *in-vitro* conditions, measurement of the salt bridge by hydrogen exchange or NOESY experiments was difficult.

The R74-E40 salt-bridge in dNEDD8 competes with an intermolecular hydrogen bond involving R74, which is required for stable association with WHB^{SD}. Deamidation-induced competition for R74 promotes extended conformations of the C-terminal tail, inhibiting the formation of a stable NEDD8-WHB^{SD} complex. Even after E2~Ub interacts with CRLs, deamidation disrupts the Q40 contacts and destabilizes the NEDD8-WHB^{SD} complex. The inability of NEDD8 to associate with WHB^{SD} may effectively lock Cullin^{CTD}-Rbx1 into a closed conformation, as suggested by XL/MS experiments (13).

Our results with Shigella flexneri deamidase OspI and E. coli deamidase Cif suggest a common inactivation mechanism of host cellular pathways by bacterial deamidases. The deamidated glutamine residue competes for functional electrostatic interactions between the target and its interacting partners. Disruption of these interactions adversely affects downstream signaling cascades and inhibits host immune responses to pathogen infection.

DATA AVAILABILITY STATEMENT

The original contributions presented in the study are included in the article/**Supplementary Material**. Further inquiries can be directed to the corresponding author.

AUTHOR CONTRIBUTIONS

PM carried out all MD simulations. KC performed the NMR experiments. RD supervised the project. PM and RD wrote the initial draft. All authors contributed to the article and approved the submitted version.

ACKNOWLEDGMENTS

We acknowledge the support of the Department of Atomic Energy, Government of India, under project identification no RTI 4006. The NMR data were acquired at the NCBS-TIFR NMR Facility, supported by the Department of Atomic Energy, Government of India, under project no RTI 4006. The work was supported by intramural grants from the Tata Institute of Fundamental Research. The NMR facility is also partially supported by the Department of Biotechnology, B-Life grant under project no dbt/pr12422/med/31/287/2014. The NCBS Central computing facility is acknowledged for Molecular Dynamics simulations.

SUPPLEMENTARY MATERIAL

The Supplementary Material for this article can be found online at: https://www.frontiersin.org/articles/10.3389/fimmu.2021.695331/full#supplementary-material

REFERENCES

1. Metzger MB, Pruneda JN, Klevit RE, Weissman AM. RING-Type E3 Ligases: Master Manipulators of E2 Ubiquitin-Conjugating Enzymes and Ubiquitination. *Biochim Biophys Acta - Mol Cell Res* (2014) 1843:47–60. doi: 10.1016/j.bbamcr.2013.05.026
2. Petroski MD, Deshaies RJ. Function and Regulation of Cullin-RING Ubiquitin Ligases. *Nat Rev Mol Cell Biol* (2005) 6:9–20. doi: 10.1038/nrm1547
3. Zheng N, Schulman BA, Song L, Miller JJ, Jeffrey PD, Wang P, et al. Structure of the Cul1-Rbx1-Skp1-F Boxskp2 SCF Ubiquitin Ligase Complex. *Nature* (2002) 416:703–9. doi: 10.1038/416703a
4. Morimoto M, Nishida T, Honda R, Yasuda H. Modification of Cullin-1 by Ubiquitin-Like Protein Nedd8 Enhances the Activity of SCF(skp2) Toward P27(Kip1). *Biochem Biophys Res Commun* (2000) 270:1093–6. doi: 10.1006/bbrc.2000.2576
5. Read MA, Brownell JE, Gladysheva TB, Hottelet M, Parent LA, Coggins MB, et al. Nedd8 Modification of Cul-1 Activates SCF(beta(TrCP))-Dependent Ubiquitination of IkappaBalpha. *Mol Cell Biol* (2000) 20:2326–33. doi: 10.1128/MCB.20.7.2326-2333.2000
6. Lyapina S. Promotion of NEDD8-CUL1 Conjugate Cleavage by COP9 Signalosome. *Sci (80-)* (2001) 292:1382–5. doi: 10.1126/science.1059780
7. Duda DM, Borg LA, Scott DC, Hunt HW, Hammel M, Schulman BA. Structural Insights Into NEDD8 Activation of Cullin-RING Ligases: Conformational Control of Conjugation. *Cell* (2008) 134:995–1006. doi: 10.1016/j.cell.2008.07.022
8. Baek K, Krist DT, Prabu JR, Hill S, Klügel M, Neumaier LM, et al. NEDD8 Nucleates a Multivalent Cullin–RING–UBE2D Ubiquitin Ligation Assembly. *Nature* (2020) 578:461–6. doi: 10.1038/s41586-020-2000-y
9. Washington EJ, Banfield MJ, Dangl JL. What a Difference a Dalton Makes: Bacterial Virulence Factors Modulate Eukaryotic Host Cell Signaling Systems *via* Deamidation. *Microbiol Mol Biol Rev* (2013) 77:527–39. doi: 10.1128/MMBR.00013-13
10. Cui J, Yao Q, Li S, Ding X, Lu Q, Mao H, et al. Glutamine Deamidation and Dysfunction of Ubiquitin/NEDD8 Induced by a Bacterial Effector Family. *Science* (2010) 329:1215–8. doi: 10.1126/science.1193844
11. Jubelin G, Frédéric T, Duda DM, Hsu Y, Samba-Louaka A, Nobe R, et al. Pathogenic Bacteria Target NEDD8-Conjugated Cullins to Hijack Host-Cell Signaling Pathways. *PloS Pathog* (2010) 6(9):e1001128. doi: 10.1371/journal.ppat.1001128

12. Winston JT, Strack P, Beer-Romero P, Chu CY, Elledge SJ, Harper JW. The SCFbeta-TRCP-Ubiquitin Ligase Complex Associates Specifically With Phosphorylated Destruction Motifs in IkappaBalpha and Beta-Catenin and Stimulates IkappaBalpha Ubiquitination *In Vitro* [Published Erratum Appears in Genes Dev 1999 Apr 15;13(8):1050]. *Genes Dev* (1999) 13:270–83. doi: 10.1101/gad.13.3.270
13. Yu C, Mao H, Novitsky EJ, Tang X, Rychnovsky SD, Zheng N, et al. Gln40 Deamidation Blocks Structural Reconfiguration and Activation of SCF Ubiquitin Ligase Complex by Nedd8. *Nat Commun* (2015) 6:1–12. doi: 10.1038/ncomms10053
14. Dunbrack RL. Rotamer Libraries in the 21. *Curr Opin Struct Biol* (2002) 12:431–40. doi: 10.1016/S0959-440X(02)00344-5
15. Pettersen EF, Goddard TD, Huang CC, Couch GS, Greenblatt DM, Meng EC, et al. UCSF Chimera—A Visualization System for Exploratory Research and Analysis. *J Comput Chem* (2004) 25:1605–12. doi: 10.1002/jcc.20084
16. Hornak V, Abel R, Okur A, Strockbine B, Roitberg A, Simmerling C. Comparison of Multiple Amber Force Fields and Development of Improved Protein Backbone Parameters. *Proteins* (2006) 65:712–25. doi: 10.1002/prot.21123
17. Best RB, Hummer G. Optimized Molecular Dynamics Force Fields Applied to the Helix-Coil Transition of Polypeptides. *J Phys Chem B* (2009) 113:9004–15. doi: 10.1021/jp901540t
18. Lindorff-Larsen K, Piana S, Palmo K, Maragakis P, Klepeis JL, Dror RO, et al. Improved Side-Chain Torsion Potentials for the Amber Ff99sb Protein Force Field. *Proteins Struct Funct Bioinforma* (2010) 78:1950–8. doi: 10.1002/prot.22711
19. Yoo J, Aksimentiev A. Improved Parametrization of Li +, Na +, K +, and Mg 2 + Ions for All-Atom Molecular Dynamics Simulations of Nucleic Acid Systems. *J Phys Chem Lett* (2012) 3:45–50. doi: 10.1021/jz201501a
20. Yoo J, Wilson J, Aksimentiev A. Improved Model of Hydrated Calcium Ion for Molecular Dynamics Simulations Using Classical Biomolecular Force Fields. *Biopolymers* (2016) 105:752–63. doi: 10.1002/bip.22868
21. Yoo J, Aksimentiev A. Improved Parameterization of Amine-Carboxylate and Amine-Phosphate Interactions for Molecular Dynamics Simulations Using the CHARMM and AMBER Force Fields. *J Chem Theory Comput* (2016) 12:430–43. doi: 10.1021/acs.jctc.5b00967
22. Miller MS, Lay WK, Li S, Hacker WC, An J, Ren J, et al. Reparametrization of Protein Force Field Nonbonded Interactions Guided by Osmotic Coefficient Measurements From Molecular Dynamics Simulations. *J Chem Theory Comput* (2017) 13:1812–26. doi: 10.1021/acs.jctc.6b01059
23. Best RB, Zheng W, Mittal J. Balanced Protein-Water Interactions Improve Properties of Disordered Proteins and non-Specific Protein Association. *J Chem Theory Comput* (2014) 10:5113–24. doi: 10.1021/ct500569b
24. Hess B, Kutzner C, van der Spoel D, Lindahl E. GRGMACS 4: Algorithms for Highly Efficient, Load-Balanced, and Scalable Molecular Simulation. *J Chem Theory Comput* (2008) 4:435–47. doi: 10.1021/ct700301q
25. Abraham MJ, Murtola T, Schulz R, Páll S, Smith JC, Hess B, et al. Gromacs: High Performance Molecular Simulations Through Multi-Level Parallelism From Laptops to Supercomputers. *SoftwareX* (2015) 1–2:19–25. doi: 10.1016/j.softx.2015.06.001
26. Peters MB, Yang Y, Wang B, Füsti-Molnár L, Weaver MN, Merz KM. Structural Survey of Zinc-Containing Proteins and Development of the Zinc AMBER Force Field (ZAFF). *J Chem Theory Comput* (2010) 6:2935–47. doi: 10.1021/ct1002626
27. Berendsen HJC, Postma JPM, Van Gunsteren WF, Dinola A, Haak JR. Molecular Dynamics With Coupling to an External Bath. *J Chem Phys* (1984) 81:3684–90. doi: 10.1063/1.448118
28. Parrinello M, Rahman A. Polymorphic Transitions in Single Crystals: A New Molecular Dynamics Method. *J Appl Phys* (1981) 52:7182–90. doi: 10.1063/1.328693
29. Bjelkmar P, Larsson P, Cuendet MA, Hess B, Lindahl E. Implementation of the CHARMM Force Field in GROMACS: Analysis of Protein Stability Effects From Correction Maps, Virtual Interaction Sites, and Water Models. *J Chem Theory Comput* (2010) 6:459–66. doi: 10.1021/ct900549r
30. Darden T, York D, Pedersen L. Particle Mesh Ewald: An N ·Log(N) Method for Ewald Sums in Large Systems. *J Chem Phys* (1993) 98:10089–92. doi: 10.1063/1.464397
31. Essmann U, Perera L, Berkowitz ML, Darden T, Lee H, Pedersen LG. A Smooth Particle Mesh Ewald Method. *J Chem Phys* (1995) 103:8577–93. doi: 10.1063/1.470117
32. Whitby FG, Xia G, Pickart CM, Hill CP. Crystal Structure of the Human Ubiquitin-Like Protein NEDD8 and Interactions With Ubiquitin Pathway Enzymes. *J Biol Chem* (1998) 273:34983–91. doi: 10.1074/jbc.273.52.34983
33. Sakata E, Yamaguchi Y, Miyauchi Y, Iwai K, Chiba T, Saeki Y, et al. Direct Interactions Between NEDD8 and Ubiquitin E2 Conjugating Enzymes Upregulate Cullin-Based E3 Ligase Activity. *Nat Struct Mol Biol* (2007) 14:167–8. doi: 10.1038/nsmb1191
34. Duda DM, Olszewski JL, Tron AE, Hammel M, Lambert LJ, Waddell MB, et al. Structure of a Glomulin-RBX1-CUL1 Complex: Inhibition of a RING E3 Ligase Through Masking of Its E2-Binding Surface. *Mol Cell* (2012) 47:371–82. doi: 10.1016/j.molcel.2012.05.044
35. Zemla A, Thomas Y, Kedziora S, Knebel A, Wood NT, Rabut G, et al. CSN-And CAND1-Dependent Remodelling of the Budding Yeast SCF Complex. *Nat Commun* (2013) 4:1641. doi: 10.1038/ncomms2628
36. Yamoah K, Oashi T, Sarikas A, Gazdoiu S, Osman R, Pan Z-Q. Autoinhibitory Regulation of SCF-Mediated Ubiquitination by Human Cullin 1's C-Terminal Tail. *Proc Natl Acad Sci USA* (2008) 105:12230–5. doi: 10.1073/pnas.0806155105
37. Mohanty P, Rashmi, Habibullah BI, Arun GS, Das R. Deamidation Disrupts Native and Transient Contacts to Weaken the Interaction Between UBC13 and RING-Finger E3 Ligases. *Elife* (2019) 8:1–62. doi: 10.7554/eLife.49223

Conflict of Interest: The authors declare that the research was conducted in the absence of any commercial or financial relationships that could be construed as a potential conflict of interest.

Publisher's Note: All claims expressed in this article are solely those of the authors and do not necessarily represent those of their affiliated organizations, or those of the publisher, the editors and the reviewers. Any product that may be evaluated in this article, or claim that may be made by its manufacturer, is not guaranteed or endorsed by the publisher.

frontiers in Immunology

ORIGINAL RESEARCH
published: 27 August 2021
doi: 10.3389/fimmu.2021.730483

Negative Regulation of RNF90 on RNA Virus-Triggered Antiviral Immune Responses Targeting MAVS

Bo Yang[1,2†], Ge Zhang[1†], Xiao Qin[1†], Yulu Huang[1], Xiaowen Ren[1], Jingliang Sun[1], Shujun Ma[1], Yanzi Liu[3], Di Song[1,4], Yue Liu[1], Yuhan Cui[1], Hui Wang[2] and Jie Wang[1,2*]*

[1] Henan Key Laboratory of Immunology and Targeted Drug, Xinxiang Medical University, Xinxiang, China, [2] Henan Collaborative Innovation Center of Molecular Diagnosis and Laboratory Medicine, School of Laboratory Medicine, Xinxiang Medical University, Xinxiang, China, [3] Department of Laboratory Medicine, the Third Affiliated Hospital of Xinxiang Medical University, Xinxiang, China, [4] Department of Laboratory Medicine, Fuwai Center China Cardiovascular Hospital, Zhengzhou, China

OPEN ACCESS

Edited by:
Éric Bergeron, Centers for Disease Control and Prevention (CDC), United States

Reviewed by:
Chunfu Zheng, University of Calgary, Canada
Congwen Wei, Academy of Military Medical Sciences (AMMS), China

***Correspondence:**
Hui Wang
wanghui@xxmu.edu.cn
Jie Wang
jiewang618@xxmu.edu.cn

†These authors have contributed equally to this work

Specialty section:
This article was submitted to Viral Immunology, a section of the journal Frontiers in Immunology

Received: *26 June 2021*
Accepted: *10 August 2021*
Published: *27 August 2021*

Citation:
Yang B, Zhang G, Qin X, Huang Y, Ren X, Sun J, Ma S, Liu Y, Song D, Liu Y, Cui Y, Wang H and Wang J (2021) Negative Regulation of RNF90 on RNA Virus-Triggered Antiviral Immune Responses Targeting MAVS. Front. Immunol. 12:730483. doi: 10.3389/fimmu.2021.730483

The antiviral innate immunity is the first line of host defense against viral infection. Mitochondrial antiviral signaling protein (MAVS, also named Cardif/IPS-1/VISA) is a critical protein in RNA virus-induced antiviral signaling pathways. Our previous research suggested that E3 ubiquitin-protein ligases RING-finger protein (RNF90) negatively regulate cellular antiviral responses by targeting STING for degradation, though its role in RNA virus infection remains unknown. This study demonstrated that RNF90 negatively regulated RNA virus-triggered antiviral innate immune responses in RNF90-silenced PMA-THP1 cells, RNF90-deficient cells (including HaCaTs, MEFs, and BMDMs), and RNF90-deficient mice. However, RNF90 regulated RNA virus-triggered antiviral innate immune responses independent of STING. RNF90 promoted K48-linked ubiquitination of MAVS and its proteasome-dependent degradation, leading to the inhibition of innate immune responses. Altogether, our findings suggested a novel function and mechanism of RNF90 in antiviral innate immunity.

Keywords: antiviral innate immune responses, ubiquitination, degradation, signaling pathway, MAVS, RNF90

INTRODUCTION

RNA viruses, which have RNA as their genetic material, including single-stranded RNA (ssRNA) viruses and double-stranded RNA (dsRNA) viruses, cause many kinds of human infectious diseases (1, 2). A lot of RNA viruses, such as human immunodeficiency virus (HIV), hepatitis C virus (HCV), Ebola virus, Zika virus, respiratory syncytial virus (RSV), influenza viruses, yellow fever virus, dengue virus, severe acute respiratory syndrome (SARS)-associated coronavirus (SARS-CoV), and SARS-CoV-2 are well-known viruses that are infectious and cause serious, even deadly, syndromes in humans (3, 4). The first line to eliminate viral invasions is the host innate immune system (5). The host antiviral immune responses are initiated by the sensing of pathogen-associated molecular patterns (PAMPs) from invading viruses by a series of pattern recognition receptors (PRRs), which results in the production of type I interferons (IFNs) and other cytokines or chemokines essential to host antiviral responses (6).

For RNA viruses, the viral nucleic acids are critical PAMPs, and the viral RNAs are recognized by TLR3 or RIG-I-like receptors (RLRs) (7). In most cell types, two RLRs, retinoic-acid-inducible

protein I (RIG-I) and Melanoma differentiation-associated gene 5 (Mda5), serve as cytosolic RNA receptors (8). Generally speaking, RIG-I is responsible for the production of type I IFNs and proinflammatory cytokines upon the infection by Newcastle disease virus (NDV), vesicular stomatitis virus (VSV), influenza virus, and Sendai virus (SeV), and Japanese encephalitis virus (JEV), whereas Mda5 was required for the responses against encephalomyocarditis virus (EMCV) and *in vitro* transcribed poly I:C (9).

Activated RIG-I and MDA5 by dsRNA engagement interact with the adaptor protein mitochondrial antiviral-signaling protein (MAVS), which is also known as caspase-activation recruitment-domain adaptor inducing I FN-β (Cardif), IFN-β promoter stimulator (IPS-1), or virus-induced signaling adaptor (VISA), *via* a caspase recruitment domain (CARD)-CARD interaction, and triggers MAVS mediating signaling pathways, including the recruitment of downstream tumor necrosis factor (TNF) receptor-associated factor (TRAF) family members, the TRAF family member-associated NF-κB activator (TANK)-binding kinase 1 (TBK1) and inducible IκB kinase (IKK-i or IKK-ϵ), leading to the activation of the transcription factor NF-κB and IRF3 (10–14). Thus, MAVS is critical to innate immunity and serves as the center of the antiviral innate immune responses against RNA viruses.

The host immune signaling pathways must be tightly controlled because its excessive activation may cause tissue damage and contribute to the pathogenesis of many human diseases (15–17). Accumulating evidence suggests that ubiquitination is part of this exquisite regulatory system and adjust the strength and duration of the immune responses in a timely and efficient way (18). Ubiquitin has seven Lys residues (K6, K11, K27, K29, K33, K48, and K63) and can be linked to its target proteins to regulate their functions by various mechanisms (19). K48-linked ubiquitination is mainly associated with proteasome-mediated degradation of proteins, whereas K63-linked modification usually regulates signaling pathways in a non-proteolytic manner (20). The process of ubiquitination was catalyzed sequentially by three different types of enzymes, E1 ubiquitin-activating enzyme, E2 ubiquitin-conjugating enzymes, and E3 ubiquitin-protein ligases (21). Human genome contains more than 600 E3 ubiquitin-protein ligases, responsible for the high selection of target proteins, including HECT-, RING- and RBP-type E3 ubiquitin-protein ligases (22).

As the center adaptor protein in the RLR signaling pathways, MAVS has been reported to be targeted by several E3 ubiquitin-protein ligases for the regulation of antiviral immune responses (23). For example, TRIM25 catalyzed K48-linked ubiquitination of MAVS and marked it for proteasomal degradation (24), whereas TRIM31 catalyzes the K63-linked polyubiquitination of MAVS and promotes its activation and subsequent induction of type I IFNs (25). In addition, our previous research suggested that TRIM44 stabilized MAVS by inhibiting the K48-linked ubiquitination and degradation of MAVS (26).

RNF90 (also called TRIM7/GNIP), was identified as a RING-type E3 ubiquitin-protein ligase in various cancer pathological conditions (27–30). In innate immunity, RNF90 positively regulates the TLR4-mediated innate response *via* its E3 ligase domain in macrophages (31). RNF90 has been reported to regulate norovirus replication (32). A recent study demonstrated that RNF90 inhibited enterovirus replication by targeting viral 2BC protein for ubiquitination and degradation (33). Our previous study indicated RNF90 deficiency protected mice from DNA virus infection and RNF90 negatively modulated DNA virus- or cytosolic DNA-triggered signaling pathway *via* the enhancement of K48-linked ubiquitination of STING and its proteasome-dependent degradation (34). A recent study showed that RNF90 promoted the Lys63 (K63)-linked polyubiquitination of the envelope protein of Zika virus, which enhances virus entry in cells and brain tissue *in vivo* (35). In this research, we investigated the role of RNF90 in RNA virus-triggered signaling pathways, and our findings suggested RNF90 as a negative regulator of the RIG-I mediated signaling pathway. RNF90 was induced during RNA virus infection, interacted with MAVS, and promoted the K48-linked ubiquitination and subsequent proteasome-dependent degradation of MAVS. RNF90 deficiency enhanced RNA virus-triggered innate immune responses and protected mice from RNA virus infection. Thus, our study demonstrated that RNF90 promoted MAVS degradation and suggest a novel mechanism that regulates antiviral immune responses of host cells against RNA virus invasion.

MATERIALS AND METHODS

Mice

We generated RNF90-deficient mice as described previously (34). The sequences of sgRNA were: K1 (GGCGGAGTTCC AAGCGCTGCGGG), K2 (GGGTCGGCTTCTAAG CCGACTGG) and K3 (CTGGATCTGGCCGCTGAGTTTGG). No RNF90 mRNA or truncated proteins were detected in the RNF90-deficient mice. Mice were housed in a facility with access to food and water and were maintained under a 12-h light/12-h dark cycle. All animal procedures were performed according to guidelines approved by the committee on animal care at Xinxiang Medical University, China. The age- and sex-matched wildtype (WT) and RNF90-deficient mice were used in the experiments.

Plasmids

Plasmids encoding human RNF90 or its deletion mutants were constructed as described previously (34). HA-Ubi, HA-K48-Ubi, HA-K63-Ubi, HA-K48R-Ubi, HA-K63R-Ubi, pIFN-β-Luc, HA/Flag-MAVS were obtained as described previously (26). HA-K6-Ubi (22900), HA-K11-Ubi (22901), HA-K27-Ubi (22902), HA-K29-Ubi (22903), HA-K33-Ubi (17607) were purchased from Addgene.

Reagents

The antibodies for immunoblot analysis or immunoprecipitation were listed as follows: anti-Flag (F3165, Sigma-Aldrich), anti-HA (901515, Biolend), anti-Myc (66004-1-Ig, Proteintech),

anti-RNF90 (sc-109107, Santa Cruz; ab170538, Abcam), anti-MAVS (14341-1-AP, Proteintech), anti-p-TBK1 (5483T, Cell Signaling Technology), anti-TBK1 (CSB-PA024154LA01HU, Flarbio), anti-p-IRF3 (4947, Cell Signaling Technology), anti-IRF3 (sc-9082, Santa Cruz), anti-p-p65 (3033, Cell Signaling Technology), anti-p65 (10745-1-AP, Proteintech), anti-STING (19851-1-AP, Proteintech), anti-Ubi (sc-8017, Santa Cruz), anti-Ubi-K48 (05-1307, Millipore), anti-Ubi-K63 (05-1313, Millipore), anti-VSVg (YM3006, Immunoway), anti-H3 (CSB-PA010109LA01HU, Flarbio), anti-β-tubulin(10068-1-AP, Proteintech), and anti-β-actin (60008-1, Proteintech). The poly (I:C) (tlrl-picw), HSV60 (tlrl-hsv60n) and cGAMP (tlrl-nacga23) were obtained from InvivoGen. The PMA (S1819) was obtained from Beyotime Biotechnology. MG132 (474790) was purchased from Millipore. 3-MA (M9281) and NH4Cl (A9434) were purchased from Sigma-Aldrich.

Cell Culture

HaCaT keratinocytes were obtained from Procell Life Science & Technology Co., Ltd., (Wuhan, China). HEK293T and THP1 cells were purchased from Stem Cell Bank, Chinese Academy of Sciences. The procedures for the generation of BMDMs and MEFs have been described previously (36, 37). THP1 STING-KO cells (thpd-kostg) were purchased from InvivoGen. RNF90-deficient HaCaT cells were generated by the Laboratory of Genetic Regulators in the Immune System in Xinxiang Medical University through CRISPR/Cas9-mediated gene editing. THP1 cells were cultured in RPMI 1640, whereas HaCaT and HEK293T cells were grown in Dulbecco's modified Eagle's medium (DMEM). Phorbol-12-myristate-13-acetate (PMA)-differentiated THP1 (PMA-THP1, a human macrophage-like cell line) cells referred to THP1 cells that were pretreated with 100ng/ml PMA for 24 h. All cells were supplemented with 10% FBS (Gibco), 4 mM L-glutamine, 100μg/ml penicillin, and 100U/ml streptomycin under humidified conditions with 5% CO_2 at 37°C. Transfection of HaCaT, HEK293T, THP1, MEFs, and BMDMs was performed with Lipofectamine 2000 (Invitrogen) according to the manufacturer's instructions.

Immunoprecipitation and Immunoblot Analysis

Immunoprecipitation and immunoblot analysis were performed as described previously (38). Briefly, cells were lysed in lysis buffer (1.0% Nonidet P-40, 20 mM Tris-HCl, 10% glycerol, 150 mM NaCl, 0.2 mM Na_3VO_4, 1mM NaF, 0.1 mM sodium pyrophosphate with a protease inhibitor 'cocktail' (Roche), pH 8.0). After centrifugation for 20 min at 14,000g, supernatants were collected and incubated with the indicated antibodies together with protein A/G Plus-agarose immunoprecipitation reagent (sc-2003, Santa Cruz) at 4°C for 3 h or overnight. After three washes, the immunoprecipitates were boiled in an SDS sample buffer for 10 min and analyzed by immunoblot.

Nuclear Extracts

The nuclear extracts were prepared as described previously (39). In short, cells were lysed with fresh buffer A (10 mM HEPES, 1.5 mM MgCl2 · 6 H2O, 10 mM KCl, 0.5 mM DTT, 0.1% Nonidet P-40, with a protease inhibitor 'cocktail' (Roche), pH 7.9). The lysate was placed on ice for 10 min and centrifuged at 10,000 rpm for 5 min at 4°C to remove cytoplasmic proteins. Nuclear proteins were extracted from the pellet in ice-cold fresh buffer C (20 mM HEPES, 1.5 mM MgCl2 · 6 H2O, 0.42 M NaCl, 0.2 mM EDTA, 25% glycerol, 0.5 mM DTT, with a protease inhibitor 'cocktail' (Roche), pH 7.9). Insoluble material was removed by centrifugation at 10,000 rpm for 5 min at 4°C. Protein concentration was measured by BCA protein assay reagent kit.

Real-Time PCR

Total RNA was extracted from the cultured cells with TRIzol reagent (Invitrogen). All gene transcripts were quantified by real-time PCR with SYBR Green qPCR Master Mix using a 7500 Fast real-time PCR system (Applied Biosystems). The relative fold induction was calculated using the $2^{-\triangle\triangle Ct}$ method. The primers used for real-time PCR were as follows:

Human IFN-β,
Forward, 5'- CACGACAGCTCTTTCCATGA -3';
Reverse, 5'- AGCCAGTGCTCGATGAATCT -3'
Human CXCL10,
Forward, 5'- GGTGAGAAGAGATGTCTGAATCC -3';
Reverse, 5'- GTCCATCCTTGGAAGCACTGCA -3'
Human TNF-α,
Forward, 5'- GGCGTGGAGCTGAGAGATAAC -3';
Reverse, 5'- GGTGTGGGTGAGGAGCACAT -3'
Human RANTES,
Forward, 5'- TACACCAGTGGCAAGTGCTC -3';
Reverse, 5'- ACACACTTGGCGGTTCTTTC -3'
Human ISG56,
Forward, 5'- GCCATTTTCTTTGCTTCCCCTA -3';
Reverse, 5'- TGCCCTTTTGTAGCCTCCTTG -3'
Human GAPDH,
Forward, 5'-TCAACGACCACTTTGTCAAGCTCA-3';
Reverse, 5'-GCTGGTGGTCCAGGTCTTACT-3'
Mouse IFN-β,
Forward, 5'- TCCTGCTGTGCTTCTCCACCACA -3';
Reverse, 5'- AAGTCCGCCCTGTAGGTGAGGTT -3'
Mouse CXCL10,
Forward, 5'- ATCATCCCTGCGAGCCTATCCT -3';
Reverse, 5'- GACCTTTTTTGGCTAAACGCTTTC -3'
Mouse TNF-α,
Forward, 5'- CGTAGGCGATTACAGTCACGG -3';
Reverse, 5'- GACCAGGCTGTCGCTACATCA -3'
Mouse ISG56,
Forward, 5'-ACAGCAACCATGGGAGAGAATGCTG-3';
Forward, 5'-ACGTAGGCCAGGAGGTTGTGCAT-3'
Mouse GAPDH,
Forward, 5'- ACGGCCGCATCTTCTTGTGCA-3';
Reverse, 5'- ACGGCCAAATCCGTTCACACC-3'.

ELISA

The culture media of BMDMs and MEFs or the serum of mice were collected for measurement of IFN-β (PBL) and TNF-α (Thermo Fisher Scientific) by ELISA according to the manufacturer's instructions.

RNA Interference

RNF90 Stealth-RNAi siRNA was designed by the Invitrogen BLOCKiT RNAi Designer. The small interfering RNA (siRNA) sequences used were as follows:

R2,

Forward, 5'-GAGGACUGUGAGGUGUUCCGGUCCA-3';

Reverse, 5'-UGGACCGGAACACCUCACAGUCCUC -3'

R3,

Forward, 5'-CAGUCUCUUCUGAGAUGAAGAAUAA-3';

Reverse, 5'-UUAUUCUUCAUCUCAGAAGAGACUG -3'

The Silencer Select negative control siRNA was obtained from Invitrogen (Catalog no.4390843). Lipofectamine 2000 was used for the transfection of PMA-THP1 or HaCaT cells with siRNA.

Viruses and Infection

Cells were infected with VSV (MOI=1) for 1.5 h. Then the cells were washed with PBS and cultured in fresh media. For the *in vivo* study, age- and sex-matched mice were intravenously or intraperitoneally infected with VSV. VSV viral titer was determined by the plaque-forming assay on Vero cells.

In Vitro Ubiquitination Assay

MAVS, RNF90, and RNF90 mutants were expressed with a TNT Quick-coupled Transcription/Translation Systems kit (L1171, Promega). *In vitro* ubiquitination assay was performed with a ubiquitination kit (BML-UW9920, Enzo Life Science) following the manufacturer's instructions.

Luciferase Reporter Gene Assay

Luciferase reporter gene assays were performed as described previously (38). In short, HEK293T cells were transfected with indicated plasmids. 24 h after transfection, cells were lysed, and reporter activity was analyzed with the Dual-Luciferase Reporter Assay System (Promega).

Confocal Microscopy

After treatment, HEK293T cells were fixed with 4% PFA in PBS, permeabilized with Triton X-100, and then blocked with 1% BSA in PBS. Nuclei were stained with 4, 6-diamidino-2-phenylindole (DAPI).

Statistics

The data are presented as the means ± SD from at least three independent experiments. The statistical comparisons between the different treatments were performed using the unpaired Student *t*-test, and $P < 0.05$ was considered statistically significant.

RESULTS

RNF90 Negatively Regulates RNA Virus-Induced Innate Immune Responses

Our previous work indicated that RNF90 negatively regulated DNA virus- or cytosolic DNA-triggered antiviral innate immune responses (34). We wondered whether RNF90 has a role in RNA virus-triggered signaling pathways. To address this issue, firstly, we examined the expression pattern of RNF90 upon poly (I:C) transfection or RNA virus infection. As shown in **Figures 1A, B**, immunoblot results indicated that RNF90 expression was induced in PMA-THP1 cells upon VSV infection (**Figure 1A**) or poly (I:C) transfection (**Figure 1B**). Then, we evaluated the effect of RNF90 on RNA virus-induced immune responses. Induction of IFN-β, CXCL10, and RANTES upon poly (I:C) transfection or VSV infection was inhibited by RNF90 overexpression in mRNA levels (**Figures 1C, D**). Next, we used the knockdown approach to further address endogenous RNF90 in RNA virus-triggered innate immune responses. PMA-THP1 cells were transfected with control siRNA (SC) or two pairs of siRNA oligonucleotides specific for RNF90 RNA (R2, R3). As shown in **Figure 2A**, both R2 and R3 inhibited endogenous RNF90 expression. In PMA-THP1 cells, real-time PCR results indicated the production of IFN-β and CXCL10 was increased in RNF90-silenced PMA-THP1 cells compared to SC-transfected cells upon poly (I:C) transfection (**Figure 2B**). Consistently, RNF90 knockdown promoted VSV-induced antiviral immune responses, including the production of IFN-β, CXCL10, and RANTES (**Figure 2C**) and the phosphorylation of TBK1, IRF3, and p65 (**Figure 2D**). In addition, standard plaque assay was performed to analyze virus titers in the cell supernatants. The results indicated RNF90 knockdown decreased VSV titers (**Figure 2E**), suggesting the VSV-triggered antiviral immune responses was inhibited by RNF90. Altogether, our results suggested a negative regulatory role of RNF90 in RNA virus-induced innate immune responses.

RNF90 Deficiency Promotes RNA Virus-Triggered Innate Immune Responses in HaCaT Cells

To further investigate the role of RNF90 in RNA virus infection, we generated the RNF90-deficient HaCaT cell line by CRISPR/Cas9 strategy. As shown in **Figure 3A**, the expression of RNF90 could not be detected in RNF90-deficient HaCaT cells by immunoblot assays. Then we stimulated the RNF90-deficient HaCaT cells and WT HaCaT cells with poly (I:C) transfection or VSV infection and evaluated the effects of RNF90 on RNA virus-triggered immune responses. Real-time PCR assays indicated that, compared to WT HaCaT cells, RNF90-deficient HaCaT cells exhibited higher IFN-β and CXCL10 production upon poly (I:C) transfection or VSV infection (**Figures 3B, C**). In addition, in RNF90-deficient HaCaT cells, the phosphorylation of TBK1, IRF3, and p65 was higher than that in WT HaCaT cells (**Figure 3D**). Finally, immunoblot results demonstrated decreased virus protein VSVg in RNF90-deficient HaCaT cells (**Figure 3E**). Altogether, our findings suggested RNF90

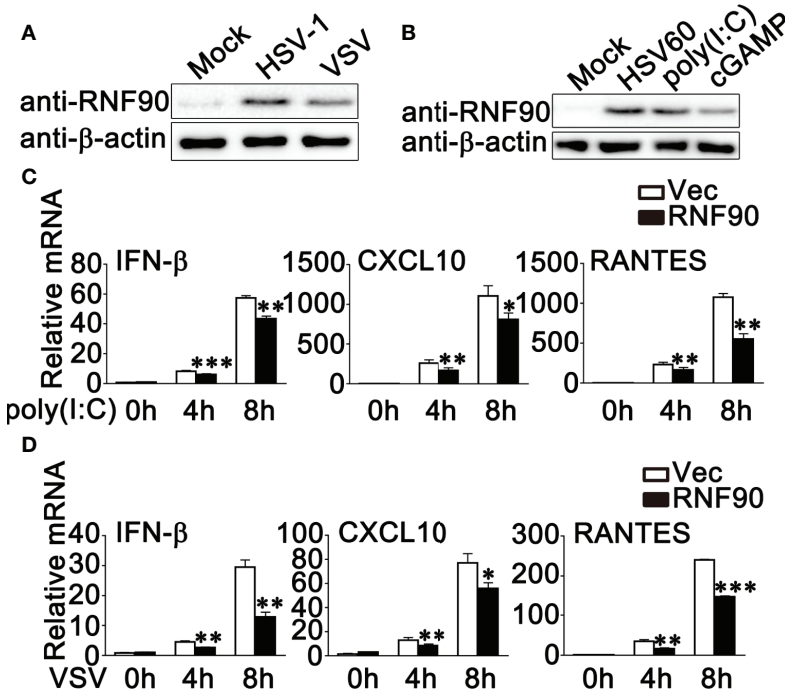

FIGURE 1 | RNF90 overexpression inhibits RNA virus-triggered innate immune responses. **(A)** PMA-THP1 cells were stimulated with HSV-1 (MOI = 1) or VSV (MOI = 1) for 8 h. Afterwards, the cells were lysed for immunoblot assays. **(B)** PMA-THP1 cells were transfected with 1 μg/ml HSV60, 2.5 μg/ml poly(I:C), or 1 μg/ml cGAMP **(B)** for 8 h. Afterwards, the cells were lysed for immunoblot assays. **(C, D)** HEK293T cells were transfected with an empty vector (Vec) or RNF90 plasmid. At 24 h after transfection, HEK293T cells were treated with poly(I:C) (2.5 μg/ml) **(C)** or VSV (MOI = 1) **(D)** for indicated time periods. Then the cells were lysed for real-time PCR analysis. β-actin was used as a loading control in all the immunoblot assays. The data are representative of three independent experiments and are presented as mean ± SEM. $^{*}P < 0.05$, $^{**}P < 0.01$, $^{***}P < 0.001$.

deficiency in HaCaT cells enhanced RNA virus-triggered innate immune responses, suggesting the inhibitory role of RNF90 in RNA virus-induced signaling pathways.

RNF90 Deficiency Promotes RNA Virus-Triggered Innate Immune Responses in Primary MEFs and BMDMs

Next, we isolated and cultured the primary MEFs and BMDMs from RNF90-deficient mice and examined the effects of RNF90 deficiency on RNA virus-triggered antiviral immune responses in primary non-immune and immune cells. As shown in **Figures 4A, B**, RNF90 deficiency enhanced the production of IFN-β, CXCL10, ISG56, and TNF-α in mRNA levels in MEFs upon the treatment of poly (I:C) transfection or VSV infection. Similar results were obtained from BMDMs isolated from RNF90-deficient mice (**Figures 5A, B**). The increase of IFN-β and ISG56 in RNF90-deficient MEFs upon VSV infection could be blocked by RNF90 transfection (**Figure S1**). Additionally, ELISA assays confirmed the increase of IFN-β, and TNF-α production in protein levels in RNF90-deficient MEFs, compared to WT MEFs, upon the treatment of poly (I:C) transfection (**Figure 4C**). Consistently, compared to the cells isolated from WT mice, RNF90-deficient MEFs and BMDMs exhibited a higher IFN-β and TNF-α production after VSV infection (**Figures 4D**, **5C**). Furthermore, in MEFs and BMDMs isolated from WT mice, the impairment of RNF90 resulted in enhanced phosphorylation of TBK1, IRF3, and p65 upon poly (I:C) transfection or VSV infection (**Figures 4E**, **5D**). VSV triggered the nuclear accumulation of IRF3, and p65 was observed in BMDMs (**Figure 5E**). In BMDMs isolated from RNF-deficient mice, the VSV-triggered nuclear accumulation of IRF3 and p65 was enhanced (**Figure 5E**). VSV infection was also suppressed by RNF90 deficiency as suggested by VSV titers using plaque assays in MEFs and VSV protein VSVg expression using immunoblot assays in BMDMs (**Figures 4F**, **5F**). Altogether, our findings in RNF90-deficient primary non-immune and immune cells confirmed that RNF90 inhibited RNA virus-triggered innate immune responses.

RNF90 Deficiency Protects Mice From RNA Virus Infection

Next, WT and RNF90-deficient mice were used to investigate the role of RNF90 in antiviral immune responses against VSV infection *in vivo*. RNF90-deficient mice exhibited prolonged survival after VSV infection, suggesting the protective role of RNF90 impairment during VSV infection in mice (**Figure 6A**). Additionally, less lung destruction was observed in the lungs from RNF90-deficient mice than that from WT mice after VSV

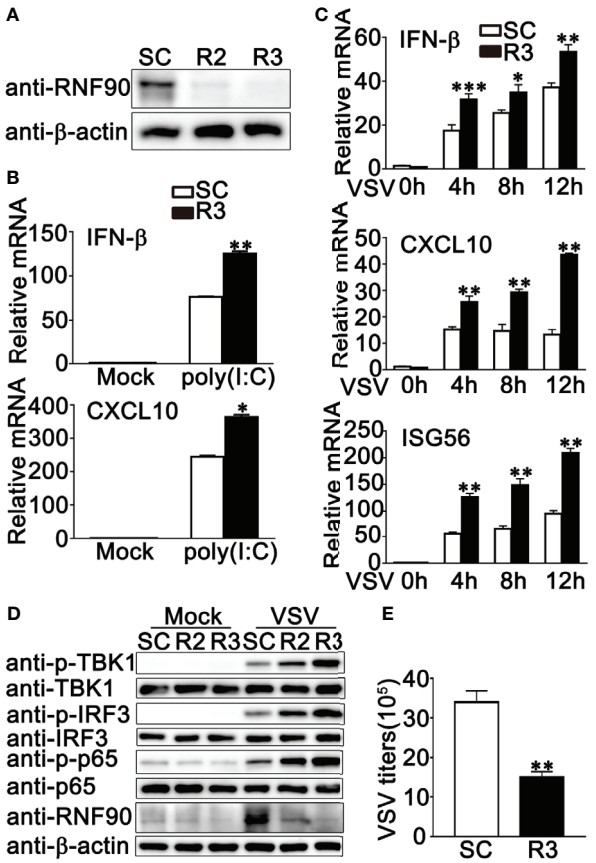

FIGURE 2 | RNF90 knockdown promotes RNA virus-triggered innate immune responses. **(A)** PMA-THP1 cells were transfected with control siRNA (SC) or RNF90-specific siRNA (R2 and R3). At 24 h after transfection, the cells were infected with VSV (MOI = 1) for 8 h and then lysed for immunoblot assay. **(B, C)** PMA-THP1 cells were transfected with control siRNA (SC) or RNF90-specific siRNA (R3). 24 h later, PMA-THP1 cells were treated with poly(I:C) (2.5 μg/ml) for 8 h **(B)** or VSV (MOI = 1) **(C)** for indicated time periods. Then the cells were lysed for real-time PCR analysis. **(D)** PMA-THP1 cells were transfected with control siRNA (SC) or RNF90-specific siRNA (R2, R3). At 24 h after transfection, the cells were infected with VSV (MOI = 1) for 8 h. Then, the cells were lysed for immunoblot analysis. **(E)** PMA-THP1 cells were transfected with control siRNA (SC) or RNF90-specific siRNA (R3). At 24 h after transfection, the cells were infected with VSV (MOI = 1) for 24 h. The titers of VSV were determined by standard plaque assay. β-actin was used as a loading control in all the immunoblot assays. The data are representative of three independent experiments and are presented as mean ± SEM. $^{*}P < 0.05$, $^{**}P < 0.01$, $^{***}P < 0.001$.

infection (**Figure 6B**). Compared to WT mice, higher IFN-β and TNF-α expression levels were observed in the serum of RNF90-deficient mice upon VSV infection (**Figure 6C**). Next, we evaluated the antiviral immune responses in different organs of mice. As shown in **Figures 6D–F**, in lung, liver, and spleen, RNF90 impairment significantly promoted VSV-triggered antiviral immune responses, as suggested by the increased production of IFN-β, CXCL10, ISG56, and TNF-α. Altogether, our findings suggested that RNF90 deficiency protected mice from RNA virus infection.

The Effect of RNF90 on RNA Virus Infection Is Independent of STING

STING has been reported to play a very important role in both RNA viruses- and DNA viruses-induced antiviral immune responses (40–43). Our previous study clarified that RNF90 negatively regulated DNA virus- or cytosolic DNA-triggered antiviral immune responses by targeting STING for degradation (34). Therefore, we wondered whether the effect of RNF90 on RNA virus-induced signaling pathways is independent of STING. To address this question, we constructed STING-deficient THP1 cells and examined the role of RNF90 in RNA virus-triggered immune responses in the absence of STING. As is shown in **Figures 7A**, **S2**, STING-deficient THP1 cells showed undetectable STING expression and impaired IFN-β production upon poly(dA:dT) or HSV60 transfection. Then, control siRNA (SC) or RNF90-specific siRNA (R3) were transfected into STING-deficient PMA-THP1 cells (**Figure 7B**). Real-time PCR assays indicated RNF90 knockdown promoted the production of IFN-β, CXCL10, and ISG56 upon poly (I:C) transfection or VSV infection in the absence of STING, suggesting RNF90 negatively regulated RNA virus-triggered immune responses targeting other proteins involved in the RLR signaling pathway. Altogether, our findings suggested that the effect of RNF90 on RNA virus-triggered antiviral immune response is independent of STING.

RNF90 Interacts With MAVS

To explore the molecular mechanisms underlying the negative regulatory role of RNF90 in RNA virus-triggered anti-viral immune responses, we first identified the target protein of RNF90 by luciferase assay. RIG-I, MAVS, TBK1, and IRF3-5D (the constitutively active mutant of IRF3) are essential to the VSV-induced antiviral signaling pathways. Thus, we examined the effects of RNF90 overexpression on IFN-β reporter activation induced by these molecules. As shown in **Figure 8A**, RNF90 overexpression inhibited IFN-β reporter activation induced by RIG-I, and MAVS, but not by TBK1 and IRF3-5D. Thus, we hypothesized that RNF90 might target MAVS to inhibit RIG-I signaling. To address this hypothesis, we investigated whether RNF90 interacted with MAVS. HA-RNF90 and Flag-MAVS were co-transfected into HEK293T cells, and co-immunoprecipitation assays revealed that RNF90 interacted with MAVS (**Figure 8B**). Additionally, confocal microscopy indicated that Flag-RNF90 colocalized with endogenous MAVS in mitochondria in HEK293T cells with or without poly (I:C) stimulation (**Figure 8C**). We further performed endogenous co-immunoprecipitation experiments, which indicated that RNF90 interacted with MAVS in untreated PMA-THP1 cells, and VSV infection enhanced the interaction at 4 h after infection (**Figure 8D**). Similar results were observed in VSV-infected HaCaT cells (**Figure 8E**). Next, we tried to figure out the region of MAVS responsible for its interaction with RNF90. As shown in **Figures 8F, G**, the residues aa180-360 of MAVS have the strongest association with RNF90, whereas aa 360-540 of MAVS lost the ability to interact with RNF90, suggesting the N-terminal of

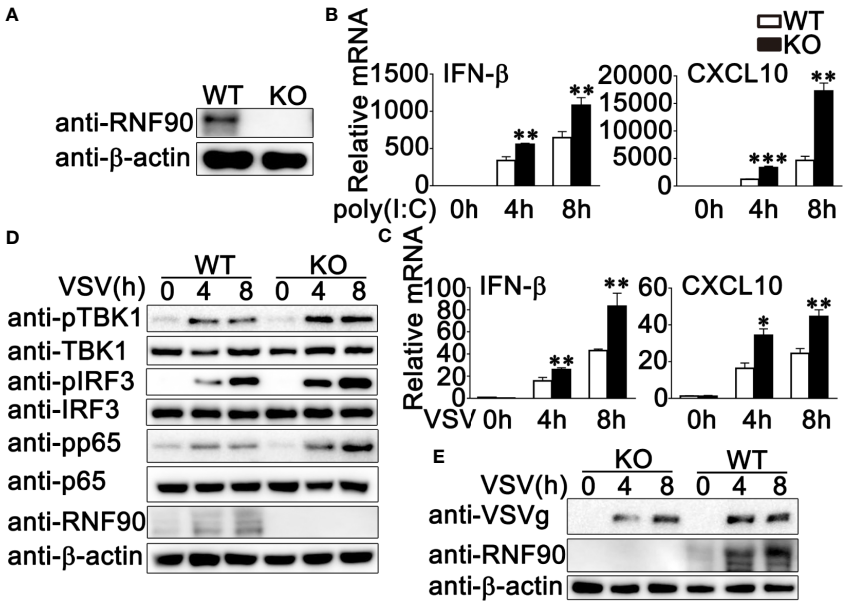

FIGURE 3 | RNF90 deficiency promotes RNA virus-triggered innate immune responses in HaCaT cells. **(A)** WT and RNF90-deficient (KO) HaCaT cells were lysed for immunoblot analysis. **(B, C)** WT and RNF90-deficient (KO) HaCaT cells were treated with poly (I:C) (2.5 μg/ml) **(B)** or VSV (MOI = 1) **(C)** for indicated time points and then lysed for real-time PCR analysis. **(D)** WT and RNF90-deficient (KO) HaCaT cells were infected with VSV (MOI = 1) for indicated time points and then lysed for immunoblot analysis. **(E)** WT and RNF90-deficient (KO) HaCaT were infected with VSV (MOI = 1) for indicated time points and then lysed for immunoblot analysis. β-actin served as a loading control in all the immunoblot assays. The data are representative of three independent experiments. $^{*}P < 0.05$, $^{**}P < 0.01$, $^{***}P < 0.001$.

MAVS is responsible for interaction with RNF90. Finally, we mapped the binding regions on RNF90 for MAVS association. As shown in **Figures 8H, I**, the aa 1-166 and aa 324-511 of RNF90 exhibited no association with MAVS, whereas aa 167-511, aa 1-323, and aa 85-511 of RNF90 maintained the association with MAVS, suggesting aa 167-323 containing the coiled-coil structure might contribute to its interaction with MAVS. Altogether, our findings suggested RNF90 interacted with MAVS.

RNF90 Promotes the Degradation of MAVS

Given that RNF90 interacted with MAVS, we next explored how RNF90 regulated the MAVS-mediated signaling pathway. The stability of MAVS was examined and the immunoblot analysis indicated that RNF90 overexpression inhibited MAVS expression in protein levels in cycloheximide (CHX) chase assay (**Figure S3**). This inhibition could be reversed by the proteasome inhibitor MG132, but not by NH4Cl or 3-MA (**Figure 9A**), suggesting RNF90 promoted MAVS degradation in a proteasome-dependent mechanism. Consistently, compared to WT cells, RNF90-deficient HaCaT cells exhibited a higher expression of MAVS upon VSV infection (**Figure 9B**).

RNF90 Promotes the K48-Linked Ubiquitination of MAVS

Next, we investigated the effect of RNF90 on the ubiquitination of MAVS. RNF90 was co-transfected with MAVS and ubiquitin, and the immunoprecipitation and immunoblot analysis indicated that RNF90 overexpression increased the ubiquitination of MAVS in a dose-dependent manner (**Figure 9C**). RING-domain containing conserved cysteine and histidine residues is essential for the activity of RING-type ubiquitin-protein ligases (22). The C29, 32A mutant of RNF90, in which the integrity of the RING domain was destroyed (30), lost the ability to promote the ubiquitination of MAVS, suggesting the important role of the RING domain in the function of RNF90 (**Figure 9D**). Additionally, *in vitro* ubiquitination assays indicated that RNF90 enhanced the ubiquitination of STING directly (**Figure 9E**). Consistently, C29, 32A mutant of RNF90, or the RNF90 mutant lacking RING domain (ΔR) could not increase the ubiquitination of STING directly (**Figure 9F**). In addition, compared to WT RNF90, C29, 32A, and ΔR mutants exhibited less inhibition on the activation of TBK1, IRF3, and p65 upon VSV infection (**Figure 9G**).

Ubiquitin contains seven Lys residues (K6, K11, K27, K29, K33, K48, and K63) and seven different polyubiquitin chains can be generated (19). Ubiquitin mutants retaining only a single lysine residue were used to determine the type of linkage enhanced by RNF90 in the ubiquitination of MAVS (**Figure 10A**). As shown in **Figure 10B**, RNF90 promoted K48 mutants (only the Lys residue 48 was retained) mediated ubiquitination of MAVS, whereas showed no detectable effect on the ubiquitination mediated by the other six types of mutants, suggesting RNF90 promoted the K48-linked ubiquitination of MAVS. To further confirm the phenomenon, two mutants of ubiquitin, K48R (only the Lys residue 48 was mutated to Arg) and K63R (only the Lys residue 63 was mutated to Arg), were transfected into HEK293T cells with MAVS and RNF90. Immunoprecipitation and immunoblot analysis indicated that RNF90 promoted K63R mediated ubiquitination of STING, but not K48R, indicating the Lys

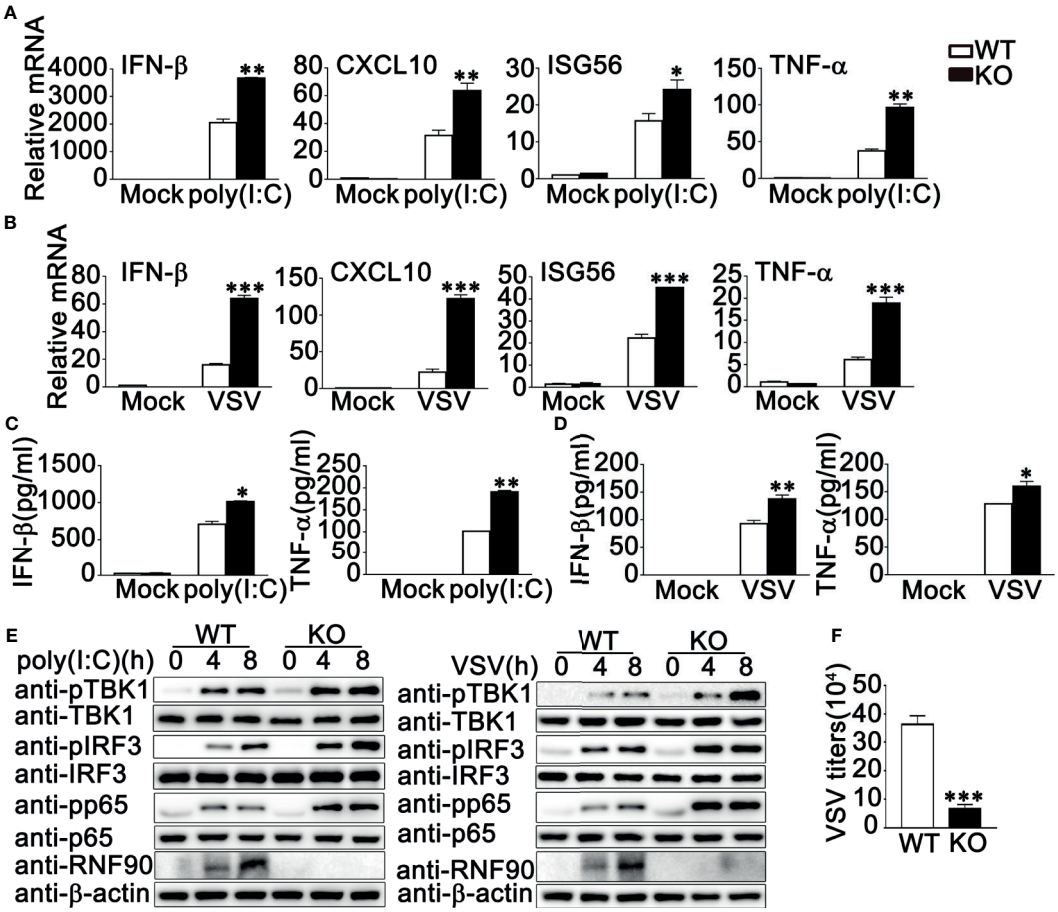

FIGURE 4 | RNF90 deficiency promotes RNA virus-triggered innate immune responses in MEFs. **(A, B)** WT and RNF90-deficient (KO) MEFs were treated with poly (I:C) (2.5 μg/ml) **(A)** or VSV (MOI = 1) **(B)** for 8 h. The cells were lysed for real-time PCR analysis. **(C, D)** WT and RNF90-deficient (KO) MEFs were stimulated with poly(I:C) (2.5 μg/ml) **(C)** or VSV (MOI = 1) **(D)** for 24 h. The supernatants were collected and subjected to ELISA analysis. **(E)** WT and RNF90-deficient (KO) MEFs were transfected with poly (I:C) (2.5 μg/ml) or VSV (MOI = 1) for indicated time points. Then the cells were lysed for immunoblot analysis. **(F)** WT and RNF90-deficient (KO) MEFs were infected with VSV for 24 h. The titers of VSV were determined by standard plaque assays. β-actin served as a loading control in all the immunoblot assays. The data are representative of three independent experiments and are presented as mean ± SEM. $^{*}P < 0.05$, $^{**}P < 0.01$, $^{***}P < 0.001$.

residue 48 was essential to the RNF90-triggered linkage of MAVS with ubiquitin (**Figure 10C**). Furthermore, RNF90-deficiency in HaCaT cells inhibited poly(I:C) transfection induced K48-linked ubiquitination of MAVS, but no significant effect of RNF90 was observed on K63-linked ubiquitination of MAVS (**Figure 10D**). Additionally, RNF90-deficient MEF cells exhibited weaker K48-linked ubiquitination of MAVS upon VSV infection (**Figure 10E**) than WT cells. Altogether, our data indicated that RNF90 promoted the K48-linked ubiquitination of MAVS and its subsequent proteasome-dependent degradation.

DISCUSSION

In recent years, accumulating evidence has demonstrated the critical role of ubiquitination in regulating antiviral innate immune responses (44). Our previous research work suggested RNF90 negatively regulated DNA virus-triggered innate immune responses targeting STING (34). Because of the important role of STING in the RNA virus-triggered signaling pathway (45), it is reasonable for us to propose the hypothesis that RNF90 could act as a negative regulator during RNA virus infection. To prove our hypothesis, first of all, we explored whether RNF90 was expressed during RNA virus infection and our findings indicated that RNF90 expression was induced upon poly (I:C) transfection or RNA virus infection. Next, we evaluated the effect of RNF90 on RNA virus-induced immune responses in cells with RNF90 overexpression, RNF90-silenced cells, RNF90-deficient cells, and RNF90-deficient mice. Firstly, RNF90 overexpression in HEK293T cells inhibited IFN-β, CXCL10, and RANTES production upon poly (I:C) transfection or VSV infection. Secondly, in RNF90-silenced PMA-THP1 cells, VSV triggered antiviral innate immune responses was promoted, compared to PMA-THP1 cells transfected with control siRNA. Thirdly, we generated RNF90-deficient HaCaT cell line by CRISPR/Cas9 strategy, in which higher expression of IFN-β and CXCL10,

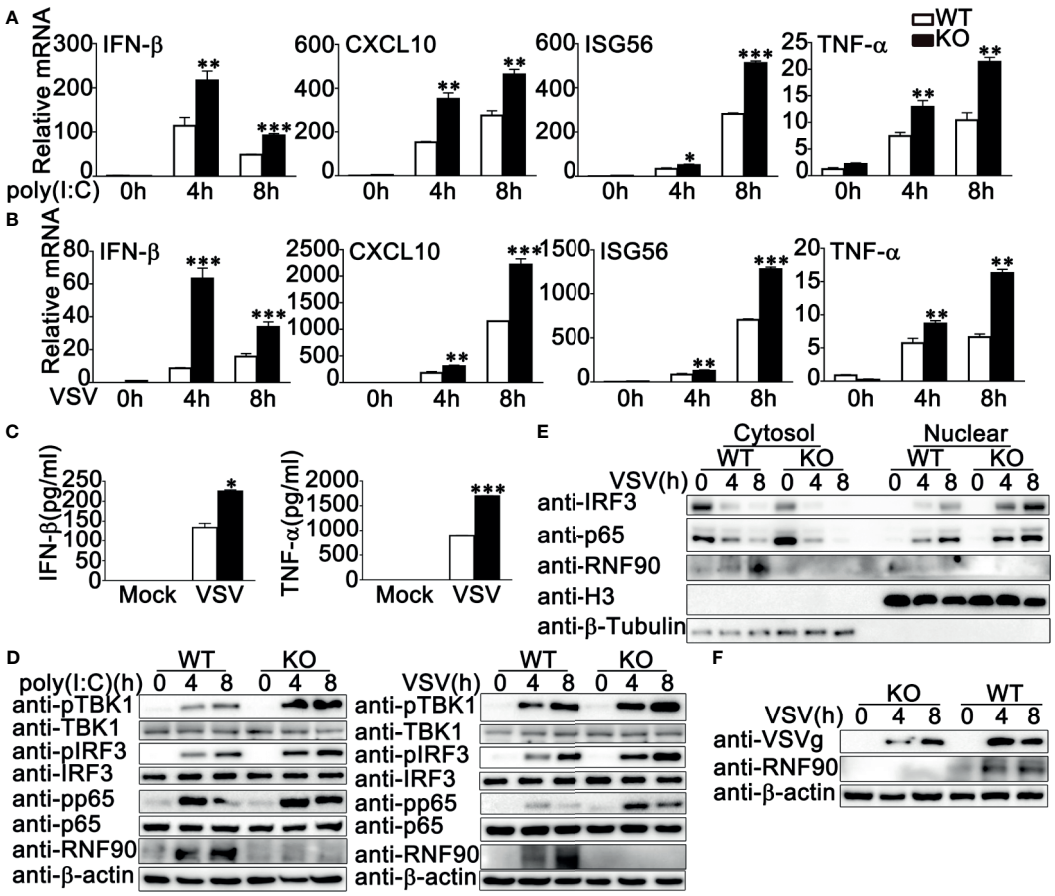

FIGURE 5 | RNF90 deficiency promotes RNA virus-triggered innate immune responses in BMDMs. **(A, B)** WT and RNF90-deficient (KO) BMDMs were treated with poly(I:C) (2.5 μg/ml) **(A)** or VSV (MOI = 1) **(B)** for indicated time periods. Then the cells were lysed for real-time PCR analysis. **(C)** WT and RNF90-deficient (KO) BMDMs were infected with VSV (MOI = 1) for 24 h. The supernatants were collected and subjected to ELISA analysis. **(D)** WT and RNF90-deficient (KO) BMDMs were treated with poly(I:C) (2.5 μg/ml) or VSV (MOI = 1) for indicated time periods. Then the cells were lysed for immunoblot analysis. **(E)** WT and RNF90-deficient (KO) BMDMs were infected with VSV (MOI = 1) for indicated time points and then fractionated into cytosolic and nuclear subfractions. The immunoblot assay was performed as indicated. **(F)** WT and RNF90-deficient (KO) BMDMs were infected with VSV (MOI = 1) for indicated time points. Then the cells were lysed for immunoblot analysis. β-actin served as a loading control in all the immunoblot assays. The data are representative of three independent experiments. $^{*}P < 0.05$, $^{**}P < 0.01$, $^{***}P < 0.001$.

enhanced activation of TBK1, IRF3, and p65, decreased expression of virus protein VSVg was observed upon VSV infection. Fourthly, we isolated and cultured the primary MEFs and BMDMs from WT and RNF90-deficient mice. Consistently, RNF90-deficient primary MEFs and BMDMs exhibited potentiated activation of TBK1, IRF3, and p65 and enhanced production of IFN-β, CXCL10, ISG56, and TNF-α after the stimulation of VSV or poly (I:C). Finally, RNF90-deficient mice exhibited prolonged survival and increased production of type I IFN and proinflammatory cytokine in the lung, liver, and spleen during VSV infection. All these data strongly demonstrated that RNF90 negatively regulated RNA virus-induced innate immune responses.

Then, we tried to explore whether the effect of RNF90 on RNA virus-triggered innate immune responses was dependent on STING. Surprisingly, in STING-deficient THP1 cells, RNF90 knockdown still affected the production of IFN-β, CXCL10, and ISG56 upon poly (I:C) transfection or VSV infection, suggesting the effect of RNF90 on RNA virus-triggered antiviral immune response is independent of STING. Thus, during the negative regulation of RNA virus-triggered immune responses by RNF90, other target proteins regulated by RNF90 needed to be identified. Then, luciferase assays were performed to identify the downstream signaling and target protein of RNF90, revealing that MAVS might be the target protein. Next, both co-immunoprecipitation assays and confocal microscopy indicated RNF90 interacted with MAVS, and this interaction was enhanced by viral infection. Considering the essential role of MAVS in the RLR signaling pathway, it was reasonable that RNF90 might target MAVS for the negative regulation of innate immune responses against RNA viruses. Our previous data have demonstrated that RNF90 promotes the K48-linked ubiquitination on K150 and degradation of STING (34), so we first examined whether RNF90 had similar effects on MAVS. As

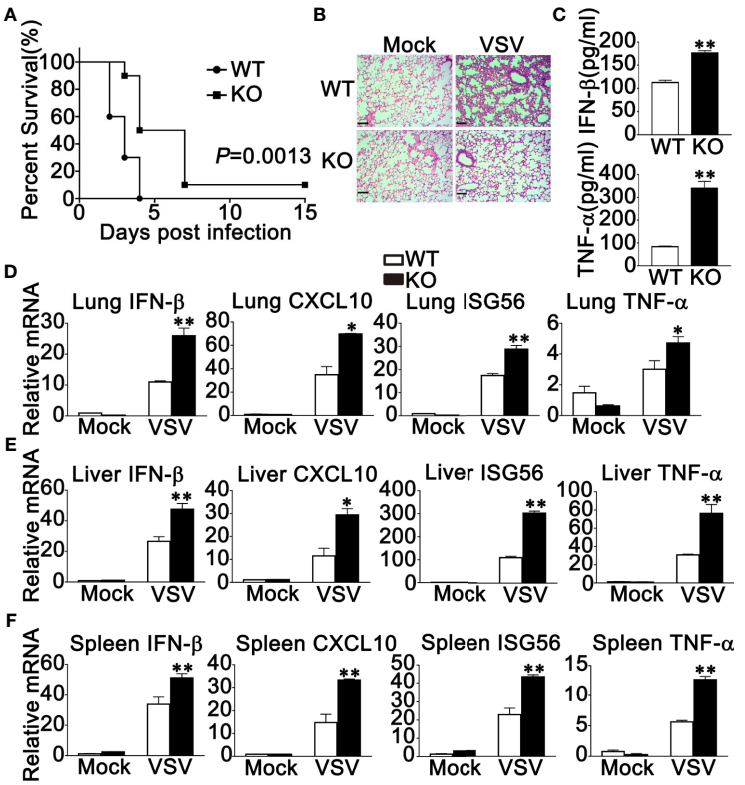

FIGURE 6 | RNF90 deficiency protects mice from RNA virus infection. **(A)** Sex and age-matched WT and RNF90-deficient (KO) mice (n = 5) were intraperitoneally (i.p.) infected with VSV [5×10^8 plaque-forming units (PFU)]. Mouse survival rates were observed and recorded for 15 days. The data were analyzed by Log-rank (Mantel-Cox) test. **(B)** Sex and age-matched WT and RNF90-deficient (KO) mice were intraperitoneally (i.p.) infected with VSV (5×10^7 PFU) for 24 h, and lung sections were analyzed by H&E staining. Scale bars, 200 μm. **(C)** ELISA of IFN-β and TNF-α in serum of WT and RNF90-deficient (KO) mice 6 h after intraperitoneal (i.p.) infection with VSV (5×10^7 PFU). **(D-F)** WT and RNF90-deficient (KO) mice were intraperitoneally infected with VSV (5×10^7 PFU) for 24 h, and then the lungs **(D)**, livers **(E)**, and spleens **(F)** of the mice were subjected to real-time PCR analysis. The data are representative of three independent experiments. $^*P < 0.05$, $^{**}P < 0.01$.

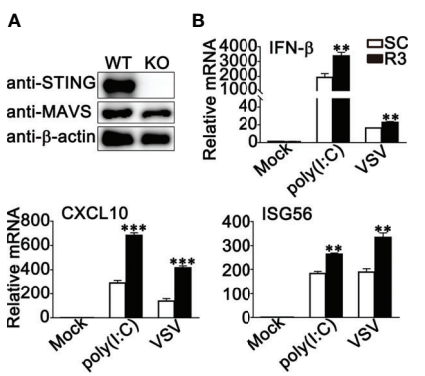

FIGURE 7 | RNF90 inhibits RNA virus-triggered innate immune responses independent of STING Signaling. **(A)** WT and STING-deficient (KO) PMA-THP1 cells were lysed for immunoblot analysis. β-actin served as a loading control. **(B)** STING-deficient (KO) PMA-THP1 cells were transfected with control siRNA (SC) or RNF90-specific siRNA (R3) for 24 h and then transfected with poly (I:C) or infected with VSV for 8 h. Then, the cells were lysed for real-time PCR assays. The data are representative of three independent experiments and are presented as mean ± SEM. $^{**}P < 0.01$, $^{***}P < 0.001$.

expected, RNF90 increased the K48-linked ubiquitination and the subsequent degradation of MAVS in a proteasome-dependent mechanism, which relied on the RING domain of RNF90. However, we did not find the motif in the sequence of MAVS similar to that contained K150 in STING. Thus, as shown in **Figure 11**, our findings suggest a novel mechanism of negative regulation of antiviral innate immune response against RNA viruses.

Whereas the essential role of STING in DNA virus- or cytosolic DNA-triggered innate immune responses has been clarified (40–43), the function and mechanisms of STING in RNA virus-triggered antiviral immune responses remain less clear (46). It seems that STING regulates innate immune responses against RNA viruses in a virus- and cell-type-specific manner (45). For example, STING-deficient MEFs exhibited high susceptibility to VSV infection, but STING-deficient BMDCs or BMDMs did not (45). Furthermore, STING-deficient mice were defective in type I IFN production upon VSV infection but not encephalomyocarditis virus (EMCV), suggesting that STING may be only involved in RIG-I, but not MDA5-mediated signaling (45). Our research findings indicated RNF90 regulated RNA-triggered immune responses targeting

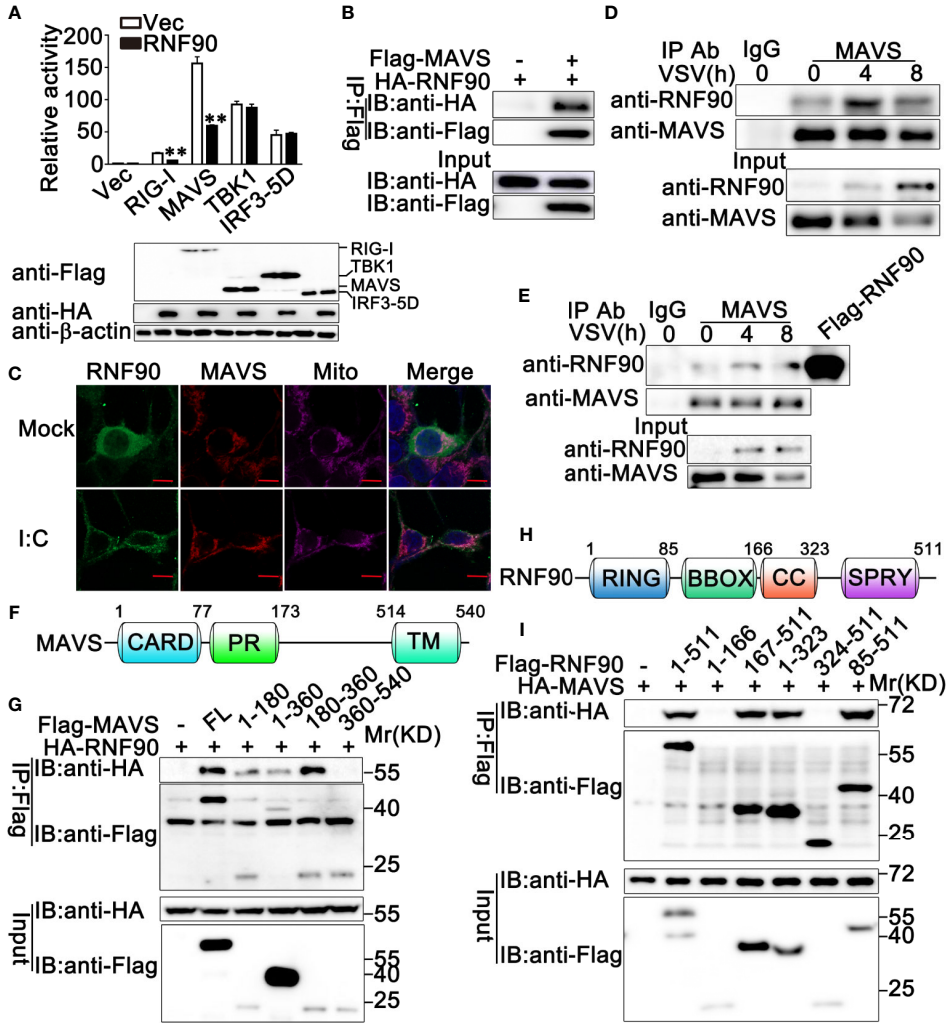

FIGURE 8 | RNF90 interacts with MAVS. **(A)** HEK293T cells were transfected with an IFN-β luciferase reporter, together with RIG-I, MAVS, TBK1, or IRF3-5D and the empty vector (Vec) or the RNF90 plasmid. At 24h after transfection, the cells were lysed for luciferase assay and immunoblot analysis. β-actin served as a loading control. $^{**}P < 0.01$. **(B)** HEK293T cells were transfected with HA-RNF90, together with the empty vector (-) or Flag-MAVS plasmid. At 24 h after transfection, the cells were lysed and subjected to immunoprecipitation (IP) and immunoblot (IB) analysis. **(C)** HEK293T cells were transfected with Flag-RNF90, at 24 h after transfection, HEK293T cells were stimulated with poly(I:C) (2.5 μg/ml) or left untreated for another 8 h. Immunofluorescence was performed using anti-Flag (green) and anti-MAVS (red). Mitochondria and Nuclei were stained with Mito Tracker or DAPI, respectively. Scale bars, 10 μm. **(D, E)** PMA-THP1 cells **(D)** or HaCaT cells **(E)** were infected with VSV (MOI = 1) for indicated time points, and then the cell lysates were subjected to immunoprecipitation (IP) and immunoblot (IB) analysis as indicated. **(F)** A schematic presentation of full-length MAVS and its mutants. **(G)** HEK293T cells were transfected with plasmids as indicated. At 24 h after transfection, the cell lysates were subjected to immunoprecipitation (IP) and immunoblot (IB) analysis as indicated. **(H)** A schematic presentation of full-length RNF90 and its mutants. **(I)** HEK293T cells were transfected with plasmids as indicated. At 24 h after transfection, the cell lysates were subjected to immunoprecipitation (IP) and immunoblot (IB) analysis as indicated. The data are representative of three independent experiments.

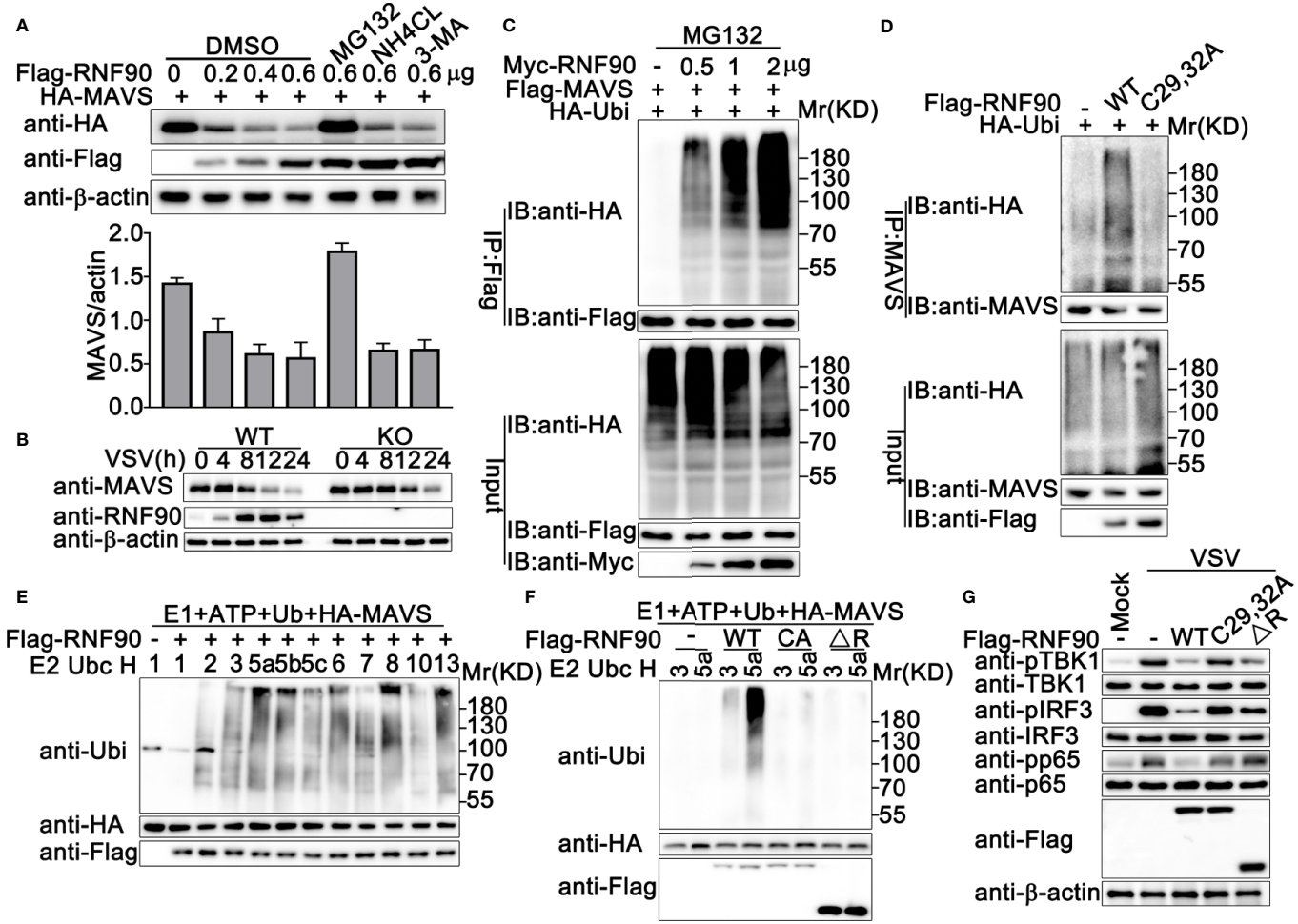

FIGURE 9 | RNF90 enhances the degradation of MAVS **(A)** HEK293T cells were transfected with HA-MAVS and the increasing amounts of RNF90 plasmids as indicated. 24 h later, cells were treated with DMSO as control, MG132 (20 mM), NH_4CL (5 mM), or 3-MA (2 mM) separately for 6 h and lysed for immunoblot assays (Top). The quantity of MAVS expression was normalized by β-actin (Bottom). **(B)** WT and RNF90-deficient (KO) HaCaT cells were infected with VSV (MOI = 1) for indicated time points, and the cell lysates were then subjected to immunoblot analysis. β-actin served as a loading control in all the immunoblot assays. **(C)** HEK293T cells were transfected with the indicated plasmids and increasing amounts of Myc-RNF90 (0, 0.5, 1, and 2 μg). 24 h later, cells were treated with MG132 (20 mM) for 6 h. Then, the cells were lysed and subjected to immunoprecipitation (IP) and immunoblot (IB) analysis. **(D)** HEK293T cells were transfected with HA-Ubiquitin (Ubi) plasmid, with empty vector (-), WT Flag-RNF90, or C29, 32A mutant plasmid. At 24 h after transfection, the cells were lysed and subjected to immunoprecipitation (IP) and immunoblot (IB) analysis. **(E, F)** Immunoblot analysis of MAVS ubiquitination *in vitro*. MAVS and WT RNF90 **(E)** or its mutants **(F)** were quickly translated *in vitro*, and the biotin-ubiquitin E1 and indicated E2s were added for the *in vitro* ubiquitination assays. Ubiquitination of MAVS was detected by anti-Ubi. **(G)** RNF90-deficient MEFs were transfected with indicated plasmids. At 24 h after transfection, the cells were infected with VSV (MOI = 1) for 4 h, and then the cell lysates were subjected to immunoblot analysis. The data are representative of three independent experiments.

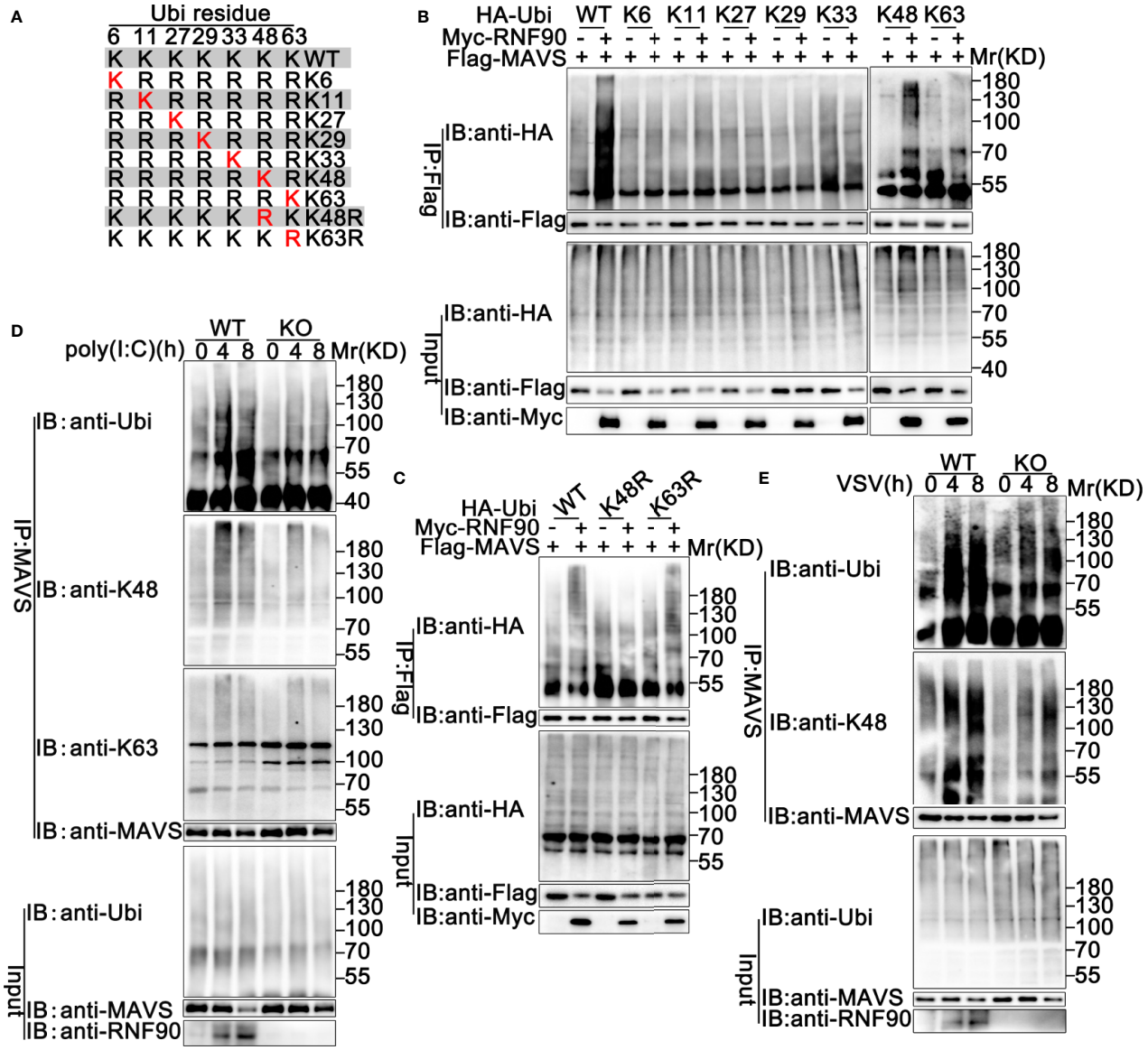

FIGURE 10 | RNF90 promotes K48-linked ubiquitination of MAVS. **(A)** A schematic presentation of Ubi and its mutants. **(B, C)** HEK293T cells were transfected with the indicated plasmids. At 24 h after transfection, immunoprecipitation (IP) and immunoblot (IB) analysis were performed as indicated. **(D)** WT and RNF90-deficient (KO) HaCaT cells were stimulated with poly(I:C) (2.5 μg/ml) for the indicated time points. Then the cells were lysed and subjected to immunoprecipitation (IP) and immunoblot (IB) analysis. **(E)** WT and RNF90-deficient (KO) MEFs were infected with VSV (MOI = 1) for the indicated time points. Then the cells were lysed and subjected to immunoprecipitation (IP) and immunoblot (IB) analysis. The data are representative of three independent experiments.

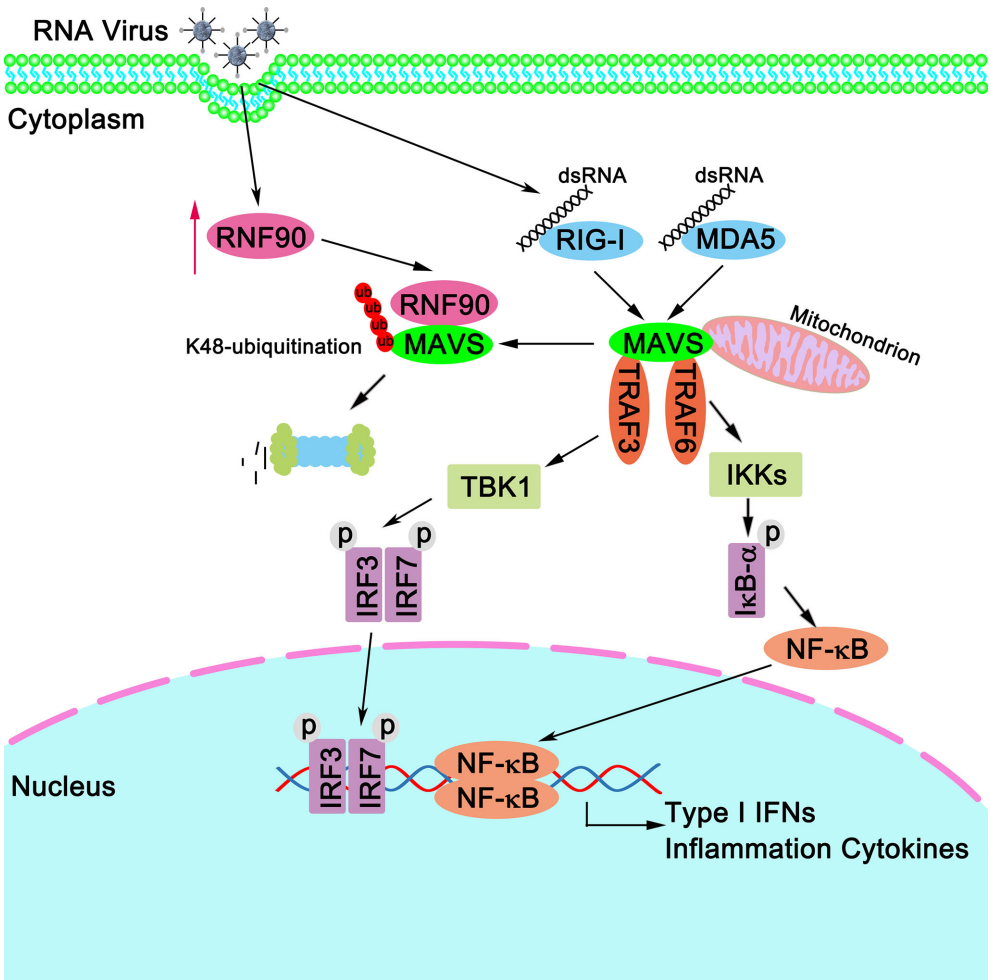

FIGURE 11 | A schematic model illustrating functional involvement of RNF90 in MAVS-mediated antiviral signaling. Upon RNA virus infection, RIG-I binds to viral dsRNA and activates MAVS. MAVS recruits TRAF3 and TRAF6 to activate type I IFN and inflammation cytokines production. Host protein RNF90, as identified in this study, ubiquitinates MAVS for degradation and tones down the responses to RNA virus infection, thereby contributing to the maintenance of balanced antiviral innate immune responses.

MAVS, independent of STING, suggesting the negative regulatory role of RNF90 in the process of RNA virus infection may be universal. Thus RNF90 has the potential to manipulate the signaling pathways mediated by both RIG-I and MDA5.

Several molecules have been identified to target MAVS to regulate the antiviral signaling pathway (47). It is unclear why different molecules are needed to control MAVS degradation to turn off the antiviral innate immune responses. It will be very interesting to investigate these regulators' expression patterns and functions during specific viral infections. Further investigations about the collaboration of these factors responsible for MAVS degradation in human diseases are also needed to address this issue.

In summary, our data suggest that RNF90, the expression of which is induced by the infection of RNA viruses, negatively regulates MAVS-mediated innate immune responses against RNA viruses. RNF90 interacts with MAVS, promotes its K48-linked ubiquitination and subsequent proteasome-dependent degradation. These results characterized a novel mechanism underlying the regulation and termination of MAVS-mediated innate immune responses against RNA viruses.

DATA AVAILABILITY STATEMENT

The raw data supporting the conclusions of this article will be made available by the authors, without undue reservation.

ETHICS STATEMENT

The animal study was reviewed and approved by committee on animal care at Xinxiang Medical University (Approval Number: XXMUSPF2017-0045).

AUTHOR CONTRIBUTIONS

BY and JW designed the experiments, analyzed the data, and wrote the manuscript. BY, JW, YuL, YC, DS, GZ, SM, YaL, MC, and FC performed the experiments. HW helped with the revision of the manuscript. All authors contributed to the article and approved the submitted version.

FUNDING

This work was supported by the National Natural Science Foundation of China Grants U1704183, 31970847, 32070949, and U2004103, Henan Medical Science and Technology Research Project LHGJ20200081, and by Henan Undergraduate Training Program for Innovation and Entrepreneurship S202010472024.

ACKNOWLEDGMENTS

We want to thank Dr. Yinming Liang for providing RNF90-deficient mice and all the members of Henan Key Laboratory of immunology and targeted drug for sharing valuable material and research support.

SUPPLEMENTARY MATERIAL

The Supplementary Material for this article can be found online at: https://www.frontiersin.org/articles/10.3389/fimmu.2021.730483/full#supplementary-material

REFERENCES

1. Poltronieri P, Sun B, Mallardo M. RNA Viruses: RNA Roles in Pathogenesis, Coreplication and Viral Load. *Curr Genomics* (2015) 16(5):327–35. doi: 10.2174/1389202916666150707160613
2. Zhu H, Zheng C. When PARPs Meet Antiviral Innate Immunity. *Trends Microbiol* (2021) 29(9):776–8. doi: 10.1016/j.tim.2021.01.002
3. Said EA, Diaz-Griffero F, Bonte D, Lamarre D, Al-Jabri AA. Immune Responses to RNA Viruses. *J Immunol Res* (2018) 2018:5473678. doi: 10.1155/2018/5473678
4. Huang C, Wang Y, Li X, Ren L, Zhao J, Hu Y, et al. Clinical Features of Patients Infected With 2019 Novel Coronavirus in Wuhan, China. *Lancet* (2020) 395(10223):497–506. doi: 10.1016/S0140-6736(20)30183-5
5. Beachboard DC, Horner SM. Innate Immune Evasion Strategies of DNA and RNA Viruses. *Curr Opin Microbiol* (2016) 32:113–9. doi: 10.1016/j.mib.2016.05.015
6. Roers A, Hiller B, Hornung V. Recognition of Endogenous Nucleic Acids by the Innate Immune System. *Immunity* (2016) 44(4):739–54. doi: 10.1016/j.immuni.2016.04.002
7. Takeda K, Kaisho T, Akira S. Toll-Like Receptors. *Annu Rev Immunol* (2003) 21:335–76. doi: 10.1146/annurev.immunol.21.120601.141126
8. Takeuchi O, Akira S. MDA5/RIG-I and Virus Recognition. *Curr Opin Immunol* (2008) 20(1):17–22. doi: 10.1016/j.coi.2008.01.002
9. Kato H, Takeuchi O, Sato S, Yoneyama M, Yamamoto M, Matsui K, et al. Differential Roles of MDA5 and RIG-I Helicases in the Recognition of RNA Viruses. *Nature* (2006) 441(7089):101–5. doi: 10.1038/nature04734
10. Kawai T, Takahashi K, Sato S, Coban C, Kumar H, Kato H, et al. IPS-1, An Adaptor Triggering RIG-I- and Mda5-Mediated Type I Interferon Induction. *Nat Immunol* (2005) 6(10):981–8. doi: 10.1038/ni1243
11. Xu LG, Wang YY, Han KJ, Li LY, Zhai Z, Shu HB. VISA Is an Adapter Protein Required for Virus-Triggered IFN-Beta Signaling. *Mol Cell* (2005) 19(6):727–40. doi: 10.1016/j.molcel.2005.08.014
12. Seth RB, Sun L, Ea CK, Chen ZJ. Identification and Characterization of MAVS, A Mitochondrial Antiviral Signaling Protein That Activates NF-KappaB and IRF 3. *Cell* (2005) 122(5):669–82. doi: 10.1016/j.cell.2005.08.012
13. Meylan E, Curran J, Hofmann K, Moradpour D, Binder M, Bartenschlager R, et al. Cardif Is an Adaptor Protein in the RIG-I Antiviral Pathway and Is Targeted by Hepatitis C Virus. *Nature* (2005) 437(7062):1167–72. doi: 10.1038/nature04193
14. Saha SK, Pietras EM, He JQ, Kang JR, Liu SY, Oganesyan G, et al. Regulation of Antiviral Responses by a Direct and Specific Interaction Between TRAF3 and Cardif. *EMBO J* (2006) 25(14):3257–63. doi: 10.1038/sj.emboj.7601220
15. Chen Q, Sun L, Chen ZJ. Regulation and Function of the cGAS-STING Pathway of Cytosolic DNA Sensing. *Nat Immunol* (2016) 17(10):1142–9. doi: 10.1038/ni.3558
16. Zhu H, Zheng C. The Race Between Host Antiviral Innate Immunity and the Immune Evasion Strategies of Herpes Simplex Virus 1. *Microbiol Mol Biol Rev* (2020) 84(4):e00099-20. doi: 10.1128/MMBR.00099-20
17. Zheng C. Protein Dynamics in Cytosolic DNA-Sensing Antiviral Innate Immune Signaling Pathways. *Front Immunol* (2020) 11:1255. doi: 10.3389/fimmu.2020.01255
18. Chiang C, Gack MU. Post-Translational Control of Intracellular Pathogen Sensing Pathways. *Trends Immunol* (2017) 38(1):39–52. doi: 10.1016/j.it.2016.10.008
19. Park Y, Jin HS, Aki D, Lee J, Liu YC. The Ubiquitin System in Immune Regulation. *Adv Immunol* (2014) 124:17–66. doi: 10.1016/B978-0-12-800147-9.00002-9
20. Liu X, Wang Q, Chen W, Wang C. Dynamic Regulation of Innate Immunity by Ubiquitin and Ubiquitin-Like Proteins. *Cytokine Growth Factor Rev* (2013) 24(6):559–70. doi: 10.1016/j.cytogfr.2013.07.002
21. Zinngrebe J, Montinaro A, Peltzer N, Walczak H. Ubiquitin in the Immune System. *EMBO Rep* (2014) 15(1):28–45. doi: 10.1002/embr.201338025
22. Vittal V, Stewart MD, Brzovic PS, Klevit RE. Regulating the Regulators: Recent Revelations in the Control of E3 Ubiquitin Ligases. *J Biol Chem* (2015) 290(35):21244–51. doi: 10.1074/jbc.R115.675165
23. Liu B, Gao C. Regulation of MAVS Activation Through Post-Translational Modifications. *Curr Opin Immunol* (2018) 50:75–81. doi: 10.1016/j.coi.2017.12.002
24. Castanier C, Zemirli N, Portier A, Garcin D, Bidere N, Vazquez A, et al. MAVS Ubiquitination by the E3 Ligase TRIM25 and Degradation by the Proteasome Is Involved in Type I Interferon Production After Activation of the Antiviral RIG-I-Like Receptors. *BMC Biol* (2012) 10:44. doi: 10.1186/1741-7007-10-44
25. Liu B, Zhang M, Chu H, Zhang H, Wu H, Song G, et al. The Ubiquitin E3 Ligase TRIM31 Promotes Aggregation and Activation of the Signaling Adaptor MAVS Through Lys63-Linked Polyubiquitination. *Nat Immunol* (2017) 18(2):214–24. doi: 10.1038/ni.3641
26. Yang B, Wang J, Wang Y, Zhou H, Wu X, Tian Z, et al. Novel Function of Trim44 Promotes an Antiviral Response by Stabilizing VISA. *J Immunol* (2013) 190(7):3613–9. doi: 10.4049/jimmunol.1202507
27. Zhou C, Zhang Z, Zhu X, Qian G, Zhou Y, Sun Y, et al. N6-Methyladenosine Modification of the TRIM7 Positively Regulates Tumorigenesis and Chemoresistance in Osteosarcoma Through Ubiquitination of BRMS1. *EBioMedicine* (2020) 59:102955. doi: 10.1016/j.ebiom.2020.102955
28. Jin J, Lu Z, Wang X, Liu Y, Han T, Wang Y, et al. E3 Ubiquitin Ligase TRIM7 Negatively Regulates NF-Kappa B Signaling Pathway by Degrading P65 in Lung Cancer. *Cell Signal* (2020) 69:109543. doi: 10.1016/j.cellsig.2020.109543
29. Zhu L, Qin C, Li T, Ma X, Qiu Y, Lin Y, et al. The E3 Ubiquitin Ligase TRIM7 Suppressed Hepatocellular Carcinoma Progression by Directly Targeting Src Protein. *Cell Death Differ* (2020) 27(6):1819–31. doi: 10.1038/s41418-019-0464-9
30. Chakraborty A, Diefenbacher ME, Mylona A, Kassel O, Behrens A. The E3 Ubiquitin Ligase Trim7 Mediates C-Jun/AP-1 Activation by Ras Signalling. *Nat Commun* (2015) 6:6782. doi: 10.1038/ncomms7782
31. Lu M, Zhu X, Yang Z, Zhang W, Sun Z, Ji Q, et al. E3 Ubiquitin Ligase Tripartite Motif 7 Positively Regulates the TLR4-Mediated Immune Response

via Its E3 Ligase Domain in Macrophages. *Mol Immunol* (2019) 109:126–33. doi: 10.1016/j.molimm.2019.01.015
32. Orchard RC, Sullender ME, Dunlap BF, Balce DR, Doench JG, Virgin HW. Identification of Antinorovirus Genes in Human Cells Using Genome-Wide CRISPR Activation Screening. *J Virol* (2019) 93(1):e01324–18. doi: 10.1128/JVI.01324-18
33. Fan W, Mar KB, Sari L, Gaszek IK, Cheng Q, Evers BM, et al. TRIM7 Inhibits Enterovirus Replication and Promotes Emergence of a Viral Variant With Increased Pathogenicity. *Cell* (2021) 184(13):3410–25.e17. doi: 10.1016/j.cell.2021.04.047
34. Yang B, Liu Y, Cui Y, Song D, Zhang G, Ma S, et al. RNF90 Negatively Regulates Cellular Antiviral Responses by Targeting MITA for Degradation. *PloS Pathog* (2020) 16(3):e1008387. doi: 10.1371/journal.ppat.1008387
35. Giraldo MI, Xia H, Aguilera-Aguirre L, Hage A, van Tol S, Shan C, et al. Envelope Protein Ubiquitination Drives Entry and Pathogenesis of Zika Virus. *Nature* (2020) 585(7825):414–9. doi: 10.1038/s41586-020-2457-8
36. Lou Y, Han M, Liu H, Niu Y, Liang Y, Guo J, et al. Essential Roles of S100A10 in Toll-Like Receptor Signaling and Immunity to Infection. *Cell Mol Immunol* (2020) 17(10):1053–62. doi: 10.1038/s41423-019-0278-1
37. Nold-Petry CA, Nold MF, Nielsen JW, Bustamante A, Zepp JA, Storm KA, et al. Increased Cytokine Production in Interleukin-18 Receptor Alpha-Deficient Cells Is Associated With Dysregulation of Suppressors of Cytokine Signaling. *J Biol Chem* (2009) 284(38):25900–11. doi: 10.1074/jbc.M109.004184
38. Wang J, Kang L, Song D, Liu L, Yang S, Ma L, et al. Ku70 Senses HTLV-1 DNA and Modulates HTLV-1 Replication. *J Immunol* (2017) 199(7):2475–82. doi: 10.4049/jimmunol.1700111
39. Yang B, Song D, Liu Y, Cui Y, Lu G, Di W, et al. IFI16 Regulates HTLV-1 Replication Through Promoting HTLV-1 RTI-Induced Innate Immune Responses. *FEBS Lett* (2018) 592(10):1693–704. doi: 10.1002/1873-3468.13077
40. Zhong B, Yang Y, Li S, Wang YY, Li Y, Diao F, et al. The Adaptor Protein MITA Links Virus-Sensing Receptors to IRF3 Transcription Factor Activation. *Immunity* (2008) 29(4):538–50. doi: 10.1016/j.immuni.2008.09.003
41. Ishikawa H, Barber GN. STING Is an Endoplasmic Reticulum Adaptor That Facilitates Innate Immune Signalling. *Nature* (2008) 455(7213):674–8. doi: 10.1038/nature07317
42. Sun W, Li Y, Chen L, Chen H, You F, Zhou X, et al. ERIS, An Endoplasmic Reticulum IFN Stimulator, Activates Innate Immune Signaling Through Dimerization. *Proc Natl Acad Sci USA* (2009) 106(21):8653–8. doi: 10.1073/pnas.0900850106
43. Jin L, Hill KK, Filak H, Mogan J, Knowles H, Zhang B, et al. MPYS Is Required for IFN Response Factor 3 Activation and Type I IFN Production in the Response of Cultured Phagocytes to Bacterial Second Messengers Cyclic-Di-AMP and Cyclic-Di-GMP. *J Immunol* (2011) 187(5):2595–601. doi: 10.4049/jimmunol.1100088
44. Heaton SM, Borg NA, Dixit VM. Ubiquitin in the Activation and Attenuation of Innate Antiviral Immunity. *J Exp Med* (2016) 213(1):1–13. doi: 10.1084/jem.20151531
45. Ran Y, Shu HB, Wang YY. MITA/STING: A Central and Multifaceted Mediator in Innate Immune Response. *Cytokine Growth Factor Rev* (2014) 25(6):631–9. doi: 10.1016/j.cytogfr.2014.05.003
46. Maringer K, Fernandez-Sesma A. Message in a Bottle: Lessons Learned From Antagonism of STING Signalling During RNA Virus Infection. *Cytokine Growth Factor Rev* (2014) 25(6):669–79. doi: 10.1016/j.cytogfr.2014.08.004
47. Yang Q, Shu HB. Deciphering the Pathways to Antiviral Innate Immunity and Inflammation. *Adv Immunol* (2020) 145:1–36. doi: 10.1016/bs.ai.2019.11.001

Conflict of Interest: The authors declare that the research was conducted in the absence of any commercial or financial relationships that could be construed as a potential conflict of interest.

Publisher's Note: All claims expressed in this article are solely those of the authors and do not necessarily represent those of their affiliated organizations, or those of the publisher, the editors and the reviewers. Any product that may be evaluated in this article, or claim that may be made by its manufacturer, is not guaranteed or endorsed by the publisher.

frontiers in Immunology

ORIGINAL RESEARCH
published: 22 September 2021
doi: 10.3389/fimmu.2021.740713

Specific Deubiquitinating Enzymes Promote Host Restriction Factors Against HIV/SIV Viruses

Wenying Gao[1†], Yajuan Rui[2†], Guangquan Li[3†], Chenyang Zhai[1], Jiaming Su[2], Han Liu[4], Wenwen Zheng[2], Baisong Zheng[1], Wenyan Zhang[1], Yongjun Yang[5], Shucheng Hua[4] and Xiaofang Yu[1,2*]*

[1] Center for Pathogen Biology and Infectious Diseases, Institute of Virology and AIDS Research, The First Hospital of Jilin University, Changchun, China, [2] Cancer Institute (Key Laboratory of Cancer Prevention and Intervention, Ministry of Education), Second Affiliated Hospital, School of Medicine, Zhejiang University, Hangzhou, China, [3] Jilin Provincial Key Laboratory on Molecular and Chemical Genetics, The Second Hospital of Jilin University, Changchun, China, [4] Department of Respiratory Medicine, The First Hospital of Jilin University, Changchun, China, [5] Key Laboratory of Zoonosis, Ministry of Education, College of Veterinary Medicine, Jilin University, Changchun, China

OPEN ACCESS

Edited by:
Soham Gupta,
Karolinska Institutet, Sweden

Reviewed by:
Jessica L. Smith,
Oregon Health and Science University, United States
Jun Zhao,
Cleveland Clinic, United States

***Correspondence:**
Xiaofang Yu
xfyu1@zju.edu.cn
Shucheng Hua
shuchenghua@126.com

[†]These authors have contributed equally to this work

Specialty section:
This article was submitted to Viral Immunology, a section of the journal Frontiers in Immunology

Received: 13 July 2021
Accepted: 31 August 2021
Published: 22 September 2021

Citation:
Gao W, Rui Y, Li G, Zhai C, Su J, Liu H, Zheng W, Zheng B, Zhang W, Yang Y, Hua S and Yu X (2021) Specific Deubiquitinating Enzymes Promote Host Restriction Factors Against HIV/SIV Viruses. Front. Immunol. 12:740713. doi: 10.3389/fimmu.2021.740713

Hijacking host ubiquitin pathways is essential for the replication of diverse viruses. However, the role of deubiquitinating enzymes (DUBs) in the interplay between viruses and the host is poorly characterized. Here, we demonstrate that specific DUBs are potent inhibitors of viral proteins from HIVs/simian immunodeficiency viruses (SIVs) that are involved in viral evasion of host restriction factors and viral replication. In particular, we discovered that T cell-functioning ubiquitin-specific protease 8 (USP8) is a potent and specific inhibitor of HIV-1 virion infectivity factor (Vif)-mediated apolipoprotein B mRNA-editing enzyme catalytic polypeptide-like 3 (APOBEC3)G (A3G) degradation. Ectopic expression of USP8 inhibited Vif-induced A3G degradation and suppressed wild-type HIV-1 infectivity even in the presence of Vif. In addition, specific DUBs repressed Vpr-, Vpu-, and Vpx-triggered host restriction factor degradation. Our study has revealed a previously unrecognized interplay between the host's DUBs and viral replication. Enhancing the antiviral activity of DUBs therefore represents an attractive strategy against HIVs/SIVs.

Keywords: USP8, deubiquitinating enzymes, antiviral activity, viral proteins, ubiquitin ligase

INTRODUCTION

Ubiquitin modification of proteins regulates their functions and is involved in virtually all aspects of cellular processes (1). Ubiquitin modification is further regulated by deubiquitinating enzymes (DUBs). DUBs have been divided according to active site homology into six broad classes (2): Ub-specific proteases (USPs), Ub C-terminal hydrolases (UCHs), ovarian tumor proteases (OTUs), Machado–Joseph disease protein domain proteases, JAMM/MPN domain-associated metallopeptidases (JAMMs), and monocyte chemotactic protein-induced proteins (MCPIPs) (3). Within the six classes of DUBs, USPs are highly diversified, consisting of more than 50 members. Many studies have reported mutations in USPs involved in multiple biological processes (4). However, the role of DUBs in the interplay between viruses and the host is poorly characterized.

Ubiquitin modification of proteins regulates their function (1, 4, 5) and the reverse process, deubiquitination, is also important for many biological events (6). The importance of deubiquitylating enzyme function is underscored by its frequent deregulation in human diseases such as cancer, infections, and neurological disease, making these enzymes potential drug targets. Also, hijacking host ubiquitin pathways is essential for the replication of diverse viruses (7, 8). The host's cytidine deaminase apolipoprotein B mRNA-editing enzyme catalytic polypeptide-like 3 (APOBEC3) proteins are potent inhibitors of virion infectivity factor (Vif)-deficient human immunodeficiency virus 1 (HIV-1ΔVif) (9, 10). APOBEC3B/DE/G/F (A3B/DE/G/F) proteins become packaged into HIV-1 virions during virus production and inhibit viral reverse transcription in newly infected target cells. Other APOBEC3 protein family members, including APOBEC3A (A3A), APOBEC3C (A3C), and APOBEC3H (A3H), also impair HIV-1 replication by packaging into virions (11). The Vif protein of HIV-1 neutralizes APOBEC3's antiviral functions by forming a viral-specific CRL5 E3 ubiquitin ligase complex consisting of CUL5, ElOB/C, and CBFβ (12–14) to promote the polyubiquitination and degradation of APOBEC3 substrates (15).

Three other HIV/simian immunodeficiency virus (SIV) accessory proteins, Vpu, Vpr, and Vpx, are also essential components of viral replication and pathogenesis. Ubiquitin modification is vital for them on the process of target protein destruction. HIV-1 Vpu hijacks CUL1 and β-TrCP to form a CRL1 E3 ubiquitin ligase complex, triggering the degradation of BST-2 (16) and PSGL-1 (17). Vpr recruits DCAF1, DDB1, and CUL4 to form the CRL4 E3 ubiquitin ligase complex to induce the degradation of HLTF (18). Vpx proteins of HIV-2Rod and certain SIVs overcome the antiviral function of SAMHD1 in myeloid cells by inducing its polyubiquitination and degradation (19, 20).

In this report, we demonstrate that DUBs are potent inhibitors of viral evasion of host restriction. We have identified various DUBs inhibiting functions of HIV Vif, Vpr, Vpu, and Vpx proteins. Collectively, our study reveals a previously unrecognized interplay between the host's DUBs and viral replication. Enhancing the antiviral activity of DUBs therefore represents an attractive strategy against HIVs/SIVs.

RESULTS

T Cell-Specific USP8 Inhibits Vif-Induced A3G Degradation and Suppresses Wild-Type HIV-1 Infectivity

The deubiquitination enzyme USP8 is a human T cell-specific factor regulating T-cell maturation and functions (21, 22), and $CD4^+$ T cells are primary targets of HIV-1 infection. HIV-1 is potently inhibited by several human cytidine deaminases that are members of human APOBEC3 proteins. HIV-1 Vif neutralizes some APOBEC3's antiviral functions by forming viral-specific CRL5 E3 ubiquitin ligase complexes (12, 13, 23, 24) to promote the polyubiquitination and degradation of APOBEC3 substrates (**Figure 1A**). Whether any host factors involved in the deubiquitination pathway can influence Vif function has not been explored.

We observed that USP8 is highly expressed in primary $CD4^+$ T cells and myeloid cells compared with HEK293T cells and RD cells (**Figures 1B, C**). Primary $CD4^+$ T cells and myeloid cells are the preferred target cells of HIV-1. We screened a library of mammalian expression vectors that encode 32 USPs twice and discovered USP8 is distinguished from the group. USP8 significantly impaired Vif-triggered APOBEC3G (A3G) degradation (**Supplementary Figures S1H, I**). To investigate whether endogenous USP8 in T cells has an effect on Vif-induced A3G degradation, we generated USP8 knocking down stable cell line in H9 T cells (**Supplementary Figure S1A**). shCon and shUSP8 H9 cells were infected with wild-type (WT) HIV-1 at the same titer or mock infected. As shown in **Figure 1D**, silencing USP8 has no effect on endogenous A3G expression (lanes 1 and 3). A3G was degraded during HIV-1 infection (lanes 1 and 2). Surprisingly, A3G degradation was enhanced in virus-infected shUSP8 H9 cells (lanes 2 and 4). In addition, cell supernatants were collected at different time points, and virus infectivity was assessed using TZM-BL indicator cells. We found that USP8 knocking down had a positive effect on HIV-1 progeny virus replication (**Figure 1E**). A similar result was also determined in primary $CD4^+$ cells (**Supplementary Figure S1B**). Since USP8 expression in HEK293T cells is lower than that in $CD4^+$ T cells, we detected whether increasing the USP8 expression could affect HIV-1 Vif function in HEK293T cells. As a result, increasing the USP8 expression effectively inhibited HIV-1 Vif-induced A3G degradation (**Figure 1F**). In the absence of exogenous USP8 expression, HIV-1 Vif induced a >70% reduction in A3G (**Figure 1F**, lane 5) when compared to control cells (**Figure 1F**, lane 4). The Vif-induced degradation of A3G was essentially abolished in the presence of increasing amounts of USP8 (**Figure 1F**, lanes 6 and 7). In the absence of Vif, A3G expression was not affected by USP8 (**Figure 1F**, lanes 1–3). Consistent with previous reports, we also observed that USP8 could rescue Vif expression in a dose-dependent manner, since Vif was ubiquitinated and degraded *via* the proteasome pathway (25) (**Figure 1F**). Furthermore, silencing endogenous USP8 expression (**Supplementary Figure S1C**) enhanced HIV-1 Vif-mediated A3G degradation in HEK293T cells (**Supplementary Figures S1C, D**). The ability of HIV-1 Vif to counteract A3G is quite conserved among different HIV-1 subtypes. To investigate whether USP8 blocking of anti-A3G activity of Vif is universal, seven viral isolates from patients representing seven HIV-1 subtypes Vif molecules were selected (26, 27), except NL4-3 Vif. We validated that USP8 has the ability to block the anti-A3G activity of Vif molecules from diverse HIV-1 subtypes (**Figure 1G**).

To examine the possible effect of USP8 on HIV-1 infection, we first co-expressed increasing amounts of USP8 with HIV-1 (NL4-3). USP8 expression had no detectable effect on viral protein expression, as determined by the expression of intracellular HIV-1 Pr55Gag in HEK293T cells (**Supplementary Figure S1E**). Virus release (**Supplementary Figure S1F**) and the infectivity of the

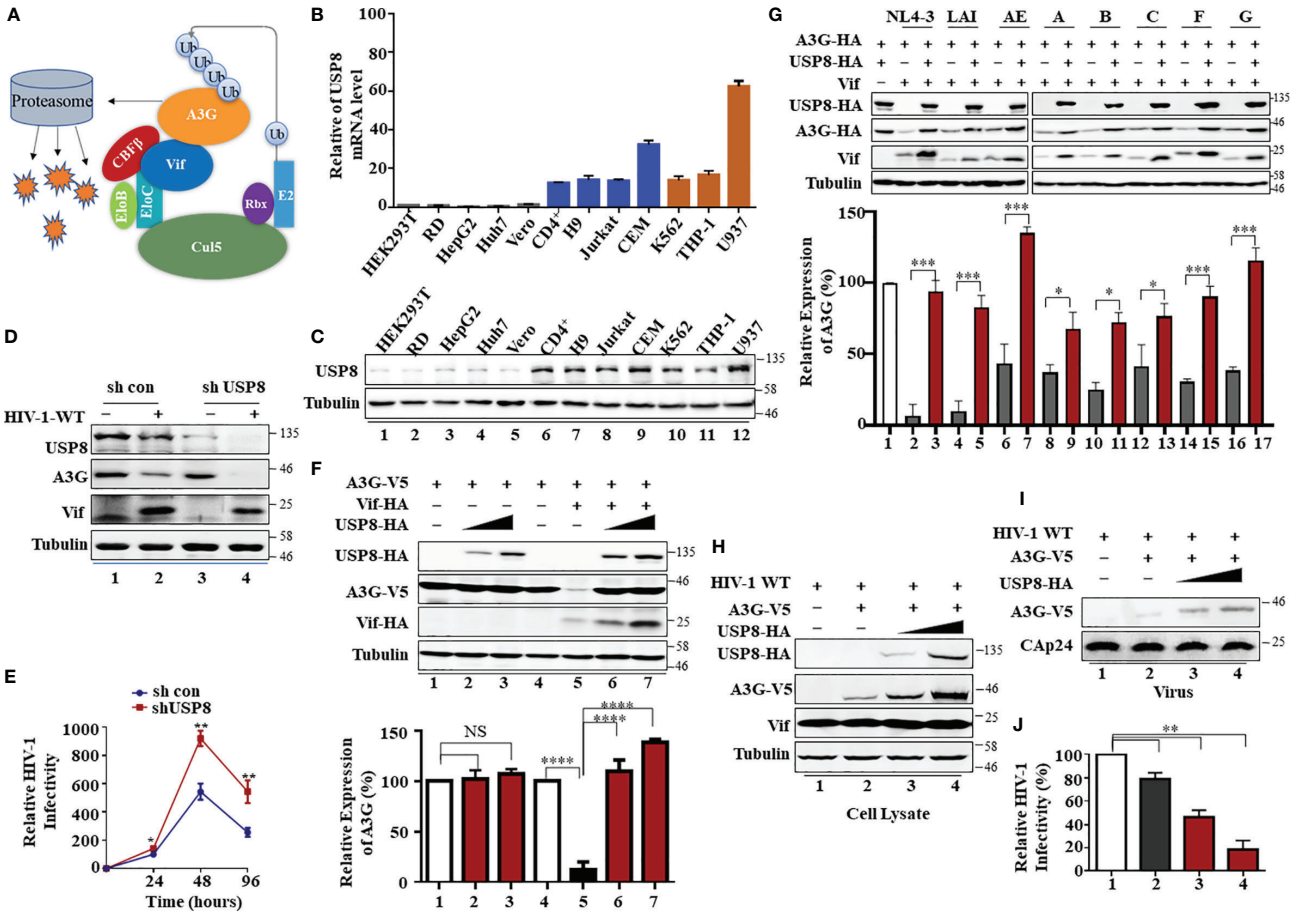

FIGURE 1 | T cell-specific ubiquitin-specific protease 8 (USP8) inhibits virion infectivity factor (Vif)-induced apolipoprotein B mRNA-editing enzyme catalytic polypeptide-like 3 (APOBEC3)G (A3G) degradation and suppresses wild-type (WT) HIV-1 infectivity. **(A)** A model of HIV Vif assembly with the Cul5, CBFβ, and EloB/C E3 components to mediate polyubiquitination and degradation of the A3G protein. **(B)** USP8 mRNA expression levels in various cell types were detected by RT-qPCR. USP8 mRNA expression in HEK293T cell line was set to 1.0. Glyceraldehyde 3-phosphate dehydrogenase (GAPDH) was used as a loading control. Orange, myeloid cell lines; blue, $CD4^+$ T cell lines; black, other cell lines. **(C)** USP8 protein expression levels in various cell types were detected by immunoblotting. **(D)** The effect of USP8 silencing on A3G expression in HIV-1-infected H9 cell. H9 USP8 silencing cells were infected with HIV or not for 48 h. Endogenous USP8 and A3G were analyzed by immunoblotting. Virus infection was determined by Pr55Gag. **(E)** The effect of USP8 silencing on HIV infectivity in H9 cell. USP8 silencing and its control H9 cells were infected with HIV for 30 h. The cells were then washed three times with phosphate buffered saline (PBS) and placed in fresh RPMI-1640 medium with 10% fetal bovine serum (FBS). Cell supernatants were then harvested after 24, 48, and 96 h of infection. Virus infectivity was assessed using TZM-BL indicator cells. **(F)** USP8 inhibits Vif-mediated A3G degradation. HEK293T cells were transfected with A3G-HA and Vif-HA or its empty vector in the presence of increasing amounts of USP8-HA. Cells were harvested 48 h after transfection. Protein expression in the cell lysates was analyzed by immunoblotting with anti-HA antibody targeting USP8-HA, A3G-HA, and Vif-HA proteins. Tubulin was used as a loading control. Quantification of A3G expression was analyzed by ImageJ2X. A3G expression alone was normalized to 100%. **(G)** USP8 repressed the anti-A3G activity of Vif molecules from diverse HIV-1 subtypes. HEK293T cells were transfected with A3G-HA and diverse HIV-1 Vif subtypes or empty vector in the presence or absence of USP8. Cells were harvested 48 h after transfection, and protein expression in the cell lysates was analyzed by immunoblotting with anti-HA antibody targeting USP8-HA, A3G-HA, and anti-Vif antibody targeting Vif proteins. Tubulin was used as a loading control. Quantification of A3G expression was analyzed by ImageJ2X. A3G expression alone was normalized to 100%. **(H–J)** HIV-1 infectivity was significantly reduced when USP8 was co-expressed with A3G. WT HIV-1 and A3G-HA or control vector were co-transfected into HEK293T cells with increasing amounts of USP8-HA. After 48 h, cells were harvested, and protein expression was analyzed by immunoblotting with anti-Pr55Gag and anti-HA antibody targeting USP8-HA and A3G-HA proteins. Tubulin was used as a loading control **(H)**. Virion particle-containing supernatants were harvested and filtered through a 0.45-μm filter, then concentrated by ultracentrifugation. Virion pellets were immunoblotted with anti-CAp24, anti-Vif, and anti-HA antibody targeting A3G-HA **(I)**. HIV-1 infectivity was assessed by TZM-bl indicator cells **(J)**. WT HIV-1 infectivity alone was set to 100% **(J)**. Column results were from n = 3 independent biological experiments **(A, F, G, J)**, and immunoblotting results are representative of n = 3 experiments **(F, H)**. Means and standard deviations are presented. The statistical significance analyses were performed using two-sided unpaired t-tests (NS, not significant, *p < 0.05, **p < 0.01, ***p < 0.001, ****p < 0.0001).

released virus (**Supplementary Figure S1G**) were also unaffected by USP8 expression in the absence of A3G. In contrast, in the presence of USP8, intracellular A3G expression (**Figure 1H**) and virion incorporation of A3G (**Figure 1I**) were increased, even in the presence of HIV-1 Vif. At the same time, the infectivity of the released HIV-1 was reduced in the presence of USP8 (**Figure 1J**), which is consistent with the increased amount of A3G virion packaging. Combined with these data, these results indicate that

USP8 exerts its potent antiviral effect through Vif. USP8 antagonized the ability of HIV-1 Vif to suppress the antiviral function of A3G, resulting in an enhanced antiviral activity of A3G against Vif-containing HIV-1.

The Active Site of the USP8 Enzyme Is Required for Inhibition of HIV-1 Vif Function

In addition to A3G, A3H-Haplotype II (hap II), which is overcome by HxB2 Vif (26), and A3F are also potent inhibitors of HIV-1 that are neutralized by Vif (13, 28, 29). We observed that USP8 can efficiently inhibit HIV-1 Vif-induced degradation of A3F (**Figures 2A, B**) and A3H-HapII (**Figures 2C, D**). The degradation of other known HIV-1 Vif targets, such as A3C (**Supplementary Figures S2A, B**) and A3DE (**Supplementary Figures S2C, D**), was also inhibited by USP8. Non-primate lentiviral Vif from bovine immunodeficiency virus (BIV) targets cow APOBEC3 proteins (30). Unlike HIV-1 Vif, non-primate lentivirus BIV Vif assembles with CUL2 and the ElOB/C E3 component (**Supplementary Figure S2E**) and is not regulated by

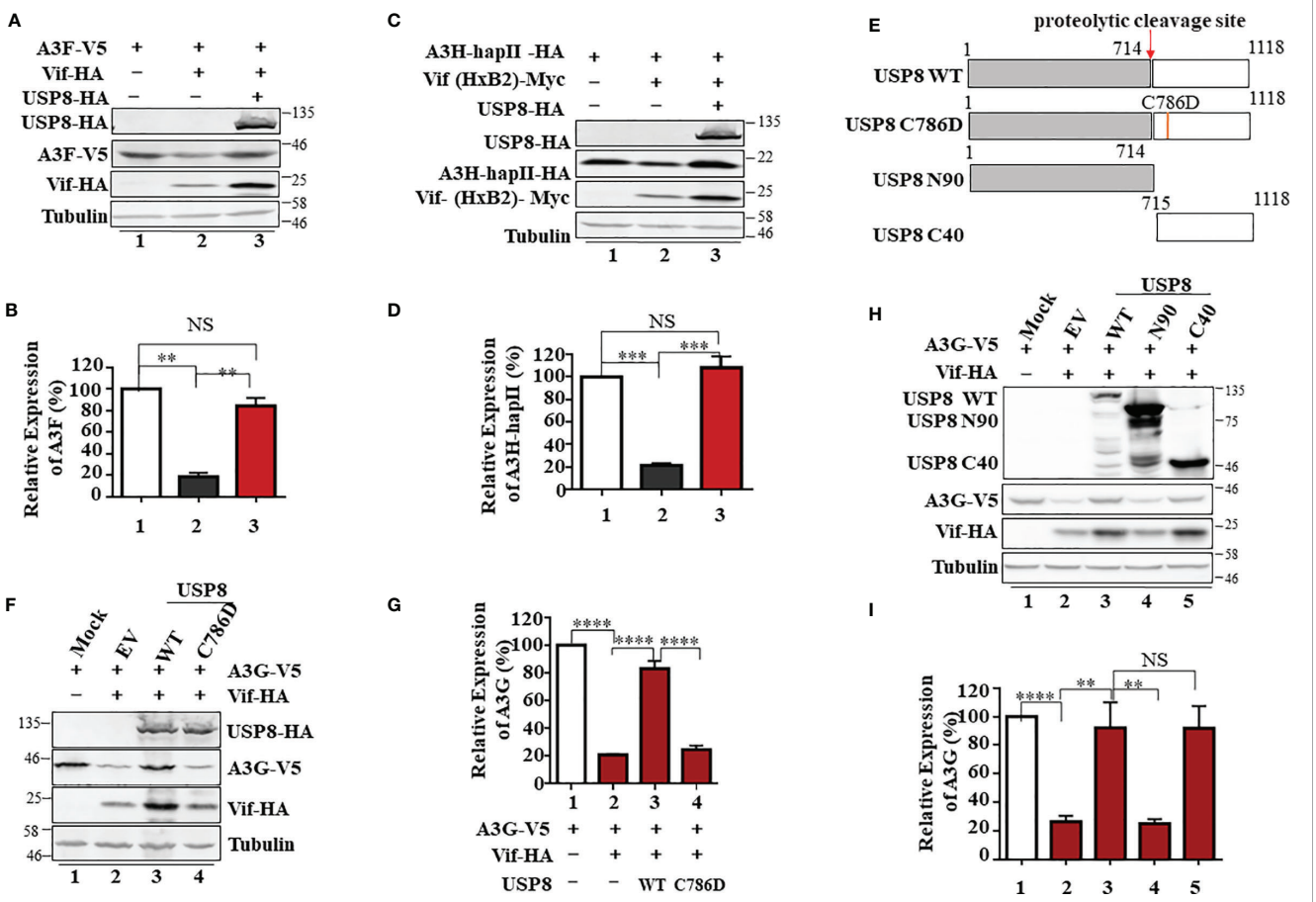

FIGURE 2 | The active site of ubiquitin-specific protease 8 (USP8) is required for inhibition of HIV-1 virion infectivity factor (Vif) function. USP8 efficiently inhibited HIV-1 Vif-induced apolipoprotein B mRNA-editing enzyme catalytic polypeptide-like 3 (APOBEC3)F (A3F) **(A)** and A3H-HapII **(C)** degradation. **(A, C)** HEK293T cells were co-transfected with expression vector as indicated. Cells were harvested 48 h after transfection. Protein expression in the cell lysates was analyzed by immunoblotting with the corresponding antibodies. Tubulin was used as a loading control. **(B, D)** Quantification of A3F or A3H-HapII expression was analyzed by ImageJ2X. A3F **(B)** or A3H-HapII **(D)** expression alone was normalized to 100%. **(E)** The schematic represents USP8 wild type (WT) and mutations used in the study. The red arrow shows the USP8 proteolytic cleavage site (p.714Arg). **(F)** The USP8C786D mutation has lost the ability to inhibit Vif-mediated degradation of A3G. HEK293T cells were transfected with A3G-V5 alone or together with Vif-HA in the presence of USP8 WT-HA, the USP8C786D-HA mutation, or empty vector (EV). Cells were harvested 48 h after transfection, and protein expression in the cell lysates was analyzed by immunoblotting with anti-V5 and anti-HA antibodies targeting A3G-V5, USP8-HA, and Vif-HA protein. Tubulin was used as a loading control. **(G)** Quantification of A3G expression was analyzed by ImageJ2X. A3G expression alone was normalized to 100%. **(H)** HEK293T cells were transfected with A3G-V5 alone or together with Vif-HA in the presence of USP8 WT-HA, a USP8 truncation, or EV. Cells were harvested after 48 h, and protein expression in the cell lysates was analyzed by immunoblotting with the corresponding antibodies. **(I)** Quantification of A3G expression was analyzed by ImageJ2X. A3G expression alone was normalized to 100%. Column results were from n = 3 **(B, D, G, I)** independent experiments, and immunoblotting results are representative of n = 3 experiments **(A, C, F, H)**. Means and standard deviations are presented. The statistical significance analyses were performed using two-sided unpaired t-tests (NS, not significant; **p < 0.01, ***p < 0.001, ****p < 0.0001).

CBFβ to trigger the degradation of bovine APOBEC3 (31). Since USP8 sequence is highly conserved between cow and human (**Supplementary Figure S2F**), human USP8 was also able to block BIV Vif-induced degradation of cow APOBEC3 in HEK293T cells (**Supplementary Figures S2G, H**). Importantly, we observed that diverse Vif expression could be enhanced by USP8 (**Supplementary Figures S2A, C, G**). Taken together, USP8 targets diverse Vif viral substrate receptors but not the E3 cellular components.

To identify whether the deubiquitinating enzymatic activity of USP8 is required for its antagonism of Vif function, a key residue Cysteine 786 of USP8 is mutated to abolish its enzymatic activity (21) (**Figure 2E**). We found that the active site mutant USP8 C786D lost the ability to inhibit Vif-mediated A3G degradation (**Figure 2F**, lane 4) when compared to wild-type USP8 (**Figure 2F**, lane 3). In the presence of USP8 C786D, Vif-mediated A3G degradation was as efficient as the no-USP8 control (**Figure 2G**, bar 4 vs. bar 2). USP8 is vital for the development and homeostasis of T cells and is cleaved in activated $CD4^+$ T cells by caspases. The C-terminal fragment of USP8, but not N-terminal fragment, possesses the enzymatic activity (21). Somatic mutations in USP8 enhance its proteolytic cleavage and are associated with Cushing's disease resulting from elevated deubiquitinase activity (22). We observed that the C-terminal fragment (C40) but not the N-terminal fragment (N90) of USP8 maintained the inhibitory activity against HIV-1 Vif (**Figures 2H, I**). Collectively, enzymatic activity of USP8 is critical for the inhibitory effect of Vif function.

USP8 Specifically Interacts With HIV-1 Vif and Reduces Vif-Triggered A3G Polyubiquitination

To explore the mechanism of USP8-mediated Vif inhibition, we employed co-immunoprecipitation (co-IP) assay to determine whether USP8 could interact with HIV-1 Vif. In the absence of Vif, USP8 was not detected in the co-IP sample (**Figure 3A**, lane 1), indicating the specificity of the assay system. In the presence of Vif, co-precipitation of USP8 with Vif was detected (**Figure 3A**, lane 3). Gads is a binding partner of USP8, which is required for USP8 in regulating the development and homeostasis of T cells (21). The interaction with HIV-1 Vif reduced the ability of USP8 binding with its functional cofactor Gads (**Supplementary Figures S3A, B**). These data establish a specific interaction between HIV-1 Vif and USP8.

Vif forms a viral-specific E3 ubiquitin ligase complex with cellular proteins CUL5, ElOB/C, and CBFβ to trigger polyubiquitination of substrates (12). Vif interacts with USP8; we next assessed whether USP8 disrupts Vif–Cullin 5–E3 ubiquitin ligase complex assembly. Interestingly, USP8 did not interact with CUL5, ElOB, or CBFβ (**Supplementary Figure S3C**) in the absence of Vif. The ability of Vif to interact with CUL5, ElOB, and CBFβ (**Figure 3B**, lane 2; **Figure 3C**) was not affected by USP8 overexpression (**Figure 3B**, lane 3; **Figure 3C**). The interaction of Vif with the target protein A3G (**Figure 3D**, lane 3; **Figure 3E**) was also not affected by USP8 (**Figure 3D**, lane 4; **Figure 3E**). However, HIV-1 Vif-induced polyubiquitination of A3G (**Figure 3F**, lane 1) was significantly reduced in the presence of USP8 (**Figure 3F**, lane 2). In contrast, enzymatically defective USP8 C786D, which could not inhibit Vif-triggered A3G degradation, was disabled in suppressing HIV-1 Vif-induced polyubiquitination of A3G (**Figure 3F**, lane 3) when compared to the WT USP8 (**Figure 3F**, lane 2). Additionally, we confirmed that USP8 repressed Vif-mediated A3G polyubiquitination *in vitro* study (**Supplementary Figures S3D–F**). Ubiquitinated A3G was purified from HEK293T cells transfected with Ub-Flag, Vif-HA, and A3G-V5 using anti-V5 affinity purification. WT USP8 and functional dominant truncation C40, which purified from HEK293T cells and incubated with ubiquitinated A3G, decreased A3G polyubiquitination, while enzymatic mutation C786D was disabled (**Supplementary Figure S3D**). USP8 C40 purified from *Escherichia coli* reduced A3G polyubiquitination in a time-dependent fashion (**Supplementary Figure S3E**). Likewise, USP8 $C40^{C786D}$, an enzymatic mutant, lost the ability of A3G deubiquitination (**Supplementary Figure S3F**). Together, these results indicated that USP8 specifically interacts with Vif and deubiquitinates the ubiquitination of A3G mediated by Vif.

HIV-1 Antagonizes USP8-Mediated Viral Suppression by Impairing USP8 Expression in $CD4^+$ Cells

Although USP8 exhibits strong inhibitory activity against Vif-mediated A3G degradation (**Figure 1F**), the anti-HIV-1 function of USP8 could be compromised during HIV-1 replication. Because USP8 expression was reduced in HIV-1-infected $CD4^+$ T cells, which is based on mass spectrometry data published by several groups (17, 32, 33). In both H9 (**Figures 4A, B** and **Supplementary Figure S4A**) and Jurkat (**Figures 4C, D** and **Supplementary Figure S4B**) $CD4^+$ T cells, HIV-1 infection resulted in depletion of USP8 proteins significantly. Moreover, the USP8 mRNA level was also reduced in HIV-1-infected T cells (**Figures 4E, F**), suggesting that down-modulation of USP8 expression by HIV-1 is at least partially the result of an alteration in USP8 mRNA transcription or RNA stability. The C-terminal fragment of USP8 contains the deubiquitining enzymatic activity (22) and is a potent inhibitor of HIV-1 Vif function (**Figure 2H**). HIV-1 Vif-triggered A3G degradation was blocked slightly more efficiently by USP8 C40 than by full-length USP8 (**Figure 4G**), which was correlated with the inhibition of HIV-1 Vif-induced A3G polyubiquitination (**Supplementary Figures S3D**, **S4C, D**). To further validate USP8 C40 function during HIV-1 infection, USP8 C40 was transduced into $CD4^+$ T cells (**Figure 4H**). Transduction with USP8 C40 in H9 cells that express endogenous APOBEC3 antiviral proteins (**Figure 4I**, lanes 3 and 4) significantly inhibited HIV-1 replication (**Figure 4J**). In contrast, USP8 C40 (**Figure 4I**, lanes 1 and 2) has no effect on HIV-1 replication (**Figure 4K**) when transduced in APOBEC3-negative Jurkat cells. These data demonstrate that modulation of USP8 function in $CD4^+$ T cells can enhance the antiviral activity of APOBEC3 cytidine deaminases against HIV-1 even in the presence of Vif.

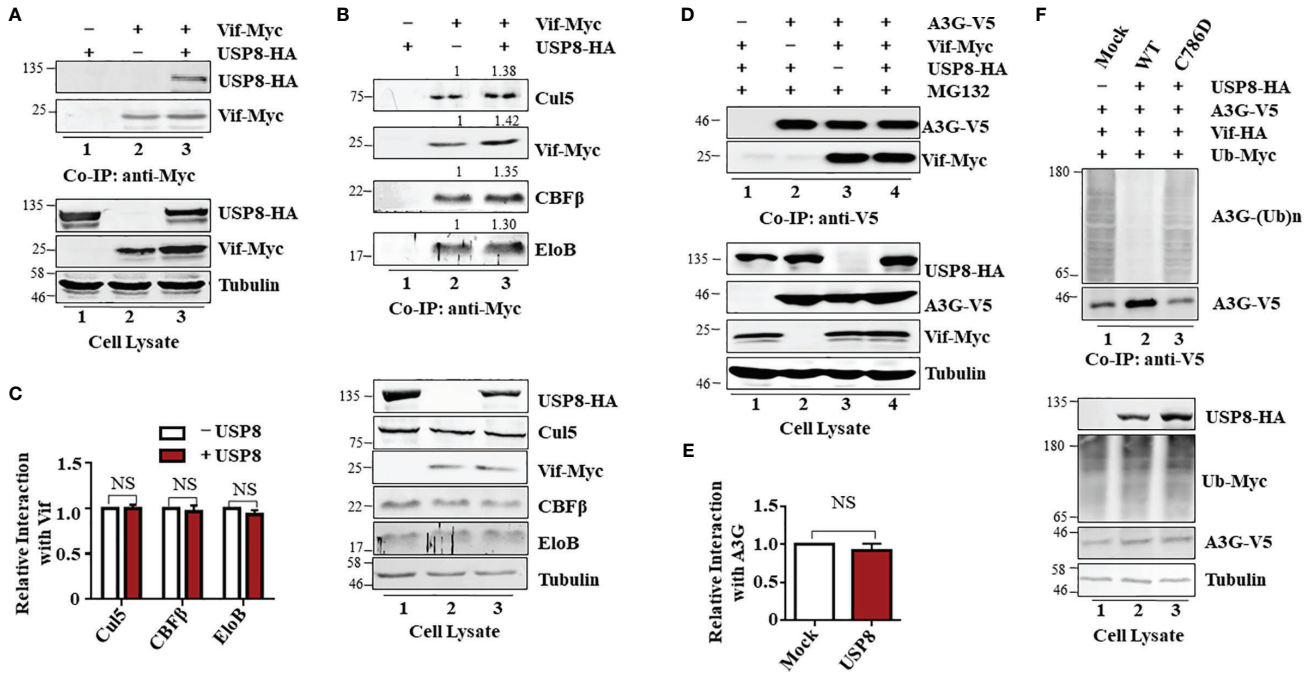

FIGURE 3 | Ubiquitin-specific protease 8 (USP8) specifically interacts with HIV-1 virion infectivity factor (Vif) and reduces Vif-triggered apolipoprotein B mRNA-editing enzyme catalytic polypeptide-like 3 (APOBEC3)G (A3G) polyubiquitination. **(A)** Co-precipitation of USP8 with Vif. HEK293T cells were transfected with USP8-HA, Vif-Myc alone, or both, as indicated. Cell lysates were prepared and immunoprecipitated using anti-Myc antibody conjugated to agarose beads 48 h after transfection. Cell lysates and precipitated samples were separated by sodium dodecyl sulfate–polyacrylamide gel electrophoresis (SDS-PAGE), transferred to nitrocellulose membranes, and reacted with an anti-HA antibody to detect USP8-HA and an anti-Myc antibody to detect Vif-Myc. Tubulin was used as the loading control for the cell lysate. **(B)** USP8 does not affect Vif–CRL5 E3 ubiquitin ligase formation. HEK293T cells were transfected with Vif-Myc, USP8-HA, or both. Cell lysates were immunoprecipitated with anti-Myc antibodies conjugated to agarose beads. Cell lysates and precipitated samples were analyzed by immunoblotting with the corresponding antibodies. Tubulin was used as the loading control for the cell lysate. **(C)** Relative binding ability of Vif with Cul5, CBFβ, and EloB in the presence or absence of USP8 was determined by ImageJ2X. Protein binding to Vif in lane 2 **(B**, upper blots**)** was set to 1.0. Data are means ± SD from n = 3 independent experiments. The statistical significance analyses were performed using two-sided unpaired t-tests (NS, not significant). **(D)** The association of Vif with A3G is also not affected by USP8. HEK293T cells were co-transfected with expression vectors as indicated. Cells were treated with 10 mM MG132 12 h before harvesting. Vif protein was immunoprecipitated from cell lysates with an anti-V5 antibody conjugated to agarose beads. Cell lysates and precipitated samples were analyzed by immunoblotting with the corresponding antibodies. Tubulin was used as the loading control for the cell lysate. **(E)** Quantification of co-precipitated Vif relative to A3G was determined by ImageJ2X. Data are means ± SD from n = 3 independent experiments. The statistical significance analyses were performed using two-sided unpaired t-tests (NS, not significant). **(F)** USP8 inhibits Vif-triggered polyubiquitination of A3G. HEK293T cells were transfected with the empty vector, Vif-HA, A3G-V5, Ub-Myc, or USP8-HA as indicated. Cells were treated with 10 mM MG132 for 12 h before harvesting. Cell lysates were prepared and immunoprecipitated using anti-V5 antibody conjugated to agarose beads 48 h after transfection. Cell lysates and precipitated samples were analyzed by immunoblotting with the corresponding antibodies. Immunoblotting results from panels **(A, B, D, F)** are representative of n = 3 independent experiments.

Specific Deubiquitinating Enzymes Suppress Different HIV/SIV Accessory Protein-Mediated Degradation of Host Restriction Factors

Ubiquitin modification is linked to many cellular processes. Diverse DUBs are involved in reversing protein ubiquitination and therefore modulate the outcome of this posttranslational modification. HIV-1 Vpr, HIV-1 Vpu, and HIV-2 Rod/SIVmac Vpx also form virus-specific E3 ubiquitin ligase complexes to mediate the polyubiquitination and degradation of various target proteins (**Supplementary Figures S5A–C**). However, in contrast to USP8-mediated Vif inhibition, USP8 had a little effect on HIV-1 Vpr-mediated HLTF degradation (**Supplementary Figure S5G**), HIV-1 Vpu-mediated BST-2 depletion (**Supplementary Figure S5H**), or HIV-2Rod/SIVmac Vpx-mediated SAMHD1 degradation (**Supplementary Figures S5I, J**). Although USP8 had little effect on HIV-1 Vpr, HIV-1 Vpu, or HIV-2 Rod/SIVmac Vpx function, we identified other potent DUB inhibitors of HIV-1 Vpr, HIV-1 Vpu, and HIV-2 Rod/SIVmac Vpx (**Figures 5A–D**) after screening 32 USPs (**Supplementary Figures S5D–F**). USP7 inhibited HIV-1 Vpr-mediated HLTF degradation (**Figure 5A**), USP33 inhibited HIV-1 Vpu-mediated BST-2 depletion (**Figure 5B**), and USP37 inhibited HIV-2 Rod/SIVmac Vpx-mediated SAMHD1 degradation (**Figures 5C, D**). Moreover, we investigated different USP functions in suitable cell lines as previously reported (16, 20, 34). Silencing USP7 in H9 T cells, HLTF degradation was more efficient in shUSP7 cells in the presence of HIV-1 infection compared with its control cells (**Figure 5E**, lanes 2 and 4). As a result, silencing USP7 promoted HIV-1 infectivity (**Supplementary Figure S5K**).

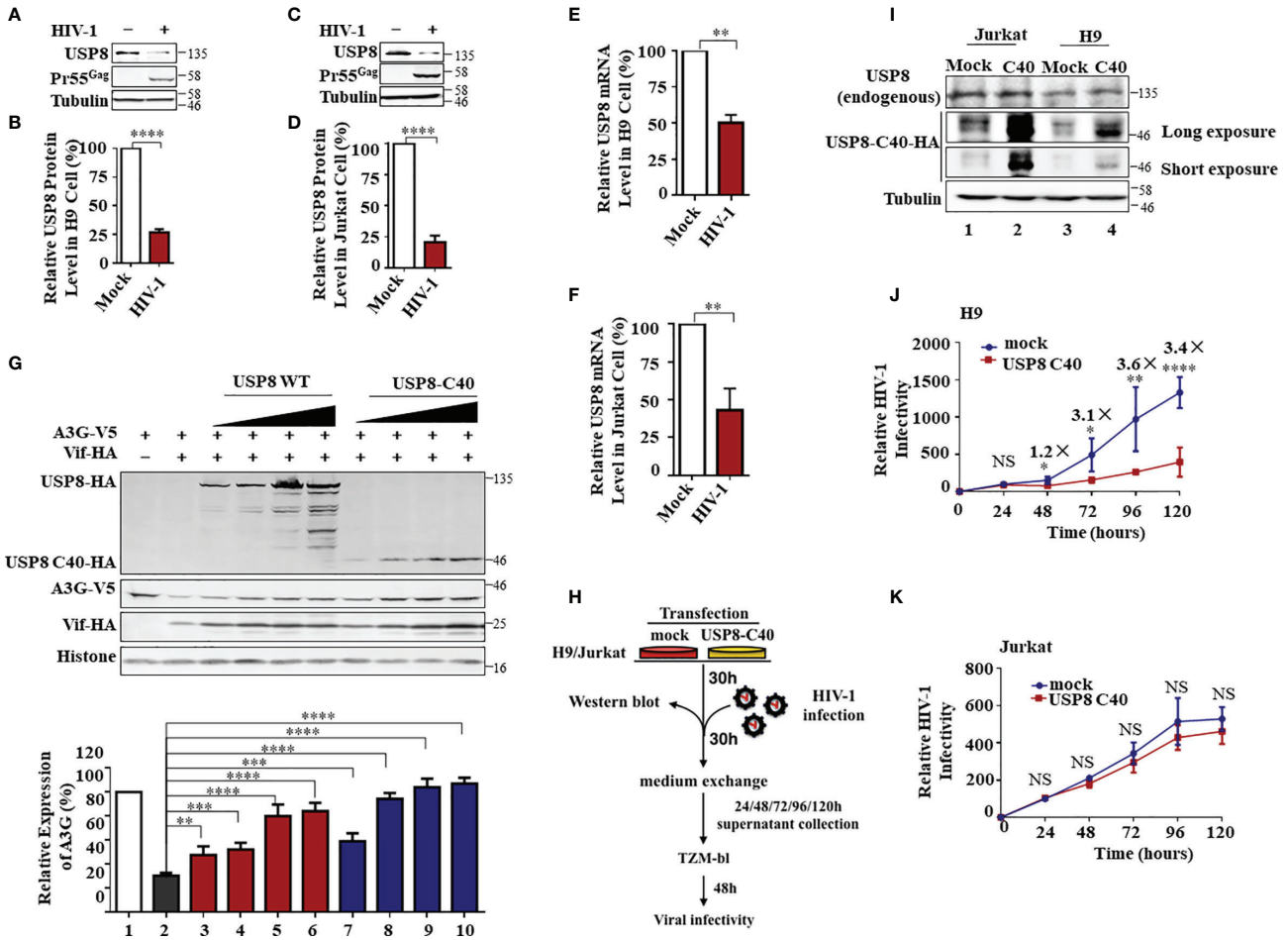

FIGURE 4 | HIV-1 antagonizes ubiquitin-specific protease 8 (USP8) suppression by lowering USP8 protein levels in CD4$^+$ cells. **(A–D)** HIV-1 suppresses USP8 expression at the protein level. H9 **(A)** and Jurkat **(C)** cells were infected or not infected with wild-type (WT) HIV for 48 h. Endogenous USP8 was analyzed by immunoblotting. Virus infection was determined by the presence of Pr55Gag. Tubulin was used as a loading control. USP8 expression was measured by ImageJ2X (mock infection was set to 100%) **(B, D)**. **(E, F)** HIV-1 suppresses USP8 expression at the mRNA level. H9 **(E)** and Jurkat **(F)** cells were infected or not infected with WT HIV for 48 h. USP8 mRNA expression was detected by RT-qPCR. Glyceraldehyde 3-phosphate dehydrogenase (GAPDH) was used as a control. **(G)** Comparison of the effect of full-length USP8 and C40-truncated USP8 on virion infectivity factor (Vif)-mediated apolipoprotein B mRNA-editing enzyme catalytic polypeptide-like 3 (APOBEC3)G (A3G) degradation. A3G-V5, together with Vif-HA or its control vector, was transfected into HEK293T cells in the presence of increasing amounts of full-length USP8 or C40-truncated USP8. Cells were harvested after 48 h, and cell lysates were heated with lysis buffer, then immunoprecipitated with the corresponding antibodies. Quantification of A3G expression was analyzed by ImageJ2X. A3G expression alone was normalized to 100%. **(H)** Workflow for USP8 C40 inhibition of HIV infectivity in H9 and Jurkat cells. **(I)** USP8-C40-HA or control vector was electro-transfected into H9 **(I)** or Jurkat **(J)** cells. After 30 h, USP8 and USP8 C40-HA expression was analyzed by immunoblotting. **(J, K)** USP8 C40-HA or control vector was electro-transfected into H9 **(K)** or Jurkat **(L)** cells. After 30 h, H9/Jurkat cells were infected with WT HIV for another 30 h. The cells were then washed three times with phosphate buffered saline (PBS) and placed in fresh RPMI-1640 medium with 10% fetal bovine serum (FBS). Cell supernatants were then harvested after 24, 48, 72, 96, and 120 h of infection. Virus infectivity was assessed using TZM-BL indicator cells. Means and standard deviations are presented. Panels **(B, D–F, J, K)** are results from n = 3 independent experiments. The statistical significance analyses were performed using two-sided unpaired t-tests (NS, not significant; *p < 0.05; **p < 0.01; ***p < 0.001; ****p < 0.0001).

Meanwhile, similar result was demonstrated in shUSP33 HeLa cells that BST2 degradation was enhanced during HIV-1 infection (**Figure 5F**, lanes 2 and 4) and subsequently promoted HIV-1 infectivity (**Supplementary Figure S5L**). HIV-1 Pr55Gag was determined to demonstrate silencing USPs has no effect on virus replication (**Figures 5E, F**). SAMHD1 was degraded in THP-1 cells when infected with SIVmac virus. As expected, SIV-induced SAMHD1 degradation was more efficient in the absence of USP37 THP-1 cells (**Figure 5G**). Collectively, specific DUBs play important roles in virus–host relationships.

DISCUSSION

APOBEC3 cytidine deaminases are host restriction factors against HIV-1 and related retroviruses. HIV-1 Vif targets

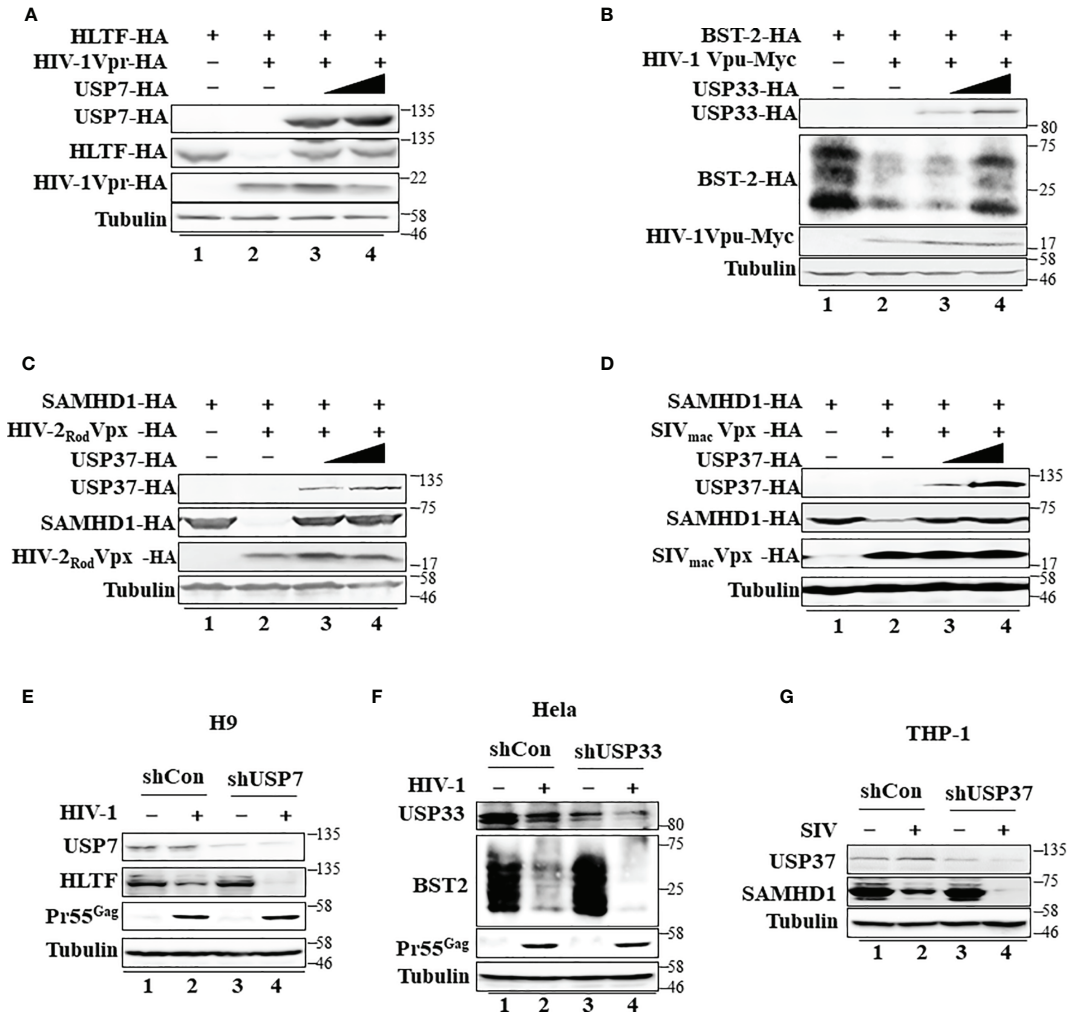

FIGURE 5 | Specific deubiquitinating enzymes suppress degradation of host restriction factors mediated by HIV/simian immunodeficiency virus (SIV) proteins. **(A)** Ubiquitin-specific protease 7 (USP7) inhibits HIV-1 Vpr-induced degradation of HLTF. HEK293T cells were transfected with expression vectors as indicated. Cell lysates were immunoblotted with the corresponding antibodies. **(B)** USP33 inhibits HIV-1 Vpu-induced BST-2 degradation. The experimental methods were the same as in panel **(A). (C, D)** USP37 inhibits HIV-2 Rod Vpx- **(C)** or SIV mac Vpx **(D)**-induced SAMHD1 degradation. The experimental methods were the same as in panel **(A). (E)** The effect of USP7 silencing on HLTF expression in WT HIV-1-infected H9 cell. H9 shUSP7 and its control cell lines were infected with WT HIV-1 or not for 48 h. Endogenous USP7 and HLTF were analyzed by immunoblotting. Virus infection was determined by Pr55Gag. **(F)** The effect of USP33 silencing on BST2 expression in WT HIV-infected Hela cell. The process is described in panel **(E). (G)** The effect of USP33 silencing on SAMHD1 expression in SIVmac-GFP-infected THP-1 cell. THP-1 cells stably expressed USP33shRNA. USP33 knockdown THP-1 cells were differentiated into macrophages by phorbol 12-myristate 13-acetate (PMA) treatment and infected with SIV mac viruses for 24 h. Endogenous USP33 and SAMHD1 were analyzed by immunoblotting. Immunoblotting results are representative of n = 3 independent experiments.

APOBEC3 for polyubiquitination and subsequent degradation to ensure successful viral replication. A3G protein degradation by ubiquitination was mediated by Vif- and cullin-RING-independent pathway. It is reported that USP49 is a new antiviral factor. USP49 increased A3G protein expression by removing ubiquitin and enhanced its anti-HIV-1 activity (35). Different from USP49, we discovered that USP8 is a potent and specific inhibitor of Vif. USP8 overexpression alone or knocking down has no effect on A3G protein stability (**Figures 1D, F**). Notably, USP8 bound Vif (**Figure 3A**) without disturbing Vif–Cullin-RING E3 complex assembly (**Figure 3B**) or Vif–A3G interaction (**Figure 3D**). USP8 blocked Vif-induced polyubiquitination and degradation of A3G (**Figures 1D–H**, **3F**). Consequently, USP8 could attenuate the infectivity of HIV-1 in the presence of A3G and suppress HIV-1 replication in $CD4^+$ T cells (**Figure 4J**). Meanwhile, both mRNA and protein expression levels of USP8 were significantly downregulated during HIV-1 infection in T cells (**Figures 4A–D** and **Supplementary Figures S4A, B**), which indicated that HIV-1 has evolved new antagonisms against USP8.

We also observed that diverse Vif expression could be enhanced by USP8 (**Figures 2A, C, F**, **3H** and **Supplementary Figures S2A, C, G**). Importantly, USP8 has the ability to block the anti-A3G activity of Vif molecules from diverse HIV-1 subtypes as well as distant related lentiviral Vif molecules (**Figure 1G** and **Supplementary Figures S2G, H**). Taken together, USP8 targets diverse Vif viral substrate receptors, but not the E3 cellular components or A3G. USP8 antagonized the ability of HIV-1 Vif to suppress the antiviral function of A3G, resulting in an enhanced antiviral activity of A3G against Vif-containing HIV-1. Next, USP8 functions in primary CD4+ T cells and monocyte-derived macrophages (MDMs) from actual patients need to be validated in the future.

Deubiquitinating enzymatic activity of USP8 is required for its antagonism of Vif function. The active site mutant USP8 C786D lost the ability to inhibit Vif-mediated A3G degradation when compared to the WT USP8 (**Figures 2F, G**). During T-cell activation, USP8 is catalytically cleaved by proteolytic enzymes into N-terminal and C-terminal fragments (22). We observed that the C-terminal fragment (C40), but not the N-terminal fragment (N90), maintains deubiquitinase activity (22) and inhibitory activity against HIV-1 Vif (**Figures 2F**, **4G**). In addition, we validated the inhibitory function of USP8 on Vif-mediated A3G polyubiquitination *in vitro* (**Supplementary Figures S3D–F**). Both WT USP8 and functional dominant truncation C40 decreased A3G polyubiquitination, while enzymatic mutation C786D was disabled (**Supplementary Figures S3D–F**).

USP8 is highly expressed in $CD4^+$ T cells and myeloid cells, which are the preferred target cells of HIV-1. USP8 is a regulatory factor of the T-cell receptor complex and plays an important role in T-cell function. HIV-1 infection could interfere with T-cell function by disturbing the expression of USP8 (**Figures 4A–F**) or its interaction with Gads5 (**Supplementary Figure S3A**). We discovered that endogenous USP8 expression is significantly reduced in HIV-1-infected H9 and Jurkat cells (**Supplementary Figures S4A, B**). It is interesting to investigate whether any auxiliary proteins of HIV may play a role in it. Unfortunately, we did not observe any significant endogenous USP8 protein expression reduction rescued by Vif-, Vpu-, or Vpx-deficient HIV. Therefore, we speculate that the reduction of USP8 by HIV may not be through its single auxiliary protein. Multiple proteins are potentially involved, including the structural proteins, which needs study in the future.

Interestingly, DUB USP8 exhibits poor activity against HIV-1 Vpr, HIV-1 Vpu, and HIV-2 Rod/SIVmac Vpx. After screening 32 USP functions, we discovered that distinct DUBs inhibit Vpr-mediated HLTF degradation, Vpu-mediated BST-2 degradation (16), and HIV-2 Rod/SIVmacVpx-mediated SAMHD1 degradation (19, 20). Vpx relieves inhibition of HIV-1 infection of myeloid cells mediated by the SAMHD1 protein (19, 20). SAMHD1 restricts reverse transcription of HIV in myeloid cells and resting T cells through its dNTP triphosphohydrolase (dNTPase) activity to repress virus replication. Different from SAMHD1, A3G and BST2/Tetherin all impair HIV-1 progeny virus replication. A3G impairs HIV-1 replication by packaging into virions during virus production and inhibits viral reverse transcription in newly infected target cells (10). BST2/Tetherin inhibits HIV-1 release by directly tethering virions to cells (16, 36). Interestingly, whether Vpr could promote HIV-1 replication in T cells is still disputable, and evidence for its role in cycling T lymphocytes has been sparse. Lahouassa et al. (18) and Yan et al. (37), using a sensitive pairwise replication competition assay, demonstrated that Vpr antagonizes HLTF to promote HIV-1 replication more fitness when coinfected with HIV-1 Vpr defective virus. In our study, the degradation of A3G, BST2, and HLTF was enhanced by HIV/SIV accessory protein when specific USPs (USP8, USP7, and USP33) were knocked down. However, we did not observe any effect on the first-round virus replication, as determined by the intracellular $Pr55^{Gag}$ expression level (**Figures 5E, F**). Importantly, USP7, USP8, or USP33 knocking down all promotes the HIV-1 progeny virus infectivity (**Figures 1D, E** and **Supplementary Figures 5K, L**). Therefore, specific USPs target different HIV/SIV accessory proteins to promote host restriction factors against HIVs/SIVs.

Ubiquitin modification of proteins and its reverse process, deubiquitination, regulate all aspects of cellular processes (1, 4, 5). Hijacking host ubiquitin pathways has been linked to the replication of diverse viruses (7). The role of DUBs in the interplay between viruses and the host has not been well characterized. In this study, we demonstrate that DUBs potently inhibit viral evasion of host restriction and viral replication (**Figure 6**). Interestingly, distinct DUBs inhibit different viral proteins with different efficacies. Enhancing the antiviral activity of certain DUBs therefore represents an attractive strategy against HIVs/SIVs.

MATERIALS AND METHODS

Plasmid Construction

USP8, USP8 N90, and USP8 C40 were constructed by PCR amplification from USP8-HA/Flag (#79639; Addgene) and then inserted between the SalI and BamHI sites of a C-terminal HA/Flag tag VR1012 vector. pET28a-USP8 C40 was constructed by PCR amplification from USP8-HA/Flag and then inserted into the pET28a-Plus vector with a 6xHis-tag at the N terminus. pET28a-USP8 C40 C786D was made from pET28a-USP8 C40 by site-directed mutagenesis. All the USP plasmids were purchased from Addgene. The infectious molecular clone pNL4-3 (WT HIV-1) (38), A3G-HA (13), A3G-V5 (13), HIV-1 NL4-3-Vif-HA (Vif-HA) (38), BIV-Vif-HA (39), A3Z2Z3-HA (39), HIV-2RodVpx (40), SIVmac Vpx-HA (40, 41), SAMHD1-HA (41), A3F-V5 (28), A3C-HA (42), A3DE-HA (42), Vpu-Myc (43) and BST-2-HA (43), A3H-hapII-HA (44), and renilla (45) were as previously described. Vifs from different HIV-1 subtypes have been previously described (26). Vpr-HA, HLTF-Flag, Vif (HxB2)-HA, Vif-Myc, and Vpx-Myc were obtained from the Institute of Virology and AIDS Research, First Hospital of Jilin University, and were as previously described (13, 38, 41).

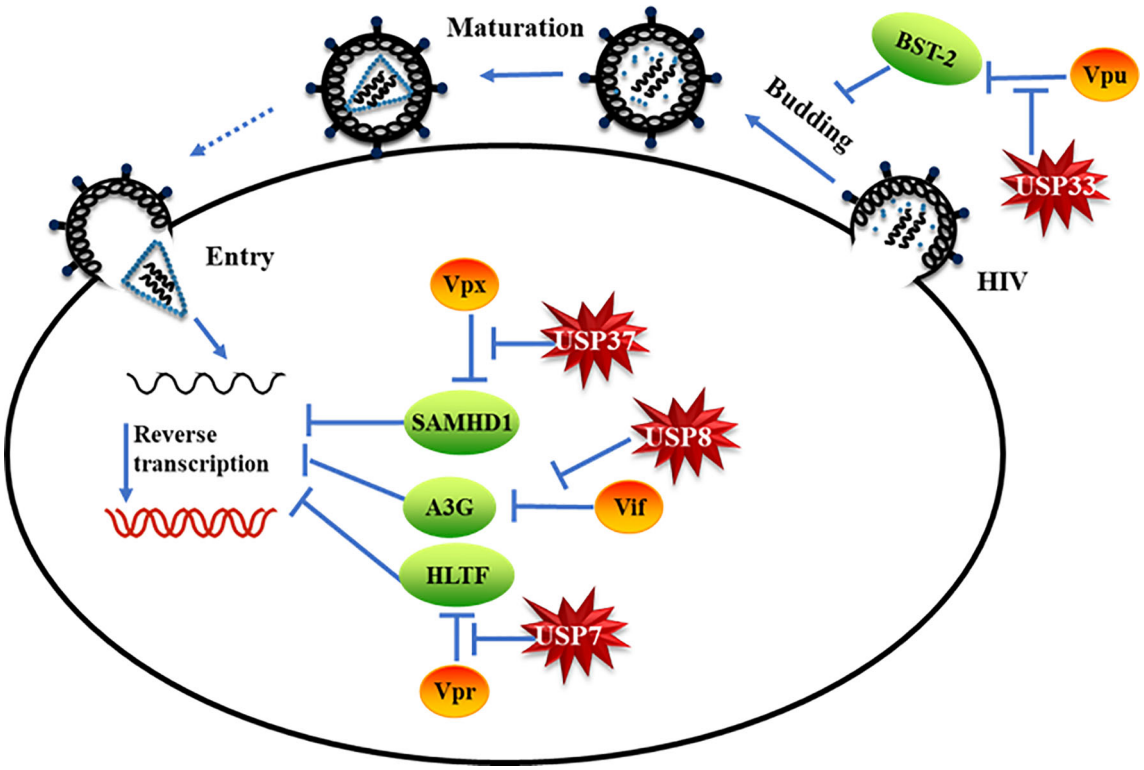

FIGURE 6 | Specific deubiquitinating enzymes suppress viral protein-mediated evasion of cell host restriction. Model of specific deubiquitinating enzymes suppressing HIV/simian immunodeficiency virus (SIV) accessory protein-mediated cell host restriction factor degradation.

Cells

HEK293T (CRL-11268; ATCC), HeLa (CRM-CCL-2; ATCC), and TZM-bl (PTA-5659; ATCC) cells were maintained in Dulbecco's modified Eagle's medium (DMEM; HyClone) containing 10% heat-inactivated fetal bovine serum (FBS, 04-001-1; Biological Industries) and penicillin/streptomycin. H9 (HTB-176; ATCC), Jurkat (TIB-152; ATCC), and THP1 (TIB-202; ATCC) cells were purchased from the ATCC and maintained in Roswell Park Memorial Institute 1640 (RPMI-1640) medium (HyClone) with 10% FBS and penicillin/streptomycin. The peripheral blood mononuclear cells (PBMCs) were isolated through Ficoll gradient centrifugation, and the $CD4^+$ T lymphocytes were then purified from the PBMCs with anti-CD4-specific antibody-coated microbeads (Miltenyi Biotec, Germany) according to the manufacturer's instructions. $CD4^+$ T lymphocytes were maintained in RPMI-1640 medium (HyClone) with 10% FBS and penicillin/streptomycin.

Transfection

DNA transfection was carried out using Lipofectamine 3000 (Invitrogen) according to the manufacturer's instructions. H9 and Jurkat cells were transfected using the Amaxa Cell Line Nucleofector Kit V (Lonza, Switzerland) with the program G-014 or X-001 according to the manufacturer's instructions.

Reagents and Antibodies

The antibodies used in this study are as follows: β-tubulin monoclonal antibody (NMS-410P; Covance), Anti-CUL5 (sc-13014; Santa Cruz Biotechnology), anti-EloB (sc-1144; Santa Cruz Biotechnology), anti-CBFb (sc-166142; Santa Cruz Biotechnology), anti-Vif (GTX80393; GeneTex), anti-USP8 (A7031; ABclonal), anti-HA (901513; Biolegend), anti-Myc (AHO0052; Invitrogen), anti-V5 (R960-25; Invitrogen), anti-SAMHD1 (TA502024; OriGene), anti-HLTF (14786-1-AP; Proteintech), anti-BST2 (13560-1-AP; Proteintech), anti-A3G (D221663;Sangon Biotech), anti-USP7 (26948-1-AP; Proteintech), anti-USP33 (20445-1-AP; Proteintech), anti-USP37 (18465-1-AP; Proteintech), anti-His (sc-8036; Santa Cruz Biotechnology). CAp24 mAb (1513) was purchased from the NIH AIDS Reagents Program. Secondary antibodies were alkaline phosphatase-conjugated anti-rabbit (115–055–045; Jackson ImmunoResearch) and anti-mouse (115–055–062; Jackson ImmunoResearch), HRP-conjugated anti-rabbit (NA934V; GE) and anti-mouse (sc-2005; Santa Cruz Biotechnology).

Immunoblot Analysis

For immunoblot analysis of cell-associated proteins, whole cell lysates were prepared as follows: Cells were collected in culture medium and centrifuged at 5,000 rpm for 5 min. Each supernatant was mixed with an appropriate volume of lysis

buffer (50 mM Tris–HCl, pH 7.8, with 150 mM NaCl, 1% NP-40, 1% sodium deoxycholate, and 4 mM EDTA) and corresponding 4× loading buffer (8% sodium dodecyl sulfate in 320 mM Tris–HCl, pH 6.8, with 40% glycerol and 0.002% bromophenol blue). Proteins were solubilized by heating for 30 min at 100°C, with occasional vortexing to shear cellular DNA. Cell lysates were subjected to sodium dodecyl sulfate–polyacrylamide gel electrophoresis (SDS–PAGE). Proteins were transferred to NC membranes (10401396; GE Whatman) and reacted with appropriate antibodies as described in the text, e.g., 1:500 rabbit polyclonal anti-USP8 to detect USP8. Membranes were then incubated with the corresponding secondary antibody, and proteins were visualized using a hypersensitive ECL chemiluminescence detection kit (Proteintech) according to the manufacturer's protocol; the assembled HIV-1 in the culture supernatants was evaluated by immunoblotting in **Figure 1I** and **Supplementary Figure S1F**. HIV-1 in the culture supernatants was filtered through a 0.45-μm filter and mixed with corresponding 4× loading buffer (described above). Proteins were solubilized by heating for 15 min at 100°C with occasional vortexing, and the HIV-1 supernatants were subjected to immunoblotting.

Co-Immunoprecipitation

In **Figure 3** and **Supplementary Figures S3** and **S4C**, HEK293T cells were co-transfected with an expression vector as indicated. In **Figures 3D, F** and **Supplementary Figure S4C**, cells were treated with 10 mM MG132 (Sigma) 12 h prior to harvesting (12, 46, 47). Cells were harvested and lysed in lysis buffer (50 mM Tris, pH 7.5, with 150 mM NaCl, 1% NP-40, and complete protease inhibitor cocktail tablets) at 4°C for 1 h, then centrifuged at 10,000×g for 30 min. Precleared cell lysates were mixed with anti-V5 antibody (**Figures 3D, F** and **Supplementary Figures S3A**, **S4C**), anti-Myc antibody (**Figures 3A, B**) or anti-HA antibody (**Supplementary Figure S3C**)-conjugated protein G agarose beads and incubated at 4°C overnight. The second day, the beads were washed six times with washing buffer (20 mM Tris, pH 7.5, with 100 mM NaCl, 0.1 mM EDTA, and 0.05% Tween-20) and centrifuged at 800×g for 1 min each time. The beads were eluted with elution buffer (0.1 M glycine-HCl, pH 3.5). The eluted materials were then analyzed by SDS-PAGE and immunoblotting as previously described.

RT-qPCR

Total RNA was extracted with TRIzol reagent (15596-026; Invitrogen) according to the manufacturer's instructions. RNA reverse transcription used EasyScript First-Strand cDNA Synthesis SuperMix (AE301; TransGen Biotech) according to the manufacturer's instructions. The quantitative real-time polymerase chain reaction (qPCR) was carried out on an Mx3005P instrument (Agilent Technologies, Stratagene, USA) using Power SYBR® Green PCR Master Mix (2x) (4367659; ABI). The primers used in this study are as follows: glyceraldehyde 3-phosphate dehydrogenase (*GAPDH*)-F: GCA AATTCCATGGCACCGT; *GAPDH*-R: TCGCCCCACTTGAT TTTGG; *USP8*-RT-F: CTGAAAGACTCTCTGAAAGCCT; *USP8*-RT-R: CCTTTCTCTTTGGTCTCACAT. Data were normalized to the housekeeping *GAPDH* gene, and the relative abundance of the transcripts was calculated using Ct models.

Chemical Synthesis of siRNA

To generate knocking down USP8 cell lines, chemically synthesized short interfering RNA (siRNA) and a nonspecific control were purchased from RiboBio Co. Ltd. (Guangzhou, China). The siUSP8 sequences are as follows: sense, #1: GCA TAAAGGTGAAGTGGCA; #2: GAAAACAGGAAGAG AGGAT; #3: GCAAAGAGGGGCAAAGAAA.

Knockdown Cell Line Construction

USP7/USP8/USP33/USP37-specific shRNAs with the following target sites were cloned in the lenti-retroviral vector pLKO.1-puro (Addgene). The shRNA sequences are as follows: USP7 shRNA: 5-CCGGCCTGGATTTGTGGTTACGTTACTCGAG TAACGTAACCACAAATCCAGGTTTTTG-3; USP8 shRNA: 5-CCGGTAAGAGTTATGTGCACAGTGCCCTCGAGGGC ACTGTGCACATAACTCTTTTTTTG-3; USP33 shRNA 5-CCGGTCTCGACAGTGGCTTAATTAACTCGAGTTAATTA AGCCACTGTCGAGATTTTTG-3; USP37 shRNA 5-CCG GCCGGATTTGCAGAAGATGATACTCGAGTATCATCTTC TGCAAATCCGGTTTTTG-3. HEK293T cells were co-transfected with sh-USP7/USP8/USP33/USP37-pLKO.1 or pLKO.1 plus RRE, REV, and VSV-G expression vectors by using Lipofectamine 3000. At 48 h after transfection, supernatants containing packaged lentivirus were harvested and used to infect H9, Hela, or THP1 cells for 96 h as indicated. Puromycin (3 μg/ml for HEK293T, 5 μg/ml for Hela, and 1.5 μg/ml for THP1) was then added into the culture to screen for stable cell lines.

HIV Infectivity and Detection

HEK293T cells were transfected with pNL4-3 (WT HIV-1) plasmid; 48 h later, the supernatant was collected and filtered through a 0.45-μm filter. Then, cells were infected with pNL4-3 virus in the presence of diethylaminoethyl-dextran hydrochloride (DEAE; 20 μg/ml) for 30 h. The culture medium was changed 30 h after infection and replaced with fresh medium and harvested at the indicated time. HIV-1 infectivity was assessed using TZM-BL indicator cells. LTR-luciferase was activated when TZM-BL cells were infected by HIV-1. TZM-BL cells were seeded in 24-well format plates (2 × 104 cells/well); 24 h later, the cells were infected with the equivalent of 0.5 ng of HIV-1 p24 antigen in the presence of 20 μg/ml DEAE. Cells were collected and lysed after 48 h. LTR-luciferase activity was measured with the Dual-Luciferase Reporter Assay System (E1910; Promega) according to the manufacturer's protocol.

In Vitro Deubiquitination Assay

Ubiquitinated A3G was isolated from HEK293T cells transfected with expression vectors of Ub-Flag, Vif-HA, and A3G-V5 and then purified from the cell extracts with anti-V5 antibody-conjugated protein G agarose beads. USP8 or its mutant was purified from HEK293T cells overexpressing USP8-HA or its mutant using anti-HA-Agarose antibody in IP buffer [1% (vol/vol) Triton X-100, 50 mM Tris–HCl pH 7.4, 50 mM EDTA,

150 mM NaCl, 10 mM NaF, 10% glycerol, and fresh protease inhibitor cocktail]. For *in vitro* deubiquitination assay, ubiquitinated A3G protein was incubated with USP8 or its mutant in the deubiquitination buffer (20 mM Tris–HCl pH 8.0, 200 mM NaCl, 1 mM EDTA, 10 mM DTT, 5% glycerol) for 1 h at 37°C. The ubiquitinated A3G was analyzed by immunoblotting.

pET28a-USP8 C40 and pET28a-USP8 C40 C786D fusion protein were expressed in the strain of *BL21(DE3)* and purified by metal-affinity chromatography on chelation resin. For *in vitro* deubiquitination assay, ubiquitinated A3G protein was incubated with USP8 C40 or its mutant in the deubiquitination buffer (mentioned above) for the indicated time courses at 37°C. The ubiquitinated A3G was analyzed by immunoblotting.

Statistical Analysis

Data from the protein quantitative analysis and luciferase reporter assays are presented as means and standard derivations. Differences among groups were analyzed by ANOVA test (Stata Corp., College 251 Station, TX, USA) (NS, not significant; *$p < 0.05$, **$p < 0.01$, ***$p < 0.001$, ****$p < 0.0001$).

DATA AVAILABILITY STATEMENT

The original contributions presented in the study are included in the article/**Supplementary Material**. Further inquiries can be directed to the corresponding authors.

ETHICS STATEMENT

Written informed consent was obtained from the individual(s) for the publication of any potentially identifiable images or data included in this article.

AUTHOR CONTRIBUTIONS

XY and WG designed the experiments. WG, GL, YR, CZ, and JS performed the experiments. XY, SH, WG, and YR analyzed the data. HL, WWZ, BZ, WYZ, and YY provided technical support. XY, WG, and YR wrote the paper with help from all authors. All authors contributed to the article and approved the submitted version.

FUNDING

This work was supported in part by funding from the National Natural Science Foundation of China (81772169; 31970151; 31900457; 31900133, 82172239, 82102384, 81701988; 81772757), the Chinese Ministry of Science and Technology (2018ZX10731-101-001-014), and the National Natural Science Foundation of Zhejiang Province (LQ21C010001).

ACKNOWLEDGMENTS

We thank Deborah McClellan, PhD, for editing the English text of a draft of this manuscript and Zhaolong Li and Hong Wang for technical assistance.

SUPPLEMENTARY MATERIAL

The Supplementary Material for this article can be found online at: https://www.frontiersin.org/articles/10.3389/fimmu.2021.740713/full#supplementary-material

Supplementary Figure 1 | Knocking down of USP8 promotes HIV-1 infectivity. **(A)** USP8 was knocked down by lentivirus infection in H9 cells. USP8 expression was analyzed by immunoblotting. **(B)** The effect of USP8 silencing on HIV infectivity in $CD4^+$ cell. **(A)** siUSP8 or si control RNA was electro-transfected into $CD4^+$cells. After 24 h, H9 cells were infected with WT HIV for another 30 h. The cells were then washed three times with PBS and placed in fresh 1640 medium with 10% FBS. Cell supernatants were then harvested after 48 h of infection. Proteins in the cell lysates were immunoblotted with the corresponding antibodies. Virus infectivity was assessed using TZM-BL indicator cells. **(C, D)** USP8 knockdown promoted Vif-triggered A3G degradation. **(D)** A3G expression from **(C)** was quantified by ImageJ2X. A3G expression alone was normalized to 100%. **(E, F)** WT HIV-1 vector was co-transfected with increasing amounts of USP8 or without USP8 in HEK293T cells. HIV-1 Pr55Gag in cells and supernatants was analyzed by immunoblotting. Tubulin was used as a loading control. **(G)** HIV-1 infectivity was assessed using TZM-bl indicator cells. The process is described in Materials and Methods. **(H)** Screening 32 USPs function on inhibiting Vif-mediated A3G degradation. HEK293T cells were transfected with A3G-V5 and Vif-HA or its empty vector in the presence of 32 USPs. Cells were harvested 48 h after transfection; protein expression in the cell lysates was analyzed by immunoblotting. Quantification of A3G expression from three independent results was analyzed by ImageJ2X. A3G expression alone was normalized to 100%. **(I)** The second-round screening of selective functional USPs in H. Quantification of A3G expression from three independent results was analyzed by ImageJ2X. A3G expression alone was normalized to 100%. Means and standard deviations are presented. Results are representative of n=3 independent experiments. The statistical significance analyses were performed using two-sided unpaired t-tests (NS, not significant, *$p < 0.05$; **$p < 0.01$; ***$p < 0.001$, ****$p < 0.0001$).

Supplementary Figure 2 | USP8 efficiently inhibits Vif-induced degradation of APOBEC3 proteins. **(A, C)** HEK293T cells were co-transfected with expression vector as indicated. Proteins in the cell lysates were immunoblotted with the corresponding antibodies. **(B, D)** Quantification of A3C or A3DE expression was analyzed by ImageJ2X. A3C/A3DE expression alone was normalized to 100%. **(E)** A model of the assembly of the BIV Vif E3 component mediating polyubiquitination and degradation of target proteins. **(F)** Sequence alignment of bovine (NM_001076126.1) and human (BC110590.2) USP8 using DNAMAN 8.0 software. **(G)** USP8 inhibits BIV Vif-induced degradation of A3Z2Z3. HEK293T cells were co-transfected with expression vector as indicated. Proteins in the cell lysates were immunoblotted with the corresponding antibodies. **(H)** Quantification of A3Z2Z3 expression was analyzed by ImageJ2X. Data are representative of at least three independent repeats. The statistical significance analyses were performed using two-tailed unpaired t-tests (***$p < 0.001$; ****$p < 0.0001$).

Supplementary Figure 3 | Vif affects the association of USP8 and Gads, and USP8 barely interacts with the CRL5 E3-ubiquitin-ligase complex. **(A)** USP8 interacts poorly with Gads in the presence of Vif. USP8-HA was co-transfected with Vif-Myc, Gads-V5 alone, or both, into HEK293T cells. Cell lysates were prepared and immunoprecipitated 48 h after transfection using anti-V5 antibody conjugated to agarose beads. Cell lysates and precipitated samples were analyzed by immunoblotting with the corresponding antibodies. Tubulin was used as the loading control for the cell lysate (n=3). **(B)** Relative binding ability of USP8 and Gads in the presence or absence of Vif. Lane 2 from A was set to 100%. **(C)** USP8-HA or Vif-HA was transfected into HEK293T cells. Cells were treated with 10 mM MG132 12 h

prior to harvesting. Cell lysates were prepared and immunoprecipitated overnight using anti-HA agarose beads. Cell lysates and precipitated samples were analyzed by immunoblotting with anti-HA, anti-Cul5, anti-CBFβ, or anti-EloB antibody. Tubulin was used as the loading control for the cell lysate (n=3). **(D)** USP8 deubiquitinates A3G *in vivo*. Ubiquitinated A3G was purified from HEK293T cells transfected with Ub-Flag,Vif-HA and A3G-V5 using anti-V5 affinity purification. HA-tagged USP8, USP8 C40 or USP8^{C786D} was purified from HEK293T cells using anti-HA affinity purification. Ubiquitinated A3G-V5 was incubated with HA-tagged USP8 or USP8^{C786D} for 1h, followed by immunoblotting using antibodies against Ub-Flag and USP8-HA. **(E)** Ubiquitinated A3G was purified from HEK293T cells transfected with Ub-Flag, Vif-HA and A3G-V5 using anti-V5 affinity purification. USP8 C40 recombinant protein was purified by Ni2+-NTA beads. Ubiquitinated A3G-V5 was incubated with His-tagged USP8C40 for indicated times, followed by immunoblotting using antibodies against Ub-Flag and USP8-His. **(F)** Ubiquitinated A3G was purified from HEK293T cells transfected with Ub-Flag, Vif-HA and A3G-V5 using anti-V5 affinity purification. USP8 C40 and USP8 C40^{C786D} recombinant protein was purified by Ni2+-NTA beads. Ubiquitinated A3G-V5 was incubated with His-tagged USP8C40 or USP8 C40^{C786D} for 1h, followed by immunoblotting using antibodies against Ub-Flag and USP8-His. Results from **(A-F)** are representative of n=3 independent experiments.

Supplementary Figure 4 | HIV-1 antagonizes USP8 suppression in CD4$^+$ cells, and USP8 C40 inhibits HIV-1 Vif-induced A3G polyubiquitination. **(A, B)** HIV-1 suppresses USP8 expression at the protein level. H9 **(A)** and Jurkat **(D)** cells were infected with WT HIV or not for 48 h and 72h. Endogenous USP8 was analyzed by immunoblotting. Virus infection was determined by the presence of Pr55Gag. Tubulin was used as a loading control. USP8 expression was measured by ImageJ2X (mock infection was set to 100%). **(C)** The C terminus of USP8 is important for the inhibition of Vif-induced A3G degradation. HEK293T cells were transfected with Vif-HA, A3G-V5, and Ub-Myc in the presence of WT USP8, a truncation (N909 or C40), or control vector. Cells were treated with 10 mM MG132 for 12 h prior to harvesting. Cell lysates were prepared and immunoprecipitated overnight using anti-V5 antibody conjugated to agarose beads. Cell lysates and precipitated samples were analyzed by immunoblotting with the corresponding antibodies. **(D)** A3G ubiquitination was measured by ImageJ2X; A3G mock was set to 100%. Means and standard deviations are from three independent experiments. The statistical significance analyses were performed using two-tailed unpaired t-tests (NS, not significant; ***p<0.001).

Supplementary Figure 5 | (A) Model showing how HIV-1 Vpr assembles E3 ubiquitin ligase complexes to target HLTF protein polyubiquitination and degradation. **(B)** Model showing how HIV-1 Vpu assembles E3 ubiquitin ligase complexes to target BST-2 protein polyubiquitination and degradation. **(C)** Model showing how HIV-2/SIV Vpx assembles E3 ubiquitin ligase complexes to target SAMHD1 protein polyubiquitination and degradation. **(D)** Screening 32 USPs function on inhibiting Vpr-mediated HLTF degradation. HEK293T cells were transfected with HLTF-HA and Vpr-HA or its empty vector in the presence of 32 USPs. Cells were harvested 48 h after transfection; protein expression in the cell lysates was analyzed by immunoblotting. Quantification of HLTF expression was analyzed by ImageJ2X. HLTF expression alone was normalized to 100%. **(E)** Screening 32 USPs function on inhibiting Vpu-mediated BST2 degradation. Quantification of BST2 expression was analyzed by ImageJ2X. BST2 expression alone was normalized to 100%. **(F)** Screening 32 USPs function on inhibiting Vpx-mediated SAMHD1 degradation. Quantification of SAMHD1 expression was analyzed by ImageJ2X. SAMHD1 expression alone was normalized to 100%. **(G)** USP8 does not inhibit HIV-1 Vpr-induced degradation of HLTF. HEK293T cells were transfected with expression vector as indicated. Proteins in the cell lysates were immunoblotted with the corresponding antibodies. The relative expression of HLTF was analyzed by ImageJ2X. HLTF expression alone was set to 100%. **(H)** USP8 does not inhibit HIV-1 Vpu-induced BST-2 degradation. **(I, J)** USP8 does not inhibit HIV-2/SIV Vpx-induced SAMHD1 degradation. **(K, L)** Virus infectivity was assessed using TZM-BL indicator cells. shCON virus infectivity was set as 100%. Results from D-J are representative of n=3 independent experiments. Means and standard deviations are from three independent experiments. The statistical significance analyses were performed using two-tailed unpaired t-tests (NS, not significant; **p < 0.01; ***p < 0.001; ****p < 0.0001).

REFERENCES

1. Swatek KN, Komander D. Ubiquitin Modifications. *Cell Res* (2016) 26:399–422. doi: 10.1038/cr.2016.39
2. Sahtoe DD, Sixma TK. Layers of DUB Regulation. *Trends Biochem Sci* (2015) 40:456–67. doi: 10.1016/j.tibs.2015.05.002
3. Clague M, Barsukov I, Coulson J, Liu H, Rigden D, Urbé S. Deubiquitylases From Genes to Organism. *Physiol Rev* (2013) 93:1289–315. doi: 10.1152/physrev.00002.2013
4. Sowa ME, Bennett EJ, Gygi SP, Harper JW. Defining the Human Deubiquitinating Enzyme Interaction Landscape. *Cell* (2009) 138:389–403. doi: 10.1016/j.cell.2009.04.042
5. Berndsen CE, Wolberger C. New Insights Into Ubiquitin E3 Ligase Mechanism. *Nat Struct Mol Biol* (2014) 21:301–7. doi: 10.1038/nsmb.2780
6. Reyes-Turcu FE, Wilkinson KD. Polyubiquitin Binding and Disassembly by Deubiquitinating Enzymes. *Chem Rev* (2009) 109:1495–508. doi: 10.1021/cr800470j
7. Calistri A, Munegato D, Carli I, Parolin C, Palu G. The Ubiquitin-Conjugating System: Multiple Roles in Viral Replication and Infection. *Cells* (2014) 3:386–417. doi: 10.3390/cells3020386
8. Osei Kuffour E, Schott K, Jaguva Vasudevan AA, Holler J, Schulz WA, Lang PA, et al. USP18 (UBP43) Abrogates P21-Mediated Inhibition of HIV-1. *J Virol* (2018) 92(20). doi: 10.1128/JVI.00592-18
9. Malim MH, Emerman M. HIV-1 Accessory Proteins–Ensuring Viral Survival in a Hostile Environment. *Cell Host Microbe* (2008) 3:388–98. doi: 10.1016/j.chom.2008.04.008
10. Harris RS, Bishop KN, Sheehy AM, Craig HM, Petersen-Mahrt SK, Watt IN, et al. DNA Deamination Mediates Innate Immunity to Retroviral Infection. *Cell* (2003) 113(6):803–9. doi: 10.1016/s0092-8674(03)00423-9
11. Wissing S, Galloway NL, Greene WC. HIV-1 Vif Versus the APOBEC3 Cytidine Deaminases: An Intracellular Duel Between Pathogen and Host Restriction Factors. *Mol Aspects Med* (2010) 31:383–97. doi: 10.1016/j.mam.2010.06.001
12. Zhang W, Du J, Evans SL, Yu Y. & Yu, X. F. T-Cell Differentiation Factor CBF-Beta Regulates HIV-1 Vif-Mediated Evasion of Host Restriction. *Nature* (2011) 481:376–9. doi: 10.1038/nature10718
13. Yu X, Yu Y, Liu B, Luo K, Kong W, Mao P, et al. Induction of APOBEC3G Ubiquitination and Degradation by an HIV-1 Vif-Cul5-SCF Complex. *Science* (2003) 302:1056–60. doi: 10.1126/science.1089591
14. Guo Y, Dong L, Qiu X, Wang Y, Zhang B, Liu H, et al. Structural Basis for Hijacking CBF-β and CUL5 E3 Ligase Complex by HIV-1 Vif. *Nature* (2014) 505:229–33. doi: 10.1038/nature12884
15. Simon V, Bloch N, Landau NR. Intrinsic Host Restrictions to HIV-1 and Mechanisms of Viral Escape. *Nat Immunol* (2015) 16:546–53. doi: 10.1038/ni.3156
16. Neil SJ, Zang T, Bieniasz PD. Tetherin Inhibits Retrovirus Release and Is Antagonized by HIV-1 Vpu. *Nature* (2008) 451:425–30. doi: 10.1038/nature06553
17. Liu Y, Fu Y, Wang Q, Li M, Zhou Z, Dabbagh D, et al. Proteomic Profiling of HIV-1 Infection of Human CD4(+) T Cells Identifies PSGL-1 as an HIV Restriction Factor. *Nat Microbiol* (2019) 4:813–25. doi: 10.1038/s41564-019-0372-2
18. Lahouassa H, Blondot ML, Chauveau L, Chougui G, Morel M, Leduc M, et al. HIV-1 Vpr Degrades the HLTF DNA Translocase in T Cells and Macrophages. *Proc Natl Acad Sci USA* (2016) 113:5311–6. doi: 10.1073/pnas.1600485113
19. Hrecka K, Hao C, Gierszewska M, Swanson SK, Kesik-Brodacka M, Srivastava S, et al. Vpx Relieves Inhibition of HIV-1 Infection of Macrophages Mediated by the SAMHD1 Protein. *Nature* (2011) 474:658–61. doi: 10.1038/nature10195
20. Laguette N, Sobhian B, Casartelli N, Ringeard M, Chable-Bessia C, Ségéral E, et al. SAMHD1 Is the Dendritic- and Myeloid-Cell-Specific HIV-1 Restriction Factor Counteracted by Vpx. *Nature* (2011) 474:654–7. doi: 10.1038/nature10117
21. Dufner A, Kisser A, Niendorf S, Basters A, Reissig S, Schönle A, et al. The Ubiquitin-Specific Protease USP8 Is Critical for the Development and Homeostasis of T Cells. *Nat Immunol* (2015) 16:950–60. doi: 10.1038/ni.3230

22. Reincke M, Sbiera S, Hayakawa A, Theodoropoulou M, Osswald A, Beuschlein F, et al. Mutations in the Deubiquitinase Gene USP8 Cause Cushing's Disease. *Nat Genet* (2015) 47:31–8. doi: 10.1038/ng.3166
23. Jäger S, Kim DY, Hultquist JF, Shindo K, LaRue RS, Kwon E, et al. Vif Hijacks CBF-Beta to Degrade APOBEC3G and Promote HIV-1 Infection. *Nature* (2011) 481:371–5. doi: 10.1038/nature10693
24. Hache G, Shindo K, Albin JS, Harris RS. Evolution of HIV-1 Isolates That Use a Novel Vif-Independent Mechanism to Resist Restriction by Human APOBEC3G. *Curr Biol* (2008) 18:819–24. doi: 10.1016/j.cub.2008.04.073
25. Fujita M, Akari H, Sakurai A, Yoshida A, Chiba T. Expression of HIV-1 Accessory Protein Vif Is Controlled Uniquely to be Low and Optimal by Proteasome Degradation. *Microbes Infect* (2004) 6:791–8. doi: 10.1016/j.micinf.2004.04.011
26. Zhao K, Du J, Rui Y, Zheng W, Kang J, Hou J, et al. Evolutionarily Conserved Pressure for the Existence of Distinct G2/M Cell Cycle Arrest and A3H Inactivation Functions in HIV-1 Vif. *Cell Cycle* (2015) 14:838–47. doi: 10.1080/15384101.2014.1000212
27. Binka M, Ooms M, Steward M, Simon V. The Activity Spectrum of Vif From Multiple HIV-1 Subtypes Against APOBEC3G, APOBEC3F, and APOBEC3H. *J Virol* (2012) 86:49–59. doi: 10.1128/jvi.06082-11
28. Liu B, Sarkis PT, Luo K, Yu Y, Yu XF. Regulation of Apobec3F and Human Immunodeficiency Virus Type 1 Vif by Vif-Cul5-ElonB/C E3 Ubiquitin Ligase. *J Virol* (2005) 79:9579–87. doi: 10.1128/JVI.79.15.9579-9587.2005
29. Zhen A, Wang T, Zhao K, Xiong Y, Yu XF. A Single Amino Acid Difference in Human APOBEC3H Variants Determines HIV-1 Vif Sensitivity. *J Virol* (2010) 84:1902–11. doi: 10.1128/JVI.01509-09
30. Larue RS, Lengyel J, Jonsson SR, Andresdottir V, Harris RS. Lentiviral Vif Degrades the APOBEC3Z3/APOBEC3H Protein of its Mammalian Host and Is Capable of Cross-Species Activity. *J Virol* (2010) 84:8193–201. doi: 10.1128/JVI.00685-10
31. Zhang J, Wu J, Wang W, Wu H, Yu B, Wang J, et al. Role of cullin-elonginB-elonginC E3 Complex in Bovine Immunodeficiency Virus and Maedi-Visna Virus Vif-Mediated Degradation of Host A3Z2-Z3 Proteins. *Retrovirology* (2014) 11:77. doi: 10.1186/s12977-014-0077-9
32. Greenwood EJ, Matheson NJ, Wals K, van den Boomen DJ, Antrobus R, Williamson JC, et al. Temporal Proteomic Analysis of HIV Infection Reveals Remodelling of the Host Phosphoproteome by Lentiviral Vif Variants. *Elife* (2016) 5. doi: 10.7554/eLife.18296
33. Matheson NJ, Sumner J, Wals K, Rapiteanu R, Weekes MP, Vigan R, et al. Cell Surface Proteomic Map of HIV Infection Reveals Antagonism of Amino Acid Metabolism by Vpu and Nef. *Cell Host Microbe* (2015) 18:409–23. doi: 10.1016/j.chom.2015.09.003
34. Decorsière A, Mueller H, van Breugel PC, Abdul F, Gerossier L, Beran RK, et al. Hepatitis B Virus X Protein Identifies the Smc5/6 Complex as a Host Restriction Factor. *Nature* (2016) 531:386–9. doi: 10.1038/nature17170
35. Pan T, Song Z, Wu L, Liu G, Ma X, Peng Z, et al. USP49 Potently Stabilizes APOBEC3G Protein by Removing Ubiquitin and Inhibits HIV-1 Replication. *eLife* (2019) 8. doi: 10.7554/eLife.48318
36. Perez-Caballero D, Zang T, Ebrahimi A, McNatt MW, Gregory DA, Johnson MC, et al. Tetherin Inhibits HIV-1 Release by Directly Tethering Virions to Cells. *Cell* (2009) 139:499–511. doi: 10.1016/j.cell.2009.08.039
37. Yan J, Shun MC, Zhang Y, Hao C, Skowronski J. HIV-1 Vpr Counteracts HLTF-Mediated Restriction of HIV-1 Infection in T Cells. *Proc Natl Acad Sci USA* (2019) 116(19):9568–77. doi: 10.1073/pnas.1818401116
38. Wang H, Liu B, Liu X, Li Z, Yu XF, Zhang W. Identification of HIV-1 Vif Regions Required for CBF-Beta Interaction and APOBEC3 Suppression. *PloS One* (2014) 9:e95738. doi: 10.1371/journal.pone.0095738
39. Zhang W, Wang H, Li Z, Liu X, Liu G, Harris RS, et al. Cellular Requirements for Bovine Immunodeficiency Virus Vif-Mediated Inactivation of Bovine APOBEC3 Proteins. *J Virol* (2014) 88:12528–40. doi: 10.1128/JVI.02072-14
40. Wei W, Guo H, Liu X, Zhang H, Qian L, Luo K. A First-in-Class NAE Inhibitor, MLN4924, Blocks Lentiviral Infection in Myeloid Cells by Disrupting Neddylation-Dependent Vpx-Mediated SAMHD1 Degradation. *J Virol* (2014) 88:745–51. doi: 10.1128/JVI.02568-13
41. Wei W, Guo H, Gao Q, Markham R, Yu XF. Variation of Two Primate Lineage-Specific Residues in Human SAMHD1 Confers Resistance to N Terminus-Targeted SIV Vpx Proteins. *J Virol* (2014) 88:583–91. doi: 10.1128/JVI.02866-13
42. Zhang W, Chen G, Niewiadomska AM, Xu R, Yu XF. Distinct Determinants in HIV-1 Vif and Human APOBEC3 Proteins Are Required for the Suppression of Diverse Host Anti-Viral Proteins. *PloS One* (2008) 3:e3963. doi: 10.1371/journal.pone.0003963
43. Lv M, Zhang B, Shi Y, Han Z, Zhang Y, Zhou Y, et al. Identification of BST-2/Tetherin-Induced Hepatitis B Virus Restriction and Hepatocyte-Specific BST-2 Inactivation. *Sci Rep* (2015) 5:11736. doi: 10.1038/srep11736
44. Zhen A, Du J, Zhou X, Xiong Y, Yu XF. Reduced APOBEC3H Variant Anti-Viral Activities Are Associated With Altered RNA Binding Activities. *PLoS One* (2012) 7:e38771. doi: 10.1371/journal.pone.0038771
45. Su J, Rui Y, Lou M, Yin L, Xiong H, Zhou Z, et al. HIV-2/SIV Vpx Targets a Novel Functional Domain of STING to Selectively Inhibit cGAS-STING-Mediated NF-kappaB Signalling. *Nat Microbiol* (2019) 4:2552–64. doi: 10.1038/s41564-019-0585-4
46. Wu HT, Kuo YC, Hung JJ, Huang CH, Chen WY, Chou TY, et al. K63-Polyubiquitinated HAUSP Deubiquitinates HIF-1alpha and Dictates H3K56 Acetylation Promoting Hypoxia-Induced Tumour Progression. *Nat Commun* (2016) 7:13644. doi: 10.1038/ncomms13644
47. Liu X, Yao Y, Ding H, Han C, Chen Y, Zhang Y, et al. USP21 Deubiquitylates Nanog to Regulate Protein Stability and Stem Cell Pluripotency. *Signal Transduct Target Ther* (2016) 1:16024. doi: 10.1038/sigtrans.2016.24

Conflict of Interest: The authors declare that the research was conducted in the absence of any commercial or financial relationships that could be construed as a potential conflict of interest.

frontiers in Immunology

REVIEW
published: 11 October 2021
doi: 10.3389/fimmu.2021.742542

An Integrated View of Deubiquitinating Enzymes Involved in Type I Interferon Signaling, Host Defense and Antiviral Activities

Guanghui Qian[1*†], *Liyan Zhu*[2†], *Gen Li*[1†], *Ying Liu*[1], *Zimu Zhang*[1], *Jian Pan*[1*] *and Haitao Lv*[1*]

[1] Institute of Pediatric Research, Children's Hospital of Soochow University, Suzhou, China, [2] Department of Experimental Center, Medical College of Soochow University, Suzhou, China

OPEN ACCESS

Edited by:
Soham Gupta,
Karolinska Institutet (KI), Sweden

Reviewed by:
Bo Zhong,
Wuhan University, China
Douglas Gray,
University of Ottawa, Canada
Emmanuel Taillebourg,
Commissariat à l'Energie Atomique et aux Energies Alternatives (CEA), France

***Correspondence:**
Guanghui Qian
ghqian@suda.edu.cn
Jian Pan
panjian2008@163.com
Haitao Lv
haitaossz@163.com

[†]These authors have contributed equally to this work

Specialty section:
This article was submitted to Viral Immunology, a section of the journal Frontiers in Immunology

Received: 16 July 2021
Accepted: 16 September 2021
Published: 11 October 2021

Citation:
Qian G, Zhu L, Li G, Liu Y, Zhang Z, Pan J and Lv H (2021) An Integrated View of Deubiquitinating Enzymes Involved in Type I Interferon Signaling, Host Defense and Antiviral Activities. Front. Immunol. 12:742542. doi: 10.3389/fimmu.2021.742542

Viral infectious diseases pose a great challenge to human health around the world. Type I interferons (IFN-Is) function as the first line of host defense and thus play critical roles during virus infection by mediating the transcriptional induction of hundreds of genes. Nevertheless, overactive cytokine immune responses also cause autoimmune diseases, and thus, tight regulation of the innate immune response is needed to achieve viral clearance without causing excessive immune responses. Emerging studies have recently uncovered that the ubiquitin system, particularly deubiquitinating enzymes (DUBs), plays a critical role in regulating innate immune responses. In this review, we highlight recent advances on the diverse mechanisms of human DUBs implicated in IFN-I signaling. These DUBs function dynamically to calibrate host defenses against various virus infections by targeting hub proteins in the IFN-I signaling transduction pathway. We also present a future perspective on the roles of DUB-substrate interaction networks in innate antiviral activities, discuss the promises and challenges of DUB-based drug development, and identify the open questions that remain to be clarified. Our review provides a comprehensive description of DUBs, particularly their differential mechanisms that have evolved in the host to regulate IFN-I-signaling-mediated antiviral responses.

Keywords: deubiquitinating enzymes, type I IFN signaling, ubiquitin, virus infection, innate immunity

INTRODUCTION

Pathogen invasions are responsible for many diseases and exert extensive effects on human health ranging from mild to potentially fatal infections. Critically, the prevalence of certain viruses, such as SARS-CoV-2, can even pose a serious threat to global human health (1). The host's immune system evolved as the first line of defense against the invasion of microbial pathogens and can also trigger various immune responses through dynamic interactions with differential cellular components (2, 3). Among all the signaling pathways examined, much attention has been given to the signaling events triggered by one class of molecules during the activation of innate immune responses, pattern-recognition receptors (PRRs). Innate immune responses are rapidly initiated when host cellular PRRs, such as Toll-like receptors (TLRs), RIG-I-like receptors (RLRs), NOD-like receptors

(NLRs), and DNA sensors encounter pathogen-associated molecular patterns (PAMPs) of fungal, bacterial, or viral origin (4, 5). Toll-like receptors, including TLR3, TLR4, TLR7, TLR8, and TLR9 can sense endosomal nucleic acids derived from pathogens and infected apoptotic cells. Specifically, TLR3 and TLR7/8 recognize double-stranded RNA (dsRNA) and single-stranded RNA (ssRNA), respectively, whereas TLR9 detects unmethylated CpG double-stranded DNA species (6). The activation of TLR3, TLR4, TLR7, TLR8, and TLR9 leads to activation of the adapter myeloid differentiation 88 (MyD88)-dependent pathway, which causes IRF7 activation through a TRAF6-dependent mechanism (TLR7/8/9) or the Toll/interleukin-1 (IL-1) receptor-domain-containing adapter-inducing IFNβ (TRIF)-dependent pathway and thus leads to IRF3 and IRF7 activation through a TBK1-dependent mechanism (TLR3/4) (7–9). RLRs are another critical sensor of virus infection. These protein family members include retinoic acid-inducible gene I (RIG-I, also known as Ddx58), melanoma differentiation-associated protein 5 (MDA5, also known as Ifih1 or Helicard), and laboratory of genetics and physiology protein 2 (LGP2) (10). Viral 5' ppp RNA, and longer double-stranded (ds) RNA are often recognized by RIG-I and MDA5, respectively, and both proteins share two N-terminal caspase activation and recruitment domains (CARDs), which are needed for interaction with the mitochondrial antiviral signaling protein (MAVS, also termed IPS-1, VISA or CARDIF). The interacting components then activate MAVS and TNF receptor-associated factors (TRAF)-mediated downstream signaling during virus infection (11). Ultimately, the viruses recognized by different host sensors induce antiviral responses by regulating multiple signaling pathways, which are characterized by rapid gene expression of inflammation-inducing molecules and/or cytokines, including interferons (12–15).

Type I IFNs (also called IFNα/β or IFN-Is), which serve as the first line of host defense against virus infection can be induced in almost all cells in the body. A dysregulated interferon-response is thus associated with many diseases, such as autoimmune diseases (16), infectious diseases (17), and the recent severe coronavirus diseases, which have caused a major ongoing pandemic worldwide (18). The critical cytosolic DNA sensor, cyclic guanosine monophosphate-adenosine monophosphate (cGAMP) synthase (cGAS) often recognizes viral DNA and triggers downstream immune responses through the molecule stimulator of interferon genes (STING, also known as MITA, MPYS, ERIS, or TMEM173) (19). STING further activates TRAFs, which in turn activate TANK-binding kinase 1 (TBK1) or IκB kinase (IKK), and this activation leads to the activation of nuclear factor-kappa enhancer-binding protein (NF-κB) or interferon regulatory factor 3 or 7 (IRF3 or IRF7, respectively). The activated IRF3 and IRF7 complex ultimately translocates the nucleus, which leads to the transcriptional induction of multiple IFNs (**Figure 1A**) (20).

Furthermore, the secreted IFN-Is bind to and signal through a heterodimeric transmembrane receptor composed of the subunits IFNAR1 and IFNAR2. The ligation of IFNAR activates the receptor-associated protein tyrosine kinases Janus kinase 1 (JAK1) and tyrosine kinase 2 (TYK2). In the canonical IFNAR-mediated downstream signaling pathway, activated JAK1 and TYK2 induce phosphorylation of the signal transducer and activator of transcription 1 (STAT1) and STAT2 molecules present in the cytosol, which leads to the dimerization, nuclear translocation, and binding of these molecules to IRF9 to form the ISG factor 3 (ISGF3) complex. This complex then enters the nucleus and binds to DNA sequences termed interferon-sensitive response elements (ISREs) (with the consensus sequence TTTCNNTTTC), which results in induction of the transcription of several hundred IFN-stimulated genes (ISGs), including Mx1, OAS, STAT1, interferon-regulatory factors (IRFs) and other antiviral genes (21) (**Figure 1B**). These ISGs function to induce an antiviral state within the cell. Thus, it can be concluded that host antiviral efficiencies are tightly regulated not only at the virus-induced IFN-I production level but also at the interferon receptor-mediated downstream signaling level.

Currently, post-translational modifications (PTMs), which involve the covalent linkage of new functional groups to amino acid chains, have remarkably expanded the functions of proteins. Over the years, an increasing number of studies have uncovered that PTMs also play pivotal roles during host innate immune responses upon virus infection (22, 23). In particular, ubiquitination (also known as ubiquitylation or ubiquitinylation) events in which 8.5-kDa ubiquitin (Ub) is conjugated to one or more lysine residues of proteins are broadly involved in antiviral signaling by regulating the stability, folding, and location of proteins or by interacting with other proteins in the signaling transduction pathway (22, 24). In general, ubiquitination involves three sequential steps: an initial activation step catalyzed by the Ub-activating enzyme (E1), an intermediate step in which Ub is covalently linked to a conjugating enzyme (E2), and a final specific step in which Ub reaches its ultimate destination of the substrate amino group through a reaction catalyzed by a ligase enzyme (E3) (25–27). Substrate-conjugated ubiquitin can be modified by additional Ub molecules to build polyubiquitin chains. The C-terminal carboxyl group of the distal Ub moiety is covalently attached to either the first methionine (M1) of the proximal Ub moiety or one of the seven lysine (K) residues K6, K11, K27, K29, K33, K48, and K63 to result in the formation of linear Ub chains or polyubiquitin chains (28–30). Homotypic polyubiquitin chains are often referred to as a single type of polyubiquitin linkage, whereas heterotypic polyubiquitin chains are characterized by the presence of at least two different types of linkages within the same polymer (31).

Similar to other PTMs, ubiquitination is reversible, and the reversal process is implemented by an array of proteases termed deubiquitinating enzymes (DUBs) or deubiquitinating peptidases. Approximately 100 DUBs encoded in the human genome. These DUBs have been categorized into at least seven families based on their homology domains and cleavage preferences: namely, ubiquitin-specific proteases (USPs), ubiquitin C-terminal hydrolases (UCHs), ovarian tumour proteases (OTUs), Machado-Joseph disease protease family members (MJDs), the motif interacting with the Ub (MIU)-containing novel DUB family (MINDYs), the JAB1/MPN/MOV34 metalloenzyme family (JAMMs, also termed MPN+), zinc fingers with UFM1-specific peptidase domain proteins (ZUFSPs), and other members

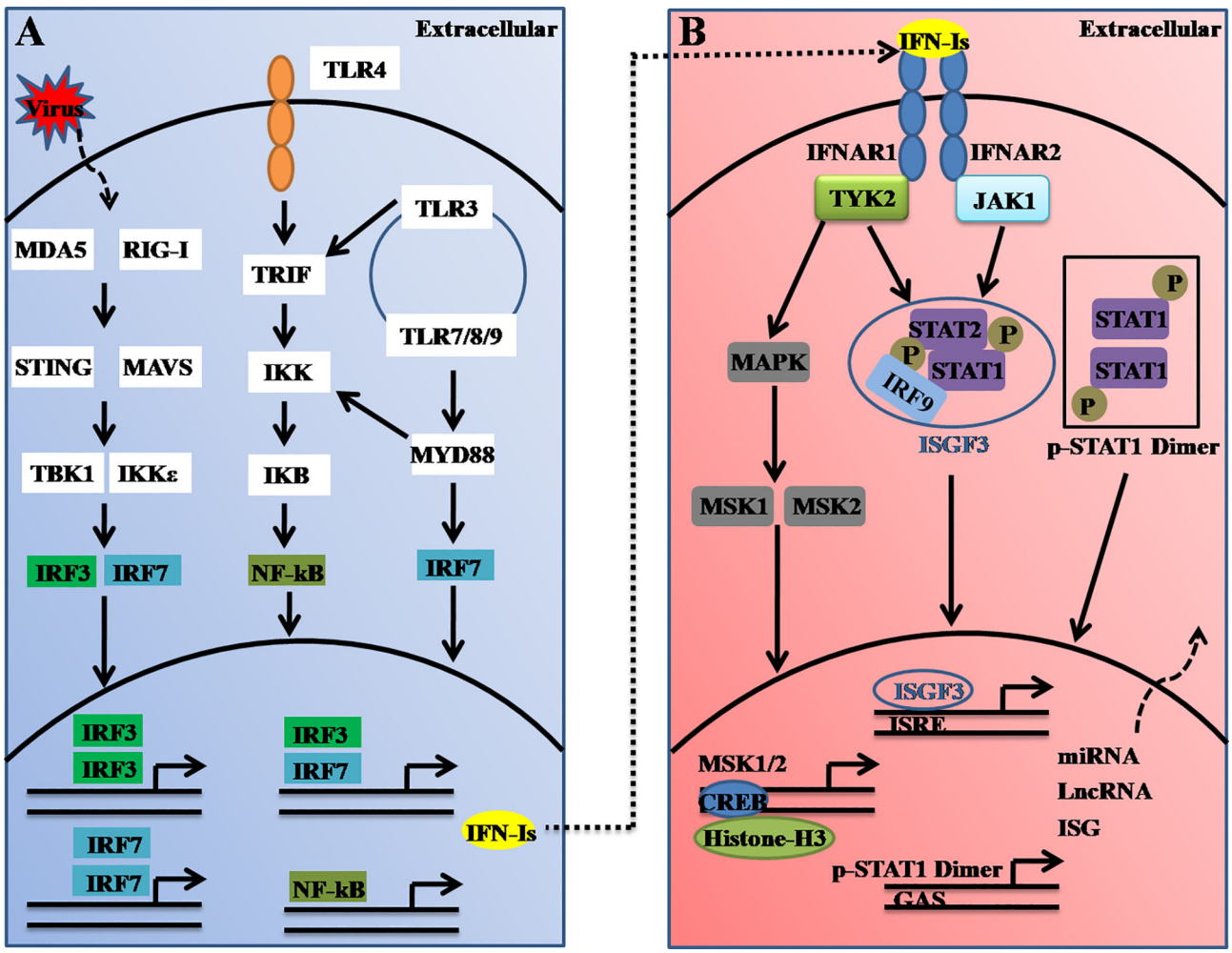

FIGURE 1 | Schematic illustration of type I interferon (IFN-I) induction and receptor signaling pathways. **(A)** Type-I IFNs are induced upon virus nucleic acid recognition by a variety of PRRs, including TLRs and cytosolic nucleic acid sensors. The activation of PRRs causes the nuclear translocation of IRFs or NF-κB, which bind to the promoter region of IFN-Is and thus induce their transcription. IRF3- and IRF7-mediated IFN-I production could be regulated by STING (*via* cGAS), RIG-I, MDA5, TLR3, and TLR4 (through TRIF), whereas the ligand engagement of TLR7/8 and TLR9 activates IRF7 *via* MyD88. **(B)** Secreted interferons bind to the IFNAR complex composed of IFNAR1 and IFNAR2, which causes cross-phosphorylation of JAK1 and TYK2 and further activation of STAT homo/heterodimers to control distinct expression profiles. ISGF3, which comprise of STAT1, STAT2, and IRF9, binds to the IFN-stimulated response element (ISRE). TYK2 activates MAPK and MSK1/2. Nuclear MSK1/2 further phosphorylates CREB and induces the transcriptional induction of hundreds of genes or noncoding RNAs.

identified recently (32–36) (**Figure 2**). These DUBs often contain a catalytic domain surrounded by one or more accessory domains, and some of these domains contribute to Ub binding and target recognition (37). One of the best-characterized functions of DUBs is the removal of monoubiquitin and polyubiquitin chains from proteins, thus ensuring that the Ub-proteasome system (UPS) functions properly and recycles free Ub for reuse to maintain the homeostasis of the polyubiquitin pool (38, 39). Analogous to the dynamic and crucial roles of ubiquitination events shown previously, DUB-mediated deubiquitination events also play important roles in the antiviral innate immune response (23, 24, 40, 41). Here, we summarize the differential regulatory roles of human DUBs involved in the IFN-I signaling transduction pathway during viral infections. Integrated analyses of DUBs involved in the IFN-I signaling transduction pathway might improve our understanding of their diverse regulatory mechanisms and host antiviral activities, and facilitate the development of therapeutic targets to improve host antiviral efficiency in the future.

DUBS REGULATE VIRUS-INDUCED IFN-I PRODUCTION AND ANTIVIRAL ACTIVITIES

Constitutively expressed RLRs often reside in the cytoplasm of uninfected cells in an auto-repressed, inactive state (42). However, upon viral infection, the master regulators RIG-I and MDA5 are

Ubiquitin C-terminal Hydrolases (UCHs)	UCHL1 UCHL3 UCHL5 BAP1
Ubiquitin Specific Proteases (USPs)	USP1 USP2A USP2B USP3 USP4 USP5 USP6 USP7B USP8 USP9 USP10 USP11 USP12 USP13 USP14 USP15 USP16 USP17 USP18 USP19 USP20 USP21 USP22 USP24 USP25 USP26 USP27 USP28 USP29 USP30 USP31 USP32 USP33 USP34 USP35 USP36 USP37 USP38 USP39 USP40 USP41 USP42 USP43 USP44 USP45 USP46 USP47 USP48 USP49 USP50 USP51 USP52 USP53 USP54 CYLD USPL1
Otubain Proteases (OTUs)	OTUB1 OTUB2 OTUD1 OTUD3 OTUD4 OTUD5 OTUD6A OTUD6B OTUD7B OTULIN YOD1 STAMBP A20 Cezanne Cezanne2 TRABID VCPIP1 FAM105A
Machado-Joseph Disease Proteases(MJDs)	Ataxin-3 Ataxin-3-like JOSD1 JOSD2 JOSD3
MINDYs	MINDY1 MINDY2 MINDY3 MINDY4
ZUFSP	ZUFSP
JAB1/MPN/Mov34 Metallo-enzymes (JAMMs)	STAMBP STAMBPL1 BRCC36 COPS5 COPS6 PSMD7 PSMD14 PRPF8 EIF3F EIF3H MPND MYSM1
Other DUBs	MCPIP1 PPPDE1

FIGURE 2 | List of DUBs identified in the human genome. These DUBs are categorized into at least seven subfamilies, namely, Ub carboxyl-terminal hydrolases (UCHs), Ub-specific proteases (USPs), ovarian tumor proteases (OTUs), Machado-Joseph disease proteases (MJDs), motifs interacting with Ub (MIU)-containing novel DUB family members (MINDYs), zinc fingers with UFM1-specific peptidase domain protein/C6orf113/ZUP1 (ZUFSP), JAB1/MPN/MOV34 metalloenzyme family members (JAMMs, also termed MPN+), and other newly identified members.

rapidly activated and then induce the transcriptional induction of multiple IFNs. Additionally, mice lacking RIG-I or MDA5 are highly susceptible to infection and fail to produce IFN-I and proinflammatory cytokines (43, 44). Given the importance of RIG-I and MDA5 in the RLR signaling pathways, the functions of the two proteins are affected by multiple PTM events, such as phosphorylation and ubiquitination. For instance, several E3 ligases, such as TRIM25 (45), RNF135 (46), RNF125 (47), RNF122 (48), TRIM40 (49), CHIP (50), and c-Cbl (51), regulate RIG-I signaling by modulating Ub chains from various signaling proteins. Among these, the K63-linked ubiquitination of RIG-I often represents a critical step in promoting the activation of IFN-I signaling (45, 46, 52). Intriguingly, IFN stimulation could also promote an increase in the expression level of RIG-I. Thus, the protein turnover and activity of RIG-I must be tightly regulated to ensure restoration to homeostasis and to avoid hyperactivation of IFN and cytokine signaling. To the best of our knowledge, at least nine DUBs, A20, CYLD, USP3, USP5, USP14, USP15, USP21, USP25, and USP27X, have been proposed to counteract the K63-linked ubiquitination of RIG-I and, thereby attenuate downstream signaling and IFN-β production (**Table 1** and **Figure 3**) (58, 76, 93). However, unlike the nine above-mentioned Dubs, USP4 and USP17 are the two DUBs that positively regulate virus-induced IFN-I signaling by increasing the stability of RIG-I (**Table 1** and **Figure 3**). Congruently, the overexpression of USP4 or USP17 significantly promotes virus-induced IFN production and thereby restricts virus replication, whereas the knockdown of USP4 or USP17 has the opposite effect (77, 87). Moreover, DUBs also exhibit different functions under different contexts. For example, the deubiquitinating enzyme USP15 negatively regulates virus-induced IFN-I production by targeting RIG-I (84). However, USP15 has also been identified to positively regulate type I IFN responses by decreasing the polyubiquitination level of TRIM25 (85, 86). Because the function of DUBs can be altered by various PTMs under differential contexts (123), the discrepancy that USP15 exerts both positive and negative effects may arise from the context-specific PTM of USP15 itself, which may allow dynamic fine-tuning of the signaling. Among the DUBs that interact with STING, five members, namely CYLD, OTUD5, USP18 (also termed UBP43), USP20, and USP44, have been

TABLE 1 | Summary on human DUBs involved in the regulation on IFN-I signaling and antiviral responses.

DUB	Substrate	Ub Model	Effect	Specific Event	References
A20	RIG-I	NA	–	Suppressing VSV through inhibition on RIG-I	(53)
A20	MAVS	NA	–	Suppressing VSV through inhibition on MAVS	(53)
A20	IRF7	K63	–	Deubiquitinating K63-Ub on IRF7 in 293 cell	(54)
A20	TRAF6	K63	NA	Deubiquitinating K63-Ub on TRAF6 in HEK293T cells	(55)
A20	IKK-γ	NA	NA	Interacting with ubiquitinated NEMO, inhibiting IKK phosphorylation and NF-κB activation	(56)
CYLD	IKK-γ	M1	NA	Suppressing NF-κB signaling	(57)
CYLD	RIG-I	K63	–	Deubiquitinating K63-Ub on RIG-I to decrease IFN production	(58)
CYLD	MAVS	NA	–	Interacting with but not deubiquitinating MAVS to negatively regulate IFN production	(58)
CYLD	TBK1	K63	–	Deubiquitinating K63-Ub on TBK1, negatively regulating RIG-I-mediated antiviral response	(58)
CYLD	STING	K48	+	Deubiquitinating K48-Ub on STING, promoting the innate antiviral response	(59)
UCHL1	TRAF3	K63	–	Deubiquitinating K63-Ub on TRAF3 in HEK293T cell, negatively regulating virus-induced IFNs production	(60)
OTUB1	TRAF3	Ub	–	Deubiquitinating Ub on TRAF3, negative regulating virus-induced IFNs signaling	(61)
OTUB2	TRAF6	Ub	–	Deubiquitinating Ub on TRAF6, negatively regulating virus-induced IFNs signaling	(61)
OTUD1	IRF3	K63	NA	Deubiquitinating K63-Ub on IRF3, inhibiting IRF3 nuclear translocation and transcriptional activity	(62)
OTUD1	IRF3	K6	–	Deubiquitinating the viral infection-induced K6-linked ubiquitination on IRF3	(63)
OTUD1	SMURF1	K48	–	Deubiquitinating K48-Ub on SMURF1, causing degradation on MAVS/TRAF3/TRAF6	(64)
OTUD3	MAVS	K63	–	Deubiquitinating K63-Ub on MAVS, inhibiting innate antiviral immune responses	(65)
OTUD4	MAVS	K48	+	Deubiquitinating K48-Ub on MAVS, promoting antiviral responses	(66)
OTUD4	MyD88	K63	NA	Suppressing TLR/NF-κB signaling	(67)
OTUD5	TRAF3	K63	–	Deubiquitinating K63-Ub on TRAF3, suppressing type I IFN production in HEK293 cells	(68)
OTUD5	STING	K48	+	Deubiquitinating K48-Ub on STING, promoting innate antiviral immunity.	(69)
OTUD7B	RIPK1	K48&K63	NA	Deubiquitinating K48 and K63-Ub on RIPK1	(70, 71)
OTUD7B	TRAF3	K48	NA	Deubiquitinating K48-Ub on TRAF3, inhibiting TRAF3 proteolysis, preventing NF-κB activation	(72)
OTUD7B	TRAF6	K63	NA	Deubiquitinating TRAF6 in HUVECs	(73)
USP1	TBK1	K48	+	Inhibiting TBK1 degradation, promoting RIG-I- induced IRF3 activation and IFN-β secretion	(74)
USP2B	TBK1	K63	–	Deubiquitinating K63-Ub on TBK1 to inhibit TBK1 kinase activity	(75)
USP3	RIG-I	K63	–	Deubiquitinating K63-Ub on RIG-I, to convert RIG-I to its inactive form in 293T	(76)
USP4	RIG-I	K48	+	Deubiquitinating K48-Ub on RIG-I to stabilize RIG-I	(77)
USP4	TRAF6	K48	NA	Deubiquitinating K48-Ub on TRAF6, positively regulating RLR-induced NF-κB activation	(78)
USP5	RIG-I	K48	–	Increasing the K48-Ub on RIG-I after SeV infection	(40)
USP7	TRIM27	K48	–	USP7 knockout destabilizes TRIM27, which increase TBK1 turnover and IFNs signaling	(79)
USP7	NF-κB	K48	NA	Stabilizing NF-κB, increasing NF-κB transcription	(80)
USP13	STING	K27	–	Inhibiting the recruitment on TBK1 to STING by deubiquitinating K27-Ub on STING	(81)
USP14	RIG-I	K63	–	Deubiquitinating K63-Ub on RIG-I in 293T cell	(82)
USP14	cGAS	K48	+	Recruited by TRIM14 to stabilize cGAS, functions as a positive feedback loop on cGAS signaling	(83)
USP15	RIG-I	K63	–	Deubiquitinating K63-Ub on RIG-I in HEK-293T cells	(84)
USP15	TRIM25	K48	+	Deubiquitinating K48-Ub on TRIM25 to maintain TRIM25 in an inactivate state	(85)
USP15	TRIM25	Ub	+	Deubiquitinating Ub on TRIM25 in haematopoietic cells and resident brain cells	(86)
USP17	RIG-I	K48&K63	+	Deubiquitinating K48-Ub on RIG-I	(87)
USP17	MDA5	K48&K63	+	Deubiquitinating K48-Ub and K63-Ub on MDA5	(87)
USP18	ISG15	NA	–	Recruiting USP20 to form a complex with STING independently on DUB activity	(88)
USP18	TAK1	K63	NA	Suppressing TLR/NF-κB signaling	(89)
USP19	TRIF	K27	–	Deubiquitinating K27-Ub on TRIF to impair the recruitment of TRIF to TLR3/4	(90)
USP20	STING	K48	+	Deubiquitinating K33- or K48 Ub on STING together with USP18	(91, 92)
USP21	RIG-I	K63	–	Deubiquitinating K63-Ub on RIG-I in HEK 293T cells	(93)
USP22	STING	K27	–	Deubiquitinating K27-Ub on STING by recruiting USP13	(40)
USP22	IRF3	K48	+	Stabilizing KPNA2, promoting IRF3 nuclear translocation	(94)
USP25	RIG-I	K48&K63	–	Deubiquitinating RIG-I in HEK-293T cells	(95)
USP25	TRAF3	K48&K63	–	Deubiquitinating TRAF3 in HEK-293T cells	(95)
USP25	TRAF6	K48&K63	–	DeubiquitinatingTRAF6 in HEK-293T cells	(95)
USP25	TRAF3	K48	+	Deubiquitinating K48-Ub in BMDCs and MEFs	(96)
USP25	TRAF6	K63	+	Deubiquitinating Ub on TRAF6	(96)
USP27X	RIG-I	K63	–	Deubiquitinating K63-Ub on RIG-I	(97)
USP27X	cGAS	K48	+	Deubiquitinating K48-Ub on cGAS to stabilize cGAS	(98)
USP29	cGAS	K48	+	Deubiquitinating and stabilizing cGAS to promote innate antiviral responses against DNA viruses	(99)
USP31	TRAF2	K48	NA	Deubiquitinating K48-Ub and stabilizing TRAF2	(100)
USP38	TBK1	K33	–	USP38 knockout increases K33-linked Ub but abrogates the K48-mediated degradation on TBK1	(101)
USP44	STING	K48	+	Preventing STING from proteasome-mediated degradation	(102)
USP49	STING	K63	–	Deubiquitinating K63-Ub on STING, inhibiting STING aggregation and the recruitment on TBK1	(103)
MYSM1	TRAF3	K63	–	Deubiquitinating K63-Ub on TRAF3	(104)
MYSM1	TRAF6	K63	–	Deubiquitinating K63-Ub on TRAF6	(104)
MYSM1	STING	K63	–	Deubiquitinating K63-Ub on STING	(105)
MCPIP1	TRAFs	K48&K63	–	Deubiquitinating TRAFs and inhibiting IRF3 nuclear translocation in HEK293T and HeLa cells	(106, 107)

(Continued)

TABLE 1 | Continued

DUB	Substrate	Ub Model	Effect	Specific Event	References
ATXN3	HDAC3	K48&K63	+	Deubiquitinating K48- and K63-Ub on HDAC3 in 293T cells	(108)
BRCC36	IFNAR1	K63	+	Deubiquitinating K63-Ub on IFNAR1 to sustain the turnover of IFNAR1 in 2fTGH cells	(109)
BRCC36	STAT1	K63	+	Maintaining the STAT1 levels by recruiting USP13 to antagonize the SMURF1-mediated degradation on STAT1	(110)
USP2A	p-STAT1	K48	+	Inhibiting K48-Ub-linked ubiquitination and degradation on pY701-STAT1 in the nucleus	(111)
USP5	SMURF1	K63	–	Deubiquitinating K63-Ub on SMURF1, inhibiting the IFN-mediated antiviral activity	(112)
USP7	SOCS1	Ub	–	Enhancing SOCS1 protein stability *via* deubiquitination effects	(113)
USP12	CBP	NA	+	Regulating CBP and TCPTP independently on the deubiquitinase activity	(114)
USP13	STAT1	K48	+	Deubiquitinating and stabilizing STAT1	(115)
USP18	JAK1	NA	–	Interacting with IFNAR2, restricting its interaction with JAK, inhibiting the tyrosine kinase activity of JAK	(116, 117)
USP39	STAT1	K6	+	Decreasing K6-linked Ub on STAT1 for degradation	(118)
MCPIP1	NA	Ub	+	Promoting IFN signaling by increasing ISRE promoter activity and ISG expression	(119)
JOSD1	SOCS1	K48	–	Deubiquitinating K48-Ub on SOCS1	(120)
COPS5	TYK2	NA	+	Stabilizing IFNAR by antagonizing the NEDD8 pathway	(121)
UCHL3	COPS5	K48&K63	+	Deubiquitinating K48- and K63-linked Ub on COPS5, increasing the IFNAR1 turnover in 293T cells	(122)

NA, not available; Ub model, the deubiquitination type on each DUB acting on the targeted proteins; effects, the DUBs positively (+) or negatively (–) regulate type I IFN signaling-mediated antiviral activity.

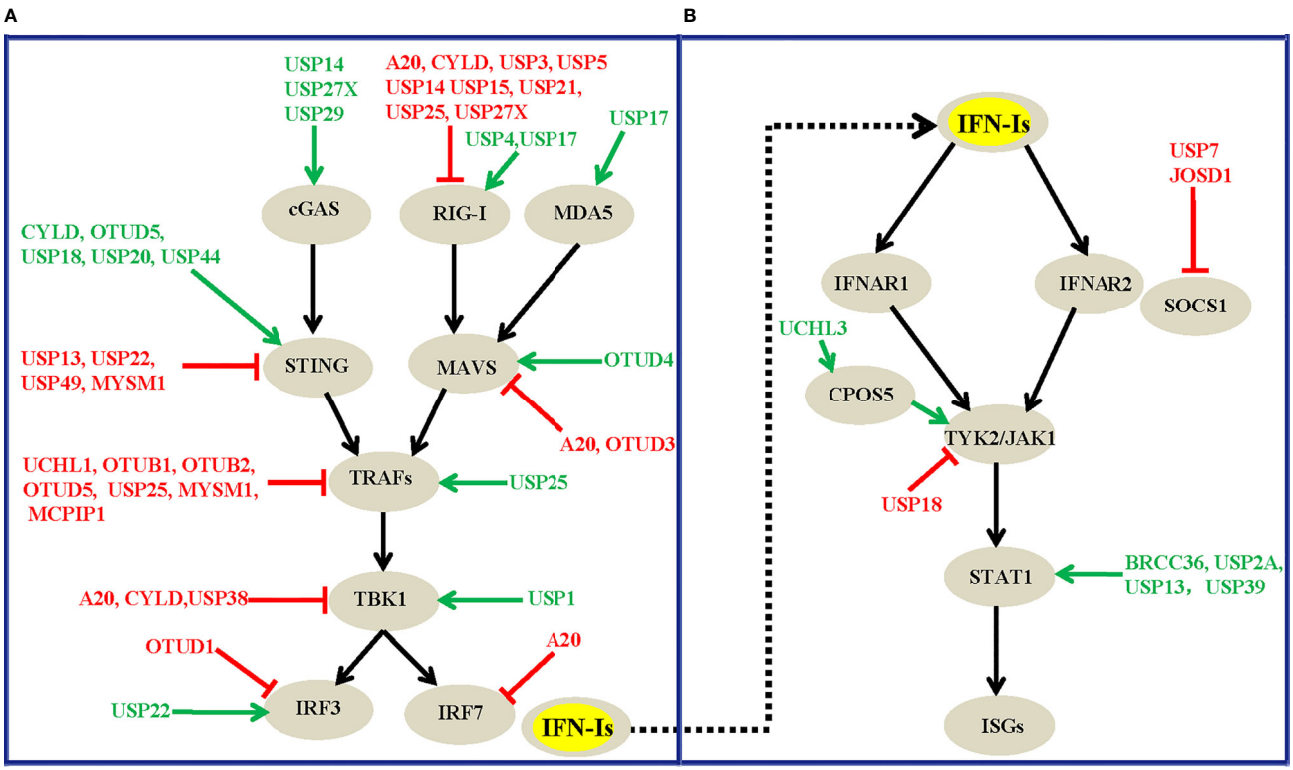

FIGURE 3 | Overview of DUBs that modulate the virus-induced IFN-I production signaling **(A)** and the IFNAR-mediated downstream signaling transduction pathway **(B)**. The green arrows and red lines respectively indicate the positive and negative regulatory roles of each DUB involved.

demonstrated to promote IFN-I production and antiviral responses. In addition, although USP18 cannot deubiquitinate STING itself, it can recruit USP20 to deubiquitinate STING and thereby suppresses virus-induced IFN-I production (91). However, the other four DUBs (USP13, USP22, USP49, and MYSM1) inhibit IFN-I-mediated antiviral activity by deubiquitinating K27- or K63-linked polyubiquitin chains of STING (40, 81, 103, 105). Consistent with this observation, USP13- and USP49-deficient mice are more resistant to lethal herpes simplex virus type 1 (HSV-1) infection than their wild-type (WT) littermates (81, 103). In addition, MYSM1 interacts with STING to cleave STING ubiquitination and attenuate the pathway, and MYSM1-deficient mice exhibit tissue damage and high mortality upon virus infection (105). Moreover, MAVS

activation and aggregation, which is promoted by K63-linked ubiquitination catalyzed by TRIM31 (124), are counteracted by OTUD3 (65). In addition, OTUD3-deficient mice also exhibit decreased morbidity after infection with vesicular stomatitis virus (VSV), which might result from increased production of cytokines and decreased viral replication (65). In addition, both OTUD3 and A20 negatively regulate the IFN-mediated antiviral response by modulating the polyubiquitination level of MAVS (125, 126). However, OTUD4 positively regulates IFN signaling and enhances host antiviral activities by deubiquitinating K48-Ub on MAVS (66).

Among the DUBs that interact with cGAS or MDA5, USP27X (98) and USP29 (99) stabilize cGAS and thus positively regulate IFN production and antiviral activities. The knockout of USP27X in mouse macrophages significantly impairs innate antiviral responses (98), whereas the knockdown or knockout of USP29 severely impairs HSV1- or cytosolic DNA-induced expression of IFN-Is and proinflammatory cytokines (99). In addition, USP17 promotes virus-induced IFN-I production by decreasing the polyubiquitination level of MDA5 (87). Notably, UCHL1, OTUB1, OTUB2, OTUD5, USP25, MYSM1, and MCPIP1 (**Figure 3A**) negatively regulate virus-induced IFN-I production and antiviral activities by cleaving K63-linked or other types of polyubiquitin chains from TRAF3 or TRAF6. Regarding the kinase TBK1, a previous study showed that the T cell anergy–related E3 Ub ligase RNF128 catalyzes the K63-linked polyubiquitination of TBK1, which causes TBK1 and IRF3 activation, and IFN-β production (127). The E3 ligases DTX4, Triad3A, and TRIP have also been identified to conjugate K48-linked polyubiquitin chains on TBK1, which results in TBK1 degradation and subsequent inhibition of IFN-Is (128–130). However, DUBs cleave the polyubiquitin chains of TBK1 to reverse the ubiquitination process mediated by E3 ligases (**Table 1** and **Figure 3**). For example, CYLD removes polyubiquitin chains from TBK1 and RIG-I and thus inhibits the IRF3 signaling pathway and IFN production triggered by RIG-I; conversely, CYLD knockdown enhances this response (58). Similarly, USP38 negatively regulates IFN-I signaling by targeting the active form of TBK1 for degradation *in vitro* and *in vivo* (101). USP19 suppresses virus-induced IFN-I production by targeting TIR domain-containing adaptor inducing interferon-β (TRIF, also known as Ticam1), which is an adaptor required for innate immune responses mediated by TLR3 and TLR4 (90). Together, these results indicate that the crosstalk between IFN-I and the Toll-like signaling pathway functions intricately in regulating host antiviral activities.

Altogether, the diversity of the mechanisms of DUB regulation enables the tight regulation of their function, which ensures an appropriate innate immune response against virus infections. To the best of our knowledge, at least twenty-four DUBs, A20, UCHL1, OTUB1, OTUB2, OTUD1, OTUD3, OTUD5, USP2B, USP3, USP5, USP7, USP13, USP14, USP15, USP18, USP19, USP21, USP22, USP25, USP27X, USP38, USP49, MYSM1, and MCPIP1, have so far been identified to negatively regulate virus-induced IFN-I production and antiviral activity. In contrast, DUBs, including CYLD, OTUD4, OTUD5, USP4, USP15, USP17, USP20, USP27X, USP29, and USP44, have been suggested to positively regulate host antiviral responses by targeting various substrates in this pathway (**Table 1**). These DUBs mainly regulate the polyubiquitination levels of RIG-I, STING, MAVS, TRAFs, and TBK1, which function at different levels of this pathway (**Figure 3A**), and this finding implies the physiological importance of these master proteins in innate immunity during viral infections. Of note, one DUB might target different proteins in the same pathway, whereas the same substrate might also be regulated by more than one DUB, which suggest the existence of dynamic and complex crosstalk between DUBs and substrates involved in IFN-I signaling-mediated antiviral activities. However, why so many DUBs are involved in host immune responses during viral infections remains unclear. One possible reason is that different DUBs may exert differential functions in response to various stimuli, and some of the Dubs might function redundantly in specific contexts. Second, the experimental tools and research biases might also contribute to the diverse roles of DUBs that have been identified. Moreover, some findings are only based on cell lines and overexpression systems and need to be confirmed *in vivo* and with genetic models in the future.

DUBS IN IFNAR-MEDIATED DOWNSTREAM SIGNALING AND THE ANTIVIRAL RESPONSE

In addition to their roles in virus-induced IFN-I production signaling, signaling molecules downstream of the IFN receptor play pivotal roles in affecting host antiviral efficiency. Because increasing the dosage of IFNs alone cannot significantly improve host antiviral efficiency, it has been proven that IFNs can induce ubiquitin-dependent degradation of the IFNAR receptor, which leads to a restriction effect on host antiviral activities (131, 132). Consequently, it is similarly important to investigate the roles of DUBs involved in the IFNAR-mediated downstream signaling pathway. However, compared with the relatively large number of DUBs that regulate virus-induced IFN-I production (**Figure 3A**), the number of DUBs that have been implicated in IFNAR-mediated downstream signaling has rarely been explored (**Figure 3B**). In most cases, the regulatory effects of DUBs are mainly focused on the STAT1 protein, which functions as an essential transcription factor in IFNAR1-mediated downstream signaling. The ubiquitination and deubiquitination regulation events of STAT1 and its associated effects on the innate immune response have been increasingly investigated in recent years. For example, the three deubiquitinating enzymes BRCC36, USP13, and USP39 interact with STAT1 and decrease the K63-, K48- and K6-linked polyubiquitin chains of STAT1 respectively (110, 115, 118). These three DUBs positively regulate IFN-mediated antiviral activities and have been proposed to antagonize the degradation rate of STAT1 mediated by two E3 ligases, SLIM (133) and SMURF1 (134). More specifically, BRCC36 deficiency leads to a rapid downregulation of STAT1 during viral infection, whereas

complementation by BRCC36 can rescue the STAT1 expression levels and suppress virus infection (110). BRCC36 sustains STAT1 protein turnover by recruiting USP13 to form a balanced complex to antagonize the SMURF1-mediated degradation of STAT1 (110). More specifically, USP13 positively regulates the antiviral activity of IFNα against DEN-2 virus replication by deubiquitinating and stabilizing STAT1 (115). Intriguingly, although USP39 was previously shown to not have deubiquitinase activity, recent studies have shown that USP39 combines with STAT1 and stabilizes its expression level by preventing the K6-linked polyubiquitination of STAT1 which promotes its degradation, and USP39 thus positively regulates IFN-I-mediated antiviral activities (118). Notably, IFN treatment could also promote USP2A to interact with pY701-STAT1 and maintain the pY701-STAT1 levels in the nucleus, which enhances IFN signaling-mediated antiviral activity (111). Unlike USP2A, the deubiquitinating enzymes BRCC36, USP13, and USP39 positively regulate IFN activities by attenuating the polyubiquitination level of STAT1, and this process is independent of IFN treatment, which suggests divergent functional roles of these DUBs under differential contexts.

Additionally, ATXN3 does not affect IFN-I production during viral infection but positively regulates IFNAR1-mediated downstream signaling by targeting HDAC3 (108). Another DUB, UCHL3, also positively regulates IFN-I-mediated antiviral activity by increasing the stability of COPS5 and IFNAR1 (121, 122). Moreover, both USP7 and JOSD1 have been identified as negative regulators of IFNAR1-mediated downstream signaling by decreasing the polyubiquitin expression level of SOCS1 and thereby enhancing the turnover of SOCS1, which is a potent suppressor of IFN-I signaling (135). The IFN-inducible deubiquitinase USP18, which functions as one of the most important DUBs in IFN signaling, can downregulate type I IFN signaling by blocking the interaction between JAK1 and IFNAR2 (88, 89, 117). In addition, USP18 has enzymatic activity in cleaving the covalently conjugated 15-kDa protein encoded by interferon-stimulated gene 15 (*ISG15*) from its targeted substrates (136), and USP18 gene-knockout mice exhibit increased susceptibility to *Salmonella typhimurium* or *Mycobacterium tuberculosis* pathogen infections (137). Intriguingly, USP18 also acts as a negative regulator of microglia activation in mice. USP18 deficiency in microglial causes destructive interferonopathy in the mouse brain, suggesting that USP18 plays a protective role in microglia function by regulating the IFNAR pathway (138). Therefore, multiple DUBs are involved in regulating IFNAR-mediated downstream signaling during viral infection. However, whether other DUBs are similarly involved remains unknown, and the connection of DUBs with immune disorders and other related diseases still needs further research.

DUBS REGULATE IFN-I-MEDIATED ANTIVIRAL RESPONSES *VIA* THEIR PROTEASE ACTIVITY

Because DUBs are proteases, it is often speculated that the DUBs functioning in antiviral immunity are dependent on their deubiquitinating enzyme activities. The Ub chains of each substrate involved in IFN-I signaling are cleaved by various DUBs through either endo- or exo cleavage activity. Although the determination of whether a DUB cleaves with endo- or exo-cleavage activity seems difficult, several studies have shown that this activity relies on both the DUB structure and the type of Ub linkage (39). Indeed, the presence of seven internal lysine residues of the Ub (K6, K11, K27, K29, K33, K48, and K63) and the α-amino-terminus of methionine1 (Met1) enable the modification of target proteins with different types of polyubiquitin chains (conjugation of Ub molecules *via* the same lysine residue), heterotypic Ub chains (conjugation through different linkage patterns), branched chains, or monoubiquitination (38). Among the different types of polyubiquitin modifications, the principal and most abundant forms are K48-linked and K63-linked polyubiquitination. However, the outcomes of these different ubiquitination events for the substrate are distinct: K48-linked polyubiquitin chains are the best characterized and trigger substrates for proteasomal degradation more frequently than other modifications (139, 140), whereas K63-linked chains play non degradative roles in cellular signaling, intracellular trafficking, the DNA damage response, and other contexts (141, 142).

The K48- and K63-linked polyubiquitin modifications are also the most common types of PTMs identified in the proteins of the IFN-I signaling pathway (**Table 1**). Although many Ub E3 ligases responsible for the K48-linked ubiquitination of proteins have been identified over the years (22, 24, 143), the corresponding DUBs in antagonizing the degradation and maintaining the protein stability of the key molecules in IFN signaling remain poorly understood (144). An overall view of the DUBs that specifically hydrolyze K48-linked polyubiquitin chains from various substrates during virus infections such as CYLD, OTUD4, OTUD5, USP1, USP4, USP14, USP15, USP20, USP25, USP27X, USP29, and USP44 is summarized in **Table 1**. These DUBs specifically hydrolyze K48-linked polyubiquitin chains from various substrates and thereby stabilize proteins and play positive roles during viral infection. More specifically, among the DUBs, CYLD deficiency promotes K48-linked polyubiquitination and degradation of STING and thereby decreases the induction of IRF3-responsive genes after HSV-1 infection. In accord with this observation, CYLD-knockout mice are more susceptible to HSV-1 infection than their wild-type littermates (59). The deubiquitinase OTUD4 interacts with MAVS to remove its K48-linked polyubiquitin chains and thereby maintains MAVS stability and promotes innate antiviral signaling. Additionally, the knockout of OTUD4 impairs RNA virus-triggered activation of IRF3 and NF-κB and the expression of their downstream target genes, and potentiates VSV replication *in vitro* and *in vivo* (66). Similarly, OTUD5 promotes the protein stability of STING *via* cleaving the K48-linked polyubiquitin chains. The knockout of OTUD5 leads to faster turnover of STING and impairs IFN-I signaling following cytosolic DNA stimulation, whereas Lyz2-Cre Otud5$^{fl/Y}$ mice and CD11-Cre Otud5$^{fl/Y}$ mice show higher susceptibility to HSV-1 infection than their corresponding control littermates (69). Among the USP members, USP1 functions as a viral infection-

induced physiological enhancer of TBK1 expression when bound to USP1 the K48-linked polyubiquitination of TBK1, resulting in enhanced TLR3/4 and RIG-I-induced IRF3 activation and IFNβ secretion (74). USP4, it positively regulates the RIG-I-mediated antiviral response by deubiquitinating K48-linked ubiquitin chains and stabilizing RIG-I (77). Interestingly, USP14, USP27X, and USP29 have been identified to positively regulate virus-induced IFN-I production by targeting the same substrate cGAS, and mechanistically, the three DUBs function by deubiquitinating K48-linked ubiquitin chains and stabilizing cGAS (83, 98, 99). Consistently, mice with the genetic ablation of USP27X and USP29 exhibit decreased levels of IFN-Is and proinflammatory cytokines after HSV-1 infection and hypersensitivity to HSV-1 infection compared with their wild-type littermates (98, 99). In addition, although both USP20 and USP44 have been shown to positively regulate virus-induced IFN-I signaling by targeting the same substrate, STING, and removing its K48-linked polyubiquitin chains, these two DUBs function differently (**Table 1**). Mechanistically, USP20 is recruited by USP18 to deconjugate K48-linked ubiquitination chains from STING and thus promotes the stability of STING and the expression of type I IFNs and proinflammatory cytokines after DNA virus infection (91). A later study, further confirmed that USP20 removes K48-linked ubiquitin chains from STING after HSV-1 infection and thereby stabilizes STING and promotes cellular antiviral responses (92). Congruently, USP20 knockout mice exhibit decreased levels of IFN-Is and proinflammatory cytokines, increased susceptibility to lethal HSV-1 infection, and aggravated HSV-1 replication compared with wild-type mice (92). The complementation of STING into Usp20 (-/-) cells remarkably restores HSV-1-triggered signaling and inhibits HSV-1 infection (92). In addition, the ectopic expression of USP15 enhances the TRIM25- and RIG-I-mediated production of type I IFN and thus suppresses RNA virus replication, whereas the depletion of USP15 causes decreased IFN production and markedly enhanced viral replication (85). Moreover, the DUB activity of USP25 is needed for virus-induced production of IFN-I and proinflammatory cytokines, because USP25 can stabilize TRAF3 by deubiquitinating K48-Ub on TRAF3 whereas the complemention of TRAF3/6 into USP25-deficient MEFs restores virus-induced signaling (96). Consistently, USP25-deficient mice are susceptible to H5N1 or HSV-1 infection than their wild-type counterparts (96).

Notably, although DUBs including OTUD1, USP5, and USP7 function to cleave K48-linked polyubiquitin chains of various substrates, the three DUBs exert opposite effects, which play negative roles in the host immune response against virus infection (**Table 1**). For example, OTUD1 upregulates the protein levels of intracellular Smurf1 by removing the K48-linked polyubiquitin chains of Smurf1, and RNA virus infection promotes the binding of Smurf1 to MAVS, TRAF3, and TRAF6, which leads to ubiquitination-dependent degradation of the three proteins and subsequent potent inhibition of IFNs production (64). In agreement with this observation, OTUD1-deficient mice produce more antiviral cytokines and are more resistant to RNA virus infection (64). In addition, a recent systematic functional screening assay revealed that USP5 inhibits IFNβ expression and promotes VSV replication by recruiting STIP1 homology and U-box containing protein 1 (STUB1) to degrade RIG-I (40). Whereas USP7 acts as a negative regulator in antiviral signaling by stabilizing TRIM27 and promoting the degradation of TBK1, the knockout of endogenous USP7 leads to enhanced TRIM27 degradation and reduced TBK1 ubiquitination and degradation (79). In the case of IFNAR-mediated downstream signaling pathway, USP2A sustains interferon antiviral activity by restricting the K48-linked ubiquitination of p-STAT1 in the nucleus (111). *Via* using RNA interference screening strategy, USP13 was found to positively regulate IFN-I signaling by deubiquitinating the K48-linked polyubiquitin chains the of STAT1 protein (115). Congruently, STAT1 ubiquitination is reduced in cells by USP13 overexpression and increased with USP13 knockdown regardless of IFNα treatment (115). JOSD1 has been identified to negatively regulate IFN-I-induced signaling and the antiviral response by deubiquitinating the K48-linked polyubiquitination of SOCS1, which is an essential negative regulator of many cytokine signaling pathways (120).

K63-linked polyubiquitin modification, it has also been identified as fundamental for both the innate and adaptive immune systems. K63-linked polyubiquitin is not only needed for the virus-induced activation of TBK1 and IRF3 (145) but also widely involved in pathways including NF-κB signaling and MAPK activation (146, 147). In NF-κB pathways, K63-linked polyubiquitin chains play pivotal roles in stabilizing the receptor signalosome on the membrane and hence facilitate the recruitment of adaptors or complexes and activating kinases (148). Critically, many E3 ligases, including TRAF6, are implicated in NF-κB pathways by catalyzing K63-linked polyubiquitination of various proteins (146). Whereas DUBs play an opposite role to E3 ligases, and various DUBs, including A20, CYLD, UCHL1, OTUD4, OTUD5, OTUD7B, USP18, USP25, and MYSM1, have been found to remove K63-linked polyubiquitin chains from various substrates (TBK1, TAK1, MyD88, TRAF3, and TRAF6) (**Table 1**). Intriguingly, unlike the aforementioned DUBs, A20 is a hybrid of a DUB and a E3 ligase and has an N-terminal OTU domain responsible for polyubiquitin cleavage and C-terminal domain-containing zinc fingers that bear E3 ligase activity. A20 cleaves the K63-linked polyubiquitin chains of TRAF6, RIP1, RIPK2, IKK-γ, and MALT1 and hence suppresses NF-κB activation. Moreover, A20 has been shown to promote the K48-linked ubiquitination of RIP1, which leads to its degradation and thereby the downregulation of NF-κB signaling (146, 149). Critically, K63-linked ubiquitination also plays a pivotal role in affecting virus-induced IFN-I production by either stabilizing substrates or by acting as a scaffold for the formation of a signaling multi complex (150). To date, a panel of 15 DUBs, such as CYLD, UCHL1, OTUD1, OTUD3, OTUD4, OTUD5, USP2B, USP3, USP14, USP15, USP21, USP25, USP27X, USP49, and MYSM1, have been identified to cleave the K63-linked polyubiquitin chains on various proteins, which results in a positive or negative effect on virus-induced IFN-I production under different contexts (**Table 1**). For example, OTUD3 removes K63-linked ubiquitin chains from MAVS and thereby inhibits MAVS aggregation and IFN-I signaling activation (65). In addition, unanchored K63

polyubiquitin chains can bind to MDA5, and this binding is important for signaling by MDA5, mutations of conserved residues in MDA5 disrupt its ubiquitin binding, and abrogate its ability to activate IRF3 (151). In the case of IFNAR1-mediated downstream signaling, BRCC36 sustains the protein turnover of IFNAR1 by removing K63-Ub from IFNAR1 (109), whereas USP5 has been identified to negatively regulate IFN-I-induced p-STAT1 activation and antiviral activities by removing K63-Ub on SMURF1 (112).

Additionally, some DUBs possess broad DUB activity against several types of Ub linkages. The DUBs OTUD7B, USP17, USP25, MCPIP1, ATXN3, and UCHL3 could simultaneously deconjugate the K48- and K63-linked Ub chains from the same protein in the IFN-I signaling pathway (**Table 1**). For instance, ATXN3 sustains IFNAR1-mediated downstream signaling by deubiquitinating both the K48- and K63-linked types of Ub chains on HDAC3 (108). However, USP13, USP19, and USP22 inhibit virus-induced IFN production by removing K27-linked polyubiquitin chains from STING (40, 81) or TRIF (90). In contrast, USP38 combines with the active form of TBK1 *via* the NLR family pyrin domain containing 4 (NLRP4) signalosome and then cleaves K33-linked Ub chains from TBK1 at Lys670, which allows DTX4 and TRIP to catalyze K48-linked ubiquitination on the same residue (101). This process causes the degradation of TBK1, thus negatively regulates IFN-I signaling. Intriguingly, USP39 promotes IFN-mediated antiviral responses by decreasing K6-linked but not canonical K48-linked polyubiquitination of STAT1 for degradation (118), eventhough K6-linked ubiquitin chains are often related to DNA damage instead of protein degradation (142). Morever, although USP5 reportedly increases K11- and K48-linked ubiquitination of RIG-I upon virus infection and thereby facilitates the degradation of RIG-I (40), the detailed mechanism used by USP5 to enhance K11-linked Ub chains of RIG-I and the exact functions of K11-linked Ub chains implicated in the RIG-I-mediated signaling pathway remain elusive. Overall, the atypical K6-, K11-, K27-, K33- and linear-linked polyubiquitin chains of proteins also play critical roles in antiviral immunity and inflammation (152). However, little is known about K29-linked polyubiquitination, and whether this type of PTM occurs on substrates involved in IFN-I signaling remains unknown and warrants further research.

DUBS REGULATE HOST ANTIVIRAL ACTIVITY INDEPENDENTLY OF THEIR PROTEASE ACTIVITY

Although many studies have demonstrated that the protease activity of DUBs is critical in regulating the Ub chains on their substrates and affecting host IFN immune responses, some studies have also shown that the catalytic activity of certain DUBs is not necessary in regulating the IFN-I signaling pathway, which implies novel strategies used by DUBs. Mechanistically, the catalytically inactive mutant sites of DUBs could not abolish their negative or positive roles during virus infection, which indicates that these DUBs function independently of their protease activity. For instance, both the wild-type and enzymatically inactive mutant of USP5 can cause a decreased polyubiquitination level of SMURF1 (112), which suggest that USP5 functions in the immune response probably independently of its protease activity. In addition, some DUBs form complexes with adaptor or scaffold proteins, which act by recruiting proteins to participate in particular biological events, attracting trafficking factors that change substrate localization, or controlling substrate activity. For instance, DUBs can regulate a specific substrate by recruiting other factors, as demonstrated by USP10 recruits and binds with monocyte chemotactic protein induced protein 1 (MCPIP1) to deubiquitinate its substrate, nuclear factor κB essential modulator (NEMO) (153). Additionally, it has been shown that A20 blocks antiviral signaling by disrupting K63-linked polyubiquitination of TBK1-IKK complex independtly of the A20 deubiquitination domain (154). Futhermore, A20 prevents the interaction between Ubc13 and both TRAF2/5 and cIAP1/2 upon TNFα stimulation, which suggest A20 functions beyond its protease activity (155). In addition, A20 suppresses TNFα-induced NF-κB signaling through a noncatalytic mechanism that involves binding to polyubiquitin chains *via* its seventh zinc finger (ZnF7) (56, 156, 157). This binding is proposed to impede the recruitment of other linear polyubiquitin binding proteins that are essential for productive signaling downstream from TNFR (157). Moreover, USP5 suppresses IFN-β expression and enhances VSV replication by recruiting STUB1 to degrade RIG-I (40). USP13, which shares ~80% sequence similarity with USP5, negatively regulates virus-induced IFN-I production by inhibiting the recruitment of TBK1 to STING by deubiquitinating the K27-linked ubiquitin chains on STING (81), whereas USP22 recruits USP13 to cleave the K27-linked polyubiquitin chains from STING (40). USP18 does not deubiquitinate STING *in vitro* but facilitates USP20 to catalyze deubiquitination of STING in a manner independently of the enzymatic activity of USP18 (91). In addition, USP18-knockout mice are more susceptible to HSV-1 infection than their wild-type littermates, and the reintroduction of STING into USP18$^{-/-}$ MEFs can restore the HSV-1-induced expression of downstream genes and cellular antiviral responses (91). In addition to being an active enzyme, USP18 can bind to the intracellular part of IFNAR2 and compete with the binding of JAK1 to the receptor, which results in negative regulation of IFNAR signaling independently of its protease activity (117). In the case of IFNAR-mediated downstream signaling, some other DUBs also implement their functions beyond their protease activities. For example, BRCC36 functions noncatalytically by recruiting USP13 to counteract the SMURF1-mediated degradation of STAT1, and this effect enhances the stability of STAT1 and improves host antiviral efficiency (110). Additionally, USP12 positively regulates IFN antiviral signaling independently of its deubiquitinase activity. Upon IFN treatment, USP12 accumulates in the nucleus, blocks the CREB-binding protein-induced acetylation of p-STAT1, and thus inhibits the dephosphorylation effects of TCPTP on p-STAT1, which ultimately maintains the nuclear p-STAT1 levels and IFN antiviral efficacy (114).

DUB INHIBITORS AND THEIR POTENTIAL ROLES IN THERAPEUTIC PURPOSES

Because DUBs play critical roles during innate antiviral responses, the development of small-molecule inhibitors that

specifically change DUB activities might be a therapeutic strategy for improving host antiviral efficiency. Over the years, inhibitors of a panel of DUBs, including USP1, USP2, USP4, USP5, USP7, USP8, USP9X, USP10, USP11, USP13, USP14, USP19, USP20, USP25/28, USP30, COPS5, STAMBP, PSMD14, UCHL1, UCHL3 and UCHL5, have been designed (158–163). However, to date, only a few small-molecule inhibitors of DUBs have been employed to investigate their functional roles in host antiviral activities. For instance, the USP7 inhibitors P5091 and P22077 have been verified to promote the type-I interferon-mediated antiviral response by destabilizing SOCS1 (113). Similarly, the USP5 inhibitor PYR41 could reduce virus replication at the mRNA and protein levels by promoting IFNAR-mediated antiviral responses (112).

Because ubiquitination and related processes are involved in myriad aspects of human cell biology and physiology, abnormalities in such events can cause many diseases. Among these events, the dysregulation of DUB activity contributes to various sporadic and genetic diseases (158, 164, 165). For instance, human USP18 deficiency underlies type 1 interferonopathy, leading to severe pseudo-TORCH syndrome which is characterized by microcephaly, enlarged ventricles, cerebral calcification, and other severe complications (166). Similarly, the homozygous mutation of USP18 also causes severe type I interferonopathy because the mutated USP18 protein results in unmitigated interferon-mediated inflammation and is lethal during the perinatal period (167). However, the treatment of these patients with ruxolitinib, a JAK 1/2 inhibitor, it significantly improves their symptoms (167). Additionally, a homozygous miss-sense mutation in STAT2 results in failure to appropriately traffic USP18 to IFNAR2 and prevents USP18 from negatively regulating responses to IFN-Is, which leads to infant death from autoinflammation disease (168). Notably, given that the current therapeutics remains incapable of achieving satisfying disease management in all patients, the therapeutic modulation of DUBs might be an attractive target in certain diseases. As has been demonstrated, although some inhibitors can treat cancer disease efficiently (169), the use of these inhibitors in the treatment of viral infectious diseases remains largely unexplored. Because DUB inhibition could promote steady-state Ub levels of specific substrates without affecting global protein or Ub levels, the development of small-molecule inhibitors targeted towards DUBs has increasingly become a promising strategy for drug discovery (170). However, because many DUBs are conserved during evolution and have a high sequence similarity, new perspectives are needed to facilitate the development of specific inhibitors. Consequently, the design of small-molecule inhibitors that interfere with the activity of DUBs or the DUB-substrate interactions accompanied by their relevance *in vivo* and related diseases remains one of the critical and challenging research areas.

CONCLUSIONS AND PERSPECTIVES

In summary, DUB-mediated regulation represents a crucial mechanism used by hosts to tightly regulate the extent of IFN signaling to achieve a balance between pathogen eradication and the prevention of excessive immune responses. However, how DUBs implement their diverse functions and interact with substrates in a dynamic, temporal, and spatial manner to ensure the most favourable outcome remains elusive. Intriguingly, some viruses also encode DUBs and other proteins that either act alone or interact with other cellular components to evade host immune surveillance (171, 172). Thus, the interplay between DUBs and pathogens might add a new sophisticated mchanism that regulates the timing and amplitude of host immune responses to viral challenges. In addition, how PTMs (such as phosphorylation, acetylation, and methylation) of DUBs and, Ub and other unconventional Ub structures modulate the functional shift of DUBs and thus affect host innate immune signaling, is still poorly understood. Future studies exploring the detailed mechanisms of DUBs, their inducers, and downstream targets during viral infections might help improve the present understanding of the mechanisms of host innate immune responses, and these findings could lead to the identification of novel targets and help guide the development of therapeutic strategies for the treatment of human diseases.

AUTHOR CONTRIBUTIONS

The table and graphs were prepared by LZ. The literature was collected and analyzed by GL and YL. JP and ZZ provided insightful comments and suggestions on the manuscript. GQ and HL wrote the paper and critically revised the draft. All authors contributed to the article and approved the submitted version.

FUNDING

Work in our laboratory is supported by grants from the National Natural Science Foundation of China (No. 31800982, No. 81971477, No. 82171797, No. 81870365, No. 82070512, No. 81702737, No. 81803116 and No. 81902534), Jiangsu Provincial Medical Young Talents (QNRC2016756), the Applied Foundational Research of Medical and Health Care of Suzhou City (SYS2019086, SYS2019083), and Gusu Health Talent Program (GSWS2020038).

ACKNOWLEDGMENTS

We thank the editor and anonymous reviewers for their constructive comments and suggestions on the article. We also apologize to colleagues in the field whose work could not be cited owing to space limitations.

REFERENCES

1. Hadjadj J, Yatim N, Barnabei L, Corneau A, Boussier J, Smith N, et al. Impaired Type I Interferon Activity and Inflammatory Responses in Severe COVID-19 Patients. *Science* (2020) 369(6504):718–24. doi: 10.1126/science.abc6027
2. Brubaker SW, Bonham KS, Zanoni I, Kagan JC. Innate Immune Pattern Recognition: A Cell Biological Perspective. *Annu Rev Immunol* (2015) 33:257–90. doi: 10.1146/annurev-immunol-032414-112240
3. Carty M, Guy C, Bowie AG. Detection of Viral Infections by Innate Immunity. *Biochem Pharmacol* (2021) 183:114316. doi: 10.1016/j.bcp.2020.114316

4. Wu J, Chen ZJ. Innate Immune Sensing and Signaling of Cytosolic Nucleic Acids. *Annu Rev Immunol* (2014) 32:461–88. doi: 10.1146/annurev-immunol-032713-120156
5. Heaton SM, Borg NA, Dixit VM. Ubiquitin in the Activation and Attenuation of Innate Antiviral Immunity. *J Exp Med* (2016) 213(1):1–13. doi: 10.1084/jem.20151531
6. Barrat FJ, Elkon KB, Fitzgerald KA. Importance of Nucleic Acid Recognition in Inflammation and Autoimmunity. *Annu Rev Med* (2016) 67:323–36. doi: 10.1146/annurev-med-052814-023338
7. Takeuchi O, Akira S. Pattern Recognition Receptors and Inflammation. *Cell* (2010) 140(6):805–20. doi: 10.1016/j.cell.2010.01.022
8. Honda K, Ohba Y, Yanai H, Negishi H, Mizutani T, Takaoka A, et al. Spatiotemporal Regulation of MyD88-IRF-7 Signalling for Robust Type-I Interferon Induction. *Nature* (2005) 434(7036):1035–40. doi: 10.1038/nature03547
9. Wang L, Zhao J, Ren J, Hall KH, Moorman JP, Yao ZQ, et al. Protein Phosphatase 1 Abrogates IRF7-Mediated Type I IFN Response in Antiviral Immunity. *Eur J Immunol* (2016) 46(10):2409–19. doi: 10.1002/eji.201646491
10. Hartmann G. Nucleic Acid Immunity. *Adv Immunol* (2017) 133:121–69. doi: 10.1016/bs.ai.2016.11.001
11. Rehwinkel J, Gack MU. RIG-I-Like Receptors: Their Regulation and Roles in RNA Sensing. *Nat Rev Immunol* (2020) 20(9):537–51. doi: 10.1038/s41577-020-0288-3
12. Kopitar-Jerala N. The Role of Interferons in Inflammation and Inflammasome Activation. *Front Immunol* (2017) 8:873. doi: 10.3389/fimmu.2017.00873
13. Fuchs SY. Ubiquitination-Mediated Regulation of Interferon Responses. *Growth Factors* (2012) 30(3):141–8. doi: 10.3109/08977194.2012.669382
14. Borden EC, Sen GC, Uze G, Silverman RH, Ransohoff RM, Foster GR, et al. Interferons at Age 50: Past, Current and Future Impact on Biomedicine. *Nat Rev Drug Discovery* (2007) 6(12):975–90. doi: 10.1038/nrd2422
15. Pestka S, Krause CD, Walter MR. Interferons, Interferon-Like Cytokines, and Their Receptors. *Immunol Rev* (2004) 202:8–32. doi: 10.1111/j.0105-2896.2004.00204.x
16. Crow MK, Olferiev M, Kirou KA. Type I Interferons in Autoimmune Disease. *Annu Rev Pathol* (2019) 14:369–93. doi: 10.1146/annurev-pathol-020117-043952
17. McNab F, Mayer-Barber K, Sher A, Wack A, O'Garra A. Type I Interferons in Infectious Disease. *Nat Rev Immunol* (2015) 15(2):87–103. doi: 10.1038/nri3787
18. Chen X, Saccon E, Appelberg KS, Mikaeloff F, Rodriguez JE, Vinhas BS, et al. Type-I Interferon Signatures in SARS-CoV-2 Infected Huh7 Cells. *Cell Death Discov* (2021) 7(1):114. doi: 10.1038/s41420-021-00487-z
19. Cheng Z, Dai T, He X, Zhang Z, Xie F, Wang S, et al. The Interactions Between cGAS-STING Pathway and Pathogens. *Signal Transduct Target Ther* (2020) 5(1):91. doi: 10.1038/s41392-020-0198-7
20. Honda K, Takaoka A, Taniguchi T. Type I Interferon [Corrected] Gene Induction by the Interferon Regulatory Factor Family of Transcription Factors. *Immunity* (2006) 25(3):349–60. doi: 10.1016/j.immuni.2006.08.009
21. Sadler AJ, Williams BR. Interferon-Inducible Antiviral Effectors. *Nat Rev Immunol* (2008) 8(7):559–68. doi: 10.1038/nri2314
22. Liu J, Qian C, Cao X. Post-Translational Modification Control of Innate Immunity. *Immunity* (2016) 45(1):15–30. doi: 10.1016/j.immuni.2016.06.020
23. Zhou Y, He C, Wang L, Ge B. Post-Translational Regulation of Antiviral Innate Signaling. *Eur J Immunol* (2017) 47(9):1414–26. doi: 10.1002/eji.201746959
24. Davis ME, Gack MU. Ubiquitination in the Antiviral Immune Response. *Virology* (2015) 479-480:52–65. doi: 10.1016/j.virol.2015.02.033
25. Ciehanover A, Hod Y. Hershko A. A Heat-Stable Polypeptide Component of an ATP-Dependent Proteolytic System From Reticulocytes. *Biochem Biophys Res Commun* (1978) 81(4):1100–5. doi: 10.1016/0006-291x(78)91249-4
26. Hershko A, Ciechanover A. The Ubiquitin System. *Annu Rev Biochem* (1998) 67:425–79. doi: 10.1146/annurev.biochem.67.1.425
27. Komander D, Rape M. The Ubiquitin Code. *Annu Rev Biochem* (2012) 81:203–29. doi: 10.1146/annurev-biochem-060310-170328
28. Ohtake F, Tsuchiya H. The Emerging Complexity of Ubiquitin Architecture. *J Biochem* (2017) 161(2):125–33. doi: 10.1093/jb/mvw088
29. Yau R, Rape M. The Increasing Complexity of the Ubiquitin Code. *Nat Cell Biol* (2016) 18(6):579–86. doi: 10.1038/ncb3358
30. Kirisako T, Kamei K, Murata S, Kato M, Fukumoto H, Kanie M, et al. A Ubiquitin Ligase Complex Assembles Linear Polyubiquitin Chains. *EMBO J* (2006) 25(20):4877–87. doi: 10.1038/sj.emboj.7601360
31. Haakonsen DL, Rape M. Branching Out: Improved Signaling by Heterotypic Ubiquitin Chains. *Trends Cell Biol* (2019) 29(9):704–16. doi: 10.1016/j.tcb.2019.06.003
32. Coleman KE, Huang TT. In a Class of Its Own: A New Family of Deubiquitinases Promotes Genome Stability. *Mol Cell* (2018) 70(1):1–3. doi: 10.1016/j.molcel.2018.03.022
33. Matsushita K, Takeuchi O, Standley DM, Kumagai Y, Kawagoe T, Miyake T, et al. Zc3h12a Is an RNase Essential for Controlling Immune Responses by Regulating mRNA Decay. *Nature* (2009) 458(7242):1185–90. doi: 10.1038/nature07924
34. Xie X, Wang X, Jiang D, Wang J, Fei R, Cong X, et al. PPPDE1 is a Novel Deubiquitinase Belonging to a Cysteine Isopeptidase Family. *Biochem Biophys Res Commun* (2017) 488(2):291–6. doi: 10.1016/j.bbrc.2017.04.161
35. Kwasna D, Abdul Rehman SA, Natarajan J, Matthews S, Madden R, De Cesare V, et al. Discovery and Characterization of ZUFSP/ZUP1, a Distinct Deubiquitinase Class Important for Genome Stability. *Mol Cell* (2018) 70(1):150–64 e6. doi: 10.1016/j.molcel.2018.02.023
36. Abdul Rehman SA, Kristariyanto YA, Choi SY, Nkosi PJ, Weidlich S, Labib K, et al. MINDY-1 Is a Member of an Evolutionarily Conserved and Structurally Distinct New Family of Deubiquitinating Enzymes. *Mol Cell* (2016) 63(1):146–55. doi: 10.1016/j.molcel.2016.05.009
37. Nijman SM, Luna-Vargas MP, Velds A, Brummelkamp TR, Dirac AM, Sixma TK, et al. A Genomic and Functional Inventory of Deubiquitinating Enzymes. *Cell* (2005) 123(5):773–86. doi: 10.1016/j.cell.2005.11.007
38. Reyes-Turcu FE, Wilkinson KD. Polyubiquitin Binding and Disassembly by Deubiquitinating Enzymes. *Chem Rev* (2009) 109(4):1495–508. doi: 10.1021/cr800470j
39. Mevissen TET, Komander D. Mechanisms of Deubiquitinase Specificity and Regulation. *Annu Rev Biochem* (2017) 86:159–92. doi: 10.1146/annurev-biochem-061516-044916
40. Liu Q, Wu Y, Qin Y, Hu J, Xie W, Qin FX-F, et al. Broad and Diverse Mechanisms Used by Deubiquitinase Family Members in Regulating the Type I Interferon Signaling Pathway During Antiviral Responses. *Sci Adv* (2018) 4(5):eaar2824. doi: 10.1126/sciadv.aar2824
41. Bhoj VG, Chen ZJ. Ubiquitylation in Innate and Adaptive Immunity. *Nature* (2009) 458(7237):430–7. doi: 10.1038/nature07959
42. Kowalinski E, Lunardi T, McCarthy AA, Louber J, Brunel J, Grigorov B, et al. Structural Basis for the Activation of Innate Immune Pattern-Recognition Receptor RIG-I by Viral RNA. *Cell* (2011) 147(2):423–35. doi: 10.1016/j.cell.2011.09.039
43. Kato H, Sato S, Yoneyama M, Yamamoto M, Uematsu S, Matsui K, et al. Cell Type-Specific Involvement of RIG-I in Antiviral Response. *Immunity* (2005) 23(1):19–28. doi: 10.1016/j.immuni.2005.04.010
44. Kato H, Takeuchi O, Sato S, Yoneyama M, Yamamoto M, Matsui K, et al. Differential Roles of MDA5 and RIG-I Helicases in the Recognition of RNA Viruses. *Nature* (2006) 441(7089):101–5. doi: 10.1038/nature04734
45. Gack MU, Shin YC, Joo CH, Urano T, Liang C, Sun L, et al. TRIM25 RING-Finger E3 Ubiquitin Ligase Is Essential for RIG-I-Mediated Antiviral Activity. *Nature* (2007) 446(7138):916–20. doi: 10.1038/nature05732
46. Oshiumi H, Matsumoto M, Hatakeyama S, Seya T. Riplet/RNF135, a RING Finger Protein, Ubiquitinates RIG-I to Promote Interferon-Beta Induction During the Early Phase of Viral Infection. *J Biol Chem* (2009) 284(2):807–17. doi: 10.1074/jbc.M804259200
47. Arimoto K, Takahashi H, Hishiki T, Konishi H, Fujita T, Shimotohno K. Negative Regulation of the RIG-I Signaling by the Ubiquitin Ligase RNF125. *Proc Natl Acad Sci USA* (2007) 104(18):7500–5. doi: 10.1073/pnas.0611551104
48. Wang W, Jiang M, Liu S, Zhang S, Liu W, Ma Y, et al. RNF122 Suppresses Antiviral Type I Interferon Production by Targeting RIG-I CARDs to Mediate RIG-I Degradation. *Proc Natl Acad Sci USA* (2016) 113(34):9581–6. doi: 10.1073/pnas.1604277113
49. Zhao C, Jia M, Song H, Yu Z, Wang W, Li Q, et al. The E3 Ubiquitin Ligase TRIM40 Attenuates Antiviral Immune Responses by Targeting MDA5 and RIG-I. *Cell Rep* (2017) 21(6):1613–23. doi: 10.1016/j.celrep.2017.10.020
50. Zhou P, Ding X, Wan X, Liu L, Yuan X, Zhang W, et al. MLL5 Suppresses Antiviral Innate Immune Response by Facilitating STUB1-Mediated RIG-I Degradation. *Nat Commun* (2018) 9(1):1243. doi: 10.1038/s41467-018-03563-8

51. Chen W, Han C, Xie B, Hu X, Yu Q, Shi L, et al. Induction of Siglec-G by RNA Viruses Inhibits the Innate Immune Response by Promoting RIG-I Degradation. *Cell* (2013) 152(3):467–78. doi: 10.1016/j.cell.2013.01.011
52. Okamoto M, Kouwaki T, Fukushima Y, Oshiumi H. Regulation of RIG-I Activation by K63-Linked Polyubiquitination. *Front Immunol* (2017) 8:1942. doi: 10.3389/fimmu.2017.01942
53. Lin R, Yang L, Nakhaei P, Sun Q, Sharif-Askari E, Julkunen I, et al. Negative Regulation of the Retinoic Acid-Inducible Gene I-Induced Antiviral State by the Ubiquitin-Editing Protein A20. *J Biol Chem* (2006) 281(4):2095–103. doi: 10.1074/jbc.M510326200
54. Ning S, Pagano JS. The A20 Deubiquitinase Activity Negatively Regulates LMP1 Activation of IRF7. *J Virol* (2010) 84(12):6130–8. doi: 10.1128/JVI.00364-10
55. Boone DL, Turer EE, Lee EG, Ahmad RC, Wheeler MT, Tsui C, et al. The Ubiquitin-Modifying Enzyme A20 Is Required for Termination of Toll-Like Receptor Responses. *Nat Immunol* (2004) 5(10):1052–60. doi: 10.1038/ni1110
56. Skaug B, Chen J, Du F, He J, Ma A, Chen ZJ. Direct, Noncatalytic Mechanism of IKK Inhibition by A20. *Mol Cell* (2011) 44(4):559–71. doi: 10.1016/j.molcel.2011.09.015
57. Zhang J, Stirling B, Temmerman ST, Ma CA, Fuss IJ, Derry JM, et al. Impaired Regulation of NF-kappaB and Increased Susceptibility to Colitis-Associated Tumorigenesis in CYLD-Deficient Mice. *J Clin Invest* (2006) 116 (11):3042–9. doi: 10.1172/JCI28746
58. Friedman CS, O'Donnell MA, Legarda-Addison D, Ng A, Cardenas WB, Yount JS, et al. The Tumour Suppressor CYLD Is a Negative Regulator of RIG-I-Mediated Antiviral Response. *EMBO Rep* (2008) 9(9):930–6. doi: 10.1038/embor.2008.136
59. Zhang L, Wei N, Cui Y, Hong Z, Liu X, Wang Q, et al. The Deubiquitinase CYLD Is a Specific Checkpoint of the STING Antiviral Signaling Pathway. *PloS Pathog* (2018) 14(11):e1007435. doi: 10.1371/journal.ppat.1007435
60. Karim R, Tummers B, Meyers C, Biryukov JL, Alam S, Backendorf C, et al. Human Papillomavirus (HPV) Upregulates the Cellular Deubiquitinase UCHL1 to Suppress the Keratinocyte's Innate Immune Response. *PloS Pathog* (2013) 9(5):e1003384. doi: 10.1371/journal.ppat.1003384
61. Li S, Zheng H, Mao AP, Zhong B, Li Y, Liu Y, et al. Regulation of Virus-Triggered Signaling by OTUB1- and OTUB2-Mediated Deubiquitination of TRAF3 and TRAF6. *J Biol Chem* (2010) 285(7):4291–7. doi: 10.1074/jbc.M109.074971
62. Lu D, Song J, Sun Y, Qi F, Liu L, Jin Y, et al. Mutations of Deubiquitinase OTUD1 Are Associated With Autoimmune Disorders. *J Autoimmun* (2018) 94:156–65. doi: 10.1016/j.jaut.2018.07.019
63. Zhang Z, Wang D, Wang P, Zhao Y, You F. OTUD1 Negatively Regulates Type I IFN Induction by Disrupting Noncanonical Ubiquitination of IRF3. *J Immunol* (2020) 204(7):1904–18. doi: 10.4049/jimmunol.1900305
64. Zhang L, Liu J, Qian L, Feng Q, Wang X, Yuan Y, et al. Induction of OTUD1 by RNA Viruses Potently Inhibits Innate Immune Responses by Promoting Degradation of the MAVS/TRAF3/TRAF6 Signalosome. *PloS Pathog* (2018) 14(5):e1007067. doi: 10.1371/journal.ppat.1007067
65. Zhang Z, Fang X, Wu X, Ling L, Chu F, Li J, et al. Acetylation-Dependent Deubiquitinase OTUD3 Controls MAVS Activation in Innate Antiviral Immunity. *Mol Cell* (2020) 79(2):304–19.e7. doi: 10.1016/j.molcel.2020.06.020
66. Liuyu T, Yu K, Ye L, Zhang Z, Zhang M, Ren Y, et al. Induction of OTUD4 by Viral Infection Promotes Antiviral Responses Through Deubiquitinating and Stabilizing MAVS. *Cell Res* (2019) 29(1):67–79. doi: 10.1038/s41422-018-0107-6
67. Zhao Y, Mudge MC, Soll JM, Rodrigues RB, Byrum AK, Schwarzkopf EA, et al. OTUD4 Is a Phospho-Activated K63 Deubiquitinase That Regulates MyD88-Dependent Signaling. *Mol Cell* (2018) 69(3):505–16.e5. doi: 10.1016/j.molcel.2018.01.009
68. Kayagaki N, Phung Q, Chan S, Chaudhari R, Quan C, O'Rourke KM, et al. DUBA: A Deubiquitinase That Regulates Type I Interferon Production. *Science* (2007) 318(5856):1628–32. doi: 10.1126/science.1145918
69. Guo Y, Jiang F, Kong L, Wu H, Zhang H, Chen X, et al. OTUD5 Promotes Innate Antiviral and Antitumor Immunity Through Deubiquitinating and Stabilizing STING. *Cell Mol Immunol* (2020) 18(8):1945–55. doi: 10.1038/s41423-020-00531-5
70. Enesa K, Zakkar M, Chaudhury H, Luong le A, Rawlinson L, Mason JC, et al. NF-kappaB Suppression by the Deubiquitinating Enzyme Cezanne: A Novel Negative Feedback Loop in Pro-Inflammatory Signaling. *J Biol Chem* (2008) 283(11):7036–45. doi: 10.1074/jbc.M708690200
71. Ji Y, Cao L, Zeng L, Zhang Z, Xiao Q, Guan P, et al. The N-Terminal Ubiquitin-Associated Domain of Cezanne Is Crucial for Its Function to Suppress NF-kappaB Pathway. *J Cell Biochem* (2018) 119(2):1979–91. doi: 10.1002/jcb.26359
72. Hu H, Brittain GC, Chang JH, Puebla-Osorio N, Jin J, Zal A, et al. OTUD7B Controls Non-Canonical NF-kappaB Activation Through Deubiquitination of TRAF3. *Nature* (2013) 494(7437):371–4. doi: 10.1038/nature11831
73. Luong le A, Fragiadaki M, Smith J, Boyle J, Lutz J, Dean JL, et al. Cezanne Regulates Inflammatory Responses to Hypoxia in Endothelial Cells by Targeting TRAF6 for Deubiquitination. *Circ Res* (2013) 112(12):1583–91. doi: 10.1161/CIRCRESAHA.111.300119
74. Yu Z, Song H, Jia M, Zhang J, Wang W, Li Q, et al. USP1-UAF1 Deubiquitinase Complex Stabilizes TBK1 and Enhances Antiviral Responses. *J Exp Med* (2017) 214(12):3553–63. doi: 10.1084/jem.20170180
75. Zhang L, Zhao X, Zhang M, Zhao W, Gao C. Ubiquitin-Specific Protease 2b Negatively Regulates IFN-Beta Production and Antiviral Activity by Targeting TANK-Binding Kinase 1. *J Immunol* (2014) 193(5):2230–7. doi: 10.4049/jimmunol.1302634
76. Cui J, Song Y, Li Y, Zhu Q, Tan P, Qin Y, et al. USP3 Inhibits Type I Interferon Signaling by Deubiquitinating RIG-I-Like Receptors. *Cell Res* (2014) 24(4):400–16. doi: 10.1038/cr.2013.170
77. Wang L, Zhao W, Zhang M, Wang P, Zhao K, Zhao X, et al. USP4 Positively Regulates RIG-I-Mediated Antiviral Response Through Deubiquitination and Stabilization of RIG-I. *J Virol* (2013) 87(8):4507–15. doi: 10.1128/JVI.00031-13
78. Xu C, Peng Y, Zhang Q, Xu XP, Kong XM, Shi WF. USP4 Positively Regulates RLR-Induced NF-kappaB Activation by Targeting TRAF6 for K48-Linked Deubiquitination and Inhibits Enterovirus 71 Replication. *Sci Rep* (2018) 8(1):13418. doi: 10.1038/s41598-018-31734-6
79. Cai J, Chen HY, Peng SJ, Meng JL, Wang Y, Zhou Y, et al. USP7-TRIM27 Axis Negatively Modulates Antiviral Type I IFN Signaling. *FASEB J: Off Publ Fed Am Soc Exp Biol* (2018) 32(10):5238–49. doi: 10.1096/fj.201700473RR
80. Colleran A, Collins PE, O'Carroll C, Ahmed A, Mao X, McManus B, et al. Deubiquitination of NF-kappaB by Ubiquitin-Specific Protease-7 Promotes Transcription. *Proc Natl Acad Sci USA* (2013) 110(2):618–23. doi: 10.1073/pnas.1208446110
81. Sun H, Zhang Q, Jing YY, Zhang M, Wang HY, Cai Z, et al. USP13 Negatively Regulates Antiviral Responses by Deubiquitinating STING. *Nat Commun* (2017) 8:15534. doi: 10.1038/ncomms15534
82. Li H, Zhao Z, Ling J, Pan L, Zhao X, Zhu H, et al. USP14 Promotes K63-Linked RIG-I Deubiquitination and Suppresses Antiviral Immune Responses. *Eur J Immunol* (2019) 49(1):42–53. doi: 10.1002/eji.201847603
83. Chen M, Meng Q, Qin Y, Liang P, Tan P, He L, et al. TRIM14 Inhibits cGAS Degradation Mediated by Selective Autophagy Receptor P62 to Promote Innate Immune Responses. *Mol Cell* (2016) 64(1):105–19. doi: 10.1016/j.molcel.2016.08.025
84. Zhang H, Wang D, Zhong H, Luo R, Shang M, Liu D, et al. Ubiquitin-Specific Protease 15 Negatively Regulates Virus-Induced Type I Interferon Signaling *via* Catalytically-Dependent and -Independent Mechanisms. *Sci Rep* (2015) 5:11220. doi: 10.1038/srep11220
85. Pauli EK, Chan YK, Davis ME, Gableske S, Wang MK, Feister KF, et al. The Ubiquitin-Specific Protease USP15 Promotes RIG-I-Mediated Antiviral Signaling by Deubiquitylating TRIM25. *Sci Signal* (2014) 7(307):ra3. doi: 10.1126/scisignal.2004577
86. Torre S, Polyak MJ, Langlais D, Fodil N, Kennedy JM, Radovanovic I, et al. USP15 Regulates Type I Interferon Response and Is Required for Pathogenesis of Neuroinflammation. *Nat Immunol* (2017) 18(1):54–63. doi: 10.1038/ni.3581
87. Chen R, Zhang L, Zhong B, Tan B, Liu Y, Shu HB. The Ubiquitin-Specific Protease 17 Is Involved in Virus-Triggered Type I IFN Signaling. *Cell Res* (2010) 20(7):802–11. doi: 10.1038/cr.2010.41
88. Ritchie KJ, Hahn CS, Kim KI, Yan M, Rosario D, Li L, et al. Role of ISG15 Protease UBP43 (USP18) in Innate Immunity to Viral Infection. *Nat Med* (2004) 10(12):1374–8. doi: 10.1038/nm1133

89. Yang Z, Xian H, Hu J, Tian S, Qin Y, Wang RF, et al. USP18 Negatively Regulates NF-kappaB Signaling by Targeting TAK1 and NEMO for Deubiquitination Through Distinct Mechanisms. *Sci Rep* (2015) 5:12738. doi: 10.1038/srep12738
90. Wu X, Lei C, Xia T, Zhong X, Yang Q, Shu HB. Regulation of TRIF-Mediated Innate Immune Response by K27-Linked Polyubiquitination and Deubiquitination. *Nat Commun* (2019) 10(1):4115. doi: 10.1038/s41467-019-12145-1
91. Zhang M, Zhang MX, Zhang Q, Zhu GF, Yuan L, Zhang DE, et al. USP18 Recruits USP20 to Promote Innate Antiviral Response Through Deubiquitinating STING/MITA. *Cell Res* (2016) 26(12):1302–19. doi: 10.1038/cr.2016.125
92. Zhang MX, Cai Z, Zhang M, Wang XM, Wang Y, Zhao F, et al. USP20 Promotes Cellular Antiviral Responses *via* Deconjugating K48-Linked Ubiquitination of MITA. *J Immunol* (2019) 202(8):2397–406. doi: 10.4049/jimmunol.1801447
93. Fan Y, Mao R, Yu Y, Liu S, Shi Z, Cheng J, et al. USP21 Negatively Regulates Antiviral Response by Acting as a RIG-I Deubiquitinase. *J Exp Med* (2014) 211(2):313–28. doi: 10.1084/jem.20122844
94. Cai Z, Zhang MX, Tang Z, Zhang Q, Ye J, Xiong TC, et al. USP22 Promotes IRF3 Nuclear Translocation and Antiviral Responses by Deubiquitinating the Importin Protein KPNA2. *J Exp Med* (2020) 217(5):1–19. doi: 10.1084/jem.20191174
95. Zhong H, Wang D, Fang L, Zhang H, Luo R, Shang M, et al. Ubiquitin-Specific Proteases 25 Negatively Regulates Virus-Induced Type I Interferon Signaling. *PloS One* (2013) 8(11):e80976. doi: 10.1371/journal.pone.0080976
96. Lin D, Zhang M, Zhang MX, Ren Y, Jin J, Zhao Q, et al. Induction of USP25 by Viral Infection Promotes Innate Antiviral Responses by Mediating the Stabilization of TRAF3 and TRAF6. *Proc Natl Acad Sci USA* (2015) 112 (36):11324–9. doi: 10.1073/pnas.1509968112
97. Tao X, Chu B, Xin D, Li L, Sun Q. USP27X Negatively Regulates Antiviral Signaling by Deubiquitinating RIG-I. *PloS Pathog* (2020) 16(2):e1008293. doi: 10.1371/journal.ppat.1008293
98. Guo Y, Jiang F, Kong L, Li B, Yang Y, Zhang L, et al. Cutting Edge: USP27X Deubiquitinates and Stabilizes the DNA Sensor cGAS to Regulate Cytosolic DNA-Mediated Signaling. *J Immunol* (2019) 203(8):2049–54. doi: 10.4049/jimmunol.1900514
99. Zhang Q, Tang Z, An R, Ye L, Zhong B. USP29 Maintains the Stability of cGAS and Promotes Cellular Antiviral Responses and Autoimmunity. *Cell Res* (2020) 30(10):914–27. doi: 10.1038/s41422-020-0341-6
100. Li S, Wang D, Zhao J, Weathington NM, Shang D, Zhao Y. The Deubiquitinating Enzyme USP48 Stabilizes TRAF2 and Reduces E-Cadherin-Mediated Adherens Junctions. *FASEB J: Off Publ Fed Am Soc Exp Biol* (2018) 32(1):230–42. doi: 10.1096/fj.201700415RR
101. Lin M, Zhao Z, Yang Z, Meng Q, Tan P, Xie W, et al. USP38 Inhibits Type I Interferon Signaling by Editing TBK1 Ubiquitination Through NLRP4 Signalosome. *Mol Cell* (2016) 64(2):267–81. doi: 10.1016/j.molcel.2016.08.029
102. Zhang HY, Liao BW, Xu ZS, Ran Y, Wang DP, Yang Y, et al. USP44 Positively Regulates Innate Immune Response to DNA Viruses Through Deubiquitinating MITA. *PloS Pathog* (2020) 16(1):e1008178. doi: 10.1371/journal.ppat.1008178
103. Ye L, Zhang Q, Liuyu T, Xu Z, Zhang MX, Luo MH, et al. USP49 Negatively Regulates Cellular Antiviral Responses *via* Deconjugating K63-Linked Ubiquitination of MITA. *PloS Pathog* (2019) 15(4):e1007680. doi: 10.1371/journal.ppat.1007680
104. Panda S, Nilsson JA, Gekara NO. Deubiquitinase MYSM1 Regulates Innate Immunity Through Inactivation of TRAF3 and TRAF6 Complexes. *Immunity* (2015) 43(4):647–59. doi: 10.1016/j.immuni.2015.09.010
105. Tian M, Liu W, Zhang Q, Huang Y, Li W, Wang W, et al. MYSM1 Represses Innate Immunity and Autoimmunity Through Suppressing the cGAS-STING Pathway. *Cell Rep* (2020) 33(3):108297. doi: 10.1016/j.celrep.2020.108297
106. Liang J, Saad Y, Lei T, Wang J, Qi D, Yang Q, et al. MCP-Induced Protein 1 Deubiquitinates TRAF Proteins and Negatively Regulates JNK and NF-kappaB Signaling. *J Exp Med* (2010) 207(13):2959–73. doi: 10.1084/jem.20092641
107. Chen X, Zhao Q, Xie Q, Xing Y, Chen Z. MCPIP1 Negatively Regulate Cellular Antiviral Innate Immune Responses Through DUB and Disruption of TRAF3-TBK1-IKKepsilon Complex. *Biochem Biophys Res Commun* (2018) 503(2):830–6. doi: 10.1016/j.bbrc.2018.06.083
108. Feng Q, Miao Y, Ge J, Yuan Y, Zuo Y, Qian L, et al. ATXN3 Positively Regulates Type I IFN Antiviral Response by Deubiquitinating and Stabilizing Hdac3. *J Immunol* (2018) 201(2):675–87. doi: 10.4049/jimmunol.1800285
109. Zheng H, Gupta V, Patterson-Fortin J, Bhattacharya S, Katlinski K, Wu J, et al. A BRISC-SHMT Complex Deubiquitinates IFNAR1 and Regulates Interferon Responses. *Cell Rep* (2013) 5(1):180–93. doi: 10.1016/j.celrep.2013.08.025
110. Cheng Q, Feng Q, Xu Y, Zuo Y, Liu J, Yuan Y, et al. BRCC36 Functions Noncatalytically to Promote Antiviral Response by Maintaining STAT1 Protein Stability. *Eur J Immunol* (2020) 51(2):296–310. doi: 10.1002/eji.202048537
111. Ren Y, Zhao P, Liu J, Yuan Y, Cheng Q, Zuo Y, et al. Deubiquitinase USP2a Sustains Interferons Antiviral Activity by Restricting Ubiquitination of Activated STAT1 in the Nucleus. *PloS Pathog* (2016) 12(7):e1005764. doi: 10.1371/journal.ppat.1005764
112. Qian G, Zhu L, Huang C, Liu Y, Ren Y, Ding Y, et al. Ubiquitin Specific Protease 5 Negatively Regulates the IFNs-Mediated Antiviral Activity *via* Targeting SMURF1. *Int Immunopharmacol* (2020) 87:106763. doi: 10.1016/j.intimp.2020.106763
113. Yuan Y, Miao Y, Zeng C, Liu J, Chen X, Qian L, et al. Small-Molecule Inhibitors of Ubiquitin-Specific Protease 7 Enhance Type-I Interferon Antiviral Efficacy by Destabilizing SOCS1. *Immunology* (2020) 159(3):309–21. doi: 10.1111/imm.13147
114. Liu J, Jin L, Chen X, Yuan Y, Zuo Y, Miao Y, et al. USP12 Translocation Maintains Interferon Antiviral Efficacy by Inhibiting CBP Acetyltransferase Activity. *PloS Pathog* (2020) 16(1):e1008215. doi: 10.1371/journal.ppat.1008215
115. Yeh HM, Yu CY, Yang HC, Ko SH, Liao CL, Lin YL. Ubiquitin-Specific Protease 13 Regulates IFN Signaling by Stabilizing STAT1. *J Immunol* (2013) 191(6):3328–36. doi: 10.4049/jimmunol.1300225
116. Sarasin-Filipowicz M, Wang X, Yan M, Duong FH, Poli V, Hilton DJ, et al. Alpha Interferon Induces Long-Lasting Refractoriness of JAK-STAT Signaling in the Mouse Liver Through Induction of USP18/UBP43. *Mol Cell Biol* (2009) 29(17):4841–51. doi: 10.1128/MCB.00224-09
117. Malakhova OA, Kim KI, Luo JK, Zou W, Kumar KG, Fuchs SY, et al. UBP43 Is a Novel Regulator of Interferon Signaling Independent of Its ISG15 Isopeptidase Activity. *EMBO J* (2006) 25(11):2358–67. doi: 10.1038/sj.emboj.7601149
118. Peng Y, Guo J, Sun T, Fu Y, Zheng H, Dong C, et al. USP39 Serves as a Deubiquitinase to Stabilize STAT1 and Sustains Type I IFN-Induced Antiviral Immunity. *J Immunol* (2020) 205(11):3167–78. doi: 10.4049/jimmunol.1901384
119. Qian L, Zuo Y, Deng W, Miao Y, Liu J, Yuan Y, et al. MCPIP1 is a Positive Regulator of Type I Interferons Antiviral Activity. *Biochem Biophys Res Commun* (2018) 498(4):891–7. doi: 10.1016/j.bbrc.2018.03.076
120. Wang X, Zhang L, Zhang Y, Zhao P, Qian L, Yuan Y, et al. JOSD1 Negatively Regulates Type-I Interferon Antiviral Activity by Deubiquitinating and Stabilizing Socs1. *Viral Immunol* (2017) 30(5):342–9. doi: 10.1089/vim.2017.0015
121. Muromoto R, Nakajima M, Hirashima K, Hirao T, Kon S, Shimoda K, et al. Jun Activation Domain-Binding Protein 1 (JAB1) Is Required for the Optimal Response to Interferons. *J Biol Chem* (2013) 288(43):30969–79. doi: 10.1074/jbc.M113.485847
122. Zhao P, Guo T, Qian L, Wang X, Yuan Y, Cheng Q, et al. Ubiquitin C-Terminal Hydrolase-L3 Promotes Interferon Antiviral Activity by Stabilizing Type I-Interferon Receptor. *Antiviral Res* (2017) 144:120–9. doi: 10.1016/j.antiviral.2017.06.002
123. Wang Y, Wang F. Post-Translational Modifications of Deubiquitinating Enzymes: Expanding the Ubiquitin Code. *Front Pharmacol* (2021) 12:685011. doi: 10.3389/fphar.2021.685011
124. Liu B, Zhang M, Chu H, Zhang H, Wu H, Song G, et al. The Ubiquitin E3 Ligase TRIM31 Promotes Aggregation and Activation of the Signaling Adaptor MAVS Through Lys63-Linked Polyubiquitination. *Nat Immunol* (2017) 18(2):214–24. doi: 10.1038/ni.3641
125. Paz S, Vilasco M, Arguello M, Sun Q, Lacoste J, Nguyen TL, et al. Ubiquitin-Regulated Recruitment of IkappaB Kinase Epsilon to the MAVS Interferon

Signaling Adapter. *Mol Cell Biol* (2009) 29(12):3401–12. doi: 10.1128/MCB.00880-08
126. Yoo YS, Park YY, Kim JH, Cho H, Kim SH, Lee HS, et al. The Mitochondrial Ubiquitin Ligase MARCH5 Resolves MAVS Aggregates During Antiviral Signalling. *Nat Commun* (2015) 6:7910. doi: 10.1038/ncomms8910
127. Song G, Liu B, Li Z, Wu H, Wang P, Zhao K, et al. E3 Ubiquitin Ligase RNF128 Promotes Innate Antiviral Immunity Through K63-Linked Ubiquitination of TBK1. *Nat Immunol* (2016) 17(12):1342–51. doi: 10.1038/ni.3588
128. Nakhaei P, Mesplede T, Solis M, Sun Q, Zhao T, Yang L, et al. The E3 Ubiquitin Ligase Triad3A Negatively Regulates the RIG-I/MAVS Signaling Pathway by Targeting TRAF3 for Degradation. *PloS Pathog* (2009) 5(11):e1000650. doi: 10.1371/journal.ppat.1000650
129. Cui J, Li Y, Zhu L, Liu D, Songyang Z, Wang HY, et al. NLRP4 Negatively Regulates Type I Interferon Signaling by Targeting the Kinase TBK1 for Degradation *via* the Ubiquitin Ligase DTX4. *Nat Immunol* (2012) 13(4):387–95. doi: 10.1038/ni.2239
130. Zhang M, Wang L, Zhao X, Zhao K, Meng H, Zhao W, et al. TRAF-Interacting Protein (TRIP) Negatively Regulates IFN-Beta Production and Antiviral Response by Promoting Proteasomal Degradation of TANK-Binding Kinase 1. *J Exp Med* (2012) 209(10):1703–11. doi: 10.1084/jem.20120024
131. Zheng H, Qian J, Varghese B, Baker DP, Fuchs S. Ligand-Stimulated Downregulation of the Alpha Interferon Receptor: Role of Protein Kinase D2. *Mol Cell Biol* (2011) 31(4):710–20. doi: 10.1128/MCB.01154-10
132. Carbone CJ, Zheng H, Bhattacharya S, Lewis JR, Reiter AM, Henthorn P, et al. Protein Tyrosine Phosphatase 1B Is a Key Regulator of IFNAR1 Endocytosis and a Target for Antiviral Therapies. *Proc Natl Acad Sci USA* (2012) 109(47):19226–31. doi: 10.1073/pnas.1211491109
133. Tanaka T, Soriano MA, Grusby MJ. SLIM is a Nuclear Ubiquitin E3 Ligase That Negatively Regulates STAT Signaling. *Immunity* (2005) 22(6):729–36. doi: 10.1016/j.immuni.2005.04.008
134. Yuan C, Qi J, Zhao X, Gao C. Smurf1 Protein Negatively Regulates Interferon-Gamma Signaling Through Promoting STAT1 Protein Ubiquitination and Degradation. *J Biol Chem* (2012) 287(21):17006–15. doi: 10.1074/jbc.M112.341198
135. Piganis RA, De Weerd NA, Gould JA, Schindler CW, Mansell A, Nicholson SE, et al. Suppressor of Cytokine Signaling (SOCS) 1 Inhibits Type I Interferon (IFN) Signaling *via* the Interferon Alpha Receptor (IFNAR1)-Associated Tyrosine Kinase Tyk2. *J Biol Chem* (2011) 286(39):33811–8. doi: 10.1074/jbc.M111.270207
136. Basters A, Geurink PP, El Oualid F, Ketscher L, Casutt MS, Krause E, et al. Molecular Characterization of Ubiquitin-Specific Protease 18 Reveals Substrate Specificity for Interferon-Stimulated Gene 15. *FEBS J* (2014) 281(7):1918–28. doi: 10.1111/febs.12754
137. Dauphinee SM, Richer E, Eva MM, McIntosh F, Paquet M, Dangoor D, et al. Contribution of Increased ISG15, ISGylation and Deregulated Type I IFN Signaling in Usp18 Mutant Mice During the Course of Bacterial Infections. *Genes Immun* (2014) 15(5):282–92. doi: 10.1038/gene.2014.17
138. Goldmann T, Zeller N, Raasch J, Kierdorf K, Frenzel K, Ketscher L, et al. USP18 Lack in Microglia Causes Destructive Interferonopathy of the Mouse Brain. *EMBO J* (2015) 34(12):1612–29. doi: 10.15252/embj.201490791
139. Wagner SA, Beli P, Weinert BT, Nielsen ML, Cox J, Mann M, et al. A Proteome-Wide, Quantitative Survey of *In Vivo* Ubiquitylation Sites Reveals Widespread Regulatory Roles. *Mol Cell Proteomics* (2011) 10(10):M111 013284. doi: 10.1074/mcp.M111.013284
140. Jiang X, Chen ZJ. The Role of Ubiquitylation in Immune Defence and Pathogen Evasion. *Nat Rev Immunol* (2011) 12(1):35–48. doi: 10.1038/nri3111
141. Clague MJ, Urbe S, Komander D. Breaking the Chains: Deubiquitylating Enzyme Specificity Begets Function. *Nat Rev Mol Cell Biol* (2019) 20(6):338–52. doi: 10.1038/s41580-019-0099-1
142. Kulathu Y, Komander D. Atypical Ubiquitylation - the Unexplored World of Polyubiquitin Beyond Lys48 and Lys63 Linkages. *Nat Rev Mol Cell Biol* (2012) 13(8):508–23. doi: 10.1038/nrm3394
143. Ebner P, Versteeg GA, Ikeda F. Ubiquitin Enzymes in the Regulation of Immune Responses. *Crit Rev Biochem Mol Biol* (2017) 52(4):425–60. doi: 10.1080/10409238.2017.1325829
144. Zong Z, Zhang Z, Wu L, Zhang L, Zhou F. The Functional Deubiquitinating Enzymes in Control of Innate Antiviral Immunity. *Adv Sci (Weinh)* (2021) 8(2):2002484. doi: 10.1002/advs.202002484
145. Zeng W, Xu M, Liu S, Sun L, Chen ZJ. Key Role of Ubc5 and Lysine-63 Polyubiquitination in Viral Activation of IRF3. *Mol Cell* (2009) 36(2):315–25. doi: 10.1016/j.molcel.2009.09.037
146. Song K, Li S. The Role of Ubiquitination in NF-kappaB Signaling During Virus Infection. *Viruses* (2021) 13(2):1–17. doi: 10.3390/v13020145
147. Ohtake F, Saeki Y, Ishido S, Kanno J, Tanaka K. The K48-K63 Branched Ubiquitin Chain Regulates NF-kappaB Signaling. *Mol Cell* (2016) 64(2):251–66. doi: 10.1016/j.molcel.2016.09.014
148. Chen J, Chen ZJ. Regulation of NF-kappaB by Ubiquitination. *Curr Opin Immunol* (2013) 25(1):4–12. doi: 10.1016/j.coi.2012.12.005
149. Wertz IE, O'Rourke KM, Zhou H, Eby M, Aravind L, Seshagiri S, et al. De-Ubiquitination and Ubiquitin Ligase Domains of A20 Downregulate NF-kappaB Signalling. *Nature* (2004) 430(7000):694–9. doi: 10.1038/nature02794
150. Chen ZJ, Sun LJ. Nonproteolytic Functions of Ubiquitin in Cell Signaling. *Mol Cell* (2009) 33(3):275–86. doi: 10.1016/j.molcel.2009.01.014
151. Jiang X, Kinch LN, Brautigam CA, Chen X, Du F, Grishin NV, et al. Ubiquitin-Induced Oligomerization of the RNA Sensors RIG-I and MDA5 Activates Antiviral Innate Immune Response. *Immunity* (2012) 36(6):959–73. doi: 10.1016/j.immuni.2012.03.022
152. van Huizen M, Kikkert M. The Role of Atypical Ubiquitin Chains in the Regulation of the Antiviral Innate Immune Response. *Front Cell Dev Biol* (2019) 7:392. doi: 10.3389/fcell.2019.00392
153. Niu J, Shi Y, Xue J, Miao R, Huang S, Wang T, et al. USP10 Inhibits Genotoxic NF-kappaB Activation by MCPIP1-Facilitated Deubiquitination of NEMO. *EMBO J* (2013) 32(24):3206–19. doi: 10.1038/emboj.2013.247
154. Parvatiyar K, Barber GN, Harhaj EW. TAX1BP1 and A20 Inhibit Antiviral Signaling by Targeting TBK1-IKKi Kinases. *J Biol Chem* (2010) 285(20):14999–5009. doi: 10.1074/jbc.M110.109819
155. Shembade N, Ma A, Harhaj EW. Inhibition of NF-kappaB Signaling by A20 Through Disruption of Ubiquitin Enzyme Complexes. *Science* (2010) 327(5969):1135–9. doi: 10.1126/science.1182364
156. Tokunaga F, Nishimasu H, Ishitani R, Goto E, Noguchi T, Mio K, et al. Specific Recognition of Linear Polyubiquitin by A20 Zinc Finger 7 Is Involved in NF-kappaB Regulation. *EMBO J* (2012) 31(19):3856–70. doi: 10.1038/emboj.2012.241
157. Verhelst K, Carpentier I, Kreike M, Meloni L, Verstrepen L, Kensche T, et al. A20 Inhibits LUBAC-Mediated NF-kappaB Activation by Binding Linear Polyubiquitin Chains *via* its Zinc Finger 7. *EMBO J* (2012) 31(19):3845–55. doi: 10.1038/emboj.2012.240
158. Harrigan JA, Jacq X, Martin NM, Jackson SP. Deubiquitylating Enzymes and Drug Discovery: Emerging Opportunities. *Nat Rev Drug Discovery* (2018) 17(1):57–78. doi: 10.1038/nrd.2017.152
159. Schauer NJ, Magin RS, Liu X, Doherty LM, Buhrlage SJ. Advances in Discovering Deubiquitinating Enzyme (DUB) Inhibitors. *J Med Chem* (2020) 63(6):2731–50. doi: 10.1021/acs.jmedchem.9b01138
160. Tomala MD, Magiera-Mularz K, Kubica K, Krzanik S, Zieba B, Musielak B, et al. Identification of Small-Molecule Inhibitors of USP2a. *Eur J Med Chem* (2018) 150:261–7. doi: 10.1016/j.ejmech.2018.03.009
161. Lopez-Castejon G, Luheshi NM, Compan V, High S, Whitehead RC, Flitsch S, et al. Deubiquitinases Regulate the Activity of Caspase-1 and Interleukin-1beta Secretion *via* Assembly of the Inflammasome. *J Biol Chem* (2013) 288(4):2721–33. doi: 10.1074/jbc.M112.422238
162. Wu HQ, Baker D, Ovaa H. Small Molecules That Target the Ubiquitin System. *Biochem Soc Trans* (2020) 48(2):479–97. doi: 10.1042/BST20190535
163. Love KR, Catic A, Schlieker C, Ploegh HL. Mechanisms, Biology and Inhibitors of Deubiquitinating Enzymes. *Nat Chem Biol* (2007) 3(11):697–705. doi: 10.1038/nchembio.2007.43
164. Catrysse L, Vereecke L, Beyaert R, van Loo G. A20 in Inflammation and Autoimmunity. *Trends Immunol* (2014) 35(1):22–31. doi: 10.1016/j.it.2013.10.005
165. Ruan J, Schluter D, Wang X. Deubiquitinating Enzymes (DUBs): DoUBle-Edged Swords in CNS Autoimmunity. *J Neuroinflamm* (2020) 17(1):102. doi: 10.1186/s12974-020-01783-8

166. Meuwissen ME, Schot R, Buta S, Oudesluijs G, Tinschert S, Speer SD, et al. Human USP18 Deficiency Underlies Type 1 Interferonopathy Leading to Severe Pseudo-TORCH Syndrome. *J Exp Med* (2016) 213(7):1163–74. doi: 10.1084/jem.20151529
167. Alsohime F, Martin-Fernandez M, Temsah MH, Alabdulhafid M, Le Voyer T, Alghamdi M, et al. JAK Inhibitor Therapy in a Child With Inherited USP18 Deficiency. *New Engl J Med* (2020) 382(3):256–65. doi: 10.1056/NEJMoa1905633
168. Gruber C, Martin-Fernandez M, Ailal F, Qiu X, Taft J, Altman J, et al. Homozygous STAT2 Gain-of-Function Mutation by Loss of USP18 Activity in a Patient With Type I Interferonopathy. *J Exp Med* (2020) 217(5):1–9. doi: 10.1084/jem.20192319
169. Kemp M. Recent Advances in the Discovery of Deubiquitinating Enzyme Inhibitors. *Prog Med Chem* (2016) 55:149–92. doi: 10.1016/bs.pmch.2015.10.002
170. Altun M, Kramer HB, Willems LI, McDermott JL, Leach CA, Goldenberg SJ, et al. Activity-Based Chemical Proteomics Accelerates Inhibitor Development for Deubiquitylating Enzymes. *Chem Biol* (2011) 18 (11):1401–12. doi: 10.1016/j.chembiol.2011.08.018
171. Hoffmann HH, Schneider WM, Rice CM. Interferons and Viruses: An Evolutionary Arms Race of Molecular Interactions. *Trends Immunol* (2015) 36(3):124–38. doi: 10.1016/j.it.2015.01.004
172. Bailey-Elkin BA, Knaap RCM, Kikkert M, Mark BL. Structure and Function of Viral Deubiquitinating Enzymes. *J Mol Biol* (2017) 429(22):3441–70. doi: 10.1016/j.jmb.2017.06.010

Conflict of Interest: The authors declare that the research was conducted in the absence of any commercial or financial relationships that could be construed as a potential conflict of interest.

Publisher's Note: All claims expressed in this article are solely those of the authors and do not necessarily represent those of their affiliated organizations, or those of the publisher, the editors and the reviewers. Any product that may be evaluated in this article, or claim that may be made by its manufacturer, is not guaranteed or endorsed by the publisher.

frontiers in Immunology

MINI REVIEW
published: 09 December 2021
doi: 10.3389/fimmu.2021.740223

Progress on Poxvirus E3 Ubiquitin Ligases and Adaptor Proteins

Haoran Cui[1,2,3†], *Yaxian Zhang*[2,3†] *and Leiliang Zhang*[1,2,3*]

[1] Department of Clinical Laboratory Medicine, The First Affiliated Hospital of Shandong First Medical University and Shandong Provincial Qianfoshan Hospital, Jinan, China, [2] Department of Pathogen Biology, School of Basic Medical Sciences, Shandong First Medical University and Shandong Academy of Medical Sciences, Jinan, China, [3] Medical Science and Technology Innovation Center, Shandong First Medical University & Shandong Academy of Medical Sciences, Jinan, China

Poxviruses have evolved a variety of innate immunity evasion mechanisms, some of which involve poxvirus-encoded E3 ubiquitin ligases and adaptor proteins. Based on their functional domains and ubiquitin transfer mechanisms, these poxvirus-encoded E3 ubiquitin ligases and adaptor proteins can be divided into five categories: PRANC, ANK/BC, BBK, P28/RING, and MARCH proteins. Although the substrates of many poxvirus E3 ubiquitin ligases remain to be discovered, most of the identified substrates are components of the innate immune system. In this review, we discuss the current research progress on poxvirus-encoded E3 ubiquitin ligases and adaptor proteins to provide mechanistic insights into the interplay between these viruses and their hosts.

Keywords: poxvirus, ubiquitin, E3 ubiquitin ligase, innate immune evasion, MARCH

OPEN ACCESS

Edited by:
Konstantin Sparrer, Ulm University Medical Center, Germany

Reviewed by:
Zheng Zhang, Second Affiliated Hospital of Southern University of Science and Technology, China
Anil Pant, Kansas State University, United States

***Correspondence:**
Leiliang Zhang
armzhang@hotmail.com

†*These authors share first authorship*

Specialty section:
This article was submitted to Viral Immunology, a section of the journal Frontiers in Immunology

Received: *12 July 2021*
Accepted: *24 November 2021*
Published: *09 December 2021*

Citation:
Cui H, Zhang Y and Zhang L (2021) Progress on Poxvirus E3 Ubiquitin Ligases and Adaptor Proteins. Front. Immunol. 12:740223. doi: 10.3389/fimmu.2021.740223

INTRODUCTION

Members of the family *Poxviridae* are double-stranded DNA viruses that replicate in the cytoplasm of the host cell. After infecting the host, poxviruses usually cause local or systemic purulent skin damage. *Poxviridae* is divided into two subfamilies: *Chordopoxvirinae* and *Entomopoxvirinae*. The typical members of the *Chordopoxvirinae* subfamily are variola virus (VARV), cowpox virus (CPXV), monkeypox virus (MPXV), vaccinia virus (VACV), orf virus (ORFV), myxoma virus (MYXV), and ectromelia virus (ECTV) (1).

The host inhibits the replication and spread of the virus through both the innate and adaptive immune systems. Therefore, immune escape mechanisms are particularly important for the survival of the virus (2). Poxviruses have gradually developed a variety of immune escape strategies during their evolution. For instance, poxviruses encode ubiquitination pathway components that modify the host proteins, directly affecting viral recognition, the generation of antiviral signals and inflammation, and the elimination of the virus.

Ubiquitin consists of 76 amino acids and can be attached to target proteins. The ubiquitination process occurs through an enzymatic cascade. First, ubiquitin needs to be activated by an E1 ubiquitin-activating enzyme; then, the activated ubiquitin is transferred to an E2 ubiquitin-conjugating enzyme; and finally, an E3 ubiquitin ligase transfers ubiquitin to a lysine residue on the target protein (**Figure 1A**) (3). Deubiquitylating enzymes (DUBs) maintain the dynamic state of the cellular ubiquitome by releasing conjugated ubiquitin from proteins and recycling it to maintain the cellular level of free ubiquitin (4). In the above series of enzymatic cascade reactions, the E3 ubiquitin ligase enzyme plays a vital role in the specific recognition of target substrates. At present, 8 types of polyubiquitination modification linkages have been reported. Seven of them involve connections of the glycine at the

C-terminus of the ubiquitin molecule to a lysine in the ubiquitin chain, specifically, K6, K11, K27, K29, K33, K48 or K63 (**Figure 1B**). Among those seven polyubiquitination modifications, those at K48 and K63 are the best studied. At least four ubiquitins linked together *via* their Lys48 residues form the ubiquitin chain that triggers degradation by the 26S proteasome (**Figure 1C**). In addition, monoubiquitination or Lys63-linked polyubiquitination functions as a nonproteolytic signal in intracellular trafficking, DNA repair, and signal transduction pathways (**Figure 1C**). The eighth type of ubiquitin linkage is linear ubiquitination, in which the amino group of the methionine residue on ubiquitin is connected to the carboxy group of the glycine residue of another ubiquitin. Ubiquitin-like proteins (UbLs), including NEDD8, SUMO, and ISG15, are biochemically similar to Ub and are also covalently attached to the lysines of their substrates. The conjugation of ubiquitin to UbL, and *vice versa*, can also occur, forming hybrid chains (5).

The E3 ubiquitin ligases in eukaryotes are mainly classified into three types based on their functional domains and ubiquitin transfer mechanisms (6). The most abundant type of ubiquitin ligase is Really Interesting New Gene (RING) E3s. They are characterized by a zinc-binding domain, called a RING domain, or a U-box domain (7). Some RING E3s, such as cullin-RING ligases (CRLs), are composed of multiple subunits. CRLs are composed of a cullin scaffold with a RING-box domain at its N-terminus, an adaptor protein and a substrate receptor. There are several subtypes of CRL ligases. One subtype contains Casitas B-Lineage Lymphoma Proto-Oncogene C (c-Cbl), Mouse Double Minute 2 (Mdm2), and Inhibitor of Apoptosis (IAP) and RING finger proteins (8). Another CRL ligase subtype comprises large protein complexes that include a minimal core element composed of cullin and RING-H2. Another subtype of CRL ligase is the Membrane-Associated RING-CH (MARCH) type. The E3 ligases of the Homologous to the E6AP Carboxyl Terminus (HECT) domain family are another E3 ligase type and are characterized by a conserved HECT domain located at the C-terminus of the protein (9). The other E3 ligase type is RING-between RING-RING (RBR) E3s, named after their two predicted RING domains (RING1 and RING2) and an

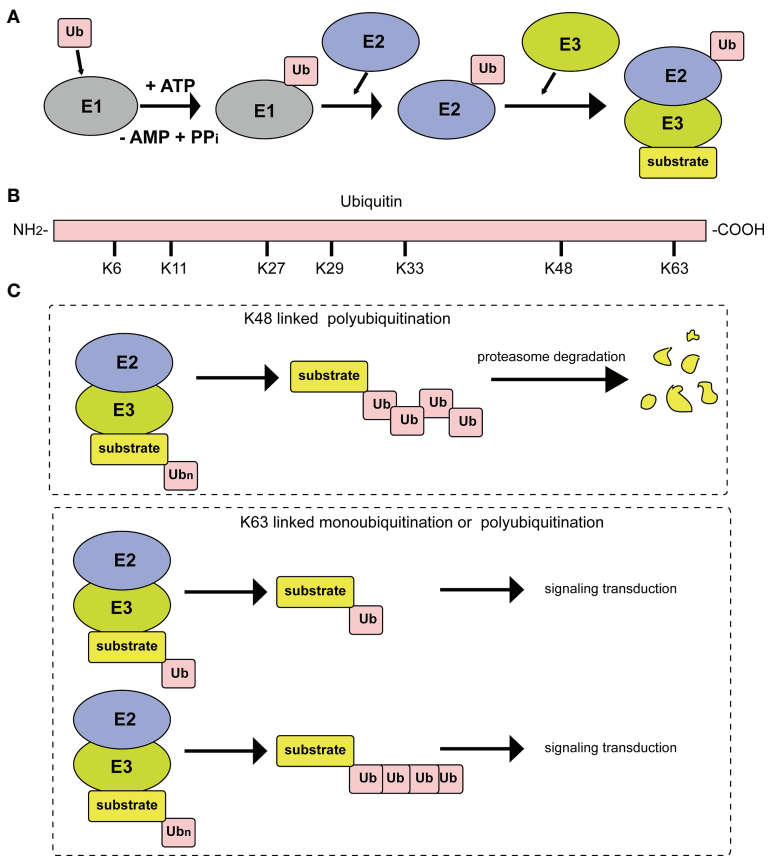

FIGURE 1 | Diagrammatic sketch of the ubiquitin cascade and E3 classification. **(A)** Illustration of the ubiquitin/26S proteome pathway. E1 is activated through ATP hydrolysis and adenosylates the ubiquitin molecule. Then, ubiquitin is successfully transferred to E3 from E1 by the catalysis of E2. With the participation of E3, substrates are modified by the ubiquitin molecule in different linkage modes. **(B)** The seven lysine residues on the ubiquitin molecule that can be ubiquitinated. **(C)** Different ubiquitin molecule linkage types. Upper panel, ubiquitin molecules connect with each other through K48 to form a polyubiquitin chain. Substrates modified by the polyubiquitin chain are degraded by the proteasome pathway. Lower panel, substrate modification by ubiquitin molecules through K63 type monoubiquitylation or polyubiquitylation, which plays important roles in signal transduction.

in-between-RING domain (IBR). In the RBR catalytic process, the RING1 domain recruits ubiquitin-charged E2, and the RING2 domain possesses a catalytic cysteine. In this review, we focus on poxvirus-encoded E3 ubiquitin ligases and adaptor proteins, which are CRL ligases.

POXVIRUS-ENCODED E3 UBIQUITIN LIGASES AND ADAPTOR PROTEINS

Poxviruses encode many proteins with E3 ubiquitin ligase functions, including pox protein repeats of ankyrin-C-terminal domain (PRANC), ankyrin repeat (ANK)/Elongin B/Elongin C (BC), BTB/Kelch (BBK), P28/RING, and MARCH. Diagrams of the E3 ubiquitin ligases and adaptor proteins encoded by poxvirus are illustrated in **Figure 2** and summarized in **Tables 1**, **2**.

PRANC Proteins

Poxviruses usually encode 4 to 5 ANK proteins. The ANK repeat domain, composed of 33 amino acid residues, mainly exists in *Chordopoxvirinae*, often functioning as a protein-protein interaction motif. Approximately 80% of ANK proteins have an F-box domain at the C-terminus, and this F-box domain is shorter than the typical F-box domain in the host cells (17). Specifically, the F-box domain encoded by poxviruses is similar in length to one or two of the three alpha helices of the cellular F-box protein. The M-T5 protein of MYXV; the VACV protein of B18R; the ORFV008, ORFV123, ORFV126, ORFV128, and ORFV129 proteins of ORFV; and EVM002, EVM005, EVM154, and EVM165 of ECTV all contain F-boxes. The Skp, Cullin, F-box (SCF) motif is the recognition motif of E3 ubiquitin ligases that mediate the ubiquitination and degradation of substrates *via* the 26S proteasome (8). In the viral ANK/F-box protein, the F-box motif binds to the N-terminus of the scaffold protein cullin-1 (Cul-1) *via* the adaptor protein S-Phase Kinase Associated Protein 1 (SKP1) (**Figure 2A**). The substrate is then ubiquitinated and degraded by binding to the substrate receptor region of the F-box protein through the degradation sequence. The SCF complex can selectively degrade regulatory proteins, thus modulating a variety of cell activities, such as signal transduction and cell cycle regulation (26).

MYXV encodes M-T5, M148R, M149R and M150, all of which are considered PRANC proteins, as they include N-terminal ANK repeats and a C-terminal F-box structure. The association of M-T5 and Cul-1 reduces P27 expression levels through 26S proteasomal degradation mediated by M-T5/SCF1. The association of M-T5 and Cul-1 maintains the protein level of Akt instead of reducing it through M-T5/SCF1-mediated 26S proteasome degradation. M-T5 can mimic the cellular protein PIKE-A, forming a complex with Akt to induce its activity. M-T5 interacts with Akt to promote the phosphorylation of P27 to regulate apoptosis and cell growth. P27/kip1 belongs to the cell cycle control protein Cip/Kip family and is a negative cell cycle regulator. The continuous phosphorylation and ubiquitination-associated degradation of P27 promote the cell cycle to cross the G0/G1 checkpoint, thereby avoiding programmed cell death due to virus infection (13, 17). The M148 protein encoded by MYXV contains 10 ankyrin repeats and is located in the cytoplasm and nucleus. M149 contains 9 of these ankyrin repeats and is unevenly distributed in the cytoplasm in the form of dots. Neither M148 nor M149 is required for virus replication in

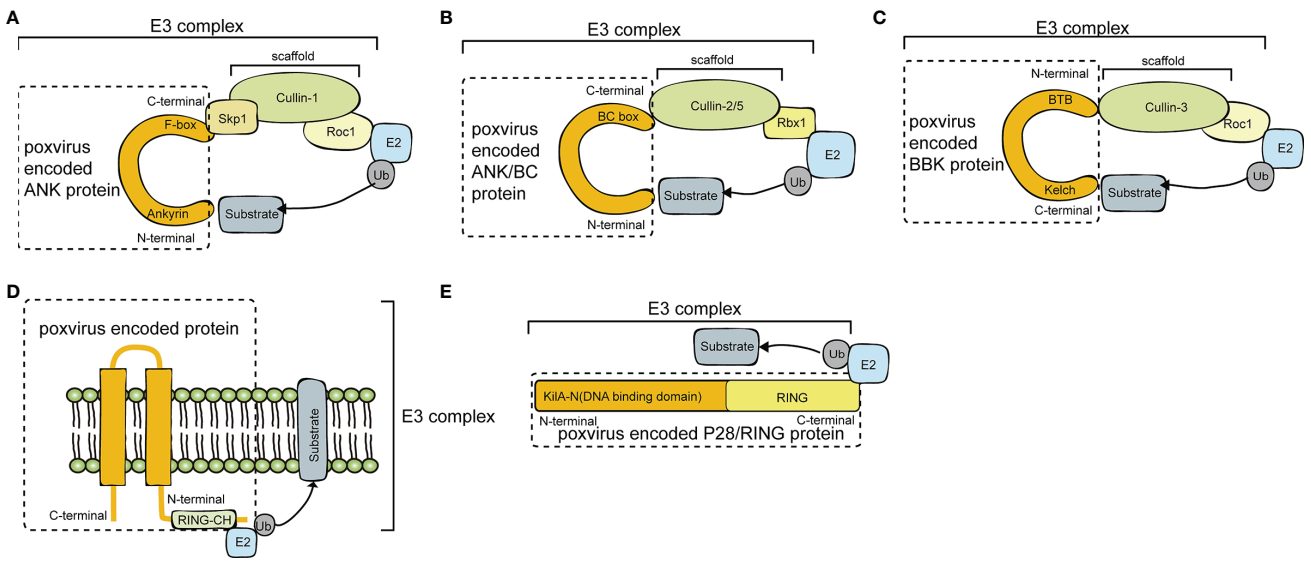

FIGURE 2 | A diagram of poxvirus E3 ubiquitin ligases and adaptor proteins. **(A)** Schematic diagram of Cullin-1 E3 Ub ligases and poxvirus-encoded pox protein repeats of ankyrin-C-terminal domain (PRANC) protein. **(B)** Schematic diagram of Cullin-2/Cullin-5 E3 Ub ligases and poxvirus-encoded ankyrin repeat (ANK)/Elongin B/Elongin C (BC) protein. **(C)** Schematic diagram of Cullin-3 E3 Ub ligases and poxvirus-encoded BTB/Kelch (BBK) protein. **(D)** Schematic diagram of P28/RING protein. **(E)** Schematic diagram of membrane-associated RING-CH (MARCH) protein.

TABLE 1 | Summary of poxvirus E3 ubiquitin ligases.

Classification	E3 ubiquitin ligase protein encoded by poxvirus	Substrates
MARCH	M153 (Myxoma virus)	CD4, CD95, MHC-I, FAS (10)
P28/RING	EVM012 (Mouse poxvirus)	not found
	M143 (Myxoma virus)	not found (11)
	P28 (Vaccinia virus)	not found (12)

tissue culture. However, when MYXV infects rabbits, it acts as a virulence factor (14). The identification of the proteins and target substrates that interact with M148, M149, and M150 requires further research. M150 is another viral protein with an ankyrin repeat sequence, containing nine ankyrin repeats in its N-terminus and an F-box in its C-terminus. This structure is necessary for the pathogenic mechanism of MYXV. The M150 protein localizes to dot-like structures in the nucleus. However, deletion of the eighth ankyrin repeat disrupts its nuclear localization. Therefore, the nuclear localization of M150 depends on the eighth ankyrin repeat. M150 colocalized with p50 of NF-κB in the nucleus in cells stimulated by tumor necrosis factor (TNF). This indicates that M150 may interfere with the NF-κB signaling pathway, but the details of this mechanism remain unclear (14).

The CPXV protein CP77 is a PRANC protein that contains nine ankyrin repeats and a 13 amino acid F-box motif at its C-terminus (15). CP77 blocks TNF-mediated nuclear translocation and activation of the NF-κB subunit p65, while it does not block IκBα phosphorylation. CP77 binds to the NF-κB subunit p65 through six ankyrin repeats in the N-terminus and binds to Cul-1 and SKP1 of the SCF complex through the C-terminal 13 amino acid F-box-like sequence. Through these two pathways, poxvirus CP77 inhibits NF-κB activation and weakens the signal transduction of the natural immune response in cells (15).

In CPXV and other orthopoxviruses, viral inducer of RIPK3 degradation (vIRD) was identified to trigger the ubiquitination and proteasome-mediated degradation of receptor interacting protein kinase 3 (RIPK3) and inhibit necroptosis (21).

ORFV belongs to the genus Parapoxvirus and causes local skin infections in goats, sheep and humans (29). The five proteins ORFV008, ORFV123, ORFV126, ORFV128 and ORFV129 encoded by ORFV all contain F-box domains (18). ORFV008, ORFV123, ORFV126, ORFV128 and ORFV129 interact with the SKP1, Cul-1 and Roc1 proteins of host cells in an F-box-dependent manner, and the interaction of ORFV008 with SCF does not inhibit the E3 ubiquitin ligase function of cellular SCF (17). In summary, poxviruses are likely to use ANK/F-box proteins to recruit target proteins to SCF1 ubiquitin ligase and degrade specific cellular proteins through the ubiquitin protease system of the host to support virus replication.

ECTV causes lethal mousepox in infected mice. The four proteins EVM002, EVM005, EVM154 and EVM165 encoded by ECTV all contain an F-box domain in the C-terminus that interacts with the host SCF complex (30). EVM005 colocalizes with Cul-1 and interacts with Cul-1, SKP1 and Roc1. Deletion of the F-box domain eliminates the interactions among EVM005, Cul-1 and SKP1 (30). One of the key steps in NF-κB activation is the ubiquitination and degradation of IκBα by the cellular SCF β-TrCP-ubiquitin ligase complex. The overexpression of EVM002, EVM005, EVM154 and EVM165 inhibited TNF- or IL-1β-stimulated IκBα degradation and NF-κB subunit p65 nuclear translocation. The inhibition of the NF-κB pathway by EVM005 depends on its F-box domain and the interaction between EVM005 and the SCF complex (19, 20). In A/NCR and C57BL/6 mouse models, virus lacking EVM005 exhibited significantly weakened virulence, indicating that EVM005 is necessary for the toxicity and immune regulation of ECTV (19).

VACV B18R is highly conserved in orthopoxviruses, containing ANK repeats and an F-box domain (16). B18R, together with two other VACV proteins, M2 and C5, has functions in uncoating and in viral DNA replication (31). Yeast two-hybrid screening experiments showed that SKP1A binds to B18R, and this interaction was confirmed by immunoprecipitation experiments, which further showed that the binding of SKP1A to B18R was dependent on the F-box (16).

VACV C9 contains 6 ANK repeats and an F-box domain near the C-terminus, which antagonizes the antiviral state induced by type I interferons (IFNs) in the early stage of VACV replication

TABLE 2 | Summary of poxvirus adaptor proteins for E3 ubiquitin ligases.

Classification	E3 adaptor protein encoded by poxvirus	Substrates
PRANC	M-T5 (Myxoma virus)	P27/Kip1 (13)
	M148, M149, M150 (Myxoma virus)	not found (14, 15)
	B18R (Vaccinia virus)	not found (16)
	ORFV008, ORFV123, ORFV126 ORFV128, ORFV129 (Orf virus)	not found (17, 18)
	EVM002, EVM005, EVM154 and EVM165 (Ectromelia virus)	IκBα (19, 20)
	CP77 (cowpox virus), C9 (Vaccinia virus)	NF-κB (15)
	viral inducer of RIPK3 degradation (vIRD)	not found (21)
ANK/BC protein	EVM010 (Ectromelia virus)	not found (22)
	MC132 (Molluscum contagiosum virus)	NF-κB p65 (23)
BBK	EVM150, EVM167, EVM18, EVM27 (Ectromelia virus)	not found (24)
	SPPV-019 (Sheeppox virus)	not found (25)
	C2L, F3L, A55R (Vaccinia virus)	not found (26)
	D11L, C18L, G3L, A57R (Vaccinia virus)	not found (27, 28)
	M006, M008, M009, M014, M140 (Myxoma virus)	not found (27, 28)

(32). When VACV infects host cells, pattern recognition receptors (PRRs) bind to pathogen-associated molecular patterns (PAMPs), activating a series of signal cascades to induce the transcription of IFN-encoding genes. Secreted IFNs act on the originating cell or on neighboring cells to activate the JAK-STAT pathway, inducing the transcription of more than 300 interferon-stimulated genes (ISGs). These genes induced by IFNs can protect the host against infection by viruses and other pathogens. Studies have found that C9 interacts with SCF and SCN (COP9 signal body/deubiquitination) complexes. C9 may interact with related proteins through both the F-box and SKP1 to mediate the proteasomal degradation of specific host proteins, such as ISGs. The degradation of ISGs antagonizes the host antiviral status induced by IFNs (32). In addition, the N- and C-terminal portions of C9 bind interferon-induced proteins with tetratricopeptide repeats (IFITs) and ubiquitin regulatory complexes, respectively. Ectopic expression of C9 rescues IFN-induced inhibition of viral DNA replication in IFIT KO cell lines (33).

VACV A49 is phosphorylated at serine 7 but not serine 12, and this phosphorylation is necessary and sufficient for its binding to β-TrCP to antagonize NF-κB (34). A49 inhibits NF-κB activation by molecular mimicry and has a motif near the N-terminus that is conserved in IκBα, β-catenin, HIV Vpu, and some other proteins (34). Phosphorylation of A49 S7 occurs when NF-κB signaling is activated by the addition of IL-1β or overexpression of TRAF6 or IKKβ, the kinase needed for IκBα phosphorylation (34). Thus, A49 is an elegant biological regulation because it becomes an NF-κB antagonist upon activation of NF-κB signaling (34). Interestingly, A49 encodes a second, smaller polypeptide that is expressed *via* leaky scanning translation from methionine 20 and is unable to block NF-κB activation (35). Viruses engineered to express either only the large protein or only the small A49 protein both have lower virulence than wild-type virus and greater virulence than an A49L deletion mutant (35).

In summary, poxviruses encode PRANC proteins that can bind SKP1. The cullin-based E3 ubiquitin ligase consists of three functional components: a catalytic component consisting of a small RING domain protein to recruit the ubiquitin-conjugating enzyme, a cullin scaffold component, and a substrate recognition component that can bind the substrate and recruit it to the vicinity of the catalytic component.

ANK/BC Proteins

In contrast to ANK repeat/F-box proteins that associate with Cul-1, noncanonical ANK protein 010 encoded by ECTV EVM010 interacts with host cullin-2 (Cul-2) *via* a C-terminal BC box (22). Bioinformatics and mass spectrometry approaches revealed that poxviral ANK ortholog groups IV and VI represent a novel class of viral ANK proteins targeting host Cul-2. In ECTV, ANK/BC proteins suppress the production of CXCL10, CCL5, and IFN, thus inhibiting innate immune signaling (22). Thus, it is speculated that the potential substrate of EVM010 is an innate immune signaling component.

MCTV MC132 was identified to associate with NF-κB subunit p65 by unbiased affinity purification. MC132 targeted p65 for ubiquitin-dependent proteasomal degradation by recruiting p65 to a host Cullin-5 (Cul-5)/BC complex, leading to effective suppression of NF-κB activity and thus benefiting virus replication (23). Poxvirus ANK/BC E3 ligase is illustrated in **Figure 2B**.

BBK Proteins

The molecular composition and function of the Cul-3-dependent E3 ligase complex has been revealed. In this complex, the binding of BTB domain-containing proteins to their substrates is mediated by Cul-3. Poxvirus is the only virus family known to encode BBK proteins, indicating that poxvirus may interact with Cul-3 to regulate the host ubiquitination pathway.

The BTB domains of the ECTV virus BBK proteins EVM150 and EVM167 bind to the N-terminal region of Cul-3 (**Figure 2C**). Moreover, EVM150 and EVM167 bind to E2-bound ubiquitin and Rocl, and the RING finger protein has the effect of an E3 ubiquitin ligase. In summary, EVM150 and EVM167 rely on Cul-3 to activate their ubiquitin ligase functions, recruiting as-yet unknown substrates for ubiquitination (24). In addition, the BBK proteins EVM18 and EVM27 also interact with Cul-3. It is not clear whether all BBK proteins in poxviruses are related to the ubiquitination pathway.

Studies have found that knocking out the BBK gene in VACV leads to a decrease in the number of mature progeny viruses (36). VACV bearing a BBK gene knockout mutation showed reduced toxicity in the nasal cavities of infected mice. VACV with BBK knockout also exhibited reduced cytopathic changes and formed fewer cell protuberances *in vitro*. The sheeppox virus BBK protein (SPPV)-019 is an important virulence factor. Calcium-independent cell adhesion is reduced in sheep infected with SPPV-019 knockout virus, indicating that SPPV-019 may regulate cell adhesion (25). When injected into sheep through the nasal cavity or an intradermal route, the SPPV-019-knockout virus was very weak, indicating that the SPPV-019 protein plays an important role in the life cycle of the poxvirus (25).

VACV encodes three BBK family proteins: C2L, F3L and A55R (26). The VACV production in mice subcutaneously injected with BBK-knockout VACV was very weak. However, the role of BBK in the ubiquitination pathway of host cells is still unclear. Previous studies showed that the N-terminal BTB-BACK (BB) domain of A55 binds directly to the Cul3 N-terminal domain (Cul3-NTD) (37). According to sequence analysis, D11L, C18L, G3L, and A57R encoded by VACV and M006, M008, M009, M014, and M140 encoded by MYXV also belong to the BBK family of proteins (27, 28).

MARCH Proteins

MYXV causes widespread lethal multiple myxomatosis in European rabbits (38). The M153R gene of MYXV encodes the E3 ubiquitin ligase M153, which contains a RING-CH domain and two transmembrane domains in its N-terminus (**Figure 2D**). Proteins with such features are referred to as MARCH proteins. In the early stage of MYXV infection, M153 is translocated from the cytoplasm to the endoplasmic reticulum, which in turn upregulates the plasma membrane levels of MHC-I, CD4, activated leukocyte cell adhesion molecule (ALCAM) and the proapoptotic factor Fas/CD95. Those

ubiquitinated substrates are then degraded by the lysosomal pathway. M153 inhibits the recognition of MHC-I and death signals by CD8 T lymphocytes and inhibits the recognition of MHC-II molecules by CD4 T lymphocytes (10). During MYXV infection, the RING-CH domain of M153 acts as a ubiquitin ligase to recognize and ubiquitinate the lysine residue in the cytoplasmic tail of CD4, which is responsible for the recognition of MHC-II molecules. Therefore, CD4 ubiquitination inhibits the recognition of MHC-II molecules. The ubiquitination and degradation of immune molecules on the cell surface induced by M153 is an important mechanism by which MYXV suppresses the immune response (10).

P28/RING Proteins

ECTV causes fatal skin damage in mice, and the P28 protein plays a key role in this process (39). P28 is a virulence factor with E3 ubiquitin ligase activity. P28 contains two functional domains, the DNA binding domain in the N-terminus and the RING domain in the C-terminus. The DNA binding domain is also called the KilA-N domain. The KilA-N domain plays an important role in the cytoplasmic localization of P28 (**Figure 2E**). Fowlpox virus (FWPV) encodes 2 functional P28 ubiquitin ligases, FWPV150 and FWPV157 (40). P28 completely loses its E3 ubiquitin ligase function when the RING domain of P28 is mutated. Therefore, the RING domain plays a role in maintaining its E3 ligase activity. Both the KilA-N domain and RING domain are crucial for the function of P28 ubiquitin ligases. ECTV and VARV P28 interact with the E2 ubiquitin-conjugating enzymes Ubc4 and UbcH5c to degrade substrates. When Ubc13/Uev1A is present, P28 can catalyze the Lys63 ubiquitination of multiple protein substrates (41).

Homologs of P28-containing proteins have also been found in other orthopoxviruses, such as VARV, CPXV, MPXV, VACV, fibroma virus (SFV) and MYXV. P28 in ECTV, M143R in MYXV (11), P28 in VACV (11) and other P28 E3 ubiquitin ligases all contain a RING finger structure. The structure of the P28/RING protein is relatively conserved among different poxviruses. Although the P28/RING protein is not essential for virus replication in cell culture, it is important for the pathogenic mechanism in virus-infected mice (12).

CONCLUSION AND PERSPECTIVE

During coevolution with their hosts, poxviruses have incorporated host cell genes into their genomes and adapted them to promote the viral life cycle. In recent years, with in-depth research on the mechanisms of host–virus interactions, research on the function of the E3 ubiquitin ligases encoded by poxviruses has made significant progress. Recently, many new proteins and protein substrates have been discovered using different approaches. For example, bioinformatics analysis and quantitative proteomics were applied to discover that ECTV protein 010 is a noncanonical ANK protein that binds to Cul-2 (22). In contrast, a small interfering RNA (siRNA) approach was used in the discovery of RIPK3 (21). In an extensive crystal structure study, the Cul2-Rbx1-EloBC-VHL complex was revealed, extending the classification of viruses encoding RING E3s (42). Many poxvirus ubiquitin E3 ligases and adapter proteins play important roles in the viral life cycle, including in replication and productive infection. The main functions of poxvirus-encoded E3 ligases are related to host immune evasion (**Tables 1**, **2**).

However, the current understanding of poxvirus E3 ubiquitin ligases is limited. More E3 ligases encoded by poxviruses will be discovered, and many poxvirus E3 ubiquitin ligase substrates remain to be explored. The homologies between genes from different poxviruses and between poxvirus genes and human genes have aided the rational discovery of new poxvirus-encoded E3 ligases, which will facilitate future studies in this field.

The known poxvirus E3 ubiquitin ligases involved in host immune invasion could be developed as potential inhibitors of the host immune system, providing new antiviral strategies. In view of the complex interactions between poxviruses and their hosts, the interplay between poxviruses and the ubiquitin system needs further exploration in the future. The identification of natural substrates of poxvirus E3 ubiquitin ligases will facilitate our understanding of host–virus interactions, and particularly the role of poxvirus E3 ubiquitin ligases in virus infection.

AUTHOR CONTRIBUTIONS

LZ conceived the work. HC and YZ draft the manuscript. LZ modified the manuscript. All authors contributed to the article and approved the submitted version.

FUNDING

This work was supported by grants from National Natural Science Foundation of China [81871663 and 82072270], Academic promotion programme of Shandong First Medical University [2019LJ001], and Natural Science Foundation of Shandong Province [ZR2021QC095].

REFERENCES

1. Van Vliet K, Mohamed MR, Zhang L, Villa NY, Werden SJ, Liu J, et al. Poxvirus Proteomics and Virus-Host Protein Interactions. *Microbiol Mol Biol Rev* (2009) 73:730–49. doi: 10.1128/MMBR.00026-09
2. Beachboard DC, Horner SM. Innate Immune Evasion Strategies of DNA and RNA Viruses. *Curr Opin Microbiol* (2016) 32:113–9. doi: 10.1016/j.mib.2016.05.015
3. Scheffner M, Nuber U, Huibregtse JM. Protein Ubiquitination Involving an E1-E2-E3 Enzyme Ubiquitin Thioester Cascade. *Nature* (1995) 373:81–3. doi: 10.1038/373081a0
4. Clague MJ, Urbé S, Komander D. Breaking the Chains: Deubiquitylating Enzyme Specificity Begets Function. *Nat Rev Mol Cell Biol* (2019) 20:338–52. doi: 10.1038/s41580-019-0099-1
5. Pérez Berrocal DA, Witting KF, Ovaa H, Mulder MPC. Hybrid Chains: A Collaboration of Ubiquitin and Ubiquitin-Like Modifiers Introducing Cross-

Functionality to the Ubiquitin Code. *Front Chem* (2019) 7:931. doi: 10.3389/fchem.2019.00931
6. Morreale FE, Walden H. Types of Ubiquitin Ligases. *Cell* (2016) 165:248–248.e1. doi: 10.1016/j.cell.2016.03.003
7. Zheng N, Shabek N. Ubiquitin Ligases: Structure, Function, and Regulation. *Annu Rev Biochem* (2017) 86:129–57. doi: 10.1146/annurev-biochem-060815-014922
8. Lorick KL, Jensen JP, Fang S, Ong AM, Hatakeyama S, Weissman AM. RING Fingers Mediate Ubiquitin-Conjugating Enzyme (E2)-Dependent Ubiquitination. *Proc Natl Acad Sci U States America* (1999) 96:11364–9. doi: 10.1073/pnas.96.20.11364
9. Huibregtse JM, Scheffner M, Beaudenon S, Howley PM. A Family of Proteins Structurally and Functionally Related to the E6-AP Ubiquitin-Protein Ligase. *Proc Natl Acad Sci USA* (1995) 92:2563–7. doi: 10.1073/pnas.92.7.2563
10. Mansouri M, Bartee E, Gouveia K, Hovey Nerenberg BT, Barrett J, Thomas L, et al. The PHD/LAP-Domain Protein M153R of Myxomavirus Is a Ubiquitin Ligase That Induces the Rapid Internalization and Lysosomal Destruction of CD4. *J Virol* (2003) 77:1427–40. doi: 10.1128/JVI.77.2.1427-1440.2003
11. Nerenberg BT, Taylor J, Bartee E, Gouveia K, Barry M, Früh K. The Poxviral RING Protein P28 Is a Ubiquitin Ligase That Targets Ubiquitin to Viral Replication Factories. *J Virol* (2005) 79:597–601. doi: 10.1128/JVI.79.1.597-601.2005
12. Senkevich TG, Koonin EV, Buller RM. A Poxvirus Protein With a RING Zinc Finger Motif is of Crucial Importance for Virulence. *Virology* (1994) 198:118–28. doi: 10.1006/viro.1994.1014
13. Johnston JB, Wang G, Barrett JW, Nazarian SH, Colwill K, Moran M, et al. Myxoma Virus M-T5 Protects Infected Cells From the Stress of Cell Cycle Arrest Through Its Interaction With Host Cell Cullin-1. *J Virol* (2005) 79:10750–63. doi: 10.1128/JVI.79.16.10750-10763.2005
14. Blanie S, Mortier J, Delverdier M, Bertagnoli S, Camus-Bouclainville C. M148R and M149R Are Two Virulence Factors for Myxoma Virus Pathogenesis in the European Rabbit. *Vet Res* (2009) 40:11. doi: 10.1051/vetres:2008049
15. Chang SJ, Hsiao JC, Sonnberg S, Chiang CT, Yang MH, Tzou DL, et al. Poxvirus Host Range Protein CP77 Contains an F-Box-Like Domain That Is Necessary to Suppress NF-kappaB Activation by Tumor Necrosis Factor Alpha But is Independent of its Host Range Function. *J Virol* (2009) 83:4140–52. doi: 10.1128/JVI.01835-08
16. Sperling KM, Schwantes A, Schnierle BS, Sutter G. The Highly Conserved Orthopoxvirus 68k Ankyrin-Like Protein is Part of a Cellular SCF Ubiquitin Ligase Complex. *Virology* (2008) 374:234–9. doi: 10.1016/j.virol.2008.02.018
17. Herbert MH, Squire CJ, Mercer AA. Poxviral Ankyrin Proteins. *Viruses* (2015) 7:709–38. doi: 10.3390/v7020709
18. Sonnberg S, Seet BT, Pawson T, Fleming SB, Mercer AA. Poxvirus Ankyrin Repeat Proteins are a Unique Class of F-Box Proteins That Associate With Cellular SCF1 Ubiquitin Ligase Complexes. *Proc Natl Acad Sci USA* (2008) 105:10955–60. doi: 10.1073/pnas.0802042105
19. Burles K, van Buuren N, Barry M. Ectromelia Virus Encodes a Family of Ankyrin/F-Box Proteins That Regulate Nfκb. *Virology* (2014) 468-470:351–62. doi: 10.1016/j.virol.2014.08.030
20. van Buuren N, Burles K, Schriewer J, Mehta N, Parker S, Buller RM, et al. EVM005: An Ectromelia-Encoded Protein With Dual Roles in NF-κb Inhibition and Virulence. *PloS Pathog* (2014) 10:e1004326. doi: 10.1371/journal.ppat.1004326
21. Liu Z, Nailwal H, Rector J, Rahman MM, Sam R, McFadden G, et al. A Class of Viral Inducer of Degradation of the Necroptosis Adaptor RIPK3 Regulates Virus-Induced Inflammation. *Immunity* (2021) 54:247–58.e7. doi: 10.1016/j.immuni.2020.11.020
22. Odon V, Georgana I, Holley J, Morata J, Maluquer de Motes C. Novel Class of Viral Ankyrin Proteins Targeting the Host E3 Ubiquitin Ligase Cullin-2. *J Virol* (2018) 92:e01374–18. doi: 10.1128/JVI.01374-18
23. Brady G, Haas DA, Farrell PJ, Pichlmair A, Bowie AG. Poxvirus Protein MC132 From Molluscum Contagiosum Virus Inhibits NF-B Activation by Targeting P65 for Degradation. *J Virol* (2015) 89:8406–15. doi: 10.1128/JVI.00799-15
24. Wilton BA, Campbell S, Van Buuren N, Garneau R, Furukawa M, Xiong Y, et al. Ectromelia Virus BTB/kelch Proteins, EVM150 and EVM167, Interact With Cullin-3-Based Ubiquitin Ligases. *Virology* (2008) 374:82–99. doi: 10.1016/j.virol.2007.11.036
25. Balinsky CA, Delhon G, Afonso CL, Risatti GR, Borca MV, French RA, et al. Sheeppox Virus Kelch-Like Gene SPPV-019 Affects Virus Virulence. *J Virol* (2007) 81:11392–401. doi: 10.1128/JVI.01093-07
26. Mercer AA, Fleming SB, Ueda N. F-Box-Like Domains are Present in Most Poxvirus Ankyrin Repeat Proteins. *Virus Genes* (2005) 31:127–33. doi: 10.1007/s11262-005-1784-z
27. Cameron C, Hota-Mitchell S, Chen L, Barrett J, Cao JX, Macaulay C, et al. The Complete DNA Sequence of Myxoma Virus. *Virology* (1999) 264:298–318. doi: 10.1006/viro.1999.0001
28. Kochneva G, Kolosova I, Maksyutova T, Ryabchikova E, Shchelkunov S. Effects of Deletions of Kelch-Like Genes on Cowpox Virus Biological Properties. *Arch Virol* (2005) 150:1857–70. doi: 10.1007/s00705-005-0530-0
29. Rohde J, Emschermann F, Knittler MR, Rziha HJ. Orf Virus Interferes With MHC Class I Surface Expression by Targeting Vesicular Transport and Golgi. *BMC Vet Res* (2012) 8:114. doi: 10.1186/1746-6148-8-114
30. van Buuren N, Couturier B, Xiong Y, Barry M. Ectromelia Virus Encodes a Novel Family of F-Box Proteins That Interact With the SCF Complex. *J Virol* (2008) 82:9917–27. doi: 10.1128/JVI.00953-08
31. Liu B, Panda D, Mendez-Rios JD, Ganesan S, Wyatt LS, Moss B. Identification of Poxvirus Genome Uncoating and DNA Replication Factors With Mutually Redundant Roles. *J Virol* (2018) 92:e02152–17. doi: 10.1128/JVI.02152-17
32. Liu R, Moss B. Vaccinia Virus C9 Ankyrin Repeat/F-Box Protein Is a Newly Identified Antagonist of the Type I Interferon-Induced Antiviral State. *J Virol* (2018) 92:e00053–18. doi: 10.1128/JVI.00053-18
33. Liu R, Olano LR, Mirzakhanyan Y, Gershon PD, Moss B. Vaccinia Virus Ankyrin-Repeat/F-Box Protein Targets Interferon-Induced IFITs for Proteasomal Degradation. *Cell Rep* (2019) 29:816–28.e6. doi: 10.1016/j.celrep.2019.09.039
34. Neidel S, Ren H, Torres AA, Smith GL. NF-κb Activation Is a Turn on for Vaccinia Virus Phosphoprotein A49 to Turn Off NF-κb Activation. *Proc Natl Acad Sci USA* (2019) 116:5699–704. doi: 10.1073/pnas.1813504116
35. Neidel S, Torres AA, Ren H, Smith GL. Leaky Scanning Translation Generates a Second A49 Protein That Contributes to Vaccinia Virus Virulence. *J Gen Virol* (2020) 101:533–41. doi: 10.1099/jgv.0.001386
36. Buller RM, Palumbo GJ. Poxvirus Pathogenesis. *Microbiol Rev* (1991) 55:80–122. doi: 10.1128/mr.55.1.80-122.1991
37. Gao C, Pallett MA, Croll TI, Smith GL, Graham SC. Molecular Basis of Cullin-3 (Cul3) Ubiquitin Ligase Subversion by Vaccinia Virus Protein A55. *J Biol Chem* (2019) 294:6416–29. doi: 10.1074/jbc.RA118.006561
38. Liu J, Wennier S, McFadden G. The Immunoregulatory Properties of Oncolytic Myxoma Virus and Their Implications in Therapeutics. *Microbes Infect* (2010) 12:1144–52. doi: 10.1016/j.micinf.2010.08.012
39. Mottet K, Bareiss B, Milne CD, Barry M. The Poxvirus Encoded Ubiquitin Ligase, P28, Is Regulated by Proteasomal Degradation and Autoubiquitination. *Virology* (2014) 468–470:363–78. doi: 10.1016/j.virol.2014.08.028
40. Bareiss B, Barry M. Fowlpox Virus Encodes Two P28-Like Ubiquitin Ligases That Are Expressed Early and Late During Infection. *Virology* (2014) 462-463:60–70. doi: 10.1016/j.virol.2014.05.018
41. Huang J, Huang Q, Zhou X, Shen MM, Yen A, Yu SX, et al. The Poxvirus P28 Virulence Factor is an E3 Ubiquitin Ligase. *J Biol Chem* (2004) 279:54110–6. doi: 10.1074/jbc.M410583200
42. Cardote TAF, Gadd MS, Ciulli A. Crystal Structure of the Cul2-Rbx1-EloBC-VHL Ubiquitin Ligase Complex. *Struct (London Engl 1993)* (2017) 25:901–11.e3. doi: 10.1016/j.str.2017.04.009

Conflict of Interest: The authors declare that the research was conducted in the absence of any commercial or financial relationships that could be construed as a potential conflict of interest.

this article, or claim that may be made by its manufacturer, is not guaranteed or endorsed by the publisher.

frontiers in Immunology

ORIGINAL RESEARCH
published: 04 January 2022
doi: 10.3389/fimmu.2021.794664

The Structure and Immune Regulatory Implications of the Ubiquitin-Like Tandem Domain Within an Avian 2'-5' Oligoadenylate Synthetase-Like Protein

Justin D. Shepard[1†], Brendan T. Freitas[2†], Sergio E. Rodriguez[3,4†], Florine E. M. Scholte[3], Kailee Baker[2], Madelyn R. Hutchison[2], Jaron E. Longo[2], Holden C. Miller[2], Brady M. O'Boyle[1], Aarushi Tandon[2], Peng Zhao[5], Neil J. Grimsey[2], Lance Wells[5,6], Éric Bergeron[2,3] and Scott D. Pegan[7*]*

[1] Department of Infectious Diseases, University of Georgia, Athens, GA, United States, [2] Department of Pharmaceutical and Biomedical Sciences, University of Georgia, Athens, GA, United States, [3] Division of High Consequence Pathogens and Pathology, Viral Special Pathogens Branch, Centers for Disease Control and Prevention, Atlanta, GA, United States, [4] Department of Microbiology and Immunology, Galveston National Laboratory, Institute for Human Infection and Immunity, University of Texas Medical Branch, Galveston, TX, United States, [5] Complex Carbohydrate Research Center, University of Georgia, Athens, GA, United States, [6] Department of Biochemistry and Molecular Biology, University of Georgia, Athens, GA, United States, [7] Division of Biomedical Sciences, University of California Riverside, Riverside, CA, United States

Post-translational modification of host and viral proteins by ubiquitin and ubiquitin-like proteins plays a key role in a host's ability to mount an effective immune response. Avian species lack a ubiquitin-like protein found in mammals and other non-avian reptiles; interferon stimulated gene product 15 (ISG15). ISG15 serves as a messenger molecule and can be conjugated to both host and viral proteins leading them to be stabilized, degraded, or sequestered. Structurally, ISG15 is comprised of a tandem ubiquitin-like domain (Ubl), which serves as the motif for post-translational modification. The 2'-5' oligoadenylate synthetase-like proteins (OASL) also encode two Ubl domains in series near its C-terminus which binds OASL to retinoic acid inducible gene-I (RIG-I). This protein-protein interaction increases the sensitivity of RIG-I and results in an enhanced production of type 1 interferons and a robust immune response. Unlike human and other mammalian OASL homologues, avian OASLs terminate their tandem Ubl domains with the same LRLRGG motif found in ubiquitin and ISG15, a motif required for their conjugation to proteins. Chickens, however, lack RIG-I, raising the question of structural and functional characteristics of chicken OASL (chOASL). By investigating chOASL, the evolutionary history of viruses with deubiquitinases can be explored and

OPEN ACCESS

Edited by:
Chaofeng Han, Second Military Medical University, China

Reviewed by:
Guanqun L. Liu, Cleveland Clinic Florida, United States
Carina De Oliveira Mann, Technical University of Munich, Germany

***Correspondence:**
Scott D. Pegan
scott.pegan@medsch.ucr.edu
Éric Bergeron
exj8@cdc.gov

[†]These authors contributed equally to this work and share first authorship

Specialty section:
This article was submitted to Molecular Innate Immunity, a section of the journal Frontiers in Immunology

Received: *13 October 2021*
Accepted: *13 December 2021*
Published: *04 January 2022*

Citation:
Shepard JD, Freitas BT, Rodriguez SE, Scholte FEM, Baker K, Hutchison MR, Longo JE, Miller HC, O'Boyle BM, Tandon A, Zhao P, Grimsey NJ, Wells L, Bergeron É and Pegan SD (2022) The Structure and Immune Regulatory Implications of the Ubiquitin-Like Tandem Domain Within an Avian 2'-5' Oligoadenylate Synthetase-Like Protein. Front. Immunol. 12:794664. doi: 10.3389/fimmu.2021.794664

drivers of species specificity for these viruses may be uncovered. Here we show that the chOASL tandem Ubl domains shares structural characteristics with mammalian ISG15, and that chOASL can oligomerize and conjugate to itself. In addition, the ISG15-like features of avian OASLs and how they impact interactions with viral deubiquitinases and delSGylases are explored.

Keywords: OASL, ISG15, UBL, avian immunity, Nairovirus, protease, ubiquitin

INTRODUCTION

Oligoadenylate synthetase (OAS) proteins are a group of enzymes that act as pattern recognition receptors (PRRs) and detect pathogen-associated molecular patterns (PAMPs) (1). Upon recognition of PAMPs, PRRs initiate signaling cascades that induce host defense mechanisms (2). One key PAMP recognized by PRRs is double-stranded RNA. The OAS family of proteins are made up of one or more OAS domains, at least one of which is catalytically active and contains an RNA binding site (3, 4). Following RNA binding, the OAS enzyme is activated and catalyzes the synthesis of 2'-5'-oligoadenylate (2-5A), which activates RNAse L, resulting in the degradation of cytoplasmic RNAs (5, 6). Another member of the OAS family, OAS-like (OASL), is also shown to play a role in antiviral responses to double-stranded RNA, but with a different mechanism of action than its OAS counterpart (3, 4, 7).

OASLs are unique members of the OAS family as they contain a single OAS domain with variable 2-5A synthetase activity across different species. The functional diversity of OASL may be exemplified by the various OAS proteins currently identified. Mouse OASL2 (mOASL2) readily catalyzes the production of 2-5As in response to cytoplasmic viral RNA; however, mOASL1 does not have the same 2-5A synthetase activity in response to viral nucleic acids (3, 5, 8). The ortholog to mOASL2, human OASL (hOASL), also lacks 2-5A synthetase activity when challenged by viral RNA (3, 5, 8), while avian (duck, goose, ostrich, and chicken) OASLs maintain their 2'-5'A synthetase activity in response to the same challenge (3, 5, 8, 9).

In addition to their single OAS domain, OASLs contain a tandem ubiquitin (Ub)-like protein (Ubl) domain at their C-terminus (3). Ub is a post-translational modifier that is conjugated to target proteins at its C-terminal LRLRGG motif. In the presence of double-stranded RNA, retinoic acid inducible gene-I (RIG-I) undergoes a conformational change that exposes its N-terminal caspase activation and recruitment domains (CARDs), which are then conjugated by K63 poly-Ub by the ligase tripartite motif containing protein 25 (TRIM25), initiating a signaling cascade that upregulates type I interferons (IFN) and IFN-stimulated genes (ISG)s such as hOASL (4). Following the upregulation of hOASL, its Ubl domain is thought to mimic poly-Ub and binds to RIG-I (4, 10). Structurally, the Ubl domains of mammalian OASL resemble that of native Ub but lack the LRLRGG motif that allows Ub to be conjugated to its target host and viral proteins. It is therefore unknown how hOASL mediates this interaction between the Ubl domain and RIG-I. In contrast, this motif is found on the Ubl domain of avian OASLs

Unlike most mammalian OASLs, avian OASLs are catalytically active and act on the OAS/RNase L pathway, and with the exception of chickens, induce RIG-I signaling in a Ubl-dependent manner (11). The Ubl domains of avian OASLs are required to activate either pathway, whereas mammalian OASLs activate RNase L in a Ubl-independent manner. The dual functionality of the avian OASLs may be due to the reduced number of OAS and OASL proteins that avian species encode compared to mammals (3, 5, 8, 9). Most birds express only OASL, with some *Ratitae* species, such as ostriches, expressing OASL and OAS1 (12). Meanwhile, mammals can have up to three OAS proteins and up to two OASLs. Both birds and mammals, however, express an OAS homologue, nucleotidyltransferase (NTase) cyclic GMP-AMP synthetase (cGAS). Beyond the predominate absence of OAS proteins, birds lack another important immunoregulatory Ubl, ISG15, that is involved in many aspects of the mammalian antiviral innate immune response (13).

ISG15 is an important regulator of the mammalian antiviral innate immune response. It is involved in the regulation of many antiviral responses including RIG-I, NF-κB, cytokine and chemokine production, and immune cell activation (14–17). Additionally, ISGylation of viral proteins signals their degradation or inactivation (18–20). The importance of ISG15 and Ub for successful antiviral responses are highlighted by the evolution of viruses encoding proteases that target these proteins such as the ovarian tumor domain proteases (OTU)s of Nairoviruses and papain-like proteases (PLpro) of coronaviruses (14, 21–23). These viral proteases reverse post-translational modifications by Ub and ISG15 by cleaving the conjugation created at their C-terminal LRLRGG motifs and generally preferentially cleave immunologically relevant poly-Ub chains and ISG15s from their virus' host species (24, 25). Based on this activity it is possible that some viral OTUs and PLpro's have adapted to target similar immunologically relevant Ubls such as OASL (26, 27).

Here we examine the structure of the domestic chicken OASL (chOASL) tandem Ubl domain and show that it contains features resembling those found in mammalian ISG15s. Analysis of OASL sequences from six diverse species indicate that these features are likely conserved among avian OASLs, just as they are among ISG15s. Sequence analysis indicates these features are likely not shared with mammalian OASLs. We also observed that chOASL do form conjugates in chicken embryonic fibroblasts

whether induced into an antiviral state or not. Nearly 900 proteins were identified, with chOASL conjugating primarily to itself when in an antiviral state. Finally, we examined the ability of OTUs and PLpro's from a diverse group of viruses to productively engage with the Ubl domain of chOASL. Several OTUs that lack deubiquitinase (DUB) and deISGylase activity were found to have moderate deOASLylase activity, with deOASLylase activity in OTUs mirroring viral host preferences. Similar species sensitivity was observed for PLpro's, which generally displayed significantly less deOASLylase activity than their OTU counterparts. Overall, the structure and covalent conjugation role of avian OASL's tandem Ubl domain was explored.

MATERIALS AND METHODS

Chemicals and Reagents

Poly-ethylene glycol (PEG) 3350 was purchased from Sigma Life Sciences, tri-ammonium citrate was purchased from Sigma Life Sciences, Ampicillin was purchased from GoldBio, dehydrated Luria-Bertani (LB) Broth was purchased from Fisher Scientific, DL-dithiothroitol (DTT) and isopropyl-β-d-thiogalactopyranoside (IPTG) were purchased from GoldBio. 4-(2-Hydroxyethyl)-1-piperazineethanesulfonic acid (HEPES) was purchased from Fisher BioReagents. Imidazole was purchased from Acros Organics; tris(hydroxymethyl)aminomethane (Tris) was purchased from Fisher Scientific. Sodium chloride (NaCl) was purchased from Fisher Chemical, and bovine serum albumin (BSA) was purchased from Sigma Life Science.

Construction, Expression, and Purification of Proteases and Ubls

The tandem Ubl domain of chOASL (342-497; Genbank ID: NP_990372) was cloned into pET-15b by Genscript and transformed into T7-expressing *E. coli*. Bacteria were cultured in 9 L of LB broth containing 100 μg/mL ampicillin at 37°C until the OD_{600} reached 0.6. Once reached, the expression was induced by the addition of 1 mM isopropyl β-d-thiogalactopyranoside (IPTG), and the culture was incubated at 18°C overnight. The culture was centrifuged at 12,000 g for 10 min, and then the pellet was collected and stored in a -80°C freezer. The cell pellet was dissolved into lysis buffer (500 mM NaCl and 50 mM Tris-HCl [pH = 7.0]) with lysozyme and then sonicated in Fisher Scientific series 150 on ice at 50% power with 5 s pulses for 6 min. The lysate was centrifuged at 64,000 g for 30 min to remove all insoluble products. The supernatant was then filtered and placed onto Ni-nitrilotriacetic agarose resin (Qiagen). The resin was washed using five column volumes of lysis buffer containing 10 mM imidazole. The protein was eluted using 5 column volumes of lysis buffer containing 300 mM imidazole. Thrombin was added to the elution to remove the 6X His-tag, and the combined solution was dialyzed in size exclusion buffer (200 mM NaCl, 50 mM Tris-HCl [pH = 7.0]) and run over a Size Exclusion Superdex 75 column (GE Healthcare, Pittsburgh PA). Purity was confirmed by gel electrophoresis. Nairovirus OTUs were expressed and purified as previously described (24).

Protease Activity Assay With proOASL

Activity assays of OTUs originating from viruses within the *Nairoviridae* genus *Orthonairovirus*, Crimean-Congo hemorrhagic fever virus (CCHFV, strain IbAr10200, Genbank: NC_005301), Dugbe virus (DUGV, strain ArD4431, Genbank: U15018), Erve virus (ERVEV, prototype, Genbank: JF911697), Nairobi sheep disease virus (NSDV, strain Jilin, Genbank: NC_034387), Ganjam virus (GANV, a Nairobi sheep disease orthonairovirus genotype called 'Ganjam virus', Genbank: EU697949), Taggert virus (TAGV, strain MI14850, Genbank: KT820205), Qalyub virus (QYBV, strain ErAg370, Genbank: NC_034511), Farallon virus (FARV, strain CalAr846, Genbank: NC_034502), Huángpí tick virus 1 (HpTV-1, strain H124-1, Genbank: NC_031135), Issyk-kul virus (ISKV, strain LEIV-315K, Genbank: KF892005), Leopards Hill virus (LPHV, strain 11SB17, Genbank: AB842088), Dera Ghazi Khan virus (DGKV, strain JD254, Genbank: NC_034520), Hazara virus (HAZV, strain JC280, Genbank: NC_038709), and Kupe virus (KUPEV, strain K611, Genbank: EU257628), with purified chOASL Ubl (*G. gallus*; NP_990372.2), Golden Eagle (*A. chrysaetos*; XP_029899442.1), or Emperor Penguin (*A. forsteri*; XP_019326421.1) were adapted from previously reported methods (25). Briefly, for 24 h, 10 μM OASL was incubated at 37°C with 20 nM of each Nairovirus OTU. At indicated timepoints, 10 μL samples were taken from the reaction tubes and quenched in 2x Laemmli buffer and boiled at 98°C for 5 min. Samples were run on BioRad Mini-PROTEAN® TGX Stain-Free™ pre-cast gels. Visualization of timepoints relied on Stain-Free technology that enhances the fluorescence of endogenous tryptophan. The gels were UV-activated for five minutes and subsequently imaged in a BioRad ChemiDoc™ Imaging system according to the manufacturer's recommendations.

Utilizing the same technique PLpros originating from viruses within the *Coronaviridae* family, porcine epidemic diarrhea virus (PEDV, strain CV777, Genbank: AF353511), Severe acute respiratory syndrome virus 1 (SARS, strain Urbani, Genbank: AY278741), (MERS, strain HCoV-EMC, Genbank: NC_019843), murine hepatitis virus (MHV, strain: JHM, Genbank: NC_006852), infectious bronchitis virus (IBV, strain Beaudette, Genbank: NC_001451), and porcine deltacoronavirus (pDCoV, strain HKU15, Genbank: NC_039208.1) were tested for their ability to process chOASL Ubl and evaluated in the same manner.

Crystallization of chOASL Tandem Ubl Domain

The Ubl domain of chOASL was screened against a series of Qiagen NeXtal suites by hanging drop using a TTP Labtech Mosquito (TTP Labtech, Herfordshire, United Kingdom). The initial screens produced spindly, starburst shaped crystals from a condition containing 0.18 M tri-ammonium citrate and 20% w/v PEG 3350. This condition was then optimized by varying concentrations of PEG 3350 and tri-ammonium citrate as well

as with additive screens. The final optimized crystal that the Ubl structure was collected from was cubic in shape and was generated through hanging drop with a final mother liquor of 0.18 M tri-ammonium citrate and 24% w/v PEG 3350, 16.3 mg/mL protein, and a 30% w/v galactose additive from Hampton research. The drop was 4 μL and contained a 4:1:5 ratio of mother liquor to additive to protein. The crystals were flash cooled in a cryoprotective solution containing 0.18 M tri-ammonium citrate and 28% w/v PEG 3350. The data set for chOASL Ubl domain was collected at the National Synchrotron Light Source II (Brookhaven National Laboratory, Upton, NY) on Life Science Biomedical Technology Research AMX beamline 17-ID-1 using a Eiger9M detector. Data were collected using wavelength 1 Å.

Data Processing and Structure Solution

All X-ray images were indexed, strategized, integrated, and scaled using HKL2000 (28). To create a cross-validation set from a random 5% of the reflections to be used throughout refinement, the CCP4 software suite was employed (29). The initial phase solution for the structure of chOASL Ubl domain was obtained by molecular replacement *via* Phaser (30). A homology model of the Ubl domain based on mouse ISG15 (5CHW) was generated using MODELLER (31) for use as a search model. The structures were refined initially using Autobuild (32), then alternating rounds of manual editing in Coot (33), and automated refinement with Phenix (34). Molprobity was used to examine the final model of each structure to confirm the quality of the structures. The data collection and refinement statistics for each structure along are listed in **Supplemental Table 1**. The structure of chOASL Ubl has been deposited in the protein data bank (PDB 7SBI).

Cell Culture

Chicken embryonic fibroblasts (CRL-12203; UMNSAH/'DF-1') (ATCC, Manassas, VA) were grown in Dulbecco's Modified Eagle Medium with GlutaMAX (DMEM) supplemented with 10% fetal bovine serum in the presence or absence (for transfections) of Penicillin-Streptomycin (10,000 U/mL) (ThermoFisher Scientific, Waltham, MA). Chicken fibroblasts were passaged using Trypsin-EDTA (0.05%) with phenol red (ThermoFisher Scientific) every two to three days for subculturing and experimental designs.

Chicken Cell Transfections, Stimulations, and Harvesting

Chicken embryonic fibroblasts (DF-1) were grown in 10 cm tissue culture-treated dishes and transfected with pcDNA 3.1(+) plasmid expressing His/FLAG-chOAS [Gene Name: DYK-cOASL_pcDNA3.1(+)] (Genscript) using TransIT-LT1 (Mirus Bio) transfection reagent. Cells were stimulated 24 h post transfection with recombinant chicken IFN-α (Bio-Rad) in optimem supplemented with 0.2% bovine serum albumin, or polyI:C (*In vivo*Gen) in Lipofectamine 2000 (ThermoFisher Scientific). Treatments with polyI:C (MilliporeSigma, St. Louis, MO) and chicken IFN-α (Bio-Rad Laboratories, Hercules, CA) were titrated and optimized on DF-1 cells to minimize cytotoxicity. Cells were harvested by scraping 24 h post stimulation in lysis buffer (137mM NaCl, 10% glycerol, 1% NP-40 Surfact-Amps [Thermo Scientific], 1X Halt Protease Inhibitor Cocktail [Thermo Scientific], 20mM Tris-HCl [pH=8.0]), centrifuged at 12,000 rpm and 4°C for 30 minutes, and the supernatant was collected in aliquots and stored at -80°C.

Western Blotting

Various antibodies raised against FLAG-Tag (MilliporeSigma), His-, HA-, and V5-Tag, and β-Actin (ThermoFisher Scientific) were used in western blotting using the Invitrogen Mini Gel System (ThermoFisher Scientific) following manufacturers protocols. Briefly, cell monolayers were lysed on ice with either NP-40 lysis buffer (ThermoFisher Scientific) or 2x Laemmli Sample Buffer (BioRad). Lysates were then heated to 95°C for 10 minutes and loaded onto 3-8% Tris-Acetate protein gels (ThermoFisher Scientific). Proteins were transferred onto nitrocellulose membranes using semi-dry transfer and probed according to Pierce Fast Western Blot Kit (ThermoFisher Scientific) manufacturer instructions. Blots were imaged on a GelDoc (BioRad).

Immunoprecipitations

The His/FLAG-chOASL plasmid construct [DYK-cOASL_pcDNA3.1(+)], was mutagenized by In-Fusion cloning PCR mutagenesis (Takara, San Jose, CA) and inhouse primers (available upon request) designed to replace the His/FLAG nucleotide sequences, with that of an HA-tag sequence. HA-tagged construct was cloned into competent cells, DNA mini-prepped (Zymo Research, Irvine, CA), restriction digest screened, next generation sequenced for confirmation of FLAG/HA swap, and DNA maxi-prepped (Zymo Research). DF-1 cell monolayers were transfected with either a FLAG- or HA-tagged version of the chOASL construct, along with a reporter plasmid (pCAGG-GFP) to standardize vector concentrations across transfected cells, as previously described. Cell monolayers were lysed on ice with Mammalian Protein Extraction Reagent (ThermoFisher Scientific) per reagent protocols, mixed at 4°C for 30 min and clarified by centrifugation. Clarified lysates were mixed separately to either Anti-FLAG M2 Magnetic Beads (MilliporeSigma) or Pierce Anti-HA Magnetic Beads (ThermoFisher Scientific) per manufacturers' instructions. Beads were eluted with 2x Laemmmli Sample Buffer and processed as previously described for western blots. Blots were probed with a monoclonal anti-FLAG M2 murine antibody conjugated to peroxidase (HRP) (MilliporeSigma).

Mass Spectrometry Analysis of chOASL Conjugates From Chicken Cells

The chOASL transfected DF-1 cell lysates were incubated with ANTI-FLAG M2 magnetic beads (Sigma-Aldrich) for 2 hr at room temperature. The flow-through was removed and the beads were washed thoroughly with TBS. The bound proteins were eluted by boiling the beads in 5% Sodium dodecyl sulfate (SDS) (Fisher Scientific) in 50 mM triethylammonium bicarbonate (TEAB) (Sigma-Aldrich) for 3 min. The eluted

proteins were then reduced by 5 mM Tris(2-carboxyethyl) phosphine hydrochloride (TCEP) (Sigma-Aldrich) at 55°C for 15 min and alkylated by 20 mM MMTS at room temperature for 10 min. The alkylated proteins were then loaded onto S-trap micro columns (PROTIFI), washed thoroughly with 100 mM TEAB in 90% methanol (Fisher Scientific), and digested by trypsin/lys-C (Promega) mix at 37°C for 16 hr. The digested peptides were eluted sequentially by 50 mM TEAB, 0.2% formic acid (Fisher Scientific), and 50% acetonitrile (Fisher Scientific). The eluted peptides were combined, dried down, and reconstituted in 0.1% formic acid.

The reconstituted peptides were separated on an Acclaim™ PepMap™ 100 C18 column (75 μm x 15 cm) and eluted into the nano-electrospray ion source of an Orbitrap Eclipse™ Tribrid™ mass spectrometer (Thermo Scientific) at a flow rate of 200 nL/min. The elution gradient consists of 1-40% acetonitrile in 0.1% formic acid over 220 min followed by 10 min of 80% acetonitrile in 0.1% formic acid. The spray voltage was set to 2.2 kV and the temperature of the heated capillary was set to 275°C. Full MS scans were acquired from m/z 200 to 2000 at 60k resolution, and MS/MS scans following collision-induced dissociation (CID) were collected in the ion trap. The raw spectra were analyzed by Proteome Discoverer (v2.5, Thermo Scientific) with mass tolerance set as 20 ppm for precursors and 0.5 Da for fragments. The search output was filtered at 0.1% false discovery rate and the spectra assigned as peptides with glycine-glycine modification were manually evaluated. The identified proteins were subjected to biological pathway analysis using Panther Classification System. Spectral counts were used to evaluate the abundances of the identified proteins as well as the abundances of glycine-glycine modification: the numbers of spectra were collected for every identified peptides, then summarized for the respective proteins those peptides were assigned to, and used to evaluate the abundances of every identified proteins; the numbers of spectra assigned to the glycine-glycine modified peptides were summarized for each modified protein and used to represent the abundances of protein glycine-glycine modification.

RESULTS

Structural Analysis of the chOASL Tandem Ubl Domain

Like Ub, OASL Ubls interact with the CARDs of RIG-I to initiate an antiviral signaling cascade in the presence of viral RNA (7, 10, 11, 35). To determine the degree to which chOASL Ubl domains resemble poly-Ub or ISG15, an X-ray crystal structure was obtained of the tandem Ubl domain of chOASL from residue 350 to 505 (**Figure 1A**; PDB 7SBI). The structure was determined to a resolution of 2.23 Å in the space group $P2_1$ (**Supplemental Table 1**). Molecular replacement phasing was performed using homology models of both β-grasp domains based on Ub. Each β-grasp was phased independently with linker regions subsequently modeled in. Two copies of the chOASL tandem Ubl domain were identified in the asymmetric unit. Electron density was found for all but the final two glycine residues which were disordered and a small density gap within a flexible region of the N-terminal β-grasp between β-sheets three and four.

The chOASL tandem Ubl domain's N-terminal β-grasp contains the typical four β-strands, forming two β–sheets, that wrap around a three-turn α-helix (**Figure 1**). Both β-grasps also contain two 3_{10}-helixes bracketing the third β-strand, which is consistent with the secondary structure topology of Ub and ISG15. The C-terminal β-grasp consists of the same secondary structure features in the same relative positioning to one another, with the addition of a short, fifth β-strand. Resembling the more compacted ISG15 rather than linear di-Ub, the two β-grasp folds are connected by a four-residue hinge region, but closely associated with each other (**Figure 1B**). In chOASL, the hinge consists of a T-E-P-Q motif that forms one internal, main chain hydrogen bond as well as a hydrogen bond to R447 (**Figure 2A**). The two β-grasp folds are oriented slightly closer together in OASL than in ISG15 and far closer than in linear di-Ub (**Figure 1B**).

The close orientation of the two Ubl domains of chOASL is largely due to Y388 of the N-terminal β-grasp (**Figure 2A**). The aromatic ring of Y388 interacts with an extremely hydrophobic pocket within the C-terminal β-grasp of the Ubl domain, while the hydroxyl group forms hydrogen bonds with the main chain of V490. PISA analysis reveals this interface to be 281.1 $Å^2$ spanned by four hydrogen bonds (36). In addition to the hydrogen bonds between Y388 and V490, H489 form bonds with R387 and W373. Because of these interactions the two Ubls adopt a compact, rigid tandem Ubl conformation rather than two distinct Ubl domains. ISG15s from all previously examined species have similar hydrophobic interactions between F41 and a hydrophobic pocket within their C-terminal β-grasp (**Figure 2B**). However, ISG15s do not appear to have conserved hydrogen bonds across the interface, and as a result the two β-grasps are more flexible in their orientation to each other. In human ISG15, this interface is 182.2 $Å^2$ and is spanned by two hydrogen bonds from E139 to the main chain of F41. While E139 is highly conserved among mammalian ISG15s, it is not always oriented in a manner that would allow for interactions across the interface. When the C-terminal β-grasps are overlaid the N-terminal β-grasp of chOASL is rotated approximately 65 degrees relative to human ISG15. The rotational difference between human ISG15 and chOASL resembles the difference between human ISG15 and bat ISG15, which is reported to be 76 degrees (37). However, despite the similarity in the rotation of the N-terminal domains of bat ISG15 and chOASL, the two do not overlap when the C-terminal domains are overlaid due to the more compact tertiary structure of chOASL.

Examination of the electrostatic surfaces of the chOASL tandem Ubl domain confirms the presence of a negatively charged pocket between the β-grasps of chOASL (**Figure 3A**). The two β-grasps are tightly packed around this charged pocket. This differs from polymeric Ub and ISG15, which do not have highly charged inter-domain interfaces and have visibly distinct Ubl domains (**Figure 3A**). Most of the surface of the C-terminal β-grasp of chOASL is positively charged. Evaluation of the level

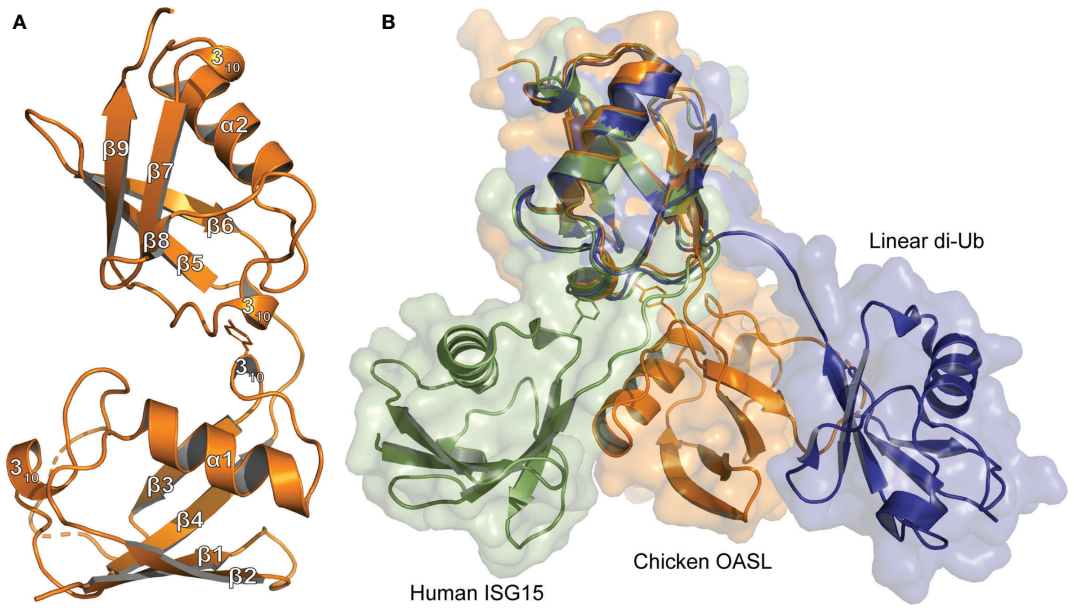

FIGURE 1 | Tertiary structure comparison of Ubls **(A)** Cartoon representation of the Ubl domain of chOASL (Orange; PDB 7SBI) with secondary structure labels corresponding to those in **Figure 4**. **(B)** Cartoon and surface representations of the chOASL Ubl domain, human ISG15 (Green; PDB 1Z2M), and linear di-Ub (Blue; PDB 2W9N) overlaid at their C-terminal β-grasps.

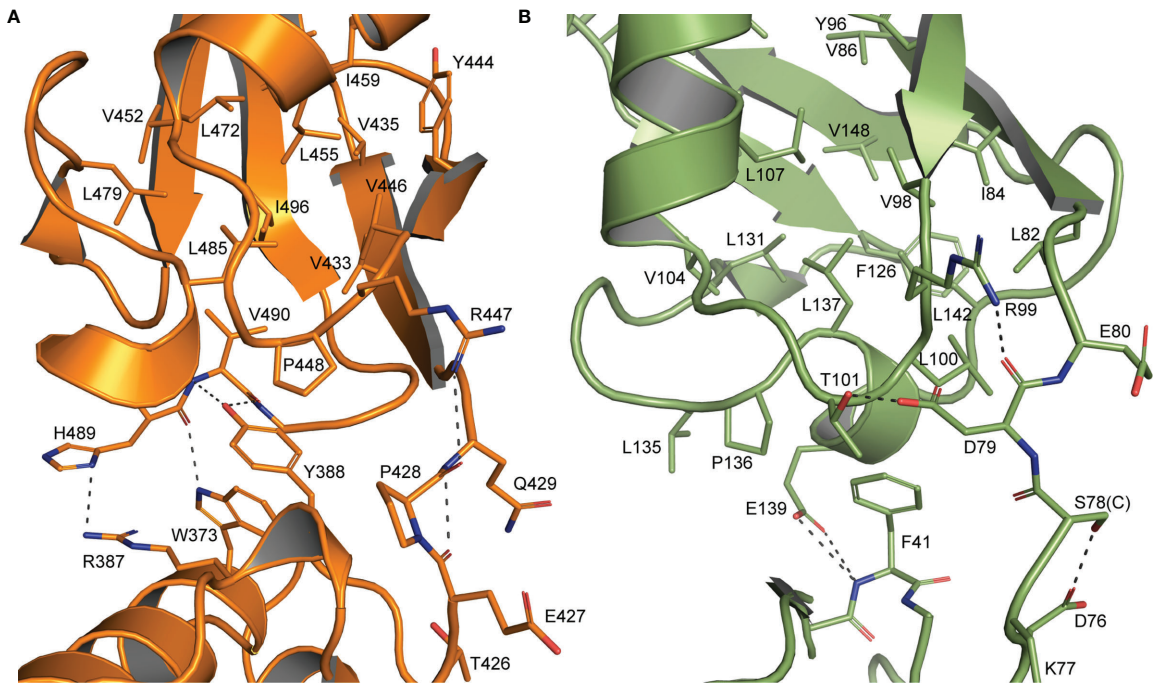

FIGURE 2 | Interdomain interactions dictate Ubl β-grasp orientation **(A)** Interactions between the two β-grasps of chOASL (Orange) along with the connecting hinge region highlighting hydrogen bonds at the interface and hydrophobic interactions between Y388 and the C-terminal hydrophobic pocket. **(B)** Similar interactions between the two β-grasps of human ISG15 (Green).

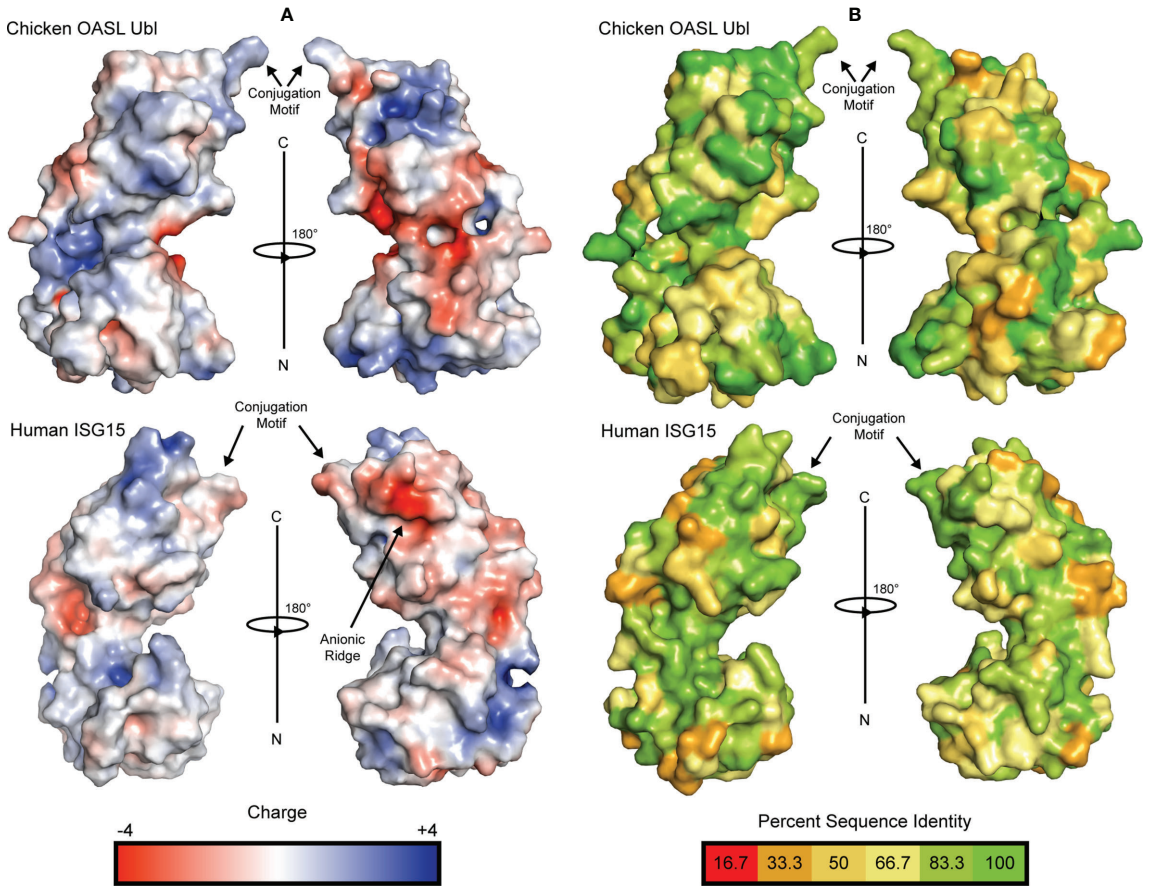

FIGURE 3 | Electrostatic surface potential and residue conservation of chOASL Ubl and human ISG15. **(A)** Surface rendering of each Ubl with surface potential ranging from +4 to -4. Negatively charged regions are shown in red and positively charged regions are shown in blue. Potentials were generated using the PDB2PQR server and the surface was rendered using the adaptive Poisson-Boltzmann solver (APBS). **(B)** Surface rendering of each Ubl with surface residues color coded to represent degree of conservation across species based on the alignments in **Figure 4**. Color scale ranges from bright green for perfectly conserved residues to orange for residues that are one third conserved.

of conservation of surface residues reveals that several of the most charged regions of chOASL, including a positively charged pocket of the C-terminus, seem to be only moderately conserved (**Figure 3B**).

Interestingly, despite avian OASL Ubl domains being approximately 55 percent conserved as a whole, their hinge regions are extremely conserved at 95.8 percent. The same region of ISG15 is only about 54 percent conserved, despite ISG15s being approximately 60 percent conserved as a whole (**Figure 4**). Closer examination reveals that not only is this region highly conserved in avian OASLs, but it is likely far more rigid as well. Specifically, this area of the hinge region is stabilized by the hydrogen bonding interaction formed by the main chain carbonyl oxygen of P428 and main chain amine of Q429 (**Figure 2**). Additionally, as these residues are highly conserved among avian OASLs, this hydrogen bond and stabilization could appear in other avian species (**Figure 4**). On the other hand, in human ISG15 none of the three hydrogen bonds being formed within this region are likely to be conserved as the residues involved have flexible side chains and show greater genetic variation among species of ISG15 (**Figures 2B** and **3**). As the hinge region connects the two β-grasp folds of ISG15 and OASL, these differences could play a role in the orientation of the two domains.

Sequence Analysis of Immunoregulatory Ubls

To identify which features of chOASL Ubl may be conserved across avian OASL, the sequences of six diverse bird species were examined. Human and mouse OASLs were also used for comparison. Upon examination of the OASL Ubl domains of these species it is apparent that some of the most highly conserved motifs of mammalian ISG15 and Ub are present in avian OASLs as well, but not in mammalian OASLs (**Figure 4**). Most notably, the LRLRGG conjugation motif is highly conserved in birds, but absent in mammalian OASL (**Figure 4A**). The presence and degree of conservation of this motif in avian OASLs, suggest a strong possibility that they are conjugating to target proteins, similar to other Ubls. Conversely, the absence of this site in mammals makes it unlikely that they

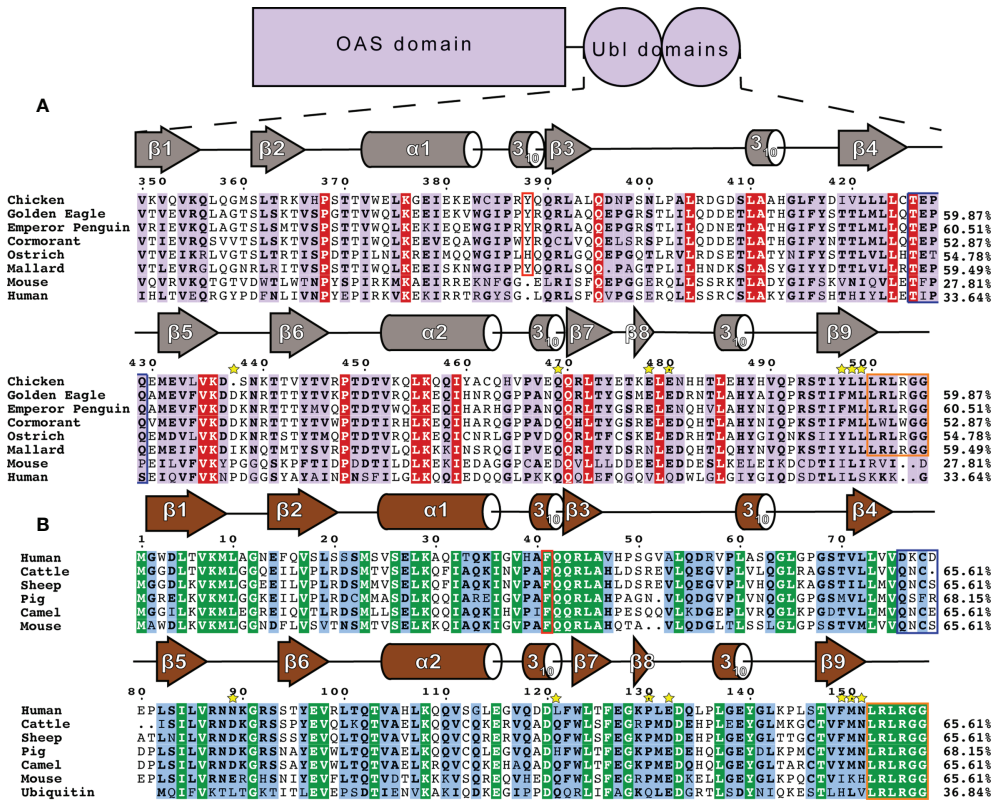

FIGURE 4 | Sequence and secondary structure comparison of OASL and ISG15 **(A)** Avian OASL Ubl domains aligned using ClustalW CLC Sequence Viewer. Percentages show the sequence identity relative to chOASL Ubl. Sequences displayed are from the following species: Domestic Chicken (*G. gallus*), Golden Eagle (*A. chrysaetos*), Emperor Penguin (*A. forsteri*), Double Crested Cormorant (*P. auratus*), Southern Ostrich (*S. camelus australis*), Mallard (*A. platyrhynchos*), House Mouse (*M. musculus*), Human (*H. sapiens*). Ubl domain secondary structure based on Define Secondary Structure of Proteins (DSSP) algorithm calculations for chOASL is shown in gray. The aromatic residue found at the interface between the domains is boxed in red and the C-terminal LRLRGG conjugation motif is boxed in purple. Yellow stars indicate residues that form interactions at known OTU selectivity determination sites. **(B)** Mammalian ISG15s and Ubiquitin aligned using ClustalW CLC Sequence Viewer. Percentages show the sequence identity relative to human ISG15. Sequences displayed are from the following species: Human (*H. sapiens*), Cattle (*B. taurus*), Sheep (*O. aries*), Boar (*S. scrofa*), Dromedary Camel (*C. dromedarius*), House Mouse (*M. musculus*), and Ubiquitin. General ISG15 secondary structure based on Define Secondary Structure of Proteins (DSSP) algorithm calculations for mouse ISG15 is shown in gray.

could conjugate to a target, indicating that if mammalian OASL Ubls are functional it would not be through conjugation in a Ub or ISG15-like manner.

Previous structural analysis of mammalian ISG15s revealed a critical phenylalanine residue at the interface of the two Ubl domains (37). In ISG15 F41 causes the two domains to more closely associate and has a profound impact of ISG15 tertiary structure (37). While F41 is not present in any OASL, avian OASLs have residues with aromatic side chains such as Y388 of chOASL. The lone outlier, ostriches, have a histidine, with an imidazole ring, at that location (**Figure 4B**). Human and mouse OASL do not contain obvious analogs to F41 or Y388. Both have aromatic side chains two positions upstream of their ISG15 counterparts, but the difference in location might place these residues outside of the domain interface. In addition to F41, ISG15s have a QQRLA motif at this site that make up a 3_{10}-helix followed by a short β-sheet (**Figure 4B**). This motif is fully conserved in Ub and the N-terminal domain of ISG15. In avian OASLs is moderately conserved on the N-terminal domain and highly conserved on the C-terminal domain. It is not well conserved on either domain of mammalian OASL.

Other similarities can be found in the degree and regions of homology between avian OASLs and ISG15s. In general, ISG15s share approximately 60% sequence identity even among distantly related mammals (24). Likewise, the base level of sequence identity between avian OASL Ubls appears to be 53-61% (**Figure 4**). The regions of conservation appear to be similar as well. In addition to those already mentioned, there are several sections of ISG15 that have highly conserved sequences across species, and while they are not all similar to the sequences found in avian OASLs, the same regions of OASL share high degrees of conservation internally.

Conjugation of Transfected chOASL in Chicken Cells

Considering chickens lack RIG-I, and chOASL contains a C-terminal sequence mirroring that of Ub, ISG15, and some other Ubls, we investigated whether chOASL formed covalent

conjugates in lieu of its RIG-I modulating role. To determine whether modification of host proteins by chOASL occurred, chicken embryonic fibroblasts (DF-1 cells) were transfected with plasmids expressing FLAG-tagged chOASL and subsequently stimulated to induce an antiviral state with synthetic double stranded RNA (poly(I:C)), or chicken IFN-α. DF-1 cells were harvested at various time points post transfection and post antiviral stimulation, and cell lysates were analyzed by western blot using FLAG-antibodies (**Figure 5A**). All analyzed time points showed the presence of protein banding at 61kDa for transfected chOASL. In addition, there were also bands displayed at approximately 90kDa and 120kDa. These results were consistent regardless of the presence or absence of antiviral stimulants. Given that chOASL might be conjugating to itself due to the presence of a 120kDa band, two chOASL tagged constructs were designed, one with a FLAG tag and another with an HA tag. Both constructs were expressed separately and combined within DF-1 cells (**Figure 5B**). Lysates from these transfected cells were immunoprecipitated with anti-FLAG or anti-HA magnetic beads. Eluents were probed with a primary antibody against FLAG. **Figure 5C** shows the presence of a 120kDa band from both anti-FLAG or anti-HA immunoprecipitations, supporting that chOASL auto-conjugates when overexpressed and/or antivirally stimulated within DF-1 cells.

Mass spectrometry was performed on cell lysates to further investigate the identity of the proteins bound by FLAG-tagged chOASL, which broadly identified 832 conjugated proteins (**Supplemental Table 2**). Of these, 580 were identified to the *Gallus gallus* (chicken) proteome using Panther Classification

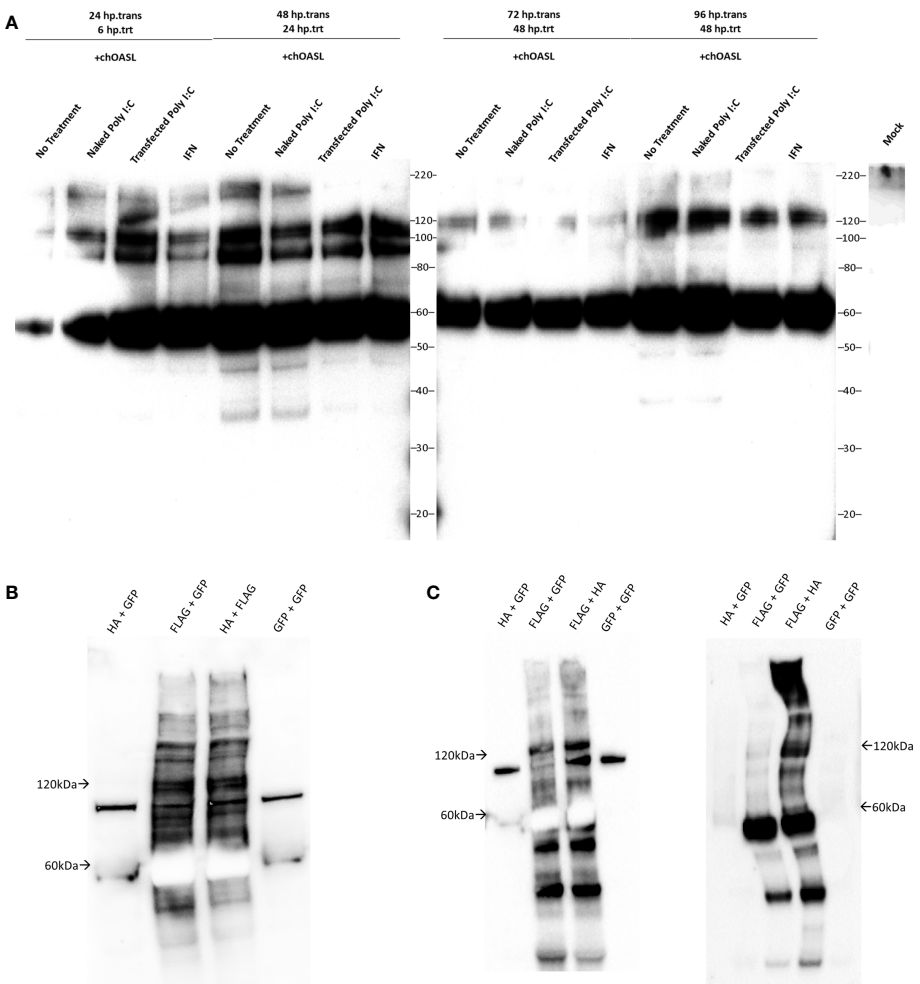

FIGURE 5 | Western blots of cell lysates or immunoprecipitation elutions from tagged chOASL transfected into DF-1 (chicken) cells. **(A)** FLAG-tagged chOASL transfected DF-1 cells were treated with various antiviral state inducing conditions (polyI:C delivered with and without transfection reagent; or chicken IFN-α), harvested at various time points, and probed with anti-FLAG antibodies on western blots. **(B)** To examine the putative chOASL-chOASL conjugations shown in **(A)**, two separate tagged constructs, one a FLAG- the other an HA-chOASL, were transfected separately or combined into DF-1 cells, for downstream immunoprecipitations, along with a GFP control plasmids as warranted. **(B)** shows these immunoprecipitation input lysates on western blot with an anti-FLAG antibody. **(C)** Left blot is of immunoprecipitations using magnetically bound beads conjugated to anti-FLAG antibodies. Right blot is of immunoprecipitations from beads conjugated to anti-HA antibodies. Both blots in **(C)** were probed with an HRP conjugated primary antibody against FLAG.

System and were grouped according to their cell processes (**Figure 6A**). Identified proteins which had the highest spectral counts (greatest in abundance, *i.e.*, most conjugated to chOASL), were also analyzed separately for pathway analysis (**Figure 6B**). Abundances for the ten highest spectral counted proteins were also analyzed (**Figure 6C**). Mass spectrometry, along with western blotting from **Figure 5**, supported that within DF-1 cells, chOASL conjugates primarily to itself, given the difference in spectral counts for OASL versus other conjugates (**Supplemental Table 2** and **Figures 5A–C**, **6C**). Conjugation of chOASL C-terminus should render an ϵ-G-G- linked peptide on chOASL modified lysines. We identified by mass spectrometry specific sites of modification on 21 out of 32 lysines on chOASL, with single site modifications on 43 other identified proteins (**Supplemental Table 2**). Given the sequence similarities between chOASL and chOAS*A (92.1% shared residue identities), we were unable to discriminate between bona fide conjugations between chOASL and chOAS*A given many of the shared modification sites (**Supplemental Table 2**). Other proteins such as glyceradldehyde-3-phosphate dehydrogenase (GAPDH), dihydropyrimidinase-related protein 2 (CRMP2A), peroxiredoxin-1 (PRDX1), dihydropyrimidinase-related protein 3 (DPYSL3), 40S ribosomal protein S3 (RPS3), Ubiquitin-like carboxyl-terminal hydrolase 18 (USP18), DNA-(apurinic or apyrimidinic site) lyase (RPS3), vigilin (HDLBP), and ubiquitin carboxyl-terminal hydrolase 5 (USP5), were identified as the most abundant conjugates to chOASL, however, they were approximately two orders of magnitude less in abundance (via spectral counts) to chOASL (**Figure 6C**).

Cleavage of chOASL Tandem Ubl Domain by Viral Proteases

Given that OASL is conjugated to target proteins in a similar fashion as Ub and ISG15 to other proteins, this presents the possibility that OASL could perform similar functions in the avian immune system to those lacking ISG15. If conjugation of OASL Ubls to a target protein has antiviral effects, there may be an evolutionary pressure for some viruses to adapt the ability to counter this mechanism, like viruses reversing ubiquitination and ISGylation. Similar to ISG15, avian OASLs are translated in an immature form with several amino acids downstream of their LRLRGG conjugation motif that would have to be cleaved off before conjugation. To explore if viral proteases may be able to process OASL, the pro-form of chOASL tandem Ubl domain was expressed with a C-terminal 6X His-Tag and was incubated with OTUs from 14 Nairovirus species for 24 hours with timepoint samples taken at specified intervals to determine approximate cleavage rate (**Figure 7**). Of the 14 OTUs tested, 7 were capable of cleaving chOASL to some degree, and 4 cleaved all chOASL within 24 hours. None fully processed the substrate in less than 2 hours. Viral OTUs demonstrate clear species preferences when processing ISG15s and the rate of cleavage demonstrated by these OTUs is similar to what is seen when known deISGylases are incubated with ISG15s from non-host species (24, 38). Specificity of OTU deOASLylase activity was additionally assessed using two distantly related avian OASLs from penguin and eagle (**Supplemental Figure 1**). Like ISG15, species to species difference within avian OASLs also seem to impact their suitability as viral protease substrates, with viral OTUs exhibiting majority deOASLylase activity against penguin OASL rather than eagle OASL (**Supplemental Figure 1**).

Beyond OTUs, six PLpro's representing all four classes of coronaviruses (α, β, γ, and δ), were evaluated for their deOASLylase activity related to chOASL as well as OASLs from penguin and eagle species (**Figure 8** and **Supplemental Figure 1**). When compared to Nairovirus OTUs, coronavirus PLpro's were less active against chOASL. In both cases, half of the enzymes tested demonstrated no activity, however the OTUs

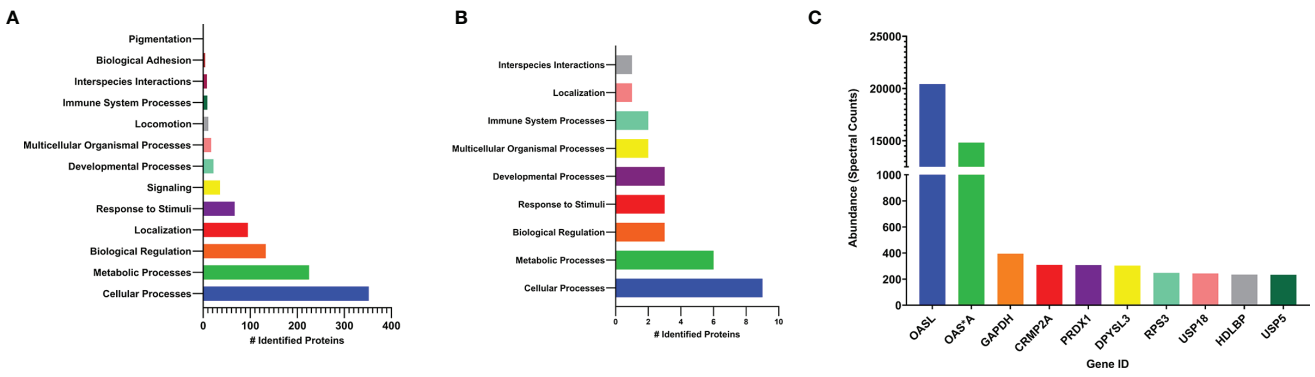

FIGURE 6 | Pathway and quantitative analysis, by mass spectrometry, of conjugated proteins to chOASL from transfected DF-1 cell lysates. **(A)** pathway analysis of total identified proteins conjugated to chOASL. **(B)** pathway analysis of highest abundance proteins (>100 spectral counts) conjugated to chOASL. **(C)** quantitative analysis of the ten most abundant conjugated proteins to chOASL. Pathway analysis of identified proteins was done using Panther Classification System (Geneontology; www.pantherdb.org) on the *Gallus gallus* proteome database. Protein abbreviations: 2'-5'-oligoadenylate synthase like protein (OASL), 2'-5'-oligoadenylate synthase (OAS*A), glyceradldehyde-3-phosphate dehydrogenase (GAPDH), dihydropyrimidinase-related protein 2 (CRMP2A), peroxiredoxin-1 (PRDX1), dihydropyrimidinase-related protein 3 (DPYSL3), 40S ribosomal protein S3 (RPS3), Ubiquitin-like carboxyl-terminal hydrolase 18 (USP18), DNA-(apurinic or apyrimidinic site) lyase (RPS3), vigilin (HDLBP), and ubiquitin. carboxyl-terminal hydrolase 5 (USP5).

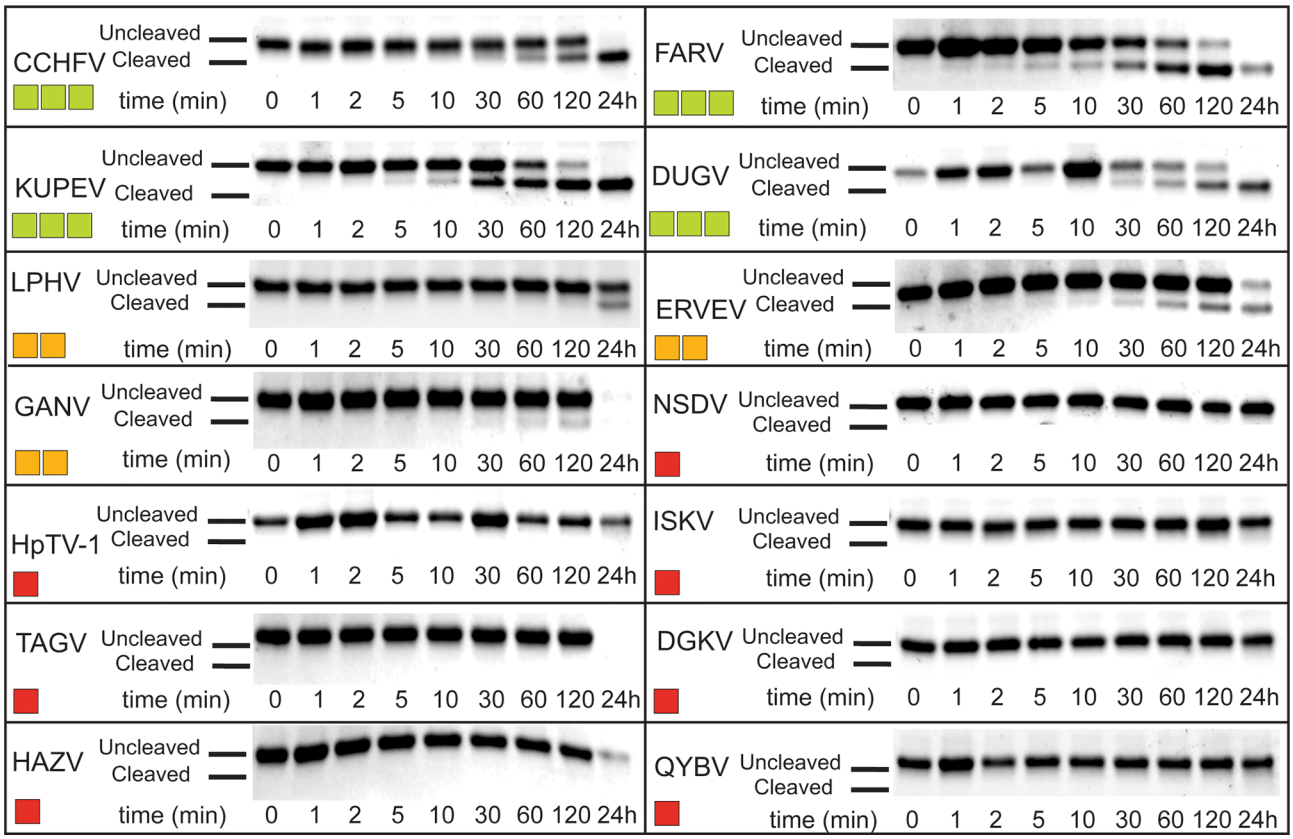

FIGURE 7 | deOASLylase activity of Nairovirus OTUs in chicken. OTUs from CCHFV, FARV, KUPEV, DUGV, LPHV, ERVEV, GANV, NSDV, HpTV-1, ISKV, TAGV, DGKV, HAZV, and QYBV were evaluated for their cleavage activity towards proOASL Ubl from chicken at 37°C, 10 μM of chOASL Ubl was incubated with 20 nM of each OTU for at least 24 h with samples taken at the time points indicated. The summary of chOASL cleavage by the different Nairovirus OTUs is presented as a heat map. Colors range from dark red (no cleavage) to light green (moderate cleavage).

that did demonstrate deOASLylase activity cleaved more than their PLpro counterparts. The three PLpro's that demonstrated some degree of deOASLylase activity were found in each genus except for *Alphacoronavirus*. Meanwhile the non-cleaving PLpro's were found in either the alpha or betacoronavirus subgroup. The most active chicken deOASLylating PLpro was from avian infectious bronchitis virus (IBV), which causes severe respiratory distress in chickens (39).

DISCUSSION

Probing the Function(s) of Avian OASL

The revelation that covalent modification of proteins by chOASL is occurring in chicken cells when induced into an antiviral state by polyI:C or IFN a is intriguing. First, unlike the small Ub, ISG15, or other Ubls that modify host proteins for signaling purposes, OASL is 59 kD in size. This dwarfs the 8-17kD size of those other protein modifiers.

The results also illustrate that chOASL gets to conjugated to many proteins (**Figures 5A, B**), however, much of the conjugation appears to be to itself (**Supplemental Table 2** and **Figures 5C**, **6C**) whether chicken cells were stimulated or not for an antiviral state (**Figure 5A**). There have been oligomerization domains proven within human OAS (3), and oligomerization between human OASL and RIG-I (4), however, this is the first report of chOASL oligomerizing with itself covalently as early as 24 hours after transfection. This conjugation of chOASL to itself was also apparent. Regardless of treatment used to induce an antiviral state (**Figure 5A**), suggesting that enzymes required for chOASL conjugation are constitutively expressed in DF-1 cells or that plasmid DNA transfection triggered their expression.

The pathway analysis of chOASL primarily involved cellular and immune response pathways, though when looking at the most abundant conjugated proteins, the pathway analysis supports that most conjugated proteins are involved in cellular and metabolic processes. With at least three of these primary conjugates, involved in immune system processes (**Figure 6B**). Of these identified proteins (aside from OASL), peroxiredoxin-1 has immune mediated pathways dealing with inflammation, oxidative stress, immune cell activations, and regulation of NFκβ signaling (40). Additionally, GAPDH has some regulatory functions that involve type I IFN production and type II IFN responses (41). With lower conjugation events also

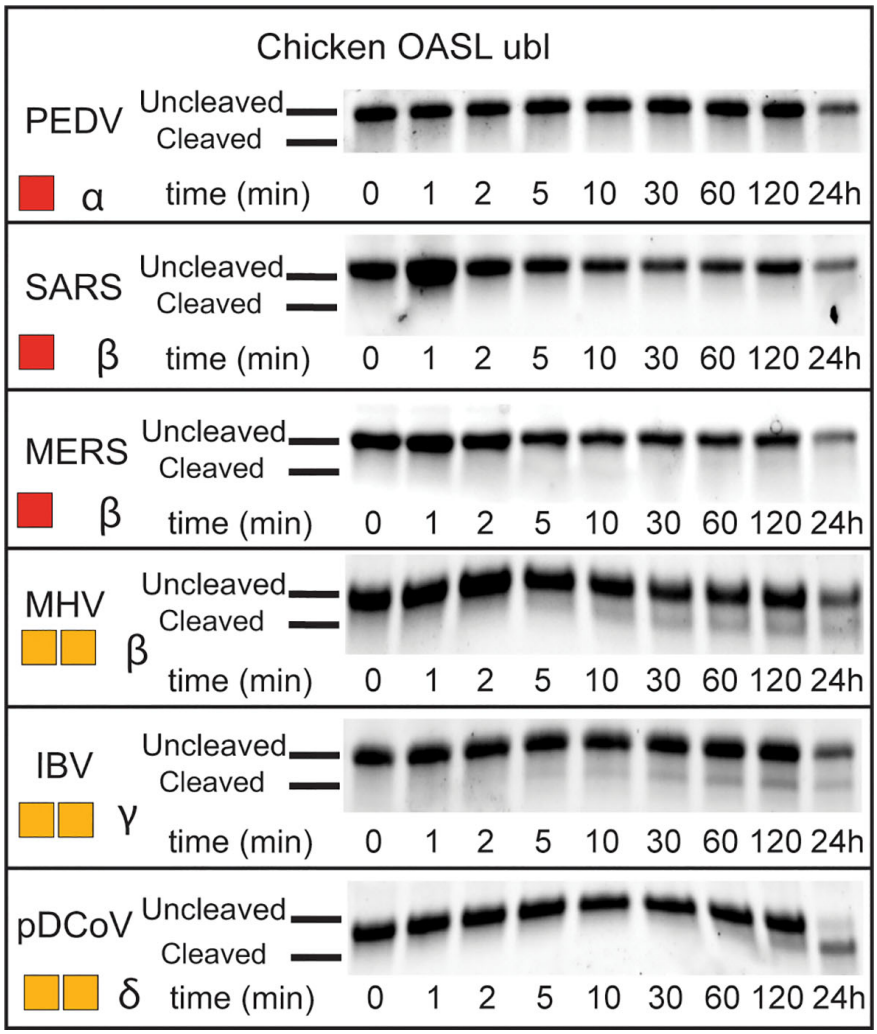

FIGURE 8 | deOASLylase activity of coronavirus PLpros in chicken. PLpros from PEDV, SARS, MERS, MHV, IBV, and were evaluated for their cleavage activity towards proOASL Ubl from chicken at 37°C, 10 μM of chOASL Ubl was incubated with 20 nM of each OTU for at least 24 h with samples taken at the time points indicated. The summary of chOASL cleavage by the different coronavirus PLpros is presented as a heat map. Colors range from dark red (no cleavage) to orange (weak cleavage). The subgroup each coronavirus belongs to is denoted next to the respective heat map.

found to other immune mediators such as STAT1, ANKRD-(-1 and -17), REL, and IFIT5 (**Supplemental Table 2**). Additionally, the results highlighted a few ubiquitin specific protease homologues that are modified by chOASL to include USP18. The chUSP18 homologue is notable because mammalian USP18 is a deISGylase regulating ISG15 antiviral activity (42). With no ISG15 in chicken cells, chUSP18s cellular substrate is likely another Ubl entity. Similar to other Ubls, the presence of OASL conjugates suggests that there are a set of enzymes required for this type of modification. Ultimately, how interactions of chOASL among these conjugates, specifically to itself, warrant further studies; specifically in relation to how viral OTU act on these conjugation events and the evolutionary arms race among viral taxa (with OTU) and animal antiviral-response elements.

Significance of the ISG15-Like Structure the chOASL Tandem Ubl Domain

Compared to linear, di-K63, and other di-Ubs, ISG15 has a relatively compact conformation but retains rotational flexibility around the interface between its domains (37). The β-grasps of chOASL's tandem Ubl domain are even more compact than those of most ISG15s, and the presence of four hydrogen bonds at the interface likely reduces rotational flexibility. Sequence data suggests that three of the four hydrogen bonds are highly conserved among tandem Ubl motifs found in bird OASLs. As the hinge region of chOASL forms a hydrogen bond with a residue on the C-terminal domain as well as one within itself, it would likely have limited flexibility. The high conservation observed between avian OASL hinge regions suggests that the

rigidity of the region would be conserved as well. Conversely, the hinge of ISG15 is flexible and highly variable (37). Interestingly, both chOASL and human ISG15 have an arginine at the same position on their C-terminal domains that forms a hydrogen bond with the hinge main chain, however this arginine is not conserved among either OASLs or ISG15s. The arginine is found in only two of the six OASLs examined and is not seen on any of the other ISG15s examined here. However, other side chains with primary amines can be found at this site with glutamines being found at this site in two of the OASLs, and two of the ISG15s, and a lysine being present on one of the OASLs.

The increased number of interactions dictating OASL tertiary structure along with the higher degree of conservation seen in these residues suggests that this conformation of the Ubl domain may contribute to the function of avian OASL. The removal of the tandem Ubl domain from duck and ostrich OASL has been shown to hinder their ability to activate not only the RIG-I pathway, but also the RNase L pathway by reducing their capacity to bind viral RNA (11). Mutation of F41 to a lysine in human ISG15 altered the conformation to the point where SARS-CoV-1 no longer bind the ISG15 effectively impeding its antiviral function (37). The evolutionary appearance of tandem Ubl domains with ISG15 and OASL as well as the negative impact of perturbing them suggest that this structural element could be key to selective recognition of these Ubls by both host and viral enzymes that seek engagement with them.

Structural Factors Potentially Affecting deOASLylase Activity of OTUs and PLpro's

When chOASL is overlaid with a structure of sheep ISG15 in complex with the KUPEV OTU as well as FARV OTU, it appears that the OASL would be capable of forming some of the same interactions that allow OTUs to cleave ISG15s and Ub. While not properly oriented in this structure due to a lack of stabilizing interactions from being bound, the LRLRGG motif would easily be accommodated within the P1-P6 binding sites adjacent to the active site (**Figure 9**). Aside from the LRLRGG binding pocket,

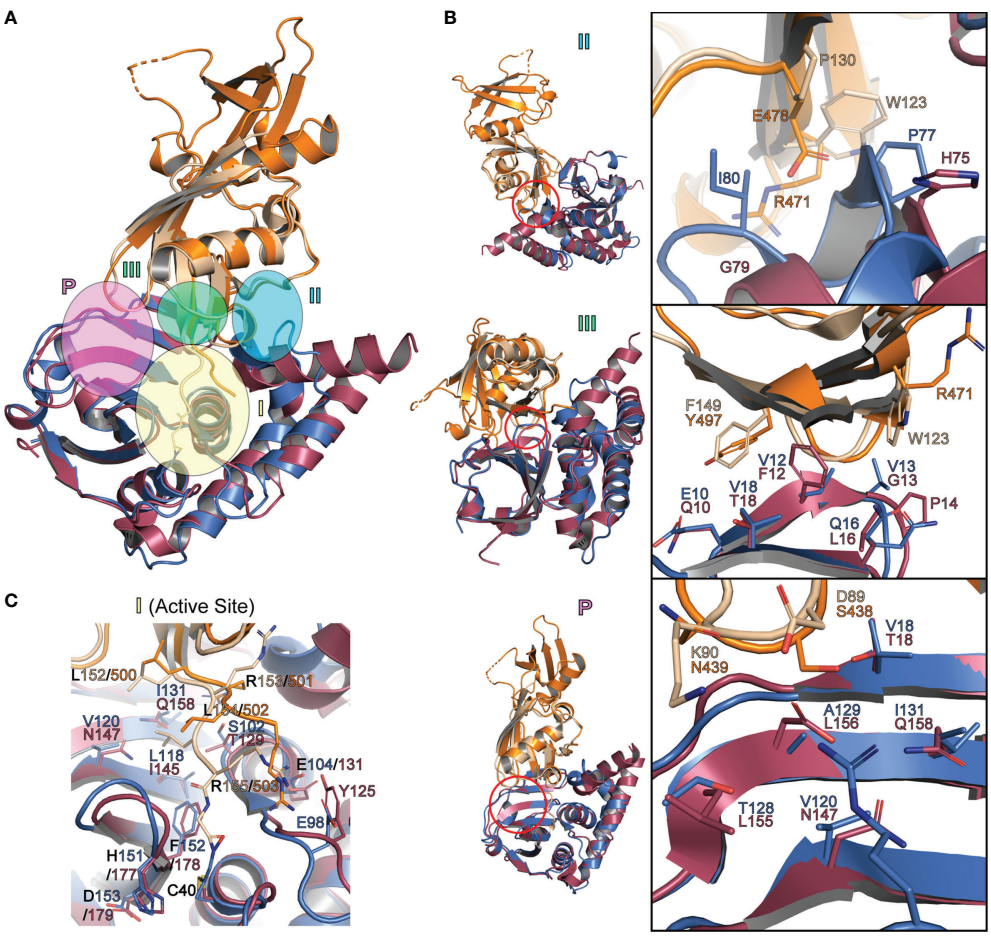

FIGURE 9 | Interactions between Ubls and OTUs that determine substrate specificity **(A)** Cartoon representation of chOASL Ubl (Orange), FARV OTU (Purple; PDB 6DX5), sheep ISG15 C-terminal domain (Beige) and KUPEV OTU (Blue; PDB 6OAR). Ubls are overlaid at their C-terminal β-grasps and OTUs are overlaid with the Ubl LRLRGG motifs within their active sites. **(B)** Close up views of OTU selectivity determination sites, highlighting interactions that determine substrate preferences. **(C)** Close of view of FARV and KUPEV OTU active sites with the C-terminus of Ubl substrates bound.

three key sites that have been determined to be important for OTU selectivity (24). OASL forms similar interaction at two of the three and neither site is identical (**Figure 9B**). The differences at these recognition sites result in KUPEV OTU having significantly higher activity toward sheep ISG15 than chOASL. While the residues at these selectivity sites are not shared between ISG15s and avian OASLs they are highly conserved within their respective groups (**Figure 4**).

When the chOASL Ubl domain is similarly overlaid with a structure K48 linked di-Ub bound to the PLpro from SARS-CoV-1 we see that the orientation of the OASL β-grasp domains prevent it from fitting into the active site of the SARS-CoV-1 PLpro (**Figure 10**). With the C-terminal chOASL β-grasp domain aligned in the active site, the N-terminal β-grasp domain sterically clashes with the zinc finger of the PLpro (**Figure 10**). The extent of this clash may vary among PLpros as this region has been shown to have some flexibility when binding Ubl substrates (43). Hence, the degree of flexibility of this PLpro region in combination with the robust domain-domain interface found here in chOASL could offer a preliminary rationale for negligible to low PLpro deOASLylase activity. However, much like that with Nairovirus OTUs, in-depth molecular investigation will have to be performed prior to having a definitive conclusion.

Potential Implications of Nairovirus OTU deOASLylase Activity

The ability of some Nairoviruses to productively process chOASL may be the result from off target activity toward a similar substrate, or the result of an evolutionary pressure on Nairoviruses to counter OASL dependent immune responses in avian species. For instance, the OTU of the Ganjam virus (GANV) has robust DUB and deISGylase activity and weak deOASLylase activity (**Figure 7**). Viewing from the standpoint that GANV OTU is one of the most efficient viral DUB and deISGylases found, having some off target activity towards another Ubl would not be that surprising (24, 44). However, the OTUs of FARV, KUPEV, and Dugbe virus (DUGV) all demonstrate moderate activity towards chOASL (**Figure 7**) and have been shown to be relatively weak DUBs, deISGylases, or

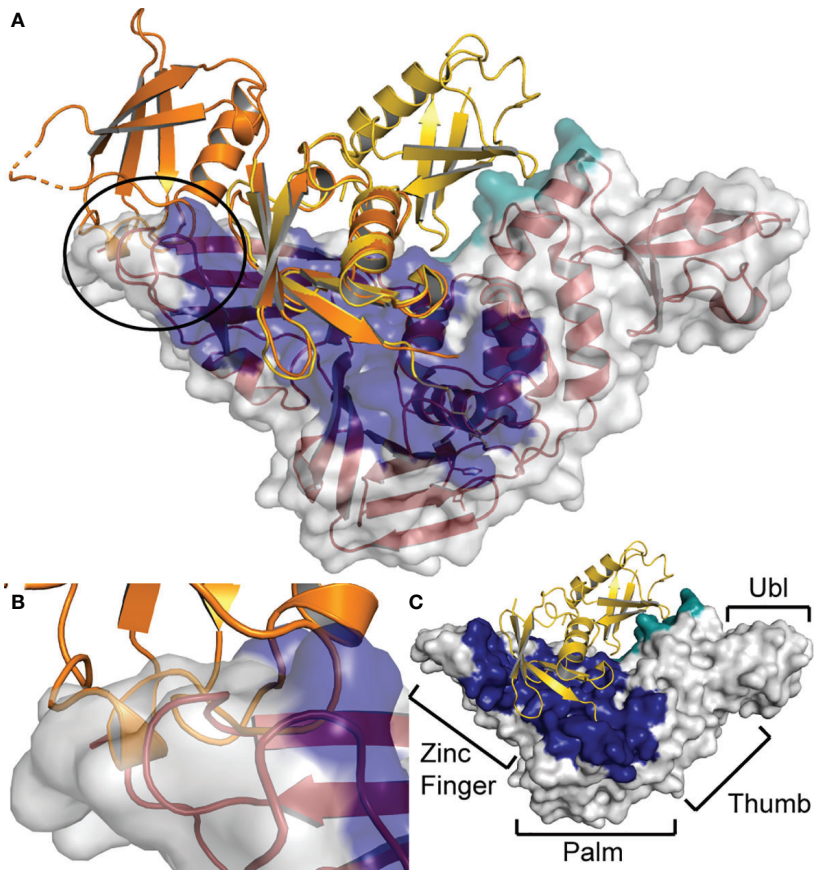

FIGURE 10 | Steric hindrance at the zinc finger prevents SARS-CoV PLpro from cleaving chOASL **(A)** chOASL Ubl domain (Orange) overlaid at the C-terminal β-grasp with K48 linked di-Ub (Yellow) bound to SARS-CoV PLpro (Red cartoon and white surface) (PDB 5E6J). **(B)** Close up view of the overlap between the PLpro zinc finger domain and N-terminal β-grasp of chOASL that causes a steric hindrance, preventing cleavage. **(C)** Surface view of SARS-CoV PLpro with the four domains labeled and the proximal Ub-binding pocket (Blue) and the distal Ub-binding pocket (Teal) highlighted.

both (24, 44). Several other viral OTUs also have negligible activity towards Ub and ISG15 (24, 44). Previously, species specificity among ISG15s, or preference for other Ubls, was suggested to be the origin of weak enzymatic activity (24). FARV OTU robust activity towards chOASL appears to highlight an example of the latter hypothesis. FARV belongs to the *Hughes* serogroup, which primarily infects seabirds (45). CCHFV deOASLylase activity might also originate from its interaction with avian species. These interactions have been recently suggested for the spread of CCHFV to western Europe (46, 47). Hence, FARV OTU as well as other OTUs may have adapted to process the OASL of certain avian species and this is reflected through activity towards related species such as chicken.

Put together, the identification of covalent bonding of avian OASLs to itself and other immunological proteins as well as OASLs tandem Ubl domain's structural similarities to that of ISG15 highlights how avian species may take a different approach to OASL immune signaling pathways. Additionally, these conjugation events may also offer a solution to the recent finding where certain Nairovirus OTUs that principally circulate within avian species lack appreciable enzymatic activity towards Ub or the more common Ubl ISG15.

PDB Accession Number

The final protein structure for chOASL Ubl was deposited in the Protein Data Bank with the ID 7SBI.

DATA AVAILABILITY STATEMENT

The datasets presented in this study can be found in online repositories. The names of the repository/repositories and accession number(s) can be found below: http://www.wwpdb.org/, 7SBI.

AUTHOR CONTRIBUTIONS

SP, EB, LW, SR, FS, and JS contributed to the conception and design of the study. BF, SR, KB, MH, JL, HCM, BO'B, AT, PZ, NG, and JS performed key experiments and the analysis of them. All authors contributed to the first draft of the manuscript and contributed to manuscript revision, read, and approved the submitted version.

ACKNOWLEDGMENTS

Data were collected the National Synchrotron Light Source II (NSLS-II) AMX-17-ID beamline at Brookhaven National Laboratory (BNL). This work was supported by NIH R01AI151006 (SP and EB) as well as DoD HDTRA 12110005 (SP). This work was also supported in part by CDC Emerging Infectious Disease Research Core Funds and by the Oak Ridge Institute for Science and Education (ORISE) through an interagency agreement between the U.S. Department of Energy (DOE) and the U.S. Department of Agriculture—Agricultural Research Service (SR). ORISE is managed by Oak Ridge Associate Universities (ORAU) under contract with DOE. The authors thank the Genetics Systems Team of the Viral Special Pathogens Branch (CDC/NCEZID/DHCPP/), specifically Drs. César Albariño and Shilpi Jain for expert assistance in next generation sequencing.

SUPPLEMENTARY MATERIAL

The Supplementary Material for this article can be found online at: https://www.frontiersin.org/articles/10.3389/fimmu.2021.794664/full#supplementary-material

REFERENCES

1. Vajjhala PR, Ve T, Bentham A, Stacey KJ, Kobe B. The Molecular Mechanisms of Signaling by Cooperative Assembly Formation in Innate Immunity Pathways. *Mol Immunol* (2017) 86:23–37. doi: 10.1016/j.molimm.2017.02.012
2. Pandey S, Kawai T, Akira S. Microbial Sensing by Toll-Like Receptors and Intracellular Nucleic Acid Sensors. *Cold Spring Harb Perspect Biol* (2014) 7(1): a016246. doi: 10.1101/cshperspect.a016246
3. Choi UY, Kang JS, Hwang YS, Kim YJ. Oligoadenylate Synthase-Like (OASL) Proteins: Dual Functions and Associations With Diseases. *Exp Mol Med* (2015) 47:e144. doi: 10.1038/emm.2014.110
4. Zhu J, Ghosh A, Sarkar SN. OASL-A New Player in Controlling Antiviral Innate Immunity. *Curr Opin Virol* (2015) 12:15–9. doi: 10.1016/j.coviro.2015.01.010
5. Kristiansen H, Gad HH, Eskildsen-Larsen S, Despres P, Hartmann R. The Oligoadenylate Synthetase Family: An Ancient Protein Family With Multiple Antiviral Activities. *J Interferon Cytokine Res* (2011) 31(1):41–7. doi: 10.1089/jir.2010.0107
6. Li XL, Ezelle HJ, Hsi TY, Hassel BA. A Central Role for RNA in the Induction and Biological Activities of Type 1 Interferons. *Wiley Interdiscip Rev RNA* (2011) 2(1):58–78. doi: 10.1002/wrna.32
7. Ibsen MS, Gad HH, Andersen LL, Hornung V, Julkunen I, Sarkar SN, et al. Structural and Functional Analysis Reveals That Human OASL Binds dsRNA to Enhance RIG-I Signaling. *Nucleic Acids Res* (2015) 43(10):5236–48. doi: 10.1093/nar/gkv389
8. Eskildsen S, Justesen J, Schierup MH, Hartmann R. Characterization of the 2'-5'-Oligoadenylate Synthetase Ubiquitin-Like Family. *Nucleic Acids Res* (2003) 31(12):3166–73. doi: 10.1093/nar/gkg427
9. Tag-El-Din-Hassan HT, Morimatsu M, Agui T. Functional Analysis of Duck, Goose, and Ostrich 2'-5'-Oligoadenylate Synthetase. *Infect Genet Evol* (2018) 62:220–32. doi: 10.1016/j.meegid.2018.04.036
10. Zhu J, Zhang Y, Ghosh A, Cuevas RA, Forero A, Dhar J, et al. Antiviral Activity of Human OASL Protein is Mediated by Enhancing Signaling of the RIG-I RNA Sensor. *Immunity* (2014) 40(6):936–48. doi: 10.1016/j.immuni.2014.05.007
11. Rong E, Wang X, Chen H, Yang C, Hu J, Liu W, et al. Molecular Mechanisms for the Adaptive Switching Between the OAS/RNase L and OASL/RIG-I Pathways in Birds and Mammals. *Front Immunol* (2018) 9:1398. doi: 10.3389/fimmu.2018.01398
12. Tatsumi R, Sekiya S, Nakanishi R, Mizutani M, Kojima S, Sokawa Y. Function of Ubiquitin-Like Domain of Chicken 2'-5'-Oligoadenylate Synthetase in Conformational Stability. *J Interferon Cytokine Res* (2003) 23(11):667–76. doi: 10.1089/107999003322558809
13. Magor KE, Miranzo Navarro D, Barber MR, Petkau K, Fleming-Canepa X, Blyth GA, et al. Defense Genes Missing From the Flight Division. *Dev Comp Immunol* (2013) 41(3):377–88. doi: 10.1016/j.dci.2013.04.010
14. Frieman M, Ratia K, Johnston RE, Mesecar AD, Baric RS. Severe Acute Respiratory Syndrome Coronavirus Papain-Like Protease Ubiquitin-Like

Domain and Catalytic Domain Regulate Antagonism of IRF3 and NF-kappaB Signaling. *J Virol* (2009) 83(13):6689–705. doi: 10.1128/JVI.02220-08
15. Napolitano A, van der Veen AG, Bunyan M, Borg A, Frith D, Howell S, et al. Cysteine-Reactive Free ISG15 Generates IL-1beta-Producing CD8alpha(+) Dendritic Cells at the Site of Infection. *J Immunol* (2018) 201(2):604–14. doi: 10.4049/jimmunol.1701322
16. Recht M, Borden EC, Knight EJr. A Human 15-kDa IFN-Induced Protein Induces the Secretion of IFN-Gamma. *J Immunol* (1991) 147(8):2617–23.
17. Swaim CD, Scott AF, Canadeo LA, Huibregtse JM. Extracellular ISG15 Signals Cytokine Secretion Through the LFA-1 Integrin Receptor. *Mol Cell* (2017) 68 (3):581–90 e5. doi: 10.1016/j.molcel.2017.10.003
18. Kim YJ, Kim ET, Kim YE, Lee MK, Kwon KM, Kim KI, et al. Consecutive Inhibition of ISG15 Expression and ISGylation by Cytomegalovirus Regulators. *PloS Pathog* (2016) 12(8):e1005850. doi: 10.1371/journal.ppat.1005850
19. Tang Y, Zhong G, Zhu L, Liu X, Shan Y, Feng H, et al. Herc5 Attenuates Influenza A Virus by Catalyzing ISGylation of Viral NS1 Protein. *J Immunol* (2010) 184(10):5777–90. doi: 10.4049/jimmunol.0903588
20. Kwon YT, Ciechanover A. The Ubiquitin Code in the Ubiquitin-Proteasome System and Autophagy. *Trends Biochem Sci* (2017) 42(11):873–86. doi: 10.1016/j.tibs.2017.09.002
21. Devaraj SG, Wang N, Chen Z, Chen Z, Tseng M, Barretto N, et al. Regulation of IRF-3-Dependent Innate Immunity by the Papain-Like Protease Domain of the Severe Acute Respiratory Syndrome Coronavirus. *J Biol Chem* (2007) 282 (44):32208–21. doi: 10.1074/jbc.M704870200
22. Frias-Staheli N, Giannakopoulos NV, Kikkert M, Taylor SL, Bridgen A, Paragas J, et al. Ovarian Tumor Domain-Containing Viral Proteases Evade Ubiquitin- and ISG15-Dependent Innate Immune Responses. *Cell Host Microbe* (2007) 2(6):404–16. doi: 10.1016/j.chom.2007.09.014
23. Holzer B, Bakshi S, Bridgen A, Baron MD. Inhibition of Interferon Induction and Action by the Nairovirus Nairobi Sheep Disease Virus/Ganjam Virus. *PloS One* (2011) 6(12):e28594. doi: 10.1371/journal.pone.0028594
24. Dzimianski JV, Scholte FEM, Williams IL, Langley C, Freitas BT, Spengler JR, et al. Determining the Molecular Drivers of Species-Specific Interferon-Stimulated Gene Product 15 Interactions With Nairovirus Ovarian Tumor Domain Proteases. *PloS One* (2019) 14(12):e0226415. doi: 10.1371/journal.pone.0226415
25. Deaton MK, Dzimianski JV, Daczkowski CM, Whitney GK, Mank NJ, Parham MM, et al. Biochemical and Structural Insights Into the Preference of Nairoviral DeISGylases for Interferon-Stimulated Gene Product 15 Originating From Certain Species. *J Virol* (2016) 90(18):8314–27. doi: 10.1128/JVI.00975-16
26. Denison MR, Perlman S. Translation and Processing of Mouse Hepatitis Virus Virion RNA in a Cell-Free System. *J Virol* (1986) 60(1):12–8. doi: 10.1128/jvi.60.1.12-18.1986
27. Bergeron E, Albarino CG, Khristova ML, Nichol ST. Crimean-Congo Hemorrhagic Fever Virus-Encoded Ovarian Tumor Protease Activity Is Dispensable for Virus RNA Polymerase Function. *J Virol* (2010) 84(1):216–26. doi: 10.1128/JVI.01859-09
28. Otwinowski Z, Minor W. [20] Processing of X-Ray Diffraction Data Collected in Oscillation Mode. *Methods Enzymol* (1997) 276:307–26. doi: 10.1016/S0076-6879(97)76066-X
29. Winn MD, Ballard CC, Cowtan KD, Dodson EJ, Emsley P, Evans PR, et al. Overview of the CCP4 Suite and Current Developments. *Acta Crystallogr D Biol Crystallogr* (2011) 67(Pt 4):235–42. doi: 10.1107/S0907444910045749
30. McCoy AJ, Grosse-Kunstleve RW, Adams PD, Winn MD, Storoni LC, Read RJ. Phaser Crystallographic Software. *J Appl Crystallogr* (2007) 40(Pt 4):658–74. doi: 10.1107/S0021889807021206
31. Webb B, Sali A. Comparative Protein Structure Modeling Using MODELLER. *Curr Protoc Bioinf* (2016) 54:5 6 1–5 6 37. doi: 10.1002/cpbi.3
32. Terwilliger TC, Grosse-Kunstleve RW, Afonine PV, Moriarty NW, Zwart PH, Hung LW, et al. Iterative Model Building, Structure Refinement and Density Modification With the PHENIX AutoBuild Wizard. *Acta Crystallogr D Biol Crystallogr* (2008) 64(Pt 1):61–9. doi: 10.1107/S090744490705024X
33. Emsley P, Cowtan K. Coot: Model-Building Tools for Molecular Graphics. *Acta Crystallogr D Biol Crystallogr* (2004) 60(Pt 12 Pt 1):2126–32. doi: 10.1107/S0907444904019158
34. Adams PD, Afonine PV, Bunkoczi G, Chen VB, Davis IW, Echols N, et al. PHENIX: A Comprehensive Python-Based System for Macromolecular Structure Solution. *Acta Crystallogr D Biol Crystallogr* (2010) 66(Pt 2):213–21. doi: 10.1107/S0907444909052925
35. Dhar J, Cuevas RA, Goswami R, Zhu J, Sarkar SN, Barik S. 2'-5'-Oligoadenylate Synthetase-Like Protein Inhibits Respiratory Syncytial Virus Replication and Is Targeted by the Viral Nonstructural Protein 1. *J Virol* (2015) 89(19):10115–9. doi: 10.1128/JVI.01076-15
36. Krissinel E, Henrick K. Inference of Macromolecular Assemblies From Crystalline State. *J Mol Biol* (2007) 372(3):774–97. doi: 10.1016/j.jmb.2007.05.022
37. Langley C, Goodwin O, Dzimianski JV, Daczkowski CM, Pegan SD. Structure of Interferon-Stimulated Gene Product 15 (ISG15) From the Bat Species Myotis Davidii and the Impact of Interdomain ISG15 Interactions on Viral Protein Engagement. *Acta Crystallogr D Struct Biol* (2019) 75(Pt 1):21–31. doi: 10.1107/S2059798318015322
38. Daczkowski CM, Dzimianski JV, Clasman JR, Goodwin O, Mesecar AD, Pegan SD. Structural Insights Into the Interaction of Coronavirus Papain-Like Proteases and Interferon-Stimulated Gene Product 15 From Different Species. *J Mol Biol* (2017) 429(11):1661–83. doi: 10.1016/j.jmb.2017.04.011
39. Cavanagh D. Coronavirus Avian Infectious Bronchitis Virus. *Vet Res* (2007) 38(2):281–97. doi: 10.1051/vetres:2006055
40. Rhee SG. Overview on Peroxiredoxin. *Mol Cells* (2016) 39(1):1–5. doi: 10.14348/molcells.2016.2368
41. Yamaguchi R, Yamamoto T, Sakamoto A, Ishimaru Y, Narahara S, Sugiuchi H, et al. Roles of Myeloperoxidase and GAPDH in Interferon-Gamma Production of GM-CSF-Dependent Macrophages. *Heliyon* (2016) 2(2): e00080. doi: 10.1016/j.heliyon.2016.e00080
42. Freitas BT, Scholte FEM, Bergeron E, Pegan SD. How ISG15 Combats Viral Infection. *Virus Res* (2020) 286:198036. doi: 10.1016/j.virusres.2020.198036
43. Daczkowski CM, Goodwin OY, Dzimianski JV, Farhat JJ, Pegan SD. Structurally Guided Removal of DeISGylase Biochemical Activity From Papain-Like Protease Originating From Middle East Respiratory Syndrome Coronavirus. *J Virol* (2017) 91(23):1–16. doi: 10.1128/JVI.01067-17
44. Dzimianski JV, Beldon BS, Daczkowski CM, Goodwin OY, Scholte FEM, Bergeron E, et al. Probing the Impact of Nairovirus Genomic Diversity on Viral Ovarian Tumor Domain Protease (vOTU) Structure and Deubiquitinase Activity. *PloS Pathog* (2019) 15(1):e1007515. doi: 10.1371/journal.ppat.1007515
45. Converse JD, Hoogstraal H, Moussa MI, Feare CJ, Kaiser MN. Soldado Virus (Hughes Group) From Ornithodoros (Alectorobius) Capensis (Ixodoidea: Argasidae) Infesting Sooty Tern Colonies in the Seychelles, Indian Ocean. *Am J Trop Med Hyg* (1975) 24(6 Pt 1):1010–8. doi: 10.4269/ajtmh.1975.24.1010
46. Spengler JR, Estrada-Pena A. Host Preferences Support the Prominent Role of Hyalomma Ticks in the Ecology of Crimean-Congo Hemorrhagic Fever. *PloS Negl Trop Dis* (2018) 12(2):e0006248. doi: 10.1371/journal.pntd.0006248
47. Palomar AM, Portillo A, Mazuelas D, Roncero L, Arizaga J, Crespo A, et al. Molecular Analysis of Crimean-Congo Hemorrhagic Fever Virus and Rickettsia in Hyalomma Marginatum Ticks Removed From Patients (Spain) and Birds (Spain and Morocco), 2009-2015. *Ticks Tick Borne Dis* (2016) 7 (5):983–7. doi: 10.1016/j.ttbdis.2016.05.004

Author Disclaimer: The findings and conclusions in this report are those of the authors and do not necessarily represent the official position of the Centers for Disease Control and Prevention.

Conflict of Interest: The authors declare that the research was conducted in the absence of any commercial or financial relationships that could be construed as a potential conflict of interest.

Publisher's Note: All claims expressed in this article are solely those of the authors and do not necessarily represent those of their affiliated organizations, or those of the publisher, the editors and the reviewers. Any product that may be evaluated in this article, or claim that may be made by its manufacturer, is not guaranteed or endorsed by the publisher.

Advantages of publishing in Frontiers

OPEN ACCESS
Articles are free to read for greatest visibility and readership

FAST PUBLICATION
Around 90 days from submission to decision

HIGH QUALITY PEER-REVIEW
Rigorous, collaborative, and constructive peer-review

TRANSPARENT PEER-REVIEW
Editors and reviewers acknowledged by name on published articles

Frontiers
Avenue du Tribunal-Fédéral 34
1005 Lausanne | Switzerland

Visit us: www.frontiersin.org
Contact us: frontiersin.org/about/contact

REPRODUCIBILITY OF RESEARCH
Support open data and methods to enhance research reproducibility

DIGITAL PUBLISHING
Articles designed for optimal readership across devices

FOLLOW US
@frontiersin

IMPACT METRICS
Advanced article metrics track visibility across digital media

EXTENSIVE PROMOTION
Marketing and promotion of impactful research

LOOP RESEARCH NETWORK
Our network increases your article's readership